frontiers | Research Topics

Women in plant nutrition 2022

Edited by
Petra Bauer, Bahar Yildiz Kutman, Stefania Astolfi and Chiou Tzyy-Jen

Published in
Frontiers in Plant Science

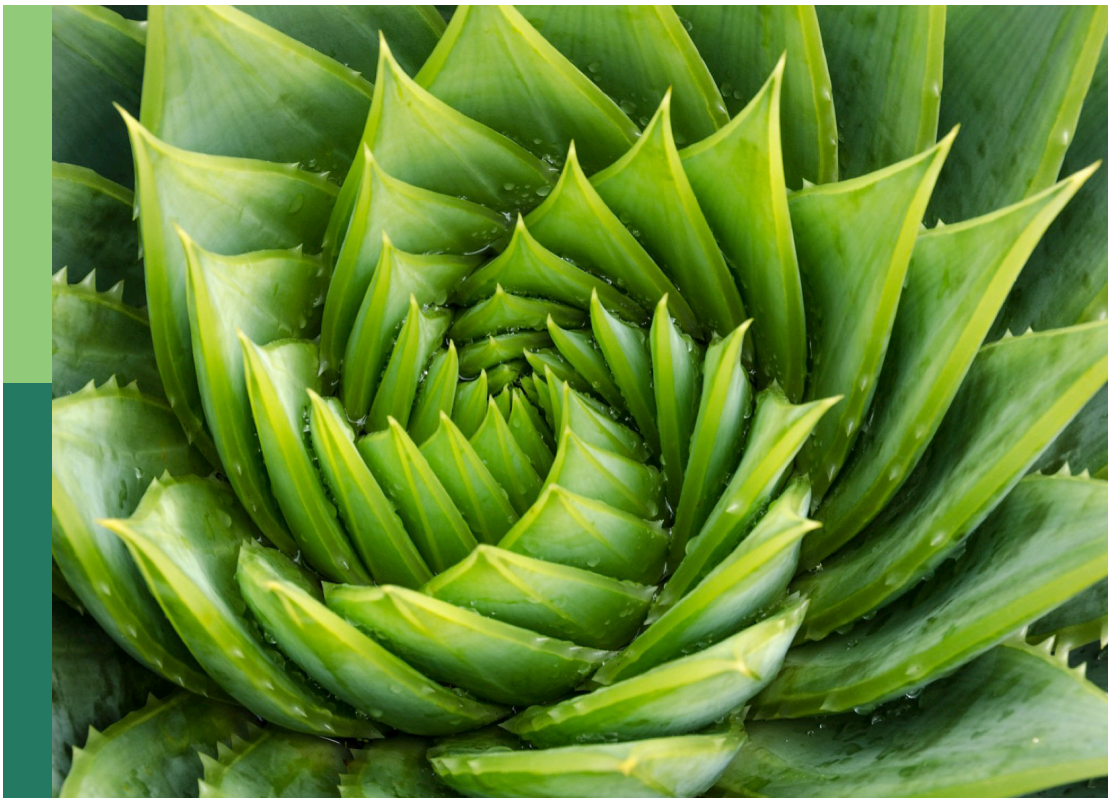

ISSN 1664-8714
ISBN 978-2-8325-3509-7
DOI 10.3389/978-2-8325-3509-7

About Frontiers

Frontiers is more than just an open access publisher of scholarly articles: it is a pioneering approach to the world of academia, radically improving the way scholarly research is managed. The grand vision of Frontiers is a world where all people have an equal opportunity to seek, share and generate knowledge. Frontiers provides immediate and permanent online open access to all its publications, but this alone is not enough to realize our grand goals.

Frontiers journal series

The Frontiers journal series is a multi-tier and interdisciplinary set of open-access, online journals, promising a paradigm shift from the current review, selection and dissemination processes in academic publishing. All Frontiers journals are driven by researchers for researchers; therefore, they constitute a service to the scholarly community. At the same time, the *Frontiers journal series* operates on a revolutionary invention, the tiered publishing system, initially addressing specific communities of scholars, and gradually climbing up to broader public understanding, thus serving the interests of the lay society, too.

Dedication to quality

Each Frontiers article is a landmark of the highest quality, thanks to genuinely collaborative interactions between authors and review editors, who include some of the world's best academicians. Research must be certified by peers before entering a stream of knowledge that may eventually reach the public - and shape society; therefore, Frontiers only applies the most rigorous and unbiased reviews. Frontiers revolutionizes research publishing by freely delivering the most outstanding research, evaluated with no bias from both the academic and social point of view. By applying the most advanced information technologies, Frontiers is catapulting scholarly publishing into a new generation.

What are Frontiers Research Topics?

Frontiers Research Topics are very popular trademarks of the *Frontiers journals series*: they are collections of at least ten articles, all centered on a particular subject. With their unique mix of varied contributions from Original Research to Review Articles, Frontiers Research Topics unify the most influential researchers, the latest key findings and historical advances in a hot research area.

Find out more on how to host your own Frontiers Research Topic or contribute to one as an author by contacting the Frontiers editorial office: frontiersin.org/about/contact

Women in plant nutrition: 2022

Topic editors

Petra Bauer — Heinrich Heine University of Düsseldorf, Germany
Bahar Yildiz Kutman — Gebze Technical University, Türkiye
Stefania Astolfi — University of Tuscia, Italy
Chiou Tzyy-Jen — Agricultural Biotechnology Research Center, Academia Sinica, Taiwan

Citation

Bauer, P., Kutman, B. Y., Astolfi, S., Tzyy-Jen, C., eds. (2023). *Women in plant nutrition: 2022*. Lausanne: Frontiers Media SA. doi: 10.3389/978-2-8325-3509-7

Table of contents

frontiers | Frontiers in Plant Science

TYPE Editorial
PUBLISHED 05 September 2023
DOI 10.3389/fpls.2023.1271399

OPEN ACCESS

EDITED AND REVIEWED BY
Antonio Lupini,
Mediterranea University of Reggio Calabria, Italy

*CORRESPONDENCE
Stefania Astolfi
sastolfi@unitus.it
Petra Bauer
petra.bauer@hhu.de
Tzyy-Jen Chiou
tjchiou@gate.sinica.edu.tw
Bahar Yildiz Kutman
bykutman@gtu.edu.tr

RECEIVED 02 August 2023
ACCEPTED 30 August 2023
PUBLISHED 05 September 2023

CITATION
Astolfi S, Bauer P, Chiou T-J and Kutman BY (2023) Editorial: Women in plant nutrition: 2022.
Front. Plant Sci. 14:1271399.
doi: 10.3389/fpls.2023.1271399

Editorial: Women in plant nutrition: 2022

Stefania Astolfi[1]*, Petra Bauer[2,3]*, Tzyy-Jen Chiou[4]* and Bahar Yildiz Kutman[5]*

[1]Department of Agriculture and Forest Sciences (DAFNE), University of Tuscia, Viterbo, Italy, [2]Institute of Botany, Heinrich Heine University, Düsseldorf, Germany, [3]Cluster of Excellence on Plant Sciences (CEPLAS), Heinrich-Heine University, Düsseldorf, Germany, [4]Agricultural Biotechnology Research Center, Academia Sinica, Taipei, Taiwan, [5]Institute of Biotechnology, Gebze Technical University, Gebze, Kocaeli, Türkiye

KEYWORDS

plant nutrition, iron, phosphorus, nitrogen, seed

Editorial on the Research Topic
Women in plant nutrition: 2022

Based on the UNESCO Institute for Statistics data (UIS—UNESCO Institute for Statistics, 2020), female scientists are a minority among researchers and less than 30% of researchers worldwide are women. For sustainable development, science and gender equality are critical concepts. To promote gender equality and highlight the significant contributions of women, Frontiers in Plant Science offered "Women in Plant Nutrition: 2022" platform to promote the work of women scientists particularly in all fields of Plant Nutrition.

The yield and quality of crop plants depend on the abilities of plants to obtain and utilize essential nutrients for their growth and development. Two vital macronutrients for plants are nitrogen and phosphorus. A crucial micronutrient is iron. Understanding the nutritional properties of these elements and how plants acquire them or react to deficiencies is essential for optimizing plant growth and ensuring sustainable agriculture practices. By understanding the mobilization and allocation of nitrogen, phosphorus, and other essential nutrients, we can cultivate healthier crops, protect the environment, and meet the increasing demands for food.

Nitrogen (N) nutrition in plants has significant implications for their growth, development, and overall productivity. The management of N nutrition requires to find a balance between providing adequate N for healthy growth and avoiding overuse that could harm the environment and alter ecological dynamics. Soil management, proper fertilization practices, and sustainable agricultural techniques can help achieve this balance while optimizing plant productivity and preserving environmental and public health. For improving the N fertilizer economy and sustainable agriculture, Padhan et al. attempt to gain an understanding of the processes and mechanisms associated with reproductive stage N remobilization and N partitioning to grain. On the other hand, Ji et al. proposed a sensor-based N-management strategy (GreenSeeker sensor) for the development and implementation of vegetable N-management strategies.

Being able to detect and protect plants from deficient phosphorous (P) is very relevant. P is taken up in the form of phosphate, that is highly relevant as macronutrient. However, phosphate stores are limited and have been only found in few countries. Knowing how

phosphate can be better acquired, mobilized, reused or recycled is a topic in several articles of this Research Topic. To increase the availability of insoluble phosphorus for plant use, Yahya et al. study the phosphate-solubilizing bacteria (PSB) by integrating soil nutritional status and meteorological conditions at the application site for sustainable wheat production. These PSB can be developed into potential biofertilizers in the future. Another mechanism by which plants achieve access to phosphate is the onset of autophagy, a controlled degradation and recycling pathway to mobilize the cells' own nutrient resources under stress and senescence. Lin et al. investigate the roles of two phosphate deficiency-induced autophagy-related proteins.

The study of Le Tougaard et al. aimed at demonstrating how phosphate deficiency can be better diagnosed in leaves in the field, especially when varying light conditions influence the symptoms differently in the various leaf developmental stages. As phytic acid (PA), the major phosphorus storage sink within the plant seeds, binds important essential minerals limiting their bioavailability, Fritelli et al. showed a genetic approach (TILLING strategy) to silence *TdMRP3* and improve micronutrients (Fe, Zn, Mn) concentration in wheat seeds through a significant reduction in PA content.

In addition to absorbing mineral nutrients directly by plant roots, most plant species can acquire nutrients such as phosphate from arbuscular mycorrhizal (AM) fungi *via* symbiotic interaction in natural conditions. The extraradical hyphal network of AM fungi facilitates the transport of nutrients, especially phosphorus, to the plant host in exchange for carbohydrates. Deng et al. characterized the nuclear factor Y (NF-Y) family members in Medicago. They found these transcription factors play crucial roles in arbuscular development and degeneration, offering new insights into the transcription program of AM symbiosis. Hsieh et al. took another aspect to investigate how AM symbiosis affects rice growth and ion homeostasis under salt stress. Their results suggest the potential interplay between phosphate-related signaling pathways and AM-enhanced salt tolerance.

Finally, seed nutritional properties are important for nutritional food security and selecting variants with the highest bio-available nutrient profiles is crucial to meet the global food demands. Iron is an essential micronutrient that frequently limits plant growth under alkaline and calcareous growth conditions. Iron is also frequently lacking in sufficient amounts in human diets. Knowing the genes impacting the uptake and allocation of iron in seeds is a milestone in improving plant-based nutrition. Lichtblau et al. describe a potential regulatory module for iron utilization and accumulation in seeds. Manipulating the amino acid residues involved in the interaction of transcription factors and regulatory proteins (including a small protein and putative E3 ligase) that can form a protein interaction complex is a novel suggested way for biofortification and coping with low Fe bioavailability. Dragicevic et al. found that nutrient properties of maize kernels depended on various kernel traits such as kernel color.

Taken together, this Research Topic highlights mechanisms for nitrogen and phosphate use, as well as potentially new mechanisms for increasing nutritional properties of seeds and kernels. These topics are important for improving nutritional food security and contributing to a better sustainable agriculatural land use system.

Author contributions

SA: Writing – original draft, Writing – review & editing. PB: Writing – original draft, Writing – review & editing. T-JC: Writing – original draft, Writing – review & editing. BK: Writing – original draft, Writing – review & editing.

Conflict of interest

The authors declare that the research was conducted in the absence of any commercial or financial relationships that could be construed as a potential conflict of interest.

The author(s) declared that they were an editorial board member of Frontiers, at the time of submission. This had no impact on the peer review process and the final decision

Publisher's note

frontiers | Frontiers in Plant Science

ORIGINAL RESEARCH
published: 10 June 2022
doi: 10.3389/fpls.2022.930049

The Iron Deficiency-Regulated Small Protein Effector FEP3/IRON MAN1 Modulates Interaction of BRUTUS-LIKE1 With bHLH Subgroup IVc and POPEYE Transcription Factors

Daniela M. Lichtblau[1†], Birte Schwarz[1†], Dibin Baby[1†], Christopher Endres[1], Christin Sieberg[1] and Petra Bauer[1,2]*

[1] *Institute of Botany, Heinrich Heine University Düsseldorf, Düsseldorf, Germany,* [2] *Cluster of Excellence on Plant Sciences, Heinrich Heine University Düsseldorf, Düsseldorf, Germany*

OPEN ACCESS

Edited by:
Marc Hanikenne, University of Liège, Belgium

Reviewed by:
Kuo-Chen Yeh, Academia Sinica, Taiwan
Takanori Kobayashi, Ishikawa Prefectural University, Japan

***Correspondence:**
Petra Bauer
petra.bauer@hhu.de

[†]These authors share first authorship

Specialty section:
This article was submitted to Plant Nutrition, a section of the journal Frontiers in Plant Science

Received: *27 April 2022*
Accepted: *19 May 2022*
Published: *10 June 2022*

Citation:
Lichtblau DM, Schwarz B, Baby D, Endres C, Sieberg C and Bauer P (2022) The Iron Deficiency-Regulated Small Protein Effector FEP3/IRON MAN1 Modulates Interaction of BRUTUS-LIKE1 With bHLH Subgroup IVc and POPEYE Transcription Factors. Front. Plant Sci. 13:930049. doi: 10.3389/fpls.2022.930049

In light of climate change and human population growth one of the most challenging tasks is to generate plants that are Fe-efficient, resilient to low Fe supply and Fe-biofortified. For such endeavors, it is crucial to understand the regulation of Fe acquisition and allocation in plants. One open question is how identified Fe-regulatory proteins comprising positive and negative regulators act together to steer Fe homeostasis. bHLH transcription factors (TFs) belonging to the subgroups IVb and IVc can initiate a bHLH cascade controlling the –Fe response in roots. In *Arabidopsis thaliana*, the –Fe-induced genes are sub-divided into several gene co-expression clusters controlled by different sets of TFs. Some of the co-expressed genes encode regulatory E3 ligase proteins BRUTUS (BTS)/BTS-LIKE (BTSL) and small proteins belonging to the group of FE UPTAKE-INDUCING PEPTIDE/IRON MAN (FEP/IMA). Recently, it was described that FEP1/IMA3 and FEP3/IMA1 proteins inhibit the repression of bHLH factors by BTS. We had postulated that –Fe-regulated co-expression clusters provide new information about regulatory protein interaction complexes. Here, we report a targeted yeast two-hybrid screen among 23 proteins of the –Fe response. This identified a novel protein interactome involving another E3 ligase, namely BTSL1, basic helix-loop-helix (bHLH) protein POPEYE (PYE) and transcription factors of the subgroup IVc as well as FEP3/IMA1. Because of the difficulty in stable BTSL1 protein expression in plant cells, we used a yeast two hybrid-based deletion mapping, homology modeling and molecular docking, to pinpoint interaction sites in BTSL1 and FEP3/IMA1. bHLH IVc TFs have similar residues at their C-terminus as FEP3/IMA1 interacting sites. FEP3/IMA1 attenuated interaction of BTSL1 and bHLH proteins in a yeast three-hybrid assay, in line with physiological data pointing to enhanced Fe acquisition and allocation in FEP3/IMA1 overexpression and *btsl1 btsl2* mutant plants. Hence, exploiting –Fe-induced gene co-expression networks identified

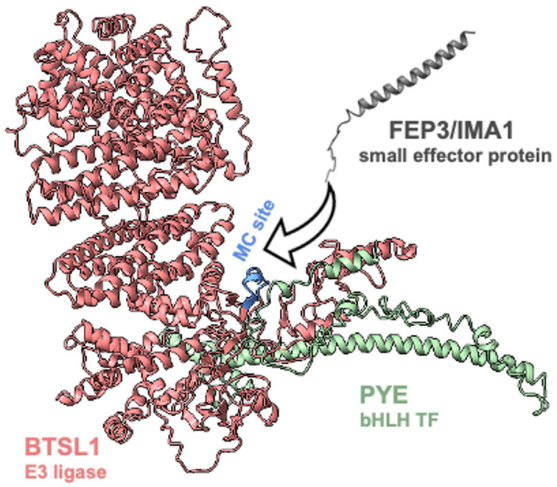

GRAPHICAL ABSTRACT

FEP3/IMA1 as a small effector protein that binds and inhibits the BTSL1 complex with PYE and bHLH subgroup IVc proteins. Structural analysis resolved interaction sites. This information helps improving models of Fe regulation and identifying novel targets for breeding of Fe-efficient crops.

Keywords: Fe deficiency, protein interaction network, bHLH, yeast three-hybrid, tripartite interaction, BRUTUS-LIKE E3 ligase, *Arabidopsis thaliana*, IRON MAN

INTRODUCTION

Generating resilient and biofortified crops for climate change and human nutrition requirements is one of the most challenging tasks for the future. The micronutrient iron (Fe) is a crucial cofactor for plant growth as it is needed for many redox and electron transfer reactions like those involved in chlorophyll synthesis and photosynthesis. Although very abundant in the soil, Fe is often not readily bio-accessible, because at neutral or basic pH it precipitates as insoluble Fe(III) oxides and hydroxides (Lindsay, 1988; Hans Wedepohl, 1995), and this will likely increase drastically with global warming and drought. To cope with low Fe bio-availability, plants mobilize Fe in the soil, either via Fe^{3+}-chelating phytosiderophores (in grasses, so-called Strategy II) or via acidification and reduction of Fe^{3+} into Fe^{2+} (Strategy I) (Marschner and Römheld, 1994). Additionally, plants mobilize internal sources of Fe and transport it toward the shoots (Connorton et al., 2017). Fe deficiency stress results in leaf chlorosis and poor growth. Elevated cellular Fe, instead, may generate radicals via the Fe-catalyzed Fenton reaction, leading to unspecific damage of cellular components. Fe homeostasis is thus very critical for the performance of plants. Plants constantly adjust Fe mobilization with plant growth and environmental stress factors (Brumbarova et al., 2015). Clearly, plants sense the Fe status, signal their demand and regulate internal allocation and uptake of external Fe. The need to orchestrate these different processes is reflected in the complex transcriptomic network of genes that are co-regulated under Fe deficiency (–Fe) and that encode metal ion transporters, enzymes for reduction and chelation of Fe, transcription factors (TFs) and other regulators that steer the coordinated Fe deficiency response (Ivanov et al., 2012; Schwarz and Bauer, 2020). The co-expression clusters allow feed-forward and feed-back regulation of Fe mobilization, and there are many open questions as to the complex interconnections and regulatory mechanisms of the encoded proteins.

A cascade of basic helix-loop-helix (bHLH) transcription factors (TFs) that is conserved at least within eudicots, up-regulates Fe acquisition in response to a –Fe signal (Gao et al., 2019b). Arabidopsis (*Arabidopsis thaliana*) has at least 12 bHLH proteins controlling Fe uptake (Gao et al., 2019b; Schwarz and Bauer, 2020). bHLH proteins have been classified into subgroups according to their bHLH domain amino acid sequences (Heim et al., 2003). Subgroup IVc bHLH TFs (bHLH034, bHLH104, ILR3/bHLH105, bHLH115) have redundant functions. Together with bHLH subgroup IVb protein URI/bHLH121 they form heterodimeric complexes and induce the –Fe response (Zhang et al., 2015; Li et al., 2016;

Abbreviations: 3AT, 3-amino-1,2,4-triazole; aa, amino acid; AD, activation domain; BD, binding domain; bHLH, basic helix-loop-helix; BiFC, bimolecular fluorescence complementation; GFP, green fluorescent protein; GUS, β-glucuronidase; HHE, hemerythrin/HHE cation-binding motif; mCherry, second generation mRFP derivative; mRFP, monomeric red fluorescent protein; ORF, open reading frame; OX, over-expression; RT-qPCR, reverse transcription quantitative PCR; SD, standard deviation (Statistics)/synthetic defined medium (Y2H); TF, transcription factor; WT, wild type; Y2H, yeast two-hybrid; Y3H, yeast three-hybrid; YFP, yellow fluorescent protein.

Liang et al., 2017; Gao et al., 2019a; Kim et al., 2019). bHLH011, another bHLH IVb TF, acts as a negative regulator of the Fe uptake machinery (Tanabe et al., 2019; Li et al., 2022). A third bHLH subgroup IVb protein named POPEYE (PYE) is also a negative regulator that down-regulates Fe distribution genes *NICOTIANAMINE SYNTHASE4* (*NAS4*), *FRO3* and *ZINC-INDUCED FACILITATOR1* (*ZIF1*) (Long et al., 2010). URI and bHLH IVc TFs up-regulate *PYE* and other co-expressed genes including *BHLH* Ib genes (Zhang et al., 2015; Liang et al., 2017; Gao et al., 2019a; Kim et al., 2019). –Fe-induced bHLH subgroup Ib proteins (bHLH038, bHLH039, bHLH100, bHLH101) form dimers with the bHLH protein FIT, and altogether they are essential for up-regulating Fe acquisition (Colangelo and Guerinot, 2004; Jakoby et al., 2004; Yuan et al., 2008; Wang et al., 2013; Trofimov et al., 2019; Cai et al., 2021). Root Fe acquisition involves the activation of *FERRIC REDUCTION OXIDASE2* (*FRO2*) encoding the Fe reductase that reduces Fe^{3+} to Fe^{2+} (Robinson et al., 1999) and *IRON-REGULATED TRANSPORTER1* (*IRT1*), which codes for the importer of Fe^{2+} (Vert et al., 2002).

The action of several bHLH subgroup IVb and IVc transcription factors is counteracted by E3 ligases that are induced by the bHLH cascade. ILR3 and bHLH115 are controlled through proteasomal degradation by their own target BRUTUS (BTS), a negative regulator of Fe uptake (Selote et al., 2015; Liang et al., 2017; Li et al., 2021). bHLH104 also interacts with BTS (Long et al., 2010; Selote et al., 2015). This paradoxical situation of incoherent regulation was explained by the need to have a shut-down mechanism for Fe re-mobilization (Hindt et al., 2017). Another hypothesis is that BTS ensures a constant turnover of TF (Selote et al., 2015). BTS has an interesting domain structure that indicates Fe-sensing functions. BTS has a C-terminal REALLY INTERESTING NEW GENE (RING) domain with E3 ligase activity and N-terminal hemerythrin/HHE-like cation-binding motifs for Fe and oxygen binding (Kobayashi et al., 2013; Selote et al., 2015). The two homologs BTS-LIKE1 (BTSL1) and BTSL2, which negatively regulate Fe uptake, have partly redundant functions, but only BTS is expressed in roots and shoots, while BTSL1 and BTSL2 are root-specific (Hindt et al., 2017). BTSL2 is tightly co-regulated with FIT, while BTSL1 is most similarly co-regulated with FIT target genes and Fe homeostasis genes for Fe allocation (Schwarz and Bauer, 2020). It was reported that FIT was degraded in the presence of BTSL2 (Rodriguez-Celma et al., 2019). What makes BTS/BTSL proteins so interesting is that they resemble FBXL5, a component of the mammalian Fe-sensing E3 ligase complex (Kobayashi et al., 2013). BTS protein stability and function are also coupled to Fe presence or absence. However, unlike FBXL5, BTS was found to be unstable in the presence of Fe (Selote et al., 2015).

A third level of regulation is exerted by small proteins. BTS was found to ubiquitinate a co-expressed and –Fe-regulated small Fe-uptake-promoting regulatory protein FE UPTAKE-INDUCING PEPTIDE3 (FEP3)/IRON MAN1 (IMA1) (Li et al., 2021). FEP/IMA are an interesting class of potential phloem-mobile small proteins. They share a 17-amino-acid C-terminal consensus sequence (Grillet et al., 2018; Hirayama et al., 2018). FEP/IMA small proteins induce Fe acquisition (Kobayashi et al., 2020), and indeed they are functionally interchangeable between species, showing that there must be likely a conserved mechanism of action (Grillet et al., 2018). When our work was initiated, no mechanism of action of FEP/IMA proteins had been known. In parallel to our work, just recently, it was described that FEP1/IMA3 and FEP3/IMA1 stabilized bHLH115 and ILR3 in the presence of BTS (Li et al., 2021). FEP/IMA proteins inhibited BTS-mediated degradation of the Fe deficiency response-inducing bHLH subgroup IVc proteins (Li et al., 2021). Interestingly, the bHLH factors have a C-terminal stretch resembling the FEP/IMA interaction region in BTS (Li et al., 2021). From this work, the question remained whether FEP/IMA proteins target BTSL proteins in similar manner. It was also unclear whether bHLH subgroup IVc TFs are targets of BTSL proteins. Moreover, little information has been available on protein complex structural aspects that explain the physiological data.

Transcriptional co-regulation in response to –Fe can be an indicator of protein-protein interaction, e.g., in the case of bHLH039/FIT (Yuan et al., 2008). We deciphered that –Fe-regulated co-expression gene clusters and their regulators serve to identify novel protein interaction complexes. We report here, that we tested protein interactions among 23 proteins of the –Fe response. Among them, we identified an interactome involving the proteins BTSL1, FEP3/IMA1, PYE, and bHLH subgroup IVc TFs. Analysis of this protein interactome showed that FEP3/IMA1 is an effector modulating the BTSL1-bHLH protein interaction.

RESULTS

A Targeted Yeast Two-Hybrid Screen Uncovered the BTSL1-bHLH-FEP3/IMA1 Interactome

To identify novel protein interaction complexes, we exploited co-expression network information from Fe deficiency transcriptomics data sets (Ivanov et al., 2012; Schwarz and Bauer, 2020) and literature to select 23 candidates for a targeted yeast two-hybrid (Y2H)-based pairwise protein interaction screen, hereafter termed targeted Y2H screen (**Supplementary Table 1**). Criteria for the selection of candidates were (i) unknown functions of cytosolic proteins during Fe deficiency responses (at the time the study was initiated) and (ii) known regulatory functions of Fe homeostasis in the cytosol or nucleus, including proteins from outside of this network and enzymatic functions. Because of the redundancy of bHLH subgroup Ib proteins, we had limited this group to bHLH039, which has the strongest effect among the four proteins (Wang et al., 2013; Trofimov et al., 2019).

At first, all 23 candidates were tested in pairwise combinations in the targeted Y2H screen (**Supplementary Table 1** and **Supplementary Figures 1**, **2**). If possible, we performed reciprocal (AD/BD and vice versa) combinations and included homodimeric interaction tests. 5–6% of tested interactions were positive and they comprised 20 heterodimeric and six

homodimeric interactions (summarized in **Figure 1**). We noted that several interactions involved BTS or BTSL proteins and bHLH factors. For example, BTSL1 interacted with PYE, ILR3, MYB72, DUF506, SDI1, PRS2, FEP3/IMA1, and UP2. Besides BTSL1, PYE interacted with UP2 and SDI1. Hence, the targeted Y2H screen provided evidence for a Fe-regulatory interactome involving PYE and bHLH subgroup IVc TFs together with FEP3/IMA1 and BTSL1. Additionally, the connection between Fe, sulfur and glucosinate metabolism via SDI interactions is suggested from the screen (Aarabi et al., 2016; Samira et al., 2018). Among the interacting pairs, we detected the expected interactions FIT + bHLH039 (Yuan et al., 2008), BTS + ILR3 (Long et al., 2010), BTS + bHLH104 (Long et al., 2010), PYE + ILR3 (Selote et al., 2015), and ILR3 + ILR3 (Li et al., 2016). The latter was found negative in another study (Selote et al., 2015). Some reported protein interactions were not picked up in our screen, bHLH104 + ILR3 (Zhang et al., 2015), FIT + BTSL2 (Rodriguez-Celma et al., 2019). On the other hand, we picked up an interaction that had been found to be negative in one previous study, namely PYE + PYE (Selote et al., 2015). The cases of interacting or non-interacting pairs, that were different from the literature can be explained by different protein fusion constructs used and technical aspects related to different experimental Y2H procedures. For example, FEP3/IMA1 interaction with BTS was previously detected using adenine selection in the Y2H assay (Li et al., 2021). Instead, our study used histidine selection and supplementation with 3AT to show that FEP3/IMA1 interacted with BTSL1 and BTSL2 but not BTS. Presumably, the stringency of Y2H conditions impacted colony growth and protein interaction.

In summary, the screen with 23 protein candidates uncovered 19 previously not known heterodimer and five homodimer interactions. We decided to focus on the

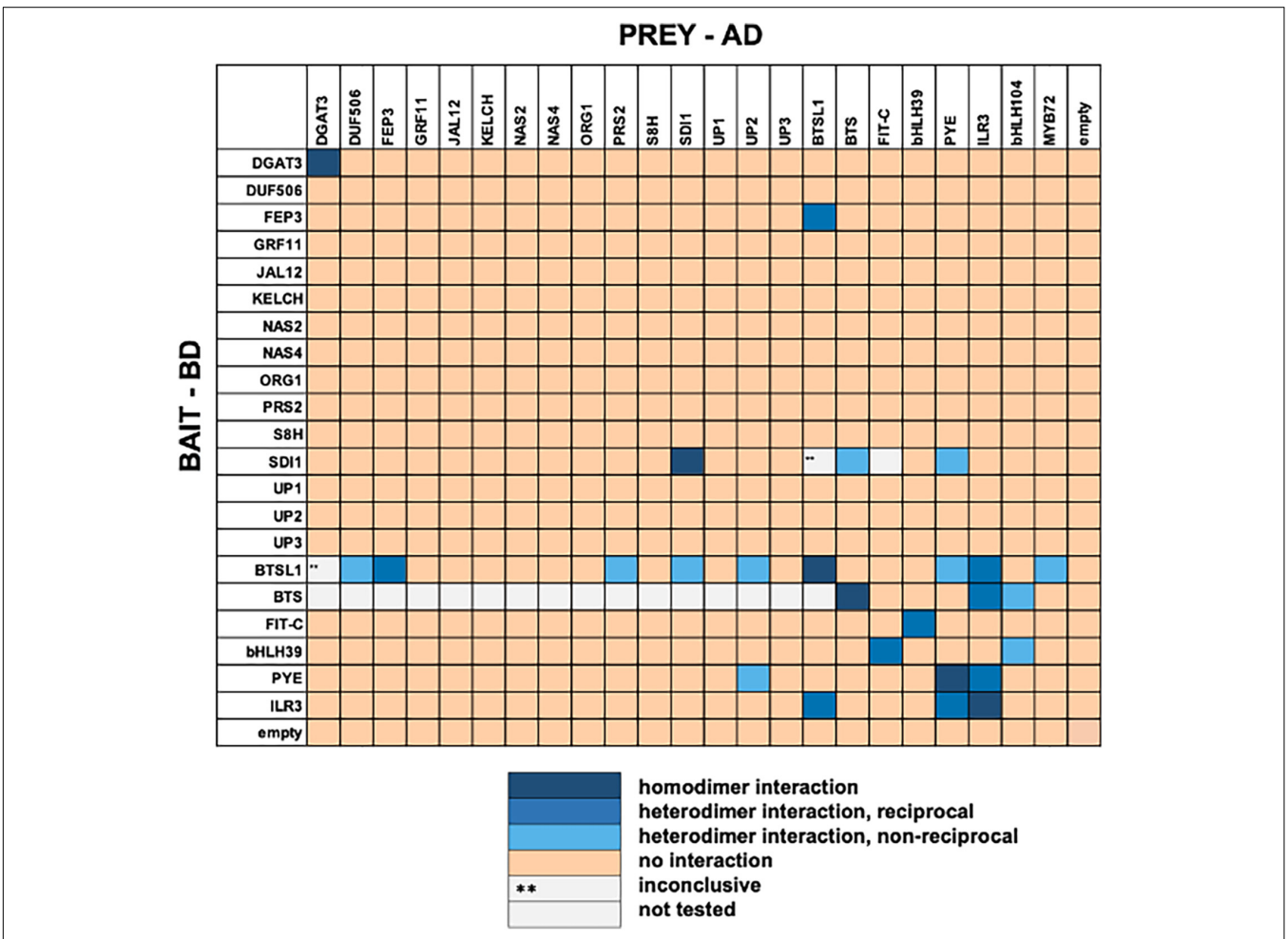

FIGURE 1 | Summary results of targeted yeast two hybrid (Y2H) screen. Twenty three protein candidates (**Supplementary Table 1**) were tested reciprocally in pairwise combinations in a targeted Y2H screen. Bait protein was fused to the GAL4 DNA-binding domain (BD), prey protein to the GAL4 activation domain (AD). The color code distinguishes homodimeric interaction (dark blue), reciprocal heterodimeric interaction (middle blue), non-reciprocal heterodimeric interaction (light blue), no interaction (light orange) or inconclusive and non-tested interactions (**, light gray). bHLH104 and Myb72 were not included as bait because of autoactivation. FIT-C was included as it is not auto-activating (Gratz et al., 2020). Original data are presented in **Supplementary Figures 1**, **2**.

BTSL1-bHLH-FEP3/IMA1 interactome. At the time the screen was conducted a mechanism of action of BTSL and FEP3/IMA1 had not been known, and we postulated a regulatory protein interaction.

Evidence for the BTSL1-bHLH-FEP3/IMA1 Interactome Was Further Studied in Targeted Assays

The discovered BTSL1-bHLH-FEP3/IMA1 interactome attracted our attention as it suggested mechanistic insight into the functions of these proteins in the context of bHLH TF action. In the validation experiments we included all TFs of the bHLH subgroup IVb and IVc group as their roles in Fe regulation were being revealed (**Figure 2** and **Supplementary Figure 3**). Deletion constructs were included to avoid auto-activation in the case of bHLH104-C, bHLH115-C and bHLH034-C (**Figures 2A,B**). BTS, BTSL1 and BTSL2 were tested against all bHLH proteins of the subgroups IVb and IVc (**Figures 2A,B**) and each other (**Supplementary Figure 3A**). bHLH proteins ILR3, bHLH104-C and PYE were also tested against each other (**Supplementary Figure 3B**). This way, we found the following positive interactions: BTS interacted with ILR3, bHLH104-C, bHLH115-C, bHLH034-C and URI (**Figure 2**), confirming the interactions of BTS with bHLH104, ILR3 and bHLH115 (Long et al., 2010; Selote et al., 2015; Li et al., 2021). Previously no interaction was found for BTS-URI (Long et al., 2010; Gao et al., 2019a) and BTS-bHLH034-C (Long et al., 2010). We did not find evidence for interaction of BTS with PYE, FEP3/IMA1, bHLH011, BTSL1, or BTSL2 (**Figure 2**), confirming published data that BTS does not interact with PYE (Long et al., 2010; Selote et al., 2015) and bHLH011 (Long et al., 2010). As mentioned above, BTS had been found to interact with FEP3/IMA1 by Li et al. (2021). BTSL1 interacted in our study with ILR3, bHLH104-C, PYE, FEP3/IMA1, bHLH115-C, and bHLH034-C (**Figure 2**). BTSL1 did not interact with bHLH011, URI, BTS and BTSL2. BTSL2 interacted with bHLH104-C, PYE and FEP3/IMA1 (**Figure 2**), while it did not interact with ILR3, BTS, and BTSL1. In a previous study, URI was also not found to interact with BTSL1 or BTSL2 (Gao et al., 2019a). We found that bHLH104-C interacted additionally with ILR3, PYE and these factors homodimerized (**Supplementary Figure 3B**). Hence, bHLH104-C indeed interacts with ILR3 (Li et al., 2016). bHLH104 homodimerizes as previously found (Li et al., 2016), and bHLH104 interacts with PYE (Selote et al., 2015). Since it was reported that BTSL1 and BTSL2 interact with FIT, but Y2H data were not yet provided (Rodriguez-Celma et al., 2019), we also re-tested specifically the interaction of BTSL1 and BTSL2 with full-length FIT and bHLH039. However, as in the targeted Y2H screen above, we did not find any proof in any combination for BTSL1 or BTSL2 interaction with FIT nor bHLH039, even though both proteins worked successfully as FIT/bHLH039 interaction pair (**Supplementary Figures 3C,D**).

Taken together, the BTSL1-bHLH-FEP3/IMA1 interactome was confirmed by targeted and extended Y2H data (summarized in **Figure 2C**). Some proteins within this group had a large set of interaction partners, e.g., bHLH104-C and BTSL1. Others had only one or none, e.g., URI and bHLH011. This shows specificity at the level of protein interactions. The interaction of BTSL1 with FEP3/IMA1 had been particularly exciting since this had offered the possibility of uncovering a novel mechanism of action for FEP3/IMA1 and BTSL1. We also focused on interacting bHLH proteins ILR3, bHLH104 and PYE. The C-termini of some of the transcription factors were sufficient for protein interactions. This was not surprising since the C-termini were also found sufficient for interactions of FIT-C (Gratz et al., 2020), bHLH034-C, bHLH104-C and ILR3-C (Li et al., 2016). Thus, BTSL1-bHLH interactions did not rely on the canonical bHLH domain.

Full-length BTS protein is unstable (Selote et al., 2015), and we suspected that because of the similar structures this might also be the case for BTSL1 and BTSL2. A reliable assay of bimolecular fluorescence complementation (BiFC) of YFP consists in simultaneous mRFP expression as control of transformation to validate novel protein interactions of Fe-regulated proteins in plant cells (Gratz et al., 2019; Khan et al., 2019). When we applied this method to study BTS/BTSL protein interactions, we detected the interaction between nY-BTSL1 and cY-PYE in a few of the transformed cells (**Supplementary Figure 4A**, top). It was not possible to detect interactions between other fusion proteins of BTSL1 and ILR3, bHLH104 or FEP3/IMA1, or any of the BTSL2 fusion proteins. In these negative cases, mRFP was detected as a control, indicating that transformation had worked (data not shown). The C-terminal part of BTS-C contains CHY- and CTCHY-type zinc (Zn) finger domains, a Zn ribbon domain and RING with E3 ligase function, and it was found sufficient for tested bHLH interactions (Selote et al., 2015). After switching to a comparable form of BTSL1-C we detected again an interaction with PYE by BiFC in a few cells (**Supplementary Figure 4A**, middle, nY-BTSL1-C + cY-PYE). mRFP signals were always present in all cells of the transformed region of the leaves (**Supplementary Figure 4A**). Interestingly, the YFP signals were present at the cell periphery rather than in the nucleus for full-length BTSL1 + PYE, while YFP signals were present in the nucleus for BTSL1-C + PYE fluorescence protein fusion (**Supplementary Figure 4A**, compare top and middle). Additionally, the interactions of BTSL1-C + ILR3 were detected in the nucleus (**Supplementary Figure 4A** bottom, nY-ILR3/cY-BTSL1-C; **Supplementary Figure 4B**). No other protein interactions could be confirmed by this method, also not FIT-BTSL1C, while mRFP was visible as positive transformation control in all cases (**Supplementary Figure 4C**, nYFP-FIT together with cY-BTSL1-C and -BTSL2-C). Overall, negative BTSL1 and BTSL2 data have to be carefully interpreted because of the low success rate for detecting protein interaction of BTSL1 and BTSL2 via BiFC, which was presumably due to their low stability.

In summary, the novel protein-protein interactions of the BTSL1-bHLH-FEP3/IMA1 interactome were also found by targeted Y2H assays. Plant cell BiFC, although a reliable assay with positive and negative controls, was not suited to confirm all protein interactions since YFP signals representing BTSL1 interactions were detected in only a few cells of the transformed regions. The differential localization of protein complexes BTSL1 + PYE and BTSL1-C + PYE by BiFC inside

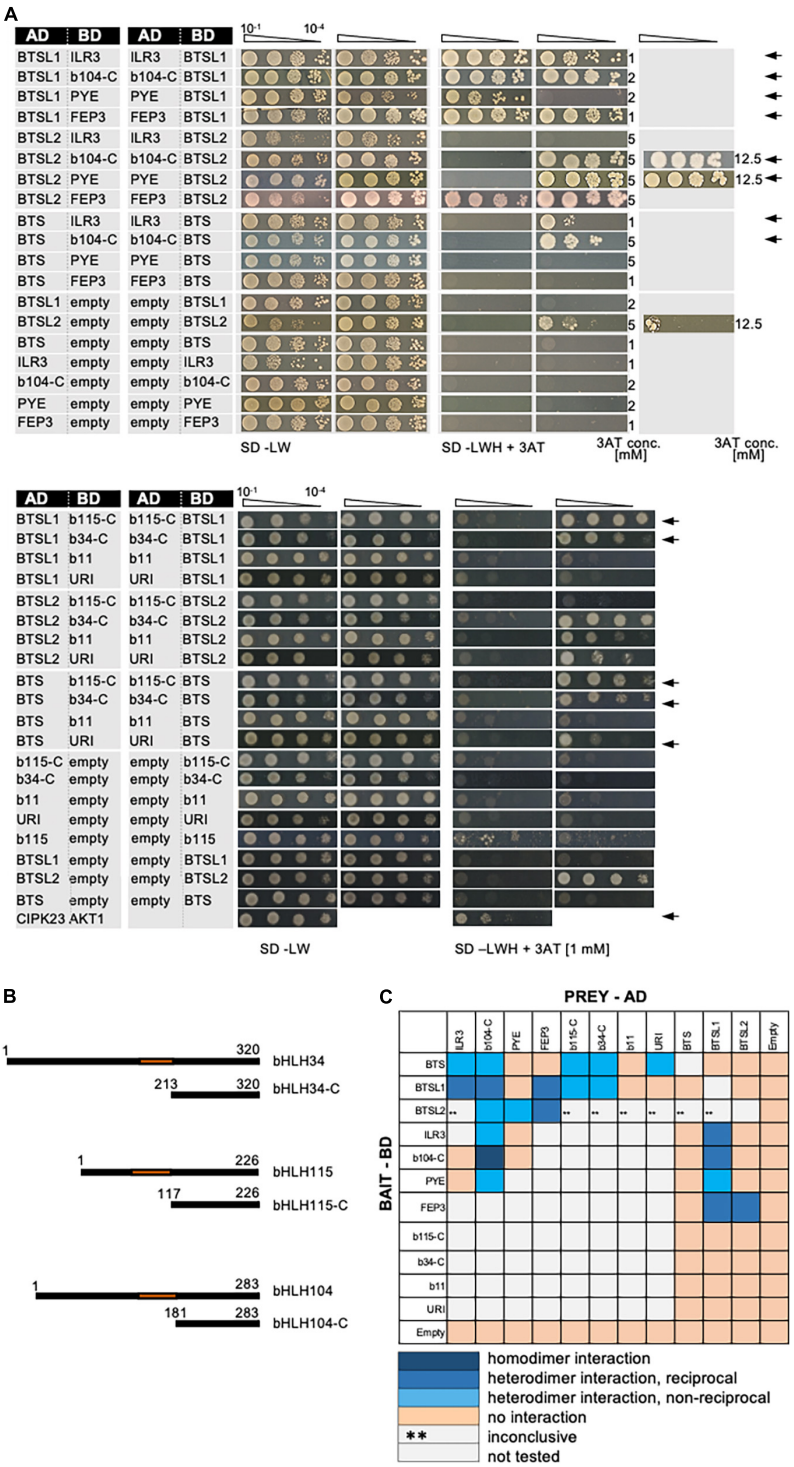

FIGURE 2 | Validation of the BTS/L-bHLH-FEP3/IMA1 interactome. **(A)** BTSL1 and BTSL2 were tested in reciprocal targeted Y2H assays against various bHLH proteins of the subgroups IVb and IVc and FEP3. Yeast co-transformed with the AD and BD combinations were spotted in 10-fold dilution series (A_{600} = 10^{-1}–10^{-4}) on SD-LW (transformation control) and SD-LWH plates supplemented with different concentrations (conc.) of 3AT as indicated on the right side (selection for protein interaction). Negative controls: empty vectors. Positive control: CIPK23 and AKT1. Arrows indicate interaction. **(B)** Schematic representation of full-length bHLH34, bHLH115, bHLH104 and their respective C-terminal parts used for Y2H. C-terminal parts lack the N-terminus and the DNA-binding domains (represented in orange). **(C)** Summary results of A. The color code distinguishes homodimeric interaction (dark blue), reciprocal heterodimeric interaction (middle blue), non-reciprocal heterodimeric interaction (light blue), no interaction (light orange) or inconclusive and non-tested interactions (**, light gray). Additional controls and Y2H validation data are presented in **Supplementary Figure 3**.

the cells showed, however, that the obtained few YFP signals were not artifacts. Presumably, it was difficult to study BTSL1 protein interactions by BiFC in plant cells because of plant factors that render the proteins unstable, as reported previously for BTS (Selote et al., 2018).

Previous PYE, ILR3, and FEP3/IMA1 fluorescent fusion protein studies showed that these proteins can be present in the same root cells in response to –Fe (Long et al., 2010; Grillet et al., 2018; Samira et al., 2018; Tissot et al., 2019). We specifically intended to localize and co-localize BTSL proteins and their interaction partners in plant cells. However, as for BiFC, these studies were also hampered by the low detection of BTSL fluorescent fusion proteins. We were only able to study intracellular localization qualitatively. Surprisingly, fluorescence protein-tagged BTSL1 localized mainly at the cell periphery and only weakly to the nucleus, as observed before in BiFC (**Supplementary Figure 4D**, YFP-BTSL1, compare with **Supplementary Figure 4A**). The fluorophore position (N-/C-terminal) did not affect BTSL1 localization (**Supplementary Figure 5**). YFP-tagged BTSL2 localized to the nucleus and the cytoplasm (**Supplementary Figure 4D**, YFP-BTSL2). Remarkably, BTSL1-C-GFP and BTSL2-C-GFP localized more to the nucleus and less to the cytoplasm compared to the full-length version, again matching the BiFC data (**Supplementary Figure 4D**, compare BTSL1-C-GFP, BTSL2-C-GFP with YFP-BTSL1 and -BTSL2, and compare with **Supplementary Figure 4A**), indicating an interesting pattern of BTSL1 and BTSL2 localization with an unexpected role of the N-terminal HHE domains in steering the intracellular localization. In contrast, YFP-BTS was localized exclusively to the nucleus (**Supplementary Figure 4D**, YFP-BTS). FEP3-GFP was localized to the nucleus and cytoplasm, with a preference for the cytoplasm (**Supplementary Figure 4**, FEP3-GFP). PYE-GFP, ILR3-GFP and YFP-bHLH104 were located in the nucleus as expected for the transcription factors (**Supplementary Figure 4D**, PYE-GFP, ILR3-GFP, YFP-bHLH104), also in accordance with previous reports (Long et al., 2010; Li et al., 2016; Samira et al., 2018). BTSL1-mCherry co-localized with ILR3-GFP in the nucleus and the same was found for BTSL1-GFP and PYE-mCherry as well as YFP-BTSL2 and PYE-mCherry (**Supplementary Figure 4E**). BTSL1-GFP and PYE-mCherry also co-localized outside the nucleus, whereby the PYE-mCherry signal at the cell periphery was weak compared with the nuclear signal (**Supplementary Figure 4E**, compare cell1 and cell 2). It was not possible to obtain fluorescence signals for BTSL1-mCherry when it was co-expressed with FEP3-GFP (not shown). Again, as was the case for BiFC, protein fluorescence detection of BTSL1 and BTSL2 was hampered by low detection of signals. In summary, these results indicate that proteins of the BTSL1-bHLH-FEP3/IMA1 interactome localize to large extent in plant cells. Aside from the nucleus interesting dynamic cytoplasmic and cell peripheral localization effects were noted for BTSL1 and BTSL2, dependent on the N-terminal part with HHE domains.

We also verified that the genes encoding the BTSL1-bHLH-FEP3/IMA1 interactome were co-expressed in the similar root cells when respective transgenic GUS plants were grown in parallel. All tested promoter-reporter activities were present in the root differentiation zone where Fe uptake occurs (**Supplementary Figure 6**). *BTSL1* promoter was mainly active in the outer root layers, in contrast to its proposed interaction partners encoded by *ILR3*, *BHLH104*, and *FEP3*, which were expressed predominantly in the root stele. Interestingly, the *BTSL1* expression pattern overlapped with the *PYE* expression pattern in the root differentiation zone in our analysis (**Supplementary Figure 6**). Hence, the tissue-specific GUS staining patterns we detected for all promoters in our growth conditions confirmed previous reports about the root-zone-related promoter regulation (Long et al., 2010; Li et al., 2016; Liang et al., 2017; Grillet et al., 2018; Samira et al., 2018; Rodriguez-Celma et al., 2019). The promoter activity does not necessarily restrict the protein to the same location. For example, FEP3/IMA1 moved long-distance from shoot to root in grafting experiments, and PYE-GFP and ILR3-GFP were located in all root tissues across the root when expressed from their promoters while the same promoter fragments conferred reporter activity mainly in the stele of the mature root zone (Long et al., 2010; Grillet et al., 2018; Samira et al., 2018).

Taken together, protein complexes of the BTSL1-bHLH-FEP3/IMA1 interactome can be formed in root cells.

Interaction Sites Between BTSL1, bHLH Proteins, and FEP3/IMA1 Were Mapped

The BTSL1-bHLH-FEP3/IMA1 interactome was very exciting and it was then interesting to better resolve the interaction. Because of the limited success in BTSL1 protein expression in plant cells, Y2H was the method of choice. The synthetic model yeast cell system is a heterologous system, broadly utilized to fine-map interaction sites in the absence of interfering plant factors in cells.

First, we mapped the required interaction site of BTSL1. It was suggested that BTS interacts with its target TFs ILR3 and bHLH115 via the RING domain (Selote et al., 2018). BTSL1 and likewise BTSL1-C interacted with bHLH factors and FEP3/IMA1 suggesting that the RING domain may also be important for BTSL1 (**Figure 3**, see also **Figure 2**). To pinpoint the specific interaction site, we used a deletion mutant approach and delimited further the C-terminal region of BTSL1 that is required for interaction with ILR3, bHLH104-C and FEP3/IMA1 (**Figure 3**). We divided BTSL1-C into further four deletion forms (BTSL1-C1 to -C.4, **Figure 3B**). BTSL1-C.1, lacking RING, Zn ribbon and the full CTCHY region, was not able to interact with ILR3, bHLH104-C or FEP3/IMA1 (**Figure 3**). The slightly longer form BTSL1-C.2 with CHY and CTCHY domains lacked RING and Zn ribbon domains and interacted with ILR3, bHLH104-C and FEP3/IMA1 (**Figure 3**). This indicates that BTSL1 RING and Zn ribbon are not needed for this interaction. A further deletion construct BTSL1-C.3 contained only the CTCHY plus RING domains, and it interacted with ILR3 and FEP3/IMA1, but not with bHLH104-C (**Figure 3**). This shows that the full CTCHY plus RING are sufficient for interaction with FEP3/IMA1 and ILR3, but not for interaction with bHLH104-C. Instead, the construct BTSL1-C.4 with only RING and Zn ribbon interacted with FEP3/IMA1 but none of the TF proteins (**Figure 3**). In

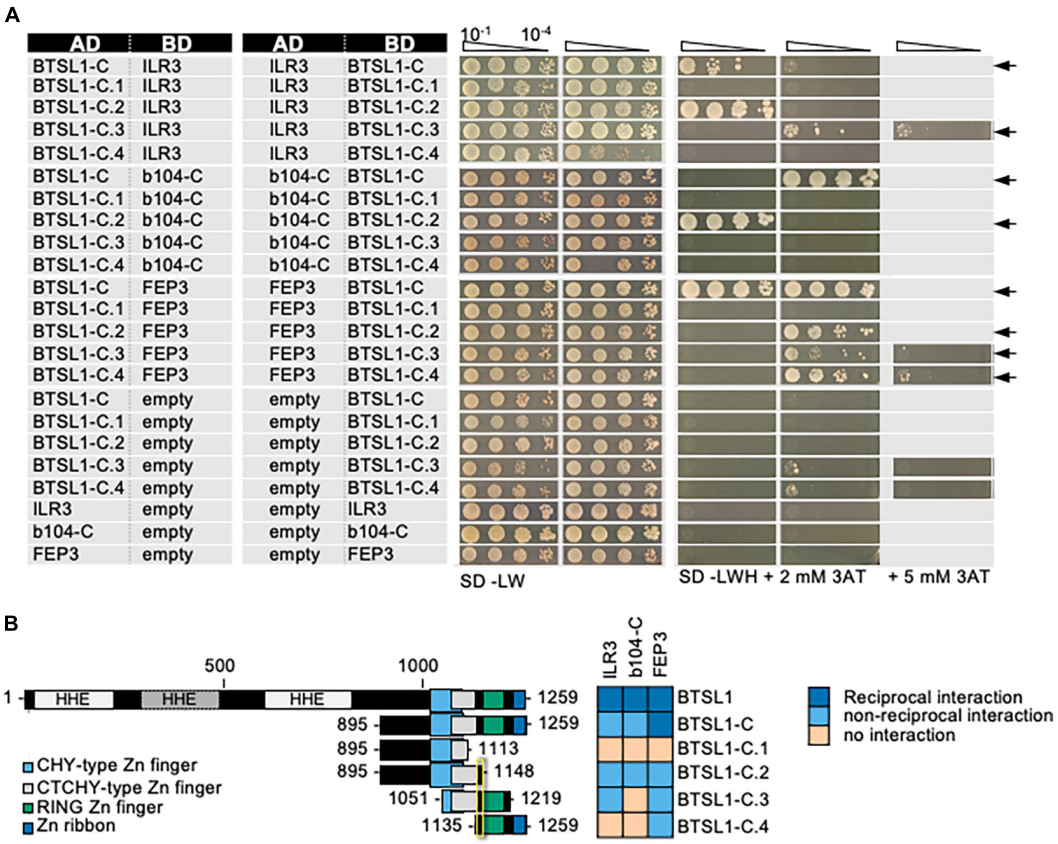

FIGURE 3 | Mapping of the interaction sites in BTSL1 by yeast two hybrid (Y2H) assays. BTSL1-C and deletion forms of BTSL1-C were tested in reciprocal targeted Y2H assays against ILR3, bHLH104-C (b104-C) and FEP3/IMA1. Yeast co-transformed with the AD and BD combinations were spotted in 10-fold dilution series (A_{600} = 10^{-1}–10^{-4}) on SD-LW (transformation control) and SD-LWH plates supplemented with different concentrations of 3AT as indicated (selection for protein interaction). Negative controls: empty vectors. Arrows indicate interaction. **(B)** Schematic representation and summary of Y2H results. Left, schematic representation of full-length BTSL1, BTSL1-C and deletion constructs of BTSL1-C.1 to –C.4, used for Y2H. The domains are indicated in color. The yellow box highlights the mapped interaction site for interaction with bHLH proteins and FEP3/IMA1. Right, summary results of panel **(A)**. The color code distinguishes reciprocal positive interactions (dark blue), non-reciprocal positive interactions (light blue), negative results on interactions (light orange).

summary, the three deletion constructs that suggest protein interaction with FEP3/IMA1 (BTSL1-C.2 to -C.4) had one common small region of 14 amino acids (aa). This small 14 aa-region was named M-C site according to the first and last aa of this 14-aa stretch. M-C is located between CTCHY and RING (**Figure 3B**, yellow box). Results were less clear for binding of ILR3 and bHLH104 to BTSL1, but CTCHY and CHY domains were needed for the interaction.

The BTSL1 M-C site was investigated in more detail and a consensus sequence within related Viridiplantae orthologs was identified (**Figure 4A**, indicated by yellow arrowhead). Deleting the M-C site in BTSL1-C (BTSL1C-dMC) abolished interactions with TFs ILR3 and bHLH104-C and FEP3/IMA1, indicating that the M-C site was essential (**Figures 4B,C**). An internal R-H part, named according to the first and last aa of an internal part, was more variable (**Figures 4A,C**, indicated in yellow), and we found that by deleting it (BTSL1-dRH), the interaction was still possible with FEP3/IMA1, but not with TFs (**Figures 4B,C**). Substituting as control the R-H part with a sextuple G residue spacer (BTSL1-6G) also resulted in interaction with FEP3/IMA1 but did not restore interaction with ILR3 and bHLH104-C (**Figures 4B,C**). Possibly, the evolutionarily conserved aa adjacent to R-H is important for interaction with FEP3/IMA1 (**Figure 4A**). Thus, FEP3/IMA1 interacts with BTSL1 at a position that is close to the interaction site of ILR3 and bHLH104-C. In summary, the 14-aa M-C site located close to the BTSL1 E3 RING domain is needed for interaction with FEP3, ILR3 and bHLH104-C. Within this region, the R-H part is essential for interaction with ILR3 and bHLH104-C, but not with FEP3/IMA1. This indicates that FEP3/IMA1 and the TFs do not bind identically to BTSL1.

Second, the interaction site within FEP3/IMA1 was mapped. As shown in previous data on FEP sequence conservation across the plant kingdom (Grillet et al., 2018), FEP3/IMA1 protein has the conserved stretch of final 17 aa at its C-terminus (**Supplementary Figure 7**). The N-terminal half and a C-terminal half of FEP3/IMA1 (termed FEP3-N and FEP3-C) were tested for their ability to interact with BTSL1, and only FEP3-C was found to be the interacting part (**Figure 5**). Next, two truncated FEP3/IMA1 versions lacking the conserved stretch (FEP3-d17) or lacking the last seven aa YDYAPAA (FEP3-d7) were tested

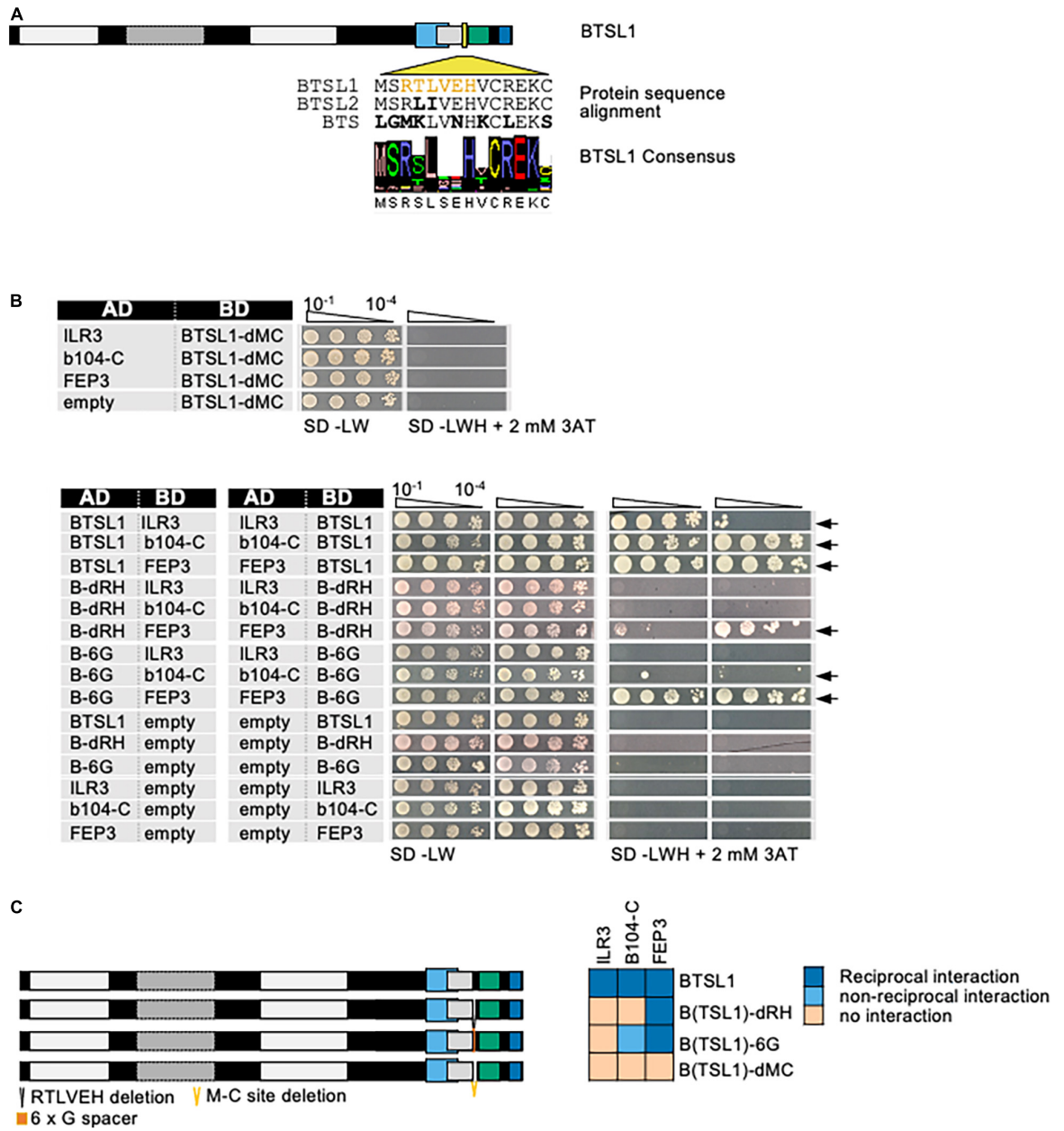

FIGURE 4 | Fine-mapping of the interaction sites in BTSL1 by yeast two hybrid (Y2H) assays. **(A)** Protein structure of BTSL1 and protein sequence alignment of the interaction M-C site within the yellow-boxed region that is highlighted, see also **Figure 3B**. A further sub-region is marked in orange letters, R-H site. The consensus sequence was obtained by identifying orthologs using blastp and comparing the sequences of the 100 best hits. **(B)** Small targeted deletion forms of BTSL1-C of or within the M-C site were tested in reciprocal targeted Y2H assays against ILR3, bHLH104-C (b104-C) and FEP3/IMA1. Yeast co-transformed with the AD and BD combinations were spotted in 10-fold dilution series (A_{600} = 10^{-1}–10^{-4}) on SD-LW (transformation control) and SD-LWH plates supplemented with 3AT as indicated (selection for protein interaction). Negative controls: empty vectors. Arrows indicate interaction. **(C)** Schematic representation and summary of Y2H results. Left, schematic representation of full-length BTSL1 and deletion constructs of and within the M-C site, used for Y2H. B-6G is a sextuple glycine spacer. The regions are indicated in color. Right, summary results of panel **(B)**. The color code distinguishes reciprocal positive interactions (dark blue), non-reciprocal positive interactions (light blue), negative results on interactions (light orange).

(**Figure 5**). Neither of the two constructs interacted with BTSL1, showing that the conserved stretch and the last seven aa in FEP3/IMA1 are crucial for FEP3/IMA1 interactions.

Third, we mapped the interaction site within the C-terminal regions of bHLH IVc proteins ILR3 and bHLH104 with BTSL1 and compared them with BTSL2 and BTS (**Figure 6**). As shown above, ILR3 interacted with BTSL1 and BTS, but not BTSL2, while bHLH104-C interacted with all three BTS/L proteins. We made an interesting observation by aligning the FEP3/IMA1 sequence with the C-termini of bHLH IVc

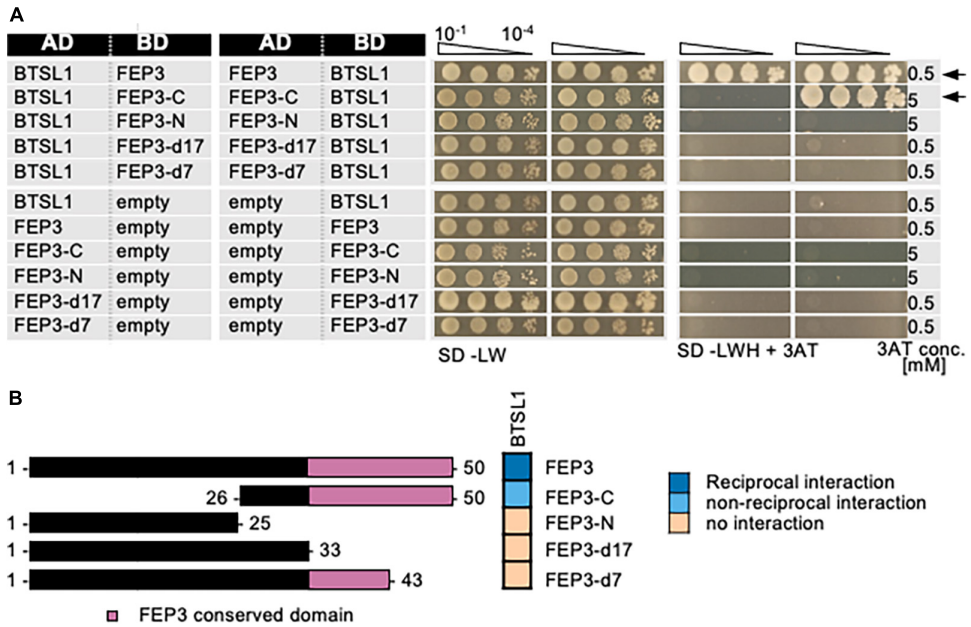

FIGURE 5 | Mapping of the interaction site in FEP3/IMA1 by yeast two hybrid (Y2H) assays. **(A)** Targeted deletion forms of FEP3/IMA1 were tested in reciprocal targeted Y2H assays against BTSL1. Yeast co-transformed with the AD and BD combinations were spotted in 10-fold dilution series (A_{600} = 10^{-1}–10^{-4}) on SD-LW (transformation control) and SD-LWH plates supplemented with different 3AT concentrations (conc.) as indicated (selection for protein interaction). Negative controls: empty vectors. Arrows indicate interaction. **(B)** Schematic representation and summary of Y2H results. Left, schematic representation of FEP3 and deletion constructs, used for Y2H. Pink color illustrates the conserved region of FEP3 (see **Supplementary Figure 5**). Right, summary results of panel **(A)**. The color code distinguishes reciprocal positive interactions (dark blue), non-reciprocal positive interactions (light blue), negative results on interactions (light orange).

protein sequences (**Supplementary Figure 8**). We found rough similarities and conserved PAA/PVA motifs at the C-terminal ends of FEP3/IMA1 and the bHLH IVc TFs (**Supplementary Figure 8**). In comparison, bHLH Ib protein C-termini did not align with FEP3/IMA1 (data not shown). We figured that one explanation for the protein interactions could be that FEP3/IMA1 mimics bHLH IVc proteins within their last 25 aa during interaction with BTSL1. To test this, we constructed ILR3-d25 and bHLH104-C-d25 that lacked the 25 aa-region aligning with FEP3/IMA1 YDYAPAA and tested their ability to interact with BTS/L proteins (**Figures 6A,B**). We found that ILR3-d25 fragment still interacted with BTSL1, but no longer with BTS, while bHLH104-C-d25 still interacted with BTSL1 and BTSL2 but also no longer with BTS. Interestingly, short fragments only consisting of the last 25 aa, ILR3-CC and bHLH104-CC, even tended to interact better with BTSL1 than the d25 fragments, while no interaction was found with BTSL2 or BTS (**Figures 6A,B**). Therefore, the last 25 aa of C-terminal ends of ILR3 and bHLH104 did not appear essential for interaction in all cases, but they were important. The importance of the last 25 aa was also reported in a study for the bHLH105 and bHLH115-BTS interaction (Li et al., 2021).

Taken together, we were able to map interaction sites for the BTSL1-bHLH-FEP3/IMA1 interactome (summarized in **Figure 6C**).

Homology modeling and molecular docking are today powerful tools that predict with high confidence protein and protein complex structures. Via AlphaFold, we obtained a protein structure that we used for theoretical molecular docking experiments considering free energy values between the mapped interaction sites of BTSL1 and FEP3. Interestingly, this theoretical approach underlined experimental data and indicated precisely the three aa residues HVC within the M-C site covering with H the last aa of the R-H site of BTSL1 (**Figure 6D**). The top model that emerged indicated that PAA of the last seven aa YDYAPAA of FEP3/IMA1 bind to BTSL1-HVC (**Figure 6D**). As described above, PAA/PVA residues are also contained at the C-terminal end of bHLH IVc factors (**Supplementary Figure 8**). Thus, theoretical modeling fit with experimental evidence. Hence, through Y2H studies and molecular docking, the interaction sites relevant for the BTSL1-bHLH-FEP3/IMA1 interactome were fine-mapped.

FEP3/IMA1 Attenuated the Interaction of BTSL1 With PYE and bHLH IVC Transcription Factors, Providing Evidence for an Effector Interaction

FEP3/IMA1 is a positive regulator of Fe uptake and potential phloem-mobile signal (Grillet et al., 2018). However, the mechanism by which FEP3/IMA1 acts had not been known. BTSL1 and BTSL2 are suspected Fe sensors and negative regulators of Fe uptake (Hindt et al., 2017). This hypothesis was strengthened by the observation, that two transgenic Arabidopsis lines over-expressing *FEP3/IMA1* (FEP3-OX#1 and

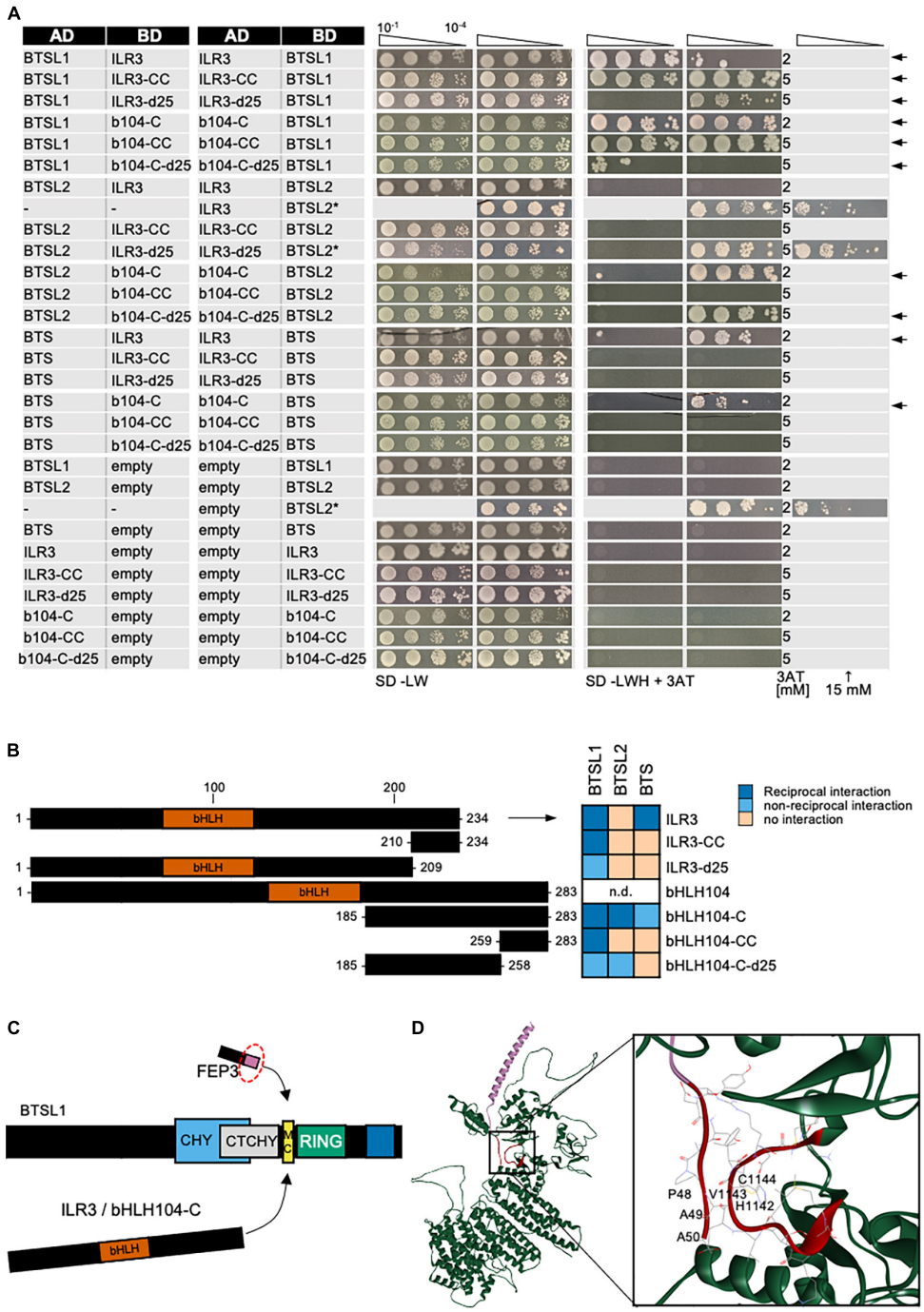

FIGURE 6 | Mapping of the interaction site in bHLH subgroup IVc proteins ILR3 and bHLH104 by yeast two hybrid (Y2H) assays. **(A)** Targeted deletion forms of bHLH proteins were tested in reciprocal targeted Y2H assays against BTSL1. Yeast co-transformed with the AD and BD combinations were spotted in 10-fold dilution series (A_{600} = 10^{-1}–10^{-4}) on SD-LW (transformation control) and SD-LWH plates supplemented with different 3AT concentrations (conc.) as indicated (selection for protein interaction). Negative controls: empty vectors. Arrows indicate interaction. BTSL2* and BTSL2 refer to two separate controls. **(B)** Schematic representation and summary of Y2H results. Left, schematic representation of bHLH and deletion constructs, used for Y2H. The color illustrates the proposed region of similarity with the C-terminus of FEP3/IMA1 (see **Supplementary Figure 8**). Right, summary results of panel **(A)**. The color code distinguishes reciprocal positive interactions (dark blue), non-reciprocal positive interactions (light blue), negative results on interactions (light orange). **(C)** Proposed mechanistic model of BTSL1-C interaction at the fine-mapped M-C site with bHLH proteins of subgroup IVb and IVc and the C-terminal conserved region of FEP3/IMA1. Compare with **Figures 4–6** for depicted functional domains. **(D)** Molecular homology modeling and molecular docking of BTSL1 and FEP3/IMA1. Left, Homology model of BTSL1 protein predicted using AlphaFold2, used for molecular docking with FEP3. Right, details of molecular docking model between BTSL1 and FEP3. The aa highlighted are HVC within the M-C region of BTSL1 and the PAA region at the C-terminus of FEP3 that shows similarity with the C-terminus of bHLH IVb and IVc proteins. The model suggests that FEP3 is an allosteric inhibitor of bHLH binding to BTSL1.

#3) had similar physiological phenotypes as loss-of-function defects in *btsl1 btsl2* mutants when comparing them side-by-side in the same growth system (for characterization of lines see **Supplementary Figure 9**). FEP3-Ox plants and *btsl1 btsl2* mutants had increased Fe contents per dry weight in seeds (**Supplementary Figure 10A**), longer roots than wild type at –Fe and partly also at +Fe (**Supplementary Figure 10B**). When examining the downstream responses of bHLH IVb and IVc TFs, *FEP3/IMA1* and *BTSL* gene expression followed the expected pattern in overexpression and mutant situations. Interestingly, *FEP3/IMA1* was not up-regulated in response to –Fe in *btsl1 btsl2* compared to wild type (**Supplementary Figure 11** upper row). In contrast, *BTS*, *BHLH038*, *BHLH039*, *PYE*, *FRO3*, and *NAS4* did not show the *FEP3/IMA1* expression pattern and hence they were not co-expressed with *FEP3/IMA1* in *btsl1 btsl2*. Instead, with exception of non-regulated *NAS4*, all these genes showed a tendency to be up-regulated in FEP3-Ox and *btsl1 btsl2* conditions compared to wild type, which was significant in the case of *BHLH038* in FEP3-Ox#1 at +Fe and in *btsl1 btsl2* at –Fe, for *BHLH039* in FEP3-Ox#3 at –Fe and in *btsl1 btsl2* at + and –Fe, for *PYE* in FEP3-Ox#1 at +Fe, and in none of the cases for *FRO3* (**Supplementary Figure 11** two middle rows). At the level of root Fe acquisition genes, *FIT* was not found differentially regulated in the mutant lines. *IRT1* and *FRO2* were co-expressed but significantly up-regulated only in the case of *IRT1* in *btsl1 btsl2* at –Fe (**Supplementary Figure 11** bottom row). Hence, except for *FEP3/IMA1* there was no other case of down-regulation. The gene expression patterns indicate that *FEP3*, *BTSL1* and *BTSL2* affect –Fe response regulation upstream of *BHLH* subgroup Ib genes at the level of bHLH IVc and URI regulation. *URI*, *BHLH011* and *BHLH115* expression did not differ between wild type and mutant lines. However, *ILR3*, *BHLH104*, and *BHLH034* were in some cases down-regulated in mutants, which was significant in the case of *ILR3* and *BHLH104* in FEP3-Ox#1 at + and –Fe, as well as in FEP3-Ox#3 at +Fe and in *btsl1 btsl2* at –Fe, and for *BHLH034* in FEP3-Ox#1 at +Fe (**Supplementary Figure 12**). Thus, *ILR3*, *BHLH104*, and *BHLH034* were transcriptionally regulated in an opposite manner as their downstream targets *BHLH038*, *BHLH039*, and *PYE* in FEP3-OX lines.

Together, these data indicate that FEP3/IMA1 acts as a positive regulator in Fe uptake, supporting published data (Grillet et al., 2018), while BTSL1/BTSL2 are negative regulators. From the gene expression, these effects happen upstream of *BHLH039* and *PYE*, and *FEP3/IMA1* does not need to be highly expressed for Fe accumulation in *btsl1 btsl2*. One possibility is that the bHLH factors ILR3, bHLH104 and bHLH034, which are positive regulators of *BHLH* subgroup Ib genes, are themselves negatively regulated downstream of FEP3/IMA1, while FEP3/IMA1 is positively affected by BTSL1 and BTSL2. Further, it is possible that FEP3/IMA1 binds BTSL1 and thereby modulates the interaction of BTSL1 with bHLH proteins. These bHLH proteins may regulate each other. Such a model predicts that FEP3/IMA1 is an effector protein that prevents or reduces BTSL1-bHLH interaction.

We tested the effect of FEP3/IMA1 on BTSL1-bHLH interactions using a quantitative yeast three hybrid (Y3H) assay. Y3H was designed to quantify ß-galactosidase activity as output of interaction between two proteins fused with AD or BD, in our case BTSL1 and a bHLH protein. Modulation of ß-galactosidase activity is quantified in the presence of an active vs. inactive so-called bridge protein, in our case FEP3/IMA1 vs. inactive FEP3-N. This assay allows testing whether the bridge protein has activating, repressing or neutral effect on the interaction complex formation of the AD/BD-fusion proteins (**Figure 7A**). By testing the effect of FEP3/IMA1 vs. FEP3-N on FIT and bHLH39 interaction, no difference was found. Instead, high b-galactosidase values indicated strong interaction of FIT and bHLH039 in all cases irrespective of FEP3/IMA1 or FEP3-N presence or absence (**Figure 7B**). This indicated that FEP3/IMA1 and FEP3-N expression had a neutral effect on the FIT-bHLH039 interaction. This was expected, based on the fact that neither bHLH039 nor FIT interacted with FEP3/IMA1. Interesting effects of FEP3/IMA1 were seen in the case of PYE, bHLH034-C and bHLH115-C, where the presence of active FEP3/IMA1 strongly impacted the protein interaction with BTSL1-C compared with the presence of inactive FEP3-N, while no difference was seen for the ILR3 interaction (**Figures 7C–G**, compare presence of FEP3 at ± Met with FEP3-N at ± Met). Additionally, the bridge protein is expressed under a methionine (Met)-repressible promoter, which allows modulating the level of FEP3/IMA1 protein in the Y3H system. We found, however, similar levels of FEP3/IMA1 protein under + and -Met in all cases (**Supplementary Figure 13**). Despite that, a difference was seen between + and -Met for PYE, bHLH034-C and bHLH115-C supporting a negative effect of FEP3/IMA1. In the case of bHLH104-C no difference was seen between + and -Met. No difference occurred for BTSL1-C and ILR3 interaction in the case of FEP3/IMA1 or FEP3N under + and -Met, either, showing that the Met regulation of FEP3/IMA1 was not as reliable as comparison with inactive FEP3-N (**Figure 7C**). The BTSL1-C + ILR3 interaction was stronger than the other tested BTSL1-C + bHLH TF interactions. We suspected that because of the strong BTSL1-C + ILR3 interaction, FEP3/IMA1 is not able to interfere as an effector with BTSL1-C and ILR3 protein interaction.

Finally, we predicted structures of BTSL1-bHLH TF-IMA protein complexes using the Alphafold-multimer tool to find an explanation for the varying degrees of attenuation of protein interaction by FEP3/IMA1. Interestingly, these predictions agreed with the molecular docking model: FEP3/IMA1 was found to bind in close proximity to the MC site of BTSL1. Moreover, structural alignment showed that all IMA proteins were predicted to bind to BTSL1 at this same MC site interface (**Supplementary Figure 14A**). Furthermore, we applied this tool to predict BTSL1-PYE, BTSL1-ILR3, BTSL1-bHLH115, and BTSL1-bHLH104 structures and aligned the predicted structures of BTSL1-bHLH-IMA1/FEP3 protein complexes (**Supplementary Figure 14**). This theoretical approach suggests that bHLH proteins bind BTSL1 at two interfaces (**Supplementary Figures 14B–E**). According to the models, a region at the N terminus of bHLH TFs binds BTSL1, designated as interface A. C-terminal regions of the TF models bind to a proximal region of the BTSL1 MC site, termed interface B. FEP3/IMA1, on the other side, only binds to interface B. PYE was found to weakly attach to BTSL1 at

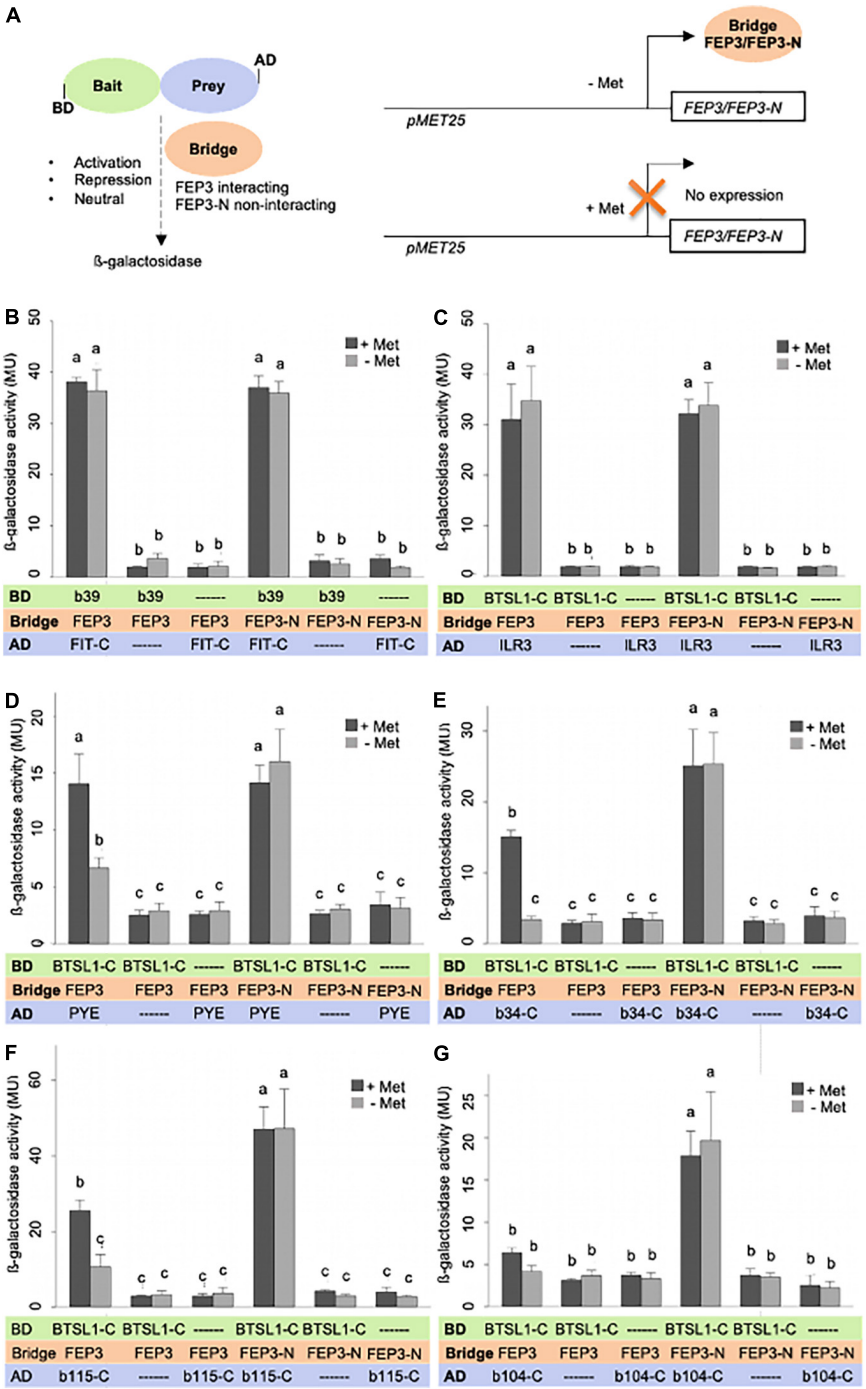

FIGURE 7 | FEP3/IMA1 effect on BTSL1-C and bHLH IVb and IVc interaction quantified by yeast three hybrid (Y3H) assay. **(A)** Schematic representation of Y3H principle and design. Left, the protein interaction strength between a bait protein (fused with Gal4 DNA binding domain, BD) and prey protein (fused with Gal4 activation domain, AD) is measured by ß-galactosidase activity, here BTSL1-C and a bHLH protein (part). The effect of a bridge protein on protein interaction is measured, here interacting FEP3/IMA1 and negative control non-interacting FEP-N, leading to either activation, repression or neutral effect on bait-prey protein interactions. Note that the term "bridge" is a neutral term, and depending in the result the "bridge" protein may act as positive or negative effector protein or have a neutral effect. Right, the Bridge protein is expressed under a pMET25 promoter by supplementation with or without methionine (+Met, -et). **(B–G)** Quantification of protein interaction strengths in absence and presence of bridge protein FEP3 or FEP3-N (±Met) of panel **(B)** FIT-C-bHLH39, **(C)** BTSL1-C-ILR3, **(D)** BTSL1-C-PYE, **(E)** BTSL1-C-bHLH34-C, **(F)** BTSL1-C-bHLH115-C, **(G)** BTSL1-C-bHLH104-C interactions. Yeast cells are grown in SD-LWM, for bridge protein expression and SD-LW for repression of bridge protein expression; ß- galactosidase activity is determined in Miller Units (MU). Data are represented as mean values with standard deviations. Different letters indicate statistically significant differences (one-way ANOVA and Tukey's *post-hoc* test, $n = 5$, $p < 0.05$). Immunoblot analysis of FEP3/IMA1 is shown in **Supplementary Figure 13**.

interface A. Instead, N terminal regions of ILR3, bHLH104, and bHLH115 were predicted to strongly attach to BTSL1 at interface A. This agrees with Y3H data. BTSL1-PYE but not BTSL1-ILR3 interaction was affected by FEP3/IMA1. PYE formed weak interaction with BTSL1 mainly via the interface B while ILR3 interacted via interfaces A and B. The C-terminal fragments bHLH104-C and bHLH115-C probably interacted weakly with BTSL1 since only interface B but not interface A was present. Thus, IMA1/FEP3 might attenuate specifically interactions that are not compensated by strong links between bHLH TFs and BTSL1 at interface A. The models also demonstrate that the bHLH factors bind to BTSL1 in an area with intrinsically disordered regions (**Supplementary Figures 14B–E**).

Taken together, FEP3/IMA1 but not FEP3-N can modulate the interaction of BTSL1 and bHLH proteins. FEP3/IMA1 attenuates the interaction of BTSL1 with bHLH factors at binding interface B, provided that the interaction of BTSL1 and bHLH proteins is moderate to weak. This can be specified by binding sites at two interfaces of BTSL1-bHLH interactions.

DISCUSSION

Little structural information has been available on how Fe-regulatory proteins interact. A targeted Y2H screen revealed the novel protein interactome BTSL1-bHLH-FEP3/IMA1, confirming that –Fe-induced co-expressed gene clusters contain information about protein interaction complexes. FEP3/IMA1 targets via its C-terminal end a small region termed M-C site within the C-terminus of BTSL1. bHLH factors bind to BTSL1 in the vicinity of this site. FEP3/IMA1 attenuates protein interactions of PYE and bHLH IVc TFs with BTSL1. The similar phenotypes of FEP3/IMA1 overexpression and *btsl1 btsl2* loss of function support that FEP3/IMA1 is a small effector protein that inhibits the BTSL1-bHLH interaction and thereby promotes Fe uptake. Hence, our study uncovered a novel mechanism of action of FEP3/IMA1.

FEP3/IMA1 Is an Effector Protein Acting on the Interaction of BTSL1 With bHLH TFs

The BTSL1-bHLH-FEP3/IMA1 interactome was uncovered in a screen, subsequently shown by targeted interaction assays combined with deletion mapping and computational docking to narrow down and confirm the protein interaction sites. Finally, quantitative protein interaction assays provided evidence about FEP3/IMA1 being a negative modulator of the BTSL1-bHLH TF interaction. The results suggest a framework for explaining structure-function relationships and a mechanism of FEP3/IMA1 action as an inhibitory protein acting upon BTSL1. FEP3/IMA1 was selective and modulated the strength of BTSL1-bHLH interactions, namely BTSL1-C-PYE, BTSL1-C-bHLH104-C, BTSL1-C-bHLH115-C, and BTSL1-C-bHLH34-C. In all these cases, FEP3/IMA1 caused repression of interaction strength, suggesting competition at the BTSL1 binding site with TF fragments, which was confirmed by theoretical prediction tools. In no case did we observe an increased strength of protein interaction in the presence of FEP3/IMA1, excluding cooperative binding effects that stimulate the interaction. Interestingly, only the weak to moderate protein interactions between BTSL1 and bHLH TFs could be altered by FEP3, but not the strong interactions, like BTSL1-C-ILR3. Clearly, the bHLH TFs differed in the number of interfaces for binding to BTSL1, whereby PYE-BTSL1 interaction appeared weaker with only interface B than that of ILR3-BTSL1 which relies on interfaces A and B. We interpret this finding to be very important in a biological context where differential interactions and their differing strengths are responsible to fine-tune Fe deficiency responses in balanced manner, depending on absence and presence of the various components of the interactome and differing binding sites. As discussed in the next paragraph the physiological data gained from FEP3/IMA1 overexpression and *btsl1 btsl2* mutants support that FEP3/IMA1 via BTSL1 targets the top of the –Fe bHLH response cascade. Since BTSL1 and BTSL2 are very similar in sequence and undergo similar protein interactions with FEP3/IMA1 and bHLH TFs, we predict that BTSL2 acts similar to BTSL1, but this requires further experiments. The related FEP1/IMA3 acts on BTS, however, the same sequence HVC is not conserved in BTS, although the PAA of the TFs were found important (Li et al., 2021), and also the M-C site of BTS shows multiple aa differences to the M-C site of BTSL1 and BTSL2. Moreover, PYE does not have the C-terminal PAA site as present in bHLH IVc TFs that interact via this motif with BTSL1. These findings together indicate that the protein interactions are far more complex and more structural details are needed to explain the various combinations and their effects. Because of the complexity of the BTSL1-bHLH-FEP3/IMA1 system, future studies need to address the competition effects and protein-ligand binding affinities and interaction strengths between all components of the BTS/BTSL, bHLH TFs and FEP/IMA system at the structural-biochemical level to decipher functional specificities of the responses.

Molecular-Physiological Integration of the BTSL1-bHLH-FEP3/IMA1 Interactome

Physiological FEP3/IMA1 overexpression resembled loss of function of *btsl1 btsl2*, supporting the inhibitory effect of FEP3/IMA1 on BTSL1, observed in the Y3H assays. The gene expression profiles demonstrate that FEP3/IMA1 and BTSL1/BTSL2 act at the top level of the –Fe response cascade to affect the downstream target genes which comprised *BHLH* subgroup Ib genes, *PYE*, their co-expressed genes and further downstream targets of those. *BHLH* subgroup Ib and *PYE* genes are controlled by URI and bHLH IVc TFs. Among them, URI did not interact with FEP3/BTSL1/BTSL2, however, bHLH subgroup IVc TFs did. Therefore, BTSL1, presumably along with BTSL2, has a negative effect on bHLH IVc factors through interaction with them, attenuated by FEP3. *FEP3/IMA1* is normally co-expressed with *BHLH* subgroup Ib and *PYE* genes, however, this was not the case in *btsl1 btsl2*. Rodriguez-Celma et al. (2019) and Li et al. (2021) proposed that TFs of the subgroups IVb or IVc repress *FEP1/IMA3* gene expression, similar as rice

homologs (Kobayashi et al., 2021). We suggest the following working model for the BTSL1-bHLH-FEP3/IMA1 interactome (**Figure 8**): BTSL1 interacts with PYE and bHLH IVc TFs to steer the top of a regulatory cascade leading to the Fe deficiency response in Arabidopsis. –Fe is sensed and bHLH IVc and URI TFs activate the –Fe response pathway in roots. *FEP3/IMA1* and *BTSL1* are up-regulated. BTSL1 protein binds PYE and bHLH IVc TFs, which downplays the –Fe response. In the presence of FEP3/IMA1, however, BTSL1 function is attenuated, allowing the TFs to be more active. Consequently, plants that constitutively up-regulate FEP3/IMA1 (in FEP3-Ox) or have no functional BTSL1 (in *btsl1 btsl2*) should accumulate Fe, which is what we observed, conform with previous studies of these mutants (Hindt et al., 2017; Grillet et al., 2018; Rodriguez-Celma et al., 2019; Li et al., 2021).

We initially struggled to explain why *ILR3* and *BHLH104* transcripts were down-regulated in FEP3-OX and *btsl1 btsl2* seedlings, although their downstream target genes were highly expressed. *ILR3/bHLH104* levels might also be controlled negatively by same TFs, possibly when the TFs are more active. This might be an additional layer of control to avoid excessive Fe uptake. This scenario actually could explain why neither *btsl1 btsl2*, nor *btsl1 btsl2 bts* triple mutants (Hindt et al., 2017) or FEP3-OX plants showed signs of severe Fe toxicity under +Fe. It was reported that PYE represses *ILR3* expression (Samira et al., 2018), hence *ILR3* down-regulation in FEP3-OX can be partly due to elevated PYE levels. In another study, ILR3 was shown to dimerize with PYE to repress *PYE* transcription (Tissot et al., 2019). Thus, bHLH IVc proteins in combination with PYE may control their own transcription. We also had expected that *PYE* and the downstream genes *NAS4*, *ZIF1*, and *FRO3* negatively regulated by PYE (Long et al., 2010) would have opposite expression patterns. However, although *PYE* was expressed at higher level in some conditions in mutant lines of this study, *NAS4* and *FRO3* were not down-regulated. This aligns with phenotypes of bHLH IVc gain-of-function lines (Zhang et al., 2015; Li et al., 2016), and indicates that PYE function can be bypassed or that bHLH IVc proteins and PYE act antagonistically to fine-tune Fe acquisition and internal Fe mobilization and allocation. Future studies need to address the network of gene regulation in plant lines with altered TF action in more detail.

This study also provided evidence that interaction of the BTSL1-bHLH system changes subcellular localization patterns. BTSL1 was mostly located at the cell periphery and only weakly in the nucleus. In contrast, BTS was located in the nucleus, as reported previously (Selote et al., 2015), except if the HHE domains were deleted, then the localization pattern shifted to the cytoplasm and was high in the root stele (Selote et al., 2015). Consistent with our results, the BTS homolog in rice, HRZ1, also localized to the nucleus while HRZ2 localized to nucleus and cytoplasm (Kobayashi et al., 2013). Interestingly, BTS and ILR3 localized and interacted in the nucleus, see also Selote et al. (2015). When BTSL1 was expressed together with PYE or ILR3 it was localized to the nucleus but still also at the cell periphery. This indicates that localization of BTSL1 is dependent on protein interaction partners in these experiments. PYE and ILR3 may be present in the cytoplasm

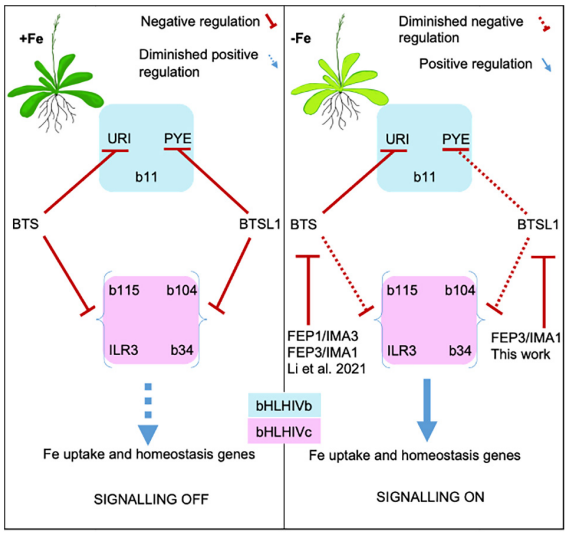

FIGURE 8 | Model of FEP1/IMA3 and FEP3/IMA1 action to prevent BTS and BTSL1 protein-mediated degradation of bHLH factors of subgroups IVb and IVc. bHLH subgroup IVb and IVc TFs elicit Fe uptake and homeostasis in response to –Fe. These TFs are targets of E3 ligases BTS and BTSL1, possibly through degradation. BTS and BTSL1 target the same bHLH IVc but different bHLH IVb proteins. BTS, BTSL1, and the small effector proteins FEP1 and FEP3 are induced upon –Fe downstream of the bHLH IVc TFs. BTS and BTSL1 receive FEP1/FEP3 signals similar to receptor-ligand interactions. Binding of FEP1/FEP3 attenuates BTS/BTSL1-mediated degradation of bHLH TFs of subgroups IVb and IVc, allowing for enhanced Fe deficiency responses. Later, increased degradation of bHLH factors may halt Fe uptake. This model is based on intricate balancing of BTS/BTSL1-TF interaction strength and FEP1/FEP3 availability, allowing the cell to rapidly switch between on/off states to adjust Fe uptake and homeostasis. BTSL1-bHLH-FEP3/IMA1 interaction was shown in this work. BTSL2 interacts with FEP3/IMA1 and with similar TF proteins of the subgroup IVb and IVc as BTSL1, and may have a similar role as BTSL1 (this work). FEP1/IMA3- and FEP3/IMA1-BTS-bHLH interactions were shown by Li et al. (2021).

or near the plasma membrane and in vicinity of plasmodesmata (Long et al., 2010; Selote et al., 2015). It might be conceivable that upon interaction with BTSL1, the entire complex shifts to the nucleus. The interaction of TFs with BTS and BTSL1 and hence their localization may depend on a combination of Fe availability and the presence of TFs. Interestingly, URI also has different localization in roots dependent on Fe supply (Gao et al., 2019a), and perhaps this pattern is also dependent on BTS. Alternatively, another factor may bind BTSL1 at the cell periphery. In this context, it is interesting to note that bHLH039 is present at the cell periphery when expressed alone, while the bHLH039-FIT complex is shifted to the nucleus (Trofimov et al., 2019). bHLH039 did not interact with BTSL1, so that it is unlikely that bHLH039 is the missing link for BTSL1 localization. The E3 ligases AtHOS1 (HIGH EXPRESSION OF OSMOTICALLY RESPONSIVE GENES1) shifts location from the cytoplasm into the nucleus during cold stress (Lee et al., 2001; Dong et al., 2006), and for AtRGLG1 (RING domain ligase 1) and AtRGLG2 it is the case upon abscisic acid or salt stress treatment (Cheng et al., 2012; Belda-Palazon et al., 2019). Because HOS1, RGLG1, and RGLG2 target nuclear proteins for degradation, the nuclear-localized E3

ligases could be the active forms during the stress conditions. FEP3/IMA1 was found distributed throughout the cell. However, we were not able to localize FEP3/IMA1 together with BTSL1. A reason might be that FEP3/IMA1 is degraded by BTSL1, in analogy to BTS that degrades FEP1/IMA3 and FEP3/IMA1 (Li et al., 2021). Taken together, future studies need to further address the localization of the interactome and its regulation by protein translocation inside the cell.

CONCLUDING REMARKS

This study identified a protein interactome of bHLH subgroup IVc and PYE TFs with BTSL1 E3-ligase modulated by the small effector protein FEP3/IMA1. FEP3/IMA1 (<100 aa) is a small ORF-encoded protein (Delcourt et al., 2018), and such small proteins can act as ligands to receptors or by modulating protein-protein interactions (Makarewich and Olson, 2017). This and other studies could not find evidence for FEP3/IMA1 cleavage and secretion, excluding that it is a processed peptide hormone (Grillet et al., 2018; Hirayama et al., 2018). Instead, full-length HA-FEP3/IMA1 protein was detectable in our plants. Therefore, FEP3/IMA1 should be regarded a small effector protein rather than a peptide. Interestingly, small protein-E3 ligase interactions are known from animal systems. For example, the Drosophila *pri* interacts with the E3 ligase Ubr3, facilitating Ubr3 binding to the TF Svb. This changes Svb function (Zanet et al., 2015). From Drosophila as well as mammals, examples are known in which small proteins alter protein localization or bind to enzymes to affect their activity, either by direct competition with the substrate or in an allosteric manner (Cabrera-Quio et al., 2016). The localization and co-localization of BTSL1 in the presence and absence of TFs indicated patterns of regulation with regard to cellular partitioning of the protein interaction complexes in plant cells.

Several open questions will be of interest for future studies: A limitation in our study is that due to the lack of BTSL1 protein detection in plant cells, we were not able to fully validate the protein interactions in plants. Using precise deletions or substitutions of different predicted functional amino acids in BTSL1 may prevent degradation of BTSL1 in plant cells. Such an approach represents a promising solution provided that an altered three-dimensional protein structure does not hamper the protein interaction capability. BTSL1 and possibly also BTSL2 may ubiquitinate and degrade bHLH subgroup IVb and IVc TFs. FEP3/IMA1 homologs, that bind BTS, may also target BTSL1 and BTSL2. This allows space for an intricate control through balanced combinations of interactions between BTS/L, bHLH, and FEP/IMA proteins. Biochemical information as to the actual structural requirements, affinities and concentrations of players and their post-translational modifications might resolve functionality of the interactomes. These factors add an unprecedented layer of complexity to the negative regulation by the FEP/IMA effector mechanism. Certainly, the interactions of BTS/L, bHLH and FEP proteins diverged from a common ancestor interaction up to the level of diversity seen in higher plants today. The complexity arising from combination possibilities between all bHLH-BTS/L and FEP/IMA proteins may allow higher land plants to adequately adjust the action of the TFs in a multitude of developmental and physiological situations. Perhaps this double negative control was driven by evolutionary constraints in response to a changing environment of the plants. Identification of interaction sites within E3 ligases offers possibilities to engineer crops with modified bHLH IVb and IVc, E3 ligase or FEP/IMA binding sites. Indeed, several of the bHLH transcription factors we studied here have roles in abiotic stress protection in plants, e.g., in photoprotection (Akmakjian et al., 2021). Mechanistic understanding of bHLH subgroup IVb and IVc factors will therefore have broad impact to adapt plants to changing climate and to unravel the ecological significance of Fe usage efficiency during climate change.

MATERIALS AND METHODS

Plant Material

Arabidopsis (*Arabidopsis thaliana*) ecotype Columbia-0 (Col-0) was used as wild type (WT) and as background for transgenic lines. Primers used are listed in **Supplementary Table 2**. The *btsl1 btsl2* loss-of-function double mutant (*btsl1-1 btsl2-2*, crossed SALK_015054 and SALK_048470) was described previously (Rodriguez-Celma et al., 2019). T-DNA insertion sites were verified with primer pairs LBb1.3/btsl1-1_RP (*btsl1*) and LBb1.3/btsl2-2_RP (*btsl2*) and homozygosity was verified with the primer pairs btsl1-1_LP/btsl1-1_RP and btsl2-2_LP/btsl2-2_RP (**Supplementary Figure 9**). For plant lines ectopically over-expressing triple HA-tagged *FEP3/IMA1* (FEP3-OX) under the control of a double CaMV 35S promoter, the coding sequence (CDS) was amplified from cDNA of Arabidopsis WT roots with primers carrying B1 and B2 attachment sites, respectively, transferred into the entry vector pDONR207 (Invitrogen) according to the manufacturer's recommendations (BP reaction, Gateway, Thermo Fisher Scientific, Life Technologies GmbH, Darmstadt, Germany). Final constructs were obtained by transferring all candidate genes subsequently into the plant binary destination vector pAlligator2 (N-terminal triple HA fusions = HA_3) (Bensmihen et al., 2004) via LR reactions (Thermo Fisher Scientific). Constructs were transformed into Agrobacteria (*Rhizobium radiobacter*) strain GV3101 (pMP90). Stable transgenic Arabidopsis lines were generated via the Agrobacterium-mediated floral dip method (Clough and Bent, 1998). Positive transformants were selected based on seed GFP expression and genotyping PCR on the transgenic cassette, selfed and propagated to T3 generation. Insertion sites of the transgenic cassettes in FEP3-OX#1 and FEP3-OX#3 were determined by thermal asymmetric interlaced (TAIL) PCR with the primers S1_AL2_LB (template: gDNA), S2_AL2_LB (template: S1_AL2_LB amplicon), S3_AL2_LB (template: S2_AL2_LB amplicon), each combined with AD1, AD2, AD3, AD4, AD5, AD6. The insertion sites were verified by genotyping PCR with primer pairs FEP3-OX1_chr5 fw/S3_AL2_LB (FEP3-OX#1), FEP3-OX3_chr1 fw/S3_AL2_LB (FEP3-OX#3). Homozygosity was determined with primer pairs FEP3-OX1_chr5 fw/FEP3-OX1_chr5 rev

(FEP3-OX#1), FEP3-OX3_chr1 fw/FEP3-OX3_chr1 rev (FEP3-OX#3). Promoter sequences of *BTS* (2,994 bp), *BTSL1* (880 bp), *PYE* (1,120) and *FEP3/IMA1* (1,614 bp) were amplified from Arabidopsis WT gDNA with primer pairs proBTS_-2994_B1 fw/proBTS_-2994_B2 rev (for *proBTS*), proBTSL1_-880_B1 fw/proBTSL1_-880_B2 rev (for *proBTSL1*), proPYE_-1120_B1 fw/proPYE_-1120_B2 rev (for *proPYE*), proFEP3_-1614_B1 fw/proFEP3_-1614_B2 rev (for *proFEP3*) and proFEP3_-1614_B1 fw/FEP3ns_B2 rev (for *proFEP3:FEP3*), respectively, cloned into pDONR207 (Invitrogen). Sequences were transferred into the vector pGWB3 (Nakagawa et al., 2007), generating *proBTS:GUS*, *proBTSL1:GUS*, *proPYE:GUS*, *proFEP3:GUS*, and *proFEP3:FEP3-GUS* constructs. Constructs were transformed into Arabidopsis WT plants as described above (Clough and Bent, 1998). Positive transformants were selected based on hygromycin resistance and genotyping PCR, selfed and propagated to T2 or T3 generation. *ProILR3:GUS*/WT and *proBHLH104:GUS*/WT Arabidopsis lines were described (Li et al., 2016).

Plant Growth Conditions

Arabidopsis seeds were surface-sterilized and stratified. For experimental analyses seeds were distributed to sterile plates containing modified half-strength Hoagland medium [1.5 mM $Ca(NO_3)_2$, 1.25 mM KNO_3, 0.75 mM $MgSO_4$, 0.5 mM KH_2PO_4, 50 μM KCl, 50 μM H_3BO_3, 10 μM $MnSO_4$, 2 μM $ZnSO_4$, 1.5 μM $CuSO_4$, 0.075 μM $(NH_4)_6Mo_7O_{24}$, 1% (w/v) sucrose, pH 5.8, and 1.4% w/v plant agar (Duchefa)] with (Fe sufficient, +Fe) or without (Fe deficient, –Fe) 50 μM FeNaEDTA and vertically grown in plant growth chambers (CLF Plant Climatics, Wertingen, Germany) under long day conditions (16 h light/8 h dark), as described in Lingam et al. (2011). Seedlings were grown for six or ten days directly on +Fe or –Fe medium [6 day (d) system/10 d system, 6-day-old/10-day-old seedlings exposed to ±Fe] (Lingam et al., 2011). Alternatively, seedlings were grown for 14 days on +Fe medium and then transferred for 3 days to either +Fe or –Fe (14 + 3 d system, 14-day-old plants exposed to ±Fe), as indicated in the text.

Yeast Assays

Targeted Yeast Two Hybrid Screen

Twenty three protein interactions were tested using N-terminal AD (pACT2-GW constructs) and BD (pGBKT7-GW constructs) fusion proteins (vectors from Clontech, Takara Bio Europe SAS, Saint-Germain-en-Laye, France). If possible, interactions were studied in both "reciprocal" combinations AD/BD and BD/AD. The interaction was considered more robust when detected in reciprocal manner than in only one direction, however, some proteins could not be tested in both situations, either because of auto-activation or steric hindrance. For Y2H assays, CDS were amplified from cDNA of Arabidopsis WT roots with primers carrying B1 and B2 attachment sites (**Supplementary Table 2**), respectively and transferred into pDONR207 (Thermo Fisher Scientific, Darmstadt, Germany). Finally, all candidate genes were transferred into destination vectors pACT2-GW and pGBKT7-GW. Yeast (*Saccharomyces cerevisiae*) strain Y187 was transformed with pACT2-GW (AD) constructs and yeast strain AH109 with pGBKT7-GW (BD) constructs via the lithium acetate (LiAc) method, based on (Gietz and Schiestl, 2007). Transformants were selected by cultivation for 2 days on minimal synthetic defined (SD) media Clontech (Takara Bio Europe SAS, Saint-Germain-en-Laye, France) lacking Leu (pACT2-GW) or Trp (pGBKT7-GW). Yeast expressing both *AD* and *BD* constructs were obtained by mating and selected on minimal SD media lacking Leu and Trp (SD-LW). To test for protein-protein interaction, a fresh diploid colony was resuspended in sterile H_2O to OD_{600} = 1 and 10 μl of the suspensions were dropped onto minimal SD media lacking Leu, Trp and His (SD-LWH), containing appropriate concentrations of 3-amino-1,2,4-triazole (3-AT). It was necessary to adjust 3-AT concentrations individually to obtain reliable and valid interaction data while avoiding auto-activation of the BD fusion proteins. Plates were cultivated at 30°C for up to 14 days. Diploid cells expressing each pACT2-GW:*X* construct in combination with an empty pGBKT7-GW and vice versa were used as negative controls. Combination of pGBT9.BS:*CIPK23* and pGAD.GH:*cAKT1* was used as a positive control of the system, FIT-C was used as it is not self-activating in the assay (Gratz et al., 2020).

Targeted Yeast Two Hybrid Assays for Validation

Selected protein pairs of the Y2H screen plus additional proteins (URI, bHLH11, bHLH34, bHLH115) and mutagenized/truncated protein versions were assayed as N-terminal AD and BD fusion proteins in both reciprocal combinations as detailed above. Mutagenized *BTSL1* versions *BTSL1-dRH*, *BTSL1-6G*, and *BTSL1-dMC* were created as described in "BTSL1 mutagenesis." Truncated versions *BTSL1-N*, *BTSL1-C*, *BTSL1-C.1*, *BTSL1-C.2*, *BTSL1-C.3*, *BTSL1-C.4*, *FEP3-N*, *FEP3-C*, *FEP3-d7*, *ILR3-d25*, *ILR3-CC*, *bHLH104-C*, *bHLH104-C-d25*, *bHLH104-CC* were amplified with primers listed in **Supplementary Table 2** and cloned into pACT2-GW and pGBKT7-GW as described in the previous section. Yeast strain AH109 was co-transformed with both pACT2-GW:*X* (AD-X) and pGBKT7-GW:*Y* (BD-Y) (including empty vector controls) as described in the previous section. X and Y represent proteins of a tested protein pair. Haploid double transformants were selected on minimal SD media lacking Leu and Trp. To select for protein-protein interaction, overnight liquid cultures were adjusted to OD_{600} = 1 and dilution series down to $OD_{600} = 10^{-4}$ were prepared. 10 μl of the suspensions were dropped onto SD media lacking Leu, Trp and His and containing the appropriate 3-AT concentration and cultivated as described in the previous section.

Yeast Three-Hybrid Assays

Genes which code for bridge protein were transferred from pDONR207 into pBRIDGE-GW using Gateway technology (Thermo Fisher Scientific, Darmstadt, Germany). Genes which code for bait proteins were cloned adjacent to Gal4-BD sequence using AQUA cloning method (Beyer et al., 2015). Prey protein constructs were prepared in pACT2-GW vector as mentioned previously. Primers are listed in **Supplementary Table 2**. Yeast (*Saccharomyces cerevisiae*) strain Y190 was transformed with pACT2-GW (AD) constructs and pBRIDGE-GW (BD-Bridge) constructs via the lithium acetate (LiAc) method, based on (Gietz and Schiestl, 2007). Co-transformants were selected by

cultivation for 2 days on minimal synthetic defined (SD) media (Clontech) lacking Leu (pACT2-GW) or Trp (pBRIDGE-GW). Beta(β)-Galactosidase assay was performed using Yeast β-Galactosidase Assay Kit (Thermo Fisher Scientific, Darmstadt, Germany), with ortho-Nitrophenyl-β-galactoside (ONPG) as substrate. Freshly grown co-transformants in SD-LT and SD-LTM were used in the assay to extract enzyme. Initially OD 600 of the cultures was measured and cells pelleted. Yeast proteins were extracted, and beta-Galactosidase assay solution was added to extract, mixed and incubated for 30 min to 3 h. Absorbance at 420 nm was measured using the Infinite 200 Pro microplate reader, TECAN. ß-galactosidase activity was calculated using Miller's formula, in Miller units (MU) ß-galactosidase activity = (1,000 * Absorbance 420)/(O.D 660* t* V); t = time in minutes of incubation, V = volume of cells used in the assay. The presence of the bridge protein HA-FEP was detected by anti-HA immunoblot analysis. Yeast proteins were harvested by agitating cells in Y-PER Yeast Protein Extraction Reagent (Thermo Fisher Scientific, Darmstadt, Germany). Equal amounts of total protein were separated on SDS-polyacrylamide gels, and transferred to a Protran nitrocellulose membrane. The membrane was blocked with 5% (w/v) milk solution in 1xTBST [150 mM NaCl, 2.7 mM KCl, 24.7 mM Tris-HCl, 0.1% (v/v) Tween 20, pH 7.4] for 30 min and subsequently incubated 1 h with anti-HA-peroxidase high-affinity monoclonal rat antibody (3F10; Roche Holding AG, Basel, Switzerland [catalog no. 12013819001]) diluted 1:1,000 in 2.5% (w/v) milk solution. After three wash steps, each for 15 min in TBST, the membrane was imaged as described in Le et al. (2016). Chemiluminescent protein bands were detected with the FluorChem Q system (ProteinSimple, San Jose, CA, United State) and images were processed with the AlphaView software (version 3.4.0.0, ProteinSimple, San Jose, CA, United State).

Histochemical β-Glucuronidase Assay

Seedlings were analyzed for β-glucuronidase (GUS) activity using 2 mM 5-bromo-4-chloro-3-indoyl-b-D-glucuronic acid (X-Gluc) as substrate and incubated at 37°C in the dark for 15 min up to 12 h. From *proBTSL1:GUS, proFEP3:GUS* and *proFEP3:FEP3-GUS* lines, four to six seedlings were fixed in ice cold 90% acetone for 1 h and washed in phosphate buffer prior to incubation in the GUS staining solution, which was vacuum infiltrated to obtain better staining. Incubation was performed as described above and stained tissue was fixed in 75% ethanol and 25% acetic acid for 2 h at RT. Chlorophyll was removed by incubation in 70% ethanol for 24 h. Seedlings were imaged with the Axio Imager M2 (Carl Zeiss AG, Oberkochen, Germany, 10× objective magnification) and images of entire seedlings assembled with the Stitching function of the ZEN 2 BLUE Edition software (Carl Zeiss AG, Oberkochen, Germany).

Subcellular (Co-) Localization

To observe subcellular localization, proteins were tagged C-terminally to GFP and/or mCherry fluorophores and/or N-terminally to YFP fluorophore and expressed transiently in tobacco leaf epidermal cells via Agrobacterium-mediated leaf infiltration. For N- and C-terminal fusions, CDSs were amplified from cDNA of Fe Arabidopsis WT roots with primers carrying B1 and B2 attachment sites (**Supplementary Table 2**), transferred into the entry vector pDONR207 (Thermo Fisher Scientific, Darmstadt, Germany) and subcloned into destination vectors pMDC83 (C-terminal GFP fusions) (Curtis and Grossniklaus, 2003), pH7WGY2 (N-terminal YFP) (Karimi et al., 2005), and β-estradiol-inducible pABind-GFP and pABind-mCherry (C-terminal GFP and mCherry, used in co-localization studies) (Bleckmann et al., 2010). The constructs were transformed into Agrobacteria as described in "Plant Material". A suspension (OD_{600} = 0.4) of Agrobacteria carrying the construct of interest in infiltration solution [2 mM NaH_2PO_4, 0.5% (w/v) glucose, 50 mM MES, 100 μM acetosyringone (in DMSO), pH 5.6] was infiltrated into tobacco leaves using a 1 ml syringe pressed to the abaxial leaf side. For co-localization corresponding Agrobacteria suspensions were mixed 1:1 (each to an OD_{600} = 0.4) prior to infiltration. For more efficient expression, Agrobacteria carrying the p19 plasmid were co-infiltrated (suppression of RNA interference) (Voinnet et al., 2003, 2015). Transformed plants were kept at RT under long day conditions (16 h light, 8 h dark) and imaged after 48–72 h with a LSM 510 meta confocal laser scanning microscope (Carl Zeiss AG, Oberkochen, Germany) or an Axio Imager M2 with ApoTome (Carl Zeiss AG, Oberkochen, Germany). GFP and YFP were imaged at an excitation wavelength of 488 nm and emission wavelength of 500–530 nm, mCherry was imaged at an excitation wavelength at 563 nm and emission wavelength of 560–615 nm. Expression of pABind constructs was induced by spraying β-estradiol mix [20 μM β-estradiol (in DMSO), 0.1% (v/v) Tween20] to the abaxial leaf side 24–48 h post-infiltration (24–48 h before imaging). The (co-) localization experiments were performed in at least two independent replicates or as indicated in the text. Plasmolysis of cells expressing *BTSL1-GFP* was achieved through treatment of the leaf sample with 1 M mannitol solution for 30 min.

Bimolecular Fluorescence Complementation

CDS of gene pairs to be tested were amplified from cDNA of Arabidopsis WT roots. Amplicons generated with primers carrying B3 and B2 attachment sites were transferred into pDONR221-P3P2 (Thermo Fisher Scientific, Darmstadt, Germany, for nYFP fusion) and amplicons generated with primers carrying B1 and B4 attachment sites were transferred into pDONR221-P1P4 (Thermo Fisher Scientific, Darmstadt, Germany, for cYFP fusion), respectively. Primer sequences are listed in **Supplementary Table 2**. In a multisite Gateway LR reaction (Thermo Fisher Scientific, Darmstadt, Germany), both genes were transferred simultaneously into destination vector pBiFCt-2in1-NN (N-terminal nYFP and cYFP fusions) (Grefen and Blatt, 2012), to create pBiFCt-2in1-NN: FEP3:BTSL1, pBiFCt-2in1-NN:PYE-BTSL1, pBiFCt-2in1-NN:PYE-BTSL1-C and pBiFCt-2in1-NN:ILR3-BTSL1-C. The constructs carry a monomeric red fluorescent protein (mRFP) as internal transformation control. As negative controls, structurally similar

proteins known to not interact were used (negative controls: pBiFCt-2in1-NN:ILR3-BTSL2-C, pBiFCt-2in1-NN:FIT-BTSL1-C) (Kudla and Bock, 2016). Constructs were transformed into Agrobacteria and subsequently infiltrated into tobacco leaves, as described above. Forty 8–52 h after infiltration, mRFP and YFP signals were detected with an Axio Imager M2 (Carl Zeiss AG, Oberkochen, Germany). YFP was imaged at an excitation wavelength of 488 nm and emission wavelength of 500–530 nm, mRFP was imaged at an excitation wavelength at 563 nm and emission wavelength of 560–615 nm. BiFC experiments were performed in at least two independent replicates with two infiltrated leaves each.

Gene Expression Analysis by RT-qPCR

Gene expression analysis was performed as described earlier (Abdallah and Bauer, 2016). In brief, mRNA was extracted from whole seedlings grown in the 6 d system ($n > 60$ per replicate) or from roots grown in the 14 + 3 d system ($n > 15$ per replicate) (see "Plant Growth Conditions") and used for cDNA synthesis. RT-qPCR was performed using the iTaq™ Universal SYBR® Green Supermix (Bio-Rad Laboratories, Hercules, CA, United States) and the SFX96 Touch™ RealTime PCR Detection System (Bio-Rad Laboratories, Hercules, CA, United States). Data was processed with the Bio-Rad SFX Manager™ software (version 3.1). Absolute gene expression values were calculated from a gene specific mass standard dilution series and normalized to the elongation factor *EF1B*α. Primers for mass standards and RT-qPCR are listed in **Supplementary Table 2**. The analysis was performed with three biological and two technical replicates.

Immunoblot Analysis

Total proteins were extracted from ground plant material (tobacco leaves or Arabidopsis whole seedlings grown in the 6 d system, n = 30-60 seedlings) with 2× Laemmli buffer [124 mM Tris-HCl, pH 6.8, 5% (w/v) SDS, 4% (w/v) dithithreitol, 20% (v/v) glycerol, with 0.002% (w/v) bromophenol blue] and denatured at 95°C for 10 min. Equal amounts of total protein were separated on SDS-polyacrylamide gels, transferred to a Protran nitrocellulose membrane and stained with PonceauS as described in Le et al. (2016). To detect HA_3-tagged FEP3/IMA1 protein, the membrane was blocked with 5% (w/v) milk solution in 1xPBST (137 mM NaCl, 2.7 mM KCl, 10.14 mM Na_2HPO_4, 1.76 mM KH_2PO_4, 0.1% (v/v) Tween® 20, pH 7.4) for 30 min and subsequently incubated 1 h with anti-HA-peroxidase antibody and detected as described in Yeast Three-Hybrid assays.

Root Length Measurement

Plants were photographed at day six. Length of primary roots of individual seedlings was measured using the JMicroVision software (version 1.2.7),[1] as described previously (Ivanov et al., 2014). For calculation of mean root lengths and standard deviations, n = 13–29 roots per line and condition were measured.

Seed Fe Content Measurement

To determine seed Fe content, 1–3 plants from each line were grown on soil under long day conditions (16 h light, 8 h dark, 21°C). Seeds were harvested, pooled by plant genotype, and dried for 16 h at 100°C. Fe was extracted from ground seed material by incubation in 500 µl 3% (v/v) HNO_3 for 16 h at 100°C. Fe content in the supernatant was determined as described (Tamarit et al., 2006). Total Fe content in the sample was calculated with the help of a standard curve and normalized to seed dry weight. Per seed pool, $n = 3$ samples were measured.

Multiple Sequence Alignments and Protein Sequence Conservation

Multiple sequence alignments were performed with ClustalX using default settings (Larkin et al., 2007). To determine conservation scores of aa in BTSL1, the full BTSL1 aa sequence was uploaded to the Basic Local Alignment Search Tool [BLAST, Altschul et al. (1990)[2]] and run against the Viridiplantae database using the standard blastp (protein-protein BLAST) algorithm. The top 100 hits were downloaded, duplicates were removed. The remaining sequences were used for multiple sequence alignment using the Clustal Omega algorithm (Sievers et al., 2011) and visualized with Jalview (Waterhouse et al., 2009).[3] The full aa sequence of FEP3/IMA1 run against the Viridiplantae database as described above. Hits were only found within the Brassicaceae family, but alignments showed sequence conservation specifically toward the C-terminus. Subsequent blastp of the C-terminal half of FEP3/IMA1 (25 aa) resulted in several angiosperm hits. FEP3/IMA1 ortholog sequence hits from exemplary angiosperm orders were downloaded and aligned.

Protein Structure Prediction and Molecular Docking

Protein structures were predicted using AlphaFold2 (Jumper et al., 2021) the Alphafold-Multimer tool (Evans et al., 2021) with protein sequences from TAIR. Multiple Sequence alignments were generated through MMseqs2 API. Molecular docking was performed in HADDOCK 2.4 (van Zundert et al., 2016; Honorato et al., 2021). Active residues were used to generate ambiguous interaction restraints. The obtained file was further processed in Discovery studio, Dassault Systems BIOVIA and UCSF Chimera.

Statistical Analysis

Null hypothesis between normally distributed groups was tested with a two-tailed Student's t-test. Null hypothesis was rejected, when the p-value (p) was below 0.05. Statistically significantly different groups are indicated by one asterisk for $p < 0.05$, two asterisks for $p < 0.01$ and three asterisks for $p < 0.001$. When comparing more than two groups, null hypotheses were tested with one-way analysis of variance (ANOVA) and a Tukey's *post-hoc* test. Null hypotheses were rejected when $p < 0.05$. Statistically

[1] http://www.jmicrovision.com

[2] https://blast.ncbi.nlm.nih.gov/

[3] http://www.jalview.org/

significantly different groups are indicated by different lowercase letters. Number of technical and biological repetitions of the individual experiments are indicated in the Figure legends.

ACCESSION NUMBERS

AKT1 (AT2G26650), BHLH11 (AT4G36060), BHLH34 (AT3G23210), BHLH38 (AT3G56970), BHLH39 (AT3G56980), BHLH100 (AT2G41240), BHLH101 (AT5G04150), BHLH104 (AT4G14410), BHLH115 (AT1G51070), BTS (AT3G18290), BTSL1 (AT1G74770), BTSL2 (AT1G18910), CIPK23 (AT1G30270), DGAT3 (AT1G48300), DUF506 (AT1G12030), FEP1 (AT2G30766), FEP3/IMA1 (AT1G47400), FIT (AT2G28160), FRO2 (AT1G01580), FRO3 (AT1G23020), GRF11 (AT1G34760), ILR3 (AT5G54680), IRT1 (AT4G19690), JAL12 (AT1G52120), KELCH (AT3G07720), MYB72 (AT1G56160), NAS2 (AT5G56080), NAS4 (AT1G56430), ORG1 (AT5G53450), PRS2 (AT1G32380), PYE (AT3G47640), SDI1 (AT5G48850), S8H (AT3G12900), TCP20 (AT3G27010), UP1 (AT3G06890), UP2 (AT3G56360), UP3 (AT5G05250), and URI (AT3G19860).

DATA AVAILABILITY STATEMENT

The original contributions presented in this study are included in the article/**Supplementary Material**, further inquiries can be directed to the corresponding author.

AUTHOR CONTRIBUTIONS

DL, BS, DB, and PB conceived the project and reviewed and edited the manuscript. DL, BS, DB, CE, and CS performed the experiments and analyzed the data. DL, BS, and PB supervised the research. BS and DL wrote the original draft. PB acquired funding and agreed to serve as the author responsible for contact and ensures communication. All authors contributed to the article and approved the submitted version.

FUNDING

This project was funded by the Deutsche Forschungsgemeinschaft (DFG, German Research Foundation) under Germany's Excellence Strategy—EXC-2048/1—project ID 390686111. This work was funded by the Deutsche Forschungsgemeinschaft GRK F020512056 (NextPlant) and the Deutsche Forschungsgemeinschaft (DFG), project ID 391465903/GRK 2466.

ACKNOWLEDGMENTS

We thank Elke Wieneke and Gintaute Matthäi for excellent technical assistance. We thank Ksenia Trofimov for help with imaging of ILR3-GFP and YFP-bHLH104. We acknowledge the contributions of Sarah Plicht, Theresa Priebe, and Kai Blaeser. We thank Janneke Balk, Norwich, United Kingdom, for *btsl1 btsl2* seeds, and Diqiu Yu, Chinese Academy of Sciences, Kunming, China, for *ProILR3:GUS*/WT and *proBHLH104:GUS*/WT Arabidopsis lines. We thank Ute Hoecker, University of Cologne, Germany, for pBRIDGE plasmid and the Y190 yeast strain, and Andreas Weber, HHU Düsseldorf, Germany, for pGWB3. pACT2-GW and pGBKT7-GW were kindly provided by Yves Jacob, Institut Pasteur, Paris, France. We thank Rumen Ivanov, Ksenia Trofimov, Inga Mohr, and Tzvetina Brumbarova for help and advice with microscopy and with the implementation of lab protocols. DL, BS, and DB were members of the international graduate school iGRAD-Plant, Düsseldorf. Funding from the German Research Foundation through the DFG International Research Training groups 1,525 and 2,466 is greatly acknowledged.

SUPPLEMENTARY MATERIAL

The Supplementary Material for this article can be found online at: https://www.frontiersin.org/articles/10.3389/fpls.2022.930049/full#supplementary-material

REFERENCES

Aarabi, F., Kusajima, M., Tohge, T., Konishi, T., Gigolashvili, T., Takamune, M., et al. (2016). Sulfur deficiency-induced repressor proteins optimize glucosinolate biosynthesis in plants. *Sci. Adv.* 2:e1601087. doi: 10.1126/sciadv.1601087

Abdallah, H. B., and Bauer, P. (2016). Quantitative reverse transcription-qPCR-Based gene expression analysis in plants. *Methods Mol. Biol.* 1363, 9–24. doi: 10.1007/978-1-4939-3115-6_2

Akmakjian, G. Z., Riaz, N., and Guerinot, M. L. (2021). Photoprotection during iron deficiency is mediated by the bHLH transcription factors PYE and ILR3. *Proc. Natl. Acad. Sci. U.S.A.* 118:e2024918118. doi: 10.1073/pnas.2024918118

Altschul, S. F., Gish, W., Miller, W., Myers, E. W., and Lipman, D. J. (1990). Basic local alignment search tool. *J. Mol. Biol.* 215, 403–410.

Belda-Palazon, B., Julian, J., Coego, A., Wu, Q., Zhang, X., Batistic, O., et al. (2019). ABA inhibits myristoylation and induces shuttling of the RGLG1 E3 ligase to promote nuclear degradation of PP2CA. *Plant J.* 98, 813–825. doi: 10.1111/tpj.14274

Bensmihen, S., To, A., Lambert, G., Kroj, T., Giraudat, J., and Parcy, F. (2004). Analysis of an activated ABI5 allele using a new selection method for transgenic Arabidopsis seeds. *FEBS Lett.* 561, 127–131. doi: 10.1016/s0014-5793(04)00148-6

Beyer, H. M., Gonschorek, P., Samodelov, S. L., Meier, M., Weber, W., and Zurbriggen, M. D. (2015). AQUA Cloning: a versatile and simple enzyme-free cloning approach. *PLoS One* 10:e0137652. doi: 10.1371/journal.pone.0137652

Bleckmann, A., Weidtkamp-Peters, S., Seidel, C. A., and Simon, R. (2010). Stem cell signaling in Arabidopsis requires CRN to localize CLV2 to the plasma membrane. *Plant Physiol.* 152, 166–176. doi: 10.1104/pp.109.149930

Brumbarova, T., Bauer, P., and Ivanov, R. (2015). Molecular mechanisms governing Arabidopsis iron uptake. *Trends Plant Sci.* 20, 124–133. doi: 10.1016/j.tplants.2014.11.004

Cabrera-Quio, L. E., Herberg, S., and Pauli, A. (2016). Decoding sORF translation - from small proteins to gene regulation. *RNA Biol.* 13, 1051–1059. doi: 10.1080/15476286.2016.1218589

Cai, Y., Li, Y., and Liang, G. (2021). FIT and bHLH Ib transcription factors modulate iron and copper crosstalk in Arabidopsis. *Plant Cell Environ.* 44, 1679–1691. doi: 10.1111/pce.14000

Cheng, M. C., Hsieh, E. J., Chen, J. H., Chen, H. Y., and Lin, T. P. (2012). Arabidopsis RGLG2, functioning as a RING E3 ligase, interacts with AtERF53 and negatively regulates the plant drought stress response. *Plant Physiol.* 158, 363–375. doi: 10.1104/pp.111.189738

Clough, S. J., and Bent, A. F. (1998). Floral dip: a simplified method for Agrobacterium-mediated transformation of Arabidopsis thaliana. *Plant J.* 16, 735–743. doi: 10.1046/j.1365-313x.1998.00343.x

Colangelo, E. P., and Guerinot, M. L. (2004). The essential basic helix-loop-helix protein FIT1 is required for the iron deficiency response. *Plant Cell* 16, 3400–3412. doi: 10.1105/tpc.104.024315

Connorton, J. M., Balk, J., and Rodriguez-Celma, J. (2017). Iron homeostasis in plants - a brief overview. *Metallomics* 9, 813–823. doi: 10.1039/c7mt00136c

Curtis, M. D., and Grossniklaus, U. (2003). A gateway cloning vector set for high-throughput functional analysis of genes in planta. *Plant Physiol.* 133, 462–469. doi: 10.1104/pp.103.027979

Delcourt, V., Staskevicius, A., Salzet, M., Fournier, I., and Roucou, X. (2018). Small proteins encoded by unannotated ORFs are rising stars of the proteome, confirming shortcomings in genome annotations and current vision of an mRNA. *Proteomics* 18:e1700058. doi: 10.1002/pmic.201700058

Dong, C.-H., Agarwal, M., Zhang, Y., Xie, Q., and Zhu, J.-K. (2006). The negative regulator of plant cold responses, HOS1, is a RING E3 ligase that mediates the ubiquitination and degradation of ICE1. *Proc. Natl. Acad. Sci. U.S.A.* 103, 8281–8286. doi: 10.1073/pnas.0602874103

Evans, R., O'Neill, M., Pritzel, A., Antropova, N., Senior, A., Green, T., et al. (2021). Protein complex prediction with AlphaFold-Multimer. *bioRxiv* [Preprint]. doi: 10.1101/2021.10.04.463034

Gao, F., Robe, K., Bettembourg, M., Navarro, N., Rofidal, V., Santoni, V., et al. (2019a). The Transcription Factor bHLH121 Interacts with bHLH105 (ILR3) and its Closest Homologs to Regulate Iron Homeostasis in Arabidopsis. *Plant Cell* 32, 508–524. doi: 10.1105/tpc.19.00541

Gao, F., Robe, K., Gaymard, F., Izquierdo, E., and Dubos, C. (2019b). The Transcriptional Control of Iron Homeostasis in Plants: A Tale of bHLH Transcription Factors? *Front. Plant Sci.* 10:6. doi: 10.3389/fpls.2019.00006

Gietz, R. D., and Schiestl, R. H. (2007). High-efficiency yeast transformation using the LiAc/SS carrier DNA/PEG method. *Nat. Protoc.* 2, 31–34. doi: 10.1038/nprot.2007.13

Gratz, R., Manishankar, P., Ivanov, R., Koster, P., Mohr, I., Trofimov, K., et al. (2019). CIPK11-Dependent phosphorylation modulates FIT activity to promote Arabidopsis Iron Acquisition in response to Calcium Signaling. *Dev. Cell* 48, 726–740.e10. doi: 10.1016/j.devcel.2019.01.006

Gratz, R., Brumbarova, T., Ivanov, R., Trofimov, K., Tunnermann, L., Ochoa-Fernandez, R., et al. (2020). Phospho-mutant activity assays provide evidence for alternative phospho-regulation pathways of the transcription factor FIT. *New Phytol.* 225, 250–267. doi: 10.1111/nph.16168

Grefen, C., and Blatt, M. R. (2012). A 2in1 cloning system enables ratiometric bimolecular fluorescence complementation (rBiFC). *Biotechniques* 53, 311–314. doi: 10.2144/000113941

Grillet, L., Lan, P., Li, W. F., Mokkapati, G., and Schmidt, W. (2018). IRON MAN is a ubiquitous family of peptides that control iron transport in plants. *Nat. Plants* 4:953. doi: 10.1038/s41477-018-0266-y

Hans Wedepohl, K. (1995). The composition of the continental crust. *Geochim. Cosmochim. Acta* 59, 1217–1232. doi: 10.1016/0016-7037(95)00038-2

Heim, M. A., Jakoby, M., Werber, M., Martin, C., Weisshaar, B., and Bailey, P. C. (2003). The basic helix-loop-helix transcription factor family in plants: a genome-wide study of protein structure and functional diversity. *Mol. Biol. Evol.* 20, 735–747.

Hindt, M. N., Akmakjian, G. Z., Pivarski, K. L., Punshon, T., Baxter, I., Salt, D. E., et al. (2017). BRUTUS and its paralogs, BTS LIKE1 and BTS LIKE2, encode important negative regulators of the iron deficiency response in Arabidopsis thaliana. *Metallomics* 9, 876–890. doi: 10.1039/c7mt00152e

Hirayama, T., Lei, G. J., Yamaji, N., Nakagawa, N., and Ma, J. F. (2018). The Putative Peptide Gene FEP1 Regulates Iron Deficiency Response in Arabidopsis. *Plant Cell Physiol.* 59, 1739–1752. doi: 10.1093/pcp/pcy145

Honorato, R. V., Koukos, P. I., Jiménez-García, B., Tsaregorodtsev, A., Verlato, M., Giachetti, A., et al. (2021). Structural Biology in the Clouds: the WeNMR-EOSC Ecosystem. *Front. Mol. Biosci.* 8:729513. doi: 10.3389/fmolb.2021.729513

Ivanov, R., Brumbarova, T., and Bauer, P. (2012). Fitting into the harsh reality: regulation of iron deficiency responses in dicotyledonous plants. *Mol. Plant* 5, 27–42. doi: 10.1093/mp/ssr065

Ivanov, R., Brumbarova, T., Blum, A., Jantke, A. M., Fink-Straube, C., and Bauer, P. (2014). SORTING NEXIN1 is required for modulating the trafficking and stability of the *Arabidopsis* IRON-REGULATED TRANSPORTER1. *Plant Cell* 26, 1294–1307.

Jakoby, M., Wang, H. Y., Reidt, W., Weisshaar, B., and Bauer, P. (2004). FRU (*BHLH029*) is required for induction of iron mobilization genes in *Arabidopsis thaliana*. *FEBS Lett.* 577, 528–534. doi: 10.1016/j.febslet.2004.10.062

Jumper, J., Evans, R., Pritzel, A., Green, T., Figurnov, M., Ronneberger, O., et al. (2021). Highly accurate protein structure prediction with AlphaFold. *Nature* 596, 583–589. doi: 10.1038/s41586-021-03819-2

Karimi, M., De Meyer, B., and Hilson, P. (2005). Modular cloning in plant cells. *Trends Plant Sci.* 10, 103–105. doi: 10.1016/j.tplants.2005.01.008

Khan, I., Gratz, R., Denezhkin, P., Schott-Verdugo, S. N., Angrand, K., Genders, L., et al. (2019). Calcium-Promoted Interaction between the C2-Domain Protein EHB1 and Metal Transporter IRT1 Inhibits Arabidopsis Iron Acquisition. *Plant Physiol.* 180, 1564–1581. doi: 10.1104/pp.19.00163

Kim, S. A., LaCroix, I. S., Gerber, S. A., and Guerinot, M. L. (2019). The iron deficiency response in Arabidopsis thaliana requires the phosphorylated transcription factor URI. *Proc. Natl. Acad. Sci. U.S.A.* 116, 24933–24942. doi: 10.1073/pnas.1916892116

Kobayashi, T., Nagano, A. J., and Nishizawa, N. K. (2020). Iron deficiency-inducible peptide-coding genes OsIMA1 and OsIMA2 positively regulate a major pathway of iron uptake and translocation in rice. *J. Exp. Bot.* 72, 2196–2211.

Kobayashi, T., Nagano, A. J., and Nishizawa, N. K. (2021). Iron deficiency-inducible peptide-coding genes OsIMA1 and OsIMA2 positively regulate a major pathway of iron uptake and translocation in rice. *J. Exp. Bot.* 72, 2196–2211. doi: 10.1093/jxb/eraa546

Kobayashi, T., Nagasaka, S., Senoura, T., Itai, R. N., Nakanishi, H., and Nishizawa, N. K. (2013). Iron-binding haemerythrin RING ubiquitin ligases regulate plant iron responses and accumulation. *Nat. Commun.* 4:2792. doi: 10.1038/ncomms3792

Kudla, J., and Bock, R. (2016). Lighting the way to protein-protein interactions: recommendations on best practices for Bimolecular Fluorescence Complementation analyses. *Plant Cell* 28, 1002–1008.

Larkin, M. A., Blackshields, G., Brown, N. P., Chenna, R., McGettigan, P. A., McWilliam, H., et al. (2007). Clustal W and clustal X version 2.0. *Bioinformatics* 23, 2947–2948.

Le, C. T. T., Brumbarova, T., Ivanov, R., Stoof, C., Weber, E., Mohrbacher, J., et al. (2016). ZINC FINGER OF ARABIDOPSIS THALIANA12 (ZAT12) Interacts with FER-LIKE IRON DEFICIENCY-INDUCED TRANSCRIPTION FACTOR (FIT) Linking Iron Deficiency and Oxidative Stress Responses. *Plant Physiol.* 170, 540–557. doi: 10.1104/pp.15.01589

Lee, H., Xiong, L., Gong, Z., Ishitani, M., Stevenson, B., and Zhu, J. K. (2001). The Arabidopsis HOS1 gene negatively regulates cold signal transduction and encodes a RING finger protein that displays cold-regulated nucleo–cytoplasmic partitioning. *Genes Dev.* 15, 912–924. doi: 10.1101/gad.866801

Li, X., Zhang, H., Ai, Q., Liang, G., and Yu, D. (2016). Two bHLH Transcription Factors, bHLH34 and bHLH104, Regulate Iron Homeostasis in Arabidopsis thaliana. *Plant Physiol.* 170, 2478–2493. doi: 10.1104/pp.15.01827

Li, Y., Lei, R., Pu, M., Cai, Y., Lu, C., Li, Z., et al. (2022). bHLH11 inhibits bHLH IVc proteins by recruiting the TOPLESS/TOPLESS-RELATED corepressors in Arabidopsis. *bioRxiv* [Preprint]. doi: 10.1101/2020.04.09.035097

Li, Y., Lu, C. K., Li, C. Y., Lei, R. H., Pu, M. N., Zhao, J. H., et al. (2021). IRON MAN interacts with BRUTUS to maintain iron homeostasis in Arabidopsis</em&gt. *Proc. Natl. Acad. Sci. U.S.A.* 118:e2109063118. doi: 10.1073/pnas.2109063118

Liang, G., Zhang, H. M., Li, X. L., Ai, Q., and Yu, D. Q. (2017). bHLH transcription factor bHLH115 regulates iron homeostasis in Arabidopsis thaliana. *J. Exp. Bot.* 68, 1743–1755. doi: 10.1093/jxb/erx043

Lindsay, W. L. (1988). "Solubility and Redox Equilibria of Iron Compounds in Soils," in *Iron in Soils and Clay Minerals*, eds J. W. Stucki, B. A. Goodman, and U. Schwertmann (Dordrecht: Springer), 37–62.

Lingam, S., Mohrbacher, J., Brumbarova, T., Potuschak, T., Fink-Straube, C., Blondet, E., et al. (2011). Interaction between the bHLH transcription factor FIT

and ETHYLENE INSENSITIVE3/ETHYLENE INSENSITIVE3-LIKE1 reveals molecular linkage between the regulation of iron acquisition and ethylene signaling in *Arabidopsis*. *Plant Cell* 23, 1815–1929. doi: 10.1105/tpc.111.084715

Long, T. A., Tsukagoshi, H., Busch, W., Lahner, B., Salt, D. E., and Benfey, P. N. (2010). The bHLH transcription factor POPEYE regulates response to iron deficiency in Arabidopsis roots. *Plant Cell* 22, 2219–2236. doi: 10.1105/tpc.110.074096

Makarewich, C. A., and Olson, E. N. (2017). Mining for Micropeptides. *Trends Cell Biol.* 27, 685–696. doi: 10.1016/j.tcb.2017.04.006

Marschner, H., and Römheld, V. (1994). Strategies of plants for acquisition of iron. *Plant Soil* 165, 261–274.

Nakagawa, T., Kurose, T., Hino, T., Tanaka, K., Kawamukai, M., Niwa, Y., et al. (2007). Development of series of gateway binary vectors, pGWBs, for realizing efficient construction of fusion genes for plant transformation. *J. Biosci. Bioeng.* 104, 34–41. doi: 10.1263/jbb.104.34

Robinson, N. J., Procter, C. M., Connolly, E. L., and Guerinot, M. L. (1999). A ferric-chelate reductase for iron uptake from soils. *Nature* 397, 694–697. doi: 10.1038/17800

Rodriguez-Celma, J., Connorton, J. M., Kruse, I., Green, R. T., Franceschetti, M., Chen, Y. T., et al. (2019). Arabidopsis BRUTUS-LIKE E3 ligases negatively regulate iron uptake by targeting transcription factor FIT for recycling. *Proc. Natl. Acad. Sci. U.S.A.* 116, 17584–17591. doi: 10.1073/pnas.1907971116

Samira, R., Li, B., Kliebenstein, D., Li, C., Davis, E., Gillikin, J. W., et al. (2018). The bHLH transcription factor ILR3 modulates multiple stress responses in Arabidopsis. *Plant Mol. Biol.* 97, 297–309. doi: 10.1007/s11103-018-0735-8

Schwarz, B., and Bauer, P. (2020). FIT, a regulatory hub for iron deficiency and stress signaling in roots, and FIT-dependent and -independent gene signatures. *J. Exp. Bot.* 71, 1694–1705. doi: 10.1093/jxb/eraa012

Selote, D., Matthiadis, A., Gillikin, J. W., Sato, M. H., and Long, T. A. (2018). The E3 ligase BRUTUS facilitates degradation of VOZ1/2 transcription factors. *Plant Cell Environ.* 41, 2463–2474. doi: 10.1111/pce.13363

Selote, D., Samira, R., Matthiadis, A., Gillikin, J. W., and Long, T. A. (2015). Iron-binding E3 ligase mediates iron response in plants by targeting basic helix-loop-helix transcription factors. *Plant Physiol.* 167, 273–286. doi: 10.1104/pp.114.250837

Sievers, F., Wilm, A., Dineen, D., Gibson, T. J., Karplus, K., Li, W. Z., et al. (2011). Fast, scalable generation of high-quality protein multiple sequence alignments using Clustal Omega. *Mol. Syst. Biol.* 7:539. doi: 10.1038/msb.2011.75

Tamarit, J., Irazusta, V., Moreno-Cermeño, A., and Ros, J. (2006). Colorimetric assay for the quantitation of iron in yeast. *Anal. Biochem.* 351, 149–151. doi: 10.1016/j.ab.2005.12.001

Tanabe, N., Noshi, M., Mori, D., Nozawa, K., Tamoi, M., and Shigeoka, S. (2019). The basic helix-loop-helix transcription factor, bHLH11 functions in the iron-uptake system in Arabidopsis thaliana. *J. Plant Res.* 132, 93–105. doi: 10.1007/s10265-018-1068-z

Tissot, N., Robe, K., Gao, F., Grant-Grant, S., Boucherez, J., Bellegarde, F., et al. (2019). Transcriptional integration of the responses to iron availability in Arabidopsis by the bHLH factor ILR3. *New Phytol.* 223, 1433–1446. doi: 10.1111/nph.15753

Trofimov, K., Ivanov, R., Eutebach, M., Acaroglu, B., Mohr, I., Bauer, P., et al. (2019). Mobility and localization of the iron deficiency-induced transcription factor bHLH039 change in the presence of FIT. *Plant Direct* 3:e00190. doi: 10.1002/pld3.190

van Zundert, G. C. P., Rodrigues, J. P. G. L. M., Trellet, M., Schmitz, C., Kastritis, P. L., Karaca, E., et al. (2016). The HADDOCK2.2 Web Server: user-Friendly Integrative Modeling of Biomolecular Complexes. *J. Mol. Biol.* 428, 720–725.

Vert, G., Grotz, N., Dedaldechamp, F., Gaymard, F., Guerinot, M. L., Briat, J. F., et al. (2002). IRT1, an Arabidopsis transporter essential for iron uptake from the soil and for plant growth. *Plant Cell* 14, 1223–1233.

Voinnet, O., Rivas, S., Mestre, P., and Baulcombe, D. (2003). An enhanced transient expression system in plants based on suppression of gene silencing by the p19 protein of tomato bushy stunt virus. *Plant J.* 84:846. doi: 10.1111/tpj.13066

Voinnet, O., Rivas, S., Mestre, P., and Baulcombe, D. (2015). An enhanced transient expression system in plants based on suppression of gene silencing by the p19 protein of tomato bushy stunt virus (Retraction of Vol 33, Pg 949, 2003). *Plant J.* 84:846. doi: 10.1111/tpj.13066

Wang, N., Cui, Y., Liu, Y., Fan, H., Du, J., Huang, Z., et al. (2013). Requirement and functional redundancy of Ib subgroup bHLH proteins for iron deficiency responses and uptake in Arabidopsis thaliana. *Mol. Plant* 6, 503–513. doi: 10.1093/mp/sss089

Waterhouse, A. M., Procter, J. B., Martin, D. M. A., Clamp, M., and Barton, G. J. (2009). Jalview version 2-a multiple sequence alignment editor and analysis workbench. *Bioinformatics* 25, 1189–1191.

Yuan, Y., Wu, H., Wang, N., Li, J., Zhao, W., Du, J., et al. (2008). FIT interacts with AtbHLH38 and AtbHLH39 in regulating iron uptake gene expression for iron homeostasis in Arabidopsis. *Cell Res.* 18, 385–397. doi: 10.1038/cr.2008.26

Zanet, J., Benrabah, E., Li, T., Pélissier-Monier, A., Chanut-Delalande, H., Ronsin, B., et al. (2015). Pri sORF peptides induce selective proteasome-mediated protein processing. *Science* 349, 1356–1358. doi: 10.1126/science.aac5677

Zhang, J., Liu, B., Li, M., Feng, D., Jin, H., Wang, P., et al. (2015). The bHLH transcription factor bHLH104 interacts with IAA-LEUCINE RESISTANT3 and modulates iron homeostasis in Arabidopsis. *Plant Cell* 27, 787–805. doi: 10.1105/tpc.114.132704

Conflict of Interest: The authors declare that the research was conducted in the absence of any commercial or financial relationships that could be construed as a potential conflict of interest.

Publisher's Note: All claims expressed in this article are solely those of the authors and do not necessarily represent those of their affiliated organizations, or those of the publisher, the editors and the reviewers. Any product that may be evaluated in this article, or claim that may be made by its manufacturer, is not guaranteed or endorsed by the publisher.

frontiers | Frontiers in Plant Science

TYPE Original Research
PUBLISHED 26 August 2022
DOI 10.3389/fpls.2022.951181

OPEN ACCESS

EDITED BY
Stefania Astolfi,
Tuscia University, Italy

REVIEWED BY
Nasim Ahmad Yasin,
University of the Punjab, Pakistan
Nazim Hussain,
Independent Researcher, Sharjah,
United Arab Emirates

*CORRESPONDENCE
Ju Min
jmin@issas.ac.cn

SPECIALTY SECTION
This article was submitted to Plant Nutrition, a section of the journal Frontiers in Plant Science

RECEIVED 23 May 2022
ACCEPTED 05 August 2022
PUBLISHED 26 August 2022

CITATION
Ji R, Shi W, Wang Y, Zhang H and Min J (2022) Development of a sensor-based site-specific N topdressing algorithm for a typical leafy vegetable. *Front. Plant Sci.* 13:951181. doi: 10.3389/fpls.2022.951181

Development of a sensor-based site-specific N topdressing algorithm for a typical leafy vegetable

Rongting Ji[1,2], Weiming Shi[1], Yuan Wang[1], Hailin Zhang[3] and Ju Min[1]*

[1]State Key Laboratory of Soil and Sustainable Agriculture, Institute of Soil Science, Chinese Academy of Sciences, Nanjing, China, [2]Nanjing Institute of Environmental Sciences, Ministry of Ecology and Environment of the People's Republic of China, Nanjing, China, [3]Department of Plant and Soil Sciences, Oklahoma State University, Stillwater, OK, United States

Precise and site-specific nitrogen (N) fertilizer management of vegetables is essential to improve the N use efficiency considering temporal and spatial fertility variations among fields, while the current N fertilizer recommendation methods are proved to be time- and labor-consuming. To establish a site-specific N topdressing algorithm for bok choy (*Brassica rapa subsp. chinensis*), using a hand-held GreenSeeker canopy sensor, we conducted field experiments in the years 2014, 2017, and 2020. Two planting densities, viz, high (123,000 plants ha^{-1}) in Year I and low (57,000 plants ha^{-1}) in Year II, whereas, combined densities in Year III were used to evaluate the effect of five N application rates (0, 45, 109, 157, and 205 kg N ha^{-1}). A robust relationship was observed between the sensor-based normalized difference vegetation index (NDVI), the ratio vegetation index (RVI), and the yield potential without topdressing (YP_0) at the rosette stage, and 81–84% of the variability at high density and 76–79% of that at low density could be explained. By combining the densities and years, the R^2 value increased to 0.90. Additionally, the rosette stage was identified as the earliest stage for reliably predicting the response index at harvest ($RI_{Harvest}$), based on the response index derived from NDVI (RI_{NDVI}) and RVI (RI_{RVI}), with R^2 values of 0.59–0.67 at high density and 0.53–0.65 at low density. When using the combined results, the RI_{RVI} performed 6.12% better than the RI_{NDVI}, and 52% of the variability could be explained. This study demonstrates the good potential of establishing a sensor-based N topdressing algorithm for bok choy, which could contribute to the sustainable development of vegetable production.

KEYWORDS

active canopy sensor, bok choy, N response index, N topdressing strategy, yield potential

Introduction

Nitrogen (N) is the key nutritional driver determining crop yield and quality, especially for vegetables (Dunn et al., 2015). However, N fertilizer use is highly inefficient, and often only 10–30% of the N applied in the field can be absorbed by the crop, with a substantial amount of N loss to the environment, resulting in soil and water quality deterioration (Zhu et al., 2005; Shi et al., 2009; Song et al., 2009). The amount and timing of the N application are the two important factors determining the N-use efficiency (NUE) (Bijay-Singh et al., 2015; Zotarelli et al., 2015). In this sense, the diagnosis of field plant N status and appropriate fertilizer-application recommendations have become a critical component of ensuring high yields and good quality vegetable crops. Since small farms characterize agriculture in many countries, as reported, 73% of farms are smaller than 1 ha and 85% are smaller than 2 ha, especially in China where over 80% of households operate less than 0.6 ha of farmland (Tan et al., 2013; Lowder et al., 2016). Fine-tuned monitoring of N status of both field and crop has been challenging, and over-fertilization is a common occurrence. In these smaller-scale operations, further complicated by variable fertility histories and rotation systems, the temporal and spatial variation in soil fertility among fields has additionally restricted efficient fertilizer-N utilization (Jin and Jiang, 2002; Lowder et al., 2016). Therefore, a site-specific topdressing N-management strategy must be developed that reflects spatial variabilities and plant N availability to improve NUE in vegetable production systems (Dobermann et al., 2003).

Numerous recommendation systems have been developed and tested for improving the N-fertilizer management of vegetable crops, such as the N_{min} methods, the Kulturbegleitenden N_{min}-Sollwerte System, and the N-Expert system (Burns, 2006; Schmidt et al., 2009). These existing systems are mainly based on soil testing and plant analysis; however, the cost and time required for soil and plant testing, the slow turnaround time, and high prediction errors among fields have limited the adoption of these methods by local farmers (Jin and Jiang, 2002; Ma et al., 2007). In recent years, significant progress in investigating remote-sensing technology as a real-time N diagnostic tool has been made, and related approaches have been applied to many crops (Samborski et al., 2009). Some proximal optical sensors, such as chlorophyll meters, Dualex instruments, and portable canopy sensors, have been used for determining the N status of vegetables (Gianquinto et al., 2011; Padilla et al., 2018). Among these, hand-held active canopy sensors have shown the potential to detect plant N status with high temporal and spatial resolution at the canopy level and have received much attention because of their superior operational efficiency over direct contact leaf sensors and relatively low cost compared to hyperspectral sensors (Raun et al., 2005; Xia et al., 2016).

One of the commonly used hand-held active canopy sensors is the GreenSeeker optical sensor, which measures reflectance from the plant canopy in the red and near-infrared wavelength region and provides two typical plant indices: the normalized difference vegetation index (NDVI) and the ratio vegetation index (RVI) (Yao et al., 2012). The canopy reflectance to visible light is primarily dependent on the chlorophyll content contained in the leaf palisade layer and the near-infrared reflectance depended upon the structure of the mesophyll cell and the cavities between cells, thus the NDVI and RVI indices can detect plant N status and make N recommendation (Olfs et al., 2005). Canopy characteristics have been used to guide the N management of many cereal crops, e.g., winter wheat, corn, and rice (Lukina et al., 2001; Barker and Sawyer, 2010; Ali et al., 2014). Although the GreenSeeker sensor has been widely used for cereal crops, there has been limited use for N-fertilizer management in vegetable crops due to their special nutritional characteristics, fertilization, regimes, and soil fertility level; therefore, it cannot be used by just replacing the crop in the equation, and the usability, application procedures, and accuracy of the GreenSeeker sensor need to be restudied in the new system (Tremblay et al., 2011; Ji et al., 2017). Previous studies have mainly focused on in-season N-status estimation of a specific vegetable, but protocols for determining the variable N-application rate considering the spatial variation of vegetable crops are urgently needed (Jones et al., 2007; Tremblay et al., 2011; Dunn et al., 2015; Padilla et al., 2018). Moreover, plant density is one of the most important agronomic factors in practice, and sensor readings and N requirements change at different densities (Raun et al., 2002). It is unknown whether a hand-held active canopy sensor like the GreenSeeker sensor can be used for the N management of leafy vegetables with different plant densities.

Bok choy (*Brassica rapa subsp. chinensis*) is a popular leafy vegetable that originated in China over 1,500 years ago. Currently, it is widely cultivated and consumed in China and north-eastern Asia for its antioxidant benefits and winter hardiness (Heimler et al., 2006; Zhang et al., 2014). In particular, it is a popular leafy vegetable in the Taihu Lake region of southern China, and compared with a previous study, there seems to be a large opportunity for N-fertilizer reduction for bok choy in this region (Zhang et al., 2016). Key questions, therefore, were whether the GreenSeeker sensor may be employed to produce N-fertilizer recommendations for bok choy and whether a sensor-based topdressing N-management strategy could reduce N-fertilizer applications without sacrificing yields. We hypothesize that the GreenSeeker sensor would be used to make N recommendation of bok choy with different densities, and the N fertilizer rate would be reduced considering temporal and spatial soil fertility. In our study, a 3-year field experiment of bok choy with different densities and N-application rates was conducted in the Taihu Lake region. The objectives were to (i) determine

whether the sensor-based N diagnosis model could be applied to bok choy with different plant densities, (ii) identify the suitable growth stage and plant index between NDVI and RVI for bok choy to make accurate predictions of yield without additional N (YP_0) and the response index (RI) with topdressing N, and (iii) develop an accurate sensor-based N-fertilizer topdressing strategy for bok choy to improve the N-use efficiency.

Materials and methods

Study site

Field experiments with bok choy (*Brassica rapa subsp. chinensis*) were conducted in 2014 (Year I), 2017 (Year II), and 2020 (Year III) in Yixing (31°16′N, 119°54′E), Jiangsu Province, which is located in the center of the Taihu Lake region in south-eastern China. This region has a sub-tropical monsoon climate, with a mean annual air temperature and rainfall of 15.7°C and 1,177 mm, respectively. The distribution of precipitation and temperature during the experimental period is shown in Figure 1. Bok choy was planted in a new vegetable field (a traditional bok choy-radish-cabbage rotation was applied in each field every year), and the soil type at the experiment site was classified as hydroagric Stagnic Anthrosol by the Chinese soil taxonomic classification (Gong, 1999), with a pH (H_2O) of 6.25, an electrical conductivity (EC) of 0.48 mS cm^{-1}, and the soil organic matter content, total N, NO_3^--N, and NH_4^+-N were 18.5 g kg^{-1}, 1.06 g kg^{-1}, 84.2 mg kg^{-1}, and 24.6 mg kg^{-1}, respectively.

Experimental design

In Years I and II, 2,680 kg ha^{-1} manure (consisting of 45 kg N ha^{-1}) and 24 kg P ha^{-1} from calcium superphosphate

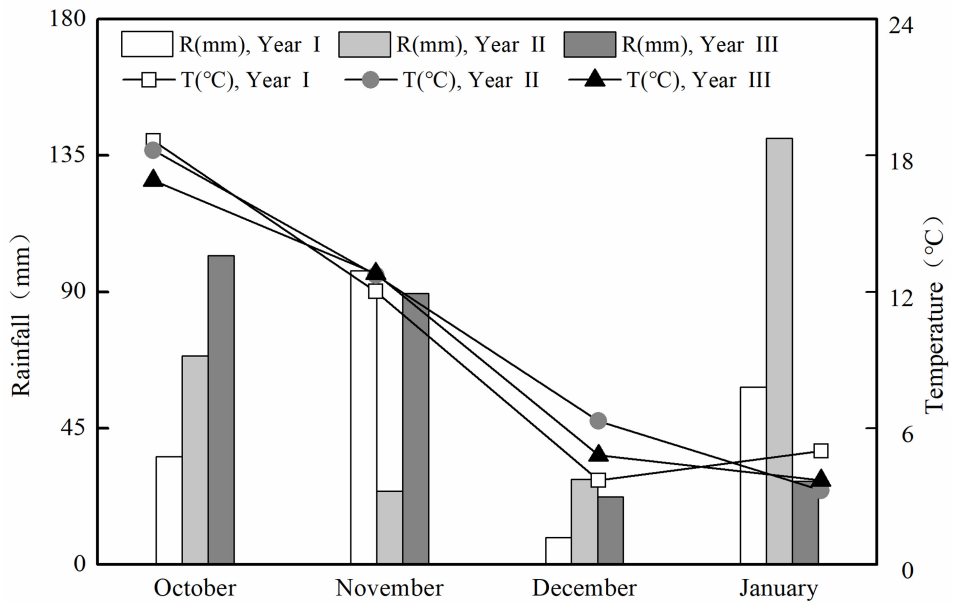

FIGURE 1
Monthly precipitation (R, mm) and average air temperature (*T*, °C) at the experiment site in cropping Years I, II, and III.

TABLE 1 Detailed experimental design.

Year	Plant density	Transplanting date	Harvest date	Nitrogen application rate (kg N ha^{-1})	Plot area (m^2)	Experimental function
Year I	123,000 plants ha^{-1}	22 October	20 December	N1 (45+0), N2 (45+64), N3 (45+112), N4 (45+160)	33.6	Modeling
Year II	57,000 plants ha^{-1}	30 October	7 January	N1 (45+0), N2 (45+64), N3 (45+112), N4 (45+160)	33.6	Modeling
Year III	123,000 and 57,000 plants ha^{-1}	3 November	13 January	N0 (0), N1 (45+0), N2 (45+64), N3 (45+112), N4 (45+160)	16.8	Modeling
Year III	87,500 plants ha^{-1}	Farmer practice	Farmer practice	Farmer practice	4.0	Validation

and 47 kg K ha^{-1} using potassium sulfate were applied to all treatments at transplanting as basal fertilizer. In addition, four chemical N rates were employed, designated as N1, N2, N3, and N4 (0, 64, 112, and 160 kg N ha^{-1}, respectively), supplied as urea. The inorganic N fertilizer was applied in two splits: 30% at transplanting and 70% at the beginning of the 5–6 true-leaf stage. A randomized complete block design with three replications was used, and each plot measured 33.6 m^2 (7.0 m × 4.8 m). To test the influence of plant densities, a high density (HD) was employed in Year I, with 123,000 plants ha^{-1}, while in Year II, a low density (LD) with 57,000 plants ha^{-1} was used. In Year III, a split experiment was conducted with two densities of HD and LD, and each plot measured 16.8 m^2 (3.5 m × 4.8 m). And two no-N fertilizer treatments (only 24 kg P ha^{-1} from calcium superphosphate and 47 kg K ha^{-1} using potassium sulfate) under HD and LD, with three replications each, were added to test the effect of soil background nitrogen supply potential.

Seedlings were grown in a small nursery first and then transplanted at the two-leaf stages into the experimental plots. In Year III, 24 plots (4.0 m^2 plot each^{-1}) located adjacent to the experiment site were established as a validation field; a moderate plant density (87,500 plants ha^{-1}) was chosen in the validation field. The N management of the validation field was designed according to local farmer practice, and the plots were arranged randomly. The corrective N-management strategy was tested to determine N fertilizer application at the rosette stage using the experimental data, and the detailed experimental design is shown in **Table 1**.

Data collection

A GreenSeeker^{TM} (Trimble Inc., Sunnyvale, CA, United States) hand-held sensor was used to collect reflectance data using red (671 ± 6 nm) and near-infrared (780 ± 6 nm) radiation. The sensor was positioned horizontally and parallel to the crop row approximately 60 cm above the crop canopy in each plot except the border rows by holding the GreenSeeker and walking at a constant speed, and the average of four measurements of independent rows from each plot was reported. Two vegetation indices (NDVI and RVI) were calculated by the internal software, and the calculations are as follows (Tremblay et al., 2009):

$$NDVI = \frac{\rho_{NIR} - \rho_{Red}}{\rho_{NIR} + \rho_{Red}} \quad (1)$$

$$RVI = \frac{\rho_{NIR}}{\rho_{Red}} \quad (2)$$

Where:

ρ_{NIR} = reflectance at the near-infrared (NIR) region;

ρ_{Red} = reflectance at the red region.

Sensor readings were collected at four growth stages (the 5–6 true-leaf, rosette, cupping, and harvest stage), and the exact sensing dates are presented in **Table 2**. The yield of each plot was determined from the aboveground fresh biomass of the bok choy adjusted to the water content of 90%. As for the validation field, the sensor readings of four stages and harvest yield were collected like those in the experimental plots. Additionally, the average N concentration of harvest bok choy was estimated by randomly sampling plants from 24 validation fields in the research region. Plant samples were oven-dried at 105°C for 30 min, then dried at 70°C to a constant weight, and later ground into fine powder to determine N concentration by a modified Kjeldahl digestion method (Xia et al., 2016).

YP_0, YP_N, RI calculation, and N-fertilizer use efficiency evaluation

To evaluate the potential of using the GreenSeeker sensor to estimate bok choy yield potential without additional N (YP_0), only treatments that received preplant N applications were used for the yield prediction model (including N1 treatment in Years I and II and N0 and N1 treatment in Year III). And YP_0 can be estimated by the empirical exponential relationship between yield and NDVI or RVI measurements of all N treatments collected by the GreenSeeker sensor, $YP_0 = a^* e^{b^* NDVI}$ or $YP_0 = a^* e^{b^* RVI}$ (Teal et al., 2006; Ji et al., 2017). The YP_N was calculated by multiplying the YP and $RI_{Harvest}$ values estimated by RI_{NDVI} (RI_{RVI}) (Raun et al., 2005; Yao et al., 2012). Johnson and Raun (2003) introduced the response index (RI) as a measure of a plant's response to additional N fertilizer. The RI is determined by comparing treatments or farm practice with a reference plot, which was traditionally used as the highest N-rate plot and represents an area where N is not a yield-limiting factor (Johnson and Raun, 2003; Lofton et al., 2012a). In our study, a 205 kg N ha^{-1} (160 kg N ha^{-1} from chemical fertilizer plus 45 kg N ha^{-1} from manure) treatment for bok choy was used as the reference plot. RI_{NDVI} (RI_{RVI}) was calculated by dividing the mean NDVI (RVI) of the reference plots by the average measurement of other N-treated plots, while $RI_{Harvest}$ was calculated by dividing the mean yield of the reference plots by the yield of other N-treated plots.

TABLE 2 Sensing dates of bok choy at the four specific growth stages.

Year	5–6 true-leaf stage	Rosette stage	Cupping stage	Harvest stage
Year I	November 10	November 22	December 2	December 15
Year II	November 15	November 27	December 14	December 28
Year III	November 17	December 2	December 20	January 11

The recovery efficiency (RE) and agronomic efficiency (AE) were computed as follows to assess the N-use efficiency of N-fertilizer input (Ali et al., 2014):

$$\mathrm{RE}(\%) = \frac{\text{total N uptake in N fertilized plot} - \text{total N in no N plot}}{\text{quantity of N fertilizer applied in N fertilized plot}} \times 100\% \quad (3)$$

$$\text{AE kg yield/kg N applied} = \frac{\text{yield in N fertilized plot} - \text{yield in no N plot}}{\text{quantity of N fertilizer applied in N fertilized plot}} \quad (4)$$

Statistical analysis

NDVI, RVI, and yield variation between different N fertilizer treatments and plant densities were subjected to one-way and two-way analyses of variance (ANOVA) and a Duncan multiple-comparison test with SPSS (ver. 20.0 for Windows, SPSS Inc., Chicago, IL, United States). All the regression coefficients in the study were calculated and plotted by Origin 8.5 (OriginLab Corporation, Northampton, MA, United States).

Results

Yield responses to different N rates and plant densities

Bok choy yields showed a significant response to different N rates and densities (Figure 2; Supplementary Table 1). The yields were greatly enhanced by increasing N rates in both years and densities. The yields of bok choy under N2, N3, and N4 treatments were increased by 31.9, 50.6, and 50.4% in Year I and 9.8, 44.4, and 48.4% in Year II. In Year III, yields under N1 to N4 treatments were 8.5–78.4% and 13.8–63.9% higher than the N0 treatment, and 29.8–64.3% and 7.9–40.9% higher than the N1 treatment at high- or low density, respectively. The yields increased as the N rate increased up to N3, but no further significant increase was observed beyond N3, suggesting that 112 kg N ha^{-1} as urea accompanied 45 kg N ha^{-1} from organic fertilizer was the optimum N rate for bok choy. As shown in Figure 2A, the yield difference between Years I and II was rather significant, and the actual yield of bok choy in Year II was 36.3–46.9% lower than that in Year I, suggesting that plant density has a significant influence on the final yields of bok choy at harvest, since the plant population in Year II was less than half of that in Year I. The yield in Year III also confirmed the effect of plant density, and 26.6–40.2% gap was observed (Figure 2B). Also, because of frost damage during the growing period, the yield in Year III was significantly lower than that in Years I and II, but a similar yield response trend was observed. Thus, the yield of bok choy was significantly increased as the N-application rate up to 157 kg N ha^{-1}, and plant densities may have a remarkable influence on yields at harvest.

In-season prediction of YP_0

Current N recommendation strategies are mainly "yield-based," and YP_0 is the possible attainable yield with no additional N (Raun et al., 2002). In practice, accurately estimating YP_0 at the early stage was the first step in determining a site-specific N-management strategy to achieve optimum yields. Compared with three common types of regression equations (Supplementary Table 2), the empirical exponential

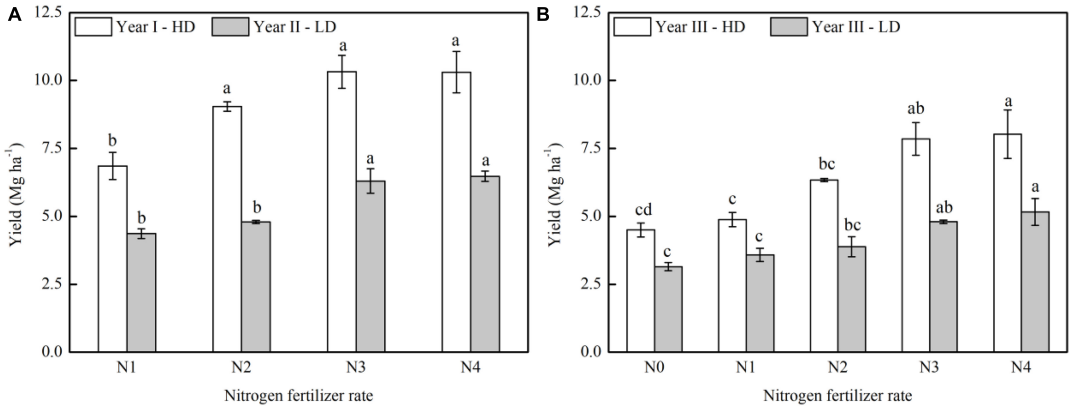

FIGURE 2
Yield responses of bok choy to different chemical N fertilizer rates in Years I, II **(A)**, and Year III **(B)**. Treatments N0, N1, N2, N3, and N4 received 0, 45, 109, 157, and 205 kg·N·ha^{-1} in the growth season, respectively. Different letters indicate significant differences among various N application rates in the specific year at the $P < 0.05$ level.

TABLE 3 Relationships between sensor-based measurements (NDVI and RVI) and yield potential without additional topdressing N application (YP_0) of bok choy at different densities of high density (HD) and low density (LD).

Growth stage	Index	HD			LD		
		Equation	R^2	RMSE[a]	Equation	R^2	RMSE
5–6 True-Leaf	NDVI	$y = 3.05e^{3.92x}$	0.68	0.73	$y = 2.60e^{1.65x}$	0.70	0.35
	RVI	$y = 1.90e^{0.63x}$	0.68	0.74	$y = 1.75e^{0.48x}$	0.72	0.34
Rosette	NDVI	$y = 1.13e^{4.01x}$	0.81	0.57	$y = 1.20e^{3.75x}$	0.79	0.31
	RVI	$y = 1.05e^{0.72x}$	0.84	0.53	$y = 0.76e^{0.86x}$	0.76	0.32
Cupping	NDVI	$y = 1.08e^{3.04x}$	0.16	1.20	$y = 5.91e^{-1.20x}$	0.03	0.64
	RVI	$y = 1.85e^{0.33x}$	0.15	1.20	$y = 6.09e^{-0.22x}$	0.03	0.64
Mature	NDVI	$y = 4.98e^{0.15x}$	0.01	1.30	$y = 0.99e^{2.88x}$	0.20	0.58
	RVI	$y = 4.64e^{0.044x}$	0.01	1.31	$y = 1.16e^{0.43x}$	0.21	0.58
Pooled	NDVI	$y = 11.76\,x - 0.062DAT + 2.72$	0.42	0.96	$y = 8.23x - 0.053DAT + 3.07$	0.36	0.65
	RVI	$y = 1.83x - 0.059DAT + 2.80$	0.40	0.98	$y = 1.43x - 0.044DAT + 2.45$	0.35	0.65

[a]RMSE means the root mean square error; DAT means days after transplanting.

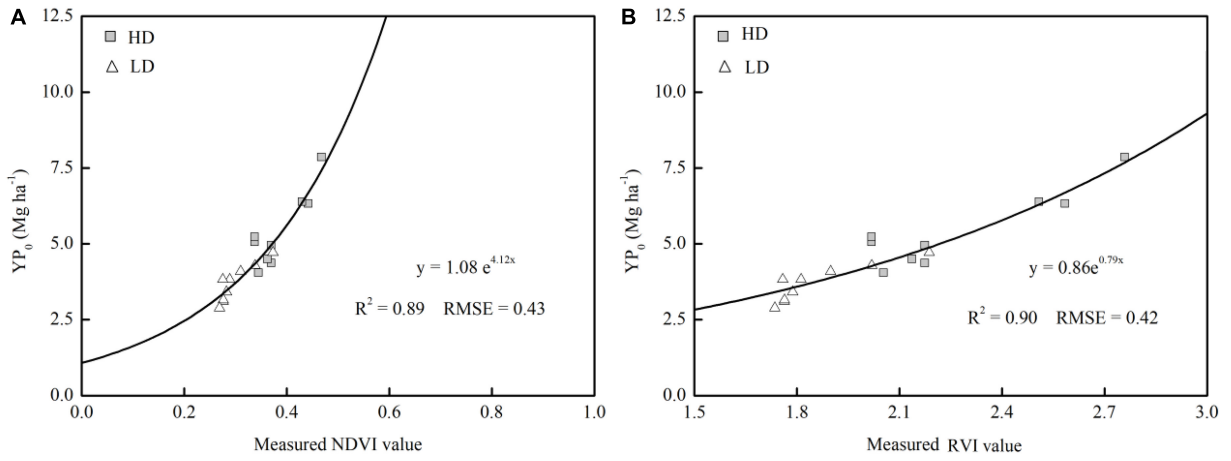

FIGURE 3
Relationship between in-season estimates of yield potential without additional N topdressing (YP_0) at the rosette stage calculated using the normalized difference vegetation index (NDVI) **(A)** and the ratio vegetation index (RVI) **(B)** in Years I, II, and III.

model was used to determine the relationship between YP_0 and the sensor-based vegetation indices (NDVI and RVI) for bok choy across growth stages (Table 3). NDVI and RVI could accurately estimate YP_0, but the relationship was not robust across all stages. At the 5–6 true-leaf stage, a low correlation was noted between sensor measurements and YP_0, and the determination coefficient ranged from 0.68 to 0.72 (Table 3). The highest R^2 was obtained at the rosette stage, and 81–84% of YP_0 of the variability under HD and 76–79% of the variability under LD could be explained by RVI and NDVI. However, at the cupping and harvest stage, a significantly weaker relationship was observed, and 1–21% of the yield variations could be explained (Table 3). In a comparison between the two sensor-based vegetation indices, NDVI and RVI, almost the same accuracy in predicting YP_0 was found at each stage.

Regression analyses (Table 3) suggest that the rosette stage was the most appropriate stage for YP_0 prediction in both years and densities, which coincides with the optimum time for topdressing N to bok choy during production. However, for practical application purposes, it would be more convenient to build a general model to predict the yield potential of vegetables with different plant densities. The fitting curves of pooled sensor readings (NDVI and RVI) and YP_0 with different densities among years at the rosette stage are presented in Figure 3. By combining all years-densities data, the sensor-based yield prediction model could explain 89–90% of the YP_0 variation. Between the two indices, RVI performed similarly to NDVI. Additionally, the plant density showed a significant effect on YP_0, and the YP_0 under HD treatments were much higher than that of LD; thus, the data points for HD treatment are located on the upper section of the line, while LD treatment data are

positioned on the lower portion of the fitting curves; however, the trend was similar for both densities (Figure 3).

In-season prediction of N response index

Aside from the accurate prediction of YP_0, the degree to which a crop responded to additional N fertilizer was also a key component in determining the appropriate N-management strategy. Table 4 shows the relationships between $RI_{Harvest}$ and RI_{NDVI} (or RI_{RVI}), which were computed from the NDVI (or RVI) readings collected at each stage. RI_{NDVI} and RI_{RVI} were significantly correlated with $RI_{Harvest}$, but the parameters were different among the stages. The sensor-based RIs can accurately predict $RI_{Harvest}$ after the 5–6 true-leaf stage, and the rosette stage was the earliest stage for which $RI_{Harvest}$ estimation was conducted, with R^2 values of 0.59–0.67 under HD treatment and 0.53–0.65 under LD treatment. After the rosette stage, a weaker relationship was observed for both RI_{NDVI} and RI_{RVI}; furthermore, those later stages were too late for topdressing N. Therefore, the rosette stage was the most appropriate stage for conducting the $RI_{Harvest}$ prediction, which was consistent with the growth stage for YP_0 prediction. After using a combined equation to explain the variation across years and densities at this stage, a weaker, but still significant, relationship was observed relative to that of individual densities. The accuracy of the RVI-based model and the RMSE value was 6.12% higher and 8.70% lower, respectively, than that seen with the NDVI-based model (Figure 4), with RVI explaining 52% of $RI_{Harvest}$ variability. This result confirms the superiority of the RVI-based model in explaining $RI_{Harvest}$ variability.

Model validation

The exponential and linear equations developed from the RVI measurements at the rosette stage were used to

TABLE 4 Relationship between RI_{NDVI} and RI_{RVI} with $RI_{Harvest}$ (y in the equations) of bok choy across years at different densities of high density (HD) and low density (LD).

Growth stage	Index	HD			LD		
		Equation	R^2	RMSE	Equation	R^2	RMSE
5–6 True-Leaf	RI_{NDVI}	$y = 1.73x-0.45$	0.31	0.27	$y = 1.13x+0.10$	0.26	0.23
	RI_{RVI}	$y = 1.88x-0.59$	0.17	0.30	$y = 1.58x-0.35$	0.16	0.24
Rosette	RI_{NDVI}	$y = 3.57x-2.44$	0.67	0.19	$y = 1.79x-0.73$	0.65	0.16
	RI_{RVI}	$y = 3.18x-2.05$	0.59	0.21	$y = 1.87x-0.76$	0.53	0.18
Cupping	RI_{NDVI}	$y = 3.11x-1.95$	0.60	0.21	$y = 1.65x-0.59$	0.57	0.17
	RI_{RVI}	$y = 1.80x-0.64$	0.62	0.20	$y = 1.47x-0.40$	0.58	0.17
Mature	RI_{NDVI}	$y = 3.20x-1.95$	0.44	0.24	$y = 2.01x-0.87$	0.52	0.18
	RI_{RVI}	$y = 0.51x-0.62$	0.59	0.21	$y = 1.44x-0.29$	0.49	0.19
Pooled	RI_{NDVI}	$y = 2.71x+0.0019DAT-1.66$	0.31	0.21	$y = 1.34x-0.0015DAT-0.19$	0.41	0.18
	RI_{RVI}	$y = -0.57x+0.0067DAT+1.68$	0.20	0.27	$y = -1.34x+0.0017DAT+2.60$	0.41	0.18

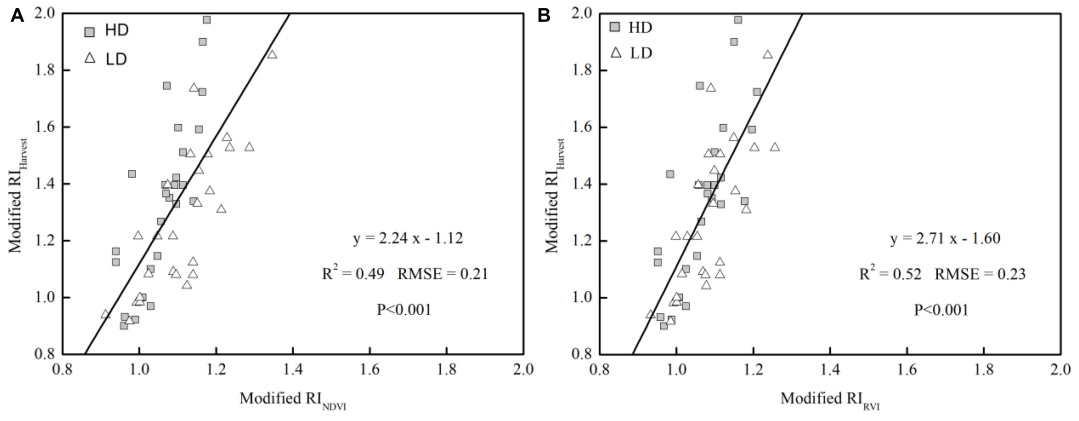

FIGURE 4
Relationships between the response index calculated with yield ($RI_{Harvest}$) and the response index calculated with NDVI (RI_{NDVI}) **(A)** and RVI (RI_{RVI}) **(B)** at the rosette stage of bok choy growth in Years I, II, and III.

predict YP_0 ($YP_0 = 0.86e^{0.79 \times RVI}$, $R^2 = 0.90$) and $RI_{Harvest}$ ($RI = 2.71 \times RI_{RVI}$-1.60, $R^2 = 0.52$) at either the high or low plant density of bok choy. To validate the reliability of the YP_0 and $RI_{Harvest}$ prediction model for different densities, we tested the model using an independent data set obtained from the validation field with a moderate plant density (87,500 plants ha^{-1}) in Year III. According to the results of the YP_0 and RI prediction models, the rosette stage was the most suitable growth stage, so RVI measurements obtained at that stage were used for validation to determine the relationship between the predicted YP_0 and $RI_{Harvest}$ and the actual values. As shown in Figure 5, the observed YP_0 was highly correlated with the predicted YP_0 ($R^2 = 0.60$) in almost a 1:1 relationship, with a slope of 0.89. For $RI_{Harvest}$, the predicted value was slightly higher than the observed results, but a good relationship ($R^2 = 0.84$) was observed, with a slope of 1.12. In general, the data points of the two validation equations were all scattered evenly around the 1:1 line. This confirms the potential of applying the in-season YP_0 and $RI_{Harvest}$ prediction model to various plant populations.

Strategy for in-season site-specific N management for bok choy

In practice, the potential yield with added N fertilization (YP_N) can be estimated by multiplying YP_0 and RI; the N requirement is then determined by multiplying the yield

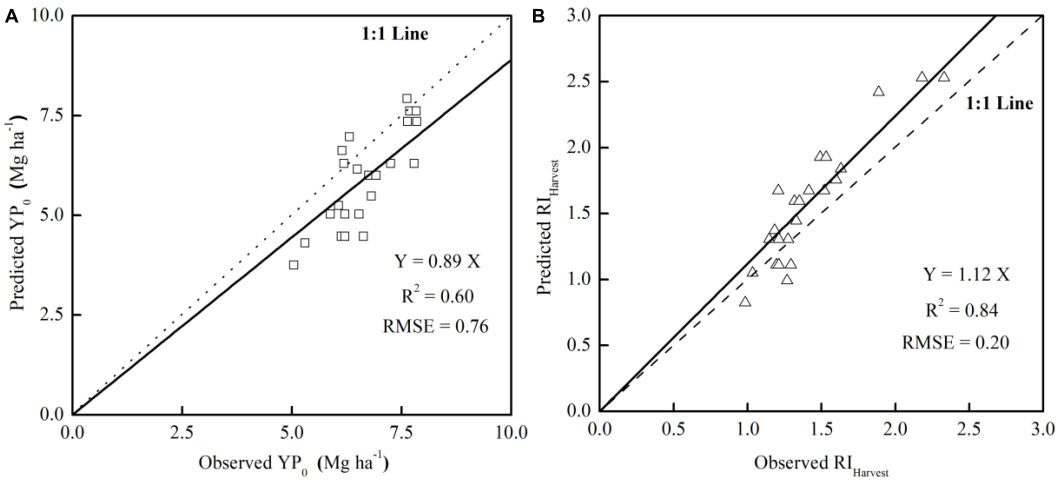

FIGURE 5
Relationship between the observed and predicted YP_0 **(A)** and $RI_{Harvest}$ **(B)** in the validation field.

TABLE 5 Estimation of sensor-based topdressing N amounts at different densities using the experimental data for bok choy.

Plot	Fertilizer N application (kg N ha^{-1})			YP_0 (Mg ha^{-1})	Yield/YP_N (Mg ha^{-1})	RE (%)	AE (yield/kg N)	Reduced nitrogen fertilizer (kg N ha^{-1})
	Fixed N rate [a]	Recommended N rate [b]	Total					
H[c]-Plot 1	109	58.77	167.77	8.33	10.74	19.49	23.18	37.23
H-Plot 2	109	54.41	163.41	8.74	11.10	20.84	25.54	41.59
H-Plot 3	109	56.99	165.99	7.86	10.19	17.88	20.12	39.01
H-Plot 4	109	48.88	157.88	5.42	7.33	9.85	17.90	47.12
H-Plot 5	109	43.41	152.41	5.48	7.17	9.64	17.54	52.59
H-Plot 6	109	47.45	156.45	5.31	7.15	9.33	16.97	48.55
L[d]-Plot 7	109	37.97	146.98	4.83	6.38	12.45	13.74	58.02
L-Plot 8	109	37.87	146.88	5.19	6.74	13.81	16.20	58.12
L-Plot 9	109	36.08	145.08	5.19	6.67	13.71	15.92	59.92
L-Plot 10	109	31.73	140.73	3.88	5.12	7.69	13.99	64.27
L-Plot 11	109	34.44	143.44	4.00	5.34	8.40	15.27	61.56
L-Plot 12	109	29.07	138.07	3.76	4.89	6.93	12.60	66.93

[a]Fixed N rate suggested the N application rate of 45 kg N ha^{-1} organic fertilizer and 19 kg N ha^{-1} chemical N fertilizer at transplanting as base fertilizer plus 45 kg N ha^{-1} chemical N fertilizer at 5–6 true-leaf stage according to the nutrient requirement pattern. [b]Recommended N rate suggested the topdressing N application rate calculated at the rosette stage by the site-specific N-topdressing algorithm. [c]H, high-density plot; [d]L, low-density plot. RE and AE stand for N recovery efficiency and agronomic efficiency.

response by plant N concentration and average NUE (Raun et al., 2005). In our study, the RVI is superior to the NDVI measurement for predicting YP_0 and $RI_{Harvest}$.

Thus, the site-specific N-topdressing algorithm for bok choy is expressed as follows (Raun et al., 2005; Yao et al., 2012):

$$N_{rate} = \frac{[(YP_0 \times RI) - YP_0] \times N\%}{NUE} \quad (5)$$

where $YP_0 = 0.86e^{0.79 \times RVI}$ and $RI = 2.71 \times RI_{RVI}$-1.60.

The NUE used in the formula is defined as the NUE of the additional N input. However, there is no consensus yet on determining the vegetables' NUE, as it depends on various soil and environmental factors, fertilizer management, and treatments applied (Barker and Sawyer, 2010; Li et al., 2017). In our study, the average NUE in the research region of vegetable crops topdressing N fertilizer was approximately 15%; thus, the NUE in the formula was initially set at 15% for bok choy. Additionally, the N% expressed in the model was the average N content of bok choy at harvest; according to our investigation, the harvested N concentration of bok choy in the Taihu Lake region was approximately 5.5% (**Supplementary Table 3**). Based on the above discussion, the NFOA for bok choy can be established.

Evaluation of the sensor-based N topdressing algorithm of bok choy

Practically, a field optimum N rate is typically recommended for the whole region and then adjusted to the specific rate for a certain field based on the spatial variation (Zhu, 2006; Yao et al., 2012). Therefore, a practical precision-driven N topdressing algorithm for bok choy was proposed for the Taihu Lake region, using 45 kg N ha^{-1} from manure as basal N fertilizer plus a 112 kg N ha^{-1} chemical N fertilizer split-applied at the transplanting and 5–6 true-leaf stage, at 30 and 40% proportion according to the nutrient requirement pattern followed by determination of the need for additional topdressing N at the rosette stage using the RVI-based NFOA (Zanão Júnior et al., 2005).

To address whether the sensor-based topdressing N-management strategy could reduce N fertilizer application without sacrificing yields, we examined the proposed N-management strategy using the plots with approximately equal N application rates in Years I, II, and III at high or low density. The data in **Table 5** show the outcomes of normal farm practice and the sensor-based N-topdressing strategy. A similar yield was obtained under the traditional farm fertilizer practice and the sensor-based topdressing strategy, at both high and low density (**Table 5**). According to our calculation, the amount of N recommended ranged from 43.41 to 58.77 kg N ha^{-1} under the high-density treatment and from 29.07 to 37.97 kg N ha^{-1} under the low-density treatment. The recommended rate was significantly lower than that employed as part of the normal farm practice, especially for the low-density treatment. When appropriately prescriptive N fertilizer amounts were applied and a sensor-based corrective N strategy was conducted, average increases of 14.91 and 31.17% of RE and 3.60 and 4.58 kg yield/kg N of AE by fertilizer N over normal farm practice were observed at high and low densities, respectively. Therefore, a reduction of 18.16–32.65% N can be achieved by using the sensor-based approach compared to N-management practice in conventional farming. Additionally, when compared with the optimum N rate at 157 kg N ha^{-1}, the amount of the sensor-based NFOA was almost equal to, or slightly less than, the optimum N rate, and the fertilizer rate gap between the NFOA-calculated fertilizer rate and the optimum N rate reflecting the soil fertility variation among plots.

Discussion

Sensor-based approaches used for assessing the crop N management of vegetable crops

Optical sensors have been a promising alternative approach for non-destructive crop monitoring (Ali et al., 2020). However, few studies have paid attention to the sensor-based N fertilizer management in vegetable production systems. This phenomenon was partly owing to the complicated canopy architecture of vegetable crops which would complicate the work of the sensor (Padilla et al., 2018). The RVI determined by the GreenSeeker sensor had a significant relationship with YP_0 (R^2 = 0.90) and $RI_{Harvest}$ (R^2 = 0.52) (**Figures 3**, **4**), the RVI performed better than the NDVI on account of its higher sensitivity *vis-a-vis* the former during the early vegetation and maturity stages, especially at high plant densities (Li et al., 2013). Given the different fitting results of the YP_0 and $RI_{Harvest}$ prediction model in Years I, II, and III, it may be influenced by the climate differences between years to some degree (**Figure 1**), and this need to have more validation (Raun et al., 2005; Ji et al., 2017). When considering the variation in yield between years, which may be due to the impact of vegetable stubble changes, pests and diseases pests during a particular year, and adverse weather, it did not influence the use of optical sensors (Liu et al., 2008; Li et al., 2017). Moreover, the YP_0 and $RI_{Harvest}$ prediction model would not be affected even if the relatively yield fluctuates (**Figures 3**, **4**). To sum up, compared with the results for rice and sugarcane, the findings of our study were as good as, or better than, the predictions for other crops (Lofton et al., 2012b; Yao et al., 2012); therefore, the YP_0 and RI index of bok choy could be reliably assessed by using the GreenSeeker sensor.

A sensor-based site-specific N topdressing strategy of bok choy

Determining the correct amount of topdressing N is a critical step toward enhancing NUE and ensuring the

productivity and quality of vegetable crops (Zhou et al., 2017). However, the complicated canopy architecture and the relatively short growth cycle of bok choy and other vegetables relative to that of grain crops (e.g., corn and rice) has caused difficulty in determining the proper timing and amounts of topdressing N for vegetables (Lukina et al., 2001; Barker and Sawyer, 2010; Lofton et al., 2012b; Ali et al., 2014; Xia et al., 2016). In addition, the coexistence model of chemical N fertilizer and organic fertilizer in the vegetable production system and the uncertainty of the N mineralization capacity of organic fertilizer significantly increases the difficulty of determining the amount of topdressing N (Chen et al., 2006; Ren et al., 2014). As found, the total yield of N4 in Years I, II, and III was slightly lower or equal to that of N3 treatment, and no significant difference was observed, therefore the N4 rate was selected as the non-N limiting treatment. And an average organic fertilizer application rate used by local farmers (about 45 kg N ha^{-1}) from manure was applied as the basal fertilizer to all treatments as part of the total N input, and, thus, the amount of topdressing N could be quantitatively assessed and the sensor-based NFOA was used in our study to establish the amount of topdressing N fertilizer at the rosette stage of bok choy Eq. 5, and the recommended N-fertilizer strategy was thus proposed for the Taihu Lake region (Zanão Júnior et al., 2005; Zhu, 2006; Yao et al., 2012). According to preliminary estimation, the sensor-based topdressing strategy could reduce the total N input by 18.16–32.65% without sacrificing yields and could improve RE by 14.91–31.17% and AE by 16.10–30.82% over traditional farming practices (**Table 5**), which is consistent with findings for rice, where site-specific sensor-based N management increased the partial factor productivity of farmers by 48% without significantly affecting grain yield (Li et al., 2009).

Effect of plant density on yield and the sensor-based prediction model

Plant density is one of the most important agro nomic management practices that influence crop yields (Lama et al., 2018; Adams et al., 2019). The yield of high-density plots (123,000 plants ha^{-1}) was 26.6–46.9% higher than that of low-density plots (57,000 plants ha^{-1}) under each N-application rate (**Figure 2**). This result is consistent with the finding for willow, where a plant density of 20,000 plants ha^{-1} resulted in a higher yield than a density of 15,000 plants ha^{-1} (Wilkinson et al., 2007). Plant density can also influence vegetation coverage and measured vegetation indices and, thus, affects sensor-based N predictions (Yao et al., 2015). In addition, as the plant population or density increases, vegetation coverage also increases, and the by-plot coefficient of variation decreases (**Supplementary Table 4**; Arnall et al., 2006), thus the effect of plant density on the YP_0 and $RI_{Harvest}$ predictions was assessed. The combined year-density fitting curves showed a more precise prediction of YP_0 than the individual ones, with the R^2 value increasing by 5.62–15.56% (**Table 3** and **Figure 3**), suggesting that plant density would affect sensor readings, and higher plant densities resulted in higher sensor values; however, plant density had no effect on YP_0 predictions. The validation result of the YP_0 and $RI_{Harvest}$ predictions, at a moderate plant density (87,500 plants ha^{-1}), confirmed the possibility of applying the estimation model to various densities (**Figure 5**), which is consistent with previous research on rice (Xue et al., 2014).

Optimum timing for making accurate YP_0 and $RI_{Harvest}$ predictions

The growth stage is an important factor in predicting YP_0 and $RI_{Harvest}$ by canopy sensors (Yao et al., 2012; Bijay-Singh et al., 2015). The NDVI and RVI had a significant relationship with YP_0, but the relationship was not stable across different stages (**Table 3**), which was similar to that for rice, where NDVI and RVI could explain at most 50% of the aboveground biomass variability due to interference from soil and water background in the early growth stages (Gnyp et al., 2014). The totally poor accuracy of the YP_0 prediction model observed under low density relative to that observed at high density was partly due to the relatively lower plant density and stronger soil background interference in the growth stages (**Table 3**; Cao et al., 2015). At the rosette stage, the accuracy of the YP_0 prediction increased for both years and densities, and the R^2 was significantly higher than that in other growth stages. However, at later stages, the relationship seemed weak, as the plant canopy began to close and the sensor became saturated at this stage and could not make satisfactory predictions (Ali et al., 2014; Ji et al., 2017). Thus, the rosette stage was the most appropriate stage for YP_0 estimation.

Similarly, the $RI_{Harvest}$ prediction was variable across stages (**Table 4**). For both the NDVI- and RVI-based $RI_{Harvest}$ prediction models, accuracy was relatively low at the 5–6 true-leaf stage for the possible effect of input N had not yet manifested. At later growth stages, the R^2 of the $RI_{Harvest}$ prediction model increased by over 90.32–150.00% that of the 5–6 true-leaf stage in experimental years. However, sensor measurements at the harvest stage were not conducted, since it is not desirable to apply N at this stage of growth (Xue et al., 2014). That is consistent with the results of Lofton et al. (2012b) for sugarcane, where a short interval after fertilization was not suitable for estimating the $RI_{Harvest}$ of cane tonnage and sugar yield, but the RI_{NDVI} at 4 and 5 weeks after fertilization could capture changes in $RI_{Harvest}$ (Lofton et al., 2012b). Therefore, the rosette stage represented the optimum stage for conducting $RI_{Harvest}$ prediction, and this period was also ideal for topdressing N if needed.

Conclusion

The development of a sensor-based N-management strategy can provide an effective tool for site-specific topdressing recommendations. It was hypothesized that the GreenSeeker sensor could be used for *in situ* N fertilizer management and topdressing recommendation of bok choy. Through the three-year field experiment, it was confirmed that the active canopy sensor could be used to reliably estimate the YP_0 and $RI_{Harvest}$ of bok choy at the rosette stage, and the RVI functioned better than the NDVI. In addition, the across-years/densities models and the validation results confirmed the potential of the sensor-based model to be applied to different plant densities. A practical and environmentally friendly N management strategy for bok choy in the Taihu Lake region is proposed, and it consists of using 45 kg N ha^{-1} from manure as basal N fertilizer and a 112 kg N ha^{-1} split-applied at the transplanting and 5–6 true-leaf stage, at 30 and 40% of the total. The remaining N should be based on the optical sensor prediction at the rosette stage. According to our estimation, a reduction of 1/5–1/3 N can be achieved by using the sensor-based approach. This strategy can improve the NUE of bok choy, is more suitable for practical applications, and has the potential to contribute to the sustainable development of vegetable crops. The current experiment represents an important field validation for the development and implementation of vegetable N-management strategies but was conducted with a limited site-year design, and NFOA parameters warrant optimization and testing with more data in future work. Further work is needed to validate the fertilizer reduction potential in on-farm applications and to explore its applicability with more site-year data.

Data availability statement

The raw data supporting the conclusions of this article will be made available by the authors, without undue reservation.

Author contributions

WS and JM conceived and designed the experiments. RJ performed the experiments and wrote the manuscript. JM and YW analyzed the data. JM contributed to the reagents, materials, and analysis tools. HZ revised the manuscript. All authors contributed to the article and approved the submitted version.

Funding

This work was supported by the National Natural Science Foundation of China (31872185) and the Enterprise Cooperation Projects (Am20210407RD).

Conflict of interest

The authors declare that the research was conducted in the absence of any commercial or financial relationships that could be construed as a potential conflict of interest.

Publisher's note

All claims expressed in this article are solely those of the authors and do not necessarily represent those of their affiliated organizations, or those of the publisher, the editors and the reviewers. Any product that may be evaluated in this article, or claim that may be made by its manufacturer, is not guaranteed or endorsed by the publisher.

Supplementary material

The Supplementary Material for this article can be found online at: https://www.frontiersin.org/articles/10.3389/fpls.2022.951181/full#supplementary-material

References

Adams, C., Thapa, S., and Kimura, E. (2019). Determination of a plant population density threshold for optimizing cotton lint yield: a synthesis. *Field Crop. Res.* 230, 11–16. doi: 10.1016/j.fcr.2018.10.005

Ali, A. M., Ibrahim, S. M., and Singh, B. (2020). Wheat grain yield and nitrogen uptake prediction using at Leaf and GreenSeeker portable optical sensors at jointing growth stage. *Inform. Process. Agriculture* 7, 375–383. doi: 10.1016/j.inpa.2019.09.008

Ali, A. M., Thind, H. S., Varinderpal, S., and Bijay, S. (2014). A framework for refining nitrogen management in dry direct-seeded rice using Greenseeker^{TM} optical sensor. *Comput. Electron. Agr.* 110, 114–120. doi: 10.1016/j.compag.2014.10.021

Arnall, D. B., Raun, W. R., Solie, J. B., Stone, M. L., Johnson, G. V., Girma, K., et al. (2006). Relationship between coefficient of variation measured by spectral reflectance and plant density at early growth stages in winter wheat. *J. Plant Nurt.* 29, 1983–1997. doi: 10.1080/01904160600927997

Barker, D. W., and Sawyer, J. E. (2010). Using active canopy sensors to quantify corn nitrogen stress and nitrogen application rate. *Agron J.* 102, 964–971. doi: 10.2134/agronj2010.0004

Bijay-Singh, B., Varinderpal-Singh, V., Jaspreet Purba, J., Purba, R. K., Sharma, R. K., Sharma, M. L., et al. (2015). Site-specific fertilizer nitrogen management in irrigated transplanted rice (*Oryza sativa*) using an optical sensor. *Precision Agric.* 16, 455–475. doi: 10.1007/s11119-015-9389-6

Burns, I. G. (2006). Assessing N fertiliser requirements and the reliability of different recommendation systems. *Acta Hort.* 700, 35–48. doi: 10.17660/ActaHortic.2006.700.2

Cao, Q., Miao, Y. X., Feng, G. H., Gao, X. W., Li, F., Liu, B., et al. (2015). Active canopy sensing of winter wheat nitrogen status: an evaluation of two sensor systems. *Comput. Electron. Agr.* 112, 54–67. doi: 10.1016/j.compag.2014.08.012

Chen, Q., Zhang, H. Y., Zhang, X. S., Li, X. L., and Liebig, H. P. (2006). Field application of N-expert system on N recommendation of autumn spinach (in Chinese with English abstract). *Acta Agriculturae Boreali-Sinica* 04, 128–134. doi: 10.1007/s11769-002-0038-4

Dobermann, A., Witt, C., Abdulrachman, S., Gines, H. C., Nagarajan, R., Son, T. T., et al. (2003). Soil fertility and indigenous nutrient supply in irrigated rice domains of Asia. *Agron. J.* 95, 913–923. doi: 10.2134/agronj2003.0913

Dunn, B., Shrestha, A., and Goad, C. (2015). Use of nondestructive sensors to quantify ornamental kale nitrogen status. *J. Plant Nurt.* 39, 1123–1130. doi: 10.1080/01904167.2015.1069342

Gianquinto, G., Orsini, F., Sambo, P., and D'Urzo, M. P. (2011). The use of diagnostic optical tools to assess nitrogen status and to guide fertilization of vegetables. *HortTechnology* 21, 287–292. doi: 10.1016/j.scienta.2011.03.038

Gnyp, M. L., Miao, Y. X., Yuan, F., Ustin, S. L., Yu, K., Yao, Y. K., et al. (2014). Hyperspectral canopy sensing of paddy rice aboveground biomass at different growth stages. *Field Crop Res.* 155, 42–55. doi: 10.1016/j.fcr.2013.09.023

Gong, Z. T. (1999). *Chinese Soil Taxonomy: Theory Approaches and Application*. Beijing: China Science Press, 160–165.

Heimler, D., Vignolini, P., Dini, M. G., Vincieri, F. F., and Romani, A. (2006). Antiradical activity and polyphenol composition of local brassicaceae edible varieties. *Food Chem.* 99, 464–469. doi: 10.1016/j.foodchem.2005.07.057

Ji, R. T., Min, J., Wang, Y., Cheng, H., Zhang, H. L., and Shi, W. M. (2017). In-season yield prediction of cabbage with a hand-held active canopy sensor. *Sensors* 17:2287. doi: 10.3390/s17102287

Jin, J. Y., and Jiang, C. (2002). Spatial variability of soil nutrients and sitespecific nutrient management in the P.R. China. *Comput. Electron. Agr.* 36, 165–172. doi: 10.1016/S0168-1699(02)00099-6

Johnson, G. V., and Raun, W. R. (2003). Nitrogen response index as a guide to fertilizer management. *J. Plant Nurt.* 26, 249–262. doi: 10.1081/PLN-120017134

Jones, C. L., Weckler, P. R., Maness, N. O., Jayasekara, R., Stone, M. L., and Chrz, D. (2007). Remote sensing to estimate chlorophyll concentration in spinach using multi-spectral plant reflectance. *Tasabe* 50, 2267–2273. doi: 10.13031/2013.24079

Lama, A. D., Klemola, T., Saloniemi, I., Niemela, P., and Vuorisalo, T. (2018). Factors affecting genetic and seed yield variability of *Jatropha curcas* (L.) across the globe: a review. *Energy Sustain Dev.* 42, 170–182. doi: 10.1016/j.esd.2017.09.002

Li, B., Bi, Z. C., and Xiong, Z. Q. (2017). Dynamic responses of nitrous oxide emission and nitrogen use efficiency to nitrogen and biochar amendment in an intensified vegetable field in southeastern China. *GCB Bioenergy* 9, 400–413. doi: 10.1111/gcbb.12356

Li, F., Jiang, X., Wang, X. F., Zhang, X. Q., Zheng, J. J., and Zhao, Q. J. (2013). Estimating grassland aboveground biomass using multitemporal MODIS data in the West Songnen Plain, China. *J. Appl. Remote Sens.* 7:073546. doi: 10.1117/1.JRS.7.073546

Li, F., Miao, Y., Zhang, F., Cui, Z., Li, R., Chen, X., et al. (2009). In-season optical sensing improves nitrogen-use efficiency for winter wheat. *Soil Sci. Soc. Am. J.* 73, 1566–1574. doi: 10.2136/sssaj2008.0150

Liu, Z. H., Jiang, L. H., Li, X. L., Hardter, R., Zhang, W. J., Zhang, Y. L., et al. (2008). Effect of N and K fertilizers on yield and quality of greenhouse vegetable crops. *Pedosphere* 18, 496–502. doi: 10.1016/S1002-0160(08)60040-5

Lofton, J., Tubana, B. S., Kanke, Y., Teboh, J., and Viator, H. (2012a). Predicting sugarcane response to nitrogen using a canopy reflectance-based response index. *Agron J.* 104, 106–113. doi: 10.2134/agronj2011.0254

Lofton, J., Tubana, B. S., Kanke, Y., Teboh, J., Viator, H., and Dalen, M. (2012b). Estimating sugarcane yield potential using an in-season determination of normalized difference vegetative index. *Sensors* 12, 7529–7547. doi: 10.3390/s120607529

Lowder, S. K., Skoet, J., and Raney, T. (2016). The number, size, and distribution of farms, smallholder farms, and family farms worldwide. *World Dev.* 87, 16–29. doi: 10.1016/j.worlddev.2015.10.041

Lukina, E. V., Freeman, K. W., Wynn, K. J., Thomason, W. E., Mullen, R. W., Stone, M. L., et al. (2001). Nitrogen fertilization optimization algorithm based on in-season estimates of yield and plant nitrogen uptake. *J. Plant Nurt.* 24, 885–898. doi: 10.1081/pln-100103780

Ma, B. L., Subedi, K. D., and Zhang, T. Q. (2007). Pre-sidedress nitrate test and other crop-based indicators for fresh market and processing sweet corn. *Agron J.* 99, 174–183. doi: 10.2134/agronj2006.0028

Olfs, H. W., Blankenau, K., Brentrup, F., Jasper, J., Link, A., and Lammel, J. (2005). Soil- and plant-based nitrogen-fertilizer recommendations in arable farming. *J. Plant Nutr. Soil Sc.* 168, 414–431. doi: 10.1002/jpln.200520526

Padilla, F. M., Gallardo, M., Pena-Fleitas, M. T., de Souza, R., and Thompson, R. B. (2018). Proximal optical sensors for nitrogen management of vegetable crops: a review. *Sensors* 18:2083. doi: 10.3390/s18072083

Raun, W. R., Solie, J. B., Johnson, G. V., Stone, M. L., Mullen, R. W., Freeman, K. W., et al. (2002). Improving nitrogen use efficiency in cereal grain production with optical sensing and variable rate application. *Agron J.* 94, 815–820. doi: 10.2134/agronj2002.0815

Raun, W. R., Solie, J. B., Stone, M. L., Martin, K. L., Freeman, K. W., Mullen, R. W., et al. (2005). Optical sensor-based algorithm for crop nitrogen fertilization. *Commun. Soil Sci. Plant.* 36, 2759–2781. doi: 10.1080/00103620500303988

Ren, T., Wang, J. G., Chen, Q., Zhang, F. S., and Lu, S. C. (2014). The effects of manure and nitrogen fertilizer applications on soil organic carbon and nitrogen in a high-input cropping system. *PLoS One* 9:e97732. doi: 10.1371/journal.pone.0097732

Samborski, S. M., Tremblay, N., and Fallon, E. (2009). Strategies to make use of plant sensors-based diagnostic information for nitrogen recommendations. *Agron J.* 101, 800–816. doi: 10.2134/agronj2008.0162Rx

Schmidt, J. P., Dellinger, A. E., and Beegle, D. B. (2009). Nitrogen recommendations for corn: an on-the-go sensor compared with current recommendation methods. *Agron J.* 101, 916–924. doi: 10.2134/agronj2008.0231x

Shi, W. M., Yao, J., and Yan, F. (2009). Vegetable cultivation under greenhouse conditions leads to rapid accumulation of nutrients, acidification and salinity of soils and groundwater contamination in south-eastern China. *Nut. Cycl. Agroecosys* 83, 73–84. doi: 10.1007/s10705-008-9201-3

Song, X. Z., Zhao, C. X., Wang, X. L., and Li, J. (2009). Study of nitrate leaching and nitrogen fate under intensive vegetable production pattern in northern China. *C. R. Biol.* 332, 385–392. doi: 10.1016/j.crvi.2008.11.005

Tan, M. L., Robinson, G. M., Li, X. B., and Xin, L. J. (2013). Spatial and temporal variability of farm size in China in context of rapid urbanization. *Chinese Geogr. Sci.* 23, 607–619. doi: 10.1007/s11769-013-0610-0

Teal, R. K., Tubana, B., Girma, K., Freeman, K. W., Arnall, D. B., Walsh, O., et al. (2006). In-season prediction of corn grain yield potential using normalized difference vegetation index. *Agron J.* 98, 1488–1494. doi: 10.2134/agronj2006.0103

Tremblay, N., Wang, Z. J., and Cerovic, Z. G. (2011). Sensing crop nitrogen status with fluorescence indicators. a review. *Agron Sustain Dev.* 32, 451–464. doi: 10.1007/s13593-011-0041-1

Tremblay, N., Wang, Z. J., Ma, B. L., Belec, C., and Vigneault, P. (2009). A comparison of crop data measured by two commercial sensors for variable-rate nitrogen application. *Precis Agric.* 10, 145–161. doi: 10.1007/s11119-008-9080-2

Wilkinson, J. M., Evans, E. J., Bilsborrow, P. E., Wright, C., Hewison, W. O., and Pilbeam, D. J. (2007). Yield of willow cultivars at different planting densities in a commercial short rotation coppice in the north of England. *Biomass Bioenerg.* 31, 469–474. doi: 10.1016/j.biombioe.2007.01.020

Xia, T. T., Miao, Y. X., Wu, D. L., Shao, H., Khosla, R., and Mi, G. H. (2016). Active optical sensing of spring maize for in-season diagnosis of nitrogen status based on nitrogen nutrition index. *Remote Sens.* 8:605. doi: 10.3390/rs8070605

Xue, L. H., Li, G. H., Qin, X., Yang, L. Z., and Zhang, H. L. (2014). Topdressing nitrogen recommendation for early rice with an active sensor in south China. *Precis Agric.* 15, 95–110. doi: 10.1007/s11119-013-9326-5

Yao, H. S., Zhang, Y. L., Yi, X. P., Hu, Y. Y., Luo, H. H., Gou, L., et al. (2015). Plant density alters nitrogen partitioning among photosynthetic components, leaf photosynthetic capacity and photosynthetic nitrogen use efficiency in field-grown cotton. *Field Crop. Res.* 184, 39–49. doi: 10.1016/j.fcr.2015.09.005

Yao, Y. K., Miao, Y. X., Huang, S. Y., Gao, L., Ma, X. B., Zhao, G. M., et al. (2012). Active canopy sensor-based precision N management strategy for rice. *Agron Sustain Dev.* 32, 925–933. doi: 10.1007/s13593-012-0094-9

Zanão Júnior, L. A., Lana, R. M. Q., and Sá, K. A. (2005). Split forms and sources of nitrogen fertilization for the flowering white cabbage production. *Hortic Bras.* 23, 965–969.

Zhang, M., Chen, Z. Z., Li, Q. L., Fan, C. H., and Xiong, Z. Q. (2016). Quantitative relationship between nitrous oxide emissions and nitrogen application rate for a typical intensive vegetable cropping system in southeastern China. *CLEAN-Soil Air Water* 44, 1725–1732. doi: 10.1002/clen.201400266

Zhang, Y. J., Chen, G. P., Dong, T. T., Pan, Y., Zhao, Z. P., Tian, S. B., et al. (2014). Anthocyanin accumulation and transcriptional regulation of anthocyanin biosynthesis in purple bok choy (*Brassica rapa* var. chinensis). *J. Agric Food Chem.* 62, 12366–12376. doi: 10.1021/jf503453e

Zhou, Z. J., Plauborg, F., Thomsen, A. G., and Andersen, M. N. (2017). A RVI/LAI-reference curve to detect N stress and guide N fertigation using combined information from spectral reflectance and leaf area measurements in potato. *Eur. J. Agron.* 87, 1–7. doi: 10.1016/j.eja.2017.04.002

Zhu, J. H., Li, X. L., Christie, P., and Li, J. L. (2005). Environmental implications of low nitrogen use efficiency in excessively fertilized hot pepper (*Capsicum frutescens* L.) cropping systems. *Agr. Ecosyst. Environ.* 111, 70–80. doi: 10.1016/j.agee.2005.04.025

Zhu, Z. L. (2006). On the methodology of recommendation for application rate of chemical fertilizer nitrogen to crops (in Chinese with English abstract). *Plant Nutr. Fert. Sci.* 12, 1–4. doi: 10.1360/aps040178

Zotarelli, L., Rens, R. L., Cantliffe, D. J., Stoffella, P. J., Gergela, D., and Burhans, D. (2015). Rate and timing of nitrogen fertilizer application on potato 'FL1867'. Part I: plant nitrogen uptake and soil nitrogen availability. *Field Crop. Res.* 183, 246–256. doi: 10.1016/j.fcr.2015.08.007

frontiers | Frontiers in Plant Science

TYPE Original Research
PUBLISHED 28 September 2022
DOI 10.3389/fpls.2022.976280

OPEN ACCESS

EDITED BY
Petra Bauer,
Heinrich Heine University of Düsseldorf, Germany

REVIEWED BY
Jose Manuel García-Garrido,
Department of Soil Microbiology and Symbiotic Systems, Experimental Station of Zaidín (CSIC), Spain
Tingting Xiao,
King Abdullah University of Science and Technology, Saudi Arabia

*CORRESPONDENCE
Wei-Yi Lin
weiyilin@ntu.edu.tw

†These authors have contributed equally to this work

SPECIALTY SECTION
This article was submitted to Plant Nutrition, a section of the journal Frontiers in Plant Science

RECEIVED 23 June 2022
ACCEPTED 06 September 2022
PUBLISHED 28 September 2022

CITATION
Deng C, Li C-J, Hsieh C-Y, Liu L-YD, Chen Y-A and Lin W-Y (2022) MtNF-YC6 and MtNF-YC11 are involved in regulating the transcriptional program of arbuscular mycorrhizal symbiosis. *Front. Plant Sci.* 13:976280. doi: 10.3389/fpls.2022.976280

MtNF-YC6 and MtNF-YC11 are involved in regulating the transcriptional program of arbuscular mycorrhizal symbiosis

Chen Deng[1†], Chun-Jui Li[2†], Chen-Yun Hsieh[2], Li-Yu Daisy Liu[2], Yi-An Chen[2] and Wei-Yi Lin[2*]

[1]Department of Horticulture and Landscape and Architecture, National Taiwan University, Taipei, Taiwan, [2]Department of Agronomy, National Taiwan University, Taipei, Taiwan

Arbuscular mycorrhizal fungi are obligate symbionts that transfer mineral nutrients to host plants through arbuscules, a fungal structure specialized for exchange for photosynthetic products. *MtNF-YC6* and *MtNF-YC11*, which encode the C subunits of nuclear factor Y (NF-Y) family in *Medicago truncatula* are induced specifically by arbuscular mycorrhizal symbiosis (AMS). A previous study showed that *MtNF-YC6* and *MtNF-YC11* are activated in cortical cells of mycorrhizal roots, but the gene functions were unknown. Herein, we identified both MtNF-YB17 and MtNF-YB12 as the interacting partners of MtNF-YC6 and MtNF-YC11 in yeast and plants. *MtNF-YB17* was highly induced by AMS and activated in cortical cells only in mycorrhizal roots but *MtNF-YB12* was not affected. The formation of B/C heterodimers led the protein complexes to transfer from the cytoplasm to the nucleus. Silencing *MtNF-YC6* and *C11* by RNA interference (RNAi) resulted in decreased colonization efficiency and arbuscule richness. Coincidently, genes associated with arbuscule development and degeneration in RNAi roots were also downregulated. *In silico* analysis showed CCAAT-binding motifs in the promoter regions of downregulated genes, further supporting the involvement of NF-Y complexes in transcriptional regulation of symbiosis. Taken together, this study identifies MtNF-YC6- or MtNF-YC11-containing protein complexes as novel transcriptional regulators of symbiotic program and provides a list of potential downstream target genes. These data will help to further dissect the AMS regulatory network.

KEYWORDS

arbuscular mycorrhizal fungus, symbiosis, nuclear factor Y, MtNF-YC6, MtNF-YC11

Introduction

Arbuscular mycorrhizal fungi (AMF), the soil-borne fungi, belong to Glomeromycota, and can form symbiotic relationships with more than 80% of land plant species (Smith and Read, 2008). These fungi are obligate symbionts that acquire mineral nutrients through extraradical hyphal network and transfer them to host plants through the specialized fungal structure and the interface (the arbuscule and peri-arbuscular space, respectively) in the inner cortical cells in exchange for photosynthetic products from host plants (Roth and Paszkowski, 2017).

After perceiving the fungal signals, a series of calcium oscillations is induced. A nuclear-localized calcium calmodulin-dependent protein kinase (CCaMK, known as DMI3 in *Medicago truncatula*) acts as decoder to decipher the calcium oscillation and activate symbiotic responses and initiate the formation of prepenetration apparatus (Takeda et al., 2012; Miller et al., 2013). CCaMK phosphorylates and interacts with CYCLOPS (known as IPD3 in *M. truncatula*) to promote symbiosis (Yano et al., 2008; Horváth et al., 2011). Several GRAS domain transcriptional regulators act downstream of CCaMK to regulate symbiotic processes, such as NSP1 and NSP2 (Delaux et al., 2013a; Hofferek et al., 2014) and RAM1 (Park et al., 2015). Genes participated in arbuscule development have been identified, including *Vapyrin* (Pumplin et al., 2010; Murray et al., 2011), *RAM2* (Wang et al., 2012; Gobbato et al., 2013), *STR and STR2* (Zhang et al., 2010), but the expression pattern of these genes are varied, suggesting that the complex regulation programs are required to ensure gene expression precisely. Although arbuscules function as a platform for nutrient exchange, the life span of this fungal structure is relatively short (Alexander et al., 1988; Alexander et al., 1989). Thus, arbuscule degeneration and new arbuscule development occur simultaneously in mycorrhizal roots to maintain an active symbiotic relationship. Currently, the knowledge about the underlying mechanism of controlling arbuscule degeneration is limited.

Medicago truncatula PT4, an AM symbiosis (AMS)-responsive phosphate transporter, is localized in a specialized cortical cell membrane that encircles an arbuscule to take up fungal phosphate. Loss of MtPT4 function did not affect arbuscule development but triggered premature arbuscule degeneration leading to less phosphate accumulation (Harrison et al., 2002; Javot et al., 2007). During the degeneration process, peroxisomes accumulate around collapsing arbuscules either to assist lipid metabolism or sequester reactive oxygen species produced at this phase (Pumplin and Harrison, 2009). MtMYB1 is the first transcriptional regulator identified involved in controlling premature arbuscule degeneration. Reducing *MtMYB1* expression in the *mtpt4* mutant restored the premature arbuscule degeneration phenotype. This transcription factor coupled with NSP1 and DELLA, participated in the transcriptional regulation of hydrolase genes associated with arbuscule degeneration (Floss et al., 2017). However, the mechanism of initiating arbuscule degeneration and the transcriptional regulation upstream to MtMyb1-mediated transcriptional program remain unclear.

The symbiosis is believed to have arisen more than 400 million years ago (Remy et al., 1994). The set of essential genes required for the formation of AMS - a symbiotic toolkit - is highly conserved in many host species. These genes usually respond specifically to AMS and are thought to be involved in AMS formation and maintenance (Delaux et al., 2013b). Through comparative phylogenomic analyses, more than 100 candidate genes that are evolutionarily conserved in host species were identified, including well-characterized AMS-responsive genes and many uncharacterized genes (Delaux et al., 2014; Favre et al., 2014; Bravo et al., 2016). Among the AMS-conserved genes, 13% are involved in transcriptional regulation (Bravo et al., 2016), and *RAM1* and *CYCLOPS* were the most well-characterized transcriptional factors involved in controlling arbuscule development. (Park et al., 2015; Floss et al., 2016; Pimprikar et al., 2016). One of the CCAAT-binding factors (CBFs) was also identified as a AMS-conserved genes and highly induced by symbiosis (Delaux et al., 2014; Favre et al., 2014; Bravo et al., 2016), but the exact role remains unclear.

CCAAT-binding factors, also named Nuclear Factor Ys (NF-Ys) or Heme Activator Proteins (HAPs), are present in all eukaryotic species. These transcriptional regulators are composed of three subunits, NF-YA, NF-YB and NF-YC. In the heterotrimeric complex, NF-YA is responsible for specific recognition of the CCAAT-binding motif in the promoter regions. NF-YB and NF-YC contain histone fold motifs, form heterodimers and interact with NF-YA to bind to the core DNA sequence (Romier et al., 2003; Petroni et al., 2012). In plants, NF-Ys are encoded by multigenic families leading to numerous kinds of heterotrimeric combinations participating in various kinds of physiological processes and rhizobium-legume symbiosis (Petroni et al., 2012; Laloum et al., 2013; Ripodas et al., 2014; Baudin et al., 2015; Zhao et al., 2016), but very few reports have demonstrated the roles of NF-Ys in AMS. Soybean *GmNF-YA1a* and *1b* were downregulated by NARK-mediated autoregulation to further reduce AMF infection events, identified as positive regulators of AMS (Schaarschmidt et al., 2013). MtNF-YC6 and MtNF-YC11 (previously designated MtCbf1 and MtCbf2) have been identified as AMS-conserved transcriptional factors (Delaux et al., 2014; Favre et al., 2014; Bravo et al., 2016). Cell-specific transcriptomic analysis and promoter analysis revealed that both genes were first induced by the contact between fungi and host plants, and the expression was also detected in arbuscule containing-cortical cells and adjacent cells when fungal hyphae extended to the cortex

(Hogekamp et al., 2011). These results imply that both genes might participate in controlling several symbiotic processes. However, their interacting partners and their roles in the AMS regulatory network await for further characterization.

In this study, we identified MtNF-YB12 and B17 as the interacting partners of MtNF-YC6/C11 and showed the activation of *MtNF-YB17* by AMS in the cortical cells of infection units. When knocking down *MtNF-YC6* and *MtNF-YC11* in mycorrhizal roots by RNA interference (RNAi), we observed a decrease in colonization efficiency and the downregulation of genes involved in the control of arbuscule development and degeneration. Furthermore, *in silico* analysis revealed the potential of these downregulated genes as the downstream targets of NF-Y complexes. Some well-characterized AMS-responsive genes also obtained more than one CCAAT-binding motif and were downregulated in RNAi roots, implying that NF-Y complexes might be involved in the control of different symbiotic processes. Our results provide new insights into the transcription program of arbuscule development.

Materials and methods

Plant growth conditions

Medicago truncatula ssp. *truncatula* ecotype Jemalong (A17) and *Nicotiana benthamiana* were used in these studies. The plants were grown in a growth chamber with 16-h light (25°C) and 8-h dark (22°C). *Medicago* seedlings were grown in cones filled with sterilized river sands and fertilized twice a week with a modified one-half strength of Hoagland's solution containing 20 μM potassium phosphate. For AMF treatment, 1 g of *Claroideoglomus etunicatum* or *Rhizophagus irregularis* inoculants (containing around 100 spores) were added before transplanting. Plants were harvested 6 weeks later for further research. *N. benthamiana* were grown in pots filled with a mixture of peat moss and vermiculite in a 9:1 ratio and fertilized with full nutrient solution once a week. At 4 weeks after transplanting, leaves were used for agroinfiltration.

Medicago truncatula root transformation

M. truncatula root transformation was conducted as described by Boisson-Dernier et al. (2001) with minor modifications. Seeds of *M. truncatula* were surface sterilized and kept in the dark at 4°C overnight. Then the seeds were transferred to germinate in a 30°C incubator for 15 h. The root tips of *Medicago* seedling were cut and co-cultivated with *Agrobacterium rhizogenes* strain Arqua1 harboring a binary vector. After cocultivation, plants were transferred to cones filled with sterilized river sands and 1 g of AMF inoculants and were grown for another 6 weeks before harvesting.

Construction for knocking down the expression of MtNF-YC6/C11 and MtNF-YB17

For generating the *MtNF-YC6/C11* and *MtNF-YB17* RNAi constructs, around 300 bp of specific sequences in the coding regions (Supplementary Figure 1) were amplified using primer pairs listed in Supplementary Table 1 and cloned into pDONR221 by Gateway BP reaction (Thermo Fisher Scientific, USA). These vectors were recombined with the pK7GWIWG(II)-RedRoot destination vector (S. Ivanov, unpublished) through Multisite Gateway LR reaction (Thermo Fisher Scientific) to generate RNAi transformation vectors under the control of the CaMV 35S promoter.

Construction for transient gene expression in *Nicotiana. benthamiana* leaves

Genes of interest were amplified using primer pairs listed in Supplementary Table 1. For detecting the subcellular localization of MtNF-YCs, MtNF-YBs and MtNF-YAs, the coding sequences were recombined with pDONR221 in the Gateway BP reaction. To express N-terminal tagged fluorescence fusion proteins, pK7WGC2, pK7WGF2 and pK7WGY2 were used to generate CFP-, GFP-, and YFP-fused proteins through Gateway LR reaction, respectively (Karimi et al., 2002).

For bimolecular fluorescence complementation (BiFC) analysis, the coding sequence of *MtNF-YC*s and *MtNF-YB*s were recombined with pUBN-nYFP, pUBC-nYFP and pUBC-cYFP (Grefen et al., 2010) to generate N-terminal YFP and C-terminal YFP tagging at either N or C terminus of target proteins.

Agrobacterium tumefaciens-mediated infiltration

Agrobacterium-mediated infiltration was performed as described (Liu et al., 2012). Briefly, the culture of *A. tumefaciens* EHA105 strain containing a binary vector was prepared in LB media incubating at 30°C overnight. The culture was resuspended in the infiltration medium (10 mM $MgCl_2$ and 10 mM MES) and diluted to an OD_{600} of 1.0. The cell suspension was kept in the dark for 2-3 h at room temperature. A mixture of cell suspension containing genes of interests was infiltrated into the leaves of *N. benthamiana*. Samples were collected 3-4 days after infiltration.

WGA staining and analysis of colonization efficiency

Medicago roots were cut into 1-cm fragments and stained with WGA-Alexa fluor 488 (Thermo Fisher Scientific) to visualize fungal structures (Park et al., 2015). The root fragments were selected randomly and examined microscopically using an Olympus SZX16 stereomicroscope (Olympus, Japan). The grid method evaluated the percentage of infected roots containing fungal structures (F%; Mcgonigle et al., 1990), the intensity of mycorrhization in the root systems (M%) and in mycorrhizal root fragments (m%), and the arbuscule abudnace in the root systems (A%) and in root fragments containing arbusucles (Trouvelot et al., 1986). The arbuscule distribution was analyzed as described (Breuillin-Sessoms et al., 2015). The arbuscules were classified based on their length and the abundance of arbuscules in difference classes was calculated as percentage.

Yeast two-hybrid assay and plasmid construction

The yeast two-hybrid assay was conducted according to the manufacturer's instructions (Clontech, USA). For testing the interaction between NF-YBs and NF-YCs, the coding sequences of *MtNF-YCs* and *MtNF-YBs* were cloned into pGBKT7-DEST and pGADT7-DEST, respectively. For testing the interaction between NF-YAs and NF-YCs, *MtNF-YC6/C11* and *MtNF-YAs* were cloned to pGADT7-DEST and pGBKT7-DEST, respectively. Primer pairs used for amplifying genes of interest are listed in Supplementary Table 1. Yeast cells cotransformed with pGADT7-T and pGBKT7-53 were positive controls while cells cotransformed with pGADT7-T and pGBKY7-Lam were negative controls. The specificity of protein-protein interactions was confirmed by the growth of yeast cells on dropout media lacking leucine, tryptophan, and histidine and supplemented 3-amino-1,2,4-triazole (3AT).

Construction for promoter analysis and GUS-staining

For analyzing the activity of the *MtNF-YB17* promoter, a 1.25-kbp fragment upstream of the start codon was amplified using primer pairs listed in Supplementary Table 1 and was cloned into pBGWFS-RedRoot which was kindly provided by Dr. Shu-Yi Yang (National Taiwan University, Taiwan).

Medicago roots were transformed with *MtNF-YB17pro:GUS* and composite roots were collected at 6 weeks after transplanting for staining. The roots were fixed in ice-cold 90% acetone for 30 min and washed three times with phosphate buffered saline (PBS). Then, the roots were incubated in GUS staining buffer (5 μM EDTA, 0.5 mM potassium ferricyanide. 0.5 mM potassium ferrocyanide and 0.5 mg ml^{-1} 5-bromo-4-chloro-3-indolyl-β-D-glucuronide cyclohexylammonium salt) at 37°C for 6 h and washed with PBS to stop the reaction. The stained roots were observed under an Olympus SZX16 stereomicroscope and a Zeiss Axio Imager M2 light microscope (Zeiss Microscopy, Germany).

Fluorescence microscopy

Fluorescence images were taken by confocal microscopy using a Leica TCS SP5 II (Leica Microsystems, Germany) with objectives HCX PL FLUOTAR 10X/0.30 DRY, HCX PL APO CS 20X/0.7 dry and HCX PL APO lambda blue 63X/1.40 OIL. The excitation and emission wavelengths for CFP were 458 nm and 465-510 nm; 475 nm and 500-520 nm for GFP; 514 nm and 520-550 nm for YFP.

RNA extraction and gene expression analysis

Total RNA was isolated using TRIzol® (Thermo Fisher Scientific) according to the manufacturer's instruction and treated with RNase-free TURBO DNase I (Thermo Fisher Scientific) to remove genomic DNA. First strand cDNAs were synthesized from 500 ng RNA using Moloney murine leukemia virus reverse transcriptase (Thermo Fisher Scientific) with oligo dT primer. Quantitative RT-PCR (qRT-PCR) was performed using iQ™ SYBR® Green Supermix (Bio-Rad, USA) on a CFX Connect Real-Time PCR Detection System (Bio-Rad). Relative expression levels ($2^{-\Delta Ct}$) were normalized to the expression of a reference gene, *MtEF1-α*. The primer pairs used for qRT-PCR are listed in Supplementary Table 2.

In silico analysis of CCAAT-binding motifs

The promoter sequences (2 kbp upstream of the start codon) of 91 differentially expressed genes in *mtpt4* mutants (Floss et al., 2017) and AMS marker genes were retrieved from *Medicago truncatula* genome database (Tang et al., 2014). The R program (version 4.1.0) was used to scan and identify CCAAT-binding motifs in the promoter regions.

Results

Identifying the NF-Y subunits that interact with MtNF-YC6 and MtNF-YC11

To identify the components in the MtNF-YC6-or MtNF-YC11-containing transcriptional complex, we first performed

yeast two-hybrid assays to test the interaction between different subunits. In the *Medicago* genome, there are 19 NF-YBs, and according to the expression profiles managed by the *M. truncatula* gene expression atlas web server (He et al., 2009), we selected *MtNF-YB7*, *B12*, *B16*, and *B17* which were induced by AMS or highly expressed in mycorrhizal roots (Supplementary Table 3) as preys to test their potential for interacting with two AMS-conserved C subunits. We found that both MtNF-YB12 and MtNF-YB17 could interact either with MtNF-YC6 or MtNF-YC11, but MtNF-YB6 and MtNF-UB17 could not interact (Figure 1A). A study on animal NF-YC pointed out an isoleucine and an aspartic acid within histone fold motif as essential residues for the interaction with B subunits (Kim et al., 1996). Thus, we generated mutated MtNF-YC6 (mC6) and MtNF-YC11 (mC11) (Supplementary Figure 2). In yeast the mutation at these two essential residues impeded the interaction with MtNF-YB12 and MtNF-YB17 (Figure 1B), supporting the importance of these two conserved residues.

To further verify the interaction *in planta*, we examined the subcellular localization of these NF-Y subunits. When transiently expressed in the leaf epidermal cells of *N. benthamiana*, both GFP-tagged MtNF-YC6 and MtNF-YC11 were observed in the cytoplasm and nuclei (Supplementary Figure 3A). Similarly, YFP-tagged MtNF-YB12 and MtNF-YB17 were also detected both in the cytoplasm and nuclei (Supplementary Figure 3B). Interestingly, when co-expressing CFP-MtNFYC6/C11 with either YFP-MtNF-YB12 or YFP-MtNF-YB17, both CFP and YFP signals were predominantly colocalized in nuclei except some weak signals of YFP-MtNF-YB12 in cytoplasm (Supplementary Figures 3C, D). Next, we performed a BiFC assay to further confirm the direct interaction *in planta*. Co-expression of C-terminal YFP (cYFP)-tagged MtNF-YC6/C11 (MtNF-YC6/C11-cYFP) either with N-terminal YFP (nYFP)-tagged MtNF-YB12 (nYFP-MtNF-YB12) or MtNF-YB17 (nYFP-MtNF-YB17) produced YFP signals exclusively in nuclei while co-expression of MtNF-YC6/C11 either with empty vector control or MtNF-YB7 or MtNF-YB16 did not give rise to any signal (Figure 1D). Likewise, co-expressing MtNF-YC6/C11-nYFP with MtNF-YB12/B17-cYFP or MtNF-YC6/C11-cYFP with MtNF-YB12/B17-nYFP also produced signals in the nucleus (Supplementary Figure 4). These results support the direct interaction of MtNF-YC6/C11 and MtNF-YB12/B17, and the formation of heterodimer brought the protein complexes from the cytoplasm to the nucleus.

The NF-YA family has eight members in *Medicago* genome. A yeast two-hybrid assay was performed to identify A subunits, which could associate either with MtNF-YC6 or MtNF-YC11. Concerning MtNF-YA1, which is a known regulator of rhizobium-legume symbiosis expressed specifically in nodules (Laloum et al., 2014; Laporte et al., 2014; Baudin et al., 2015), only seven A subunits were included in the assay. These results show the relatively strong interaction of MtNF-YC6/C11 with MtNF-YA4/A8 and weak interaction with MtNF-YA3/A5 (Figure 1C). Due to the failure of YFP-tagged MtNF-YA8 construction for unknown reasons, we only examined the localization of MtNF-YA4. Like other plant NF-YAs, MtNF-YA4 was localized in the nucleus (Supplementary Figure 5A). When transiently overexpressing CFP-MtNF-YC6/C11, MtNF-YB12/B17, and YFP-MtNF-YA4 simultaneously in the leaves of *N. benthamiana*, most CFP and YFP signals were exclusively colocalized in the nuclei (Supplementary Figure 5B), but co-expressing CFP-MtNF-YC6, MtNF-YB17 and YFP-MtNF-YA4 did not give rise to any fluorescence signal (data not shown). These results supported the interaction between these subunits and their function in the nucleus.

The responses of NF-Ys to AMS

After identifying the components which were able to interact with MtNF-YC6 and MtNF-YC11, we investigated the responses of these components to AMS at transcript levels. First, the expression of *MtNF-YC6, MtNF-YC11*, *MtNF-YB12*, *MtNF-YB17*, *MtNF-YA3*, *MtNF-YA4*, and *MtNF-YA8* in the roots of mock-treated and *C. etunicatum*- or *R. irregularis*-inoculated plants were examined by qRT-PCR. Like the previous report by Hogekamp et al. (2011), we did observe the significant induction of *MtNF-YC6* and *MtNF-YC11* in AMF-treated roots and the expression level of *MtNF-YC11* was much lower than *MtNF-YC6* in mycorrhizal roots. Intriguingly, the induction level of both genes was higher in *C. etunicatum*-colonized roots than in *R. irregularis*-colonized roots (Figure 2C) even though the colonization efficiency and the expression of the AMS marker gene, *MtPT4*, in *Medicago* roots by two different AMF species were similar (Figures 2A, B). The expression of *MtNF-YB17* was also upregulated by AMS but *MtNF-YB12* was not. Different from the expression pattern of *MtNF-YC6* and *C11*, the transcript levels of both genes were not affected by the difference in AMF species (Figure 2D). Unexpectedly, both *MtNF-YA3* and *MtNF-YA4* were downregulated by AMS except in *C. etunicatum*-inoculated roots *MtNF-YA4* was not affected. The expression of *MtNF-YA8* was much lower than *MtNF-YA3* and *MtNF-YA4*, and in contrast, it was upregulated by *C. etunicatum*-inoculation but did not respond to *R. irregularis* colonization (Figure 2E).

The analysis of *MtNF-YB17* transcripts suggested that it was co-activated with *MtNF-YC6/C11* by AMS. To determine the expression pattern of *MtNF-YB17* in colonized roots, promoter analysis was used to detect its expression at the tissue level. The GUS activity in composite roots expressing *MtNF-YB17pro:GUS* was analyzed. Blue staining was only observed in the vascular tissues in mock-treated roots (Figures 3A, B). But in *R. irregularis*-inoculated roots, strong blue staining was observed in the cortex of colonized regions (Figures 3C–G) while in non-

10.3389/fpls.2022.976280

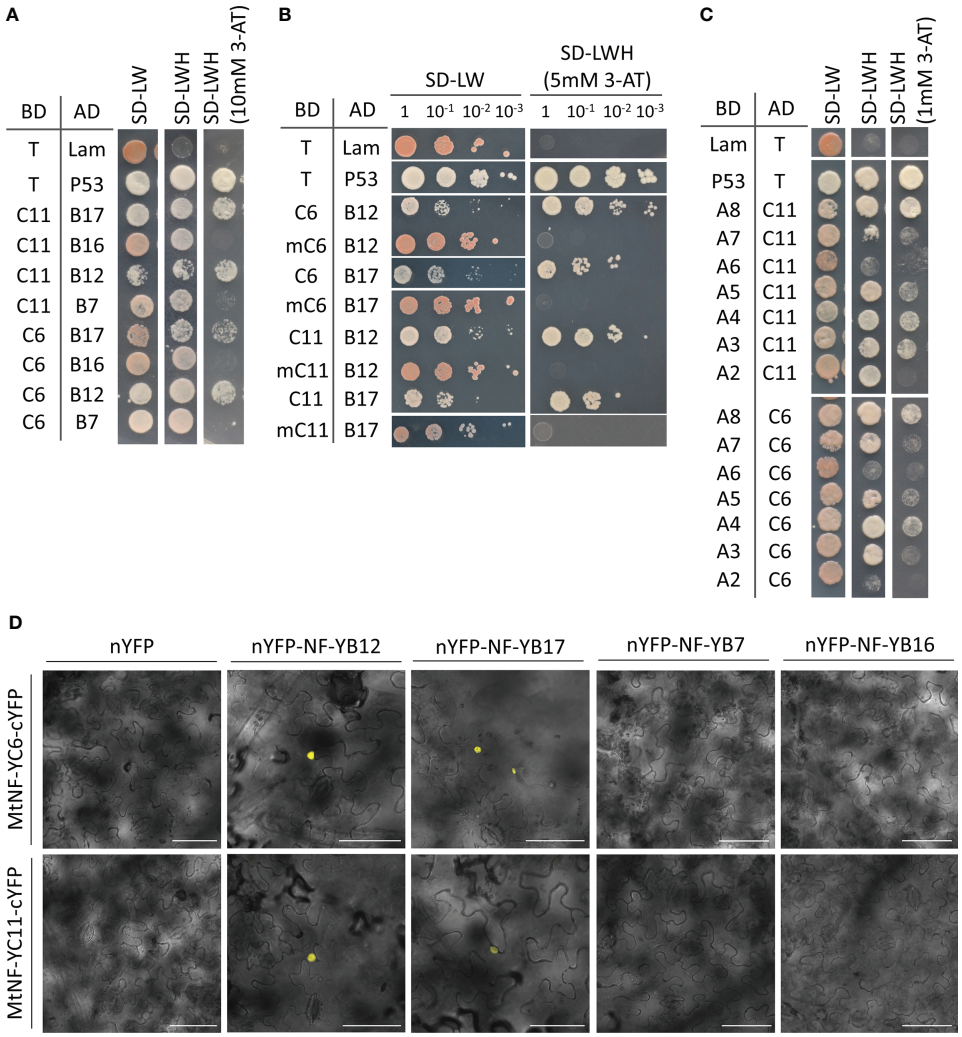

FIGURE 1
Identification of the interacting partners of MtNF-YC6 and MtNF-YC11 using yeast two-hybrid and BiFC assays. **(A)** Interaction of MtNF-YC6 (C6) or MtNF-YC11 (C11) with four different MtNF-YBs (B7, B12, B16, and B17). **(B)** Interaction of wild type or mutated MtNF-YC6 (mC6) and MtNF-YC11 (mC11) either with MtNF-YB12 (B12) or MtNF-YB17 (B17). **(C)** Interaction of MtNF-YC6 or MtNF-YC11 with seven different MtNF-YAs. Interactions of T with p53 and Lam were used as a positive and negative control, respectively. BD, Gal4 binding domain. AD, Gal4 activation domain. **(D)** Co-expressing C-terminal YFP (cYFP)-tagged MtNF-YC6 or MtNF-YC11 either with N-terminal YFP (nYFP)-tagged MtNF-YB7, B12, B16 or B17 in *N. benthamiana* leaves. The images were the overlay of bright field and YFP. Bar = 75 μm.

colonized regions GUS staining was predominantly observed in vascular tissues (Figures 3H, I). In summary, our results suggest that the expression of *MtNF-YB17* was induced by AMS and might function with MtNF-YC6/C11 in the root cortex.

Functional characterization of MtNF-YC6/C11-containing protein complex during AMS

To illustrate the role of MtNF-YC6/C11-containing protein complexes in AMS, the RNAi technique was used to knock down the expression of either *MtNF-YC6/C11* or *MtNF-YB17* in *Medicago* roots. First, we designed an RNAi construct to knock down *MtNF-YB17* in *R. irregularis*-inoculated roots (Supplementary Figure 1A). In RNAi roots, the expression of *MtNF-YC17* was significantly reduced. Although the sequence identity between *MtNF-YB12* and *MtNF-YB17* was not as high as that between *MtNF-YC6* and *C11* (Supplementary Figure 1), the expression of *MtNF-YB12* in *MtNF-YB17* RNAi roots was also slightly decreased (Supplementary Figure 6A). The frequency of AMF colonization was not affected by the decreased expression of these two B subunits (Supplementary Figure 6B). *PT4* and *BCP1*, well-known AMS marker genes, are

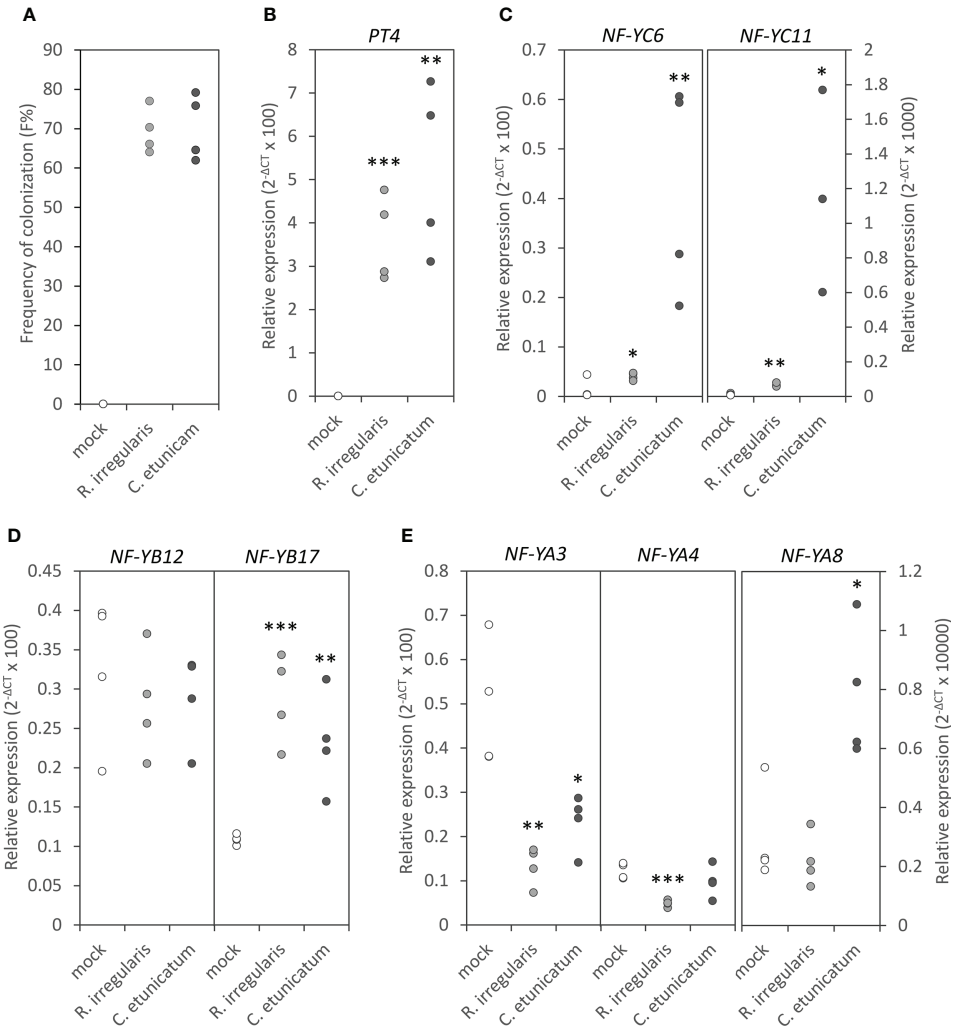

FIGURE 2
The responses of *MtNF-YC6*, *MtNF-YC11* and their interacting *NF-Y* subunits to AMS. **(A)** The frequency of colonization in AMF-colonized roots. **(B)** The relative expression level of *MtPT4*. **(C-E)** The relative expression level of *MtNF-YC6* and *C11* **(C)**, MtNF-YB12 and B17 **(D)** and *MtNF-YA3*, *A4*, and *A8* **(E)** in mock- and AMF-treated roots. n=4. Student's t test evaluated the difference between mock- and AMF-treated roots. *p<0.05, **p<0.01, ***p<0.001.

widely-used symbiotic marker genes. The expression of these two marker genes was also unchanged in RNAi roots (Supplementary Figure 6C). We also examined the expression of *MYB1*, a marker gene of arbuscule degeneration that encodes a MYB-type transcription factor (Floss et al., 2017). Similarly, it was not affected by the downregulation of *MtNF-YB17* (Supplementary Figure 6D). These results suggest that a few MtNF-YB17 proteins in RNAi roots were sufficient to exert its function or downregulation of *MtNF-YB17* and *MtNF-YB12* was insufficient to affect the AMS process.

We then investigated the importance of MtNF-YC6 and MtNF-YC11. High sequence similarity between these two genes implied the possibility of functional gene redundancy. Thus, we selected a 300 bp-conserved sequence in the coding sequence to design an RNAi construct (Supplementary Figure 1B) to simultaneously knock down both genes. Due to the higher induction level of these two genes in *C. etunicatum*- than in *R. irregularis*-colonized roots, we used *C. etunicatum* as the inoculants to test the roles of these two C subunits in AMS. In RNAi roots, *MtNF-YC6* was significantly downregulated, and *MtNF-YC11* was also decreased by RNAi but not statistically significant (Figure 4A). The expression of other members in *MtNF-YC* family was also examined except *MtNF-YC3* and *MtNF-YC10* which do not express in roots. None of family members was affected in RNAi roots (Supplementary Figure 7). On average, the AMF colonization frequency (F%), the intensity of mycorrhization (M%) and the arbuscule richness in the colonized roots (a%) were significantly decreased in RNAi roots,

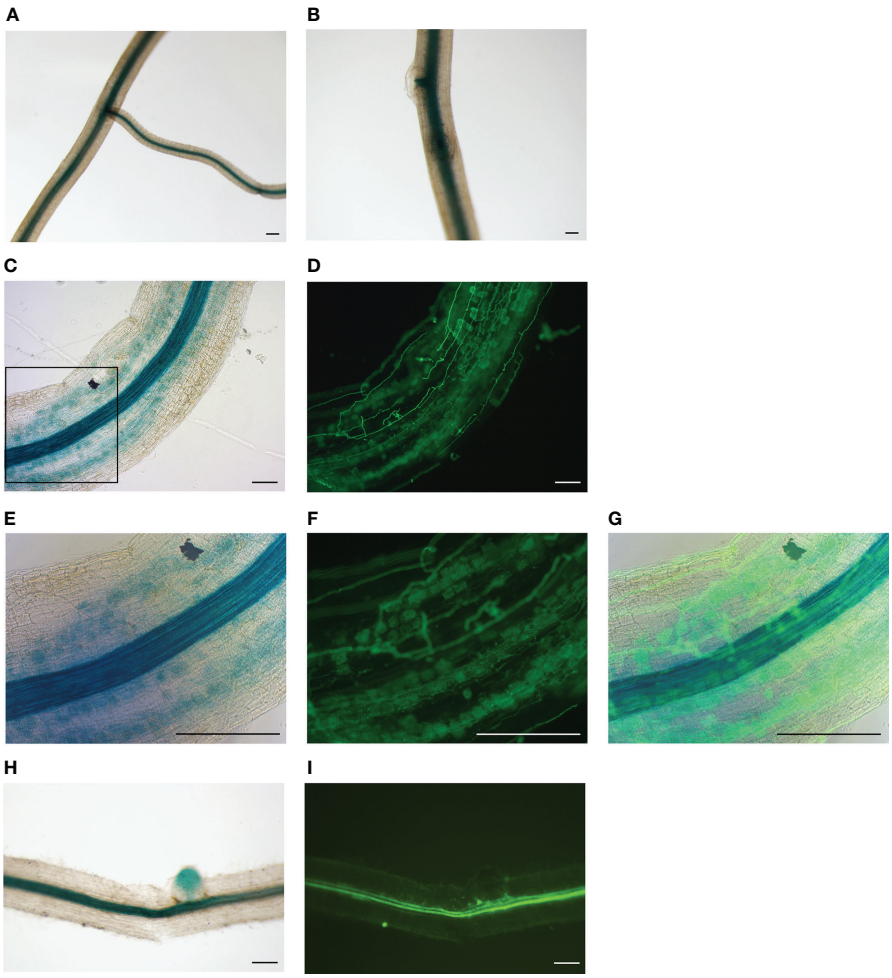

FIGURE 3
The expression pattern of *MtNF-YB17* in Medicago roots. **(A, B)** GUS staining of roots expressing *MtNF-YB17pro:GUS* from mock-treated root system. **(C-I)** GUS staining of *R. irregularis*-inoculated roots expressing *MtNF-YB17pro:GUS* **(C, E, H)**. Corresponding fluorescence images showing fungal structure stained with WGA at exactly the same region **(D, F, I)**. **(E-G)** Magnification image corresponding to the black rectangle in **(C)**. **(G)** The merged image of bright field and fluorescence. **(H, I)** Non-colonized root fragments expressing *MtNF-YB17pro:GUS* from *R. irregularis*-treated root system. Bar = 200 μm.

compared to roots transformed with an empty vector (Figure 4B) but the size distribution and morphology of arbuscules were not affected (Figure 4C and Supplementary Figure 8).

Because silencing *MtNF-YC6* and *MtNF-YC11* resulted in the decrease of colonization frequency and intensity, we further investigated the impacts on the expression of AMS marker genes at different symbiotic processes, including *DMI3* and *IPD3* which participate in the symbiotic signaling pathway (Horváth et al., 2011; Miller et al., 2013) and genes involved in the control of arbuscule development such as *Vapyrin* (Pumplin et al., 2010; Murray et al., 2011), *RAM1* (Gobbato et al., 2012; Park et al., 2015), *RAM2* (Wang et al., 2012; Gobbato et al., 2013), *STR*, *STR2* (Zhang et al., 2010), *NSP1*, *NSP2* (Delaux et al., 2013a; Hofferek et al., 2014), and *BCP1* (Pumplin and Harrison, 2009). Transcripts of *RAM1*, *RAM2*, *STR*, *STR2*, and *NSP1* were significantly reduced in RNAi roots compared to empty vector control, whereas *DMI3*, *IPD3*, *Vapyrin*, and *BCP1* were not affected (Figures 4D, E). We also examined *PT4* and *MYB1*, and intriguingly, these two genes were also significantly downregulated in RNAi roots though the reduction level of *PT4* transcripts was not statistically significant (Figure 4F). Because of the involvement of PT4 and MYB1 in the arbuscule degeneration, we further analyzed the expression of hydrolase genes associated with this process, including cysteine protease genes (*CP*s), chitinase genes, a triacylglycerol lipase gene (*TGL*) and a S1/P1 type nuclease gene (*S1/P1*) (Floss et al., 2017). Coincidently, the expression of *CP4/CP5*, two of *chitinase* genes, *TGL* and *S1/P1* was significantly reduced in RNAi roots, whereas the transcript levels of *CP2*, *CP3* and the other chitinase genes were slightly decreased in RNAi roots but not significant

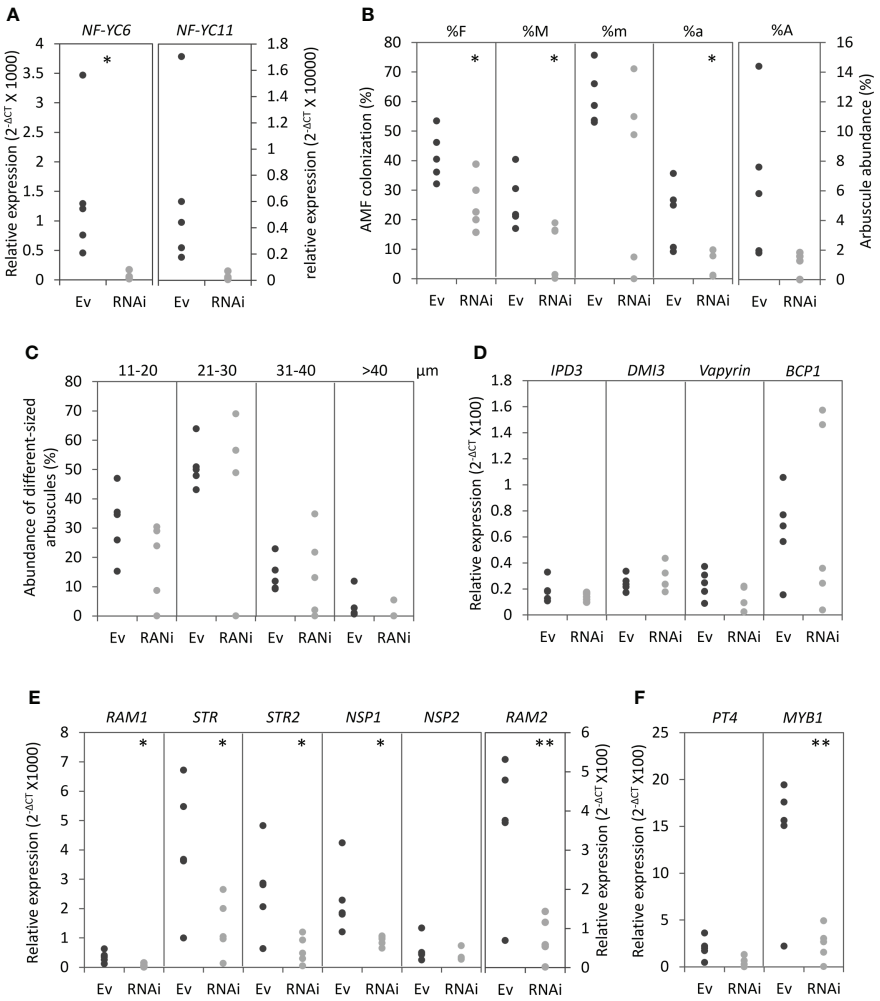

FIGURE 4
The phenotypic analysis of *MtNF-YC6* and *MtNF-YC11* RNAi roots. **(A)** The relative expression level of *MtNF-YC6* and *C11* in empty vector control (Ev) and RNAi roots (RNAi). **(B, C)** Parameters of AMF colonization **(B)** and the size distribution of arbuscules **(C)** in Ev and RNAi roots. **(D-F)** The relative expression level of AMS marker genes which participated in symbiotic signaling pathway, arbuscule development and arbuscule degeneration. The dark and light gray dots mean Ev and RNAi samples, respectively. n = 5. Student's t test evaluated the difference between Ev and RNAi. *p<0.05, **p<0.01.

(Figures 5A, B). Although *MtNF-YC6* or *MtNF-YC11* were not simultaneously downregulated in all RNAi roots, the phenotype suggested the involvement of these two genes in regulating the transcriptional program of arbuscule development.

In silico analysis of CCAAT motifs in the promoter regions of AMS-induced genes

Mutations in *Medicago PT4* result in decreased colonization efficiency and a premature arbuscule degeneration phenotype (Harrison et al., 2002; Javot et al., 2007). By analyzing transcriptome associated with arbuscule degeneration, 91 differentially expressed genes (DEG) were identified in *mtpt4* mutant compared to wild type (Floss et al., 2017). The downregulation of *MYB1* and hydrolase genes suggested that MtNF-YC6 and MtNF-YC11 might regulate genes involved in arbuscule degeneration. To understand the importance of NF-Y complexes in the transcriptional regulation at this phase, we performed *in silico* analysis to see the presence of CCAAT-binding motifs in the 2-kbp region upstream of the start codon of 91 DEGs.

We found that 71 DEGs contained at least one CCAAT-binding motif in the promoter regions. Among 71 DEGs, 15 were AMS-conserved genes, including *PT4* and *RAM2*. *MYB1* and several hydrolase genes were also identified as potential downstream targets of NF-Y complexes, such as *CP2*, *CP3*, *CP5*, *TGL*, *S1/P1*, and three chitinase genes which we examined in this

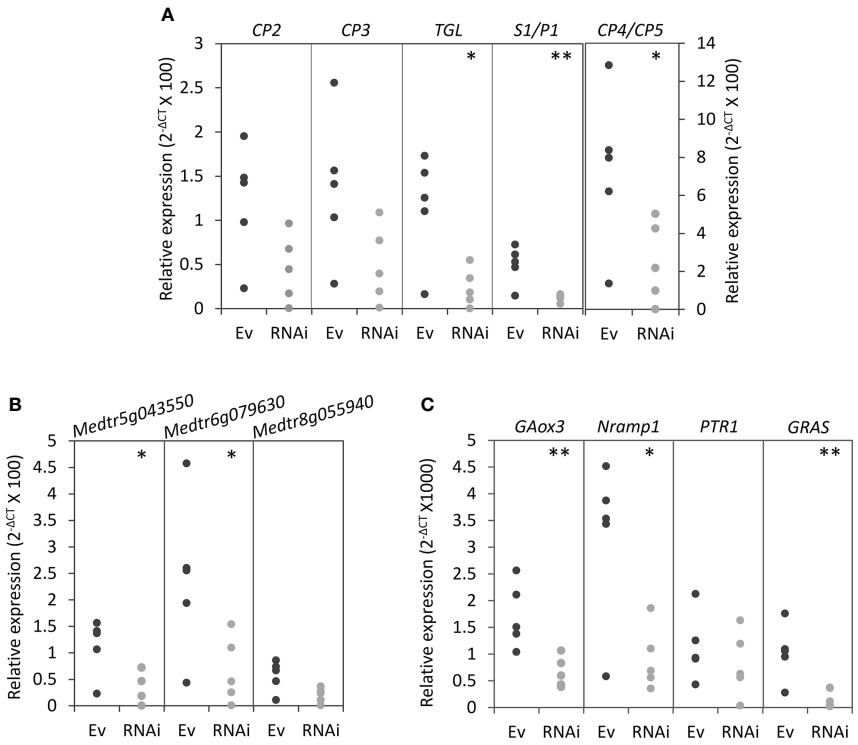

FIGURE 5
Transcript levels of genes associated with arbuscule degeneration and potential target genes of NF-Y protein complexes in *MtNF-YC6/C11* RNAi roots. **(A)** The relative expression level of cysteine protease genes (*CPs*), triacylglycerol lipase (*TGL*) and nuclease S1 (*S1/P1*). **(B)** The relative expression level of chitinase genes. **(C)** The relative expression level of potential target genes of NF-Y complexes. The dark and light gray dots mean Ev and RNAi samples, respectively. n = 5. Student's t test evaluated the difference between Ev and RNAi. *p<0.05, **p<0.01.

study. In addition to *MtPT4*, there were some transporter genes obtained CCAAT-binding motifs in the promoter region, such as *Nramp1*, *PTR1* and *NIP1* (Table 1). The location and the number of CCAAT-binding motifs were variable. *MtMYB1* contains four CCAAT-binding motifs in the promoter regions and two of them are located within 200 bp upstream of the start codon. *TGL* had two motifs and one is located 256 bp upstream of the start codon. Both *CP3* and *CP5* contained one motif within 1.5 kbp upstream, and *S1/P1* had three motifs within 500 bp upstream of the start codon (Table 1).

Our data had already shown the significant downregulation of *MYB1*, *PT4*, *RAM2*, *CP5*, *TGL*, *S1/P1* and *chitinases* in *MtNF-YC6/C11* RNAi lines (Figures 4F, 5). We further examined other potential downstream genes, including *Nramp1*, *GA3 hydroxylase* (*GA3ox*), *PTR1* and a gene encoding a GRAS transcription factor (*GRAS*). *Nramp1 GR3ox* and *GRAS* genes were significantly downregulated when *MtNF-YC6/C11* were repressed, but *PTR1*, which encodes a peptide transporter, was not affected (Figure 5C). We also analyzed CCAAT motifs in the promoter regions of AMS marker genes we examined in this study and found that all the genes have at least one motif no matter the transcript levels were affected by RNAi construct or not (Table 2). These results reveal potential target genes of NF-Y protein complexes, which might be associated with the arbuscule development and degeneration processes. Further validation is required to elucidate the detailed function of NF-Y in the regulatory network.

Discussion

The involvement of NF-Y protein complexes has been demonstrated in a wide range of processes, such as drought stress response (Nelson et al., 2007), nutrient acquisition (Qu et al., 2015), flower development (Chen et al., 2007) and nodulation process (Laloum et al., 2014; Laporte et al., 2014; Baudin et al., 2015). Two of the C subunits in the *Medicago* NF-Y family, MtNF-YC6 and MtNF-YC11, are specifically induced by AMS and expressed in the epidermal and cortical cells of colonized roots (Hogekamp et al., 2011), but their roles in AMS processes were unclear. Herein, we identify the interacting partners of these two proteins using *in vitro* and *in vivo* interaction assays and reveal their potential function in the transcriptional program of arbuscule development and degeneration.

TABLE 1 The location of CCAAT motifs were extracted from the 2 kbp upstream region of differentially expressed genes in *mtpt4* mutants.

Gene accession[a]	Location of CCAAT motif	Gene annotation
Medtr0021s0370	-1545; -1337; -1193; -1055; -851; -408; -215; -98	signal peptidase 1 (Tau)
Medtr1g011580	-976; -500; -169; -103	gibberellin 3 oxidase
Medtr1g014160	-1721; -1009	tubby C2 protein
Medtr1g028600	-622; -560	high affinity inorganic phosphate transporter (MtPT4)
Medtr1g040500	-817; -702	glycerol-3-phosphate acyltransferase (RAM2)
Medtr1g061540	-1006; -128	T32M21-140 protein
Medtr1g062970	-261; -171	heparan-alpha-glucosaminide N-acetyltransferase-like protein
Medtr1g090440	-1820; -1666; -1646; -621	C3HC4-type RING zinc finger protein
Medtr1g099310	-166	acidic chitinase
Medtr1g110510	-492; -471; -268	nuclease S1 (S1/P1 nuclease family protein)
Medtr2g012790	-901; -687; -380	F-box/kelch-repeat plant protein, putative
Medtr2g017750	-791; -284; -50	peptide transporter PTR1 (peptide/nitrate transporter)
Medtr2g055250	-1652; -322; -262; -60	F-box protein
Medtr2g062430	-1324; -1005; -505	DUF946 family protein
Medtr2g075830	-168	cysteine protease (CP1)
Medtr2g086630	-1614	germin-like protein
Medtr2g091215	-1029; -322; -160	DUF538 family protein
Medtr2g104800	-839	DUF4228 domain protein
Medtr3g022830	-1992; -709; -644; -497; -249	GRAS family transcription factor
Medtr3g035700	-1199; -1063; -470	50S ribosomal protein L2, chloroplastic
Medtr3g079190	-1719; -1130; -183	neutral ceramidase (Cer)
Medtr3g082200	-945; -233	subtilisin-like serine protease
Medtr3g088460	-1114; -753	NRAMP metal ion transporter (Nramp1)
Medtr3g109160	-1974; -1669	SAUR-like auxin-responsive family protein
Medtr3g109420	-1019	Hemoglobin
Medtr3g109610	-1697; -630; -294; -265; -23	carotenoid cleavage dioxygenase (MAX4/CCD8a)
Medtr4g005230	-1620; -1555; -1538; -1509; -370; -120	cytochrome P450 superfamily protein
Medtr4g006650	-1997; -1926; -1084; -469	heavy metal-associated transporter
Medtr4g047610	-1836; -1602; -1571; -1489; -1461; -1094; -713	papain family cysteine protease
Medtr4g077180	-961	lipid transfer protein
Medtr4g079770	-1580	cysteine protease (CP5)
Medtr4g079800	-1991; -1066; -381	cysteine protease (CP6)
Medtr4g080700	-1365; -1055	papain family cysteine protease
Medtr4g080730	-1674; -696	cysteine proteinase superfamily protein
Medtr4g091000	-1694; -753; -669; -189; -110	carbohydrate-binding module family 50 protein

[a]Genes which marked in bold are AMS-conserved genes.

TABLE 2 The location of CCAAT motifs extracted from 2 kbp upstream region of AMS marker genes included in this study.

Gene accession	Location of CCAAT motif	Gene annotation
Medtr1g105130	-427; -498; -1261; -1461	BCP1
Medtr3g072710	-209; -648	NSP2
Medtr5g026850	-775; -1771	IPD3
Medtr5g030910	-1480; -1551; -1595	STR2
Medtr6g027840	-171; -467; -590; -1215; -1446; -1807	Vapyrin
Medtr7g027190	-298; -815; -1214; -1289	RAM1
Medtr8g020840	-437; -633; -1171	NSP1
Medtr8g043970	-1517; -1542; -1565	DMI3
Medtr8g107450	-580	STR

Using yeast two-hybrid and BiFC assays, we identified MtNF-YB12 and B17 as the interacting partners of MtNF-YC6 and C11 (Figure 1). When expressing these proteins individually in *N. benthamiana* epidermal cells, we observed all the fluorescence signals both in the nucleus and cytoplasm (Supplementary Figures 3A, B). But co-expressing either one of the B subunits with MtNF-YC6 or C11 led to nuclear-dominant fluorescence signals (Supplementary Figures 3C, D). Unlike animal NF-YB, the subcellular localization of plant NF-YB subunits is variable. For example, *Arabidopsis* NF-YB2 is localized predominantly in the nucleus (Cai et al., 2007); AtNF-YB3 and AtNF-YB10 are in the cytoplasm (Liu and Howell, 2010; Hackenberg et al., 2012); while *Medicago* MtNF-YB16, rice OsNF-YB1 and OsNF-YB9 are both in the nucleus and cytoplasm (Baudin et al., 2015; E et al., 2018). Similarly, nuclear- and nucleocytoplasmic-localized NF-YCs were observed *in planta* (Hackenberg et al., 2012; Baudin et al., 2015; E et al., 2018). For cytoplasmic-localized B and C subunits of the NF-Y family, heterodimer formation usually results in the translocation of NF-YB/C heterodimers to the nucleus (Liu and Howell, 2010; Hackenberg et al., 2012; Baudin et al., 2015; E et al., 2018). In this study, we also observed the change of subcellular location from the cytoplasm to the nucleus when co-expressing MtNF-YC6/C11 either with MtNF-YB12 or MtNF-YB17. Meanwhile, no interaction was observed when co-expressing these two C subunits with MtNF-YB7 or MtNF-YB16 in the BiFC assay (Figure 1), implying the specificity of protein-protein interaction. However, the interaction specificity between B and C subunits in the NF-Y family remains subject to debate. Among all the NF-YB/C combinations in *Arabidopsis*, most of the possible interactions can be verified by yeast two-hybrid assays in Calvenzani et al. (2012), but only 31% of B/C heterodimerization can be observed in the study by Hackenberg et al. (2012). In the yeast two-hybrid system, the candidate genes are overexpressed in the cells which increases the possibility of protein-protein interaction. *In planta*, the dimerization depends on the abundance and the expression pattern of proteins. It has been shown that *MtNF-YC6* and *C11* were activated in arbuscule-containing cortical cells and adjacent cells (Hogekamp et al., 2011), and in this study, we observed the strong promoter activity of *MtNF-YB17* in the cortex of colonized root fragments (Figure 3), supporting that MtNF-YB17 might function with these two C subunits in colonized roots.

Among the four B subunits we chose for the protein-protein interaction test, the amino acid sequence identity between MtNF-YB12 and B17 is the highest (77%; Supplementary Table 4). Moreover, the phylogenetic analysis found that these two proteins were derived from the same legume-specific gene duplication events while MtNF-YB7 and MtNF-YB16 were in different subgroups (Laloum et al., 2013), implying that MtNF-YB12 and MtNF-YB17 might have similar functions. It has been shown that MtNF-YB16 forms heterotrimeric complexes with MtNF-YC1/C2 and MtNF-YA1/A2 to control nodule formation (Baudin et al., 2015) but the function of MtNF-YB7, B12, and B17 has not yet been characterized. Our study showed that only *MtNF-YB17* was upregulated in roots either inoculated with *R. irregularis* or *C. etunicatum* relative to mock-treated roots (Figure 2D), further supporting our speculation about the involvement of MtNF-YB17 in the control of AMS processes. Although *MtNF-YB12* did not respond to AMS at transcript level, we cannot exclude its role in symbiosis without examining the expression at the protein and tissue levels. In RNAi roots, the expression level of *MtNF-YB17* and *MtNF-YB12* was reduced to 1/5 and 1/2, respectively, relative to the empty vector control; however, neither AMF colonization efficiency nor the expression of AMS marker genes was affected (Supplementary Figure 6). The high expression level of *MtNF-YB16* in nodules and the interaction with NF-Y subunits involved in controlling nodule development supported its role in nitrogen-fixation symbiosis. But reducing its expression or even the other three close-related B subunits in roots did not affect symbiotic processes (Baudin et al., 2015). According to expression profiles shown in the *M. truncatula* gene atlas (Carrere et al., 2021), *MtNF-YB12* and *B17* are also expressed in other tissues and are induced by other kinds of treatments, while *MtNF-YC6* and *C11* are more specifically upregulated by AMS, implying that the B subunits might function in several physiological or developmental processes, and other B subunits might function redundantly to complement the partial loss of *MtNF-YB12* and *B17*. Our results suggest that, due to the functional redundancy and relatively low interaction specificity, it might not be enough to influence physiological processes by reducing the expression of one or a few close-related genes in the same family.

The transcripts and expression pattern of *MtNF-YC6*/*C11* are shown in this study and in Hogekamp et al. (2011) suggested their involvement in regulating all stages of AMS. Reducing their expression by RNAi decreased the frequency of AMF colonization, intensity of mycorrization and arbuscule abundance but the size distribution of arbuscule was not affected (Figures 4B, C). At molecular level, the expression of genes involved in arbuscule development was downregulated in RNAi roots coincided with the symbiotic phenotype. But the transcript levels of *DMI3* and *IPD3* which function in the initiation of cell redifferentiation and the induction of downstream symbiotic-related genes (Takeda et al., 2012; Takeda et al., 2015) were not changed by RNAi construct (Figures 4D, E). Hogekamp et al. (2011) concluded that MtNF-YC6 and C11 function at all AMS stages, but interestingly, in later symbiotic stages the promoter activities of *MtNF-YC6* and *C11* were restricted in cells containing arbuscules or adjacent cortical cells. In this study, the composite roots were harvested at later AMS stages. It is possible that MtNF-YC6 and C11 play more important roles in regulating gene expression in inner cortical cells rather than in epidermal cells, thus genes involved in early symbiotic signaling

was not significantly affected by RNAi construct. Previous studies showed that mutation at genes involved in controlling arbuscule development such as *RAM1*, *RAM2*, *STR* and *STR2* resulted in the reduction of colonization and the malformed arbuscules (Zhang et al., 2010; Gobbato et al., 2012; Wang et al., 2012; Delaux et al., 2013a; Gobbato et al., 2013; Hofferek et al., 2014; Park et al., 2015). Although these genes were significantly downregulated by *MtNF-YC6/C11* RNAi construct, the proteins which remain in the roots might still function properly to promote arbuscule development. Thus, we did not observe the significant change of size distribution of arbuscules (Figure 4C). Besides, the RNAi construct was designed to silence both genes simultaneously, but the level of reduction of these two genes was different between composite roots. Because of the potential of gene functional redundancy and linkage between two genes on chromosome 2, gene editing technique will be useful for generating double mutants for future functional studies.

In addition to genes involved in arbuscule development, transcripts of genes associated with arbuscule degeneration were also reduced in *MtNF-YC6/C11* RNAi roots. The knowledge is about the regulation of arbuscule degeneration is limited. Loss-of PT4 function or overexpressing *MYB1* enhanced hydrolase gene expression, resulting in premature arbuscule degeneration (Javot et al., 2007; Floss et al., 2017). In contrast, reducing *MYB1* transcripts only did not affect the arbuscular phenotype and the expression of AMS marker gene, *MtPT4*, and the fungal *α-tubulin* gene, but the transcript levels of hydrolase genes were significantly decreased (Floss et al., 2017), which was similar to what we observed in *MtNF-YC6/C11* RNAi roots. *In silico* analysis showed that *PT4*, *MYB1*, and hydrolase genes had at least one CCAAT-binding motif (Table 1). The downregulation of *MYB1*, *CP4/CP5*, *TGL*, *S1/P1* and chitinase genes in *MtNF-YC6/C11* RNAi roots (Figures 4F, 5) implied that NF-Y complexes might directly or indirectly regulate these genes at the transcript levels. Although no premature arbuscule degeneration was observed in *MtNF-YC6/C11* RNAi roots, considering the transcript levels of *MYB1* and hydrolase genes shown in this study and the phenotype of *myb1* single mutant as described by Floss et al. (2017), we speculated that MtNF-YC6/C11-containing protein complexes participated in regulating the transcriptional program of arbuscule degeneration. But we still cannot exclude the possibility that the downregulation of *MYB1* and hydrolase genes in RNAi roots was due to the decrease of AMF colonization and arbuscule richness. Further validation by chromatin immunoprecipitation and genetic studies may give more insights into the role of the NF-Y complex in the regulatory network of arbuscule degeneration.

In silico analysis showed that all the AMS marker genes and the potential target genes we examined in this study have at least one CCAAT motif, but the transcript levels of these genes were not always well-correlated to the expression of *MtNF-YC6/C11*. It is possible that *MtNF-YC6/C11*-containing protein complexes are not the key regulators of these genes, or the regulation by other factors compensates the role of NF-Ys in RNAi roots. Another possible reason is the variation of NF-Y binding affinity on different genes. It has been shown that the epigenetic markers on the CCAAT motifs, the distance between two motifs and the flanking sequences affect the NF-Y binding affinity *in vivo*. For example, methylation on the motifs interferes the formation of protein-DNA complex (Bi et al., 1997). The sequence logo analysis showed that C-A-G was moderately prevalent in the downstream of CCAAT motifs of validated target genes (Zambelli and Pavesi, 2017). Further investigation will be required to decipher the binding specificity and affinity of NF-Ys.

Another interesting thing is the responses of *MtNF-YA3*, *MtNF-YA4*, and *MtNF-YA8* to AMS. These A subunits were able to interact either with MtNF-YC6 or MtNF-YC11 in yeast, but the transcript levels of *MtNF-YA3* and *MtNF-YA4* were reduced by AMS while *MtNF-YA8* was not affected or upregulated by *C. etunicatum* symbiosis (Figure 2E). The expression level of *MtNF-YA8* was relatively low compared to *MtNF-YA3* and *A4*, and the response was the same as the data shown in the *M. truncatula* gene expression atlas (Supplementary Table 3). Transcriptomic analysis showed that *MtNF-YA8* was induced more than 4 folds at 48 h after rhizobium inoculation (Schiessl et al., 2019), suggesting that it might play a more important role in rhizobium-legume symbiosis than in AMS. The opposite expression pattern of *MtNF-YA3* and *A4* compared to *MtNF-YC6/C11* and *MtNF-YB17* implied that they might function differently during AMS. Arabidopsis NF-YB9 acts as an enhancer of hypocotyl elongation through physical association with PHYTOCROME-INTERACTING FACTOR 4 (PIF4) (Huang et al., 2015), while NF-YCs and NF-YAs function in the opposite. Intriguingly, overexpressing most *AtNF-YA*s led to shortened hypocotyl phenotype under continuous dark conditions, but the responses of these *AtNF-YA*s to dark treatment at the transcript level was different; some were increased while others were decreased or not affected (Myers et al., 2016). These results suggest that different NF-Y compositions might activate or silence physiological processes, and their roles do not always directly coincide with the transcriptional expression. In addition, several reports showed the interaction of NF-YB/NF-YC heterodimer with other transcription factors and the involvement of these heterotrimeric complexes in regulating downstream targets through other *cis*-acting elements (Yamamoto et al., 2009; Kumimoto et al., 2013). In these regulatory mechanisms, NF-YAs may act as a competitor to suppress the formation of trimeric complexes, interfering with the downstream transcriptional regulation (Adrian et al., 2010). In this study, we only examined the expression of three A subunits in response to AMS. Whether these genes play a positive or negative role in symbiosis will need to be addressed in further studies.

MtNF-YC6 and *MtNF-YC11* are AMS-induced genes. Interestingly, the induction level in roots inoculated with two

different AMF species was varied even though the colonization efficiency was similar (Figure 2C). We also observed the reduction of *MtNF-YA4* in *R. irregularis*-colonized roots but not in *C. etunicatum*-colonized roots and induction of *MtNF-YA8* only in *C. etunicatum*-colonized roots but not in *R. irregularis*-colonized roots (Figure 2E). By comparing the transcript level of AMS-responsive genes in the roots colonized by three different AMF species, Grunwald et al. (2009) found that among common AMS-regulated genes, only a few genes showed overlapping regulation patterns in different AMF-colonized roots, hinting that phylogenetic relationship of AMF species not only determines the fungal morphology and physiology but also affects molecular responses in host plants.

Conclusion

This study identified the interacting partners of MtNF-YC6 and MtNF-YC11 and potential downstream targets of NF-Y complexes during AMS. The AMF colonization phenotype and AMS marker gene expression demonstrate the involvement of these two genes in the regulation of arbuscule development. This information will help to build up the regulatory network of AMS in the future.

Data availability statement

The original contributions presented in the study are included in the article/Supplementary Materials. Further inquiries can be directed to the corresponding author.

Author contributions

CD and W-YL performed conceptualization and did methodology. CD, C-JL, C-YH, Y-AC and W-YL did validation and investigation. L-YDL and W-YL performed formal analysis. W-YL did data curation, prepared original draft preparation and contributed to writing—review and editing. W-YL did supervision and funding acquisition. All authors contributed to the article and approved the submitted version.

Funding

This research was funded by Ministry of Science and Technology, Taiwan (grant number most-108-2313-B-002-023-MY3) and College of Bioresources and Agriculture, NTU, Taiwan (grant number T111T6000009).

Acknowledgments

We thank Dr. Maria J. Harrison (Boyce Thompson Institute for Plant Research, USA), Dr. Tzyy-Jen Chiou (Academia Sinica, Taiwan) and Dr. Shu-Yi Yang (National Taiwan University, Taiwan) for kindly providing vectors. We thank Dr. Jui-Chang Huang (Tainan District Agricultural Research and Extension Station, Taiwan) for providing AMF inoculants, Dr. Chang-Lin Chen (National Chung Hsing University, Taiwan) for helping composite root generation, and Dr. Yu-Chang Tsai (National Taiwan University, Taiwan) for assistance in fluorescence light microscopy.

Conflict of interest

The authors declare that the research was conducted in the absence of any commercial or financial relationships that could be construed as a potential conflict of interest.

Publisher's note

All claims expressed in this article are solely those of the authors and do not necessarily represent those of their affiliated organizations, or those of the publisher, the editors and the reviewers. Any product that may be evaluated in this article, or claim that may be made by its manufacturer, is not guaranteed or endorsed by the publisher.

Supplementary material

The Supplementary Material for this article can be found online at: https://www.frontiersin.org/articles/10.3389/fpls.2022.976280/full#supplementary-material

References

Adrian, J., Farrona, S., Reimer, J. J., Albani, M. C., Coupland, G., and Turck, F. (2010). *Cis*-regulatory elements and chromatin state coordinately control temporal and spatial expression of *FLOWERING LOCUS t* in *Arabidopsis*. *Plant Cell* 22 (5), 1425–1440. doi: 10.1105/tpc.110.074682

Alexander, T., Meier, R., Toth, R., and Weber, H. C. (1988). Dynamics of arbuscule development and degeneration in mycorrhizas of *Triticum aestivum* l. and *Avena sativa* l. with reference to *Zea mays* l. *New Phytol.* 110 (3), 363–370. doi: 10.1111/j.1469-8137.1988.tb00273.x

Alexander, T., Toth, R., Meier, R., and Weber, H. C. (1989). Dynamics of arbuscule development and degeneration in onion, bean, and tomato with reference to vesicular–arbuscular mycorrhizae in grasses. *Can. J. Bot.* 67 (8), 2505–2513. doi: 10.1139/b89-320

Baudin, M., Laloum, T., Lepage, A., Ripodas, C., Ariel, F., Frances, L., et al. (2015). A phylogenetically conserved group of NF-y transcription factors interact to control nodulation in legumes. *Plant Physiol.* 169 (4), 2761–2773. doi: 10.1104/pp.15.01144

Bi, W. M., Wu, L., Coustry, F., deCrombrugghe, B., and Maity, S. N. (1997). DNA Binding specificity of the CCAAT-binding factor CBF/NF-y. *J. Biol. Chem.* 272 (42), 26562–26572. doi: 10.1074/jbc.272.42.26562

Boisson-Dernier, A., Chabaud, M., Garcia, F., Becard, G., Rosenberg, C., and Barker, D. G. (2001). Agrobacterium rhizogenes-transformed roots of *Medicago truncatula* for the study of nitrogen-fixing and endomycorrhizal symbiotic associations. *Mol. Plant Microbe Interact.* 14 (6), 695–700. doi: 10.1094/MPMI.2001.14.6.695

Bravo, A., York, T., Pumplin, N., Mueller, L. A., and Harrison, M. J. (2016). Genes conserved for arbuscular mycorrhizal symbiosis identified through phylogenomics. *Nat. Plants* 2, 15208. doi: 10.1038/nplants.2015.208

Breuillin-Sessoms, F., Floss, D. S., Gomez, S. K., Pumplin, N., Ding, Y., Levesque-Tremblay, V., et al. (2015). Suppression of arbuscule degeneration in *Medicago truncatula* phosphate transporter4 mutants is dependent on the ammonium transporter 2 family protein AMT2;3. *Plant Cell* 27 (4), 1352–1366. doi: 10.1105/tpc.114.131144

Cai, X. N., Ballif, J., Endo, S., Davis, E., Liang, M. X., Chen, D., et al. (2007). A putative CCAAT-binding transcription factor is a regulator of flowering timing in *Arabidopsis*. *Plant Physiol.* 145 (1), 98–105. doi: 10.1104/pp.107.102079

Calvenzani, V., Testoni, B., Gusmaroli, G., Lorenzo, M., Gnesutta, N., Petroni, K., et al. (2012). Interactions and CCAAT-binding of *Arabidopsis thaliana* NF-y subunits. *PloS One* 7 (8), e42902. doi: 10.1371/journal.pone.0042902

Carrere, S., Verdier, J., and Gamas, P. (2021). MtExpress, a comprehensive and curated RNAseq-based gene expression atlas for the model legume *Medicago truncatula*. *Plant Cell Physiol.* 62 (9), 1494–1500. doi: 10.1093/pcp/pcab110

Chen, N. Z., Zhang, X. Q., Wei, P. C., Chen, Q. J., Ren, F., Chen, J., et al. (2007). AtHAP3b plays a crucial role in the regulation of flowering time in *Arabidopsis* during osmotic stress. *J. Biochem. Mol. Biol.* 40 (6), 1083–1089. doi: 10.5483/bmbrep.2007.40.6.1083

Delaux, P. M., Becard, G., and Combier, J. P. (2013a). NSP1 is a component of the myc signaling pathway. *New Phytol.* 199 (1), 59–65. doi: 10.1111/nph.12340

Delaux, P. M., Sejalon-Delmas, N., Becard, G., and Ane, J. M. (2013b). Evolution of the plant-microbe symbiotic 'toolkit'. *Trends Plant Sci.* 18 (6), 298–304. doi: 10.1016/j.tplants.2013.01.008

Delaux, P. M., Varala, K., Edger, P. P., Coruzzi, G. M., Pires, J. C., and Ané, J. M. (2014). Comparative phylogenomics uncovers the impact of symbiotic associations on host genome evolution. *PloS Genet.* 10 (7), e1004487. doi: 10.1371/journal.pgen.1004487

E, Z. G., Li, T. T., Zhang, H. Y., Liu, Z. H., Deng, H., Sharma, S., et al. (2018). A group of nuclear factor y transcription factors are sub-functionalized during endosperm development in monocots. *J. Exp. Bot.* 69 (10), 2495–2510. doi: 10.1093/jxb/ery087

Favre, P., Bapaume, L., Bossolini, E., Delorenzi, M., Falquet, L., and Reinhardt, D. (2014). A novel bioinformatics pipeline to discover genes related to arbuscular mycorrhizal symbiosis based on their evolutionary conservation pattern among higher plants. *BMC Plant Biol.* 14 (1), 333. doi: 10.1186/s12870-014-0333-0

Floss, D. S., Gomez, S. K., Park, H. J., MacLean, A. M., Muller, L. M., Bhattarai, K. K., et al. (2017). A transcriptional program for arbuscule degeneration during AM symbiosis is regulated by MYB1. *Curr. Biol.* 27 (8), 1206–1212. doi: 10.1016/j.cub.2017.03.003

Floss, D. S., Levesque-Tremblay, V., Park, H. J., and Harrison, M. J. (2016). DELLA proteins regulate expression of a subset of AM symbiosis-induced genes in *Medicago truncatula*. *Plant Signal Behav.* 11 (4), e1162369. doi: 10.1080/15592324.2016.1162369

Gobbato, E., Marsh, J. F., Vernie, T., Wang, E., Maillet, F., Kim, J., et al. (2012). A GRAS-type transcription factor with a specific function in mycorrhizal signaling. *Curr. Biol.* 22 (23), 2236–2241. doi: 10.1016/j.cub.2012.09.044

Gobbato, E., Wang, E., Higgins, G., Bano, S. A., Henry, C., Schultze, M., et al. (2013). *RAM1* and *RAM2* function and expression during arbuscular mycorrhizal symbiosis and *Aphanomyces euteiches* colonization. *Plant Signal Behav.* 8 (10), e26049. doi: 10.4161/psb.26049

Grefen, C., Donald, N., Hashimoto, K., Kudla, J., Schumacher, K., and Blatt, M. R. (2010). A ubiquitin-10 promoter-based vector set for fluorescent protein tagging facilitates temporal stability and native protein distribution in transient and stable expression studies. *Plant J.* 64 (2), 355–365. doi: 10.1111/j.1365-313X.2010.04322.x

Grunwald, U., Guo, W., Fischer, K., Isayenkov, S., Ludwig-Muller, J., Hause, B., et al. (2009). Overlapping expression patterns and differential transcript levels of phosphate transporter genes in arbuscular mycorrhizal, pi-fertilised and phytohormone-treated *Medicago truncatula* roots. *Planta* 229 (5), 1023–1034. doi: 10.1007/s00425-008-0877-z

Hackenberg, D., Wu, Y., Voigt, A., Adams, R., Schramm, P., and Grimm, B. (2012). Studies on differential nuclear translocation mechanism and assembly of the three subunits of the *Arabidopsis thaliana* transcription factor NF-y. *Mol. Plant* 5 (4), 876–888. doi: 10.1093/mp/ssr107

Harrison, M. J., Dewbre, G. R., and Liu, J. Y. (2002). A phosphate transporter from *Medicago truncatula* involved in the acquisiton of phosphate released by arbuscular mycorrhizal fungi. *Plant Cell* 14 (10), 2413–2429. doi: 10.1105/tpc.004861

He, J., Benedito, V. A., Wang, M. Y., Murray, J. D., Zhao, P. X., Tang, Y. H., et al. (2009). The *Medicago truncatula* gene expression atlas web server. *BMC Bioinform.* 10, 441. doi: 10.1186/1471-2105-10-441

Hofferek, V., Mendrinna, A., Gaude, N., Krajinski, F., and Devers, E. A. (2014). MiR171h restricts root symbioses and shows like its target NSP2 a complex transcriptional regulation in *Medicago truncatula*. *BMC Plant Biol.* 14, 199. doi: 10.1186/s12870-014-0199-1

Hogekamp, C., Arndt, D., Pereira, P. A., Becker, J. D., Hohnjec, N., and Kuster, H. (2011). Laser microdissection unravels cell-type-specific transcription in arbuscular mycorrhizal roots, including CAAT-box transcription factor gene expression correlating with fungal contact and spread. *Plant Physiol.* 157 (4), 2023–2043. doi: 10.1104/pp.111.186635

Horváth, B., Yeun, L. H., Domonkos, A., Halasz, G., Gobbato, E., Ayaydin, F., et al. (2011). *Medicago truncatula* IPD3 is a member of the common symbiotic signaling pathway required for rhizobial and mycorrhizal symbioses. *Mol. Plant Microbe Interact.* 24 (11), 1345–1358. doi: 10.1094/Mpmi-01-11-0015

Huang, M. K., Hu, Y. L., Liu, X., Li, Y. G., and Hou, X. L. (2015). Arabidopsis LEAFY COTYLEDON1 mediates postembryonic development *via* interacting with PHYTOCHROME-INTERACTING FACTOR4. *Plant Cell* 27 (11), 3099–3111. doi: 10.1105/tpc.15.00750

Javot, H., Penmetsa, R. V., Terzaghi, N., Cook, D. R., and Harrison, M. J. (2007). A *Medicago truncatula* phosphate transporter indispensable for the arbuscular mycorrhizal symbiosis. *Proc. Natl. Acad. Sci. U.S.A.* 104 (5), 1720–1725. doi: 10.1073/pnas.0608136104

Karimi, M., Inze, D., and Depicker, A. (2002). GATEWAY vectors for *Agrobacterium*-mediated plant transformation. *Trends Plant Sci.* 7 (5), 193–195. doi: 10.1016/s1360-1385(02)02251-3

Kim, I. S., Sinha, S., deCrombrugghe, B., and Maity, S. N. (1996). Determination of functional domains in the c subunit of the CCAAT-binding factor (CBF) necessary for formation of a CBF-DNA complex: CBF-b interacts simultaneously with both the CBF-a and CBF-c subunits to form a heterotrimeric CBF molecule. *Mol. Cell Biol.* 16 (8), 4003–4013. doi: 10.1128/MCB.16.8.4003

Kumimoto, R. W., Siriwardana, C. L., Gayler, K. K., Risinger, J. R., Siefers, N., and Holt, B. F. (2013). NUCLEAR FACTOR y transcription factors have both opposing and additive roles in ABA-mediated seed germination. *PloS One* 8 (3), e59481. doi: 10.1371/journal.pone.0059481

Laloum, T., Baudin, M., Frances, L., Lepage, A., Billault-Penneteau, B., Cerri, M. R., et al. (2014). Two CCAAT-box-binding transcription factors redundantly regulate early steps of the legume-rhizobia endosymbiosis. *Plant J.* 79 (5), 757–768. doi: 10.1111/tpj.12587

Laloum, T., De Mita, S., Gamas, P., Baudin, M., and Niebel, A. (2013). CCAAT-box binding transcription factors in plants: Y so many? *Trends Plant Sci.* 18 (3), 157–166. doi: 10.1016/j.tplants.2012.07.004

Laporte, P., Lepage, A., Fournier, J., Catrice, O., Moreau, S., Jardinaud, M. F., et al. (2014). The CCAAT box-binding transcription factor NF-YA1 controls rhizobial infection. *J. Exp. Bot.* 65 (2), 481–494. doi: 10.1093/jxb/ert392

Liu, J. X., and Howell, S. H. (2010). bZIP28 and NF-y transcription factors are activated by ER stress and assemble into a transcriptional complex to regulate stress response genes in *Arabidopsis*. *Plant Cell* 22 (3), 782–796. doi: 10.1105/tpc.109.072173

Liu, T. Y., Huang, T. K., Tseng, C. Y., Lai, Y. S., Lin, S. I., Lin, W. Y., et al. (2012). PHO2-dependent degradation of PHO1 modulates phosphate homeostasis in *Arabidopsis*. *Plant Cell* 24 (5), 2168–2183. doi: 10.1105/tpc.112.096636

Mcgonigle, T. P., Miller, M. H., Evans, D. G., Fairchild, G. L., and Swan, J. A. (1990). A new method that gives an objective measure of colonization of roots by vesicular-arbuscular mycorrhizal fungi. *New Phytol.* 115 (3), 495–501. doi: 10.1111/j.1469-8137.1990.tb00476.x

Miller, J. B., Pratap, A., Miyahara, A., Zhou, L., Bornemann, S., Morris, R. J., et al. (2013). Calcium/calmodulin-dependent protein kinase is negatively and positively regulated by calcium, providing a mechanism for decoding calcium responses during symbiosis signaling. *Plant Cell* 25 (12), 5053–5066. doi: 10.1105/tpc.113.116921

Murray, J. D., Muni, R. R. D., Torres-Jerez, I., Tang, Y. H., Allen, S., Andriankaja, M., et al. (2011). Vapyrin, a gene essential for intracellular progression of arbuscular mycorrhizal symbiosis, is also essential for infection by rhizobia in the nodule symbiosis of *Medicago truncatula*. *Plant J.* 65 (2), 244–252. doi: 10.1111/j.1365-313X.2010.04415.x

Myers, Z. A., Kumimoto, R. W., Siriwardana, C. L., Gayler, K. K., Risinger, J. R., Pezzetta, D., et al. (2016). NUCLEAR FACTOR y, subunit c (NF-YC) transcription factors are positive regulators of photomorphogenesis in *Arabidopsis thaliana*. *PloS Genet.* 12 (9), e1006333. doi: 10.1371/journal.pgen.1006333

Nelson, D. E., Repetti, P. P., Adams, T. R., Creelman, R. A., Wu, J., Warner, D. C., et al. (2007). Plant nuclear factor y (NF-y) b subunits confer drought tolerance and lead to improved corn yields on water-limited acres. *Proc. Natl. Acad. Sci. U.S.A.* 104 (42), 16450–16455. doi: 10.1073/pnas.0707193104

Park, H. J., Floss, D. S., Levesque-Tremblay, V., Bravo, A., and Harrison, M. J. (2015). Hyphal branching during arbuscule development requires *Reduced arbuscular Mycorrhiza1*. *Plant Physiol.* 169 (4), 2774–2788. doi: 10.1104/pp.15.01155

Petroni, K., Kumimoto, R. W., Gnesutta, N., Calvenzani, V., Fornari, M., Tonelli, C., et al. (2012). The promiscuous life of plant NUCLEAR FACTOR y transcription factors. *Plant Cell* 24 (12), 4777–4792. doi: 10.1105/tpc.112.105734

Pimprikar, P., Carbonnel, S., Paries, M., Katzer, K., Klingl, V., Bohmer, M. J., et al. (2016). A CCaMK-CYCLOPS-DELLA complex activates transcription of *RAM1* to regulate arbuscule branching. *Curr. Biol.* 26 (8), 987–998. doi: 10.1016/j.cub.2016.01.069

Pumplin, N., and Harrison, M. J. (2009). Live-cell imaging reveals periarbuscular membrane domains and organelle location in *Medicago truncatula* roots during arbuscular mycorrhizal symbiosis. *Plant Physiol.* 151 (2), 809–819. doi: 10.1104/pp.109.141879

Pumplin, N., Mondo, S. J., Topp, S., Starker, C. G., Gantt, J. S., and Harrison, M. J. (2010). *Medicago truncatula* vapyrin is a novel protein required for arbuscular mycorrhizal symbiosis. *Plant J.* 61 (3), 482–494. doi: 10.1111/j.1365-313X.2009.04072.x

Qu, B., He, X., Wang, J., Zhao, Y., Teng, W., Shao, A., et al. (2015). A wheat CCAAT box-binding transcription factor increases the grain yield of wheat with less fertilizer input. *Plant Physiol.* 167 (2), 411–423. doi: 10.1104/pp.114.246959

Remy, W., Taylor, T. N., Hass, H., and Kerp, H. (1994). Four hundred-million-year-old vesicular arbuscular mycorrhizae. *Proc. Natl. Acad. Sci. U.S.A.* 91 (25), 11841–11843. doi: 10.1073/pnas.91.25.11841

Ripodas, C., Clua, J., Battaglia, M., Baudin, M., Niebel, A., Zanetti, M. E., et al. (2014). Transcriptional regulators of legume-rhizobia symbiosis: nuclear factors ys and GRAS are two for tango. *Plant Signal Behav.* 9 (5), e28847. doi: 10.4161/psb.28847

Romier, C., Cocchiarella, F., Mantovani, R., and Moras, D. (2003). The NF-YB/NF-YC structure gives insight into DNA binding and transcription regulation by CCAAT factor NF-y. *J. Biol. Chem.* 278 (2), 1336–1345. doi: 10.1074/jbc.M209635200

Roth, R., and Paszkowski, U. (2017). Plant carbon nourishment of arbuscular mycorrhizal fungi. *Curr. Opi Plant Biol.* 39, 50–56. doi: 10.1016/j.pbi.2017.05.008

Schaarschmidt, S., Gresshoff, P. M., and Hause, B. (2013). Analyzing the soybean transcriptome during autoregulation of mycorrhization identifies the transcription factors GmNF-YA1a/b as positive regulators of arbuscular mycorrhization. *Genome Biol.* 14 (6), R62. doi: 10.1186/gb-2013-14-6-r62

Schiessl, K., Lilley, J. L. S., Lee, T., Tamvakis, I., Kohlen, W., Bailey, P. C., et al. (2019). *NODULE INCEPTION* recruits the lateral root developmental program for symbiotic nodule organogenesis in *Medicago truncatula*. *Curr. Biol.* 29 (21), 3657–3668. doi: 10.1016/j.cub.2019.09.005

Smith, S. E., and Read, D. (2008). ""INTRODUCTION," in *Mycorrhizal symbiosis*, *3rd ed*. Eds. S. E. Smith and D. Read (London: Academic Press), 1–9.

Takeda, N., Handa, Y., Tsuzuki, S., Kojima, M., Sakakibara, H., and Kawaguchi, M. (2015). Gibberellins interfere with symbiosis signaling and gene expression and alter colonization by arbuscular mycorrhizal fungi in *Lotus japonicus*. *Plant Physiol.* 167 (2), 545–557. doi: 10.1104/pp.114.247700

Takeda, N., Maekawa, T., and Hayashi, M. (2012). Nuclear-localized and deregulated calcium- and calmodulin-dependent protein kinase activates rhizobial and mycorrhizal responses in *Lotus japonicus*. *Plant Cell* 24 (2), 810–822. doi: 10.1105/tpc.111.091827

Tang, H. B., Krishnakumar, V., Bidwell, S., Rosen, B., Chan, A. N., Zhou, S. G., et al. (2014). An improved genome release (version Mt4.0) for the model legume *Medicago truncatula*. *BMC Genomics* 15, 312. doi: 10.1186/1471-2164-15-312

Trouvelot, A., Kough, J. L., and Gianinazzi-Pearson, V. (1986). ""Measurement of VA mycorrhizal rate of a root system estimation methods research with functional significance,"," in *Physiological and genetical aspects of mycorrhizae* (Paris, France: INRA), 217–221.

Wang, E. T., Schornack, S., Marsh, J. F., Gobbato, E., Schwessinger, B., Eastmond, P., et al. (2012). A common signaling process that promotes mycorrhizal and oomycete colonization of plants. *Curr. Biol.* 22 (23), 2242–2246. doi: 10.1016/j.cub.2012.09.043

Yamamoto, A., Kagaya, Y., Toyoshima, R., Kagaya, M., Takeda, S., and Hattori, T. (2009). Arabidopsis NF-YB subunits LEC1 and LEC1-LIKE activate transcription by interacting with seed-specific ABRE-binding factors. *Plant J.* 58 (5), 843–856. doi: 10.1111/j.1365-313X.2009.03817.x

Yano, K., Yoshida, S., Muller, J., Singh, S., Banba, M., Vickers, K., et al. (2008). CYCLOPS, a mediator of symbiotic intracellular accommodation. *Proc. Natl. Acad. Sci. U.S.A.* 105 (51), 20540–20545. doi: 10.1073/pnas.0806858105

Zambelli, F., and Pavesi, G. (2017). Genome wide features, distribution and correlations of NF-y binding sites. *Biochim. Biophys. Acta Gene Regul. Mech.* 1860 (5), 581–589. doi: 10.1016/j.bbagrm.2016.10.007

Zhang, Q., Blaylock, L. A., and Harrison, M. J. (2010). Two *Medicago truncatula* half-ABC transporters are essential for arbuscule development in arbuscular mycorrhizal symbiosis. *Plant Cell* 22 (5), 1483–1497. doi: 10.1105/tpc.110.074955

Zhao, H., Wu, D., Kong, F., Lin, K., Zhang, H., and Li, G. (2016). The *Arabidopsis thaliana* nuclear factor y transcription factors. *Front. Plant Sci.* 7. doi: 10.3389/fpls.2016.02045

frontiers | Frontiers in Plant Science

TYPE Original Research
PUBLISHED 21 November 2022
DOI 10.3389/fpls.2022.1027618

OPEN ACCESS

EDITED BY
Stefania Astolfi,
University of Tuscia, Italy

REVIEWED BY
Mohamed Ait El Mokhtar,
Université Hassan II Mohammedia, Morocco
Corina Carranca,
Instituto Nacional Investigaciao Agraria e Veterinaria (INIAV), Portugal

*CORRESPONDENCE
Vesna Dragičević
vdragicevic@mrizp.rs

†These authors have contributed equally to this work

SPECIALTY SECTION
This article was submitted to Plant Nutrition, a section of the journal Frontiers in Plant Science

RECEIVED 25 August 2022
ACCEPTED 02 November 2022
PUBLISHED 21 November 2022

CITATION
Dragičević V, Brankov M, Stoiljković M, Tolimir M, Kanatas P, Travlos I and Simić M (2022) Kernel color and fertilization as factors of enhanced maize quality. *Front. Plant Sci.* 13:1027618. doi: 10.3389/fpls.2022.1027618

Kernel color and fertilization as factors of enhanced maize quality

Vesna Dragičević[1*†], Milan Brankov[1†], Milovan Stoiljković[2], Miodrag Tolimir[1], Panagiotis Kanatas[3], Ilias Travlos[4] and Milena Simić[1†]

[1]Group for Agro-ecology and Cropping Practices, Department for Breeding, Maize Research Institute "Zemun Polje", Belgrade, Serbia, [2]Laboratory of Physical Chemistry, Vinča Institute of Nuclear Sciences, Belgrade, Serbia, [3]Department of Crop Science, University of Patras, Patras, Greece, [4]Laboratory of Agronomy, Agricultural University of Athens, Athens, Greece

Maize is an important staple crop and a significant source of various nutrients. We aimed to determine the macronutrients, antioxidants, and essential elements in maize genotypes (white, yellow, and red kernel) using three different fertilizers, which could be used as a basis to increase the nutrient density of maize. The fertilizer treatments used bio- and organic fertilizers as a sustainable approach, urea, as a commonly used mineral fertilizer, and the control (no fertilization). We evaluated the yield, concentration of macronutrient (protein, oil, and starch), nonenzymatic antioxidants (phenolics, yellow pigment, total glutathione (GSH), and phytic phosphorus), and reduction capacity of the 2,2-diphenyl-1-picrylhydrazyl (DPPH) radical, as well as essential elements that are commonly deficient in the diet (Mg, Ca, Fe, Mn, Zn, Cu, and S) and their relationships with phytic acid. The genotype expressed the strongest effect on the variability of grain yield and the analyzed grain constituents. The red-kernel hybrid showed the greatest accumulation of protein, oil, phenolics, and essential elements (Ca, Fe, Cu, and S) than a yellow and white hybrid, especially in the biofertilizer treatment. The yellow kernel had the highest concentrations of yellow pigment, GSH, phytic phosphorous, Mg, Mn, and Zn (19.61 μg g^{-1}, 1,134 nmol g^{-1}, 2.63 mg g^{-1}, 1,963 μg g^{-1}, 11.7 μg g^{-1}, and 33.9 μg g^{-1}, respectively). The white kernel had a greater starch concentration (2.5% higher than that in the red hybrid) and the potential bioavailability of essential metals, particularly under no fertilization. This supports the significance of white maize as a staple food in many traditional diets across the world. Urea was important for the enhancement of the antioxidant status (with 88.0% reduction capacity for the DPPH radical) and increased potential Zn bioavailability in the maize kernels (13.3% higher than that in the biofertilizer treatment). This study underlines the differences in the yield potential and chemical composition of red, yellow, and white-kernel maize and their importance as a necessary part of a sustainable human diet. This information can help determine the most appropriate genotype based on the antioxidants and/or essential elements targeted for kernel improvement.

KEYWORDS

bio-fertilizer, organic fertilizer, kernel composition, essential elements, antioxidants, potential bio-availability, yield

Introduction

Maize (*Zea mays* L.) is an important crop and a staple food worldwide. It is a source of many phytonutrients, mainly carbohydrates, as well as highly valuable proteins, oils, mineral nutrients, vitamins, secondary metabolites, phenolic compounds, and phytosterols. Zein, as the main protein in maize kernels, has significant applications in pharmacy and nutraceuticals, and resistant starch confers health benefits that may reduce the risk of some cancers, atherosclerosis, and metabolic syndrome (Sha et al., 2016). It is also important to emphasize that maize kernels are gluten-free and have a low glycemic index; thus, they could be included in various diets (Giuberti et al., 2015). While breeding was mainly focused on the yield potential rather than the chemical composition of the maize kernels, current trends in sustainable nutrition have improved the nutrient density of food. Because genotypes high in protein and antioxidants are low in yield (Mahan et al., 2013), maintaining a balance between yield potential and quality could become an important trait in the future.

Owing to the increased popularity of secondary metabolites and their antioxidant properties, genotypes with various kernel colorations, ranging from intense yellow to red, purple, or even blue and black, have received considerable attention (Žilić et al., 2012; Sha et al., 2016; Suriano et al., 2021); this explains the high antioxidant activity of maize flour than wheat flour (Nikolić et al., 2019). Nevertheless, in some regions, the white kernel is mainly used for human nutrition. The synthesis of antioxidants is primarily driven by environmental factors and genotype × environment interactions; thus, stressful conditions could increase the concentration of antioxidants, such as glutathione, phenolics, yellow pigment, and phytic acid (Phy), in the crop's vegetative parts and grains (Brankovic et al., 2015; Dragičević et al., 2017; Saini and Keum, 2018).

Because a majority of soils are depleted and lack several essential elements, the deficiency of these nutrients (mainly Fe, Zn, I, and vitamin A) has resulted in the prevalence of "hidden hunger" worldwide. Addressing the need for nutrient-dense food requires strategies that improve food quality and benefit developing and developed countries (Lowe, 2021; FAO, 2022). Soils should receive significant attention as the nutrients in food originate here and as a resource with a limited or depleted nutrient budget. Therefore, the production system should integrate different practices, such as biofortification, which affect the mineral balance of the plants (Sofo et al., 2016). Fertilizers, such as organic fertilizers that are rich in various nutrients (in highly or less accessible forms) and biofertilizers, can enrich the soil with organic matter, promote soil microbiota, restore soil fertility, and increase crop fitness and growth. Roychowdhury et al. (2017) and Mishra et al. (2012) considered biofertilizers to be one of the best modern tools as an alternative to mineral fertilizers, with a beneficial impact on the environment and fulfilling the optimal supply of nutrients (P, Ca, Cu, and Zn) to the crops. Crop–microbiota relations are dynamic and depend on various factors. The diversity and number of rhizosphere microbiota are highly dependent on the crop phenophase and the type and amount of fertilizer used (Vollú et al., 2018). Furthermore, nutrient absorption and remobilization are highly dependent on the genotype (Ray et al., 2020), which should also be considered when nutrient-dense yields are the goal.

Although grain enrichment with essential elements has been targeted in previous studies, the factors that promote or reduce their bioavailability in the digestive organs of humans and monogastric animals must also be considered. In this context, phytic acid is the chief antinutrient. It is primarily a phosphorus reserve in seeds and grains, with the ability to bind minerals, proteins, and starch, limiting their bioavailability. However, its benefits are reflected in its high antioxidant activity, preventing lipid peroxidation and, thus, preserving food by preventing it from changing color and spoiling (Feizollahi et al., 2021). It can also reduce the risk of certain cancers, support heart health, and manage renal stones. It was ascertained that an increase in the phytic acid concentration in plants is also related to climate change, i.e., the atmospheric CO_2 rise, which additionally decreases the accessibility of mineral elements (Chaturvedi et al., 2017; Perera et al., 2018). Therefore, to increase the bioavailability of essential elements, it is important to determine their distribution in grains and seeds and their ratio with phytic acid (Johnson et al., 2013; Wang et al., 2015). For example, P, K, Ca, and Fe are mainly present in the rice aleurone; Zn is distributed from the aleurone to the inner endosperm, and Cu is mainly located in the inner endosperm and is not associated with P (Iwai et al., 2012).

The nutritional quality of the maize grain, especially for genotypes with different kernel colors, was narrowly described, with no data regarding essential elements and factors that promote/reduce their potential bioavailability. Consequently, this study aimed to determine the macronutrients, antioxidants, and essential elements in three different maize genotypes (white, yellow, and red) under the influence of three types of fertilizer treatments, which could be used as a basis for increasing the nutrient density of maize. The fertilization practices included sustainable fertilizers, bio- and organic fertilizers, and urea, as a commonly used mineral fertilizer. The effects of the treatments were determined by evaluating yield, macronutrients (protein, oil, and starch), various nonenzymatic antioxidants (phenolics, yellow pigment, total glutathione, phytic phosphorus, and the reduction capacity of the 1,1-diphenyl-2-picrylhydrazyl (DPPH) radical), and essential elements that are commonly deficient (Mg, Ca, Fe, Mn, Zn, Cu, and S) and their relations with phytic acid, including the potential bioavailability.

Material and methods

Trial settings and soil properties

The experiment was conducted during the maize vegetative period in 2018–2020 under dry farming conditions in Zemun Polje, Serbia (44° 52′ N, 20° 20′ E). The soil was slightly calcareous chernozem, containing 53.0% sand, 30.0% silt, and 17.0% clay. The preceding crop was always winter wheat (*Triticum vulgare* L.). Each year, at the beginning of April, the soil was sampled, and the chemical composition, including the pH, soil organic matter content (SOM), and contents of the available elements, were determined (Table 1). The variations in the contents of the mineral elements were slight and could be owing to the soil conditions of the experimental area, the previous crop, and/or the meteorological conditions and variability in the growing conditions.

The experimental trial included maize hybrids with different kernel colors: red (ZP 5048*c*), white (ZP 522*b*), and intense yellow (ZP 737). The sowing was performed in the spring (last week of April) in all 3 years. Together with seed-bed preparation (2–3 days before sowing), the fertilizer treatments were applied and incorporated into the soil according to the manufacturer's recommendations: biofertilizer (BF; Team Micorriza Plus), 3 kg ha^{-1} (0.5 kg 100 L^{-1} water); organic fertilizer (OF; Fertor), 2.5 t ha^{-1}; mineral fertilizer (urea; 46% N), 200 kg ha^{-1}; and control (Con; no fertilization). Team Micorriza Plus is an inoculum in powder form that contains the arbuscular mycorrhizal fungi *Rhizophagus intraradices* (150 spores g^{-1}) and *Glomus mosseae* (150 spores g^{-1}) and rhizosphere bacteria (1×10^7 UFC g^{-1}) with 56% organic matter content. It improves plant nutrient absorption, increases the crop's tolerance to abiotic and biotic stresses, and maintains soil fertility. Fertor is a fertilizer in pellet form, produced from chicken manure and plant-based organic matter. It contains NPK (4.5:2.7:2.3) + 1.1% Mg + 9.3% Ca and other macro- and micronutrients, which are partly soluble and available to plants, whereas insoluble parts enable the continual release of nutrients during vegetation. Standard cropping practices were applied, according to the manufacturer's requirements. Both fertilizers, Team Micorriza Plus and Fertor, are permitted for use in organic agriculture. After harvest (during the second half of October), the maize grain yield was measured and calculated at 14% moisture, and the grains were used for further analyses.

Chemical analyses

The concentrations of protein, oil, and starch in the maize kernels were determined using a near-infrared analyzer (Infraneo, Chopin, France) and were presented as a percentage. The kernel samples (100 g) were milled on the Perten 120 (Perten, Stockholm, Sweden; particle size < 500 μm). The antioxidants, such as phytic phosphorus (Pphy) and total glutathione (GSH), were determined after extraction with 5% trichloroacetic acid. The extract was centrifuged at 12,000 rpm for 15 min (Model Velocity 18R Versatile Centrifuge, Rotor TA15-24-2; Dynamica Scientific, Livingston, UK) at 4°C, and the absorbance was measured using a spectrophotometer (Biochrom Libra S22 UV/Vis Spectrophotometer, Biochrom, Cambridge, UK). The Pphy concentration was determined using the method described by Dragičević et al. (2011), which is based on the pink color formed upon the reaction between ferric ion and sulfosalicylic acid from the Wade reagent; the absorbance was measured at λ = 500 nm. The GSH was determined using the method proposed by Sari-Gorla et al. (1993), by adding 0.2 M potassium phosphate buffer (pH = 8.0) and 10 mM 5.5′-dithio (2-nitrobenzoic acid) to the extract and measuring the absorbance at 415 nm.

Water-soluble phenolics were determined after extraction with double-distilled water and centrifugation at 12,000 rpm for 15 min, using the method proposed by Simić et al. (2004). After adding 0.05M $FeCl_3$ in 0.1 M HCl and 0.008 M $K_3Fe(CN)_6$ to the sample solution, the absorbance was measured at λ = 722 nm, and the concentration of phenolics was expressed in micrograms of ferulic acid equivalent. The yellow pigment (YP) was determined using the method proposed by Vancetovic et al. (2014) after extraction with 1-butanol and centrifugation at 10,000 rpm for 5 min; the absorbance was measured at λ = 436 nm and expressed in micrograms of β-carotene per gram.

The scavenging activity, i.e., the reduction capacity of free radicals, was determined using the method suggested by Abe et al. (1998). After extraction with 70% acetone, the difference between the blank and the sample containing the added DPPH

TABLE 1 The soil composition, including soil organic matter (SOM) content and available forms of mineral elements.

	N	pH	SOM	P	K	Mg	Ca	Fe	Mn	Zn	Cu	S
	kg ha^{-1}		%	kg ha^{-1}				mg kg^{-1}				
Depth (cm)	0–90						0–30					
2018	166.4	7.17	2.82	57.9	158.2	385.2	736.4	21.98	23.5	3.86	3.31	451.54
2019	153.9	7.19	2.88	60.5	160.2	394.75	695.0	18.83	17.4	4.32	4.65	448.49
2020	167.5	7.16	3.13	61.2	162.1	342.08	732.39	24.64	18.54	5.42	4.61	448.87

radical was measured, and the reduction capacity was displayed as the percentage of DPPH reduction capacity. The concentrations of the essential elements Mg, Ca, Fe, Mn, Zn, Cu, and S were determined after wet digestion with an $HClO_4$ + HNO_3 mixture, using inductively coupled plasma-optical emission spectrometry (Spectroflame, 27.12 MHz and 2.5 kW, model P, Spectro Analytical Instruments, Kleve, Germany).

Meteorological conditions

Each experimental season in 2018–2020 was characterized by an optimal total precipitation amount (Table 2), ranging from 327.7 (2020) to 366.0 mm (2019). However, the distribution was unequal, with lower values in April and September of 2018 and 2020 (the minimum value was achieved in April 2020, with only 4.7 mm precipitation). Similarly, a low precipitation amount occurred in August–September 2019. With respect to temperature fluctuations, 2018 had the highest temperature on average. The highest values mainly occurred in August in all 3 years, and the highest value was 25.9°C in 2019.

Statistical analyses

The data were processed using an analysis of variance (*F*-test), with a significance level of $p < 0.05$. Moreover, a correlation analysis (Pearson's coefficients) included the correlation between the GY and analyzed elements (Mg, Ca, Fe, Mn, Zn, Cu, and S) and between the DPPH reduction capacity and concentration of the analyzed antioxidants (Pphy, GSH, phenolics, and YP), at $p < 0.05$. The results for the element removal with yield and the relation between Phy and the essential metals were presented as a mean ± standard error. Furthermore, the interdependence between the applied treatments and genotypes with respect to the kernel chemical composition was analyzed using a principal component analysis (PCA) as a dimensionality-reduction method, and the analysis was performed using SPSS for Windows Version 15.0 (SPSS, 2006).

Results

Impact of the year, fertilization treatments, and kernel color on the variation in the yield and chemical composition of the maize kernels

The sources, such as the year, fertilizer, genotype, and their interaction, exhibited a significant impact on the variability of the tested parameters (Table 3). In 2018, the highest average levels of GY and oil concentration were recorded (17.5% and 0.17%, respectively, greater compared to the levels in 2020), as well as Pphy, DPPH reduction capacity, GSH, Mn, and Zn (5.8%, 4.1%, 7.4%, 10.0%, and 27.6%, respectively, higher compared to the levels in 2019); protein, phenolics, YP, Ca, and Cu had the greatest values in 2020 (to 0.74%, 12.2%, 33.8%, 57.5%, and 55.9%, respectively, greater compared to the values in2018), as well as Fe and S (to 20.9% and 12.3%, respectively, compared to values in 2020). With regard to the fertilizer treatments, the highest average values for GY, Fe, and Zn were achieved in the BF treatment (2.4%, 40.0%, and 12.9% respectively, greater than those for the control); the greatest accumulation of protein, oil, Mg, Ca, Mn, Cu, and S occurred in the OF treatment (to 0.38%, 0.17%, 8.5%, 25.6%, 12.8%, 31.7%, and 12.4% respectively, greater than control); and the highest values for Pphy, phenolics, GSH, and DPPH were in the urea treatment (to 1.8%, 8.0%, 23.4%, and 0.5%, respectively, greater than for control). The control only showed an increase in the average starch and YP values.

The year did not significantly affect the variation in the starch concentration in the maize grain, and the fertilizer did not significantly affect the variation in the concentrations of the oil, Pphy, phenolics, YP, and DPPH. The genotype effect was insignificant in terms of the variation in the concentrations of Ca and Cu and the year × fertilizer interaction for the variation in the oil and starch concentration. The results indicate that white-kernel maize had a higher starch concentration on average (71.9%), whereas yellow kernel had the greatest average values for Pphy, YP, GSH, Mg, Mn, and Zn (2.63 mg g^{-1}, 19.61 μg g^{-1},

TABLE 2 The mean temperature (°C) and precipitation sum (mm) at Zemun Polje during the maize growing period in 2018–2020.

Months	Average temperature (°C)			Precipitation sum (mm)		
	2018	2019	2020	2018	2019	2020
April	18.0	14.6	14.4	24.6	51.3	4.7
May	21.7	15.7	16.9	39.0	129.6	79.9
June	22.7	24.2	21.3	150.1	113.7	125.9
July	23.6	24.1	23.3	61.9	31.0	34.8
August	25.7	25.9	25.2	44.0	19.8	66.3
September	19.8	18.6	21.9	16.9	20.6	16.1
Average/sum	21.9	20.5	20.5	336.5	366	327.7

TABLE 3 The analysis of variance includes the effect of the year (Y), fertilizer treatment (F), genotype (G), and their interaction on the grain yield (GY), protein, oil, starch, phytic phosphorus (Pphy), phenolics (Phen), yellow pigment (YP), and glutathione (GSH) contents, reduction capacity of the DPPH radical (DPPH), and concentrations of Mg, Ca, Fe, Mn, Zn, Cu, and S in maize grains with different kernel colors.

SOF	*df*	GY	Protein	Oil	Starch	Pphy	Phen.	YP	GSH	DPPH	Mg	Ca	Fe	Mn	Zn	Cu	S
Repl.	4								F								
Y	2	464.4*	27.94*	3.17*	0.55	42.47*	7.07*	17.32*	0.74*	10.53*	26.66*	101.85*	6.56*	6.40*	78.15*	159.44*	68.08*
G	2	0.95*	28.22*	312.54*	30.62*	8.49*	87.49*	84.46*	2.24*	48.69*	20.16*	0.82	9.92*	22.85*	2.98*	0.01	3.68*
F	3	0.05	2.03*	0.36	1.09*	0.30	0.17	0.04	2.07*	0.16	3.89*	2.87*	24.18*	7.08*	5.01*	3.06*	4.24*
Y × G	35	210.74*	134.15*	176.09*	45.38*	37.93*	89.91*	792.53*	2.35*	55.48*	55.16*	29.81*	7.32*	34.75*	47.35*	51.01*	30.08*
Y × F	47	64.85*	6.80*	0.71	0.57	8.58*	1.60*	2.92*	1.74*	2.07*	7.56*	43.19*	13.85*	3.80*	24.09*	77.92*	37.59*
G × F	47	64.82*	7.93*	67.9*	6.99*	2.06*	16.49*	14.25*	2.08*	10.46*	5.83*	1.13*	12.12*	8.34*	2.04*	0.88*	2.04*
Y × G × F	143	47.99*	21.09*	81.34*	19.20*	30.43*	101.11*	338.52*	3.12*	224.87*	321.12*	1,201.6*	612.22*	131.04*	420.65*	863.88*	1,939.1*
									$p_{0.05}$								
Y		0.000	0.000	0.046	0.578	0.000	0.001	0.000	0.478	0.000	0.000	0.000	0.000	0.002	0.000	0.000	0.000
G		0.395	0.000	0.000	0.000	0.000	0.000	0.000	0.111	0.000	0.000	0.443	0.000	0.000	0.055	0.986	0.028
F		0.995	0.114	0.779	0.355	0.803	0.919	0.991	0.108	0.925	0.011	0.040	0.000	0.000	0.003	0.032	0.007
Y × G		0.000	0.000	0.000	0.000	0.000	0.000	0.000	0.023	0.000	0.000	0.000	0.000	0.000	0.000	0.000	0.000
Y × F		0.000	0.000	0.727	0.852	0.000	0.110	0.002	0.076	0.030	0.000	0.000	0.000	0.000	0.000	0.000	0.000
G × F		0.000	0.000	0.000	0.000	0.031	0.000	0.000	0.029	0.000	0.000	0.345	0.000	0.000	0.033	0.560	0.033
Y × G × F		0.000	0.000	0.000	0.000	0.000	0.000	0.000	0.000	0.000	0.000	0.000	0.000	0.000	0.000	0.000	0.000
CV (%)	3.08	3.42	4.57	2.42	4.51	5.14	4.99	4.57	6.64	4.30	4.74	2.30	1.60	2.06	4.64	1.72	
		t ha^{-1}		%		mg g^{-1}	µg g^{-1}		nmol g^{-1}	%			µg g^{-1}				
2018		9.79	9.39	4.65	70.1	2.53	328.7	9.87	1,075	88.3	1,938	111.7	38.62	11.53	36.66	3.47	2,417
2019		10.30	10.13	4.59	70.9	2.38	374.5	14.92	995	84.7	1,706	262.9	47.11	10.38	26.55	7.86	2,465
2020		8.08	9.40	4.48	71.0	2.60	356.8	10.21	1,055	89.7	1,997	220.0	48.84	10.62	33.88	3.57	2,755
White		7.93	9.09	4.12	71.9	2.50	322.0	1.20	1,125	84.5	1,719	185.8	38.24	9.73	30.77	4.96	2,178
Yellow		9.51	9.84	4.22	70.7	2.63	245.8	19.61	1,134	79.5	1,963	199.3	45.01	11.69	33.90	4.92	2,505
Red		10.73	10.00	5.38	69.4	2.38	492.3	14.20	866	98.8	1,959	209.5	51.33	11.11	32.41	5.01	2,954
BF		9.68	9.48	4.61	70.8	2.51	324.8	11.50	932	87.0	1,941	212.5	58.39	11.36	34.74	4.80	2,524
OF		9.46	9.86	4.65	70.5	2.52	359.6	11.67	1,013	87.5	1,946	220.1	45.13	11.52	33.84	5.89	2,748
Urea		8.97	9.74	4.48	70.4	2.52	379.6	11.54	1,258	88.0	1,855	196.6	40.84	10.45	30.60	5.14	2,504
Con		9.45	9.48	4.56	70.9	2.47	349.4	11.97	964	87.8	1,779	163.7	35.08	10.04	30.26	4.02	2,407

*5%, significant at the probability level. SOF, source of variation; df, degrees of freedom; BF, biofertilizer; OF, organic fertilizer; Con, control (no fertilizer); CV, coefficient of variation.

10.3389/fpls.2022.1027618

1,134 nmol g^{-1}, 1,963 μg g^{-1}, 11.69 μg g^{-1}, and 33.9 μg g^{-1}, respectively); the red kernel had the greatest average GY and was also the highest in proteins, oils, phenolics, DPPH, Ca, Fe, Cu, and S (10.73 t ha^{-1}, 10.0%, 5.38%, 492.3μg g^{-1}, 98.8%, 209.5 μg g^{-1}, 51.33 μg g^{-1}, 5.01 μg g^{-1}, and 2954 μg g^{-1}, respectively).

Correlation between the yield and essential elements

We found differences in the correlation between the GY and the concentration of the essential elements in the kernels (Table 4). In general, a significant and negative correlation was observed between the GY and S in the kernels of white and yellow maize (−0.38 and −0.85, respectively). An increase in the GY was followed by a significant increase in the concentration of Mg and Cu in yellow-kernel maize (by 0.56 and 0.57, respectively) and by a significant increase in the concentrations of Mg, Fe, Mn, Zn, and Cu (by 0.53, 0.44, 0.34, 0.53, and 0.66, respectively) in the red maize kernels.

Across fertilizer treatments, the only significantly negative correlation was observed between GY and Ca in the OF treatment (−0.39). Moreover, a positive correlation was observed between GY and Cu in the OF treatment (0.47), and Mn, Cu, and S were positively correlated with GY in the BF treatment (0.69, 0.49, and 0.55, respectively). In addition, Fe, Mn, and S were positively correlated with GY in the urea treatment (0.57, 0.48, and 0.36, respectively), and Fe and Cu were positively correlated with GY in the control (0.69 and 0.44, respectively).

Influence of the kernel color and fertilizers on the removal of the essential elements with kernel yield

The removal of mineral elements from the soil with grain yield is an important trait. Fertilizer treatments, genotype, as well as their interaction, expressed a significant impact on the removal of all examined elements with yield (Table 5). The average values indicated BF as the treatment with the highest average removal of Mg, Fe, Mn, and Zn (with 10.7%, 41.0%, 13.9%, and 14.7%, respectively, in comparison with control), whereas OF contributed to the greater removal of S (with 13.4% in comparison with control), and urea contributed to the greater removal of Ca and Cu (with 24.9% and 31.6%, respectively, in comparison with control). When the kernel color was considered, red-kernel maize had the highest values of removal for all the examined elements, on average.

When the combinations of maize with different kernel colors and fertilizer treatments were considered, the highest removal of Mg, Mn, Zn, Cu, and S was achieved with the yield of red-kernel maize and OF treatment (19.36, 0.11, 0.32, 0.057, and 28.09 kg ha^{-1}, respectively). Ca and Fe followed a similar trend, where the highest removal was with the red-kernel maize and BF treatment (2.09 and 0.58 kg ha^{-1}, respectively). Following the combination of red-kernel maize and BF/OF, slightly lower values were obtained for the combination of yellow-kernel maize and BF, having values of 18.17, 1.79, 0.51, 0.10, 0.31, and 23.72kg ha^{-1} for Mg, Ca, Fe, Mn, Zn, and S, respectively.

Influence of the kernel color and fertilizers on the potential bioavailability of the essential elements and DPPH reduction capacity

The potential bioavailability of the metals was reflected through their molar relation with Phy and followed the variations in the concentrations of Phy and the metals in the maize kernels. Notably, all ratios were significantly affected by the genotype, fertilizer type, and their interaction (Table 6). Only in the case of Phy/Mg and Phy/Ca ratios were insignificant variations obtained under the influence of fertilizer, and the Phy/Ca and Phy/Cu ratios were insignificant for genotype. Thus, in

TABLE 4 The correlation between grain yield (GY) and concentrations of the analyzed elements in maize with different kernel colors under different fertilizer treatments [biofertilizer (BF); organic fertilizer (OF); urea; control (Con; no fertilizer)].

Element		Mg	Ca	>Fe	Mn	Zn	Cu	S
Genotype								
White	GY	0.08	−0.23	0.15	0.07	0.14	0.14	−0.38*
Yellow		0.56*	−0.1	0.26	0.18	−0.22	0.57*	−0.85*
Red		0.53*	0.16	0.44*	0.34*	0.53*	0.66*	0.09
Fertilizer treatment								
BF	GY	0.05	0.14	−0.04	0.69*	−0.24	0.49*	0.55*
OF		−0.01	−0.39*	0.13	0.19	−0.16	0.47*	0.29
Urea		0.08	0.34	0.57*	0.48*	−0.02	0.19	0.36*
Con		0.1	0.29	0.69*	0.3	−0.17	0.44*	0.15

*0.05, significance level.

TABLE 5 Effect of different fertilizer treatments (biofertilizer (BF); organic fertilizer (OF); urea; control (Con; no fertilizer)) and maize kernel colors on the removal of the analyzed elements with the grain yield (kg ha^{-1}) (average of 2018–2020).

	Mg	Ca	Fe	Mn	Zn	Cu	S
White							
BF	12.26 b ± 1.08	1.45 b ± 0.25	0.30 d ± 0.35	0.070 b ± 0.22	0.24 b c ± 0.50	0.036 a b ± 0.13	16.58 a ± 2.43
OF	12.52 b ± 1.07	1.57 b c ± 0.20	0.25 b ± 0.22	0.072 b ± 0.20	0.22 b ± 0.42	0.041 b ± 0.12	18.95 a ± 2.56
Urea	10.99 a ± 1.15	1.05 a ± 0.28	0.22 a ± 0.24	0.061 b ± 0.23	0.18 a ± 0.48	0.033 a b ± 0.15	15.83 b ± 2.90
Con	11.13 a ± 1.04	1.01 a ± 0.18	0.20 a ± 0.20	0.061 b ± 0.20	0.19 a ± 0.42	0.025 a ± 0.09	16.11 a ± 2.49
Yellow							
BF	18.17 e ± 1.31	1.79 b c ± 0.25	0.51 e ± 0.38	0.109 e ± 0.28	0.31 d ± 0.53	0.040 b ± 0.12	23.72 d ± 2.83
OF	15.88 c ± 1.23	1.71 b c ± 0.26	0.35 c ± 0.27	0.099 d ± 0.25	0.28 d ± 0.48	0.046 b ± 0.13	23.05 b c ± 2.77
Urea	14.99 c ± 1.25	1.62 b c ± 0.26	0.32 c ± 0.29	0.086 c ± 0.28	0.25 b c ± 0.52	0.037 a b ± 0.15	20.28 c d ± 3.01
Con	15.22 c ± 1.17	1.39 b ± 0.20	0.30 c ± 0.24	0.088 c ± 0.24	0.26 c ± 0.46	0.037 a b ± 0.12	21.16 c ± 2.69
Red							
BF	18.44 e f ± 1.28	2.09 c ± 0.28	0.58 f ± 0.42	0.107 e ± 0.26	0.31 d ± 0.51	0.044 b ± 0.15	24.76 d ± 2.86
OF	19.36 f ± 1.21	2.07 c ± 0.26	0.52 e ± 0.31	0.111 e ± 0.24	0.32 d ± 0.45	0.057 c ± 0.10	28.09 d ± 2.81
Urea	17.22 d ± 1.28	1.95 c ± 026	0.43 d ± 0.36	0.096 d ± 0.27	0.27 c ± 0.49	0.049 b ± 0.13	24.10 e ± 3.09
Con	17.30 d ± 1.17	1.62 b ± 0.21	0.36 c ± 0.26	0.197 d ± 0.23	0.29 c d ± 0.46	0.036 a b ± 0.12	23.39 d ± 2.62
Mean							
White	11.72 A ± 1.09	1.27 A ± 0.23	0.26 A ± 0.25	0.066 A ± 0.22	0.21 A ± 0.45	0.034 A ± 0.13	16.87 A ± 2.59
Yellow	16.06 B ± 1.24	1.63 A B ± 0.24	0.37 B ± 0.30	0.106 B ± 0.26	0.28 B ± 0.50	0.040 A ± 0.14	22.05 B ± 2.83
Red	18.08 C ± 1.24	1.93 B ± 0.25	0.47 C ± 0.34	0.103 C ± 0.20	0.30 B ± 0.48	0.046 B ± 0.13	25.08 C ± 2.85
BF	16.29 b ± 1.23	1.78 b ± 0.26	0.49 c ± 0.39	0.095 b ± 0.25	0.29 b ± 0.51	0.040 a ± 0.12	21.69 b ± 2.71
OF	15.92 a ± 1.23	1.78 a b ± 0.27	0.37 a b ± 0.30	0.094 a ± 0.26	0.28 a ± 0.50	0.048 a ± 0.15	23.36 a ± 3.00
Urea	14.43 b ± 1.17	1.54 b ± 0.20	0.32 b ± 0.27	0.081 b ± 0.23	0.24 b ± 0.45	0.040 b ± 0.13	20.07 b ± 2.72
Con	14.55 a ± 1.12	1.34 a ± 0.20	0.29 a ± 0.23	0.082 a ± 0.22	0.25 a ± 0.45	0.033 a ± 0.10	20.22 a ± 2.60

Values are presented as mean ± SD. Numbers followed by the same letter do not differ based on the LSD test at $p< 0.05$.

the white-kernel maize Con treatment, Phy/Mg, Phy/Ca, Phy/Fe, Phy/Mn, Phy/Zn, and Phy/Cu had the lowest values when compared to that in the red-kernel hybrid in BF/OF treatment, which achieved the highest values (to 25.1%, 36.3%, 54.6%, 27.7%, 22.2%, and 42.1%, respectively). Additionally, slightly higher values were obtained in the same treatment (Con) with yellow-kernel maize. Nevertheless, when red-kernel maize was considered, the lowest values for Phy/Ca and Phy/Cu were obtained in the control, whereas reduced values of Phy/Mg, Phy/Fe, Phy/Mn, and Phy/Zn were noted in the urea treatment. Thus, on average, a trend of a reduction in the Phy/metals ratio was observed in the white-kernel maize and control, with the exception of Phy/Zn, which had a lower value in the urea treatment.

The results from Table 7 pointed to the presence of a significant and positive correlation between the reduction capacities of the DPPH radical, Pphy, and GSH in the white- (0.68 and 0.44, respectively) and yellow-kernel maize (0.74 and 0.38, respectively), whereas there was a negative correlation with YP (−0.74 in hybrid with yellow kernels). In the red-kernel maize, there was a significant and positive correlation between the DPPH, phenolics, and GSH (0.46 and 0.55, respectively). When the fertilizer treatments were considered, a positive correlation between the DPPH and phenolics was observed in all treatments. Furthermore, there was a significant and negative correlation between the DPPH, Pphy, and GSH in the OF (−0.64 and −0.44, respectively) and Con (−0.57 and −0.70, respectively) treatments, and there was only a significantly negative correlation with GSH in the urea treatment (−0.41).

Interdependence between the kernel color, fertilizer treatments, and GY and the chemical composition

The PCA, as a dimension reduction method, indicated that the first axis explained 48.1% of the total variability, the second axis explained 25.0%, the third axis explained 10.5%, and the fourth axis explained 7.6%. The GY and protein, oil, YP, Mg, Ca, Fe, Mn, Zn, and Cu concentrations correlated significantly and positively with the first axis, whereas starch was negatively correlated. Furthermore, a significant and positive correlation was found between the second axis and Pphy, whereas it was negatively correlated with the phenolics and DPPH reduction capacity. Only Cu was significantly positively correlated with the third axis.

Considering the mutual impact of the kernel color and fertilizer treatments on the variability of each trait, it is notable

TABLE 6 Effect of different fertilizer treatments (biofertilizer (BF); organic fertilizer (OF); urea; control (Con; no fertilizer)) on the molar ratios between phytic acid (Phy) and essential elements, Phy/Mg, Phy/Ca, Phy/Fe, Phy/Mn, Phy/Zn, and Phy/Cu (average for 2018–2020).

	Phy/Mg	Phy/Ca	Phy/Fe	Phy/Mn	Phy/Zn	Phy/Cu
White						
BF	7,276 a b ± 11.28	1,418 b ± 4.51	514 e ± 2.40	94.1 b ± 0.55	387 c d ± 0.97	55.7 b c ± 0.42
OF	7,519 b ± 12.02	1,558 b ± 5.10	352 b c ± 1.69	98.2 b ± 0.59	359 b ± 0.93	64.3 c ± 0.50
Urea	6,999 a b ± 11.15	1,097 a ± 3.58	316 a ± 1.51	88.3 a ± 0.53	316 a ± 0.81	55.3 b c ± 0.43
Con	6,706 a ± 10.79	1,007 a ± 3.32	279 a ± 1.35	83.7 a ± 0.50	310 a ± 0.81	39.6 a ± 0.31
Yellow						
BF	8,282 b c ± 13.68	1,348 b ± 4.55	534 e ± 2.65	112.5 e ± 0.69	385 c d ± 1.02	47.1 a b ± 0.38
OF	7,666 b ± 13.02	1,364 b ± 4.75	390 c ± 1.99	108.4 d ± 0.69	369 c ± 0.94	58.2 b c ± 0.48
Urea	7,794 b c ± 12.86	1,387 b ± 4.69	379 b c ± 1.88	101.3 c ± 0.62	354 b c ± 0.90	50.8 b ± 0.41
Con	7,251 a ± 12.14	1,088 a ± 3.73	330 b ± 1.66	94.9 b ± 0.59	331 a b ± 0.97	46.6 a b ± 0.38
Red						
BF	8,484 c ± 13.89	1,581 b ± 5.11	615 f ± 2.92	111.2 e ± 0.66	386 c d ± 0.96	53.0 b ± 0.41
OF	8,955 c ± 13.37	1,576 b ± 4.82	550 e ± 2.47	115.7 e ± 0.65	399 d ± 0.87	68.4 c ± 0.49
Urea	8,137 b c ± 12.60	1,522 b ± 4.83	466 d ± 2.17	102.1 c ± 0.59	346 b ± 0.89	60.2 b ± 0.45
Con	8,551 c ± 12.12	1,321 b ± 3.86	413 c ± 1.77	108.4 d ± 0.57	388 c d ± 0.93	46.1 a b ± 0.32
Mean						
White	7,125 A ± 11.31	1,270 n.s. ± 4.13	365 A ± 1.74	91.1 A ± 0.54	343 A ± 0.88	53.7 n.s. ± 0.41
Yellow	7,749 A B ± 12.91	1,297 n.s. ± 4.43	408 A ± 2.05	104.3 B ± 0.65	360 A ± 0.98	50.7 n.s. ± 0.41
Red	8,532 B ± 12.89	1,500 n.s. ± 4.66	511 B ± 2.33	109.3 B ± 0.62	380 B ± 0.90	56.9 n.s. ± 0.42
BF	8,014 n.s. ± 12.77	1,449 n.s. ± 4.72	554 d ± 2.65	105.9 b ± 0.63	386 b ± 0.99	52.0 a b ± 0.40
OF	8,047 n.s. ± 12.80	1,499 n.s. ± 4.89	431 c ± 2.05	107.4 b ± 0.64	375 b ± 0.97	63.6 b ± 0.49
Urea	7,644 n.s. ± 12.21	1,335 n.s. ± 4.37	387 b ± 1.86	97.2 a ± 0.58	339 a ± 0.87	55.4 b ± 0.43
Con	7,503 n.s. ± 11.70	1,139 n.s. ± 3-64	341 a ± 1.59	95.6 a ± 0.56	343 a ± 0.86	44.1 a ± 0.33

Values are presented as mean ± SD. Numbers followed by the same letter do not differ based on the LSD test at $p < 0.05$; n.s., not significant.

that the highest variability in the starch concentration and GSH was in the white-kernel maize, mainly in the urea and control treatments and to a lesser degree in the BF and OF treatments (Figure 1). The starch concentration in the yellow- and red-kernel hybrids in the control and in the GSH in the OF treatment also showed slight variability. Greater variability in the GY, oil, phenolics, and reduction capacity of the DPPH radical was observed in the yellow-kernel maize in all fertilizer treatments. Moreover, the GY variability was slightly affected by the urea treatment for all three kernel colors. Variability in the Pphy concentration was mainly caused by the BF and urea treatments, and a slight variation was caused by no fertilization (Con) in the red-kernel hybrid. Greater variability occurred in the YP, Zn, Mn, Mg, Ca, and S in the red kernel and OF combination.

TABLE 7 The correlation between the reduction capacity of the DPPH radical, concentration of the analyzed antioxidants in maize with different kernel colors, and the application of different fertilizers (biofertilizer (BF); organic fertilizer (OF); urea; control (Con; no fertilizer)).

Antioxidant		Pphy	Phenolics	GSH	YP
Genotype					
White	DPPH	0.68*	0.04	0.44*	−0.13
Yellow		0.74*	−0.14	0.38*	−0.74*
Red		−0.09	0.46*	0.55*	0.1
Fertilizer treatment					
BF	DPPH	−0.28	0.89*	−0.36	−0.2
OF		−0.64*	0.85*	−0.44*	0.09
Urea		−0.27	0.84*	−0.41*	−0.09
Con		−0.57*	0.78*	−0.70*	−0.08

*0.05, significance level.

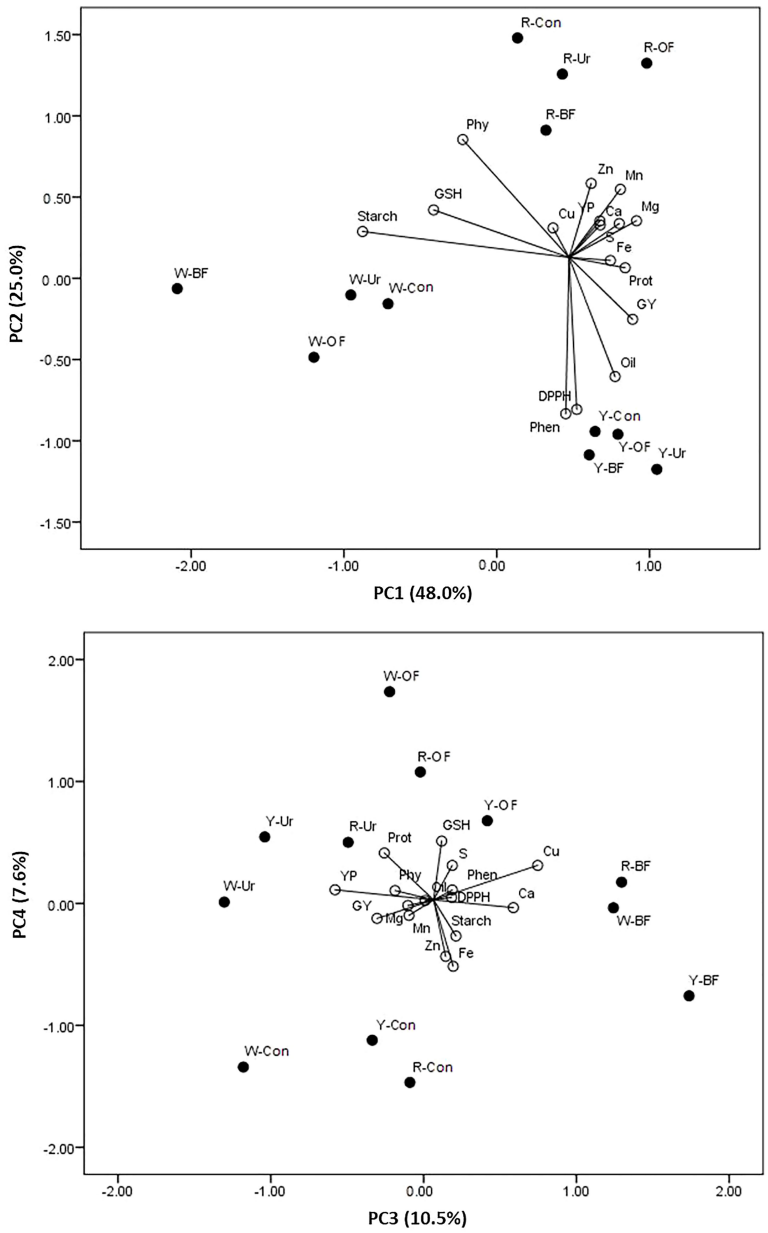

FIGURE 1
Principal component analysis of the grain yield (GY), protein (Prot), oil, starch, phytic phosphorus (Phy), phenolics (Phen), yellow pigment (YP), and glutathione (GSH) contents, reduction capacity of the DPPH radical (DPPH), and concentrations of Mg, Ca, Fe, Mn, Zn, Cu, and S in maize with different kernel colors (W, white; Y, yellow; R, red), under different fertilizer treatments(BF, biofertilizer; OF, organic fertilizer; Ur, urea; Con, control).

Discussion

The maize kernel plays an important role in the human diet in many regions globally. Genotypes with various kernel colorations, ranging from intense yellow to red, purple, or even blue and black, are very popular (Žilić et al., 2012; Sha et al., 2016; Suriano et al., 2021); however, in some regions, the white kernel is mainly used for human nutrition. Owing to a lack of information on the status of the other important nutrients, such as essential elements, this study provides valuable information on the ability to enhance the concentrations of essential elements and also improve their potential bioavailability from kernels of differently colored maize, aided by fertilization.

Year as a source of variation

As the experiment was performed under dry farming conditions, we demonstrated that the year and its interaction with other factors, such as the genotype, had the greatest impact on the variability of kernel characteristics. It is well known that meteorological variations, especially drought, are of great importance for maize yield as well as protein storage, including the absorption and accumulation of mineral elements from the soil (Ben Mariem et al., 2021). Dry conditions could severely affect crop growth and kernel filling and, thus, yield potential; however, they could also have a positive impact on the nutritional quality by increasing the protein level and accumulation of some antioxidants and mineral elements in the kernels (Saini and Keum, 2018). Even phytate, as a genotype characteristic, varied significantly across the years, confirming that climate could affect its concentration in the cereal grain (Perera et al., 2018).

Variability in the yield and chemical composition based on the kernel color

With respect to grain yield and macronutrients, it appears that red-kernel maize has greater yield potential and could be considered a good source of protein and oil and, therefore, should be a valuable part of the human diet (Sha et al., 2016). Considering the other two hybrids, white-kernel maize could be a good source of starch. It is also high in phenolics and GSH but low in essential nutrients, making it a good source of antioxidants but not minerals.

When comparing the kernels of different colors, it was obvious that the yellow kernel was richer in yellow pigment, as was expected, and in phytate and GSH, as important antioxidants, which supported the positive increasing trend of the scavenging capacity of the DPPH radical. This implies that maize is a good source of various antioxidants (Žilić et al., 2012; Sha et al., 2016; Suriano et al., 2021); our study indicates that the yellow kernel shows favorable characteristics in this regard. Additionally, the yellow-kernel maize was also high in the essential elements Mg, Mn, and Zn. However, slightly lower values of removal were found for this hybrid, particularly in Mg and Cu, which were positively correlated with the grain yield increase. In contrast to the metals, only S was negatively correlated with the grain yield increase in the white- and yellow-kernel hybrids. However, the red kernel was superior with respect to phenolics and scavenging capacity of the DPPH radical, as well as a high concentration of GSH, emphasizing a greater phenolic level in terms of the antioxidant activity of the maize kernel, when compared to other antioxidants (Žilić et al., 2012; Das and Singh, 2016). The same genotype was also high in Ca, Fe, Cu, and S. Thus, these differences again provided evidence that nutrient remobilization from the vegetative parts into the grain is highly dependent on the genotype (Ray et al., 2020) and could be the main reason for the highest removal of mineral nutrients with yield. This finding was additionally supported by the significantly positive correlation of the grain yield and all the examined essential elements, except for Ca and S. Interestingly, despite having the highest S level, the red-kernel maize had the lowest concentration of thiolic protein, GSH. Nevertheless, the white-kernel maize was still relatively high in the GSH, phenolics, phytic P, and the scavenging capacity of the DPPH radical, which was positively linked with the increasing level of phytic P and GSH.

Greater accumulation of the essential elements in the maize kernels does not necessarily indicate greater accessibility for humans and monogastric animals, which is mainly dependent on the concentrations of the various antinutrients, such as phytic acid, in the grain (Iwai et al., 2012; Brouns, 2021; Feizollahi et al., 2021). Thus, it is important to know the molar ratio between phytic acid and the essential metals as an indicator of their potential bioavailability (Johnson et al., 2013; Wang et al., 2015). Even though the red-kernel maize had the lowest average phytic acid concentration, the value of the phytic acid/essential metals ratio was the greatest in its kernels. Considering that a high level of phenolics could interfere with the accessibility of essential metals (Johnson et al., 2013), it can be assumed that the potential bioavailability, mainly of Ca, Fe, Cu, and other elements, from the red-kernel maize, was compromised, weakening its potential as a highly accessible source of essential elements. Nevertheless, fertilization, such as with urea and organic fertilizer, significantly reduced the ratio of phytic acid and essential elements in the kernel of this genotype, implying that fertilization practices could be successfully used to enhance the chemical composition of desirable traits in the kernels. Compared to the red-kernel maize, the yellow-kernel hybrid had a slightly lower phytic acid/essential metals ratio and the lowest phytic acid/Cu ratio, in combination with the greatest values for the promoters, yellow pigment, and GSH (which enhance the bioavailability of the essential metals), which could emphasize the yellow hybrid as a highly accessible source of Cu and potentially Mg, Mn, and Zn as well. Some elements are considerably lacking in diets worldwide (Lowe, 2021). When compared to the red- and yellow-kernel hybrids, the white-kernel hybrid had the lowest phytic acid/essential metals ratio, making it a desirable choice for highly available essential elements.

Variability in the yield and chemical composition, governed by fertilizer type

Fertilization is an important practice to optimize crop growth, fitness, and yield potential, as well as boost the synthesis and accumulation of important nutrients in the edible parts of plants, such as the grain in maize, thus improving their nutritional quality. Until now, fertilization has

mainly considered the application of macronutrients, such as N, P, and K. Meanwhile, the rising trend in soil devastation and the increasing requirements for the production of nutrient-dense crops (FAO, 2022) necessitate sustainable strategies that will increase efficiency and faster absorption of nutrients. Both organic and biofertilizers are used to sustain/improve soil fertility and uphold crop growth through improved nutrient absorption efficiency. They also overlap in benefits in terms of increasing the diversity and number of beneficial soil microbiota (Du et al., 2022).

The findings of this study showed that biofertilizer had a positive impact on the average grain yield as well as Fe and Zn accumulation in the maize grain, demonstrating that by promoting the activity of soil microbiota, the absorption of essential elements, increased crop fitness, and grain yield could be realized. Consequently, biofertilizer contributed to the greater removal of essential elements with yield, mainly with the red-kernel hybrid, such as Ca and Fe, whereas organic fertilizer was effective for Mg, Mn, Zn, Cu, and S removal. Similar findings were reported for sweet maize, which was grown after cover crops and biofertilizer, and dent maize, which was intercropped with soybean and biofertilizer (Dragicevic et al., 2015; Dragicevic et al., 2021). Notably, the incorporation of Zn fertilizers into the soil can enhance microbial metabolism, positively affecting Zn absorption, whole-plant metabolism, and promoting further pollen viability and kernel number, thus increasing the yield; however, this effect is highly dependent on the genotype (Liu et al., 2020; Xiao et al., 2022). This could explain the highest grain yield achieved by the red-kernel hybrid in biofertilizer treatment. Although organic fertilizer was important to increase macronutrient accumulation in the maize kernels (oils and proteins), it also enhanced the absorption and accumulation efficiency of essential elements, such as Mg, Ca, Mn, Cu, and S. Nevertheless, the findings revealed that urea is essential for the antioxidant status of maize kernels, as it improved the scavenging capacity of the DPPH radical and increased the accumulation of Pphy, phenolics, and GSH. The phenolics were positively correlated with the scavenging capacity of the DPPH radical in all the treatments, confirming their importance in the antioxidant response. It is well known that urea promotes the absorption and accumulation of Zn and Fe in the grains of various crops (Yuan et al., 2017; Pal et al., 2021). In this study, urea parallel increased the grain yield and Fe, Mn, and S in the maize grain.

The phytic P concentrations in the treatments with organic fertilizer and urea were very similar, indicating that P, as well as N, can play an important role in phytic acid accumulation (Ning et al., 2009; Kaplan et al., 2019). Even though phytic acid is an important antioxidant and, thus, can considerably increase the antioxidant potential of plants (Akin-Idowu et al., 2017; Pramitha et al., 2021), in this study, it negatively correlated with the scavenging capacity of the DPPH radical in the organic fertilizer and control treatments. This indicated that apart from the genotype, other cropping practices could influence the share of phytic acid, affecting antioxidant activity. It is well known that urea is successfully used for biofortification to enhance Zn and Fe accumulation in crop grains (Pal et al., 2021; Kaur and Singh, 2022). In this study, urea primarily decreased the ratio of phytic acid with Mg, Fe, Mn, and Zn even in red-kernel maize, thereby contributing to their better potential accessibility.

The study limitations are attributed to the fact that only one soil type, the chernozem soil type, was considered, and the inclusion of soils lacking in multiple elements could more extensively explain the potential impact of applied fertilizers. From the viewpoint of potential bioavailability, further research comprising experiments *in vitro* and *in vivo* could provide a new avenue for research and integrate results from agricultural and nutritional/medical sciences regarding the nutritional value of variously colored maize kernels with elevated concentrations of essential elements under real-time conditions.

Conclusion

The importance of maize as a staple crop and a source of various nutrients was supported by this study. The contribution of maize was determined by comparing the yield and chemical composition of differently colored kernels, with a focus on different fertilizer types as a possible tool for agronomic biofortification.

When the hybrids with differently colored kernels were compared, the white kernel was the best in terms of variability in the starch and GSH concentrations, while the yellow-kernel hybrid had a greater potential for achieving a high grain yield, oil and phenolic concentrations, and greater scavenging capacity of the DPPH radical. The red-kernel hybrid had the highest potential to enhance the kernel composition, based on greater variability in all the examined essential elements and yellow pigment, and there was a greater potential for reducing the phytic acid concentration, which could lead to an increase in its potential bioavailability. Thus, the impact of the genotype on the variability in the examined traits was significant.

The fertilizer type, such as bio- and organic fertilizers, also played an important role in improving kernel quality with respect to the accumulation of essential elements and their greater removal with yield. From such viewpoint, biofertilizer was beneficial for grain yield as well as greater accumulation of proteins, Fe, Cu, and S and antioxidants status, particularly when red-kernel hybrid was considered, while organic fertilizer was mainly efficient for greater accumulation of macronutrients in the kernels, too, including essential elements, such as Mg, Ca, Mn, Cu, and S. Although urea is a less sustainable fertilizer, it was important in enhancing the antioxidant status and

increasing the potential Zn bioavailability from the maize kernels.

The results of this study can be used to determine an appropriate genotype based on the antioxidants and/or essential elements targeted for kernel enhancement. We recommend that, in general, all three genotypes should be included in human diets in a cyclical manner and that the share of maize products, as a rich source of phytonutrients, should be increased.

Data availability statement

The original contributions presented in the study are included in the article. Further inquiries can be directed to the corresponding author.

Author contributions

VD and MSi contributed to the experiment design. VD and MSt conducted the chemical analysis. VD, MB, and PK conducted the statistical analyses. VD, MB, and Msi wrote the manuscript. MB, Msi, and MT organized the experiment. PK, Msi, and IT edited the manuscript. Msi initiated the experiment. Msi and MT acquired equipment and funding. All the authors contributed to the revision of the manuscript and read and approved the final version.

Funding

This research was supported by the Ministry of Education, Science and Technological Development, Republic of Serbia, under Grant no. 451-03-68/2022-14/200040.

Acknowledgments

The authors are grateful to Branka Radovanović, Biljana Noro, Milan Kostić, and Miroslav Maksimović for their effort and dedication in conducting the experiment.

Conflict of interest

The authors declare that the research was conducted in the absence of any commercial or financial relationships that could be construed as a potential conflict of interest.

Publisher's note

All claims expressed in this article are solely those of the authors and do not necessarily represent those of their affiliated organizations, or those of the publisher, the editors and the reviewers. Any product that may be evaluated in this article, or claim that may be made by its manufacturer, is not guaranteed or endorsed by the publisher.

References

Abe, N., Murata, T., and Hirota, A. (1998). Novel DPPH radical scavengers, bisorbicillinol and demethyltrichodimerol, from a fungus. *Biosci. Biotechnol. Biochem.* 62, 661–666. doi: 10.1271/bbb.62.661

Akin-Idowu, P. E., Odunola, O. A., Gbadegesin, M. A., Ademoyegun, O. T., Aduloju, A. O., and Olagunju, Y. O. (2017). Nutritional evaluation of five species of grain amaranth – an underutilized crop. *Int. J. Sci.* 3, 18–27. doi: 10.18483/ijSci.1131

Ben Mariem, S., Soba, D., Zhou, B., Loladze, I., Morales, F., and Aranjuelo, I. (2021). Climate change, crop yields, and grain quality of c_3 cereals: A meta-analysis of [CO_2], temperature, and drought effects. *Plants (Basel).* 10, 1052. doi: 10.3390/plants10061052

Brankovic, G., Dragičević, V., Dodig, D., Zoric, M., Knežević, D., Žilić, S., et al. (2015). Genotype x environment interaction for antioxidants and phytic acid contents in bread and durum wheat as influenced by climate. *Chil. J. Agric. Res.* 75, 139–146. doi: 10.4067/S0718-58392015000200001

Brouns, F. (2021). Phytic acid and whole grains for health controversy. *Nutrients* 14, 25. doi: 10.3390/nu14010025

Chaturvedi, A. K., Bahuguna, R. N., Pal, M., Shah, D., Maurya, S., and Jagadish, K. S. V. (2017). Elevated CO_2 and heat stress interactions affect grain yield, quality and mineral nutrient composition in rice under field conditions. *Field Crops Res.* 206, 149–157. doi: 10.1016/j.fcr.2017.02.018

Das, A. K., and Singh, V. (2016). Antioxidative free and bound phenolic constituents in botanical fractions of Indian specialty maize (*Zea mays* l.) genotypes. *Food Chem.* 201, 298–306. doi: 10.1016/j.foodchem.2016.01.099

Dragičević, V., Oljača, S., Simić, M., Dolijanović, Z., Kresović, B., and Brankov, M. (2017). Content of some antioxidants in intercropped maize and soybean grain. *J. Agric. Sci. BGD.* 62, 31–40. doi: 10.2298/JAS1701031D

Dragičević, V., Sredojević, S., Perić, V., Nišavić, A., and Srebrić, M. (2011). Validation study of a rapid colorimetric method for the determination of phytic acid and inorganic phosphorus from seeds. *Acta Per. Tech.* 42, 11–21. doi: 10.2298/APT1142011D

Dragicevic, V., Dolijanović, Ž., Janosevic, B., Brankov, M., Stoiljkovic, M., Dodevska, M. S., et al. (2021). Enhanced nutritional quality of sweet maize kernel in response to cover crops and bio-fertilizer. *Agronomy* 11, 981. doi: 10.3390/agronomy11050981

Dragicevic, V., Oljaca, S., Stojiljkovic, M., Simic, M., Dolijanovic, Z., and Kravic, N. (2015). Effect of the maize–soybean intercropping system on the potential bioavailability of magnesium, iron and zinc. *Crop Pasture Sci.* 66, 1118. doi: 10.1071/CP14211

Du, T.-Y., He, H.-Y., Zhang, Q., Lu, L., Mao, W.-J., and Zhai, M. (2022). Positive effects of organic fertilizers and biofertilizers on soil microbial community composition and walnut yield. *Appl. Soil Ecol.* 175, 104457. doi: 10.1016/j.apsoil.2022.104457

FAO (2022). *Soils for nutrition, state of the art* (Rome, Italy: Food and Agriculture Organization).

Feizollahi, E., Mirmahdi, R. S., Zoghi, A., Zijlstra, R. T., Roopesh, M. S., and Vasanthan, T. (2021). Review of the beneficial and anti-nutritional qualities of phytic acid, and procedures for removing it from food products. *Food Res. Int.* 143, 110284. doi: 10.1016/j.foodres.2021.110284

Giuberti, G., Fortunati, P., Cerioli, C., and Gallo, A. (2015). Gluten free maize cookies prepared with high-amylose starch: *In vitro* starch digestibility and sensory characteristics. *J. Nutr. Food Sci.* 5, 424. doi: 10.4172/2155-9600.1000424

Iwai, T., Takahashi, M., Oda, K., Terada, Y., and Yoshida, K. T. (2012). Dynamic changes in the distribution of minerals in relation to phytic acid accumulation

during rice seed development. *Plant Physiol.* 160, 2007–2014. doi: 10.1104/pp.112.206573

Johnson, C. R., Thavarajah, D., and Thavarajah, P. (2013). The influence of phenolic and phytic acid food matrix factors on iron bioavailability potential in 10 commercial lentil genotypes (*Lens culinaris* l.). *J. Food Compost. Anal.* 31, 82–86. doi: 10.1016/j.jfca.2013.04.003

Kaplan, M., Karaman, K., Kardes, Y. M., and Kale, H. (2019). Phytic acid content and starch properties of maize (*Zea mays* l.): Effects of irrigation process and nitrogen fertilizer. *Food Chem.* 283, 375–380. doi: 10.1016/j.foodchem.2019.01.029

Kaur, A., and Singh, G. (2022). Zinc and iron application in conjunction with nitrogen for agronomic biofortification of field crops – a review. *Crop Pasture Sci.* 73. doi: 10.1071/CP21487

Liu, D. Y., Zhang, W., Liu, Y. M., Chen, X. P., and Zou, C. Q. (2020). Soil application of zinc fertilizer increases maize yield by enhancing the kernel number and kernel weight of inferior grains. *Front. Plant Sci.* 11. doi: 10.3389/fpls.2020.00188

Lowe, N. M. (2021). The global challenge of hidden hunger: Perspectives from the field. *Proc. Nutr. Soc* 80, 283–289. doi: 10.1017/S0029665121000902

Mahan, A. L., Murray, S. C., Rooney, L. W., and Crosby, K. M. (2013). Combining ability for total phenols and secondary traits in a diverse set of colored (red, blue, and purple) maize. *Crop Sci.* 53, 1248–1255. doi: 10.2135/cropsci2012.06.0385

Mishra, D. J., Singh, R., Mishra, U. K., and Shahi, S. K. (2012). Role of bio-fertilizer in organic agriculture: A review. *Res. J. Recent Sci.* 2, 39–41.

Nikolić, N., Mitrović, J., Karabegović, I., Savić, S., Petrović, S., Lazić, M., et al. (2019). A comparison between wheat and different kinds of corn flour based on minerals, free phenolic acid composition and antioxidant activity. *Qual. Assur. Saf. Crops Foods.* 11, 341–349. doi: 10.3920/QAS2018.1411

Ning, H., Liu, Z., Wang, Q., Lin, Z., Chen, S., Li, G., et al. (2009). Effect of nitrogen fertilizer application on grain phytic acid and protein concentrations in japonica rice and its variations with genotypes. *J. Cereal Sci.* 50, 49–55. doi: 10.1016/j.jcs.2009.02.005

Pal, V., Singh, G., and Dhaliwal, S. S. (2021). A new approach in agronomic biofortification for improving zinc and iron content in chickpea (*Cicerar ietinum* l.) grain with simultaneous foliar application of zinc sulphate, ferrous sulphate and urea. *J. Soil Sci. Plant Nutr.* 21, 883–896. doi: 10.1007/s42729-021-00408-0

Perera, I., Seneweera, S., and Hirotsu, N. (2018). Manipulating the phytic acid content of rice grain toward improving micronutrient bioavailability. *Rice (N Y).* 11, 4. doi: 10.1186/s12284-018-0200-y

Pramitha, J. L., Rana, S., Aggarwal, P. R., Ravikesavan, R., Joel, A. J., and Muthamilarasan, M. (2021). Diverse role of phytic acid in plants and approaches to develop low-phytate grains to enhance bioavailability of micronutrients. *Adv. Genet.* 107, 89–120. doi: 10.1016/bs.adgen.2020.11.003

Ray, K., Banerjee, H., Dutta, S., Sarkar, S., Murrell, T. S., Singh, V. K., et al. (2020). Macronutrient management effects on nutrient accumulation, partitioning, remobilization, and yield of hybrid maize cultivars. *Front. Plant Sci.* 11. doi: 10.3389/fpls.2020.01307

Roychowdhury, D., Mondal, S., and Banerjee, S. K. (2017). The effect of biofertilizers and the effect of vermicompost on the cultivation and productivity of maize – a review. *Adv. Crop Sci. Tech.* 05, 261. doi: 10.4172/2329-8863.1000261

Saini, R. K., and Keum, Y. S. (2018). Significance of genetic, environmental, and pre- and postharvest factors affecting carotenoid contents in crops: A review. *J.Agric. Food Chem.* 66, 5310–5324. doi: 10.1021/acs.jafc.8b01613

Sari-Gorla, M., Ferrario, S., Rossini, L., Frova, C., and Villa, M. (1993). Developmental expression of glutathione-s-transferase in maize and its possible connection with herbicide tolerance. *Euphytica* 67, 221–230. doi: 10.1007/BF00040624

Sha, H. T. R., Prasad, K., and Kumar, P. (2016). Maize–a potential source of human nutrition and health: A review. *Cogent Food Agric.* 2, 1166995. doi: 10.1080/23311932.2016.1166995

Simić, A., Sredojević, S., Todorović, M., Đukanović, L., and Radenović, C. (2004). Studies on the relationship between the content of total phenolics in exudates and germination ability of maize seed during accelerated aging. *Seed Sci. Technol.* 32, 213–218. doi: 10.15258/sst.2004.32.1.22

Sofo, A., Lundegårdh, B., Mårtensson, A., Manfra, M., Pepe, G., Sommella, E., et al. (2016). Different agronomic and fertilization systems affect polyphenolic profile, antioxidant capacity and mineral composition of lettuce. *Sci. Hortic.* 204, 106–115. doi: 10.1016/j.scienta.2016.04.003

SPSS Inc (2006). *SPSS For windows, version 15.0* (Chicago: SPSS Inc).

Suriano, S., Balconi, C., Valoti, P., and Redaelli, R. (2021). Comparison of total polyphenols, profile anthocyanins, color analysis, carotenoids and tocols in pigmented maize. *LWT* 144, 111257. doi: 10.1016/j.lwt.2021.111257

Vancetovic, J., Zilic, S., Bozinovic, S., and Ignjatovic-Micic, D. (2014). Simulating of top-cross system for enhancement of antioxidants in maize grain. *Span. J. Agric. Res.* 12, 467–476. doi: 10.5424/sjar/2014122-5222

Vollú, R. E., Cotta, S. R., Jurelevicius, D., Leite, D., Parente, C., Malm, O., et al. (2018). Response of the bacterial communities associated with maize rhizosphere to poultry litter as an organomineral fertilizer. *Front. Environ. Sci.* 6. doi: 10.3389/fenvs.2018.00118

Wang, Z., Liu, Q., Pan, F., Yuan, L., and Yin, X. (2015). Effects of increasing rates of zinc fertilization on phytic acid and phytic acid/zinc molar ratio in zinc bio-fortified wheat. *Field Crops Res.* 184, 58–64. doi: 10.1016/j.fcr.2015.09.007

Xiao, Y. S., Zhou, B., Han, Z., Liu, S., Ding, C., Jia, F., et al. (2022). Microbial mechanism of zincfertilizer input on rice grain yield and zinc content of polished rice. *Front. Plant Sci.* 13. doi: 10.3389/fpls.2022.962246

Yuan, L., Zhang, Z., Yang, J., Yang, Y., Ma, X., and Wu, L. (2017). Coated urea enhances iron and zinc concentrations in rice grain under different cultivation methods. *J. Plant Nutr.* 40, 841–850. doi: 10.1080/01904167.2016.1250907

Žilić, S., Serpen, A., Akıllıoğlu, G., Gökmen, V., and Vančetović, J. (2012). Phenolic compounds, carotenoids, anthocyanins, and antioxidant capacity of colored maize (*Zea mays* l.) kernels. *J. Agric. Food Chem.* 60, 1224–1231. doi: 10.1021/jf204367z

frontiers | Frontiers in Plant Science

TYPE Original Research
PUBLISHED 19 December 2022
DOI 10.3389/fpls.2022.1072171

OPEN ACCESS

EDITED BY
Chiou Tzyy-Jen,
Agricultural Biotechnology Research Center, Academia Sinica, Taiwan

REVIEWED BY
Rupam Kapoor,
University of Delhi, India
Natalia Requena,
Karlsruhe Institute of Technology (KIT), Germany

*CORRESPONDENCE
Shu-Yi Yang
shuyiyang@ntu.edu.tw

†These authors have contributed equally to this work

SPECIALTY SECTION
This article was submitted to Plant Nutrition, a section of the journal Frontiers in Plant Science

RECEIVED 17 October 2022
ACCEPTED 05 December 2022
PUBLISHED 19 December 2022

CITATION
Hsieh C, Chen Y-H, Chang K-C and Yang S-Y (2022) Transcriptome analysis reveals the mechanisms for mycorrhiza-enhanced salt tolerance in rice.
Front. Plant Sci. 13:1072171.
doi: 10.3389/fpls.2022.1072171

Transcriptome analysis reveals the mechanisms for mycorrhiza-enhanced salt tolerance in rice

Chen Hsieh [1†], Yun-Hsin Chen [2†], Kai-Chieh Chang [2†] and Shu-Yi Yang [2*]

[1]Department of Horticulture and Landscape Architecture, National Taiwan University, Taipei, Taiwan, [2]Institute of Plant Biology, National Taiwan University, Taipei, Taiwan

More than half of the global population relies on rice as a staple food, but salinization of soil presents a great threat to rice cultivation. Although previous studies have addressed the possible benefits of arbuscular mycorrhizal (AM) symbiosis for rice under salinity stress, the underlying molecular mechanisms are still unclear. In this study, we found that mycorrhizal rice had better shoot and reproductive growth and a significantly higher K^+/Na^+ ratio in the shoot. The reactive oxygen species (ROS) scavenging capacity in rice shoots was also improved by AM symbiosis. To elucidate the molecular mechanisms required for AM-improved salt tolerance, transcriptome analysis revealing the differentially expressed genes (DEGs) based on the response to AM symbiosis, salinity or specific tissue was performed. Thirteen percent of DEGs showed tissue-preferred responses to both AM symbiosis and salt stress and might be the key genes contributing to AM-enhanced salt tolerance. Gene Ontology (GO) enrichment analysis identified GO terms specifically appearing in this category, including cell wall, oxidoreductase activity, reproduction and ester-related terms. Interestingly, GO terms related to phosphate (Pi) homeostasis were also found, suggesting the possible role of the Pi-related signaling pathway involved in AM-enhanced salt tolerance. Intriguingly, under nonsaline conditions, AM symbiosis influenced the expression of these genes in a similar way as salinity, especially in the shoots. Overall, our results indicate that AM symbiosis may possibly use a multipronged approach to influence gene expression in a way similar to salinity, and this modification could help plants be prepared for salt stress.

KEYWORDS

Arbuscular mycorrhizal symbiosis, salinity, transcriptome, *Oryza sativa L.*, Pi homeostasis, cell wall

Introduction

Rice (*Oryza sativa L.*), belonging to the family Gramineae (Poaceae), is a major food crop for more than half of the global population and is very susceptible to saline soil, which is one of the most important obstacles to crop production worldwide (Flowers and Yeo, 1995; Porcel et al., 2012). In view of the evidence from a recent study, up to 50% of cultivated land will be degraded by 2050 due to salinization (Hossain, 2019). Sodium (Na^+) is the main toxic ion in salinized soil (Wakeel, 2013). Many cytosolic enzyme activities are activated by potassium but inhibited by sodium (Flowers et al., 1977). Salt stress can also reduce photosynthesis efficiency and induce changes in cell wall properties, ionic toxicity (primary effect) and osmotic stress (secondary effect), leading to the accumulation of reactive oxygen species (ROS) (Shomer et al., 2003; Sudhir and Murthy, 2004; Sharma et al., 2012; Singh et al., 2014). To increase tolerance to stress, plants have evolved a variety of physiological and biochemical mechanisms in response to salt damage. Regarding cell wall modification, previous studies have reported that monocot and dicot expansins play positive roles in plant resistance to salt stress (Yan et al., 2014; Li et al., 2015; Jadamba et al., 2020). To remove excess ROS, plants have developed a system including nonenzymatic and enzymatic antioxidants (Ahmad et al., 2010; Das and Roychoudhury, 2014). To mitigate the damage of toxic ions, mediating roles of transporters in Na^+ absorption from root to shoot and Na^+ compartmentalization within leaf tissues and cells, including Na^+/H^+ antiporter SOS1 (salt overly sensitive), Na^+/K^+ transporter HKT (high affinity potassium transporter) and vacuolar Na^+/H^+ antiporter NHX (sodium/hydrogen exchanger), are critical for salinity tolerance (Horie et al., 2007; Olias et al., 2009; Keisham et al., 2018). The role of osmoprotectants and hormones in salt stress tolerance has also been discussed (Gupta and Huang, 2014)

Arbuscular mycorrhizal (AM) fungi can form mutualistic symbiotic relationships with more than 80% of terrestrial plant species and 90% of agricultural plants (Smith and Read, 2010). These symbiotic relationships can enhance plant nutrient uptake from the soil, thereby improving growth and stress tolerance (Porras-Soriano et al., 2009; Kapoor et al., 2013; Rivero et al., 2018; Begum et al., 2019). AM fungi increase photosynthetic efficiency, secondary metabolite production, antioxidant activity and accessibility of water and nutrients to the plant and maintain ion balance under salt stress (Porcel et al., 2012; Evelin and Kapoor, 2014; Sarwat et al., 2016; Evelin et al., 2019). Moreover, AM symbiosis helps to prevent excessive Na^+ uptake and transport from roots to shoots, enhancing the absorption of essential cations, such as K^+, Ca^{2+}, and Mg^{2+}, and increasing the K^+/Na^+ or Mg^{2+}/Na^+ ratio in host plants under saline conditions (Giri et al., 2003; Giri and Mukerji, 2004; Colla et al., 2008; Evelin et al., 2019). AM-enhanced salt stress tolerance of rice has also been reported (Porcel et al., 2015; Porcel et al., 2016; Tisarum et al., 2020). The AM fungus *Claroideoglomus etunicatum* enhances the quantum yield of the rice plant (*O. sativa* L. cv. puntal) for photosystem II and decreases nonphotochemical quenching (NPQ) under salt stress, thereby improving the carbon dioxide (CO_2) fixation efficiency (Porcel et al., 2015). Moreover, upland rice plants inoculated with AM fungi (*Glomus etunicatum*) have a higher level of photosynthetic abilities, photosynthetic pigment, stomatal conductance, transpiration rate, osmolyte production (e.g., total soluble sugar and free proline), osmotic potential and grain yield under salt stress (Tisarum et al., 2020). Furthermore, the expression of rice transporter genes (*OsSOS1*, *OsNHX3*, *OsHKT2;1* and *OsHKT1;5*), which are involved in vacuolar sodium sequestration and Na^+ recirculation from shoots to roots, is upregulated in AM-colonized plants in a saline environment (Porcel et al., 2016). These studies all report the positive effects of AM symbiosis on salt stress tolerance in rice using phenomic approaches (Porcel et al., 2015; Porcel et al., 2016; Tisarum et al., 2020). Even though ample evidence has demonstrated that AM symbiosis has positive effects on plant physiological responses under salinity stresses, the underlying mechanism of how AM symbiosis manipulates its host plant to manage salt stress is still limited. A more recent RNA-seq-based transcriptome analysis revealed that the positive effects of AM symbiosis at the transcriptional level of *Sesbania cannabina* alleviate salt stress, which is mainly enriched in photosynthesis, ROS scavenging and specific transcription factors (Ren et al., 2019). Transcriptome analysis revealed that AM-induced genes in the roots of *Casuarina glauca* under salinity were enriched in antioxidant enzyme activity, carbohydrate metabolism, cell wall and ion transport (Wang et al., 2021). However, such comprehensive transcriptome analysis to reveal how AM symbiosis alleviates salt damage in rice has not yet been performed.

In this work, we investigated the effect of AM symbiosis on the growth and ion homeostasis of rice plants under salt stress. By using transcriptome analysis, we focused on differentially expressed genes (DEGs) showing tissue-preferred responses to both AM symbiosis and salt stress to illustrate how the transcriptome regulation of mycorrhizal rice plants responds to salt stress.

Materials and methods

Plant materials and growth conditions

Seeds of rice (*O. sativa L. japonica* cv. Nipponbare) were sterilized and germinated on 1/2 Murashige and Skoog (MS) medium with 0.8% agar. After one week, rice seedlings were transferred and grown in plastic tubes containing sterilized

sands without (mock) or with sand inoculum containing spores of *Rhizophagus irregularis* (Ri, purchased from *Mycorise*®*ASP*, *Premier Tech*, Rivière-du-Loup, Québec, Canada). Plants were grown in a phytochamber with a 12-h day/night cycle at 30/28°C and 70% air humidity. The plants were regularly watered for the first week after inoculation and fertilized every second day with one-half Hoagland solution containing 25 µM phosphate (Pi). At five weeks postinoculation (5 wpi), mock and mycorrhizal plants were divided into two batches, in which one batch was treated with fertilizer solution supplemented with 150 mM NaCl (saline condition) and the other batch was grown under nonsaline conditions. At 8 wpi, shoots and roots were collected and separated to detect the physiological, biochemical and molecular responses. One biological replicate was the combination of two plants, and three biological replicates were collected from each treatment.

Mycorrhizal quantification

Root samples were stained with Trypan blue, and mycorrhizal colonization was quantified with a modified gridline intersection procedure as described (Paszkowski et al., 2006).

Plant phenotyping

For biomass measurement, the dry weight was measured after two days at 70°C in a hot-air oven. To monitor the tissue ion content, 0.05 g of chopped dry samples was digested with 2 ml 65% HNO_3 and 0.5 ml H_2O_2 (both Suprapur; Merck) in a MarsXpress microwave digestion system (CEM, Matthews, NC, USA). After that, the samples were diluted with Milli-Q water (Millipore Co., MA, USA) to 20 ml, filtered using a 0.45-µm membrane filter and injected into an inductively coupled plasma (ICP) analyzer. The elemental profile of plant samples was determined using inductively coupled plasma-optical emission spectrometry (ICP-OES; PerkinElmer OPTIMA 5300) according to a previously described method with some modification (Shanmugam et al., 2011). The relative ion concentration (mg/L) of each sample was obtained based on the wavelength intensity and calibration standard curve. For 3,3'-diaminobenzidine (DAB) staining, the youngest fully expanded leaves detached from 8-week-old plants were soaked in DAB solution (0.1%) overnight and then decolorized in bleaching solution (96% ethanol:acetic acid:glycerol = 3:1:1) at 70°C until the brown spots appeared clearly. To statistically present the H_2O_2 content visualization by DAB staining, all pictures were first transformed into 8-bit grayscale images. The percentage of brown area (the area of brown spots divided by the area of whole leaf) was quantified by using ImageJ.

RNA extraction, cDNA synthesis, RT–PCR and RT–qPCR

RNA extraction, cDNA synthesis, RT–PCR, and RT–qPCR were performed as previously reported (Gutjahr et al., 2008). Total RNA was extracted from 100 mg shoot or root tissue by using TRIzol Reagent (Invitrogen™) following the manufacturer's instructions. For the following gene expression analysis, genomic DNA was removed from total RNA using DNase I (RNase-free, Invitrogen™). After DNase I treatment, purified RNA samples were reverse transcribed using the Moloney murine leukemia virus reverse transcriptase kit (Invitrogen™) with oligo (dT) primers for cDNA synthesis. The RT-qPCRs were performed with SYBR® Green Supermix (2X) (Bio-Rad) on a CFX Connect Real-Time PCR Detection System (Applied Biosystems) as described in the manufacturer's protocol. Transcript levels were normalized to constitutively expressed *Cyclophilin2* (Gutjahr et al., 2008). The RT–qPCR primers were designed using Primer3 web version 4.1.0 (http://primer3.ut.ee/). All RT–qPCR primers are listed in Supplementary Table S9.

Illumina library preparation, sequencing and functional annotation

A total amount of RNA (≥ 4 µg) per sample was used for transcriptome sequencing. The quantity and purity of the purified RNA was assessed using a NanoDrop ND-2000 (Thermo Scientific, Wilmington, MA, USA) and an Agilent 2100 Bioanalyzer (Agilent Technologies, Inc., Santa Clara, CA, USA) before Illumina NGS sequencing. To construct the sequencing libraries, only high-quality RNA samples were used (OD260/280 = 1.8~2.0, OD260/230 ≥ 2.0, RIN ≥ 7.0). After purification, end repair, and ligation to sequencing adapters, strand-specific sequencing libraries were constructed by using the Illumina HiSeq 4000 platform (2 × 150 bp paired end) and following the handbook for the NEBNext® Ultra™ RNA Library Prep Kit for Illumina® (Genomics Biotechnology Co., Ltd, Taipei, Taiwan). The read depth is 6 Gb. The quality control of raw reads was evaluated using FastQC software v0.11.8 (http://www.bioinformatics.babraham.ac.uk/projects/fastqc/). The low-quality reads (Q-value < 20) and adaptors were removed using the sequence preprocessing tool Trimmomatic v0.39 (Bolger et al., 2014). After low-quality reads and adaptors were removed, all reads were mapped to *Oryza sativa* v7.0 from Phytozome 13 (Goodstein et al., 2012) with STAR (Dobin et al., 2013) and quantified with

Salmon (Patro et al., 2017) using the nf-core/rnaseq pipeline (Ewels et al., 2020).

Differentially expressed gene analysis

Genes with low expression (log2CPM < -3) were filtered out based on the CPM value. DEGs were identified using the edgeR (empirical analysis of DGE in R) package v3.10.5 by comparing the counts per million (CPM) values between treatment groups (Robinson et al., 2010). Three treatment groups (salt, AM and tissue) were categorized to identify DEGs responding to salt, AM symbiosis or tissue from pairwise comparison between samples with one factor difference. For example, salt-responsive genes were identified between the same tissues with the same mycorrhizal treatment but grown under control and salinity conditions. AM-responsive genes were identified between the same tissues with the same salinity treatment but grown under mock and mycorrhizal conditions. Tissue-responsive genes were identified between roots and shoots with the same salinity and mycorrhizal treatment. In each group, four pairwise comparisons were performed. An adjusted p value and false discovery rate (FDR) < 0.05 and an absolute value of log2-fold-change > 1 were considered significant thresholds. To further analyze the overlap of DEGs among different treatment groups, a custom Python script was used to plot the Venn diagram of the DEGs responsive to salt, AM symbiosis and tissue.

GO enrichment analysis

After obtaining the DEGs in each region from Venn diagram analysis, a gene ontology (GO) enrichment analysis of the DEGs was performed with CARMO, a web-based tool for GO analysis (Wang et al., 2015) with "MSU RGAP ID" selected. The output GO list from CARMO was submitted to REVIGO (Supek et al., 2011) for visualization for interpretation. The bubble plot in the manuscript was plotted with a custom Python script using the scatterplot function from the package seaborn (Waskom et al., 2017). The GO terms from each region were sorted by FDR and filtered based on FDR < 0.05. Only the top 15 terms were visualized on the bubble plot.

Gene expression heatmap visualization

Fold change values were calculated by edgeR (Robinson et al., 2010). TPM values were calculated by Salmon (Patro et al., 2017). Custom Python scripts were used to visualize the fold change value of the selected genes with the clustermap function from the seaborn package (Waskom et al., 2017).

Statistical analysis

The experiment to observe phenotypic data was arranged with three to seven biological replicates in each treatment. The mean values were compared using two-way ANOVA followed by a least significant differences (LSD) *post hoc* test and analyzed by R software.

Accession numbers

Sequence data from this article can be found in the Michigan State University Rice Genome Annotation Project database (http://rice.plantbiology.msu.edu) using the following accession numbers: *granule-bound starch synthase II* (*OsGBSSII*) (LOC_Os07g22930), *xyloglucan endotransglucosylase/hydrolases 19* (*OsXTH19*) (LOC_Os03g01800), *low phosphate root 5* (*OsLPR5*) (LOC_Os01g03640), *purple acid phosphatase 7* (*OsPAP7*) (LOC_Os11g34720) and *OsCyclophilin2* (LOC_Os02g02890). The sequencing files discussed in this publication have been deposited in NCBI's Gene Expression Omnibus (Edgar et al., 2002) and are accessible through Gene Expression Omnibus (GEO) Series accession number GSE200863 (https://www.ncbi.nlm.nih.gov/geo/query/acc.cgi?acc=GSE200863).

Results

Phenotypic changes in mock and mycorrhizal plants under salt stress

To examine whether mycorrhizal rice plants could maintain better growth under salt stress, 5-week-old rice seedlings inoculated with the AM fungus *R. irregularis* (Ri) or without (mock) were grown under nonsaline (0 mM NaCl) or saline (150 mM NaCl) conditions for another three weeks. To investigate the effect of salinity on fungal growth, the fungal colonization level was quantified. Mock plants did not show the presence of AM fungi under either saline or nonsaline conditions (data not shown). The average fungal colonization levels reached 91% and 93% under nonsaline and saline conditions, respectively, indicating that AM fungi successfully colonized rice roots. The abundance of vesicles was slightly reduced by salinity, and the level of extraradical hyphae was higher under salt stress. The levels of the remaining fungal structures were not significantly different between nonsaline and saline conditions (Figure 1A). These results indicated that salt stress had a mild impact on AM symbiosis.

Mycorrhizal plants showed fewer wilted blade tips than mock plants under saline conditions (Figure 1B). Under nonsaline conditions, both the shoot and root biomass of mock plants and mycorrhizal plants were not different

10.3389/fpls.2022.1072171

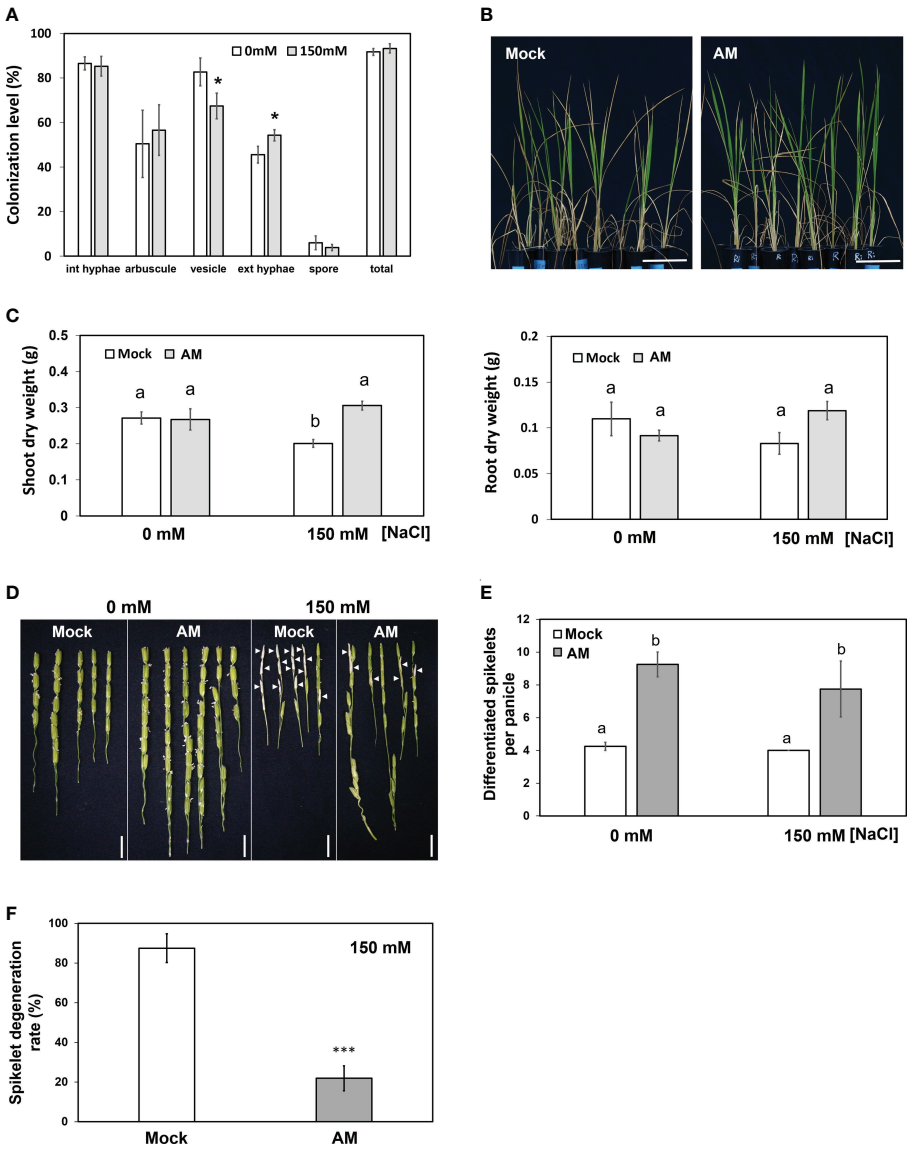

FIGURE 1
Physiological and agronomic traits of mock and mycorrhizal plants under salt stress. **(A)** Fungal colonization levels expressed as a percentage of colonized roots. **(B)** Phenotype of rice plants under salt stress. **(C)** Dry weight of shoots and roots. **(D)** Spikelet phenotype. Arrowheads indicate the typical salt-injured spikelets. **(E)** Comparison of spikelet number per panicle in mock and mycorrhizal plants. **(F)** Spikelet degeneration rate of mock and mycorrhizal plants under salt stress. The spikelet degeneration rate was defined as the degenerated spikelet number divided by the total number of spikelets per panicle. Rice plants were grown without (mock) or with the AM fungus *R. irregularis* (AM) for 5 weeks and then treated with normal (0 mM NaCl) or salt solution (150 mM NaCl) for 3 weeks. Standard error is derived from 3-7 biological replicates. One plant was considered one biological replicate in **(C-F)**, and two plants were considered one biological replicate in **(A)**. Different letters represent significant differences at $p < 0.05$ (two-way ANOVA followed by a least significant differences *post hoc* test). $*p < 0.05$, $***p < 0.001$ for Student's t test. Scale bar = 10 cm in **(B)** and 1 cm in **(D)**.

(Figure 1C), reflecting the fact that rice is an AM-nonresponsive plant (Smith et al., 2004; Li et al., 2006; Hata et al., 2010; Smith and Read, 2010). On the other hand, under saline conditions, the shoot biomass of mock plants but not mycorrhizal plants was severely decreased by salt stress (Figure 1C). The dry weight of mycorrhizal plant shoots was significantly higher than that of the mock group (1.5-fold) under salt stress. In contrast, AM symbiosis did not influence root biomass significantly under either nonsaline or saline conditions (Figure 1C). These results suggested that AM symbiosis may help rice plants maintain better shoot growth under salt stress.

We then aimed to further examine whether AM symbiosis also had positive effects on reproductive growth (panicle development) under salt stress. Compared with the mock

10.3389/fpls.2022.1072171

plants, the mycorrhizal plants showed a 2.17- and 1.93-fold increase in differentiated spikelet numbers under control and salt stress conditions, respectively (Figure 1E). In addition, AM-colonized plants contained fewer salt-injured spikelets (Figure 1D), and the spikelet degeneration rate (number of salt-injured spikelets divided by total number of spikelets) in mycorrhizal plants was significantly lower than that in mock plants under salt stress (Figure 1F). These results further indicated that AM symbiosis could enhance spikelet tolerance to salt stress.

To evaluate the effect of salt stress on nutrient content, the concentrations of Na^+, K^+ and P were measured. Under salt stress, the Na^+ concentration significantly increased compared to nonsaline conditions in both mock and mycorrhizal plants. Strikingly, mycorrhizal shoots presented a lower concentration of Na^+ than mock shoots under salt stress (Supplementary Figure S1A). The ability to maintain a high cytosolic K^+/Na^+ ratio is an indicator of plant salt tolerance (Gregorio and Senadhira, 1993; Wu et al., 2013), so the K^+ concentration was also measured to calculate the K^+/Na^+ ratio. The only difference in K^+ concentration between mock and mycorrhizal plants was found in shoot tissue under salt stress, in which mock shoots accumulated more K^+ than mycorrhizal shoots (Supplementary Figure S1B). Salt stress significantly reduced the K^+/Na^+ ratio in both mock and mycorrhizal plants. In roots, the K^+/Na^+ ratio of mycorrhizal plants was significantly higher than that of mock plants under nonsaline conditions (Supplementary Figure S1C). However, in shoots, the K^+/Na^+ ratio of mycorrhizal plants was significantly higher than that of mock plants under saline conditions (Supplementary Figure S1D). Even though the shoot/root Na^+ ratio was significantly increased by salt stress, the shoot/root Na^+ ratio was significantly lower in mycorrhizal plants than in mock plants, suggesting that mycorrhizal plants restrict sodium movement from roots to shoots (Supplementary Figure S1E). Previous studies showed that phosphate enhanced plant growth under saline conditions (Okusanya and Fawole, 1985). Therefore, we also measured the phosphorus content of plants. The results showed that the phosphorus content in mycorrhizal plants significantly increased in both shoots and roots compared with mock plants under both nonsaline and saline conditions (Supplementary Figure S1F). The positive effect of AM symbiosis not only enhanced salt tolerance, as shown by the K^+/Na^+ ratio, but also increased the efficiency of phosphate uptake.

Since AM symbiosis maintained shoot growth under salt stress (Figure 1C), whether the ROS level was different between mock and mycorrhizal shoots was further analyzed by visualizing H_2O_2 content histochemical stained with 3,3′-diaminobenzidine (DAB). It was obvious that the area of brown coloration was larger in mock shoots than in mycorrhizal shoots under salt stress (Figure 2). The results suggested that AM symbiosis may enhance the reduction in H_2O_2 levels in the shoots to protect the rice plant from oxidative damage under salt stress.

Identification of differentially expressed genes regulated by AM symbiosis in response to salt stress

To better understand the salt tolerance mechanism in mycorrhizal plants at the molecular level, RNA sequencing was used to investigate differential gene expression in response to AM symbiosis under salt stress. RNA-seq data were generated from the roots and shoots of mock and mycorrhizal plants grown under nonsaline and saline conditions with two to three biological replicates. Twenty-two paired-end libraries (Supplementary Table S1) were generated, and 683,233,862 and 656,077,984 paired-end 150 bp raw reads were obtained from the control and salt treatment samples, respectively. After removing the low-quality raw reads (Q-value < 20) and trimming adaptor sequences, a total of 671,602,666 cleaned reads with > 90% Q30 bases from nonsaline samples and 635,393,116 from saline samples were selected as high-quality reads for further analysis (Supplementary Table S1). All the high-quality reads served as input to the nfcore/rnaseq pipeline. The genome reference of *Oryza sativa* v7.0 was downloaded from Phytozome 13 (https://phytozome-next.jgi.doe.gov/). Sample correlation matrix analysis revealed a strong similarity between the biological replicates (Supplementary Figure S2).

Differentially expressed genes (DEGs) affected by one of the three factors, salinity, AM symbiosis and tissue, were identified with cutoffs of $|\log_2(\text{fold-change})| > 1$ and FDR < 0.05. For tissue-preferred expression, approximately nine thousand genes showed differential expression patterns between shoots and roots in each condition, and among these genes, approximately 45% showed higher expression in the roots than in the shoots. Moreover, this ratio was similar and not affected by salinity or AM symbiosis (Figure 3A). For AM-regulated expression, the number of DEGs regulated by AM symbiosis varied. For example, 2025 and 135 genes were regulated by AM symbiosis in the shoots grown under control and salinity conditions, respectively, and 1480 and 818 genes were regulated by AM symbiosis in the roots grown under control and salinity conditions, respectively. The number of AM-regulated DEGs was dramatically reduced in the roots and shoots grown under salt stress compared to those under control condition. Interestingly, more genes were downregulated in shoots but upregulated in roots by AM symbiosis under both control and salinity conditions (Figure 3B). For salinity-regulated expression, the number of DEGs regulated by salinity also varied. For example, 4058 and 676 genes were regulated by salinity in the shoots under mock and mycorrhizal conditions, respectively, and 1702 and 1223 genes

10.3389/fpls.2022.1072171

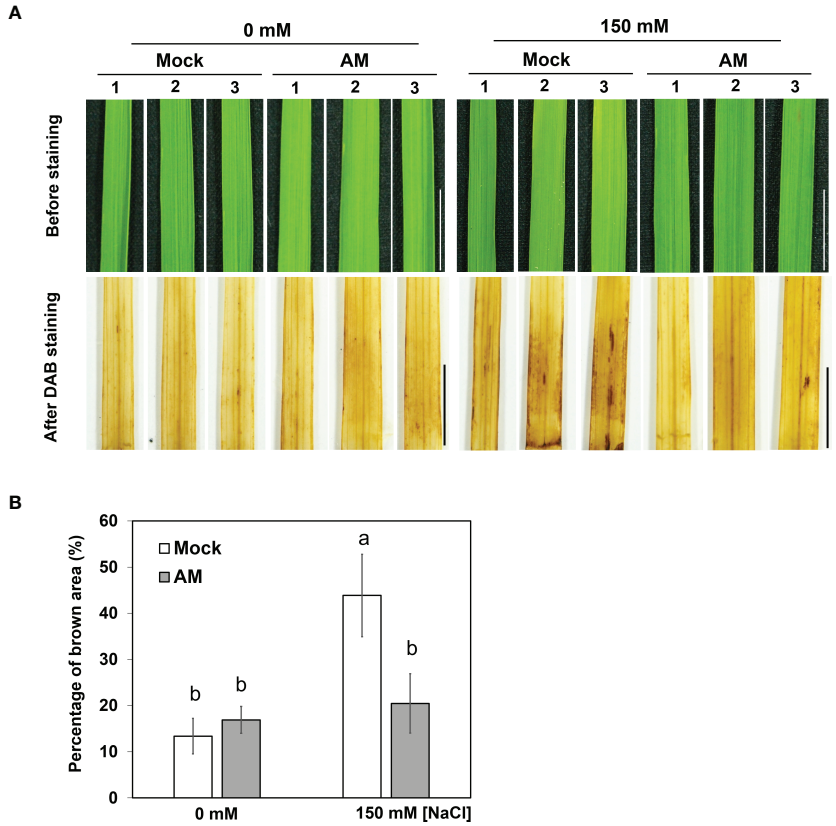

FIGURE 2
DAB staining in rice shoots under salt stress **(A)** Accumulation of H_2O_2 visualized in leaf blades by DAB staining after 3 weeks of salt stress. The eighth fully expanded leaves from 5-6 plants were detached and incubated in DAB solution for 16 hrs, and representative leaves from 3 plants are presented. Mock, nonmycorrhizal plants; AM, mycorrhizal plants inoculated with *R. irregularis*. Scale bar = 1 cm. **(B)** The percentage of brown area (the area of brown spots divided by the area of whole leaf) of DAB staining was quantified by using ImageJ. The standard error was derived from 5-6 biological replicates (one plant was considered one biological replicate). Different letters represent significant differences at $p < 0.05$ (two-way ANOVA followed by a least significant differences *post hoc* test).

were regulated by salinity in the roots under mock and mycorrhizal conditions, respectively. The number of salinity-regulated DEGs was significantly reduced in the tissues colonized by AM fungi, especially in shoots. In addition, salinity stress upregulated more genes in roots than no stress under both mock and mycorrhizal conditions. However, more genes were downregulated by salinity stress in mock shoots but upregulated in mycorrhizal shoots (Figure 3C). These results showed that the effect of AM symbiosis and salinity on gene expression was less pronounced under salinity and mycorrhizal conditions, respectively. In addition, compared to mock shoots, mycorrhizal shoots showed differential responses to salt stress.

In total, 15,679 DEGs were identified from the three treatment groups (Figure 3A). To further reveal the difference in DEGs among the three treatments, a Venn diagram was generated, and these DEGs were categorized into the seven regions (Figure 3D). In region 1, 8,123 genes (51.81%) were differentially expressed between shoots and roots and were not regulated by AM symbiosis or salinity treatment. In region 2, 172 genes (1.10%) were regulated by AM symbiosis but did not show tissue-preferred or salinity-responsive expression patterns. In region 3, 605 genes (3.86%) were regulated by salt stress but did not show tissue-preferred or AM-responsive expression patterns. In region 4, 1,289 genes (8.22%) showed AM-responsive and tissue-preferred expression patterns but did not respond to salinity treatment. In region 5, 3,380 genes (21.56%) showed salt-responsive and tissue-preferred expression patterns but did not respond to AM symbiosis. In region 6, 134 genes (0.85%) were regulated by both AM symbiosis and salinity but showed similar expression levels in both shoots and roots. In

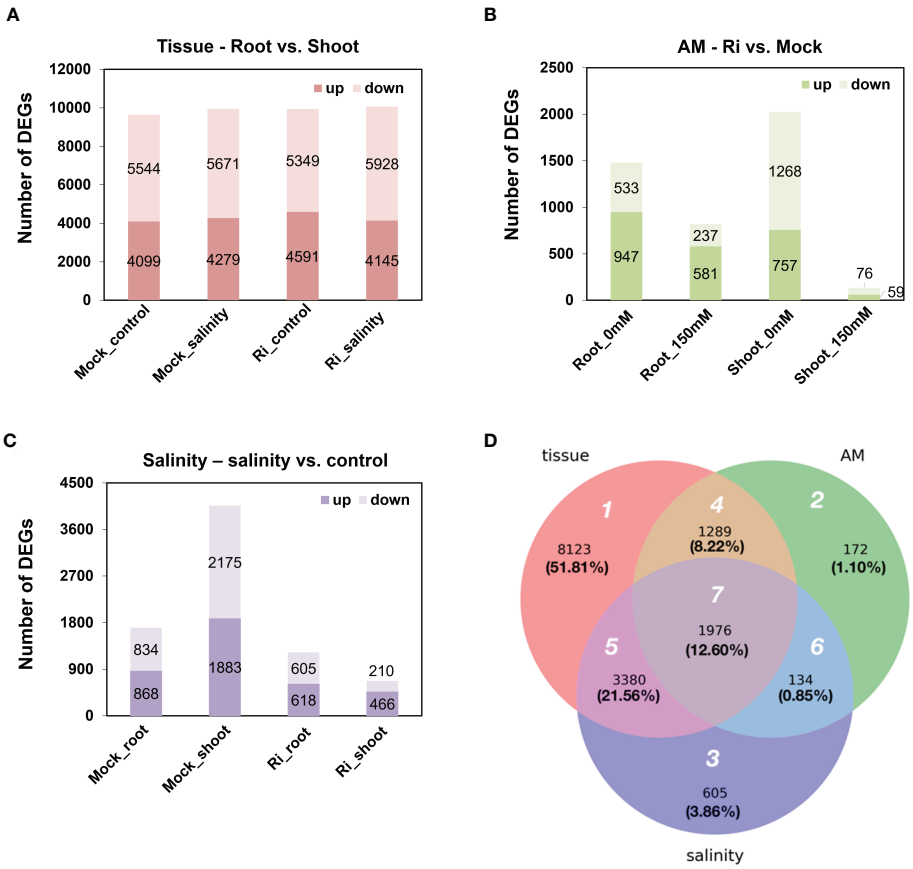

FIGURE 3
Differentially expressed genes (DEGs) regulated by tissue, AM symbiosis, and salinity stress **(A)** The number of up- and downregulated DEGs in roots compared to shoots. Upregulated referred to higher expression in roots compared to shoots and vice versa. **(B)** The number of up- and downregulated DEGs by AM symbiosis. Upregulated referred to higher expression in mycorrhizal (Ri) tissues than mock tissues and vice versa. **(C)** The number of up- and downregulated DEGs by salinity. Upregulated referred to higher expression in tissues grown under salinity conditions (150 mM) than under control conditions (0 mM) and vice versa. A total of 8 groups of samples were pairwise compared to identify DEGs regulated by tissue, AM symbiosis or salinity with cutoffs of $\log_2$(fold-change)> 1 and FDR < 0.05. **(D)** Venn diagram showing the overlap of DEGs among the three treatment groups. White number: region number; black number: number of DEGs; black number inside parenthesis, percentage of the total DEGs.

region 7, 1,976 genes (12.60%) were not only responsive to AM symbiosis and salt stress but also showed either shoot- or root-preferred expression patterns (Figure 3D).

Gene ontology enrichment analysis showed the functional profiles of AM-regulated genes

To identify the functional categories of each region, DEGs of each region in Figure 3D were submitted to CARMO for GO enrichment analysis. Enriched GO terms with FDR < 0.05 were retained for inspection and visualization. Only region 1, region 4, region 5, and region 7 obtained enriched GO terms that were significant (Supplementary Table S2). In region 1, genes showing tissue-preferred expression patterns were enriched in terms such as "thylakoid membrane organization", "photosynthesis", and "ATP binding" (Supplementary Table S2). In region 4, genes showing AM-responsive and tissue-preferred expression patterns were enriched in terms such as "biosynthetic process", "lipid metabolic process" and "sequence-specific DNA binding transcription factor activity" (Supplementary Table S2). In region 5, genes showing salinity-responsive and tissue-preferred expression patterns were enriched in terms such as "secondary metabolic process", "response to abiotic stimulus" and "electron carrier activity" (Supplementary Table S2). In region 7, genes showing tissue-preferred expression in response to both AM symbiosis and salinity might be important for AM-enhanced salt stress tolerance. Among the 10-15 GO terms with the smallest FDR value belonging to either the cellular component (CC), biological process (BP), or molecular function (MF) category, several GO terms contained

10.3389/fpls.2022.1072171

similar descriptions. For example, four and two GO terms contained "membrane" and "cell wall", respectively. Three and two GO terms contained "transport" and "hydrolase activity", respectively. Six GO terms were related to signal transduction, including "protein tyrosine kinase activity" and "protein serine/threonine kinase activity". In addition, the most enriched GO term is "cytoplasmic membrane-bounded vesicle" (Supplementary Table S2 and Figure 4).

Since we are interested in how AM symbiosis enhanced salt stress tolerance, a 3-way Venn diagram of the enriched GO terms from region 4 (tissue-preferred and AM-responsive), region 5 (tissue-preferred and salinity-responsive), and region 7 (tissue-preferred and AM/salinity-responsive) was generated to find specific GO terms derived from each region (Supplementary Figure S3 and Table S3). The GO terms that overlapped between the three regions (g7 region in Supplementary Figure S3) included more general terms such

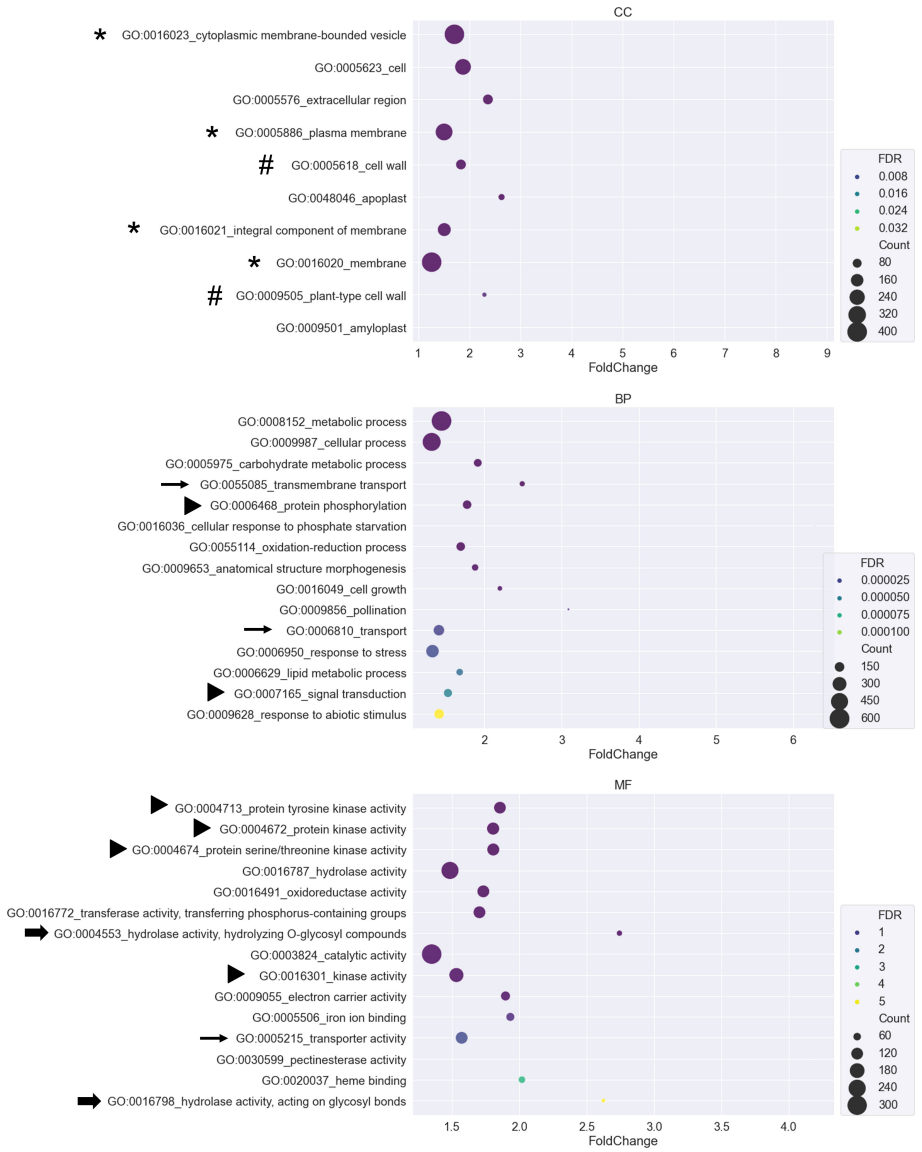

FIGURE 4
GO enrichment analysis for DEGs from region 7 A bubble plot was used to visualize the Gene Ontology (GO) enrichment analysis of DEGs belonging to region 7. GO terms from the cellular component (CC), biological process (BP), and molecular function (MF) categories were plotted. The X-axis represents the fold change of the GO enrichment level of the gene set over the background. The size of the bubbles represents the number of genes. The color of the bubbles represents the false discovery rate (FDR). GO terms with FDR greater than 0.05 were removed from the list. Only the 10-15 GO terms with the smallest FDR value were visualized in each category. Symbols in front of GO terms showed that these GO terms shared similar descriptions.

as "carbohydrate metabolic process", "catalytic activity", "cation binding", "hydrolase activity", "metabolic process", and "transport". Stress-related terms such as "response to abiotic stimulus" and "response to stress" and signaling-related terms such as "protein kinase activity", "protein phosphorylation", "protein serine/threonine kinase activity" and "protein tyrosine kinase activity" were also found (Supplementary Table S3). The GO terms that were specific to tissue-preferred and AM-responsive DEGs (g1 region in Supplementary Figure S3) included "ATPase activity", "fatty acid biosynthetic process" and "transmembrane receptor protein serine/threonine kinase signaling pathway" (Supplementary Table S3). The GO terms that were specific to tissue-preferred and salinity-responsive DEGs (g2 region in Supplementary Figure S3) included transport-related terms such as "amino acid transport", "divalent metal ion transport" and "sugar transmembrane transporter activity". Secondary metabolite-related terms such as "secondary metabolic process" and "ent-kaurene synthase activity" and photosynthesis-related terms such as "photosynthesis, light harvesting" and "photosynthesis, light reaction" were also found. Interestingly, reproduction-related terms such as "pollen–pistil interaction", "recognition of pollen" and "stamen development" were also identified (Supplementary Table S3). Finally, GO terms specific to DEGs representing tissue-preferred and AM/salinity-responsive expression patterns might be involved in AM-enhanced salt tolerance (g3 region in Supplementary Figure S3). In the g3 region, GO terms could be classified into several categories. One category was related to esters, such as "carboxylic ester hydrolase activity" and "hydrolase activity, acting on ester bonds". Another category was related to reproduction, such as "pollen tube growth" and "pollination". GO terms related to the cell wall, such as "cell wall modification", "cellular glucan metabolic process", "glucan biosynthetic process", "pectinesterase activity" and "xyloglucan: xyloglucosyl transferase activity", were also found. Intriguingly, many GO terms related to Pi homeostasis were found in the g3 region, such as "acid phosphatase activity", "cellular phosphate ion homeostasis", "cellular response to phosphate starvation", "myo-inositol hexakisphosphate biosynthetic process", "phosphate ion transport" and "positive regulation of cellular response to phosphate starvation" (Supplementary Table S3). The expression pattern of genes belonging to GO terms specific to the g3 region will be closely investigated in future studies.

Genes related to cell wall modification, ester-related, reproduction and oxidoreductase activity are involved in the response to AM symbiosis and salt stress

The expression of DEGs belonging to region 7-specific GO terms (g3 region) was visualized by heatmap. Most genes belonging to cell wall-related GO terms, such as "cell wall modification", "cellular glucan metabolic process" and "glucan biosynthetic process", showed higher expression in shoots than in roots (Figure 5 and Supplementary Table S4), suggesting their possible critical role in the shoots. Interestingly, in the shoots, the expression patterns of these genes in response to salinity and AM symbiosis were similar. For example, pectinesterase (LOC_Os01g21034) was induced by salinity in the mock shoots (salinity (Mock_shoot) column) and upregulated by AM symbiosis in the shoots under control conditions (Ri (control_shoot) column) (Figure 5 and Supplementary Table S4). These results implied that under control conditions, AM symbiosis already had a similar effect as salinity on the expression of these genes. Similar results were also observed in the expression pattern of genes belonging to "ester-related" or "oxidoreductase activity, acting on CH-OH group of donors" GO terms (Figure 6 and Supplementary Table S5) and those belonging to reproduction-related GO terms (Supplementary Figure S4 and Supplementary Table S6). To closely investigate the expression pattern and validate RNA-seq data, the expression profile from RNA-seq data and the corresponding RT–qPCR results for two genes were represented. For *granule-bound starch synthase II (GBSSII)* (Baysal et al., 2020) identified from the "glucan biosynthetic process" GO term, its expression was downregulated by AM symbiosis under control conditions and by salinity under mock conditions in both shoots and roots. Therefore, its expression was similar in mock and mycorrhizal tissue under salt stress. The RT–qPCR results were consistent with the RNA-seq findings (Supplementary Figure S5). For *xyloglucan endotransglucosylase/hydrolases 19 (XTH19)* (Yokoyama et al., 2004) identified from the "cellular glucan metabolic process" GO term, salinity or AM symbiosis did not influence the expression in the roots. However, its expression was upregulated by AM symbiosis under control conditions and by salinity under mock conditions in the shoots. Therefore, its expression was similar in mock and mycorrhizal shoots under salt stress. The RT–qPCR results were consistent with the RNA-seq findings (Supplementary Figure S5).

Phosphate-related pathways may play important roles in AM-enhanced salt tolerance

Several region 7-specific GO terms related to Pi homeostasis were selected for closer examination. For genes belonging to the GO terms "GO: 0016036 cellular response to phosphate starvation", "GO:0006817 phosphate ion transport" and "GO:0003993 acid phosphatase", most genes showed higher expression in the roots than in the shoots (Figure 7 and Supplementary Table S7). Interestingly, similar to the genes mentioned above, the expression patterns of these genes in response to salinity and AM symbiosis were similar in the

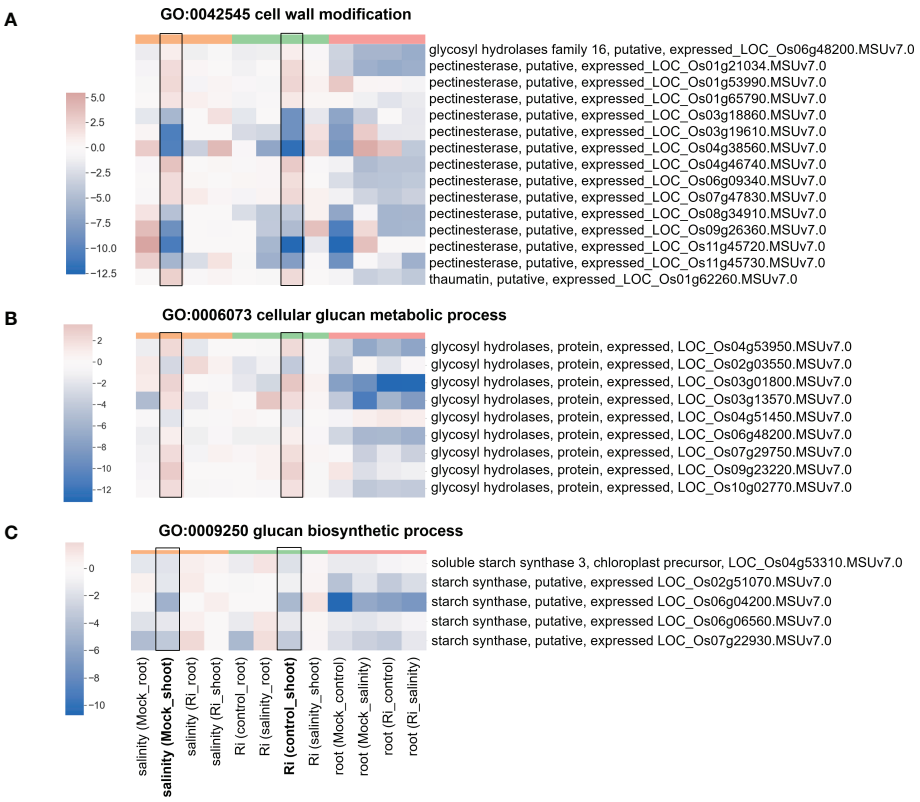

FIGURE 5
Heatmap showing the fold change of DEGs belonging to cell wall-related GO terms **(A)** Expression profile of DEGs from region 7 with the GO term "GO:0042545 cell wall modification". **(B)** Expression profile of DEGs from region 7 with the GO term "GO:0006073 cellular glucan metabolic process". **(C)** Expression profile of DEGs from region 7 with the GO term "GO:0009250 glucan biosynthetic process". The log2(fold change) values of DEGs from the selected GO terms were visualized with a heatmap. The color bar on top of the heatmap indicates the DE comparison groups: orange – salinity effect; green – AM symbiosis; pink – tissue difference. On the x-axis, each column represents a pairwise comparison to show the effect causing the DE, and inside the parentheses are the condition.

shoots. For example, SPX domain containing protein (LOC_Os10g25310) and Ser/Thr protein phosphatase family protein (LOC_Os11g34720) were repressed or induced by salinity in the mock shoots (salinity (Mock_shoot) column) and repressed or induced by AM symbiosis in the shoots under control conditions (Ri (control_shoot) column), respectively (Figure 7 and Supplementary Table S7). These results implied that under nonsaline conditions, AM symbiosis influenced the expression of these genes in a similar way as salinity. Among these genes, the expression of *low phosphate root 5 (LPR5)* (Cao et al., 2016) identified from the "cellular response to phosphate starvation" GO term was downregulated by AM symbiosis under control conditions and by salinity under mock conditions in both shoots and roots. Therefore, its expression was similar in mock and mycorrhizal tissues under salt stress. The RT–qPCR results were consistent with the RNA-seq findings (Supplementary Figure S5). For *purple acid phosphatase 7 (PAP7)* (Zhang et al., 2011) identified from the "acid phosphatase" GO term, salinity or AM symbiosis did not influence its expression in the roots. However, its expression was upregulated by AM symbiosis under control conditions and by salinity under mock conditions in the shoots. Therefore, its expression was similar in mock and mycorrhizal shoots under salt stress. The RT–qPCR results were consistent with the RNA-seq findings (Supplementary Figure S5). Overall, these data implied that AM symbiosis influenced the expression of genes belonging to cell wall modification, ester-related, reproduction, oxidoreductase activity and phosphate-related pathways as salinity did, and this mediation might help plants prepare while encountering salinity stress.

AM-regulated genes under salinity stress may be involved in AM-enhanced salt tolerance

To identify AM-regulated genes under salt stress, especially from the g3 region, the cutoff of log2(fold change) was set to one

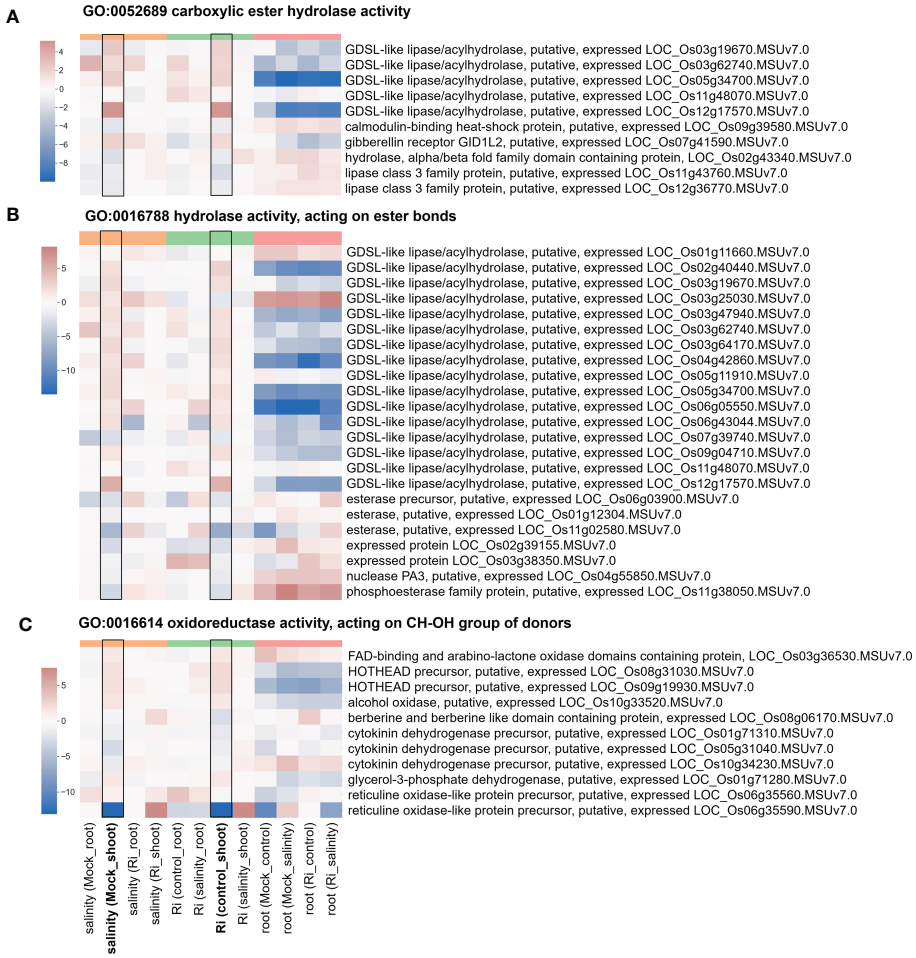

FIGURE 6
Heatmap showing the fold change of DEGs belonging to ester-related and oxidoreductase activity GO terms **(A)** Expression profile of DEGs from region 7 with the GO term "GO:0052689 carboxylic ester hydrolase activity". **(B)** Expression profile of DEGs from region 7 with the GO term "GO:0016788 hydrolase activity, acting on ester bonds". **(C)** Expression profile of DEGs from region 7 with the GO term "GO:0016614 oxidoreductase activity, acting on CH-OH group of donors". The log2(fold change) values of DEGs from the selected GO terms were visualized with a heatmap. The color bar on top of the heatmap indicates the DE comparison groups: orange – salinity effect; green – AM symbiosis; pink – tissue difference. On the x-axis, each column represents a pairwise comparison to show the effect causing the DE, and inside the parentheses are the condition.

to obtain AM-up or downregulated genes under salt stress. AM-upregulated genes, especially in the roots under salinity, included AMP-binding enzyme, GRETCHEN HAGEN 3.2 (GH3.2), glucose-1-phosphate adenylyltransferase, inorganic phosphate transporter, multicopper oxidase and starch synthase. AM-downregulated genes, especially in the roots under salinity, included kinases such as calcium/calmodulin dependent protein kinase (CAMK) and receptor-like protein kinase; Ser/Thr protein phosphatase; and cell wall-related genes such as endoglucanase, expansin and pectinesterase (Supplementary Figure S6 and Table S8). AM-upregulated genes, especially in the shoots under salinity, included cation/hydrogen exchanger 15 (CHX15); Pi-related genes, such as SPX domain-containing protein, inorganic phosphate transporter and multicopper oxidase; cell wall-related genes, such as endoglucanase, expansin and pectinesterase; inositol-3-phosphate synthase; and potassium channel Arabidopsis K^+ transporters 2/3 (AKT2/3). Fewer genes were downregulated by AM symbiosis, especially in shoots under salt stress, and a high proportion of terpene synthase was identified from this category (Supplementary Figure S7 and Table S8). Interestingly, AM symbiosis also had a similar effect as salinity on the expression of these genes under control conditions, especially in the shoots (Supplementary Figures S6 and S7 and Table S8).

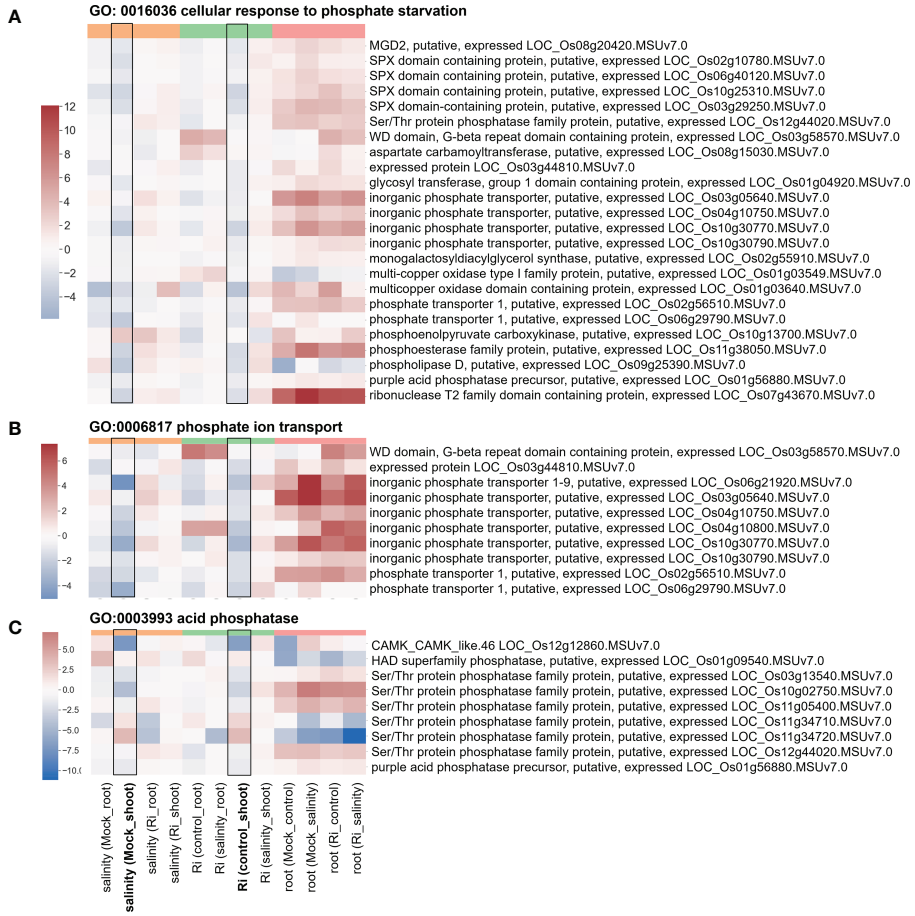

FIGURE 7
Heatmap showing the fold change of DEGs belonging to Pi homeostasis-related GO terms **(A)** Expression profile of DEGs from region 7 with the GO term "GO: 0016036 cellular response to phosphate starvation". **(B)** Expression profile of DEGs from region 7 with the GO term "GO:0006817 phosphate ion transport". **(C)** Expression profile of DEGs from region 7 with the GO term "GO:0003993 acid phosphatase". The log2(fold change) values of DEGs from the selected GO terms were visualized with a heatmap. The color bar on top of the heatmap indicates the DE comparison groups: orange – salinity effect; green – AM symbiosis; pink – tissue difference. On the x-axis, each column represents a pairwise comparison to show the effect causing the DE, and inside the parentheses are the condition.

Discussion

We found that AM symbiosis did not affect shoot and root dry weight under nonsaline conditions (Figure 1C). Most importantly, we found that the shoot dry weight of rice colonized by *R. irregularis* was significantly higher than that of the mock rice under salt stress (Figure 1C), which is in accordance with previous studies in rice cv. Puntal colonized by *Claroideoglomus etunicatum* (Porcel et al., 2015; Porcel et al., 2016), and in *Solanum lycopersicum* colonized by *R. irregularis* (Hajiboland et al., 2010; Khalloufi et al., 2017). Thus, we proved that AM symbiosis could improve rice shoot growth under salt stress. In addition, we further proved that AM symbiosis could also enhance reproductive growth under salinity (Figures 1D–F).

Our mineral nutrient analysis showed that mycorrhizal plants colonized with *R. irregularis* exhibited lower shoot Na^+ concentrations under salt stress, consistent with previous research in *Trigonella foenumgraecum* colonized by *R. irregularis* (Evelin et al., 2012) and in rice cv. Leum Pua (Indica rice) colonized by *Glomus. geosporum* or *G. mosseae* (Tisarum et al., 2020). However, the Na^+ concentration in the shoot tissues of rice cv. Puntal (Indica rice) was not affected by the AM fungi *C. etunicatum* (Porcel et al., 2016). These results suggest that different combinations of rice cultivars, AM fungal species, and salinity treatment might result in distinct outcomes. Furthermore, the reduced root-to-shoot Na^+ distribution in mycorrhizal plants under salt stress (Supplementary Figure S1E) was consistent with the finding that the AM fungus *C.*

etunicatum reduced the root-to-shoot Na^+ distribution in rice cv. Puntal (Porcel et al., 2016). Under salt stress, increased shoot K^+/Na^+ ratio by *R. irregularis* colonization was observed in rice (our study), *S. lycopersicum* (Hajiboland et al., 2010) and *T. foenumgraecum* (Evelin et al., 2012). Moreover, previous studies have shown that AM fungi (Ri) alleviate the stress impact by reducing ROS accumulation (Benhiba et al., 2015; He et al., 2017; Haddidi et al., 2020), which is consistent with our results (Figure 2).

Changes in plants' ability to respond or tolerate salt stress may be achieved through regulation of gene expression. Surprisingly, our results showed that AM symbiosis influenced the expression of genes belonging to cell wall GO term in a similar way as salinity did, especially in the shoots under nonsaline conditions, and several expasin and pectinesterase were upregulated by AM symbiosis under salt stress in shoots (Figure 5 and Supplementary Figure S7). Cell wall is the first organelle that senses and responds to salt stress (Evelin et al., 2019). Pectinesterase was identified as a promising candidate gene involved in salinity tolerance from an integrative meta-analysis approach in rice (Mansuri et al., 2020). Glycosyl hydrolase has been reported to be a potential biomarker for salinity tolerance in tomato varieties (Reyes-Pérez et al., 2019). Overexpression of expansin can enhance the tolerance of crop plants to salt stress (Han et al., 2012; Jadamba et al., 2020). Under salinity, lipid metabolism can be associated with extreme alterations in cell membrane integrity and function (Evelin et al., 2019). AM symbiosis upregulated the expression of most GDSL-like lipase/acylhydrolase belonging to ester-related GO terms in the shoots under nonsaline condition in a similar way as salinity did (Figure 6), and the positive role of AtLTL1 in salt tolerance has been reported (Naranjo et al., 2006). Myo-inositol and its derivative metabolites, such as inositol-3-phophate, are essential in diverse signal transduction responding to stress conditions (Jia et al., 2019). We found that AM symbiosis also had a similar effect as salinity on the expression of inositol-3-phosphate synthase in the shoots under control conditions. Moreover, the expression of this gene was upregulated by AM symbiosis under salt stress in the shoots (Supplementary Figure S7). Previous studied also showed that salt tolerance could be enhanced by the overexpression of inositol-3-phosphate synthase in rice (Kusuda et al., 2015). Phytohormones have been reported to play important roles in salt stress tolerance (Fahad et al., 2015). Our results found that AM symbiosis also had a similar effect as salinity on the expression of *GH3.2* under control conditions in the shoots. Moreover, the expression of this gene was upregulated by AM symbiosis under salt stress in the roots (Supplementary Figures S6). The GH3 protein family, which is responsible for binding free indole-3-acetic acid (IAA) to amino acids, has been reported to play a positive role in salt stress tolerance in cotton (Kirungu et al., 2019). Flavonoids could act as the nonenzymatic ROS scavenger (Yang and Guo, 2018), and 4CL proteins belonging to the AMP-binding protein family and regulating a pathway that contributes to flavonoid synthesis may contribute to salinity tolerance in two desert poplars (Zhang et al., 2015). Our data showed that AM symbiosis also had a similar effect as salinity on the expression of AMP-binding enzymes under control conditions in the shoots, and the expression of these genes was upregulated by AM symbiosis under salt stress in the roots (Supplementary Figures S6). Starch has been considered a key factor in plant fitness under abiotic stress, such as salinity (Kanai et al., 2007; Wang et al., 2013; Thalmann and Santelia, 2017). For example, the expression of glucose-1-phosphate adenylyltransferase, which encodes a starch building enzyme, was upregulated by salt stress in *Neochloris oleoabundans* (De Jaeger et al., 2018). The expression of starch synthase was also upregulated by salt stress in different plant species (Thalmann and Santelia, 2017). We found that AM symbiosis upregulated the expression of starch synthase and glucose-1-phosphate adenylyltransferase in the roots under salt stress (Figure 5 and Supplementary Figure S6), which could be beneficial for salinity tolerance. However, AM symbiosis downregulated the expression of these genes in the shoots under nonsaline condition similar as the effect caused by salinity (Figure 5 and Supplementary Figure S6). Reduced starch synthesis or increased starch remobilization might be helpful to provide sugars as osmoprotectants to mitigate the negative effect of stress (Thalmann and Santelia, 2017).

Maintain ionic homeostasis is important for plant salt stress tolerance (Yang and Guo, 2018; Evelin et al., 2019). "Cytoplasmic membrane-bounded vesicle" is the most enriched GO term among genes showed tissue-preferred expression in response to both AM symbiosis and salinity (Supplementary Table S2). It has been shown that intracellular membrane dynamics have played roles in plant salt tolerance. Under salt stress, regulation of vesicle trafficking and increase of cytoplasmic vesicles by accelerating endocytosis may be helpful for Na^+ compartmentalization (Yang and Guo, 2018; Wang et al., 2020). Our results also showed that AM symbiosis and salinity regulated genes involved in Pi homeostasis in a similar way in shoots, and AM symbiosis upregulated the expression of genes such as inorganic Pi transporter and multicopper oxidase under salinity in both roots and shoots (Figure 7 and Supplementary Figures S6, 7). Salinity-reduced Pi uptake has been reported in several plant species, suggesting the negative role of salt stress on Pi uptake (Martinez and Lauchli, 1994; Navarro et al., 2001). Many genes involved in the Pi starvation response are also regulated by salinity or play important roles in salt stress tolerance, suggesting crosstalk between the Pi starvation response and the salt stress signaling pathway (Baek et al., 2017). These findings support that many Pi homeostasis-related genes were regulated by salinity in our transcriptome analysis. In addition, previous studies showed that salt stress tolerance could be enhanced by exogenous Pi application or in Pi-accumulating mutants (Okusanya and Fawole, 1985; Miura et al., 2011; Sun et al., 2018). The increased Pi content in mycorrhizal roots and shoots and upregulated expression of Pi homeostasis-related genes by AM symbiosis observed in our study

might be the key factor for AM-enhanced salt stress tolerance (Supplementary Figures S1, S6, S7). AM symbiosis also had a similar effect as salinity on the expression of cation/H^+ exchanger (CHX) and Arabidopsis K^+ transporter (AKT2/3) in the shoots under control conditions, and AM-upregulated expression of these two genes was observed in the shoots under salt stress (Supplementary Figures S7). The contribution of the CHX channel to salt stress tolerance has been reported in soybean (Jia et al., 2017). AKT2 channels play a major role in phloem K^+ loading and unloading, and the fact that AKT2 is regulated by two positive regulators of salt stress tolerance, calcineurin B-like-interacting protein kinase 6 (CIPK6) and calcineurin B-like 4 (CBL4), suggests that AKT2 is involved in the adaptation to salt stress (Chérel and Gaillard, 2019).

Overall, our results indicate that AM symbiosis might possibly use a multipronged approach to influence gene expression in a way similar to salinity did, especially in the shoots under nonsaline conditions. This modification might help plants be prepared for salt stress. However, the underlying molecular mechanism to mediate this regulation is still unclear, and the relevance of this regulation on salt stress tolerance is also unknown. In addition, under salt stress, AM symbiosis also upregulated the expression of several genes involved in cell wall and lipid modification, inositol-3-phophate and starch synthesis, and auxin and ionic homeostasis. These genes may play positive roles in salt stress tolerance and the growth of mycorrhizal plants might be further maintained under salinity.

Data availability statement

The datasets presented in this study can be found in online repositories. The names of the repository/repositories and accession number(s) can be found in the article/Supplementary material.

Author contributions

Y-HC and S-YY designed the experiments. Y-HC and K-CC performed the experiments and analyzed the data. CH performed the RNA sequencing analysis. CH, Y-HC and S-YY wrote the article. All authors read and approved the final manuscript. All authors contributed to the article and approved the submitted version.

Funding

Grants from the Ministry of Science and Technology of Taiwan (MOST 107-2311-B-002-001-MY2, MOST 108-2311-B-002-006-MY3 and MOST 111-2311-B-002 -005 -MY3) and Ministry of Education of Taiwan (NTU-CC-108L893108).

Acknowledgments

We acknowledge Genomics Biotechnology Co., Ltd. (Taipei, Taiwan) for assistance in RNA sequencing and sample processing and the Technology Commons (TechComm) of the College of Life Sciences at National Taiwan University (NTU) for technical support. We sincerely thank Yi-Chian Tang and Dr. Kuo-Chen Yeh (Agricultural Biotechnology Research Center, Academia Sinica, Taiwan) for excellent technical assistance and help with the ICP-OES operation. We also thank Dr. Yu-Chang Tsai, Dr. Ying-Chung Lin, Dr. Hieng-Ming Ting and Dr. Chin-Mei Lee for their helpful comments on this research.

Conflict of interest

The authors declare that the research was conducted in the absence of any commercial or financial relationships that could be construed as a potential conflict of interest.

Publisher's note

Supplementary material

The Supplementary Material for this article can be found online at: https://www.frontiersin.org/articles/10.3389/fpls.2022.1072171/full#supplementary-material

References

Ahmad, P., Jaleel, C. A., Salem, M. A., Nabi, G., and Sharma, S. (2010). Roles of enzymatic and nonenzymatic antioxidants in plants during abiotic stress. *Crit. Rev. Biotechnol.* 30, 161–175. doi: 10.3109/07388550903524243

Baek, D., Chun, H. J., Yun, D. J., and Kim, M. C. (2017). Cross-talk between phosphate starvation and other environmental stress signaling pathways in plants. *Molecules Cells* 40, 697–705. doi: 10.14348/molcells.2017.0192

Baysal, C., He, W., Drapal, M., Villorbina, G., Medina, V., Capell, T., et al. (2020). Inactivation of rice starch branching enzyme IIb triggers broad and unexpected changes in metabolism by transcriptional reprogramming. *Proc. Natl. Acad. Sci. United States America* 117, 26503–26512. doi: 10.1073/pnas.2014860117

Begum, N., Qin, C., Ahanger, M. A., Raza, S., Khan, M. I., Ashraf, M., et al. (2019). Role of arbuscular mycorrhizal fungi in plant growth regulation: implications in abiotic stress tolerance. *Frontier Plant Sci.* 19, 1068. doi: 10.3389/fpls.2019.01068

Benhiba, L., Fouad, M. O., Essahibi, A., Ghoulam, C., and Qaddoury, A. (2015). Arbuscular mycorrhizal symbiosis enhanced growth and antioxidant metabolism in date palm subjected to long-term drought. *Trees* 29, 1725–1733. doi: 10.1007/s00468-015-1253-9

Bolger, A., Lohse, M., and Usadel, B. (2014). Trimmomatic: a flexible trimmer for illumina sequence data. *Bioinformatics* 30, 2114–2120. doi: 10.1093/bioinformatics/btu170

Cao, Y., Ai, H., Jain, A., Wu, X., Zhang, L., Pei, X., et al. (2016). Identification and expression analysis of OsLPR family revealed the potential roles of OsLPR3 and 5 in maintaining phosphate homeostasis in rice. *BMC Plant Biol.* 16, 210. doi: 10.1186/s12870-016-0853-x

Chérel, I., and Gaillard, I. (2019). The complex fine-tuning of K^+ fluxes in plants in relation to osmotic and ionic abiotic stresses. *Int. J. Mol. Sci.* 20, 715. doi: 10.3390/ijms20030715

Colla, G., Rouphael, Y., Cardarelli, M., Tullio, M., Rivera, C. M., and Rea, E. (2008). Alleviation of salt stress by arbuscular mycorrhizal in zucchini plants grown at low and high phosphorus concentration. *Biol. Fertility Soils* 44, 501–509. doi: 10.1007/s00374-007-0232-8

Das, K., and Roychoudhury, A. (2014). Reactive oxygen species (ROS) and response of antioxidants as ROS-scavengers during environmental stress in plants. *Front. Environ. Sci.* 2, 53. doi: 10.3389/fenvs.2014.00053

De Jaeger, L., Carreres, B. M., Springer, J., Schaap, P. J., Eggink, G., Dos Santos, V., et al. (2018). Neochloris oleoabundans is worth its salt: Transcriptomic analysis under salt and nitrogen stress. *PloS One* 13, e0194834. doi: 10.1371/journal.pone.0194834

Dobin, A., Davis, C. A., Schlesinger, F., Drenkow, J., Zaleski, C., Jha, S., et al. (2013). STAR: ultrafast universal RNA-seq aligner. *Bioinformatics* 29, 15–21. doi: 10.1093/bioinformatics/bts635

Edgar, R., Domrachev, M., and Lash, A. (2002). Gene expression omnibus: NCBI gene expression and hybridization array data repository. *Nucleic Acids Res.* 30, 207–210. doi: 10.1093/nar/30.1.207

Evelin, H., Devi, T. S., Gupta, S., and Kapoor, R. (2019). Mitigation of salinity stress in plants by arbuscular mycorrhizal symbiosis: current understanding and new challenges. *Front. Plant Sci.* 12, 470. doi: 10.3389/fpls.2019.00470

Evelin, H., Giri, B., and Kapoor, R. (2012). Contribution of glomus intraradices inoculation to nutrient acquisition and mitigation of ionic imbalance in NaCl-stressed trigonella foenum-graecum. *Mycorrhiza* 22, 203–217. doi: 10.1007/s00572-011-0392-0

Evelin, H., and Kapoor, R. (2014). Arbuscular mycorrhizal symbiosis modulates antioxidant response in salt-stressed trigonella foenum-graecum plants. *Mycorrhiza* 24, 197–208. doi: 10.1007/s00572-013-0529-4

Ewels, P. A., Peltzer, A., Fillinger, S., Patel, H., Alneberg, J., Wilm, A., et al. (2020). The nf-core framework for community-curated bioinformatics pipelines. *Nat. Biotechnol.* 38, 276–278. doi: 10.1038/s41587-020-0439-x

Fahad, S., Nie, L., Chen, Y., Wu, C., Xiong, D., Saud, S., et al. (2015). "Crop plant hormones and environmental stress," in *Sustainable agriculture reviews*. Ed. E. Lichtfouse (Cham: Springer), 371–400.

Flowers, T., Troke, P., and Yeo, A. (1977). The mechanism of salt tolerance in halophytes. *Annu. Rev. Plant Physiol.* 28, 89–121. doi: 10.1146/annurev.pp.28.060177.000513

Flowers, T., and Yeo, A. (1995). Breeding for salinity resistance in crop plants: where next? *Funct. Plant Biol.* 22, 875–884. doi: 10.1071/PP9950875

Giri, B., Kapoor, R., and Mukerji, K. (2003). Influence of arbuscular mycorrhizal fungi and salinity on growth, biomass, and mineral nutrition of acacia auriculiformis. *Biol. Fertility Soils* 38, 170–175. doi: 10.1007/s00374-003-0636-z

Giri,, and Mukerji, K. G. (2004). Mycorrhizal inoculant alleviates salt stress in sesbania aegyptiaca and sesbania grandiflora under field conditions: evidence for reduced sodium and improved magnesium uptake. *Mycorrhiza* 14, 307–312. doi: 10.1007/s00572-003-0274-1

Goodstein, D. M., Shu, S., Howson, R., Neupane, R., Hayes, R. D., Fazo, J., et al. (2012). Phytozome: a comparative platform for green plant genomics. *Nucleic Acids Res.*, (40), D1178–D1186. doi: 10.1093/nar/gkr944

Gregorio, G., and Senadhira, D. (1993). Genetic analysis of salinity tolerance in rice (Oryza sativa l.). *Theor. Appl. Genet.* 86, 333–338. doi: 10.1007/BF00222098

Gupta, B., and Huang, B. (2014). Mechanism of salinity tolerance in plants: physiological, biochemical, and molecular characterization. *Int. J. Genomics* (2014), 701596. doi: 10.1155/2014/701596

Gutjahr, C., Banba, M., Croset, V., An, K., Miyao, A., An, G., et al. (2008). Arbuscular mycorrhiza–specific signaling in rice transcends the common symbiosis signaling pathway. *Plant Cell* 20, 2989–3005. doi: 10.1105/tpc.108.062414

Haddidi, I., Duc, N. H., Tonk, S., Rápó, E., and Posta, K. (2020). Defense enzymes in mycorrhizal tomato plants exposed to combined drought and heat stresses. *Agronomy* 10, 1657. doi: 10.3390/agronomy10111657

Hajiboland, R., Aliasgharzadeh, N., Laiegh, S., and Poschenrieder, C. (2010). Colonization with arbuscular mycorrhizal fungi improves salinity tolerance of tomato (Solanum lycopersicum l.) plants. *Plant Soil* 331, 313–327. doi: 10.1007/s11104-009-0255-z

Han, Y., Xiu Li, A., Li, F., Rong Zhao, M., and Wang, W. (2012). Characterization of a wheat (Triticum aestivum l.) expansin gene, TaEXPB23, involved in the abiotic stress response and phytohormone regulation. *Plant Physiol. Biochem.* 54, 49–58. doi: 10.1016/j.plaphy.2012.02.007

Hata, S., Kobae, Y., and Banba, M. (2010). "Interactions between plants and arbuscular mycorrhizal fungi," in *International review of cell and molecular biology* (Netherlands: Elsevier), 1–48.

He, F., Sheng, M., and Tang, M. (2017). Effects of rhizophagus irregularis on photosynthesis and antioxidative enzymatic system in robinia pseudoacacia l. under drought stress. *Front. Plant Sci.* 8, 183. doi: 10.3389/fpls.2017.00183

Horie, T., Costa, A., Kim, T. H., Han, M. J., Horie, R., Leung, H. Y., et al. (2007). Rice OsHKT2; 1 transporter mediates large na+ influx component into k+-starved roots for growth. *EMBO J.* 26, 3003–3014. doi: 10.1038/sj.emboj.7601732

Hossain, M. S. (2019). Present scenario of global salt affected soils, its management and importance of salinity research. *Int. Res. J. Biol. Sci.* 1, 1–3. Available at: https://scirange.com/abstract/irjbs.2019.1.3

Jadamba, C., Kang, K., Paek, N.-C., Lee, S. I., and Yoo, S.-C. (2020). Overexpression of rice Expansin7 (Osexpa7) confers enhanced tolerance to salt stress in rice. *Int. J. Mol. Sci.* 21, 454. doi: 10.3390/ijms21020454

Jia, Q., Kong, D., Li, Q., Sun, S., Song, J., Zhu, Y., et al. (2019). The function of inositol phosphatases in plant tolerance to abiotic stress. *Int. J. Mol. Sci.* 20, 3999. doi: 10.3390/ijms20163999

Jia, B., Sun, M., Duanmu, H., Ding, X., Liu, B., Zhu, Y., et al. (2017). GsCHX19.3, a member of cation/H+ exchanger superfamily from wild soybean contributes to high salinity and carbonate alkaline tolerance. *Sci. Rep.* 7, 9423. doi: 10.1038/s41598-017-09772-3

Kanai, M., Higuchi, K., Hagihara, T., Konishi, T., Ishii, T., Fujita, N., et al. (2007). Common reed produces starch granules at the shoot base in response to salt stress. *New Phytol.* 176, 572–580. doi: 10.1111/j.1469-8137.2007.02188.x

Kapoor, R., Evelin, H., Mathur, P., and Giri, B. (2013). "Arbuscular mycorrhiza: approaches for abiotic stress tolerance in crop plants for sustainable agriculture," in *Plant acclimation to environmental stress* (New York: Springer), 359–401.

Keisham, M., Mukherjee, S., and Bhatla, S. C. (2018). Mechanisms of sodium transport in plants–progresses and challenges. *Int. J. Mol. Sci.* 19, 647. doi: 10.3390/ijms19030647

Khalloufi, M., Martínez-Andújar, C., Lachaâl, M., Karray-Bouraoui, N., Pérez-Alfocea, F., and Albacete, A. (2017). The interaction between foliar GA3 application and arbuscular mycorrhizal fungi inoculation improves growth in salinized tomato solanum lycopersicum l. plants by modifying the hormonal balance. *J. Plant Physiol.* 214, 134–144. doi: 10.1016/j.jplph.2017.04.012

Kirungu, J. N., Magwanga, R. O., Lu, P., Cai, X., Zhou, Z., Wang, X., et al. (2019). Functional characterization of Gh_A08G1120 (GH3.5) gene reveal their significant role in enhancing drought and salt stress tolerance in cotton. *BMC Genet.* 20, 62. doi: 10.1186/s12863-019-0756-6

Kusuda, H., Koga, W., Kusano, M., Oikawa, A., Saito, K., Hirai, M. Y., et al. (2015). Ectopic expression of myo-inositol 3-phosphate synthase induces a wide range of metabolic changes and confers salt tolerance in rice. *Plant Sci.* 232, 49–56. doi: 10.1016/j.plantsci.2014.12.009

Li, A., Han, Y. Y., Wang, X., Chen, Y. H., Zhao, M. R., Zhou, S.-M., et al. (2015). Root-specific expression of wheat expansin gene TaEXPB23 enhances root growth and water stress tolerance in tobacco. *Environ. Exp. Bot.* 110, 73–84. doi: 10.1016/j.envexpbot.2014.10.002

Li, A., Smith, S. E., Holloway, R. E., Zhu, Y., and Smith, F. A. (2006). Arbuscular mycorrhizal fungi contribute to phosphorus uptake by wheat grown in a phosphorus-fixing soil even in the absence of positive growth responses. *New Phytol.* 172, 536–543. doi: 10.1111/j.1469-8137.2006.01846.x

Mansuri, R. M., Shobbar, Z. S., Jelodar, N. B., Ghaffari, M., Mohammadi, S. M., and Daryani, P. (2020). Salt tolerance involved candidate genes in rice: an integrative meta-analysis approach. *BMC Plant Biol.* 20, 452. doi: 10.1186/s12870-020-02679-8

Martinez, V., and Lauchli, A. (1994). Salt-induced inhibition of phosphate uptake in plants of cotton (Gossypium hirsutum l.). *New Phytol.* 125, 609–614. doi: 10.1111/j.1469-8137.1994.tb02955.x

Miura, K., Sato, A., Ohta, M., and Furukawa, J. (2011). Increased tolerance to salt stress in the phosphate-accumulating arabidopsis mutants siz1 and pho2. *Planta* 234, 1191–1199. doi: 10.1007/s00425-011-1476-y

Naranjo, M. A., Forment, J., RoldÑn, M., Serrano, R., and Vicente, O. (2006). Overexpression of arabidopsis thaliana LTL1, a salt-induced gene encoding a GDSL-motif lipase, increases salt tolerance in yeast and transgenic plants. *Plant Cell Environ.* 29, 1890–1900. doi: 10.1111/j.1365-3040.2006.01565.x

Navarro, J. M., Botella, M. A., Cerdá1, A., and Martinez, V. (2001). Phosphorus uptake and translocation in salt-stressed melon plants. *J. Plant Physiol.* 158, 375–381. doi: 10.1078/0176-1617-00147

Okusanya, O., and Fawole, T. (1985). The possible role of phosphate in the salinity tolerance of lavatera arborea. *J. Ecol.* (73), 317–322. doi: 10.2307/2259785

Olias, R., Eljakaoui, Z., Li, J., De Morales, P. A., Marín-Manzano, M. C., Pardo, J. M., et al. (2009). The plasma membrane Na+/H+ antiporter SOS1 is essential for salt tolerance in tomato and affects the partitioning of na+ between plant organs. *Plant Cell Environ.* 32, 904–916. doi: 10.1111/j.1365-3040.2009.01971.x

Paszkowski, U., Jakovleva, L., and Boller, T. (2006). Maize mutants affected at distinct stages of the arbuscular mycorrhizal symbiosis. *Plant J.* 47, 165–173. doi: 10.1111/j.1365-313X.2006.02785.x

Patro, R., Duggal, G., Love, M. I., Irizarry, R. A., and Kingsford, C. (2017). Salmon provides fast and bias-aware quantification of transcript expression. *Nat. Methods* 14, 417–419. doi: 10.1038/nmeth.4197

Porcel, R., Aroca, R., Azcon, R., and Ruiz-Lozano, J. M. (2016). Regulation of cation transporter genes by the arbuscular mycorrhizal symbiosis in rice plants subjected to salinity suggests improved salt tolerance due to reduced na+ root-to-shoot distribution. *Mycorrhiza* 26, 673–684. doi: 10.1007/s00572-016-0704-5

Porcel, R., Aroca, R., and Ruiz-Lozano, J. M. (2012). Salinity stress alleviation using arbuscular mycorrhizal fungi. a review. *Agron. Sustain. Dev.* 32, 181–200. doi: 10.1007/s13593-011-0029-x

Porcel, R., Redondo-Gómez, S., Mateos-Naranjo, E., Aroca, R., Garcia, R., and Ruiz-Lozano, J. M. (2015). Arbuscular mycorrhizal symbiosis ameliorates the optimum quantum yield of photosystem II and reduces non-photochemical quenching in rice plants subjected to salt stress. *J. Plant Physiol.* 185, 75–83. doi: 10.1016/j.jplph.2015.07.006

Porras-Soriano, A., Soriano-Martín, M. L., Porras-Piedra, A., and Azcón, R. (2009). Arbuscular mycorrhizal fungi increased growth, nutrient uptake and tolerance to salinity in olive trees under nursery conditions. *J. Plant Physiol.* 166, 1350–1359. doi: 10.1016/j.jplph.2009.02.010

Ren, C.-G., Kong, C.-C., Yan, K., and Xie, Z.-H. (2019). Transcriptome analysis reveals the impact of arbuscular mycorrhizal symbiosis on sesbania cannabina expose to high salinity. *Sci. Rep.* 9, 1–9. doi: 10.1038/s41598-019-39463-0

Reyes-Pérez, J. J., Ruiz-Espinoza, F. H., Hernández-Montiel, L. G., De Lucía, B., Cristiano, G., and Murillo-Amador, B. (2019). Evaluation of glycosyl-hydrolases, phosphatases, esterases and proteases as potential biomarker for NaCl-trsess tolerance in solanum lycopersicum l. varieties. *Molecules* 24, 2488. doi: 10.3390/molecules24132488

Rivero, J., Ñlvarez, D., Flors, V., Azcón-Aguilar, C., and Pozo, M. J. (2018). Root metabolic plasticity underlies functional diversity in mycorrhiza-enhanced stress tolerance in tomato. *New Phytol.* 220, 1322–1336. doi: 10.1111/nph.15295

Robinson, M. D., Mccarthy, D. J., and Smyth, G. K. (2010). edgeR: a bioconductor package for differential expression analysis of digital gene expression data. *Bioinformatics* 26, 139–140. doi: 10.1093/bioinformatics/btp616

Sarwat, M., Hashem, A., Ahanger, M. A., Abd_Allah, E. F., Alqarawi, A., Alyemeni, M. N., et al. (2016). Mitigation of NaCl stress by arbuscular mycorrhizal fungi through the modulation of osmolytes, antioxidants and secondary metabolites in mustard (Brassica juncea l.) plants. *Front. Plant Sci.* 7, 869. doi: 10.3389/fpls.2016.00869

Shanmugam, V., Lo, J. C., Wu, C. L., Wang, S. L., Lai, C. C., Connolly, E. L., et al. (2011). Differential expression and regulation of iron-regulated metal transporters in arabidopsis halleri and arabidopsis thaliana–the role in zinc tolerance. *New Phytol.* 190, 125–137. doi: 10.1111/j.1469-8137.2010.03606.x

Sharma, P., Jha, A. B., Dubey, R. S., and Pessarakli, M. (2012). Reactive oxygen species, oxidative damage, and antioxidative defense mechanism in plants under stressful conditions. *J. Bot.* 2012. doi: 10.1155/2012/217037

Shomer, I., Novacky, A. J., Pike, S. M., Yermiyahu, U., and Kinraide, T. B. (2003). Electrical potentials of plant cell walls in response to the ionic environment. *Plant Physiol.* 133, 411–422. doi: 10.1104/pp.103.024539

Singh, M., Kumar, J., Singh, V., and Prasad, S. (2014). Proline and salinity tolerance in plants. *Biochem. Pharmacol.* 3, e170. doi: 10.4172/2167-0501.1000e170

Smith, S. E., and Read, D. J. (2010). *Mycorrhizal symbiosis* (New York:Academic press).

Smith, S. E., Smith, F. A., and Jakobsen, I. (2004). Functional diversity in arbuscular mycorrhizal (AM) symbioses: the contribution of the mycorrhizal p uptake pathway is not correlated with mycorrhizal responses in growth or total p uptake. *New Phytol.* 162, 511–524. doi: 10.1111/j.1469-8137.2004.01039.x

Sudhir, P., and Murthy, S. (2004). Effects of salt stress on basic processes of photosynthesis. *Photosynthetica* 42, 481–486. doi: 10.1007/S11099-005-0001-6

Sun, Y., Mu, C., Zheng, H., Lu, S., Zhang, H., Zhang, X., et al. (2018). Exogenous pi supplementation improved the salt tolerance of maize (Zea mays l.) by promoting na+ exclusion. *Sci. Rep.* 8, 16203. doi: 10.1038/s41598-018-34320-y

Supek, F., Bošnjak, M., Škunca, N., and Šmuc, T. (2011). REVIGO summarizes and visualizes long lists of gene ontology terms. *PloS One* 6, e21800. doi: 10.1371/journal.pone.0021800

Thalmann, M., and Santelia, D. (2017). Starch as a determinant of plant fitness under abiotic stress. *New Phytol.* 214, 943–951. doi: 10.1111/nph.14491

Tisarum, R., Theerawitaya, C., Samphumphuang, T., Polispitak, K., Thongpoem, P., Singh, H. P., et al. (2020). Alleviation of salt stress in upland rice (Oryza sativa l. ssp. indica cv. leum pua) using arbuscular mycorrhizal fungi inoculation. *Front. Plant Sci.* 11, 348. doi: 10.3389/fpls.2020.00348

Wakeel, A. (2013). Potassium–sodium interactions in soil and plant under saline-sodic conditions. *J. Plant Nutr. Soil Sci.* 176, 344–354. doi: 10.1002/jpln.201200417

Wang, X., Chang, L., Wang, B., Wang, D., Li, P., Wang, L., et al. (2013). Comparative proteomics of thellungiella halophila leaves from plants subjected to salinity reveals the importance of chloroplastic starch and soluble sugars in halophyte salt tolerance. *Mol. Cell. Proteomics* 12, 2174–2195. doi: 10.1074/mcp.M112.022475

Wang, Y., Dong, F., and Tang, M. (2021). Transcriptome analysis of arbuscular mycorrhizal casuarina glauca in damage mitigation of roots on NaCl stress. *Microorganisms* 10, 15. doi: 10.3390/microorganisms10010015

Wang, M., Li, X., Luo, S., Fan, B., Zhu, C., and Chen, Z. (2020). Coordination and crosstalk between autophagosome and multivesicular body pathways in plant stress responses. *Cells* 9, 119. doi: 10.3390/cells9010119

Wang, J., Qi, M., Liu, J., and Zhang, Y. (2015). CARMO: a comprehensive annotation platform for functional exploration of rice multi-omics data. *Plant J.* 83, 359–374. doi: 10.1111/tpj.12894

Waskom, M., Botvinnik, O., O'kane, D., Hobson, P., Lukauskas, S., Gemperline, D. C., et al. (2017). *Mwaskom/seaborn: v0.8.1 (September 2017) (v0.8.1)* (Zenodo).

Wu, H., Shabala, L., Barry, K., Zhou, M., and Shabala, S. (2013). Ability of leaf mesophyll to retain potassium correlates with salinity tolerance in wheat and barley. *Physiologia Plantarum* 149, 515–527. doi: 10.1111/ppl.12056

Yang, Y., and Guo, Y. (2018). Elucidating the molecular mechanisms mediating plant salt-stress responses. *New Phytol.* 217, 523–539. doi: 10.1111/nph.14920

Yan, A., Wu, M., Yan, L., Hu, R., Ali, I., and Gan, Y. (2014). AtEXP2 is involved in seed germination and abiotic stress response in arabidopsis. *PloS One* 9, e85208. doi: 10.1371/journal.pone.0085208

Yokoyama, R., Rose, J. K. C., and Nishitani, K. (2004). A surprising diversity and abundance of xyloglucan endotransglucosylase/hydrolases in rice. classification and expression analysis. *Plant Physiol.* 134, 1088–1099. doi: 10.1104/pp.103.035261

Zhang, C. H., Ma, T., Luo, W. C., Xu, J. M., Liu, J. Q., and Wan, D. S. (2015). Identification of 4CL genes in desert poplars and their changes in expression in response to salt stress. *Genes* 6, 901–917. doi: 10.3390/genes6030901

Zhang, Q., Wang, C., Tian, J., Li, K., and Shou, H. (2011). Identification of rice purple acid phosphatases related to phosphate starvation signalling. *Plant Biol.* 13, 7–15. doi: 10.1111/j.1438-8677.2010.00346.x

frontiers | Frontiers in Plant Science

TYPE Original Research
PUBLISHED 12 January 2023
DOI 10.3389/fpls.2022.1074383

OPEN ACCESS

EDITED BY
Stefania Astolfi,
University of Tuscia, Italy

REVIEWED BY
Amitava Rakshit,
Banaras Hindu University, India
Vesna Dragicevic,
Maize research Institute Zemun Polje, Serbia

*CORRESPONDENCE
Sumera Yasmin
sumeraimran2012@gmail.com
Tesfaye Wubet
tesfaye.wubet@ufz.de
Mahreen Yahya
mahreenyahya@yahoo.com

SPECIALTY SECTION
This article was submitted to Plant Nutrition, a section of the journal Frontiers in Plant Science

RECEIVED 19 October 2022
ACCEPTED 18 November 2022
PUBLISHED 12 January 2023

CITATION
Yahya M, Rasul M, Hussain SZ, Dilawar A, Ullah M, Rajput L, Afzal A, Asif M, Wubet T and Yasmin S (2023) Integrated analysis of potential microbial consortia, soil nutritional status, and agro-climatic datasets to modulate P nutrient uptake and yield effectiveness of wheat under climate change resilience.
Front. Plant Sci. 13:1074383.
doi: 10.3389/fpls.2022.1074383

Integrated analysis of potential microbial consortia, soil nutritional status, and agro-climatic datasets to modulate P nutrient uptake and yield effectiveness of wheat under climate change resilience

Mahreen Yahya[1]*, Maria Rasul[1,2], Sayed Zajif Hussain[3], Adil Dilawar[4,5], Midrar Ullah[6], Lubna Rajput[7], Aftab Afzal[8], Muhammad Asif[9], Tesfaye Wubet[10,11]* and Sumera Yasmin[1]*

[1]Soil and Environmental Biotechnology Division, National Institute for Biotechnology and Genetic Engineering College, Pakistan Institute of Engineering and Applied Sciences (NIBGE-C, PIEAS), Punjab, Pakistan, [2]Department of Environment and Energy, Sejong University, Neungdong-ro, Gwangjin-gu, Republic of Korea, [3]Department of Chemistry and Chemical Engineering, Syed Babar Ali-School of Science and Engineering (SBA-SSE), Lahore University of Management Sciences (LUMS), Punjab, Pakistan, [4]State Key Laboratory of Resources and Environmental Information System, Institute of Geographic Sciences and Natural Resources Research, Chinese Academy of Sciences, Beijing, China, [5]University of Chinese Academy of Sciences (UCAS), Beijing, China, [6]Department of Biotechnology, Shaheed Benazir Bhutto University, Khyber Pakhtunkhwa, Pakistan, [7]Plant Physiology and Biotechnology Agricultural Research Centre, Sindh, Pakistan, [8]Department of Botany, Hazara University Mansehra, Khyber Pakhtunkhwa, Pakistan, [9]Agricultural Biotechnology Division, National Institute for Biotechnology and Genetic Engineering College, Pakistan Institute of Engineering and Applied Sciences (NIBGE-C, PIEAS), Punjab, Pakistan, [10]Department of Community Ecology, Helmholtz Centre for Environmental Research (UFZ), Halle, Germany, [11]German Centre for Integrative Biodiversity Research (iDiv) Halle-Jena-Leipzig, Leipzig, Germany

Climate change has a devastating effect on wheat production; therefore, crop production might decline by 2030. Phosphorus (P) nutrient deficiency is another main limiting factor of reduced yield. Hence, there is a dire need to judiciously consider wheat yield, so that human requirements and nutrition balance can be sustained efficiently. Despite the great significance of biostimulants in sustainable agriculture, there is still a lack of integrated technology encompassing the successful competitiveness of inoculated phosphate-solubilizing bacteria (PSB) in agricultural systems in the context of climatic conditions/meteorological factors and soil nutritional status. Therefore, the present study reveals the modulation of an integrated P nutrient management approach to develop potential PSB consortia for recommended wheat varieties by considering the respective soil health and agro-climatic conditions. The designed consortia were found to maintain adequate viability for up to 9 months, verified through field emission scanning electron microscopy and viable count. Furthermore, a significant

increase in grain yield (5%–8%) and seed P (4%) content was observed in consortia-inoculated wheat plants with 20% reduced Diammonium phosphate (DAP) application under net house conditions. Fluorescence *in situ* hybridization analysis of roots and amplification of the *gcd* gene of *Ochrobactrum* sp. SSR indicated the survival and rhizosphere competency of the inoculated PSB. Categorical principal component analysis (CAT-PCA) showed a positive correlation of inoculated field-grown wheat varieties in native soils to grain yield, soil P content, and precipitation for sites belonging to irrigated plains and seed P content, soil organic matter, and number of tillers for sites belonging to Northern dry mountains. However, the impact of inoculation at sites belonging to the Indus delta was found significantly correlated to soil potassium (K) content, electrical conductivity (EC), and temperature. Additionally, a significant increase in grain yield (15%) and seed P (14%) content was observed in inoculated wheat plants. Thus, the present study demonstrates for the first time the need to integrate soil biological health and agro-climatic conditions for consistent performance of augmented PSB and enhanced P nutrient uptake to curtail soil pollution caused by the extensive use of agrochemicals. This study provides innovative insights and identifies key questions for future research on PSB to promote its successful implementation in agriculture.

KEYWORDS

soil-specific consortia, rhizoscanning, soil organic matter, root architecture, climatic conditions, fluorescence *in situ* hybridization, field emission scanning electron microscopy

Introduction

Global warming is causing a rapid increase in the Earth's surface temperature, leading agriculture to face multiple challenges (Camaille et al., 2021). In addition, climate change is the major uncontrollable factor, adversely affecting global food production (Farooq et al., 2022). Climate change is likely to increase the intensity of extreme climate events that will affect patterns of agricultural production, water cycle, and eventually food security (Muluneh, 2021). All of these events resulted in increasing floods, declining food production and quality, and increasing food prices. Such events caused substantial yield losses in major cereal crops such as 5.5% yield reduction in wheat (Shah et al., 2021). On the other hand, global food demand is expected to increase by 60% with the increasing global population (Bijl et al., 2018). Therefore, there is a pressing need at this crucial time to transit toward sustainable crop production that enables crops to grow well under resource-limited environmental challenging conditions with optimum yields across a wide array of environmental conditions (Reynolds et al., 2021).

Today, novel and advanced techniques such as smart irrigation, fertilizers with enhanced efficiency, integration fertilizers, and pest management have been adapted for sustainable crop production (Ahmad et al., 2022). The challenge faced by 40% of the global phosphorus (P)-deficient soil has been addressed by the application of phosphatic chemical fertilizers in recent years. However, most of these chemical fertilizers applied to the soil become unavailable to the plant, and their excessive application to overcome the P deficiency leads to environmental pollution concerning contamination of groundwater and eutrophication (Alori et al., 2017). Rock phosphate (RP), on the other hand, is the primary source of P, but it is a nonrenewable resource that is progressively exhausted worldwide (Pavinato et al., 2022). RP has low agronomic effectiveness due to its crude nature, high reactivity, and less solubility in the soil (Soumare et al., 2020).

Integration of plant growth-promoting bacteria in agriculture biotechnology represents a promising solution for improved soil fertility and crop yield. A group of microorganisms called phosphate-solubilizing bacteria (PSB) is the key component to increasing the availability of insoluble P for plant use. Nowadays, PSB-based biofertilizers are considered crucial constituents that contribute to sustainable production in agro-ecosystems (Mitter et al., 2021). The persistence of PSB is the most important underlying factor in designing successful bioinoculants because it indicates the interaction of the

microbial inoculation with the host plant, its capability to compete with indigenous microbes and cope with abiotic conditions that depend on soil type, its characterization, and agro-climatic conditions (Finkel et al., 2017). Therefore, designing climate-smart biofertilizers and evaluating their persistence in native soil and climate would be a potential approach to boost plant growth and substantial resilience in agriculture.

To the best of our knowledge, a holistic approach to disentangle the system in the context of climatic conditions/meteorological factors and soil nutritional status is scarce. As previous microbial inocula are either being evaluated under controlled conditions (Chen and Liu, 2019; Elhaissoufi et al., 2020) or if conducted under field conditions (Sedri et al., 2022; Liu et al., 2022), no emphasis is usually given to the native microbial bacteria, soil nutrient status, and climatic conditions of the agricultural site. Most of the previous studies are based on identifying microbes in the wheat rhizosphere and application of the same bacteria to different environments (Mahoney et al., 2017; Ullah et al., 2022; Sedri et al., 2022); however, studies on the development of soil-specific PSB consortia and their application in respective climatic zones are entirely missing.

Hence, the present study is the first comprehensive report in which soil-specific consortia were developed, composed of indigenous PSB from wheat-growing agro-climatic zones of Pakistan, and implemented in their respective soils under field conditions for wheat. It was thus hypothesized (H1) that the application of soil-specific consortium along with recommended wheat varieties can improve wheat yield predominantly by relating to the soil nutritional status and meteorological conditions to ensure the survival of inoculated native PSB in the wheat rhizosphere. A positive correlation might exist (H2) between meteorological and soil nutritional factors and wheat yield that might result in improved wheat production.

Materials and methods

Sample collection, soil physicochemical analysis, and environmental data

Soil samples were collected from different provinces of Pakistan. Province 1, i.e., Site 1: Faisalabad (31°23'45.1"N, 73° 01'3.4"E), Site 2: Nankana Sahib (31°27′0″N, 73°42′24″E), and Site 3: Pindi Bhattian (31°6'954"N, 73°18'66"E); Province 2, i.e., Site 4: Hazara (34°25′12″N, 73°15′0″E); and Province 3, i.e., Site 5: Husri (25°19′0″N, 68°25′0″E) and Site 6: Tando Jam (25°25′ 40.21″N, 68°31′40.4″E) were selected for the study. Soil samples from each site were collected at the depth of 20 cm and analyzed for soil physicochemical properties. Soil pH and electrical conductivity (EC) were measured using a pH meter (PHS-3C, REX, Shanghai) and an electrical conductivity meter (DDS-307A, REX, Shanghai), respectively (Rhoades, 1993). The wet oxidation method was used to determine soil organic matter (Nelson and Sommers, 1996). Soil total nitrogen (N) was determined by the Kjeldahl method (Bremner and Mulvaney, 1983). Soil-available P was measured by the sodium bicarbonate method (Olsen, 1954). Sodium content and soil exchangeable potassium (K) were determined using a flame photometer (Model 410, Corning, Halstead, UK; Simard, 1993). Meteorological data of each site were collected from Pakistan Meteorological Department (PMD) (https://www.pmd.gov.pk/en/).

Bacterial strains used

Bacterial strains used in this study are a subset of a large collection of PSB isolated from the rhizosphere soil of wheat grown in different agro-ecological zones of Pakistan (Yahya et al., 2021). PSB, i.e., *Bacillus* sp. TAYB, *Enterobacter* spp. ZW9, *Enterobacter* spp. ZW32, *Enterobacter* spp. D1, *Ochrobactrum* sp. SSR, *Pantoea* sp. S1, and *Pseudomonas* sp. TJA were used in the study for consortium development and obtained from the National Institute for Biotechnology and Genetic Engineering (NIBGE) Biotech Resource Center (NBRC: http://www.nibge.org/Default.aspx). The 16S rRNA gene sequences of these strains were deposited to NCBI GenBank (https://www.ncbi.nlm.nih.gov/). *Enterobacter* spp. ZW32 (accession number: MK817561), *Ochrobactrum* sp. SSR (accession number: MK422612), and *Enterobacter* spp. ZW9 (accession number: MK024209) were isolated from Province 1 (Punjab). *Enterobacter* spp. D1 (accession number: MK422618) and *Pantoea* sp. S1 (accession number: MK422619) were isolated from Province 2 [Khyber Pakhtunkhwa (KPK)]. While *Bacillus* sp. TAYB (accession number: MN754081) and *Pseudomonas* sp. TJA (accession number: MK422620) were isolated from Province 3 (Sindh).

All of the strains used in the present study have multiple plant growth-promoting attributes, i.e., phosphate solubilization, zinc solubilization, indole acetic acid production, and organic acid production (Yahya et al., 2021).

Development of bioformulation with soil-specific consortia

Three different consortia were designed by selecting soil-/site-specific PSB for recommended wheat varieties to that particular site. Wheat variety-1 Faislabad-2008 recommended for Province 1 (Punjab) was inoculated with consortium-1, i.e., *Enterobacter* spp. ZW32, *Ochrobactrum* sp. SSR, and *Enterobacter* spp. ZW9. Consortium-2 comprising *Enterobacter* spp. D1, *Ochrobactrum* sp. SSR, and *Pantoea* sp. S1 was designed for wheat variety-2 (Fakhr-e-Sarhad) recommended for Province 2 (KPK). Whereas consortium-3 comprising *Bacillus* sp. TAYB, *Ochrobactrum* sp.

SSR, and *Pseudomonas* sp. TJA was used for wheat variety-3 (TD1) recommended for Province 3 (Sindh).

For the preparation of the inoculum, a loopful of each bacterial culture was transferred to 25 ml of Luria-Bertani (LB) broth medium separately and grown anaerobically on a rotatory shaker at 28°C ± 2°C for 24 to 48 h. Bacterial cultures for each consortium were mixed separately to make a suspension (1×10^9 CFU ml^{-1}).

Three filter mud (FM) and soil-specific consortia-based bioformulations were developed. FM, an agro-industrial by-product of sugar cane (Yahya et al., 2022), was ground and sieved through a 2-mm sieve and further autoclaved before inoculation. The bacterial suspension (300 ml) of each consortium (1×10^9 CFU ml^{-1}) was then aseptically and uniformly mixed in 700 g of FM, packed in polythene bags, and incubated at 28°C (Pastor-Bueis et al., 2019). Uninoculated control was prepared by mixing LB broth (300 ml) with sterilized FM (700 g).

Field emission scanning electron microscopy of bioformulations

Field emission scanning electron microscopy (FESEM) was used to assess the presence of inoculated PSB in the tested formulations up to 270 days post-inoculation (DPI). Furthermore, the viability of inoculated bacteria was estimated from each bioformulation on LB agar medium and National Botanical Research Institute's phosphate (NBRIP) agar medium by the serial dilution method (Nautiyal, 1999).

Evaluation of soil-specific consortia in earthen pots under net house conditions

The effect of three bioformulations was assessed on wheat variety Faisalabad 2008 using native soil collected from Faisalabad (loamy soil texture, available P 1.87 mg kg^{-1}, organic matter 0.57%, and pH 8) in earthen pots under net house conditions. Seeds were sterilized with 1.5% sodium hypochlorite (NaOCl) solution for 5 min and washed with autoclaved sterilized water five times. Sterilized seeds were pelleted with bioformulation (2 kg of carrier per 50 kg seeds) comprising respective consortium suspension (1×10^9 CFU ml^{-1}). Seeds were then incubated for 30 min. Seeds pelleted with uninoculated sterilized FM were used as controls. Six seeds were sown per pot (30 cm diameter) containing 5 kg of soil and arranged in a completely randomized design. All inoculated treatments were supplemented with 80% DAP, i.e., 20% reduced amount of DAP, and two uninoculated controls supplemented with 80% or 100% DAP.

Measurement of plant growth parameters and soil nutrient analysis

Plants were uprooted after 35 DPI to evaluate plant growth parameters, i.e., root length, shoot length, and dry weight of plant. Plants were harvested at maturity, and data regarding plant height, number of tillers, grain yield, plant biomass, and plant P content (Tandon, 1993) were recorded. Six plants were selected from each replicate of each treatment for analysis. Rhizospheric soil was analyzed for available P by the molybdenum blue method (Olsen, 1954) and alkaline phosphatase activity by p-nitrophenyl method (Tabatabai and Bremner, 1969).

Detection of inoculated Phosphate Solubilizing bacteria (PSB)

The survival of inoculated Phosphate Solubilizing bacteria (PSB) was assessed by viable count (Somasegaran and Hoben, 2012). Root colonization and persistence of inoculated PSB were studied by fluorescence *in situ* hybridization (FISH). FLUOS-labeled green probe EUB338 was used to detect the PSB population. Reisolated colonies of PSB were identified by comparing morphological characteristics and P solubilization to that of pure colonies (Yasmin et al., 2016). Morphologically similar colonies of SSR obtained from all inoculated treatments were further validated by amplification of the *gcd* gene (MK883703) specific for *Ochrobactrum* strain SSR (Rasul et al., 2021).

Evaluation of soil-specific consortia for wheat yield parameters in multilocational field trials

The developed consortia were further evaluated under different wheat-growing agro-climatic field conditions during the winter season of 2019–2020 in Province 1 (Punjab), i.e., NIBGE field, Faisalabad, Pindi Bhattian, Nankana Sahib; Province 2 (KPK), i.e., Hazara; and Province 3 (Sindh), i.e., Husri and Tando Jam (Figure 1). All three consortia were prepared as described in the above section. Bacterial cultures for each consortium were mixed separately to make a suspension (1×10^9 CFU ml^{-1}), then mixed uniformly with FM (700 g) and incubated at 28°C (Pastor-Bueis et al., 2019). Three treatments composed of consortium-inoculated seeds supplemented with 80% of the recommended dose of DAP (i.e., 20% reduced DAP) and two uninoculated controls supplemented with 80% or 100% of DAP (i.e., recommended dose of DAP) were considered for multilocation trials.

Experiments were carried out in a randomized complete block design. Each treatment consisted of three replicates and a plot size of 4 m × 6 m at NIBGE, 4 m × 4 m at Pindi Bhattian, 6 m × 6 m at Nankana Sahib and Hazara, and 4 m × 5 m at Husri and Tando Jam. Seeds were sown by the drill method using a hand drill. The experiment was conducted under standard agronomic practices. At maturity, plants were harvested and data were recorded for

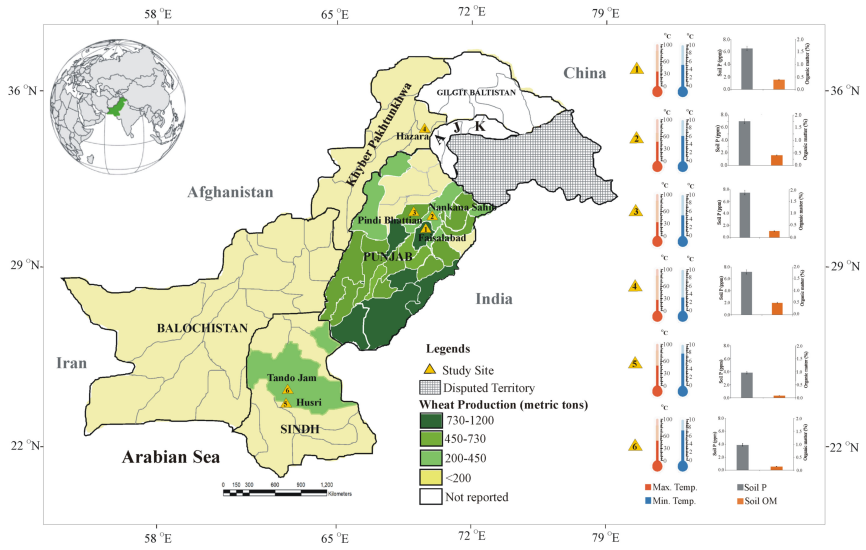

FIGURE 1
Map of Pakistan with multilocation trials targeted in the present study for evaluation of soil-specific consortia on recommended wheat varieties. Different shades of green colors highlight the region showing wheat production in the main wheat districts of Pakistan (source: https://ipad.fas.usda.gov/countrysummary/Default.aspx?id=PK&crop=Wheat). Thermometers and bar graphs show climatic temperature (Pakistan Meteorological Department; source: https://www.pmd.gov.pk/en/) soil available P and organic matter of the soil of study sites.

grain yield, plant biomass, harvest index (HI), plant height, number of tillers, and seed P. Soil-available P (Olsen, 1954) and alkaline phosphatase activity (Tabatabai and Bremner, 1969) were determined according to standard protocols.

Statistical analysis

Data were statistically analyzed using ANOVA. Least significant difference (LSD) compared variations between the treatments at a 5% level of confidence using Statistix 10 software (Tallahassee, FL, USA). Principal component analysis (PCA) was performed using SPSS 23.0 software (SPSS Inc., USA).

Results

Soil physicochemical analysis and environmental data

Biochemical analysis of soil parameters revealed the difference in soil properties for all of the soils from five different sites belonging to major wheat-growing areas (Table 1). Organic matter of the soils from the Indus delta (Sindh) was below 1%. While in soils from the Northern irrigated plains (Punjab) and in particular from the Northern dry mountains Khyber Pakhtunkhwa (KPK), the organic matter was up to 1.7%. As Pakistani soils are alkaline calcareous in nature, the pH of the soils ranged from 7 to 8.5. Soil EC was much higher in soils belonging to the Indus delta (3.42 dS m^{-1}) and lower in soils of the Northern dry mountains (1.1 dS m^{-1}). Whereas soil N, P, and K content were higher in the KPK soils and much lower in soils belonging to Sindh.

Shelf life of the bioformulations

Three FM-based soil-specific consortia were evaluated for shelf life under controlled conditions. The survival of all PSB included in the three consortia was confirmed up to 270 DPI as indicated by both viable count and visualization of PSB by FESEM (Figure 2; Table S1). Maximum viability of soil-specific consortia was maintained (up to 2 × 10^9 CFU ml^{-1}) at 90 DPI for consortium-1 (Table S1).

Evaluation of soil-specific consortia in earthen pots under net house conditions

All PSB consortia improved wheat growth significantly in the pot experiment under net house conditions (Figure 3). Consortium-1 showed the maximum increase in grain yield (5.95 g $plant^{-1}$) followed by consortium-2 (5.83 g $plant^{-1}$) and

TABLE 1 Physicochemical properties of soils collected and environmental data of the experimental field sites.

Parameters		Experimental sites					
		Site 1 Faisalabad	Site 2 Nankana Sahib	Site 3 Pindi Bhattian	Site 4 Hazara	Site 5 Husri	Site 6 Tando Jam
Physico-chemical Properties	pH	7.94 ± 0.41	7.98 ± 0.42	7.62 ± 0.38	7.50 ± 0.52	8.20 ± 0.41	8.50 ± 0.43
	EC (dS m^{-1})	1.25 ± 0.06	1.51 ± 0.08	1.45 ± 0.07	1.10 ± 0.05	2.16 ± 0.41	3.42 ± 0.17
	Organic matter (%)	1.57 ± 0.03	1.60 ± 0.03	1.06 ± 0.03	1.71 ± 0.05	0.32 ± 0.04	0.56 ± 0.05
	Available P (µg kg^{-1})	4.21 ± 0.29	4.73 ± 0.36	4.45 ± 0.31	4.60 ± 0.31	3.27 ± 0.22	3.52 ± 0.28
	Total N (%)	0.030 ± 0.002	0.327 ± 0.002	0.031 ± 0.001	0.042 ± 0.003	0.017 ± 0.001	0.025 ± 0.001
	Extractable K (mg kg^{-1})	153 ± 7.65	149 ± 7.45	129 ± 6.45	125 ± 6.57	181 ± 9.05	145 ± 7.25
	Soil Texture	Sandy Loam	Loam	Sandy Loam	Loam	Clay Loam	Clay Loam
Climatic Conditions	Rain fall (mm)	225.67 ± 11.28	254.50 ± 12.73	244.50 ± 12.23	166.43 ± 8.32	7.53 ± 0.38	8.07 ± 0.40
	Average min Temp(°C)	12.08 ± 0.60	11.75 ± 0.59	11.49 ± 0.57	9.80 ± 0.49	13.23 ± 0.66	13.87 ± 0.69
	Average max Temp(°C)	24 ± 1.20	23.50 ± 1.18	23.50 ± 1.18	23.60 ± 1.18	27.60 ± 1.38	27.73 ± 1.39
	Relative Humidity (%)	62.87 ± 3.14	64.40 ± 3.22	64.17 ± 3.21	63.00 ± 3.15	55.83 ± 2.79	56.17 ± 11.95
	Sunshine Duration (hours/month)	195.33 ± 9.77	183.67 ± 9.18	182.53 ± 9.13	157.37 ± 7.87	239.00 ± 11.95	237 ± 11.85

Physicochemical properties of soils collected from different sites of wheat-growing areas, Pakistan. Values are an average of six biological replicates EC, Eclectic conductivity; KPK, Khyber Pakhtunkhwa.

consortium-3 (5.77 g $plant^{-1}$) as compared to 80% and 100% uninoculated controls. A significant increase (3.6%–4.1%) in seed P was observed in inoculated plants compared to uninoculated controls. Upon inoculation with the consortia, an increase in available soil P (5.7–6.25 µg g^{-1} soil) and phosphatase activity (22–24 µmol g^{-1} soil h^{-1}) was observed (Table S2).

The presence of inoculated PSB was detected on wheat roots from the earthen pot experiment at 35 DPI (Figure 4). The highest density of PSB was observed in roots inoculated with consortium-1 and consortium-3 (Figures 4B, D). Reisolated PSB colonies were identified based on their morphological characteristics and phosphate solubilization (233–359 µg ml^{-1}). Furthermore, one of the PSB strains, *Ochrobactrum* SSR, was validated by the amplification of the strain-specific *gcd* gene that confirmed the presence of inoculated bacteria in consortia-inoculated soil (Figure S1).

Evaluation of soil-specific consortia on wheat yield parameters in multilocational field trials

Soil-specific consortia improved various plant growth parameters of wheat under respective soil conditions. Maximum grain yield (5,390 kg ha^{-1}) was observed as a result of consortium-1 inoculation at site 2 followed by site 3 (5,240 kg ha^{-1}) and site 1 (4,806 kg ha^{-1}). In the case of consortium-2, grain yield of 5,174 kg ha^{-1} was observed at site 4 with a 20% reduced application of DAP. Maximum grain yield (5,324 kg ha^{-1}) was observed as a result of consortium-2 inoculation at site 6 followed by site 5 (4,806 kg ha^{-1}). HI ranged from 30% to 36%.

Inoculation of consortium-1 increased (up to 15%) grain yield at site 2 followed by site 3 (12%) and site 1 (2%). However, inoculation of consortium-2 increased the grain yield by 8% at

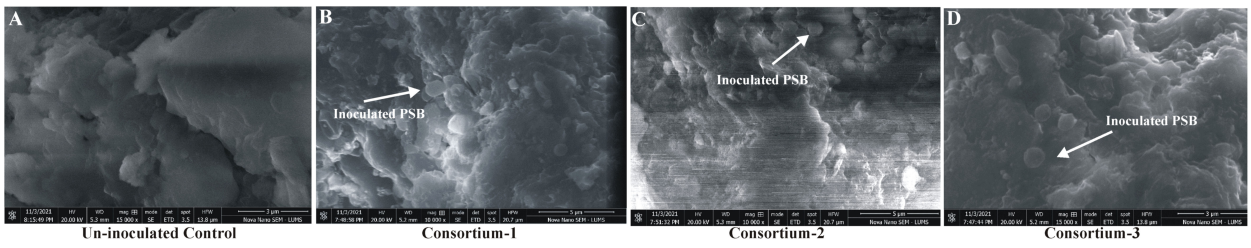

FIGURE 2
Shelf life study of filter mud-based formulation inoculated with soil-specific consortia under controlled conditions. Field emission scanning electron microscopic (FESEM) analysis of uninoculated filter mud-based bioformulations **(A)** and inoculated filter mud-based bioformulations with consortium-1 **(B)**, consortium-2 **(C)**, and consortium-3 **(D)**.

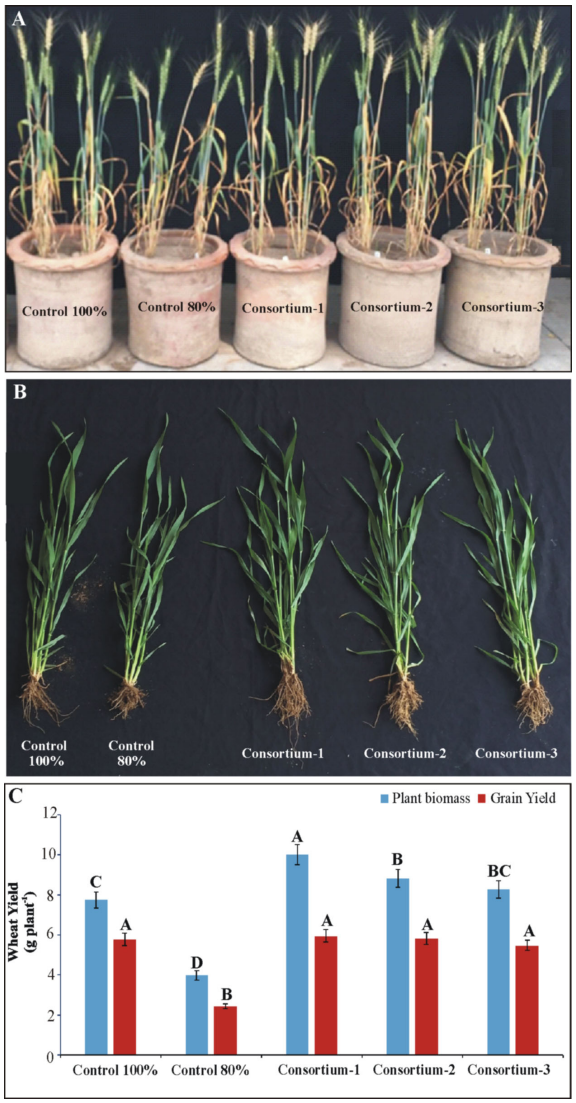

FIGURE 3
Evaluation of soil-specific consortia for plant yield parameters of wheat grown in pots under net house conditions **(A, B)**. Effects of bioformulation on plant biomass **(C)** and grain yield were recorded. Mean values denoted by the same letter are not significantly different at P = 0.05 according to LSD.

site 4 as compared to 80% control. The increase in grain yield was 5% at site 5 and 14% at site 6 in inoculated treatments with consortium-3 as compared to 80% control (Table 2).

Effect of PSB inoculation on plant P content

A significant increase in plant P content was observed as a result of PSB inoculation. The PSB-inoculated treatments showed a significant increase in plant seed P content compared to the 80% and 100% controls. The plant P content was significantly higher (4%–4.9%) in inoculated treatments at sites 1, 2, and 3 followed by sites 4, 6, and 5 (Table 2). Maximum plant P content (4.9%) was observed at site 2 followed by site 1 (4.5%) in PSB-inoculated treatment as compared to both 80% and 100% controls, whereas plant P content at site 6 (3.7%) and site 5 (3.5%) also increased as compared to both controls.

Effect of PSB inoculation on soil-available P and phosphatase activity

Soil phosphatase activity was also significantly higher in PSB-inoculated treatments. There was a pronounced increase in soil phosphatase activity at sites 2, 3, and 1, followed by sites 4, 6, and 5. Maximum soil phosphatase activity (26 μmoles g^{-1} soil h^{-1}) was observed for site 1 in consortium-1-inoculated treatment as compared to both 80% and 100% controls. The maximum soil phosphatase activity (24 μmoles g^{-1} soil h^{-1}) was for site 4 in consortium-2-inoculated treatment. While soil phosphatase activity (17 μmoles g^{-1} soil h^{-1}) for sites 5 and 6 in consortium-3-inoculated treatment was higher as compared to both 80% and 100% controls (Table 2).

Trends and variations of meteorological factors at multilocational field sites

The trends in the change of key meteorological factors were analyzed during the wheat season 2019–2020 at the six field sites with respect to precipitation and temperature (Figure 4). Maximum precipitation was recorded at site 4 during the month of March. However, precipitation was recorded during the months of January, February, and April at site 4. Minimum precipitation was recorded at sites 5 and 6, which was almost negligible. Whereas a moderate level of precipitation was recorded for sites 1, 2, and 3 throughout the wheat season except for the month of March. On the other hand, the maximum temperature was observed at sites 5 and 6, while the minimum temperature was recorded at site 4 (Figure 5).

Correlation between growth parameters, soil physicochemical attributes, and meteorological factors

Plant growth parameters were subjected to categorical principal component analysis (CAT-PCA). The PCA plot showed the correlation between the wheat yield parameters, with the two principal components (PCs) contributing up to 73% to the variance on the x-axis (PC1 = 51%) and y-axis (PC2 = 22%). Inoculated plants had a significant (positive) effect on grain yield, plant tillers, soil-available P, soil phosphatase activity, and seed P content. No parameter was found negatively affected by the PSB inoculation. The analysis demonstrated the treatment differences in all six soils. Among the six soils, the effect of treatments was pronounced at sites 2, 3, 5, and 6. PCA showed a pronounced effect of soil-specific

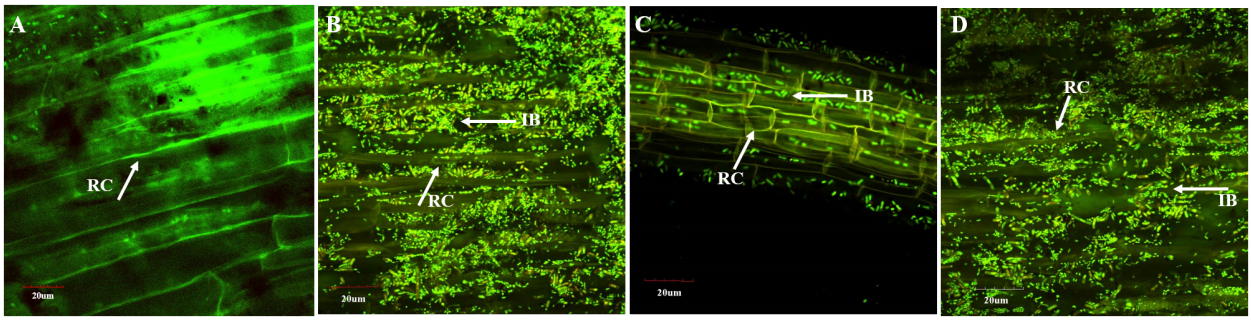

FIGURE 4
Confocal laser scanning microscopy of wheat roots at 35 days after inoculation of consortia in pot experiment under net house conditions. Oligonucleotide probes labeled with FLUOS dye showed green fluorescent signals for the entire bacterial population in the uninoculated control **(A)** and in wheat inoculated with consortium-1 **(B)**, consortium-2 **(C)**, and consortium-3 **(D)**. IB, inoculated bacteria; RC, root cells.

consortium on plant growth parameters and soil parameters (Figure 6). Regression analysis confirmed a positive correlation between wheat yield parameters, i.e., seed P content, wheat grain yield, and soil-available P as a result of PSB consortium application in multilocational field trials (Figure S2).

Furthermore, CAT-PCA of wheat yield parameters, soil physicochemical analysis, and meteorological factors revealed that the success of each consortium was the result of varying factors associated with the meteorological conditions and soil nutritional status of that site (Figure 7). A total of 71% variation was explained by PCA, where 64% variance was accounted for by PC1 and 7% by PC2. A positive correlation of PSB-inoculated field-grown wheat to grain yield, soil P content, and precipitation was observed for sites 2 and 3 belonging to irrigated plains. While seed P content, soil organic matter, and number of tillers were found positively correlated with site 4 belonging to Northern dry mountains. However, the impact of inoculation at sites 5 and 6 belonging to the Indus delta was found considerably correlated to soil K content, EC, and temperature.

Discussion

The burgeoning global biofertilizer market for agricultural use is driven by the pressure to surge sustainable crop production. The success of biofertilizers is primarily dependent upon the ability of inoculants to persist and perform effectively under natural environmental conditions (Lopes et al., 2021). Although an elite bacterial strain is essential for the efficacious development of inoculants, non-biological components are the foremost dynamics for the consistent performance of inoculum under field conditions (Mendoza-Suárez et al., 2021). Extensive field evaluation of inoculum has rarely been evaluated under a range of soils and environmental conditions and is urgently needed to foster successful implementation by farmers or growers. The potential impact of the environment on inoculation is usually neglected. Therefore, this study provides the first holistic report on the development of soil-specific PSB consortia and their application in respective agro-climatic conditions.

Three consortia were designed for their native soils and respective recommended wheat varieties by using the most efficient PSB having multiple plant growth-promoting traits such as indole acetic acid production, zinc solubilization, and siderophore production (Yahya et al., 2021). This is because native microorganisms are more adaptable and persist longer in native soils (Souza et al., 2015). A shelf-life study of three consortia up to 270 DPI indicated that these are the elite PSB strains and that FM had significantly maintained a higher bacterial load. This also suggests that the carrier material based on FM provides a more suitable microenvironment for inoculated PSB and has a longer shelf life. This is an essential property of carrier materials for maintaining microbial viability (Soumare et al., 2020).

Therefore, for designing the optimal inoculant formulation, a well-characterized FM-based carrier material was used in the study. Other contributing factors for the maintenance of microbial viability are the constitutional essential elements in FM, predominantly silicon (Si), iron (Fe), P, calcium (Ca), magnesium (Mg), carbon (C), and oxygen (O) (Yahya et al., 2022). Studies showed that a significant amount of Si, Fe, P, Ca, and Mg in FM made it a suitable product as a source of nutrients (Dotaniya et al., 2016).

To investigate the contribution of these PSB bioformulations to crop yield, a pot experiment was performed with Faisalabad 2008 variety of wheat grown under net house conditions. Significant increase (up to 1.4%) in grain yield, plant biomass (1-1.3%), seed P content (up to 4.32%), and soil phosphatase activity (up to 24%) and subsequent P availability in the soil (up to 6.25%) was observed in inoculated plants treated with reduced (20%) application of DAP.

The survivability of inoculated PSB in wheat rhizosphere was verified by viability and FISH, indicating that inoculated PSB were rhizosphere-competent phosphobacteria. Furthermore, the P-

TABLE 2 Effect of PSB consortia on various wheat yield and soil parameters in multilocational field trials.

Province	Sites	Districts	Treatments	No. of tillers (tillers m^{-2})	Plant height(cm)	Plant biomass (kg ha^{-1})	Grain yield (kg ha^{-1})	[1]Seed P (%)	[2]Soil Available P	[3]Phosphatase Activity	Harvest Index(%)
Province 1 (Punjab)	**1**	Faisalabad	Inoculated	373 ± 19 A	107 ± 5.51 A	14,500 ± 725 A	4,806 ± 240 A	4.50 ± 0.23 A	6.30 ± 0.31 A	26.33 ± 1.32 A	33
			80% Control	321 ± 16 A	104 ± 5.22 A	14,300 ± 715 A	4,728 ± 236 A	4.00 ± 0.20 B	5.60 ± 0.28 B	23.20 ± 1.16 B	33
			100% Control	338 ± 17 A	105 ± 5.25 A	14,400 ± 720 A	4,789 ± 239 A	4.17 ± 0.21AB	5.97 ± 0.29 AB	24.20 ± 1.21 AB	33
	2	Nankana Sahib	Inoculated	480 ± 24 A	110 ± 5.57 A	17,050 ± 852 A	5,390 ± 270 A	4.50 ± 0.23 A	6.37 ± 0.32 A	27.00 ± 1.32 A	32
			80% Control	370 ± 19 B	105 ± 5.00 B	14,333 ± 717 B	4,610 ± 231 B	4.05 ± 0.20 B	5.64 ± 0.28 A	24.20 ± 0.50 B	32
			100% Control	407 ± 20 B	108 ± 5.03 AB	15,250 ± 763 B	4,810 ± 247 AB	4.13 ± 0.21 AB	6.07 ± 0.30 A	25.20 ± 0.96 B	32
	3	Pindi Bhattian	Inoculated	340 ± 17 A	109 ± 5.43 A	17,167 ± 858 A	5,240 ± 262 A	4.00 ± 0.20 A	5.33 ± 0.27 A	27.00 ± 1.35 A	31
			80% Control	262 ± 13 B	105 ± 5.25 A	15,167 ± 758 B	4,590 ± 230 B	3.65 ± 0.18 B	4.99 ± 0.25 B	23.63 ± 1.18 B	30
			100% Control	277 ± 14 B	108 ± 5.38 A	16,033 ± 767 B	5,020 ± 251 A	3.81 ± 0.19 AB	5.08 ± 0.25 AB	25.30 ± 1.27 AB	31
Province 2 (KPK)	**4**	Hazara	Inoculated	440 ± 22 A	107 ± 5.35 A	14,489 ± 724 A	5,174 ± 259 A	3.55 ± 0.18 A	4.52 ± 0.23 A	24.67 ± 1.24 A	36
			80% Control	342 ± 17 B	105 ± 5.25 A	13,051 ± 653 C	4,747 ± 237 C	3.20 ± 0.16 B	4.13 ± 0.21 B	21.33 ± 1.07 B	36
			100% Control	357 ± 18 B	106 ± 5.30 A	13,905 ± 698 B	4,954 ± 248 B	3.25 ± 0.16 B	4.30 ± 0.22 AB	22.00 ± 1.10 AB	36
Province 3 (Sindh)	**5**	Husri	Inoculated	351 ± 19 A	85 ± 4.25 A	15,075 ± 841 A	4,806 ± 240 A	2.91 ± 0.15 A	3.95 ± 0.20 A	20.07 ± 1.00 A	32
			80% Control	322 ± 16 A	82 ± 4.24 A	14,789 ± 703 A	4,550 ± 228 B	2.62 ± 0.13 B	3.58 ± 0.18 B	18.17 ± 0.91 B	31
			100% Control	338 ± 17 A	85 ± 4.12 A	14,855 ± 708 A	4,642 ± 232 B	2.79 ± 0.14 AB	3.61 ± 0.18 B	15.33 ± 0.96 AB	31
	6	Tando Jam	Inoculated	373 ± 19 A	89 ± 4.47 A	16,276 ± 813 A	5,324 ± 266 A	3.05 ± 0.15 A	4.50 ± 0.23 A	21.33 ± 1.07 A	33
			80% Control	328 ± 16 B	81 ± 3.75 A	14,089 ± 704 B	4,587 ± 229 B	2.72 ± 0.14 B	4.14 ± 0.21 B	19.67 ± 0.98 B	33
			100% Control	347 ± 17 AB	85 ± 3.77 A	14,389 ± 719 B	4,712 ± 236 B	2.80 ± 0.14 B	4.37 ± 0.22 AB	20.17 ± 1.01 B	33

Data are an average of three replicates.
[1]Plant P content is given in % of total plant weight.
[2]Soil-available P is presented in μg g^{-1} soil.
[3]Soil phosphatase activity is presented in μmoles g^{-1} soil h^{-1}.
± represents standard deviation. Means with significant differences ($P < 0.05$) among treatments are represented by different letters. KPK, Khyber Pakhtunkhwa.

10.3389/fpls.2022.1074383

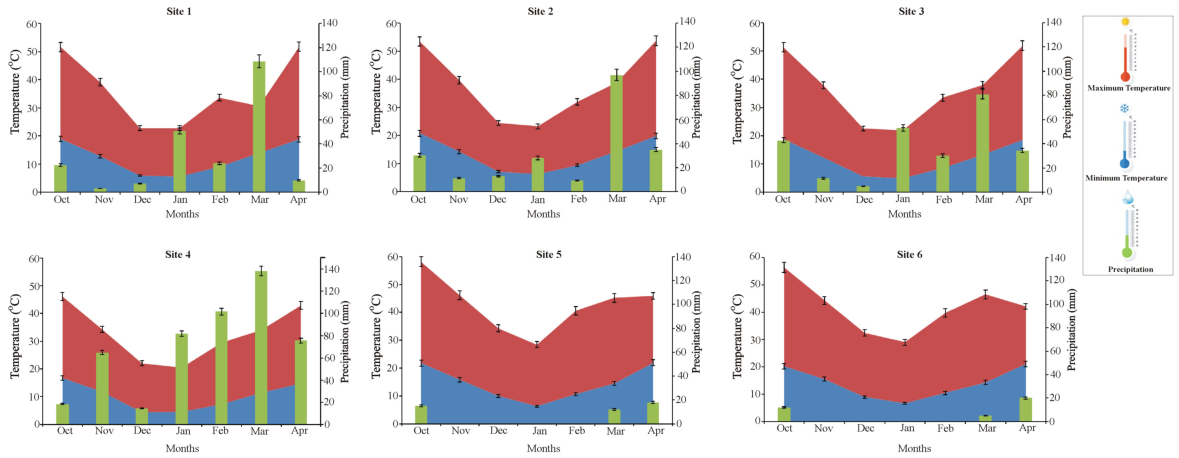

FIGURE 5
Trends of meteorological factors at multilocation field sites with respect to precipitation (green), minimum temperature (blue) and maximum temperature (red) during the wheat season 2019-20. Site1: Faisalabad, Site 2: Nankana Sahib, Site 3: Pindi Bhattian, Site 4: Hazara, Site 5: Husri and Site 6: TandoJam.

solubilizing ability of reisolated PSB was compared to their pure cultures, indicating the persistence of inoculated PSB. Morphologically similar reisolated colonies of SSR obtained from inoculated treatments were further validated by amplification of the *gcd* gene (MK883703) specific for *Ochrobactrum* strain SSR (Rasul et al., 2021). As SSR is one of the most potent strains for which strain-specific primers were available. Persistent colonization of PGPR in the rhizosphere indicates that bacteria can perform their functions (Lopes et al., 2021) and form associations with local microbial communities (Santoyo et al., 2021).

The P-solubilizing efficacy of the three PSB consortia was further evaluated under field conditions in their respective wheat-growing areas and recommended wheat varieties. The results showed an increase in grain yield (2%–14%) and seed P content

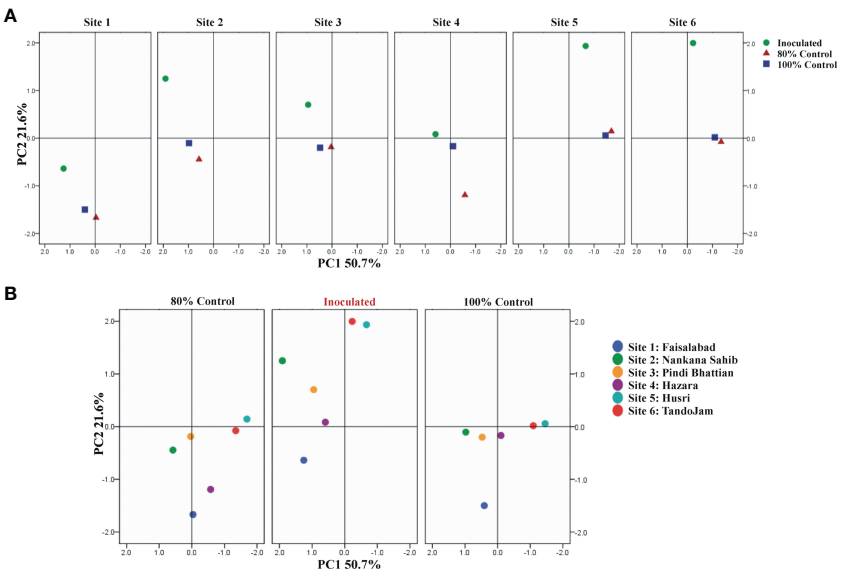

FIGURE 6
Principal component analysis (PCA) of wheat varieties inoculated with PSB and reduced application of DAP; treatment-wise **(A)** and location-wise analysis **(B)**. Treatments: inoculation of soil-specific consortia and uninoculated controls. Site 1: Faisalabad, Site 2: Nankana Sahib, Site 3: Pindi Bhattian, Site 4: Hazara, Site 5: Husri, and Site 6: Tando Jam.

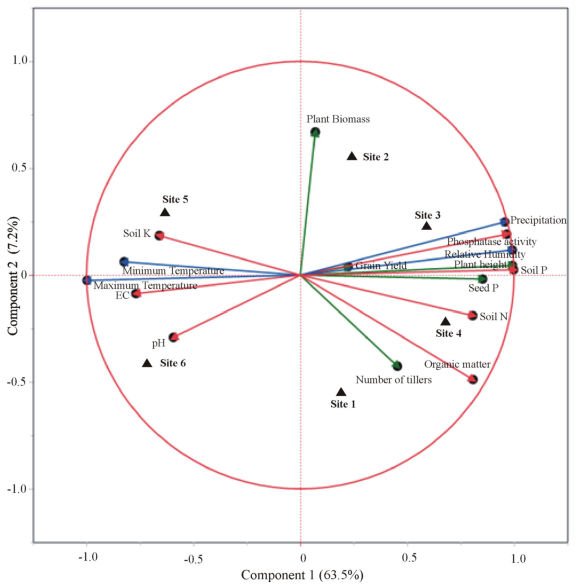

FIGURE 7
Categorical principal component analysis (CAT-PCA) of wheat yield parameters, seed P content, soil nutrient parameters, and climatic/meteorological conditions at the trial sites in response to inoculation of phosphate-solubilizing bacteria. Site 1: Faisalabad, Site 2: Nankana Sahib, Site 3: Pindi Bhattian, Site 4: Hazara, Site 5: Husri, and Site 6: Tando Jam.

(3%–5%) in inoculated treatments with a reduced application of DAP as compared to uninoculated controls. Previous studies indicated that P-solubilizing microorganisms showed the best effect with reduced application of DAP fertilizers (Rasul et al., 2019; Rosa et al., 2020; Yahya et al., 2022). Higher seed P content might be due to P translocation to seed because of PSB inoculation (Feng et al., 2021). Maximum grain yield (5,390 kg ha^{-1}) was observed as a result of consortium-1 inoculation at site 2 followed by site 3 (5,240 kg ha^{-1}) and site 1 (4,806 kg ha^{-1}). In the case of consortium-2, a grain yield of 5,174 kg ha^{-1} was observed at site 4 with a 20% reduced application of DAP. An increase in grain yield (5,324 kg ha^{-1}) was observed as a result of consortium-3 inoculation at site 6 followed by site 5 (4,806 kg ha^{-1}).

CAT-PCA of wheat yield parameters, soil physicochemical analysis, and meteorological factors revealed a positive correlation of PSB-inoculated field-grown wheat to grain yield, soil P content, and precipitation at irrigated plains, while seed P content, soil organic matter, and number of tillers were found positively correlated to sites belonging to the northern dry mountains. However, the impact of inoculation at sites belonging to the Indus delta was found to correlate with soil K content, EC, and temperature. The higher grain yield at site 4 may be due to higher soil organic matter and N contents that favor the persistence of inoculated PSB in dry mountainous soils. For instance, the organic matter of site 2 was higher (0.6%) as compared to that of site 3 and site 1 belonging to the irrigated plains. Similarly, the organic matter of site 6 was higher (0.56%) as compared to site 5 belonging to the Indus delta. This is due to the soils having a high organic matter that have higher microbial dynamics and thus eventually need lesser requirements for chemical fertilizers (Backer et al., 2018). The increase in soil organic matter is the key factor in maintaining soil fertility and plant nutrient uptake (Gerke, 2022). This can sustain agricultural productivity by restricting the use of chemical fertilizers (Allam et al., 2022). Therefore, it could be more important to amend the soil with organic matter instead of seed pelleting to augment the soil with appropriate soil fertility. Other than organic matter, soil pH, carbon content, and water availability are the important determinants for successful inoculum survival in soil under field conditions (Hartmann et al., 2015; Mahoney et al., 2017; Cao et al., 2021; Gao et al., 2021). It also depends on the soil type and the growing season (Bolyen et al., 2019; Khandare et al., 2020; Yan et al., 2020). Hence, it is essential to take into account all of these factors so that bacteria can colonize efficiently in native environmental conditions.

Secondly, the other factors that can contribute to wheat production are the climatic conditions, i.e., temperature (minimum and maximum), rainfall, relative humidity, and sunshine. These climate changes directly affect the productivity and stability of the agriculture sector (Lobo et al., 2019). Studies have shown that the most influential climatic factors in wheat production in Pakistan are relative humidity, maximum temperature, and rainfall. Maximum temperature negatively influenced the wheat yield (Ghani et al., 2021). In this study, a similar trend was observed, for example, the minimum yield was observed for sites 5 and 6, which have maximum average temperature throughout the wheat season, whereas the minimum temperature is reported to have a significant positive impact on wheat yield. Likewise, the minimum temperature was observed at site 4 with concomitant enhanced wheat yield. On the other hand, precipitation can influence the effectiveness of biofertilizers, which usually depends on soil properties. Biofertilizers are more effective in arid climates than in snowy climates (Jennifer et al., 2018). In the present study, a positive correlation of field-grown PSB-inoculated wheat with grain yield, soil P content, and precipitation was observed for sites 2 and 3, which belong to the semiarid zone. However, bacterial communities can be distinct for each site or ecosystem along the precipitation gradient (Bachar et al., 2010).

Soil microbial activity largely depends upon the temperature and soil moisture level in rain-fed agriculture (Cookson et al., 2002). The practical implication of moisture and temperature requirements is needed optimally around the establishment of crops in Mediterranean climates (Gupta et al., 2011). Studies indicated that the successful use of inoculants can only be possible for arid environments when they are applied in a timely manner (Rubin et al., 2017; Chandran et al., 2021), since rapid wetting and drying cycles can be detrimental to the survival of the inoculum (Vriezen et al., 2007). Therefore, the

inoculum must be applied to soil when the moisture content is adequate for seed germination and colony propagation.

Knowing the soil's nutritional status guides the sensible use of the inoculum. Subsequently, it is important to identify soil deficiencies in concert with the application of the inoculum. The interaction between soil C and N should also be considered, since inoculants capable of building soil organic C and improving soil structure only have this potential if soil-available N is adequate (Callaghan et al., 2022). Soil properties that can disrupt the microbial community and strategic cultivation could provide an opportunity to balance the soil conditions in favor of inoculated microbe. Hence, this study is of significant worth, and for the first time, it reports the development and application of soil-specific biofertilizers for agroecological zones of wheat. Meanwhile, it integrates soil nutritional status and agro-climatic conditions simultaneously which are found to be the key factors for consistent performance of augmented PSB. The potential *gcd* gene containing phosphobacteria used in the study was found promising for P biofortification; therefore, these might be used in the future for the development of potential biofertilizers to foster sustainable wheat production in diverse agro-climatic zones.

Conclusion

Despite the significance of the growing biofertilizer market, microbial inoculants still failed to deliver on their potential except for a few products. To the best of our knowledge, this study provides innovative insights into the imminent significance of soil-specific biofertilizers for sustainable wheat production by integrating soil nutritional status and meteorological conditions at the site of application. These consortia were found promising for P biofortification; hence, these will be used for the development of potential biofertilizers. However, the persistence and efficacy of inoculated microbe are the key components to harnessing their potential. Therefore, targeted application of biofertilizers in native soils will provide a sound basis for the efficacious inoculants.

Furthermore, new approaches like metabarcoding should be opted for the selection of a potential native PGPR consortium that can survive and establish in complex microbial communities. Research priorities are needed to allow greater exploitation of microbiomes in sustainable agriculture including core microbiomes and metagenomes of target crops. Nevertheless, metabarcoding is a powerful tool to estimate soil microbial biodiversity. There is a dire need to integrate other crucial environmental factors to obtain a full picture of biodiversity attributes that can influence the functioning of ecosystems. This could lead to developing potential soil-specific consortia with concomitant adaptability under native agro-climatic conditions and soil nutritional status.

Data availability statement

The original contributions presented in the study are included in the article/Supplementary Material. Further inquiries can be directed to the corresponding authors.

Author contributions

MY analyzed the data and wrote the manuscript. SY and TW performed data analysis and review the manuscript. SZ performed SEM analysis. AD helped in making the map. MU, LR, AA and MA helped to conduct multilocation trials. MY executed statistical analysis. SY conceived and supervised the whole study and edited the manuscript. All authors contributed to the article and approved the submitted version.

Acknowledgments

The research work was supported by "NRPU Higher Education Commission (HEC) Projects 3813 and 14919" and Pakistan Science Foundation project # PSF/CRP/T-helx-188. We are thankful to Mr. Asghar Ali, Mr. Muhammad Sarwar, Mr. Muhammad Imran and Zakir Hussain for their assistance in net house and field experiments. Thanks is due to Mr. Zahid Iqbal Sajid for plant and soil analysis.

Conflict of interest

The authors declare that the research was conducted in the absence of any commercial or financial relationships that could be construed as a potential conflict of interest.

Publisher's note

Supplementary material

The Supplementary Material for this article can be found online at: https://www.frontiersin.org/articles/10.3389/fpls.2022.1074383/full#supplementary-material

References

Ahmad, U., Alvino, A., and Marino, S. (2022). Solar fertigation: A sustainable and smart IoT-based irrigation and fertilization system for efficient water and nutrient management. *Agronomy* 12, 1012. doi: 10.3390/agronomy12051012

Allam, M., Radicetti, E., Quintarelli, V., Petroselli, V., Marinari, S., and Mancinelli, R. (2022). Influence of organic and mineral fertilizers on soil organic carbon and crop productivity under different tillage systems: A meta-analysis. *Agriculture.* 12, 464. doi: 10.3390/agriculture120404

Alori, E. T., Glick, B. R., and Babalola, O.O. (2017). Microbial phosphorus solubilization and its potential for use in sustainable agriculture. *Front. Microbiol.* 8, 971. doi: 10.3389/fmicb.2017.00971

Bachar, A., Al-Ashhab, A., Soares, M. I. M., Sklarz, M. Y., Angel, R., Ungar, E. D., et al. (2010). Soil microbial abundance and diversity along a low precipitation gradient. *Microbial Ecology.* 60 (2), 453–461. doi: 10.1007/s00248-010-9727-1

Backer, R., Rokem, J. S., Ilangumaran, G., Lamont, J., Praslickova, D., Ricci, E., et al. (2018). Plant growth-promoting rhizobacteria: Context, mechanisms of action, and roadmap to commercialization of biostimulants for sustainable agriculture. *Front. Plant Sci.* 9. doi: 10.3389/fpls.2018.01473

Bijl, D. L., Biemans, H., Bogaart, P. W., Dekker, S. C., Doelman, J. C., Stehfest, E., et al. (2018). A global analysis of future water deficit based on different allocation mechanisms. *Water Resources Res.* 54 (8), 5803–5824. doi: 10.3389/fpls.2018.01473

Bolyen, E., Rideout, J. R., Dillon, M. R., Bokulich, N. A., Abnet, C. C., Al-Ghalith, G. A., et al. (2019). Reproducible, interactive, scalable and extensible microbiome data science using QIIME 2. *Nat. Biotechnol.* 37 (8), 852–857. doi: 10.1038/s41587-019-0209-9

Bremner, J., and Mulvaney, C. (1983). "Nitrogen-total. methods of soil analysis. part 2," in *Chemical and microbial properties. no. 9.* Eds. A. L. Page, R. H. Miller and D. R. Keeney (Madison. Wisconsin: American Society of Agronomy and Soil Science Society of America. Inc). doi: 10.2134/agronmonogr9.2.2ed.c31

Callaghan, M., Ballard, R.A., and Wright, D. (2022). Soil microbial inoculants for sustainable agriculture: Limitations and opportunities. *Soil Use Management* 38, 1340–1369. doi: 10.1111/sum.12811

Camaille, M., Nicolas, F., Christophe, C., and Barka, E.A. (2021). "Advances in wheat physiology in response to drought and the role of plant growth promoting rhizobacteria to trigger drought tolerance". *Microorganisms* 4, 687. doi: 10.3390/microorganisms9040687

Cao, Q., Sun, X., Rajesh, K., Chalasani, N., Gelow, K., Katz, B., et al. (2021). Effects of rare microbiome taxa filtering on statistical analysis. *Front. Microbiol.* 11, 607325. doi: 10.3389/fmicb.2020.607325

Chandran, H., Meena, M., and Swapnil, P. (2021). Plant growth-promoting rhizobacteria as a green alternative for sustainable agriculture. *Sustainability.* 13 (19), 10986. doi: 10.3390/su131910986

Chen, Q., and Liu, S. (2019). Identification and characterization of the phosphate-solubilizing bacterium *Pantoea* sp. S32 in reclamation soil in shanxi, China. *Front. Microbiol.* 10, 2171. doi: 10.3389/fmicb.2019.02171

Cookson, W.R., Cornforth, I.S., and Rowarth, J.S. (2002). Winter soil temperature effects on nitrogen transformations in clover green manure amended or unamended soils; a laboratory and field study. *Soil Biol. Biochem.* 34, 1401–1415. doi: 10.1016/S0038-0717(02)00083-4

Dotaniya, M. L., Datta, S. C., Biswas, D. R., Dotaniya, C. K., Meena, B. L., Rajendiran, S., et al. (2016). Use of sugarcane industrial by-products for improving sugarcane productivity and soil health. *Int. J. Recycl. Org. Waste Agricult.* 5 (3), 185–194. doi: 10.1007/s40093-016-0132-8

Elhaissoufi, W., Khourchi, S., Ibnyasser, A., Ghoulam, C., Rchiad, Z., Zeroual, Y., et al. (2020). Phosphate solubilizing rhizobacteria could have a stronger influence on wheat root traits and aboveground physiology than rhizosphere p solubilization. *Front. Plant Sci.* 11. doi: 10.3389/fpls.2020.00979

Farooq, M. S., Uzair, M., Raza, A., Habib, M., Xu, Y., Yousuf, M., et al. (2022). Uncovering the research gaps to alleviate the negative impacts of climate change on food security: A review. *Front. Plant Sci.* 13. doi: 10.3389/fpls.2022.927535

Feng, Y.Y., He, J., Jin, Y., and Li, F.M. (2021). High phosphorus acquisition and allocation strategy is associated with soybean seed yield under water-and p-limited conditions. *Agronomy* 11, 574. doi: 10.3390/agronomy11030574

Finkel, O. M., Castrillo, G., Herrera Paredes, S., Salas González, I., and Dangl, J. L. (2017). Understanding and exploiting plant beneficial microbes. *Curr. Opin. Plant Biol.* 38, 155–163. doi: 10.1016/j.pbi.2017.04.018

Gao, C. H., Cao, H., Cai, P., and Sørensen, S. J. (2021). The initial inoculation ratio regulates bacterial coculture interactions and metabolic capacity. *ISME J.* 15 (1), 29–40. doi: 10.1038/s41396-020-00751-7

Gerke, J. (2022). The central role of soil organic matter in soil fertility and carbon storage. *Soil Systems* 6, 33. doi: 10.3390/soilsystems6020033

Ghani, M. J., Akhtar, K., Khaliq, S., Akhtar, N., and Ghauri, M.A. (2021). Characterization of humic acids produced from fungal liquefaction of low-grade thar coal. *Process Biochem.* 107, 1–12. doi: 10.1016/j.procbio.2021.05.003

Gupta, V. V., Rovira, A. D., and Roget, D. K. (2011). "Principles and management of soil biological factors for sustainable rainfed farming systems," in *Rainfed farming systems*. Eds. P. Tow, I. Cooper, I. Partridge and C. Birch (Springer Netherlands: Springer), 149–184.

Hartmann, M., Frey, B., Mayer, J., Mäder, P., and Widmer, F. (2015). Distinct soil microbial diversity under long-term organic and conventional farming. *ISME J.* 9 (5), 1177–1194. doi: 10.1038/ismej.2014.210

Jennifer, E. S., Amélie, C., and Gaudin, M. (2018). What is the agronomic potential of biofertilizers for maize? a meta-analysis. *FEMS Microbiol. Ecol.* 94, 7. doi: 10.1093/femsec/fiy094

Khandare, R. N., Chandra, R., Pareek, N., and Raverkar, K. P. (2020). Carrier-based and liquid bioinoculants of azotobacter and PSB saved chemical fertilizers in wheat (*Triticum aestivum* l.) and enhanced soil biological properties in mollisols. *J. Plant Nutr.* 43 (1), 36–50. doi: 10.1080/01904167.2019.1659333

Liu, J., Zhang, J., Zhu, M., Wan, H., Chen, Z., Yang, N., et al. (2022). Effects of plant growth promoting rhizobacteria (PGPR) strain *Bacillus licheniformis* with biochar amendment on potato growth and water use efficiency under reduced irrigation regime. *Agronomy* 12, 1031. doi: 10.3390/agronomy12051031

Lobo, C. B., Tomás, M. S. J., Viruel, E., Ferrero, M. A., and Lucca, M. E. (2019). Development of low-cost formulations of plant growth-promoting bacteria to be used as inoculants in beneficial agricultural technologies. *Microbiol. Res.* 219, 12–25. doi: 10.1016/j.micres.2018.10.012

Lopes, M., J., S., Dias-Filho, M.B., and Gurgel, E.S.C. (2021). Successful plant growth-promoting microbes: inoculation methods and abiotic factors. *Front. Sustain. Food Syst.* 5. doi: 10.3389/fsufs.2021.606454

Mahoney, A. K., Yin, C., and Hulbert, S.H. (2017). Community structure, species variation, and potential functions of rhizosphere-associated bacteria of different winter wheat (*Triticum aestivum*) cultivars. *Front. Plant Sci. 8*, 132. doi: 10.3389/fpls.2017.00132

Mendoza-Suárez, M., Andersen, S. U., Poole, P. S., and Sánchez-Cañizares, C. (2021). Competition, nodule occupancy, and persistence of inoculant strains: Key factors in the Rhizobium-legume symbioses. *Front. Plant Sci.*, 1684.

Mitter, E. K., Tosi, M., Obregon, D., Dunfield, K. E., and Germida, J.J. (2021). Rethinking crop nutrition in times of modern microbiology: Innovative biofertilizer technologies. *Front. Sustain. Food Syst.* 5. doi: 10.3389/fsufs.2021.606815

Muluneh, M. G. (2021). Impact of climate change on biodiversity and food security: a global perspective–a review article. *Agric. Food Secur.* 10, 36. doi: 10.1186/s40066-021-00318-5

Nautiyal, C. S. (1999). An efficient microbiological growth medium for screening phosphate solubilizing microorganisms. *FEMS Microbiol. Lett.* 170, 265–270. doi: 10.1111/j.1574-6968.1999.tb13383.x

Nelson, D., and Sommers, L. E. (1983). Total carbon, organic carbon, and organic matter. methods of soil analysis: Part 2 chemical and microbiological properties 9, 539–579.

Nelson, D., and Sommers, L. E. (1996). "Total carbon, organic carbon, and organic matter," In D. L. Sparks, et al Eds. *Methods of Soil Analysis: Part 3 Chemical Methods* (Madison, WI: ASA and SSSA)5, 961–1010. Available at: https://agris.fao.org/agris-search/search.do?recordID=US9423626.

Olsen, S. R. (1954). *Estimation of available phosphorus in soils by extraction with sodium bicarbonate* (Washington, DC: US Department of Agriculture).

Pastor-Bueis, R., Sánchez-Cañizares, C., James, E. K., and González-Andrés, F. (2019). Formulation of a highly effective inoculant for common bean based on an autochthonous elite strain of rhizobium leguminosarum bv. phaseoli, and genomic-based insights into its agronomic performance. *Front. Microbio.* 10. doi: 10.3389/fmicb.2019.02724

Pavinato, P. S., Sánchez-Rodríguez, A. R., and Tiecher, T. (2022). Editorial: Sustainable phosphorus use in agriculture. *Front. Agron.* 4. doi: 10.3389/fagro.2022.899924

Rasul, M., Yasmin, S., Suleman, M., Zaheer, A., Reitz, T., Tarkka, M. T., et al. (2019). Glucose dehydrogenase gene containing phosphobacteria for biofortification of phosphorus with growth promotion of rice. *Microbiol. Res.* 223, 1–12. doi: 10.1016/j.micres.2019.03.004

Rasul, M., Yasmin, S., Yahya, M., Breitkreuz, C., Tarkka, M., and Reitz, T. (2021). The wheat growth-promoting traits of ochrobactrum and pantoea species, responsible for solubilization of different p sources, are ensured by genes encoding enzymes of multiple p-releasing pathways. *Microbiol. Res.* 246, 126703. doi: 10.1016/j.micres.2021.126703

Reynolds, M. P., Lewis, J. M., Ammar, K., Basnet, B. R., Crespo-Herrera, L., Crossa, J., et al. (2021). Harnessing translational research in wheat for climate resilience. *J. Exp. Bot.* 72 (14), 5134–5157. doi: 10.1093/jxb/erab256

Rhoades, J. D. (1993). Electrical conductivity methods for measuring and mapping soil salinity. *Adv. Agron.* 49, 201–251. doi: 10.1016/S0065-2113(08) 60795-6

Rosa, P. A. L., Mortinho, E. S., Jalal, A., Galindo, F. S., Buzetti, S., Fernandes, G. C., et al. (2020). Inoculation with growth-promoting bacteria associated with the reduction of phosphate fertilization in sugarcane. *Front. Environ. Sci.* 8, 32. doi: 10.3389/fenvs.2020.00032

Rubin, R. L., van Groenigen, K. J., and Hungate, B. A. (2017). Plant growth promoting rhizobacteria are more cost effective under drought: a meta-analysis. *Plant Soil* 416, 309–323. doi: 10.1016/j.heliyon.2020.e05106

Santoyo, G., Gamalero, E., and Glick, B. R. (2021). Mycorrhizal-bacterial amelioration of plant abiotic and biotic stress. *Front. Sustain. Food Syst.* 5. doi: 10.3389/fsufs.2021.672881

Sedri, M. H., Niedbała, G., Roohi, E., Niazian, M., Szulc, P., Rahmani, H. A., et al. (2022). Comparative analysis of plant growth-promoting rhizobacteria (PGPR) and chemical fertilizers on quantitative and qualitative characteristics of rainfed wheat. *Agronomy* 12 (7), 1524. doi: 10.3390/agronomy12071524

Shah, H., Hellegers, P., and Siderius, C. (2021). Climate risk to agriculture: A synthesis to define different types of critical moments. *Clim. Risk Manage.* 34, 100378. doi: 10.1016/J.CRM.2021.100378

Simard, R. (1993). Ammonium acetate-extractable elements. *Soil sampling Methods Anal.* 1, 39–42. Available at: https://books.google.com.pk/books?hl=en&lr=&id=54lYLsV49zIC&oi=fnd&pg=PA39&dq=Simard,+R.+(1993).+Ammonium+acetate-extractable+elements.+Soil+sampling+Methods+Anal.+1,+39%E2%80%9342.&ots=K4lFZEH4yO&sig=yz2bytLGaBQWdZdL7MtbP5gwT7w&redir_esc=y#v=onepage&q&f=false.

Somasegaran, P., and Hoben, H. J. (2012). *Handbook for rhizobia: methods in legume-rhizobium technology* (Berlin: Springer Science and Business Media).

Soumare, A., Boubekri, K., Lyamlouli, K., Hafidi, M., Ouhdouch, Y., and Kouisni, L. (2020). From isolation of phosphate solubilizing microbes to their formulation and use as biofertilizers: status and needs. *Front. Bioeng. Biotechnol.* 7. doi: 10.3389/fbioe.2019.00425

Souza, R. D., Ambrosini, A., and Passaglia, L. M. (2015). Plant growth-promoting bacteria as inoculants in agricultural soils. *Genet. Mol. Biol.* 38, 401–419. doi: 10.1590/S1415-475738420150053

Tabatabai, M., and Bremner, J. (1969). Use of p-nitrophenyl phosphate for assay of soil phosphatase activity. *Soil Biol. Biochem.* 1, 301–307. doi: 10.1016/0038-0717(69

Tandon, H. L. S. (1993). *Methods of analysis of soils, plants, waters, and fertilizers* (New Delhi: Fertiliser Development and Consultation Organization).

Ullah, S., Asghari, B., Asad, U., Muhammad, A. S., and Naeem, K. (2022). A comparative study of plant growth promoting rhizobacteria (PGPR) and sowing methods on nutrient availability in wheat and rhizosphere soil under salinity stress. *Rhizosphere* 23, 100571. doi: 10.1016/j.rhisph.2022.100571

Vriezen, J. A., Bruijn, F. J., and Nüsslein, K. (2007). Responses of rhizobia to desiccation in relation to osmotic stress, oxygen, and temperature. *Appl. Environ. Microbiol.* 73 (11), 3451–3459. doi: 10.1128/AEM.02991-06

Yahya, M., Islam, E., Rasul, M., Farooq, I., Mahreen, N., Tawab, A., et al. (2021). Differential root exudation and architecture for improved growth of wheat mediated by phosphate solubilizing bacteria. *Front. Microbiol.* 12. doi: 10.3389/fmicb.2021.744094Y

Yahya, M., Rasul, M., Sarwar, Y., Suleman, M., Tariq, M., Hussain, S. Z., et al. (2022). Designing synergistic biostimulants formulation containing autochthonous phosphate-solubilizing bacteria for sustainable wheat production. *Front. Microbiol.* 13. doi: 10.3389/fmicb.2022.889073

Yan, A., Wang, Y., Tan, S. N., Mohd Yusof, M. L., Ghosh, S., and Chen, Z. (2020). Phytoremediation: A promising approach for revegetation of heavy metal-polluted land. *Front. Plant Sci.* 11, 359. doi: 10.3389/fpls.2020.00359

Yasmin, S., Zaka, A., Imran, A., Zahid, M. A., Yousaf, S., Rasul, G., et al. (2016). Plant growth promotion and suppression of bacterial leaf blight in rice by inoculated bacteria. *PloS One* 11, e0160688. doi: 10.1371/journal.pone.0160688

frontiers | Frontiers in Plant Science

TYPE Original Research
PUBLISHED 18 January 2023
DOI 10.3389/fpls.2023.1079559

OPEN ACCESS

EDITED BY
Matthew John Milner,
National Institute of Agricultural Botany (NIAB), United Kingdom

REVIEWED BY
Yi Chen,
John Innes Centre, United Kingdom
Ajay Kumar Pandey,
National Agri-Food Biotechnology Institute, India

*CORRESPONDENCE
Francesco Sestili
francescosestili@unitus.it

SPECIALTY SECTION
This article was submitted to Plant Nutrition, a section of the journal Frontiers in Plant Science

RECEIVED 25 October 2022
ACCEPTED 04 January 2023
PUBLISHED 18 January 2023

CITATION
Frittelli A, Botticella E, Palombieri S, Masci S, Celletti S, Fontanella MC, Astolfi S, De Vita P, Volpato M and Sestili F (2023) The suppression of TdMRP3 genes reduces the phytic acid and increases the nutrient accumulation in durum wheat grain. *Front. Plant Sci.* 14:1079559. doi: 10.3389/fpls.2023.1079559

The suppression of TdMRP3 genes reduces the phytic acid and increases the nutrient accumulation in durum wheat grain

Arianna Frittelli[1], Ermelinda Botticella[2], Samuela Palombieri[1], Stefania Masci[1], Silvia Celletti[1], Maria Chiara Fontanella[3], Stefania Astolfi[1], Pasquale De Vita[4], Mirko Volpato[5] and Francesco Sestili[1]*

[1]Department of Agriculture and Forest Science (DAFNE), University of Tuscia, Viterbo, Italy, [2]Institute of Sciences of Food Production (ISPA), National Research Council (CNR), Lecce, Italy, [3]Department for Sustainable Process, Faculty of Agriculture, Food and Environmental Science (DiSTAS), Università Cattolica, Piacenza, Italy, [4]Council for Agricultural Research and Economics, Research Centre for Cereal and Industrial Crops (CREA-CI), Foggia, Italy, [5]Grandi Molini Italiani, Venezia, Italy

Micronutrient malnutrition affects more than half of the world population. Reduced bioavailability of microelements in the raw materials is considered one of the main causes of mineral deficiency in populations whose diet is largely based on the consumption of staple crops. In this context, the production of low phytic acid (*lpa*) cereals is a main goal of the breeding programs, as phytic acid (PA) binds essential mineral cations such as iron (Fe), zinc (Zn), manganese (Mn), potassium (K), calcium (Ca) and magnesium (Mg) precipitating in the form of phytate salts poorly digested by monogastric animals, including humans, due to the lack of phytases in the digestive tract. Since PA limits the bioavailability of microelements, it is widely recognized as an anti-nutritional compound. A Targeting Induced Local Lesions IN Genomes (TILLING) approach has been undertaken to silence the genes encoding the TdABCC13 proteins, known as Multidrug-Resistance associated Proteins 3 (TdMRP3), transporters involved in the accumulation of PA inside the vacuole in durum wheat. The TdMRP3 complete null genotypes showed a significant reduction in the content of PA and were able to accumulate a higher amount of essential micronutrients (Fe, Zn, Mn) compared to the control. The number of spikelets and seeds per spike, traits associated with the agronomic performances, were reduced compared to the control, but the negative effect was in part balanced by the increased grain weight. The TdMRP3 mutant lines showed morphological differences in the root apparatus such as a significant decrease in the number of root tips, root length, volume and surface area and an increase in root average diameter compared to the control plants. These materials represent a promising basis for obtaining new commercial durum wheats with higher nutritional value.

KEYWORDS

durum wheat, genetic biofortification, micronutrients, mutagenesis, phytic acid, tilling

1 Introduction

Wheat, along with rice and maize, is one of three major cereals cultivated worldwide. The adaptability to a wide range of conditions, the good nutritional profile, along with its unique dough visco-elastic properties are the main reasons for its success (Shewry, 2009).

Durum wheat (*Triticum turgidum ssp. Durum*), the second wheat species most cultivated worldwide, is a key raw material in a wide variety of traditional foods largely consumed in the Mediterranean basin as a part of a diet style recognized as one of the healthiest in absolute terms (Willett et al., 1995; Sofi et al., 2010).

Where diets rely on plant-derived foods, it is crucial to increase the amount of health-promoting compounds (i.e. fibres, proteins, vitamins, antioxidants, minerals) in durum wheat as a valuable strategy to maintain good health and to prevent important non-communicable diet-related diseases (obesity, diabetes, cardiovascular disorders, osteoporosis, cancer), along with those associated to "hidden hunger". In this regard, hidden hunger indicates a particular form of undernutrition that occurs when the intake and absorption of micronutrients are not enough for the daily requirement. This pathology affects almost one-third of the population, triggering serious diseases such as anaemia, weak bones, fatigue and weakened immune system and a few hidden impacts on the general well-being, lowering the life quality and increasing the risk of new pathologies (Lockyer et al., 2018; Vitamin and Mineral Nutrition Information System (VMNIS), 2022).

Genetic biofortification of staple crops represents an effective and sustainable strategy to boost essential minerals (i.e. iron, magnesium, calcium, potassium and zinc) in the human diet as it does not require the addition of fertilizers during the cultivation or additives in food production giving, as result, a stable over generations crop enriched in the target compound (Vasconcelos et al., 2017; Roberts and Mattoo, 2019).

Myo-inositol-1,2,3,4,5,6-hexakisphosphate ($InsP_6$) is a ubiquitous component of eukaryotic cells that plays several regulatory roles (Shears, 2001). Also known as phytic acid (PA), it is the major phosphorus storage sink within the plant seeds and other plant tissues and organs such as pollen, roots, tubers and turions. The amount and distribution of PA within the kernel depend on the plant species. In barley, rice and wheat about 80% of PA is stored in the aleuronic layer and bran, whereas in maize and Arabidopsis mainly in the embryo and scutellum (O'Dell et al., 1972). Differently from cereals and Arabidopsis, about 95% of PA is accumulated in the cotyledons in legumes (Ariza-Nieto et al., 2007).

Due to its negative charges, PA binds important mineral cations such as zinc, iron, potassium, magnesium and calcium precipitating in the form of phytate salts poorly digested by monogastric animals, including humans, due to the lack of phytases inside the digestive tract. As it chelates ions the bioavailability of phosphorus and minerals is decreased and PA is considered an anti-nutritional compound. In addition, the excretion of undigested phosphate contributes to environmental pollution by accelerating the eutrophication of the soil (Raboy, 2009; Secco et al., 2017).

In plants, phytic acid biosynthesis is carried out through two metabolic pathways (Sparvoli and Cominelli, 2015). The lipid-dependent pathway acts in all plant tissues, while the lipid-independent pathway is mainly active in seeds. In the first step, glucose-6-phosphate is converted into myo-inositol-3-phosphate (Ins(3)P_1) by myo-inositol-3-phosphate synthase (MIPS). The subsequent steps involve sequential phosphorylation of the inositol ring through various enzymes (inositol phosphate kinase 2, IPK2; inositol 1,3,4-trisphosphate 5-/6 kinase, ITPK; inositol polyphosphate 2- kinase, IPK1). The synthesized phytic acid is accumulated into globoids, spherical inclusions found within protein bodies (Krishnan, 2008; Regvar et al., 2011), and stored inside the vacuoles where it is transported by specific PA protein transporters, such as the *Multidrug-Resistance associated Proteins* (MRPs) (Sparvoli and Cominelli, 2014; Colombo et al., 2020; Cominelli et al., 2020a).

Previous breeding programs focused on the reduction of PA to increase the mineral content of food and the sustainability of agricultural production in different crops (Raboy, 2020). *Low phytic acid* (*lpa*) genotypes have been produced in all major grain crops using different strategies. In this regard, *lpa* mutants can be divided into three classes according to the step where the mutations affect the PA biosynthetic pathway or transport: 1) the first biosynthetic step in which glucose-6-phosphate is converted into Ins(3)P_1 by MIPS; 2) the last biosynthetic step in which IPK1 phosphorylates $InsP_5$ in the 2-position to synthesize PA; 3) the transport and storage of phytic acid into the vacuole through the targeting of MRP transporters (Sparvoli and Cominelli, 2015; Colombo et al., 2020).

In bread wheat TaMRP3 homeoalleles are located on the long arm of the 5A, 4B and 4D chromosomes and encode multidrug resistance-associated proteins belonging to the ABCC cluster of plant ATP-binding cassette (ABC) transporters (Bhati et al., 2014). MRP proteins are characterized by a common structure consisting of two soluble nucleotide-binding domains (NBD1 and NBD2), two hydrophobic transmembrane domains (TMD1 and TMD2) and an additional hydrophobic N-terminal extension (TMD0) connected by a cytosolic loop to the rest of protein (Sparvoli and Cominelli, 2014; Colombo et al., 2020). *Lpa* mutants were produced by targeting *MRP* genes in *Arabidopsis thaliana*, rice, soybean and common beans (Colombo et al., 2020), demonstrating that MRP proteins are involved in the transport of PA within the vacuole (Shi et al., 2007; Nagy et al., 2009).

Interestingly, Bhati et al., 2016 previously reported a partial suppression of *TaMRP3* genes by RNA interference (RNAi) and demonstrated its functional role in bread wheat. Due to its central role in PA transport, TdMRP3 is an attractive target for increasing the accumulation of minerals in durum wheat through a non-transgenic genetic approach focused on its inactivation.

In this paper, the genes encoding TdABCC13 (TdMRP3) were completely disrupted at DNA level through a Targeting Induced Local Lesions in Genomes (TILLING) strategy, a highly processive non-transgenic reverse genetics technique that combines chemical mutagenesis with a PCR-based screening for the identification of mutations in the gene of interest (McCallum et al., 2000).

We show that the effect of *TdMRP3* silencing was a significant reduction in PA content, resulting in an improved capability to accumulate micronutrients (Fe, Zn, Mn) in wheat seeds. In addition, it was tested whether the suppression of *TdMRP3* genes in durum wheat generates modifications in root system architecture with significant consequences on root ability to acquire water and nutrients.

To the best of our knowledge, this study represents the first example of a genetic approach that successfully reduced the accumulation of phytic acid and increased the bioavailability of essential minerals in durum wheat kernel.

2 Material and methods

2.1 Isolation of genes coding TdMRP3 from genomic databases

To identify the sequences of the *TdMRP3* genes, the orthologous genes of *T. aestivum* (TraesCS5A02G512500 and TreasCS4B02G343800) were used as queries in two independent approaches. In the first approach the two queries were blasted against *Triticum turgidum* ssp *durum* cv Svevo genome in Ensembl Plants database (https://plants.ensembl.org/index.html).

In the second one the orthologous query sequences were individually blasted against the Svevo Platinum genome available at the Svevo Platinum Genome Consortium (data unpublished). The exon/intron structure of the two identified durum wheat homeoalleles (*TdMRP3-A1* and *TdMRP3-B1*) was predicted by GENESCAN web tool (Burge and Karlin, 1997).

2.2 Bioinformatic analysis of TdMRP3 proteins

Domain topology and organization were predicted by analyzing and comparing the full-length amino acid sequence of each TdMRP3 protein in the UniProt database.

The orthologous sequences of the major grass species were identified by blasting the TdMRP3 protein sequences in NCBI BLASTP software (https://blast.ncbi.nlm.nih.gov/Blast.cgi). The orthologous sequence of *Arabidopsis thaliana*, used as an outsider, was isolated from TAIR database.

The multiple sequence alignment of MRP proteins (orthologous of TdMRP3) was performed by accurate Multiple Sequence Alignment (MSA) with PSI-Coffee 11.0 tool (Chang et al., 2012).

The phylogenetic analysis of MRP proteins was carried out by MEGA11 software (Tamura et al., 2021). The evolutionary history and distance among the selected taxa were deduced using the Neighbor-Joining (NJ) method with p-distance method and pairwise deletion option. The bootstrap consensus tree was inferred from 1000 replicates.

2.3 Plant materials

A preliminary *in silico* study allowed the identification of two durum wheat mutant lines possessing deleterious mutations on the two *TdMRP3* homeoalleles through the platform WheatTILLING available at the University of Davis (https://dubcovskylab.ucdavis.edu/home; Krasileva et al., 2017). In detail, the line Kronos 3179 has a splice site mutation located in the 5' region of the intron 4 of *TdMRP3-A1*, while the line Kronos 4443 has a nonsense mutation in the exon 4 of *TdMRP3-B1* (Supplementary Figure S1). The presence of the two mutations was confirmed by Sanger sequencing.

The pyramiding of the two mutations was carried out by crossing the identified mutant lines TdMRP3-A1$^-$ and TdMRP3-B1$^-$. The partial and complete null mutants along with the controls (cv Kronos and wild-type sib lines derived by the cross) were grown in a controlled growth chamber with initial vernalization at 4-5°C for 3 weeks, followed by 18-26°C day and 16-18°C night temperature with a 16 h light period.

2.4 DNA extraction

Genomic DNA was extracted from leaves using the commercial kit NucleoSpin® Plant II (Macherey-Nagel, Düren, Germany) according to the manufacturer's instructions. The DNA was used as template for the genotyping analysis.

2.5 High resolution melting genotyping

High Resolution Melting (HRM) analysis was performed on *TdMRP3* gene amplicons including the targeted mutations, amplified from the genomic DNA of F_2 progeny of the cross described in the "Plant materials" paragraph. Amplicons were produced by a nested PCR strategy. The first PCR was carried out to amplify genome-specific fragments of 514 bp and 409 bp for *TdMRP3-A1* and *TdMRP3-B1* homeoalleles, respectively, using the primer pairs reported in Supplementary Table S1. The reaction was performed in a 20 µl volume using the following conditions: 10 µl of 2X GoTaq® G2 Hot Start Colorless Master Mix (Promega, Madison, USA), 0.5 µM of each primer, 20 ng of template DNA and nuclease-free water up to 20 µl volume, with the following conditions: 95°C for 2 min, followed by 38 cycles at 95°C for 30 s, 58°C for 30 s, 72°C for 1 min and a final extension at 72°C for 5 min. The first PCR reaction was diluted 60-fold and 2 µl were used as a template for the second PCR reaction for HRM analysis. The second reaction was carried out using the primer pairs reported in Supplementary Table S1 and was prepared as follows: 2 µl of diluted DNA template, 5 µl of 2X GoTaq® G2 Hot Start Colorless Master Mix (Promega), 0.5 µM of each primer, 1 µL LC Green Plus (Idaho Technology Inc., Salt Lake City, USA) and nuclease-free water up to 10 µl volume. The PCR program was carried out following these conditions: 95°C for 2 min, followed by 39 cycles at 95°C for 30 s, 60°C for 20 s, 72°C for 20 s and a final extension at 72°C for 5 min. At the end of the final extension step, the reaction was held at 95°C for 30 s, then at 25°C for 60 s. The PCR reaction was carried out in 96-well Frame-Star plates (4titude Ltd., Surrey, UK) overlaid with 10 µl of mineral oil (Sigma-Aldrich, St. Louis, MO, USA). The Light Scanner instrument (Idaho Technology, Inc.) was used to analyse the melting curves.

2.6 Determination of phytic acid

PA was determined in mature seeds of the selected F_4 partial and complete null mutant lines (MRP3-A1$^-$, MRP3-B1$^-$ and MRP3-A1$^-$ B1$^-$) along with the controls (cv. Kronos and WT sibling lines) using a

commercial kit (K-PHYT kit, Megazyme Inc, Bray, Ireland). The grains were grounded to fine powder by a laboratory Cycline Mill (Cyclotec 1093, FOSS, Hilleröd, Sweden). One gram of the powder was suspended in 20 ml of 0.66 M HCl with continuous stirring overnight. The supernatant was then used for the colorimetric procedure according to the manufacturer's protocol. PA content has been expressed in the form of mean values of three biological replicates ± standard error. Three technical replicates were carried out for each biological replicate. Significant differences between mean values were identified by applying a one-way analysis of variance and the *post hoc* Tukey's HSD test, p-value< 0.01.

2.7 Visualization of iron deposits in seeds using the Perls stain

The *Perls* method is used to determine the localization of ferric iron (Fe^{3+}) deposits stained in blue in the tissues (Krishnan et al., 2001; Prom-u-Thai et al., 2003). Briefly, the mature F_4 seeds were soaked in dH_2O for 5 hours. Then, the seeds were cut transversely and longitudinally and placed in Petri dishes, submerged in freshly prepared Perls staining solution (2% hydrochloric acid mixed with 2% potassium ferrocyanide) for 30 minutes. The seeds were then gently washed continuously in dH_2O for 5 minutes. The intensity of staining was rated under a stereo microscope.

2.8 Determination of nutrients concentration

Mature F_4 seeds of the selected mutant lines along with controls (cv. Kronos and WT sibling lines) were grounded to fine powder and oven-dried at 80°C to constant weight. Samples were introduced in polypropylene tubes (digiTUBES, SCP Science, Champlain, NY, USA) with 3 mL of concentrated nitric acid and 1 mL of concentrated hydrogen peroxide and heated in a block system (DIGIPREP, SCP Science, Champlain, NY, USA) for 120 min at 95° C. After digestion, the extracts were filtered by a 0.45 µm teflon filter (DigiFILTER, SCP Science, Champlain, NY, USA). After cooling down, the digests were diluted with dH_2O and analyzed by inductively coupled plasma-mass spectrometry (ICP-MS 7900, Agilent Technologies, Santa Clara, CA, USA) with Octopole Reaction System (ORS). Phosphorous and sulfur in the digested solutions were determined by inductively coupled plasma-optical emission spectrometer (ICP-OES 5100 Agilent Technologies, Santa Clara, CA, USA). Data have been expressed as mean values of three biological replicates ± standard error. Three technical replicates were carried out for each biological replicate. The ICP-MS operating conditions are summarized in Supplementary Table S2.

2.9 Analysis of root morphological traits

The mature F_4 seeds of the selected mutant lines along with control plants (cv. Kronos and WT sibling lines) were soaked in dH_2O for 1 hour. Then they were transferred in Petri dishes and left to germinate for 5 days in the dark at room temperature. After germination, uniform seedlings were transferred to a plastic pot filled with 2 L of a continuously aerated nutrient solution (Celletti et al., 2016) and were placed in a growth chamber under 27/20°C and 14/10 h day/night cycles with a relative humidity of 80% and 200 µmol m^{-2} s^{-1} PAR at leaf level for 5 days. Roots were excised from the stem and subsequently placed in a Perspex tray with a shallow film of water to minimize root overlapping. Root systems were analysed using the WinRHIZO™ scanning equipment and software (EPSON1680, WinRHIZO Pro2003b Software; Regent Instruments Inc., Quebec, Canada) to determine their volume and surface area, total root length, root diameter and number of root tips. Data have been expressed as mean values of three biological replicates ± standard error. Three technical replicates were carried out for each biological replicate.

2.10 Field trial evaluation of yield-related traits

The experimental field trial was carried out at CREA-CI (Foggia, Italy) during the 2021-2022 growing season using standard agronomic practices. For this experiment, grains from two different genotypes were used: wild-type (cv. Kronos) and double null TdMRP3 mutant. Each genotype was seeded in single plots, consisting of 1-m rows, 30 cm apart, with 30 germinating seeds per plot, and following a randomized complete block design with three replications. Plots were hand-harvested at maturity and yield-related traits (i.e. Spike weight, g; Spike length, cm; Spikelets number per spike; Kernels per spike and Kernel weight per spike, g), measured from ten randomly selected spikes per row, were recorded.

3 Results

3.1 In silico analysis of TdMRP3 transporters

A blast search of *TaMRP3-A1* and *TaMRP3-B1* (TraesCS5A02G512500 and TraesCS4B02G343800) run against the durum wheat genome in Ensembl Plants revealed a high identity with TRITD5Av1G244640 and TRITD4Bv1G193220 both coding for proteins with ATP binding and ABC-type transporter activity. The comparison of the deduced protein sequences with TaMRP3 proteins showed that both TdMRP3 proteins lack the TDM0 domain and present a shorter IPR011527 ABCC1_TM domain (data not shown).

A second blast of the orthologous *TaMRP3* homeoalleles was performed against the Svevo Platinum Genome and allowed the identification of two sequence hits with high identity values, located on the chromosomes 5A and 4B, respectively. The *TdMRP3* sequences of Svevo include 11 exons and 10 introns (Supplementary Figures S1A, S2). The deduced amino acid sequences contain 1510 and 1505 aa for TdMRP3-A1 and TdMRP3-B1, respectively; both proteins showed five domains in the forward orientation typical of ABCC transporters: TMD0-TMD1-NBD1_TMD2-NBD2 (Supplementary Figures S1B, S3). The analysis performed by I-TASSER 3D model program confirmed the presence of five transmembrane α-helices in TMD0, six α-helices in each TMD1 and TMD2 and the presence of Walker A and B motifs in

the two cytosolic nucleotide-binding domains NBD1 and NBD2 (Supplementary Figure S1B).

A Multiple Sequence Alignment (MSA) of MRP proteins of major cereals and the model species *Arabidopsis thaliana* highlighted that the five domains of TdMRP3-A1 and TdMRP3-B1 were highly conserved among the orthologous proteins of the different species except for TDM0 (Supplementary Figure S3). In Figure 1 the phylogenetic tree shows the evolutionary relationships of MRP transporters (orthologous of TdMRP3) among the grasses. TdMRP3 transporters showed phylogenetic proximity with other *Triticinae* (*Triticum aestivum*, *Triticum dicoccoides*) and barley (*Hordeum vulgare*). Noteworthy the amino acid sequences of the TdMRP3-A1 and TdMRP3-B1 were identical to those of bread wheat (TaMRP3-A1 and TaMRP3-B1, respectively). In addition, a higher homology was observed between the homeologous sequences of the genomes B and D compared to that of the A genome.

A second phylogenetic cluster was constituted by the MRP proteins isolated from *Oryza sativa*, *Zea mays*, *Sorghum bicolor*, *Panicum hallii*, *Panicum virgatum*, *Setalia italica*, *Setaria viritis*. Although the last cluster was more divergent from durum wheat sequences, the structure (domains) and the amino acid composition were strongly conserved among the different species considered for the phylogenetic tree (Figure 1; Supplementary Figure S3).

3.2 Identification and pyramiding of TdMRP3 mutations: selection of *lpa* mutants

Two knock out mutant lines for *TdMRP3* genes (one for each homeoallele), described in the "Material and methods" section, were identified through an *in silico* search on the "Wheat TILLING" platform (Krasileva et al., 2017). The single null mutant lines Kronos 3179 (TdMRP3-A1$^-$) and Kronos 4443 (TdMRP3-B1$^-$) were crossed to pyramid the two mutations and the F_2 progenies genotyped by an HRM-genotyping assay (Wittwer et al., 2003), able to distinguish among heterozygous, homozygous and wild type genotypes for both the homeoalleles (Supplementary Figure S4). The analysis led to identifying four F_2 homozygous double null mutants. In addition, three independent sister lines were identified for each single null mutant genotype (TdMRP3-A1$^-$ and TdMRP3-B1$^-$) and for the control line (wild type at each *MRP3* homeoallele-WT sibling lines). The different genotypes were confirmed by Sanger sequencing (Supplementary Figure S4).

3.3 Effect of the TdMRP3 suppression on the accumulation of phytic acid and nutrients in the kernel

To evaluate the effect of silencing of *TdMRP3* genes, mature grains were assessed for PA content in the whole set of mutants plus the controls. The complete null genotypes (TdMRP3-A1$^-$B1$^-$) showed a strong reduction in PA compared to the control (cv. Kronos) and WT sibling lines (-84.5% and – 86.5%, respectively), while no differences were observed in the single mutants (Figure 2).

In light of the interaction between PA and cationic nutrients, the localization of iron deposits and micro/macronutrient accumulation were analysed in the mature seeds of the set of TdMRP3 mutants compared to the control. The intensity of iron deposits appeared strongly increased in the double null TdMRP3 mutants, interesting the scutellum, even more in the aleuronic layer and also evident in the endosperm (Figure 3). The single null genotypes (TdMRP3-A1$^-$ and

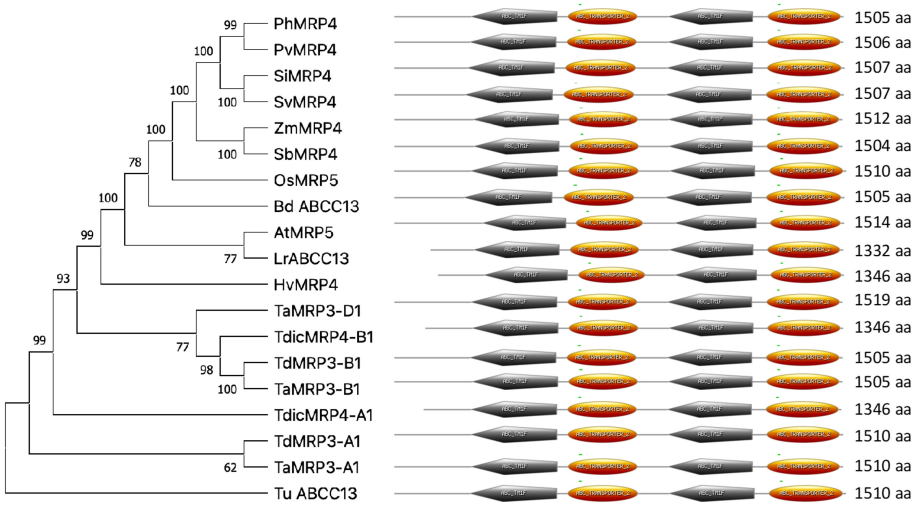

FIGURE 1
Phylogenetic tree of the ABCC multidrug resistance-associated protein (ABCC-MRP) in different plant species. Td: *Triticum turgidum ssp durum* MRP3-A1 (SVEVO PLATINUM SEQUENCE), MRP3-B (VEVO PLATINUM SEQUENCE), Ta: *Triticum aestivum* MRP3-A (XP_044384038 _TraesCS5A02G512500), MRP3-B (XP_044371728 TraesCS4B02G343800), MRP3-D (XP_044377018_TraesCS4D02G339000); Tu: *Triticum urartu* ABCC13 XP_048531007.1; Tdic: *Triticum dicoccoides* MRP4-A (XP_037437166.1), MRP4-B (XP_037426738.1); Hv: *Hordeum vulgare* MRP4 (XP 044983147.1); Bd: *Brachypodium distachyon* ABCC13 (XP_003558836.1); Zm: *Zea mays* MRP4 (EF586878); Sb: *Sorghum bicolor* MRP4 (XP 002468528.2); Pah: *Panicum hallii* MRP4 (XP 025794868.1); Pav: *Panicum virgatum* MRP4 (XP_039780041.1); Si: *Setaria italica* MRP4 (XP 004985744.1); Os: *Oryza sativa Japonica group* MRP5 (XP 015630971.1); At: *Arabidopsis thaliana* MRP5 (AT1G04120.1); Sv: *Setaria viridis* MRP4 (XP_034572896.1); Lr: *Lolium rigidum* ABCC13 like (XP_047089394.1). The tree constructed by the Neighbor-joining (NJ) method with pairwise deletion option and p-distance matrix in MEGA XI (Tamura et al., 2021). Bootstrap values (1000 replicates) were shown at each node.

10.3389/fpls.2023.1079559

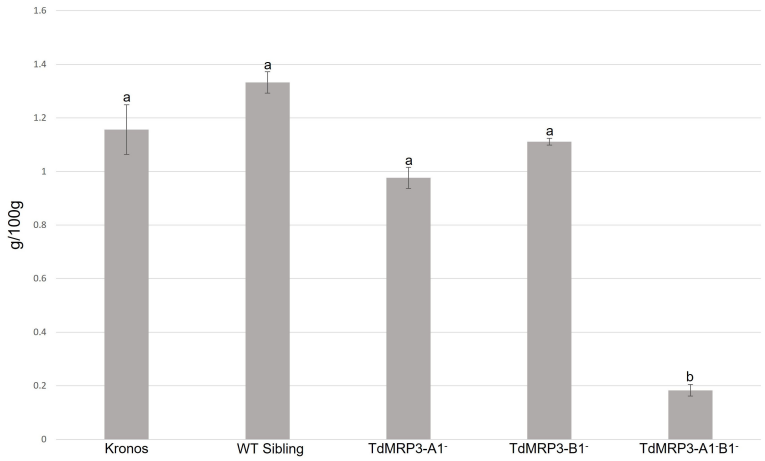

FIGURE 2
Phytic acid content in *lpa* mutants, WT sibling lines and cv. Kronos. Mean values of three biological replicates, error bars indicate standard error. Values followed by different letters differ signifcantly from one another (one-way ANOVA, Tukey HSD test, p<0.01).

TdMRP3-B1$^-$) also revealed visible differences in respect to the control, but less pronounced than the completely null genotypes (Figure 3).

The analysis of macro- and micro-nutrients in seeds highlighted differences among the genotypes. With regard to macronutrients, a higher accumulation of Mg and S was observed in the complete null TdMRP3 genotype compared to both the partial mutants and the controls (Figure 4). In detail, the whole grain of the complete null TdMRP3 genotypes showed a raise of 38.4% for Mg and 32.6% for S compared to the cv. Kronos.

No significant differences were detected for K in the mutant lines (either for partial or complete null genotypes), except for TdMRP3-A1$^-$, which showed a slight decrease (-23.5%).

More interesting, a significant raise in micronutrient accumulation was recorded in the TdMRP3-A1$^-$B1$^-$ genotype (Fe

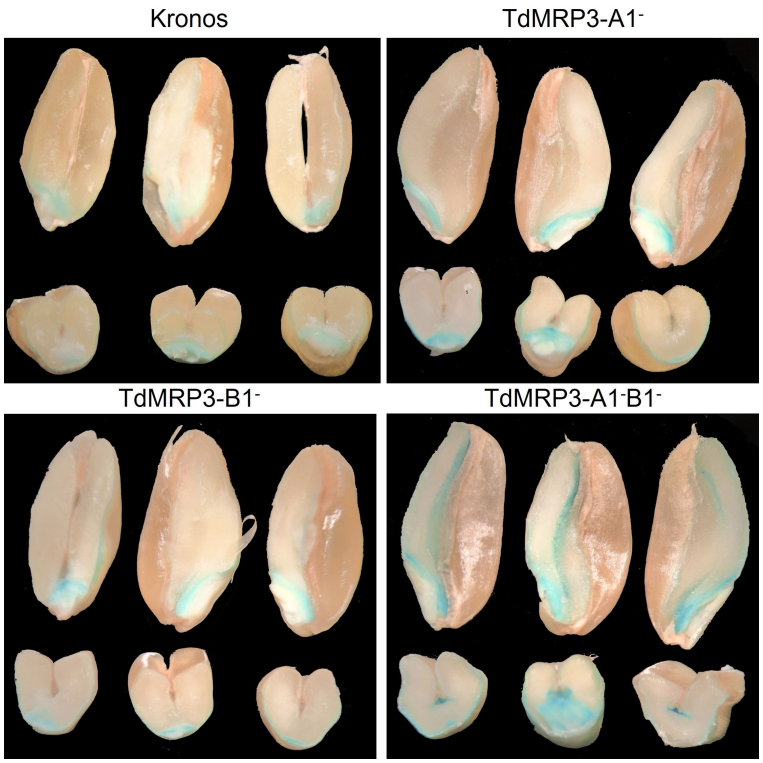

FIGURE 3
Visualization of iron deposits within the kernel using the *Perls* staining. In each image there are the longitudinal sections (top) and the transversal sections (bottom), of the seeds of cv. Kronos, TdMRP3-A1$^-$, TdMRP3-B1$^-$, TdMRP3-A1$^-$B1$^-$.

10.3389/fpls.2023.1079559

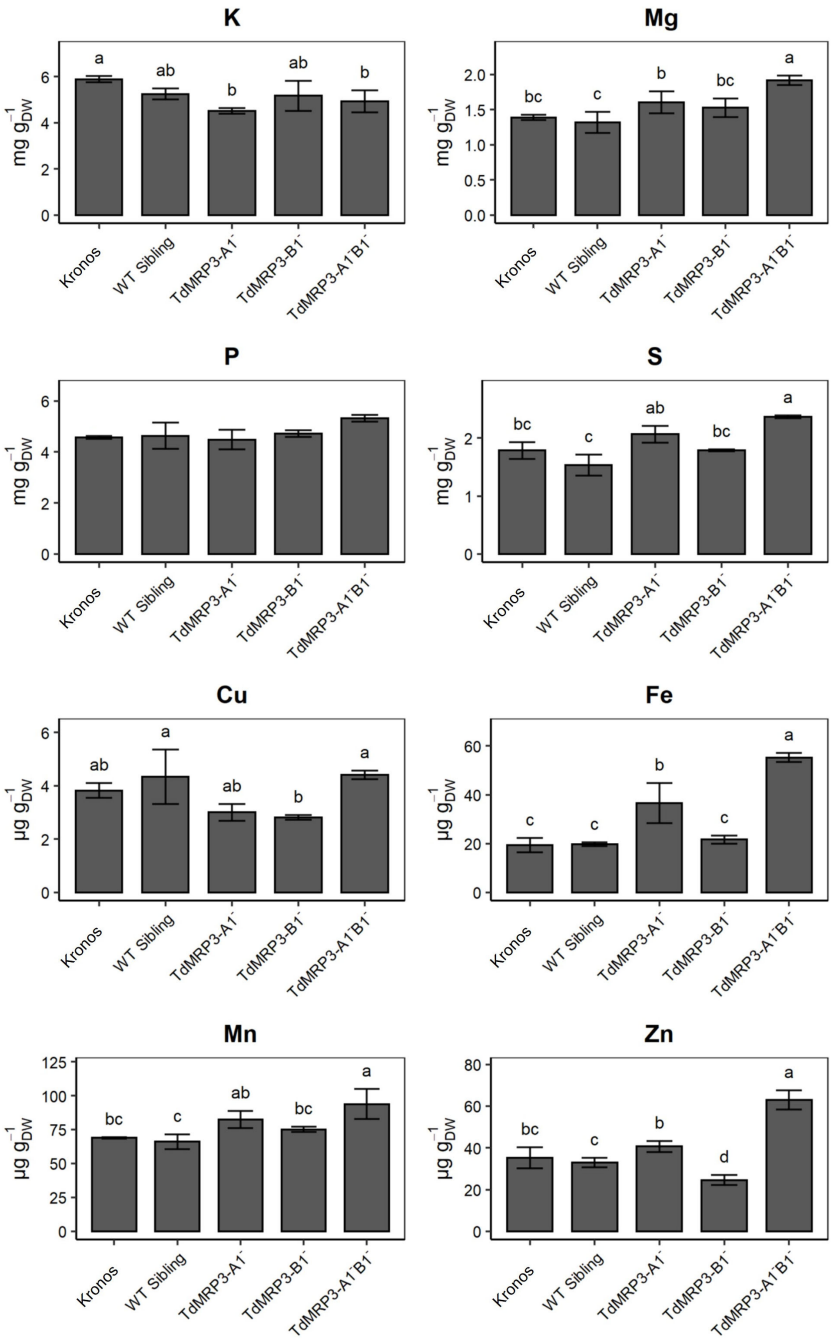

FIGURE 4
Concentration of nutrients in *lpa* mutants, WT sibling lines and cv. Kronos. Mean values of three biological replicates ± St. Dev. One-way ANOVA, LSD *post hoc* test, p <0.05.

+186.3%, Zn +78.4%, and Mn +36.3%), with the exception of Cu that maintained a concentration similar to the control (Figure 4). On the other hand, the accumulation pattern of micronutrients in partial genotypes was non-uniform. In particular, the accumulation of Fe did not change in the TdMRP3-B1$^-$ mutant, whereas it increased by 89.3% in the other partial mutant TdMRP3-A1$^-$. A different trend was also observed for Zn accumulation: it was reduced in the TdMRP3-B1$^-$ genotype (-30.3%) and not significantly affected in TdMRP3-A1$^-$.

3.4 Effects of TdMRP3 silencing on the agronomic performance and root morphology

The agronomic performances of TdMRP3 mutant lines were evaluated in field by measuring a set of yield-related parameters of plant growth. No significant differences were registered for spike weight, spike length and kernel weight for spike between the control and TdMRP3 complete null mutant genotypes

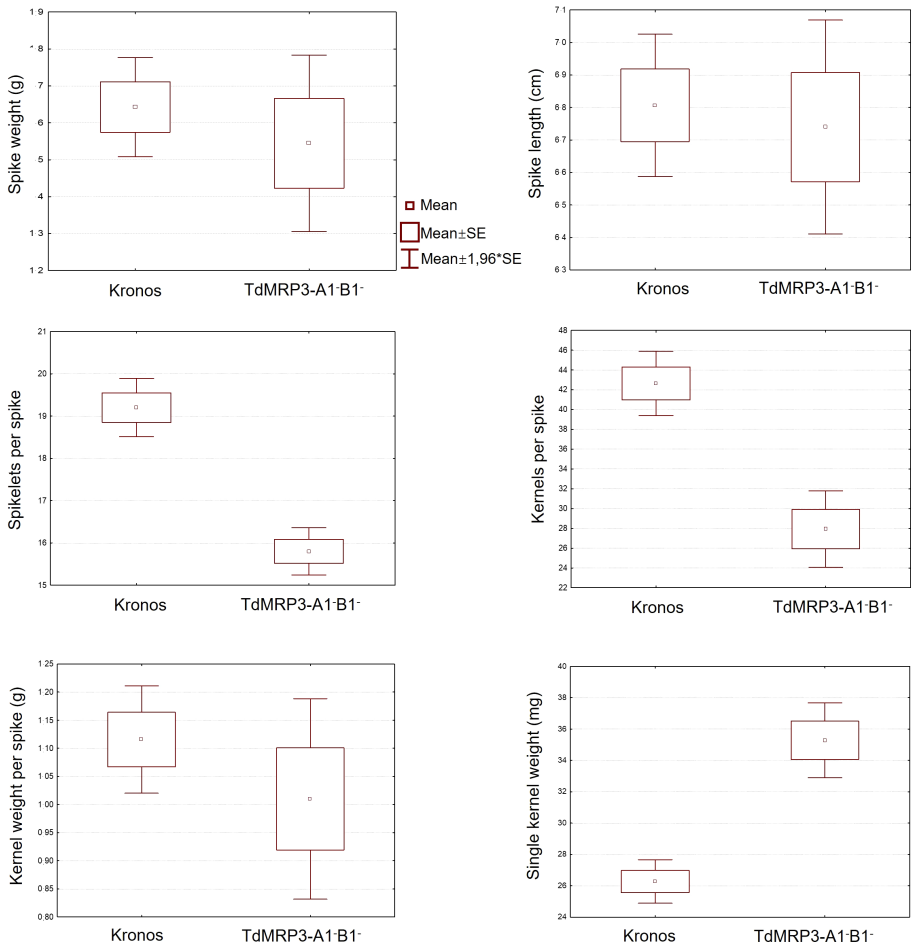

FIGURE 5
Agronomic traits analysis performed on: Spike weight (g), Spike length (cm), Spikelets per spike, Kernels per spike, Kernel weight per spike (g), Single kernel weight (mg). In each image there is the analysis of the seeds of cv. Kronos compared to TdMRP3-A1⁻B1⁻.

(Figure 5). Otherwise, TdMRP3-A1⁻B1⁻ mutant lines showed a reduction in the number of spikelets per spike (-17.7%) and a more significant reduction in the number of kernels per spike (-34.5%), while no significant differences for the grain weight per spike were recorded. Single kernel weight was increased by 34.2% in the TdMRP3-A1⁻B1⁻ mutant lines. No significant differences were observed between the single null lines and the wild type (data not shown).

As ABCC proteins are involved in several aspects of plant growth and root development, the root architecture of the set of mutant lines was analysed and compared to the control, considering the following parameters: root length, number of root tips, root surface area, volume and diameter (Figure 6). The mutant plants TdMRP3-A1⁻B1⁻ showed a significant decrease in the number of root tips (-83.5%), root length (-61.2%), volume (-16.8%), and surface area (-40.6%) compared to the cv. Kronos. A decrease in the number of root tips and an increase in root volume were observed in both the partial mutant genotypes, while no significant differences were detected in the root length and root surface area. Noteworthy, root average diameter significantly increased in all the mutants and increased by 45.8% in the TdMRP3-A1⁻B1⁻ (Figure 6).

4 Discussion and conclusions

Hidden hunger is a global health issue, that involves more than 3 billion people around the world, mostly in Africa, Asia, and Latin America. Diets poor in essential vitamins and minerals (micronutrients), typical of some countries of the above-cited continents, are the main driver of the hidden hunger. The development of biofortified staple crop varieties is an effective and low-cost strategy pursued by several major public and private sector organizations (such as Universities, INRA, CIMMYT and ICARDA) in Southern America, Asia and Africa. In this context, Harvest Plus is a big initiative focused on the development of bio-fortified wheat varieties, that involves partners from dozens of countries (Wani et al., 2022). Although numerous efforts have been focused on the realization of biofortified wheat genotypes, it remains still challenging.

In plants, PA is stored in the vacuole and functions as a Pi sink to aid plant growth upon seed germination. Due to its negative charge, PA chelates the cations forming poorly bioavailable phytate salts and limiting mineral ion bioavailability, thus promoting mineral deficiencies in the body (Grases et al., 2017; Samtiya et al., 2020). For this reason, boosting the bioavailability of minerals in plant food can be achieved by reducing PA. *Lpa* mutants can be produced by the

10.3389/fpls.2023.1079559

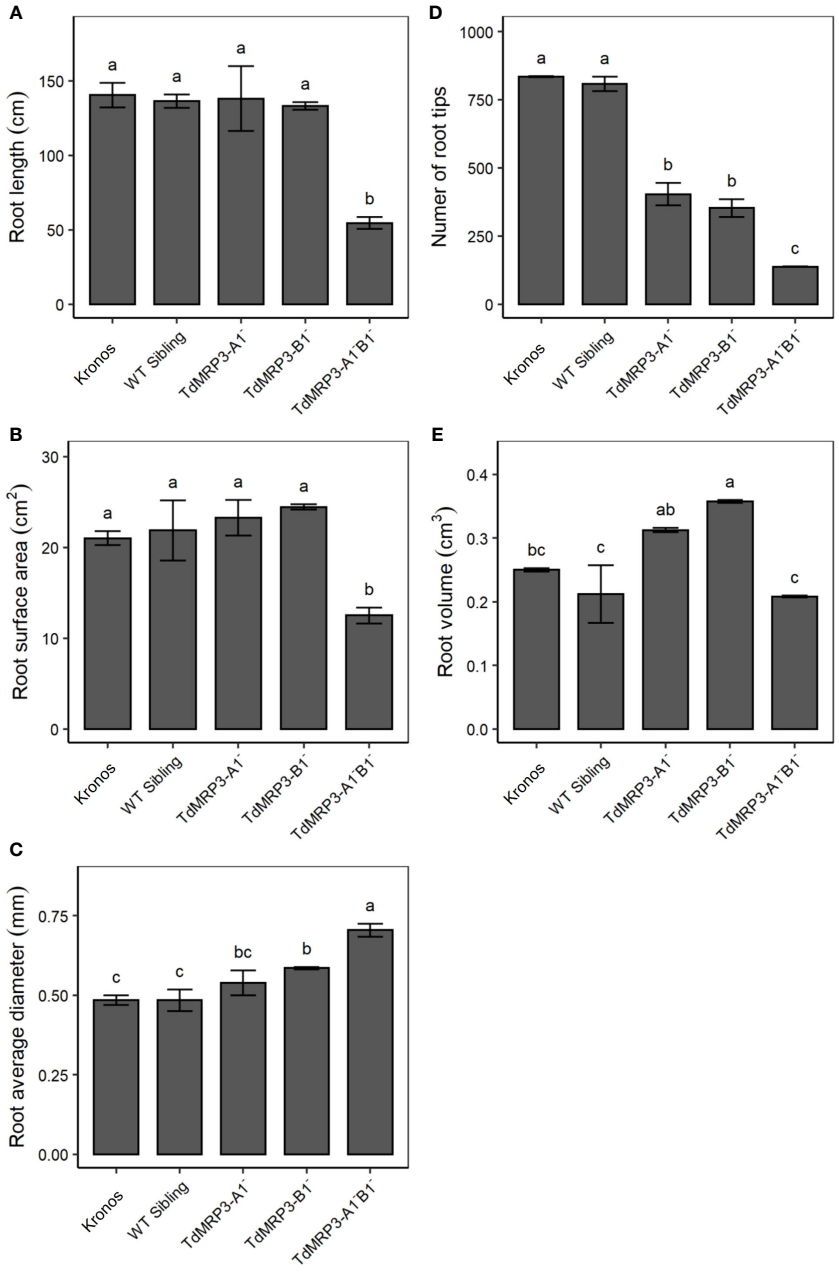

FIGURE 6
Root morphological traits: length **(A)**, surface area **(B)**, diameter **(C)**, number of root tips **(D)** and volume **(E)** in *lpa* mutants, WT sibling lines and cv. Kronos. Mean values of three biological replicates ± St. Dev. One-way ANOVA, LSD *post hoc* test, p <0.05.

impairment of the transport and storage of PA into the vacuole: in the cytosol PA is exposed to a dephosphorylation process carried out by cytosolic phosphatases, decreasing the final amount of phytates and increasing free Pi and cations (Sparvoli and Cominelli, 2015; Colombo et al., 2020). *Lpa* mutants were developed in wheat *via* ethyl methane sulfonate mutagenesis, and germplasm derived from these mutants was used for breeding purposes (Guttieri et al., 2004; Guttieri et al., 2006; Venegas et al., 2022).

Here, *lpa* mutants were generated in durum wheat targeting *TdMRP3* genes by TILLING, thereby causing the impairment of PA into the vacuole. TILLING strategy (McCallum et al., 2000) is a reverse genetics approach widely used in functional studies and breeding programs in numerous species, including bread and durum wheat (Slade et al., 2005; Botticella et al., 2011; Hazard et al., 2014; Sestili et al., 2015; Sestili et al., 2019; Garcia Molina et al., 2021) as it offers the big advantage to expand the genetic variability and to produce nontransgenic plants, that can be used for commercial purposes.

Our *in silico* analysis showed that the protein structure of MRP transporters was highly conserved among the major cereals. In detail, all the analysed sequences had the typical domains of ABCC transporters in forward orientation (Colombo et al., 2020), with a high identity degree in according to previous studies (Bhati et al., 2016; Cominelli et al., 2020b). Preliminary analysis on Ensembl database highlighted that durum wheat MRP3 proteins from Svevo genome v1 were different in length with respect to bread wheat and

other cereal sequences. These durum wheat proteins missed an N-terminal region that included the TMD0 domain and part of the TMD1. Differently, the two durum wheat MRP3 sequences isolated by means of the new Svevo Platinum sequence showed the same length of TaMRP3 proteins (1510 and 1505 aa) and a perfect amino acid identity, sharing high phylogenetic proximity with other cereal species.

TdMRP3-A1 and -B1 were clustered into the same subgroup and were closer to the MRP proteins of *Triticinae* and barley and more divergent from other species, including the major cereals (rice and maize). Our data are in agreement with previous comparative studies that showed a high level of synteny in several gene loci among wheat, barley and other members of the *Triticeae* (Linde-Laursen et al., 1997; Mayer et al., 2011). Although the MRP3 sequences are highly conserved among the A, B, and D genomes of wheat, small amino acidic differences were identified. Unexpectedly a higher synteny was observed between the homeologous sequences encoded by the B and D genomes compared to MRP3-A1. In this regard, previous studies demonstrated higher synteny levels between A and D genome homeologues compared to those of the B genome (Akhunov et al., 2003; Pont et al., 2013).

In TdMRP3 double null mutants, PA was reduced by roughly 85% compared to the control in line with what was observed in *lpa* genotypes produced in legumes and other cereals, like maize and rice that showed a reduction of 80 and 90%, respectively (Silva et al., 2021). Differently, partial suppression of *TaMRP3* genes targeted by RNAi resulted in a modest reduction of PA content (in the range from -22 to -34%) in bread wheat. These differences can be explained by the different efficiency of silencing of the two approaches: full silencing in TILLING mutants, and reduction in the range of 40-72% of *TaMRP3* transcripts in the case of RNAi plants (Bhati et al., 2016). Accordingly, the accumulation of Fe, Zn and Mn in the grain was significantly raised in the TdMRP3 null mutants than in the transgenic RNAi lines (about +186% vs +18% for Fe; about +36% vs 0% for Mn; +78% vs +13% for Zn).

Generally, the phytic acid mutants described in many plant species were presented as agronomically poor for the low yields and for the poor germination capacity of the seeds (Raboy, 2020). In bread wheat, previous studies conducted on EMS mutants showed a reduction in PA of 30 to 40% (Guttieri et al., 2004), and a more contained loss of yield (from 8 to 25%).

In our study, the reduction in yield was comparable to bread wheat, although the reduction in PA was much higher (>85%). Actually, Guttieri et al. (2006) showed the absence of consistent effects on yield and yield-related traits in wheat *lpa* mutants, depending on the different genetic backgrounds in which the trait was transferred. In particular, in the soft white spring genetic background, the kernel weight of the *lpa* mutants was greater than that of the control wild type, confirming our findings, in which the partial reduction in yield, due to the reduction in the number of spikelets and kernels for spike, was compensated by a greater kernel weight. This suggested that the negative agronomic effects of the *lpa* genotype can be mitigated by adopting an adequate genetic improvement strategy.

In maize the suppression of *ZmMRP4* was associated with ungerminability and seed weight loss (Pilu et al., 2005; Cerino Badone et al., 2012). Pilu et al., 2005 found a decreased content of PA in maize mutant lines and showed that kernels with less than 20% of PA are unable to germinate. The same pleiotropic effects were reported in rice with the suppression of *OsMRP5*, orthologous of *TdMRP3* and *ZmMRP4* (Xu et al., 2009). In detail, the T-DNA knock line, in which *OsMRP5* was disrupted, showed a strong reduction of PA (>90%) and an inability to germinate.

Non-lethal *lpa* mutants were obtained in soybean and common bean through the silencing of the orthologous genes of *TdMRP3* (Oltmans et al., 2005; Cominelli et al., 2018). PA dropped between 75 and 90% in both the species but only in common bean no pleiotropic effect on yield traits and plant phenotype was observed.

The morphology of the root apparatus was markedly altered in our complete null TdMRP3 mutant line. In detail, the root length, volume and surface area and the number of tips, were decreased, while the root diameter was increased compared to the control plants. The morphological alteration of the root apparatus is a common adaptive strategy used by plants to cope with suboptimal nutrients (mainly nitrogen, sulfur and phosphate) and water availability (Aiken and Smucker, 1996; López-Bucio et al., 2003; Péret et al., 2011). The root diameter generally matches the elongation rate, which stops when the root reaches the minimal diameter (Pagès et al., 2020). Accordingly, shorter roots generally have a larger diameter.

It is well known that the plants face phosphate starvation by modifying the root system architecture through the inhibition of primary root growth, the increase of the lateral root formation and the growth and production of root hairs, thus allowing their root systems to efficiently utilize Pi from soils (Vance et al., 2003; Hinsinger et al., 2009; Péret et al., 2011). Besides soil P concentration, also plant Pi status can trigger morphological root responses (Vance et al., 2003; Lambers et al., 2006). Thus, the short-root phenotype showed by our mutants could be attributed to changes in Pi homeostasis induced by *TdMRP3* silencing resulting in increased availability of free phosphate in the cells and lower Pi demand from the soil. Moreover, MRP3 transporters are known to be expressed in several plant tissues including roots. So, we cannot rule out the possibility that the silencing of MRP3 transporter may have a more direct effect on anatomical root differences known to impact tolerance to Pi deficiency.

From a future perspective, it could be interesting to develop novel approaches able to limit the silencing of the *TdMRP3* expression to the seed to minimize the pleiotropic effects associated with *lpa* mutants. Bhati et al. (2016), using a different silencing technology, did not find a significant difference in the root length between the control and the RNAi transgenic plants. Moreover, they observed that the number of lateral roots was higher in the transgenic lines compared to the control plants. We could interpret these contrasting results by considering that the critical P supply and plant status for the activation of P-deficiency response, including root alterations, differ among plant species (Teng et al., 2013).

In conclusion, this study shed light on the functional role of TdMRP3 in durum wheat. In detail, it confirmed that the reduction of PA through the silencing of MRP transporters is a good strategy to obtain durum wheat genotypes biofortified in essential minerals and with acceptable agronomic performances. To date, to the best of our knowledge, this represents the first study in wheat allowing at the same time to increase the accumulation of essential minerals such as Zn, Fe and Mn.

Noteworthy, the plant lines can be used as starting material in breeding programs focused on mineral biofortification without any legal restriction associated with genetically modified organisms.

Data availability statement

The datasets presented in this study can be found in online repositories. The names of the repository/repositories and accession number(s) can be found in the article/Supplementary Material.

Author contributions

AF, SP, SC, MF and PV: investigation. EB and FS: conceptualization. FS and MV: funding acquisition. AF, SP and FS: data curation. SA, FS, PV and SM: visualization and validation. AF and FS: writing-original draft preparation. PV, EB, SA, SM and SM: writing-review & editing. FS: project administration. All authors contributed to the article and approved the submitted version.

Funding

This research was partially funded by the Italian Ministry of Education, University, and Research (MIUR) in the frame of the MIUR initiative "Departments of excellence", Law 232/2016 and by Grandi Molini Italiani SpA.

Acknowledgments

The authors wish to thank Prof. Jorge Dubcovsky (University of Davis) for providing the mutant lines of Kronos TILLING platform; Dr. Annamaria Gallo for her technical assistance in making wheat crosses and Svevo Platinum Genome Consortium for the access to the sequencing of the genome of Svevo (v. 2).

Conflict of interest

Author MV is employed by Grandi Molini Italiani SpA.

FS, AF, EB, MV are coinventors of the Italian patent application no. 102022000008315 "Wheat mutant plant with a reduced content of phytic acid".

The authors declare that this study received funding from Grandi Molini Italiani SpA. The funder was not involved in the study design, collection, analysis, interpretation of data, the writing of this article, or the decision to submit it for publication.

Publisher's note

Supplementary material

The Supplementary Material for this article can be found online at: https://www.frontiersin.org/articles/10.3389/fpls.2023.1079559/full#supplementary-material

References

Aiken, R. M., and Smucker, A. J. M. (1996). Root system regulation of whole plant growth. *Annu. Rev. Phytopathol.* 34 (1), 325–346. doi: 10.1146/annurev.phyto.34.1.325

Akhunov, E. D., Akhunova, A. R., Linkiewicz, A. M., Dubcovsky, J., Hummel, D., Lazo, G., et al. (2003). Synteny perturbations between wheat homoeologous chromosomes caused by locus duplications and deletions correlate with recombination rates. *Proc. Natl. Acad. Sci.* 100 (19), 10836–10841. doi: 10.1073/pnas.1934431100

Ariza-Nieto, M., Blair, M. W., Welch, R. M., and Glahn, R. P. (2007). Screening of iron bioavailability patterns in eight bean (Phaseolus vulgaris l.) genotypes using the caco-2 cell *in vitro* model. *J. Agric. Food Chem.* 55 (19), 7950–7956. doi: 10.1021/jf070023y

Bhati, K. K., Aggarwal, S., Sharma, S., Mantri, S., Singh, S. P., Bhalla, S., et al. (2014). Differential expression of structural genes for the late phase of phytic acid biosynthesis in developing seeds of wheat (Triticum aestivum l.). *Plant Sci.* 224, 74–85. doi: 10.1016/j.plantsci.2014.04.009

Bhati, K. K., Alok, A., Kumar, A., Kaur, J., Tiwari, S., and Pandey, A. K. (2016). Silencing of ABCC13 transporter in wheat reveals its involvement in grain development, phytic acid accumulation and lateral root formation. *J. Exp. Bot.* 67 (14), 4379–4389. doi: 10.1093/jxb/erw224

Botticella, E., Sestili, F., Hernandez-Lopez, A., Phillips, A., and Lafiandra, D. (2011). High resolution melting analysis for the detection of EMS induced mutations in wheat sbella genes. *BMC Plant Biol.* 11 (1), 1–14. doi: 10.1186/1471-2229-11-156

Burge, C., and Karlin, S. (1997). Prediction of complete gene structures in human genomic DNA. *J. Mol. Biol.* 268 (1), 78–94. doi: 10.1006/jmbi.1997.0951

Celletti, S., Pii, Y., Mimmo, T., Cesco, S., and Astolfi, S. (2016). The characterization of the adaptive responses of durum wheat to different fe availability highlights an optimum fe requirement threshold. *Plant Physiol. Biochem.* 109, 300–307. doi: 10.1016/j.plaphy.2016.10.010

Cerino Badone, F., Amelotti, M., Cassani, E., and Pilu, R. (2012). Study of low phytic acid1-7 (lpa1-7), a new ZmMRP4 mutation in maize. *J. Hered.* 103 (4), 598–605. doi: 10.1093/jhered/ess014

Chang, J. M., Di Tommaso, P., Taly, J. F., and Notredame, C. (2012). Accurate multiple sequence alignment of transmembrane proteins with PSI-coffee. *BMC Bioinf.* 13 (4), 1–7. doi: 10.1186/1471-2105-13-S4-S1

Colombo, F., Paolo, D., Cominelli, E., Sparvoli, F., Nielsen, E., and Pilu, R. (2020). MRP transporters and low phytic acid mutants in major crops: Main pleiotropic effects and future perspectives. *Front. Plant Sci.* 11, 1301. doi: 10.3389/fpls.2020.01301

Cominelli, E., Confalonieri, M., Carlessi, M., Cortinovis, G., Daminati, M. G., Porch, T. G., et al. (2018). Phytic acid transport in phaseolus vulgaris: A new low phytic acid mutant in the PvMRP1 gene and study of the PvMRPs promoters in two different plant systems. *Plant Sci.* 270, 1–12. doi: 10.1016/j.plantsci.2018.02.003

Cominelli, E., Galimberti, M., Pongrac, P., Landoni, M., Losa, A., Paolo, D., et al. (2020b). Calcium redistribution contributes to the hard-to-cook phenotype and increases PHA-l lectin thermal stability in common bean low phytic acid 1 mutant seeds. *Food Chem.* 321, 126680. doi: 10.1016/j.foodchem.2020.126680

Cominelli, E., Pilu, R., and Sparvoli, F. (2020a). Phytic acid and transporters: what can we learn from low phytic acid mutants? *Plants* 9 (1), 69. doi: 10.3390/plants9010069

Garcia Molina, M. D., Botticella, E., Beleggia, R., Palombieri, S., De Vita, P., Masci, S., et al. (2021). Enrichment of provitamin a content in durum wheat grain by suppressing β-carotene hydroxylase 1 genes with a TILLING approach. *Theor. Appl. Genet.* 134 (12), 4013–4024. doi: 10.1007/s00122-021-03944-6

Grases, F., Rafel, M. P., and Costa-Bauza, A. (2017). "Dietary phytate and interactions with mineral nutrients," in *Clinical aspects of natural and added phosphorus in foods* (New York, NY: Springer), 175–183.

Guttieri, M., Bowen, D., Dorsch, J. A., Raboy, V., and Souza, E. (2004). Identification and characterization of a low phytic acid wheat. *Crop Sci.* 44 (2), 418–424. doi: 10.2135/cropsci2004.4180

Guttieri, M. J., Peterson, K. M., and Souza, E. J. (2006). Agronomic performance of low phytic acid wheat. *Crop Sci.* 46 (6), 2623–2629. doi: 10.2135/cropsci2006.01.0008

Hazard, B., Zhang, X., Naemeh, M., and Dubcovsky, J. (2014). Registration of durum wheat germplasm lines with combined mutations in SBEIIa and SBEIIb genes conferring increased amylose and resistant starch. *J. Plant registrat.* 8 (3), 334–338. doi: 10.3198/jpr2014.02.0007crg

Hinsinger, P., Bengough, A. G., Vetterlein, D., and Young, I. M. (2009). Rhizosphere: biophysics, biogeochemistry and ecological relevance. *Plant Soil* 321 (1), 117–152. doi: 10.1007/s11104-008-9885-9

Krasileva, K. V., Vasquez-Gross, H. A., Howell, T., Bailey, P., Paraiso, F., Clissold, L., et al. (2017). Uncovering hidden variation in polyploid wheat. *Proc. Natl. Acad. Sci.* 114 (6), E913–E921. doi: 10.1073/pnas.1619268114

Krishnan, H. B. (2008). Preparative procedures markedly influence the appearance and structural integrity of protein storage vacuoles in soybean seeds. *J. Agric. Food Chem.* 56 (9), 2907–2912. doi: 10.1021/jf0735228

Krishnan, S., Ebenezer, G. A. I., and Dayanandan, P. (2001). Histochemical localization of storage components in caryopsis of rice (Oryza sativa l.). *Curr. Sci.* 80 (4), 567–571.

Lambers, H., Shane, M. W., Cramer, M. D., Pearse, S. J., and Veneklaas, E. J. (2006). Root structure and functioning for efficient acquisition of phosphorus: matching morphological and physiological traits. *Ann. Bot.* 98 (4), 693–713. doi: 10.1093/aob/mcl114

Linde-Laursen, I., Heslop-Harrison, J. S., Shepherd, K. W., and Taketa, S. (1997). The barley genome and its relationship with the wheat genomes. a survey with an internationally agreed recommendation for barley chromosome nomenclature. *Hereditas* 126 (1), 1–16. doi: 10.1111/j.1601-5223.1997.00001.x

Lockyer, S., White, A., and Buttriss, J. L. (2018). Biofortified crops for tackling micronutrient deficiencies–what impact are these having in developing countries and could they be of relevance within Europe? *Nutr. Bull.* 43 (4), 319–357. doi: 10.1111/nbu.12347

López-Bucio, J., Cruz-Ramırez, A., and Herrera-Estrella, L. (2003). The role of nutrient availability in regulating root architecture. *Curr. Opin. Plant Biol.* 6 (3), 280–287. doi: 10.1016/S1369-5266(03)00035-9

Mayer, K. F., Martis, M., Hedley, P. E., Šimková, H., Liu, H., Morris, J. A., et al. (2011). Unlocking the barley genome by chromosomal and comparative genomics. *Plant Cell* 23 (4), 1249–1263. doi: 10.1105/tpc.110.082537

McCallum, C. M., Comai, L., Greene, E. A., and Henikoff, S. (2000). Targeting induced local lesions IN genomes (TILLING) for plant functional genomics. *Plant Physiol.* 123 (2), 439–442. doi: 10.1104/pp.123.2.439

Nagy, R., Grob, H., Weder, B., Green, P., Klein, M., Frelet-Barrand, A., et al. (2009). The arabidopsis ATP-binding cassette protein AtMRP5/AtABCC5 is a high affinity inositol hexakisphosphate transporter involved in guard cell signaling and phytate storage. *J. Biol. Chem.* 284 (48), 33614–33622. doi: 10.1074/jbc.M109.030247

O'Dell, B. L., De Boland, A. R., and Koirtyohann, S. R. (1972). Distribution of phytate and nutritionally important elements among the morphological components of cereal grains. *J. Agric. Food Chem.* 20 (3), 718–723. doi: 10.1021/jf60181a021

Oltmans, S. E., Fehr, W. R., Welke, G. A., Raboy, V., and Peterson, K. L. (2005). Agronomic and seed traits of soybean lines with low–phytate phosphorus. *Crop Sci.* 45 (2), 593–598. doi: 10.2135/cropsci2005.0593

Pagès, L., Bernert, M., and Pagès, G. (2020). Modelling time variations of root diameter and elongation rate as related to assimilate supply and demand. *J. Exp. Bot.* 71 (12), 3524–3534. doi: 10.1093/jxb/eraa122

Péret, B., Clément, M., Nussaume, L., and Desnos, T. (2011). Root developmental adaptation to phosphate starvation: better safe than sorry. *Trends Plant Sci.* 16 (8), 442–450. doi: 10.1016/j.tplants.2011.05.006

Pilu, R., Landoni, M., Cassani, E., Doria, E., and Nielsen, E. (2005). The maize lpa241 mutation causes a remarkable variability of expression and some pleiotropic effects. *Crop Sci.* 45 (5), 2096–2105. doi: 10.2135/cropsci2004.0651

Pont, C., Murat, F., Guizard, S., Flores, R., Foucrier, S., Bidet, Y., et al. (2013). Wheat syntenome unveils new evidences of contrasted evolutionary plasticity between paleo-and neoduplicated subgenomes. *Plant J.* 76 (6), 1030–1044. doi: 10.1111/tpj.12366

Prom-u-Thai, C., Dell, B., Thomson, G., and Rerkasem, B. (2003). Easy and rapid detection of iron in rice grain. *ScienceAsia* 29, 203–207. doi: 10.2306/scienceasia1513-1874.2003.29.203

Raboy, V. (2009). Approaches and challenges to engineering seed phytate and total phosphorus. *Plant Sci.* 177 (4), 281–296. doi: 10.1016/j.plantsci.2009.06.012

Raboy, V. (2020). Low phytic acid crops: Observations based on four decades of research. *Plants* 9 (2), 140. doi: 10.3390/plants9020140

Regvar, M., Eichert, D., Kaulich, B., Gianoncelli, A., Pongrac, P., Vogel-Mikuš, K., et al. (2011). New insights into globoids of protein storage vacuoles in wheat aleurone using synchrotron soft X-ray microscopy. *J. Exp. Bot.* 62 (11), 3929–3939. doi: 10.1093/jxb/err090

Roberts, D. P., and Mattoo, A. K. (2019). Sustainable crop production systems and human nutrition. *Front. Sustain. Food Syst.* 3, 72. doi: 10.3389/fsufs.2019.00072

Samtiya, M., Aluko, R. E., and Dhewa, T. (2020). Plant food anti-nutritional factors and their reduction strategies: an overview. *Food Product. Process. Nutr.* 2 (1), 1–14. doi: 10.1186/s43014-020-0020-5

Secco, D., Bouain, N., Rouached, A., Prom-u-Thai, C., Hanin, M., Pandey, A. K., et al. (2017). Phosphate, phytate and phytases in plants: from fundamental knowledge gained in arabidopsis to potential biotechnological applications in wheat. *Crit. Rev. Biotechnol.* 37 (7), 898–910. doi: 10.1080/07388551.2016.1268089

Sestili, F., Garcia-Molina, M. D., Gambacorta, G., Beleggia, R., Botticella, E., De Vita, P., et al. (2019). Provitamin a biofortification of durum wheat through a TILLING approach. *Int. J. Mol. Sci.* 20 (22), 5703. doi: 10.3390/ijms20225703

Sestili, F., Palombieri, S., Botticella, E., Mantovani, P., Bovina, R., and Lafiandra, D. (2015). TILLING mutants of durum wheat result in a high amylose phenotype and provide information on alternative splicing mechanisms. *Plant Sci.* 233, 127–133. doi: 10.1016/j.plantsci.2015.01.009

Shears, S. B. (2001). Assessing the omnipotence of inositol hexakisphosphate. *Cell. signal.* 13 (3), 151–158. doi: 10.1016/S0898-6568(01)00129-2

Shewry, P. R. (2009). Wheat. *J. Exp. Bot.* 60 (6), 1537–1553. doi: 10.1093/jxb/erp058

Shi, J., Wang, H., Schellin, K., Li, B., Faller, M., Stoop, J. M., et al. (2007). Embryo-specific silencing of a transporter reduces phytic acid content of maize and soybean seeds. *Nat. Biotechnol.* 25 (8), 930–937. doi: 10.1038/nbt1322

Silva, V. M., Putti, F. F., White, P. J., and Dos Reis, A. R. (2021). Phytic acid accumulation in plants: Biosynthesis pathway regulation and role in human diet. *Plant Physiol. Biochem.* 164, 132–146. doi: 10.1016/j.plaphy.2021.04.035

Slade, A. J., Fuerstenberg, S. I., Loeffler, D., Steine, M. N., and Facciotti, D. (2005). A reverse genetic, nontransgenic approach to wheat crop improvement by TILLING. *Nat. Biotechnol.* 23 (1), 75–81. doi: 10.1038/nbt1043

Sofi, F., Abbate, R., Gensini, G. F., and Casini, A. (2010). Accruing evidence on benefits of adherence to the Mediterranean diet on health: an updated systematic review and meta-analysis. *Am. J. Clin. Nutr.* 92 (5), 1189–1196. doi: 10.3945/ajcn.2010.29673

Sparvoli, F., and Cominelli, E. (2014). "Phytate transport by MRPs," in *Plant ABC transporters* (Berlin, Germany: Springer, Cham), 19–38.

Sparvoli, F., and Cominelli, E. (2015). Seed biofortification and phytic acid reduction: a conflict of interest for the plant? *Plants* 4 (4), 728–755. doi: 10.3390/plants4040728

Tamura, K., Stecher, G., and Kumar, S. (2021). MEGA11: molecular evolutionary genetics analysis version 11. *Mol. Biol. Evol.* 38 (7), 3022–3027. doi: 10.1093/molbev/msab120

Teng, W., Deng, Y., Chen, X. P., Xu, X. F., Chen, R. Y., Lv, Y., et al. (2013). Characterization of root response to phosphorus supply from morphology to gene analysis in field-grown wheat. *J. Exp. Bot.* 64 (5), 1403–1411. doi: 10.1093/jxb/ert023

Vance, C. P., Uhde-Stone, C., and Allan, D. L. (2003). Phosphorus acquisition and use: critical adaptations by plants for securing a nonrenewable resource. *New Phytol.* 157 (3), 423–447. doi: 10.1046/j.1469-8137.2003.00695.x

Vasconcelos, M. W., Gruissem, W., and Bhullar, N. K. (2017). Iron biofortification in the 21st century: setting realistic targets, overcoming obstacles, and new strategies for healthy nutrition. *Curr. Opin. Biotechnol.* 44, 8–15. doi: 10.1016/j.copbio.2016.10.001

Venegas, J., Guttieri, M. J., Boehm, J. D.Jr., Graybosch, R., Bai, G., St. Amand, P. C., et al. (2022). Genetic architecture of the high-inorganic phosphate phenotype derived from a low-phytate mutant in winter wheat. *Crop Sci* 62 (3), 1228–1241. doi: 10.1002/csc2.20738

Vitamin and Mineral Nutrition Information System (VMNIS) (2022). Available at: https://www.who.int/teams/nutrition-and-food-safety/databases/vitamin-and-mineral-nutrition-information-system (Accessed August 2022).

Wani, S. H., Gaikwad, K., Razzaq, A., Samantara, K., Kumar, M., and Govindan, V. (2022). Improving zinc and iron biofortification in wheat through genomics approaches. *Mol. Biol. Rep.* 49, 1–17. doi: 10.1007/s11033-022-07326-z

Willett, W. C., Sacks, F., Trichopoulou, A., Drescher, G., Ferro-Luzzi, A., Helsing, E., et al. (1995). Mediterranean Diet pyramid: a cultural model for healthy eating. *Am. J. Clin. Nutr.* 61 (6), 1402S–1406S. doi: 10.1093/ajcn/61.6.1402S

Wittwer, C. T., Reed, G. H., Gundry, C. N., Vandersteen, J. G., and Pryor, R. J. (2003). High-resolution genotyping by amplicon melting analysis using LCGreen. *Clin. Chem.* 49 (6), 853–860. doi: 10.1373/49.6.853

Xu, X. H., Zhao, H. J., Liu, Q. L., Frank, T., Engel, K. H., An, G., et al. (2009). Mutations of the multi-drug resistance-associated protein ABC transporter gene 5 result in reduction of phytic acid in rice seeds. *Theor. Appl. Genet.* 119 (1), 75–83. doi: 10.1007/s00122-009-1018-1

frontiers | Frontiers in Plant Science

TYPE Original Research
PUBLISHED 03 March 2023
DOI 10.3389/fpls.2023.1093581

OPEN ACCESS

EDITED BY
Stefania Astolfi,
University of Tuscia, Italy

REVIEWED BY
Ju Min,
Institute of Soil Science (CAS), China
Xiang Gao,
Japan International Research Center for Agricultural Sciences (JIRCAS), Japan

*CORRESPONDENCE
Lekshmy Sathee
lekshmyrnair@gmail.com

SPECIALTY SECTION
This article was submitted to Plant Nutrition, a section of the journal Frontiers in Plant Science

RECEIVED 09 November 2022
ACCEPTED 31 January 2023
PUBLISHED 03 March 2023

CITATION
Padhan BK, Sathee L, Kumar S, Chinnusamy V and Kumar A (2023) Variation in nitrogen partitioning and reproductive stage nitrogen remobilization determines nitrogen grain production efficiency (NUEg) in diverse rice genotypes under varying nitrogen supply. *Front. Plant Sci.* 14:1093581. doi: 10.3389/fpls.2023.1093581

Variation in nitrogen partitioning and reproductive stage nitrogen remobilization determines nitrogen grain production efficiency (NUEg) in diverse rice genotypes under varying nitrogen supply

Birendra K. Padhan[1], Lekshmy Sathee[1*], Santosh Kumar[2], Viswanathan Chinnusamy[1] and Arvind Kumar[3,4]

[1]Division of Plant Physiology, ICAR-Indian Agricultural Research Institute, New Delhi, India, [2]Division of Crop Research, Indian Council of Agricultural Research (ICAR) Research Complex for Eastern Region, Patna, Bihar, India, [3]International Rice Research Institute (IRRI) South Asia Regional Centre (ISARC), Varanasi, Uttar Pradesh, India, [4]International Crops Research Institute for the Semi-Arid Tropics, Patancheru, Telangana, India

Nitrogen (N) is an important macronutrient needed for grain yield, grain N and grain protein content in rice. Grain yield and quality are significantly determined by N availability. In this study, to understand the mechanisms associated with reproductive stage N remobilization and N partitioning to grain 2 years of field experiments were conducted with 30 diverse rice genotypes during 2019-Kharif and 2020-Kharif seasons. The experiments were conducted with two different N treatments; N deficient (N0-no external N application, available soil N; 2019-234.15 kgha-1, 2020-225.79 kgha-1) and N sufficient (N120-120 kgha-1 external N application, available soil N; 2019-363.77 kgha-1, 2020-367.95 kgha-1). N application increased the NDVI value, biomass accumulation, grain yield, harvest index and grain N accumulation. Post-anthesis N uptake and N remobilization from vegetative tissues to grain are critical for grain yield and N harvest index. Rice genotypes, Kalinga-1, BAM-4234, IR-8384-B-B102-3, Sahbhagi Dhan, BVD-109 and Nerica-L-42 showed a higher rate of N remobilization under N sufficient conditions. But, under N deficiency, rice genotypes-83929-B-B-291-3-1-1, BVD-109, IR-8384-B-B102-3 and BAM-4234 performed well showing higher N remobilization efficiency. The total amount of N remobilization was recorded to be high in the N120 treatment. The harvest index was higher in N120 during both the cropping seasons. RANBIR BASMATI, BAM-832, APO, BAM-247, IR-64, Vandana, and Nerica-L-44 were more efficient in N grain production efficiency under N deficient conditions. From this study, it is evident that higher grain N accumulation is not always associated with higher yield. IR-83929-B-B-291-3-1-1, Kalinga-1, APO, Pusa Basmati-1, and Nerica-L-44 performed well for different N

use efficiency component traits under both N deficient (N0) and N sufficient (N120) conditions. Identifying genotypes/donors for N use efficiency-component traits is crucial in improving the fertilizer N recovery rate and site specific N management.

KEYWORDS

Nitrogen remobilization efficiency (NRE), Nitrogen Harvest Index (NHI), Nitrogen grain production efficiency (NUEg), Nitrogen use efficiency, Rice, NUE, Nitrogen deficiency, Optimum Nitrogen

Introduction

Rice (*Oryza sativa* L.) is an important food crop and a major dietary source of energy and proteins (Glangchai and Rangsri, 2021). Nitrogen (N) is an indispensable macronutrient for rice production and is responsible for protein accumulation in rice grains. N is directly associated with photosynthesis, biomass accumulation, tillering activity, spikelet formation, grain growth, and grain quality (Yoshida et al., 2006). N is one of the most critical yield-limiting factors in rice production and improving its utilization efficiency is essential for sustainable agriculture (Tilman et al., 2002; Hirel et al., 2007). However, crop intensification in the past with excessive N application and the decrease in the crop N recovery rate (<50%) has led to several environmental problems (Tilman et al., 2002). Indian soils are deficient in N (Dey and Sekhon, 2016) and more than 50% yield loss is common under N scarcity (Satyanarayana et al., 2012). Exogenous application of N fertilizer is mandatory to obtain higher yield returns from modern rice cultivars (Kraiser et al., 2011; Chamely et al., 2015). N fertilization at an adequate amount is critical for vegetative and reproductive growth in rice, and a better response to applied fertilizer is achieved in rice genotypes with higher yield potential (Rahman et al., 2007). However, excessive application of chemical fertilizers may have a negative environmental impact leading to pollution, biodiversity as well as yield loss (Cassman et al., 1998). It is estimated that ~ 60% of N inputs are in excess for major cereals including rice, and only 30%- 50% of applied N is taken up, and the unused N is lost to the environment (West et al., 2014; Herrera et al., 2016). Enhancing crop N use efficiency (NUE) will help in increasing yield under limited N conditions with minimum environmental impact (Moll et al., 1982). From a physiological point of view, NUE can be evaluated by the N utilization efficiency (NUtE) or N grain production efficiency (NUEg) (Ciampitti and Vyn, 2014). Of all the cereals, rice and wheat cropping systems have the lowest levels of nitrogen use efficiency (NUE), less than 30–40% (Norton et al., 2015; Taulemesse et al., 2015; Herrera et al., 2016). An additional amount of N fertilizer is applied to compensate for the effect of a lower uptake rate and to achieve higher grain yield (Elbasyoni et al., 2019). Reproductive stage N remobilization (NR) from the storage pool to sink organs is an important determinant for grain N recovery at harvest (Gaju et al., 2011). N assimilation associated with enhanced remobilization during seed filling leads to better yield, grain N accumulation, and protein content. N fertilizer management has a profound effect on grain yield and protein content (Zebarth et al., 2007). Improving the coordination between supply and crop demand, fertilizer management is a critical approach for simultaneously increasing grain yield and protein content (Chen et al., 2011). Better N management leads to higher absorption and a higher N harvest index (NHI) at crop maturity (Zheng et al., 2017). Experiments by Zhang et al. (2020) reported that adequate N supply increases post-anthesis N uptake and N remobilization to grain. The nutritional value of rice grain is largely determined by its protein content (Duan and Sun, 2005; Wenefrida et al., 2009). nutritional quality simultaneously in rice is a major challenge for researchers (Debata and Murty, 1986; Lim and Quah, 2007; Peng et al., 2007; Chen et al., 2012; Bhullar and Gruissem, 2013; Peng et al., 2014; Li et al., 2018).

Recycling of nutrients and metabolites takes place during grain filling along with the progression of leaf senescence. During the vegetative stage, young leaves are the major sink organs for N and metabolism, but during the reproductive stage, developing grain is the most important sink for the N pool. N is transported in the form of amino acids and serves as a precursor for the GS1-NADH-GOGAT reassimilation pathway in sink tissues. Most of the protein found in seeds is derived from the amino acids translocated after proteolysis from source organs. In rice and wheat, 80% of the total grain N is remobilized from leaves and other vegetative parts (Tabuchi et al., 2007; Xu et al., 2014). N in leaves is recycled following protein hydrolysis and exported to grains, 60% to 95% of grain N comes from the remobilization of N stored in shoots before anthesis. A less important fraction of seed N directly comes from post-flowering N uptake. The plant N status during the panicle initiation stage influences spikelet differentiation and yield. Before panicle emergence, most of the N is found in the leaves of rice. Following anthesis, there is a rapid transfer of leaf N to the developing panicles. Studies on the uptake and partitioning of N in rice showed that most of the N was distributed to new, actively growing organs. Deficiency in post-flowering N availability leads to a significant reduction in grain size and grain N content (DuPont and Altenbach, 2003). Zhang et al. (2020) found that the split application of N fertilizers increased N accumulation, which subsequently increased the protein content in grain. Proportionate allocation of N to component plant parts is important for higher efficiency of N translocation to the grain. Partitioning of N to vegetative plant parts during the vegetative stage is dependent on its availability in the soil, and its remobilization to the grain after anthesis is dependent on the N storage pool; the higher the storage of N in active vegetative organs the higher is the N remobilization activity (Nooden et al., 1997; Barraclough et al., 2014; He at al., 2016; He et al., 2016; Kumari et al., 2021).

Findings from various studies suggest that the NUE of rice cultivars varies in response to N fertilizer dose, which brings the

opportunity and possibility to screen diverse rice genotypes for NUE component traits. We previously evaluated a set of 300 diverse rice genotypes in hydroponics and identified 30 genotypes with improved NUE (unpublished). The selected 30 genotypes were evaluated in the field for N utilization efficiency and variation in N assimilation (Jagadhesan et al., 2020; Jagadhesan et al., 2022). In this study, the selected 30 diverse genotypes were evaluated for NUE component traits in two consecutive seasons in the field. The aim was to understand the variations in vegetative greenness, biomass accumulation, harvest index, nitrogen and protein content, N remobilization efficiency, and N partition to different organs. The better-performing donor lines for different NUE component traits and surrogate traits are identified.

Materials and methods

Estimation of available soil nitrogen

In both the cropping seasons (2019-*Kharif* and 2020-*Kharif*) soil N availability was estimated following the Kjeldahl method (Bremner, 1960). The soil sample was collected from the field before cropping and was air-dried and soil N availability (kgha^{-1}) was determined after digestion, distillation, and titration.

Field experiments

Field experiments were conducted during the 2019-*Kharif* and 2020-*Kharif* seasons at the ICAR-Indian Agricultural Research Institute, New Delhi. A total of 30 diverse rice genotypes were selected to study reproductive stage nitrogen remobilization and associated traits with two different nitrogen application rates: N deficient (N0-without N application) and N sufficient (N120-N application at120 kgha^{-1}). N was applied in split doses: 50% basal, 25% at active tillering, and 25% at booting. Phosphorous and potassium were applied as basal doses in both the treatments (N0 and N120) at 60 kg ha^{-1} P (SSP) and at 60 kg ha^{-1} K (MOP). In both seasons, soil N availability was estimated before and after crop growth.

Estimation of biomass accumulation, partitioning, and yield-associated traits

Biomass accumulation was recorded from different plant parts: flag leaf, lower leaf, stem, and panicle after harvesting. Total biomass accumulation and biomass partitioning to individual part was recorded. The harvest Index was also calculated.

Harvest Index (HI)= (Panicle yield/Biological yield)*100

Estimation of tissue nitrogen content

Tissue N content was estimated using the Kjeldahl method (Nelson and Sommers, 1980) from the samples collected during the 2019-*Kharif* season. Plant samples from different parts were collected separately (flag leaf, lower leaf, stem, and panicle) at two different stages: anthesis and maturity. Samples were oven dried to constant dry weight and made into powder to make the sample digestion easier. Protein content per plant was derived from the tissue N content using a conversion factor of 6.25 (Salo-vaananen and Koivistoinen, 1996; Mariotti et al., 2008).

Estimation of nitrogen uptake and nitrogen grain production efficiency

To estimate the total N uptake, N content (mgg^{-1}) was multiplied by total plant biomass. The result obtained was expressed as N uptake per plant. Nitrogen grain production efficiency was calculated as follows:

Nitrogen grain production efficiency (NUEg) = Panicle yield per plant/total nitrogen accumulation per plant

Determination of N remobilization-associated traits

Different parameters associated with N movement within the plant parts were calculated (Cox et al., 1986). N Remobilization (NR) (mg plant^{-1}) = N content at anthesis -N content at maturity; N Remobilization Efficiency (NRE) (%) = (N remobilization/N content at anthesis)*100; N lost or gained (kg ha^{-1}) = N content at maturity - N content at anthesis; N at anthesis lost or gained (%) = (N lost or gained/N content at anthesis) × 100; N Harvest Index (NHI) = Grain N/total N content of aboveground parts at maturity; and N partitioning (%)= (N content in plant part/Total nitrogen content per plant)*100

Statistical analysis

Two-way analysis of variance (ANOVA) of three biological replicates was carried out in GraphPad Prism version 8 (La Jolla, California, USA) with a variety of N treatments as treatment effects to compute adjusted P values and level of significance. Mean separation was done using Sidak's multiple comparisons test following one-way ANOVA. Graphs and heat maps were prepared using GraphPad Prism version 8 (La Jolla, California, USA). A correlation study among different parameters was performed using a correlation plot package in R studio.

Results

Biomass accumulation, biomass partitioning, and Harvest Index

Soil nitrogen availability in both the experimental plots during the 2019 and 2020 seasons was in the low to medium range as shown in Supplementary Table 1. For 2019, N0-**234.15** kgha^{-1}, and N120-**363.77** kgha^{-1} and for 2020, N0-**225.79** kgha^{-1}, and N120-**367.95** kgha^{-1}. Weather parameters were at optimum during the crop growing period

(Supplementary Figure 1). Higher total biomass accumulation was recorded in both the cropping seasons in rice genotypes with N120 treatments in comparison to N0 (Supplementary Figure 2). During 2019, the highest biomass was recorded in APO (**72.94** g) in the N120 treatment and the lowest in Pusa Sugandh-5 (**14.65** g) in the N0 treatment. In 2020, the highest value of biomass accumulation was found in APO (**56.68** g) with the N120 treatment. But, the lowest value was found in KUSHAL (**15.76** g) with the N0 treatment. Total biomass accumulation among the genotypes was variable and was associated with Harvest Index and N remobilization activity. Biomass partitioning to different plant parts was also variable between treatments, stages, and genotypes. During the anthesis stage, the highest biomass partitioning to stem was recorded with the N120 treatment and lowest in the case of flag leaf in both treatments (Figure 1A). However, at harvest the result was different, and the highest biomass partitioning to panicle was recorded in both treatments (Figure 1B). A higher value was recorded in N120 in comparison to N0. Remobilization of stem reserve and photo-assimilate from leaves resulted in higher biomass partitioning to panicle resulting in higher yield. At the harvest stage, the lowest biomass partitioning was also found in the case of flag leaf under both treatments.

N120 treatments maintained higher HI in comparison to N0 during both seasons (Figure 2). Though higher panicle yield was recorded in N120 treatments, HI was almost similar among the N treatments. Genotypes such as BAM-1812, Shabhagi Dhan, and APO accumulated higher vegetative biomass at harvest under N-deficient conditions. Higher HI values were obtained in the rice genotypes Nerica-L-44, Kalinga-1, and Shusk Samrat under the N0 condition. In terms of total biomass yield, the genotypes Kalinga-1, APO, and Shabhagi Dhan performed well in the N0 treatment.

Nitrogen uptake, nitrogen remobilization

Nitrogen uptake was higher in the N120 treatments in comparison to N0 at both pre-anthesis as well as post- anthesis stages (Figures 3A, B). Out of the total N taken up during the crop growth, a major part(~ 50-70%) was taken up before anthesis. Post-anthesis N uptake was 30-40% with few exceptions (RANBIR BASMATI, NAN-GAUN-ZHANG, BAM-832, Pusa Sugandh-2, BAM-4234, BAM-759, Nerica-L-44, and Rasi). The total N uptake at harvest was significantly higher in the N120 treatment than in the N0 treatment in all the genotypes (Figure 3C). RANBIR BASMATI, APO, Rasi, and Kalinga-1 displayed the highest N uptake among all the genotypes under N-sufficient conditions. The higher magnitude of post-anthesis N uptake contributed to the high total N uptake in these genotypes. A higher level of pre-anthesis uptake resulted in high N remobilization from vegetative organs to developing organs throughout the grain-filling stage. High N availability and storage in vegetative organs (flag leaf, lower leaf, and stem) resulted in higher N remobilization to developing grains. A significant difference in N remobilization activity was found between treatments in rice genotypes. Genotypes in the N120 treatment displayed higher total remobilization activity in comparison to N0 (Figure 4A). The highest values of N remobilization recorded were **348.79** mgplant^{-1}**, 344.53** mgplant^{-1}, and **331.84** mgplant^{-1} in APO, Kalinga-1, and Anjali, respectively (N120 treatment). The lowest values observed were **34.85** mgplant^{-1}**, 38.22** mgplant^{-1}, and **39.22** mgplant^{-1} in RANBIR BASMATI, KUSHAL, and BAM-759, respectively (N0 treatment). However, the N remobilization efficiency value was different from the total N remobilization (Figure 4B). Kalinga-1 **(75.76%)**, BAM-4234 **(74.48%)**, and IR-8384-B-B102-3 **(68.73%)** displayed the highest N remobilization efficiency under N-sufficient conditions. However, genotypes grown under N120 were more efficient in N remobilization. Total N remobilization and NRE were not always positively correlated across the genotypes studied. Some genotypes, such as IR-8384-B-B102-3, IR-83929-B-B-291-3-1-1, Pusa Basmati-1, BAM-4234, Nerica-L-42 and Vandana, with low total N remobilization under N deficient condition showed higher NRE. These results were more prevalent under the N0 condition. Some genotypes in the N0 treatment showed higher remobilization efficiency in comparison to the N120 treatment. The efficiency of N

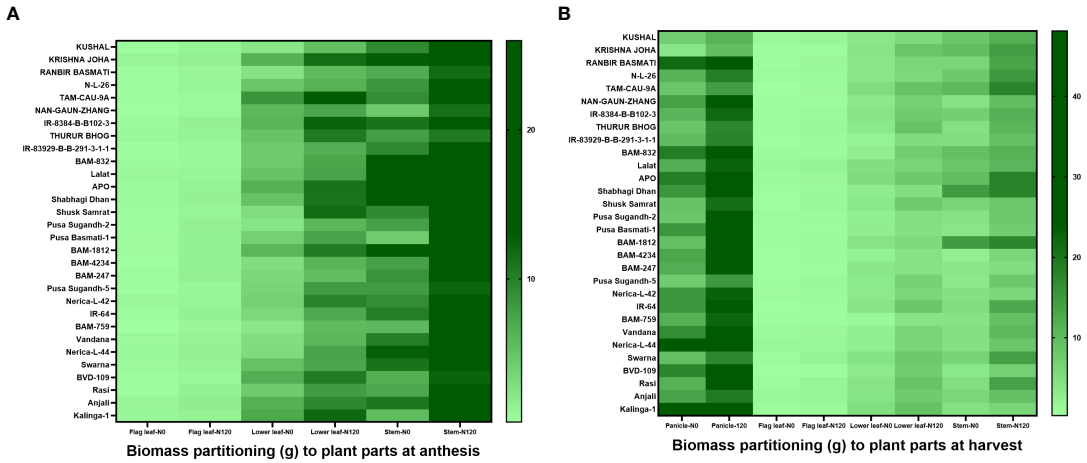

FIGURE 1
Effect of nitrogen deficient (0 kg ha-1 fertilizer N: N0) and nitrogen sufficient (120 kg ha-1 fertilizer N: N120) field conditions on biomass partitioning to plant parts at **(A)** anthesis (flag leaf, lower leaf, and stem) stage and **(B)** harvest (panicle, flag leaf, lower leaf, and stem) stage in field- grown diverse rice genotypes during the 2019-kharif season. Values presented are Mean±SE with three replications.

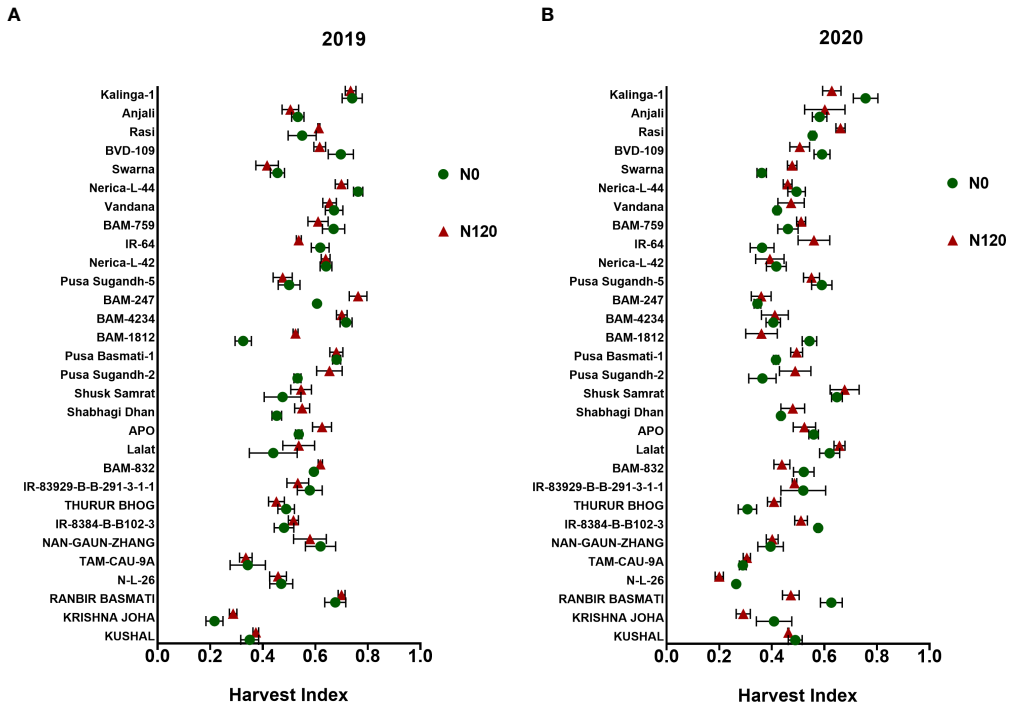

FIGURE 2
Effect of nitrogen deficient (0 kg ha-1 fertilizer N: N0) and nitrogen sufficient (120 kg ha-1 fertilizer N: N120) field conditions on Harvest Index during **(A)** the 2019-kharif and **(B)** the 2020-kharif seasons in field field-grown diverse rice genotypes. Values presented are Mean±SE with three replications.

remobilization was between **31.15%** (N0) to **75.76%** (N120) across genotypes.

N remobilization from vegetative plant parts, such as flag leaf, lower leaf, and stem, to grain was variable between treatments, between plant parts, and among genotypes (Figure 5). Among plant organs, the quantity of N remobilization was highest in the lower leaf followed by the stem and was at its lowest in the flag leaf. However, a higher value of N remobilization was observed among individual plant organs in the N120 treatment. Nitrogen remobilization percentage from the total N was highly variable (Supplementary Figure 3). The highest N remobilization percentage was observed in the flag leaf. Lower leaf and stem showed lesser N remobilization percentage from the total N content in the organs. In the case of the stem, a negative value in N remobilization was observed in some genotypes due to N losses from the plant system after anthesis. The total amount of N remobilization per plant stem contributed the highest percentage due to high stem biomass in comparison to flag leaf and lower leaf (Supplementary Figure 4). Flag leaf and lower leaf contributed a lesser percentage in N remobilization. However, the highest value was recorded in the flag leaf N remobilization percentage from the total N content in the flag leaf followed by the lower leaf and the lowest value was found in the stem.

Based on N remobilization efficiency, the rice genotypes can be classified into three groups: 1. High N remobilization (>60%), 2. Moderate N remobilization (40-60%), and 3. Low N remobilization (<40%). Genotypes such as IR-8384-B-B102-3, IR-83929-B-B-291-3-1-1, APO, Shabhagi Dhan, Shusk Samrat, Pusa Basmati-1, BAM-4234, Pusa Sugandh-5, Nerica-L-42, IR-64, Vandana, Nerica-L-44, BVD-109, Anjali, and Kalinga-1 fell under the high N remobilization category. Genotypes that fell under the medium N remobilization category were KUSHAL, KRISHNA JOHA, N-L-26, TAM-CAU-9A, THURUR BHOG, BAM-832, Lalat, Shabhagi Dhan, Shusk Samrat, Pusa Sugandh-2, BAM-1812, BAM-247, Pusa Sugandh-5, IR-64, BAM-759, Vandana, Nerica-L-44, Swarna, Rasi, and Anjali. RANBIR BASMATI was the only genotype that was included in the low N remobilization category. In terms of total N remobilization, the results were different. IR-8384-B-B102-3, APO, Shabhagi Dhan, Anjali, and Kalinga-1 displayed higher values in total N remobilization (> 300 mgplant^{-1}) (Figure 4A). Concerning N uptake, genotypes such as APO and Kalinga-1 were more efficient under N-deficient conditions. NRE was found highest in IR-8384-B-B102-3, IR-83929-B-B-291-3-1-1, BAM-4234, and Pusa Basmati-1 with N0 treatment.

Nitrogen Harvest Index, nitrogen partitioning, and total grain nitrogen accumulation

The NHI value ranges between **0.31** to **0.90** in the N0 treatment and between **0.45** to **0.89** in the N120 treatment among rice genotypes. Results were variable between treatments (N0 and N120) and among genotypes (Figure 6A). Higher NHI was reflected as lower N partitioning to vegetative parts and vice versa (Figure 6B). In the genotypes KRISHNA JOHA, TAM-CAU-9A, APO, Swarna, and Rasi total N accumulation in vegetative tissue was higher, but the NHI value was lower. Whereas the NHI value was higher in the genotypes Pusa Basmati-1, BAM-4234, BAM-759, BVD-109, and Kalinga-1. N

10.3389/fpls.2023.1093581

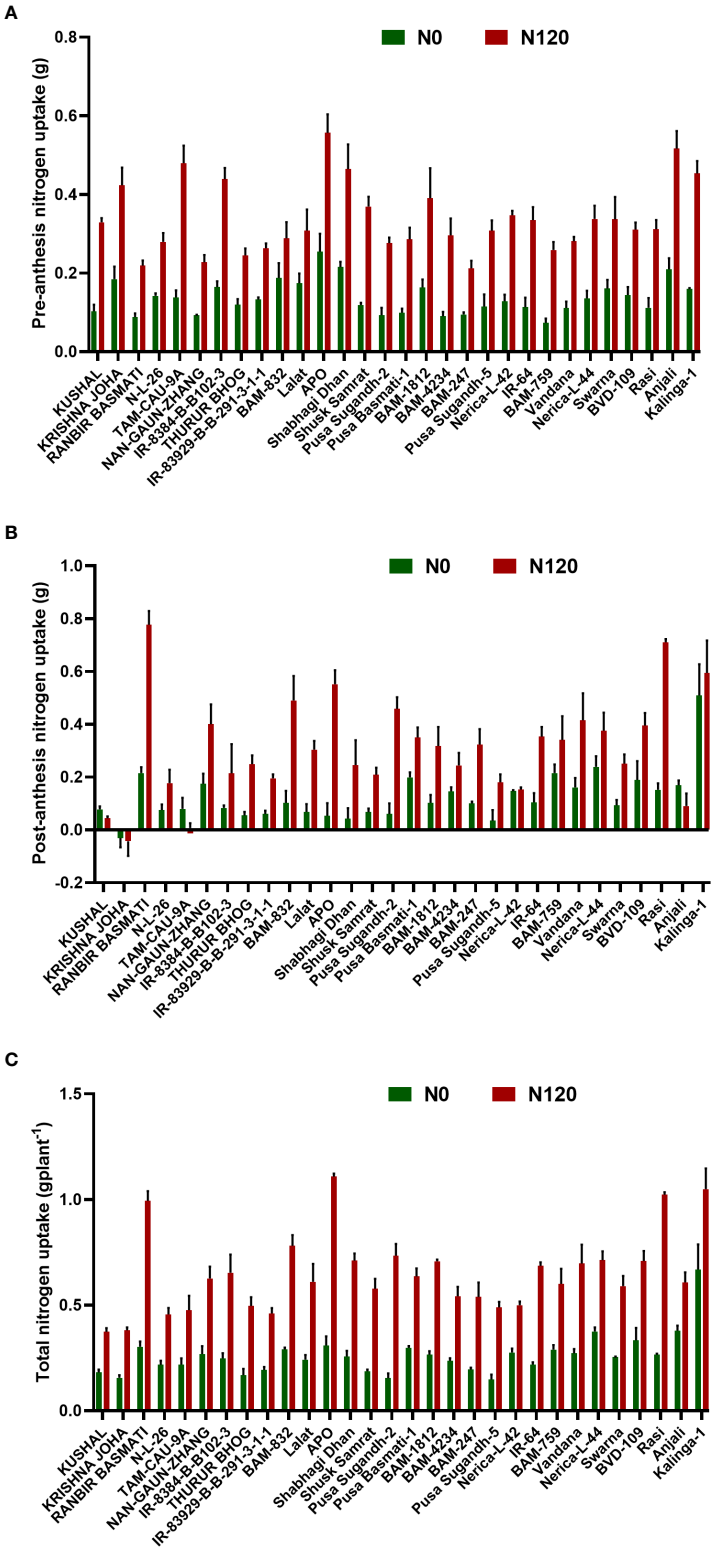

FIGURE 3
Effect of nitrogen deficient (0 kg ha-1 fertilizer N: N0) and nitrogen sufficient (120 kg ha^{-1} fertilizer N: N120) field conditions on **(A)** pre-anthesis nitrogen uptake and **(B)** post-anthesis nitrogen uptake, and **(C)** total nitrogen uptake in field- grown diverse rice genotypes during the 2019-kharif season. Values presented are Mean±SE with three replications.

content in vegetative tissue in these genotypes was lower. The NHI values were higher in the N0 treatment, whereas total vegetative N content was higher in the N120 treatment. Kalinga-1, Pusa Basmati-1, BAM-759, and BAM-4234 showed higher NHI values under the N0 condition. Variability in N partitioning to different vegetative plant parts, such as flag leaf, lower leaf, and stem, was observed. The total amount of N partitioned to stem was highest at the anthesis stage (Figure 7A) as well as at the harvest stage (Figure 7B). During the

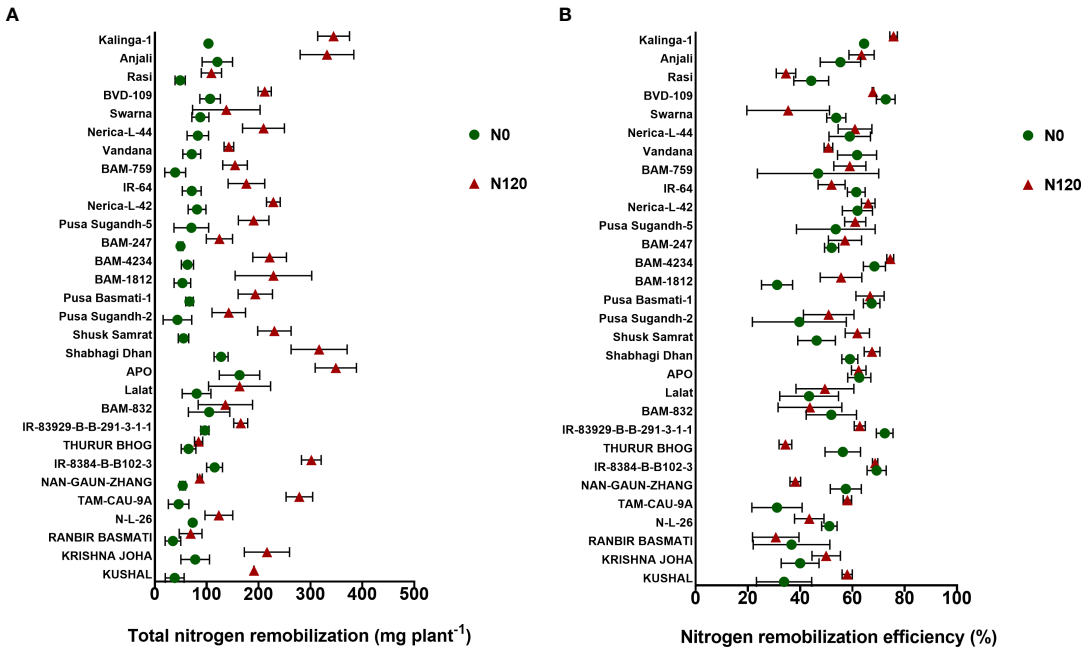

FIGURE 4
Effect of nitrogen deficient (0 kg ha-1 fertilizer N: N0) and nitrogen sufficient (120 kg ha-1 fertilizer N: N120) field conditions on **(A)** Total nitrogen remobilization and **(B)** Nitrogen remobilization efficiency in field-grown diverse rice genotypes during the 2019-kharif season. Values presented are Mean ±SE with three replications.

anthesis stage, higher N partitioning to vegetative parts was observed. During anthesis, the highest N partitioning was observed in the stem, followed by the lower leaf, and the lowest N partitioning value was observed in the flag leaf per total biomass of individual plant organs. The N partitioning per unit of biomass behaved in a reverse manner. The highest value was recorded for the flag leaf, followed by the lower leaf and the lowest N partitioning was observed in the stem. At maturity, the highest N partitioning was recorded from the panicle, represented as Nitrogen Harvest Index (Figure 6A). The NHI was positively correlated with total N accumulation in grain across genotypes. Higher NHI resulted in higher grain N accumulation. In both the cropping seasons, 2019 and 2020, total grain N accumulation was higher in the N120 treatment in comparison to the N0 treatment (Figure 8). During 2019, total grain N accumulation was between **0.10** g to **0.61** g in the N0 treatment and between **0.17** g to **0.93** g in the N120 treatment. During 2020, the value ranged between **0.10** g to

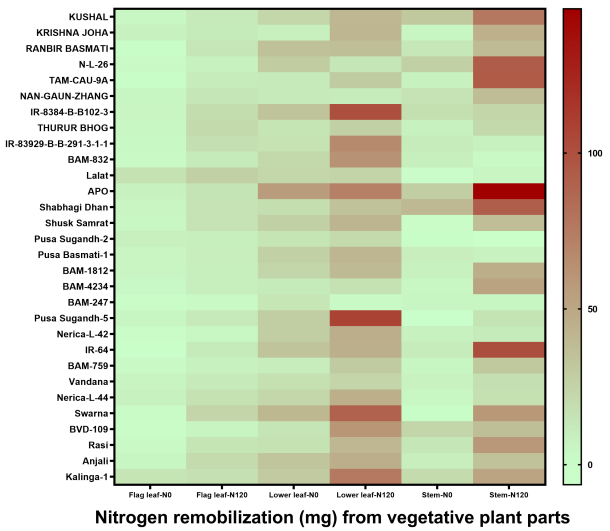

FIGURE 5
Effect of nitrogen deficient (0 kg ha-1 fertilizer N: N0) and nitrogen sufficient (120 kg ha-1 fertilizer N: N120) field conditions on nitrogen remobilization from vegetative plant parts (flag leaf, lower leaf, and stem) to grain in field- grown diverse rice genotypes during the 2019-kharif season. Values presented are Mean±SE with three replications.

0.56 g in the N0 treatment and between **0.2565 g** to **0.78 g** in the N120 treatment. During 2019, higher total grain N accumulation was recorded in comparison to 2020. In both seasons, Kalinga-1 showed the highest total grain N accumulation under N-deficient conditions. Percentage of N contributions from different vegetative parts to total grain N accumulation was found variable (Figure 9). Flag leaf contributed the lowest percentage of N to total grain N. Highest percentage of N was from the stem, followed by the lower leaf.

Nitrogen grain production efficiency (NUEg), nitrogen loss or gain

Nitrogen grain production efficiency (NUEg) was expressed as g grain produced per total N accumulation per plant. NUEg values were between **25.05** and **73.03** g grain/g N uptake (Figure 6C). Genotypes with the N0 treatment showed a higher value of NUEg in comparison to the N120 treatment. Genotypes without N application were more efficient in grain production with lesser N accumulation and grain produced per unit of available N was higher in comparison to genotypes with sufficient N application and higher tissue N content. However, the genotypes KRISHNA JOHA, BAM-1812, and BAM-247 performed well under N-sufficient conditions. Higher NUEg was observed with high N accumulation. Classifying all the genotypes studied into two groups, higher in NUEg and lower in NUEg (based on nitrogen grain production efficiency), the rice genotypes that fell under the higher NUEg group (>60 g grain/g N uptake) were RANBIR BASMATI, BAM-832, APO, BAM-247, IR-64, Vandana, and Nerica-L-44. The remaining genotypes could be placed in the lower NUEg group. The rice genotypes that displayed higher NUEg values under the N0 condition were RANBIR BASMATI, Nerica-L-44, IR-64, and BAM-832. In some genotypes, N absorbed during the vegetative stage was lost from the plant system after anthesis, resulting in lesser remobilization activity to developing grains during the reproductive stage. With few exceptions, in most of the genotypes, gain in N content was observed after anthesis (Figure 10). In KRISHNA JOHA (N0 and N120) and TAM-CAU-9A (N120), N loss was recorded. The gain in N content was predominant in N120 treated genotypes. However, the percentage gain in N was almost similar or also higher in the N0 treatments. The genotypes RANBIR BASMATI (N120), BAM-759 (N0), and Kalinga-1 (N0) showed exceptional percentage gain in N content after anthesis.

Correlation among different NUE component traits

Under the N deficient condition (N0), total N uptake was correlated to N remobilization, N Harvest Index, grain N accumulation, Harvest Index, and NUEg (Figure 11A). Under the N sufficient condition (N120), N uptake was positively correlated to all these parameters including total vegetative N. However, N uptake was strongly correlated to grain N accumulation under both N conditions. Pre-anthesis N uptake was strongly correlated to N remobilization under both conditions. However, post-anthesis N uptake showed a strong correlation with N remobilization and grain N accumulation under both N conditions. Pre-anthesis N uptake and post-anthesis N uptake showed negative correlations under both N conditions. With the N0 treatment, pre-anthesis N uptake showed a negative correlation with NHI, HI, and NUEg. Post-anthesis N uptake showed a negative correlation with total vegetative nitrogen (Figure 11A). With the N120 treatment, pre-anthesis N uptake showed a negative correlation with NHI, HI, and NUEg (Figure 11B). Post-anthesis N uptake showed a negative correlation with total vegetative N under the N0 treatment and with N remobilization and total vegetative N under the N120 treatment. NUEg was negatively correlated with pre-anthesis N uptake, N remobilization, and total vegetative N under the N120 condition (Figure 11B).

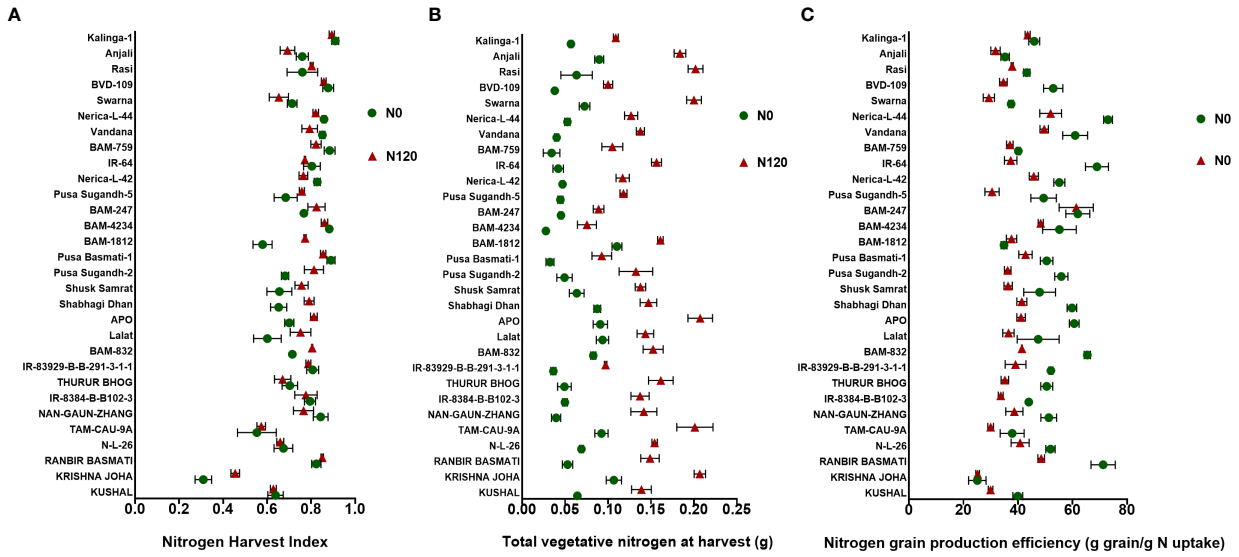

FIGURE 6
Effect of nitrogen deficient (0 kg ha-1 fertilizer N: N0) and nitrogen sufficient (120 kg ha-1 fertilizer N: N120) field conditions on **(A)** Nitrogen Harvest Index, **(B)** Total vegetative nitrogen at harvest, and **(C)** Nitrogen grain production efficiency in field- grown diverse rice genotypes during the 2019-kharif season. Values presented are Mean±SE with three replications.

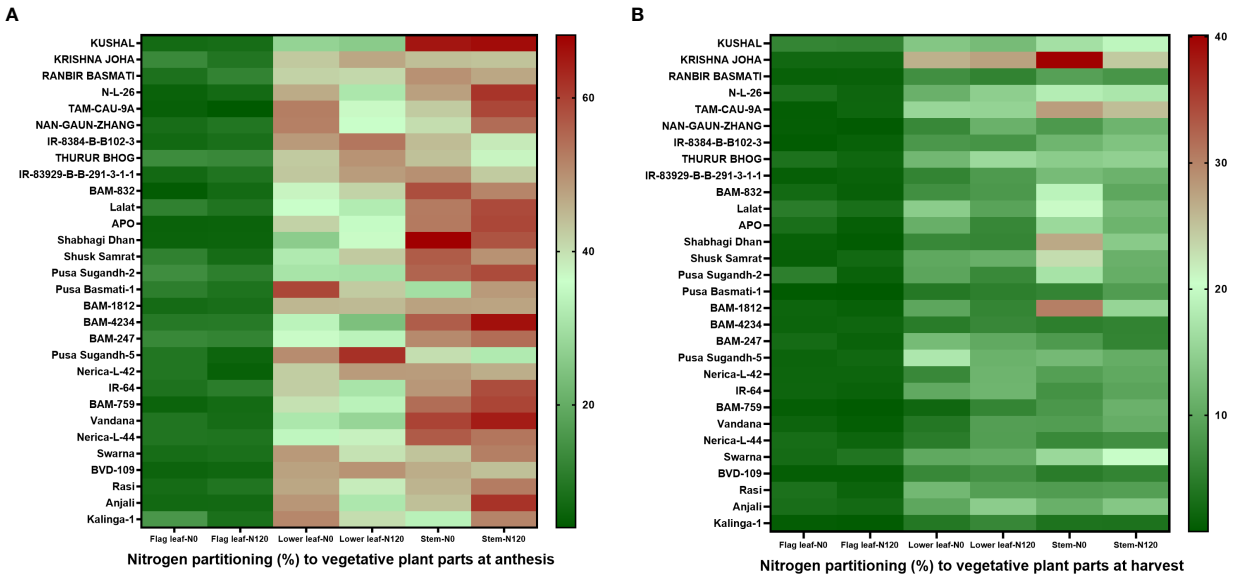

FIGURE 7
Effect of nitrogen deficient (0 kg ha-1 fertilizer N: N0) and nitrogen sufficient (120 kg ha-1 fertilizer N: N120) field conditions on nitrogen partitioning to vegetative plant parts (flag leaf, lower leaf, and stem) at **(A)** anthesis stage and at **(B)** harvest stage in field- grown diverse rice genotypes during the 2019-kharif season. Values presented are Mean±SE with three replications.

Discussion

Nitrogen uptake, partitioning to different parts, and its remobilization during the reproductive stage towards the sink, i.e., developing grains, is important in improving N grain production efficiency, grain N, and grain protein accumulation (Good et al., 2004; Lin et al., 2006; Zhang et al., 2013; Hajibarat and Saidi, 2022; Khwankaew et al., 2022; Liu et al., 2022). Nitrogen recycling or remobilization from senescing plant parts and from the storage organs to sink tissues is accomplished after the onset of flowering and during the progress towards maturity (Lemaitre et al., 2008; Masclaux-Daubresse et al., 2008; Masclaux-Daubresse et al., 2010; He et al., 2016; Asibi et al., 2019; Melino et al., 2022). The major N storage organs include the stem, leaf, and petiole. The efficiency of remobilization is determined by the N uptake capacity and sink activity in developing grains (Martinoia et al., 1981; Lin et al., 2006). N remobilization or partitioning to grains and post-anthesis N uptake directly affects grain yield and quality (Ntanos and Koutroubas, 2002; Martin et al., 2006; Uauy et al., 2006; Masoni et al., 2007; Tabuchi et al., 2007; Xue and Yang, 2008; Li et al., 2013; Raddatz et al., 2020). Understanding the mechanisms controlling N remobilization during grain development and in response to stress and identifying the genotypes performing better under such environments is required to improve the N fertilizer economy.

Nitrogen uptake improves biomass panicle yield, and Harvest Index

Nitrogen availability during vegetative growth is important for better reproductive stage development, yield, and a high Harvest Index. Higher N availability during the reproductive stage increases its partitioning to panicle as the developing grain acts as a sink increasing the demand for N from storage organs and remobilization activity (Dingkuhn, 1996; He et al., 2016; Kumari et al., 2021). Findings from previous studies showed that differential N application rates have a strong effect on source-sink activity in rice (Debata and Murty, 1986; Debata and Murty, 1988; Dingkuhn, 1996; Hameed et al., 2019; Chen et al., 2023). In our study, the soil N availability estimated in the experimental plots was between **200** $kgha^{-1}$ to **400** $kgha^{-1}$, which is not sufficient for optimum plant growth. An external source of N was supplied to study the effect on uptake, partitioning, remobilization, and grain growth of rice genotypes. The results showed a positive effect on biomass growth upon N application. N application promoted physiological activities and provided an optimum environment for plant growth. An increase in tiller number associated with plant growth in terms of height, leaf area, and leaf thickness culminated in high vegetative biomass. Few genotypes displayed better growth and biomass in low N, showing their efficiency and adaptability to the low N environment. Vegetative growth in the N0 treatment was supported by the soil N availabillity. Higher biomass accumulation accomplished due to high N availability and uptake resulted in high panicle yield and a higher Harvest Index value was obtained. Variability obtained in the HI was probably due to high vegetative N accumulation and lower level in partitioning to grain, which reduced the panicle biomass and HI. However, a higher HI was displayed with external N application supporting reproductive growth and better panicle yield. Withdrawal of N application to the field resulted in lower panicle yield and HI (Bahrani et al., 2011; Fageria, 2014; Qun et al., 2023).

Post-anthesis nitrogen uptake and nitrogen remobilization were associated with Nitrogen Harvest Index, total nitrogen accumulation in grain, and panicle yield

Pre-anthesis N uptake is associated with remobilization and post-anthesis N uptake contributes to grain development and grain N and

10.3389/fpls.2023.1093581

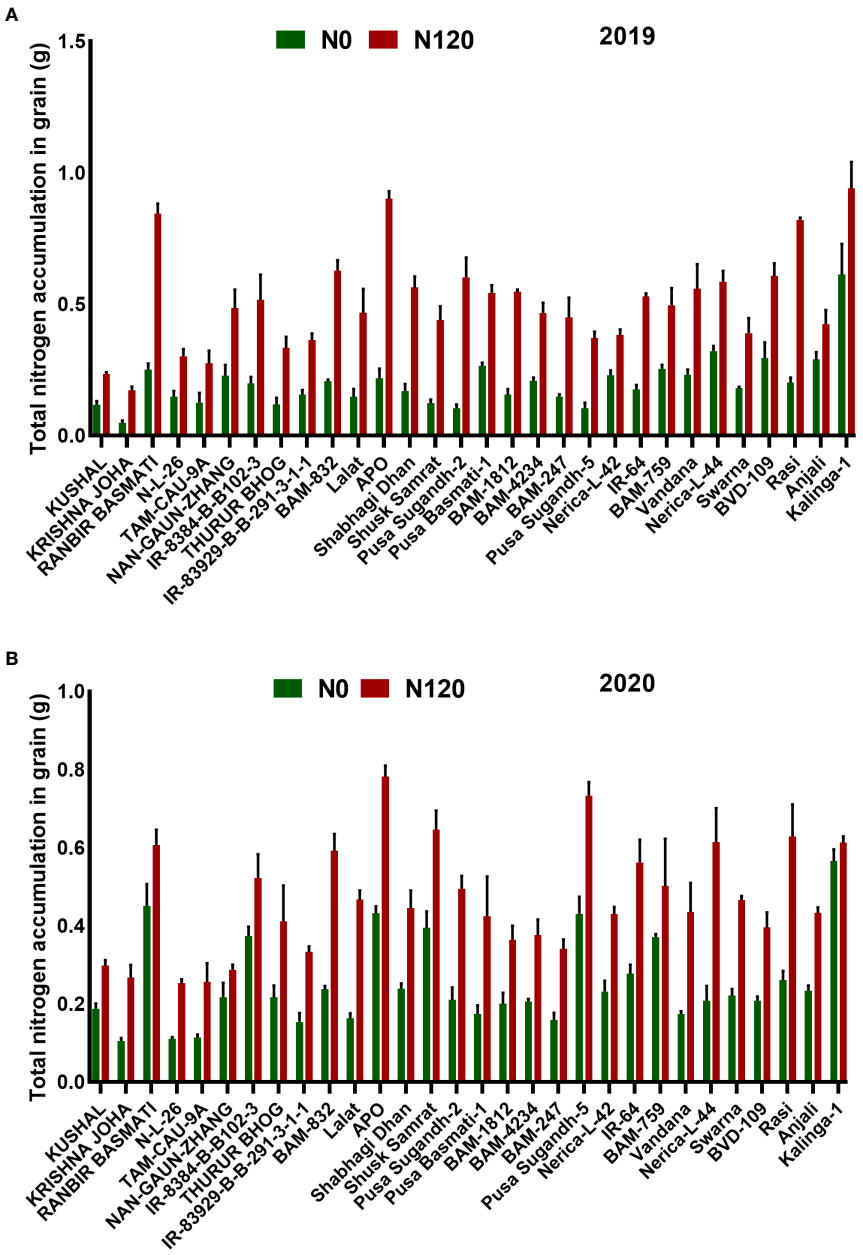

FIGURE 8
Effect of nitrogen deficient (0 kg ha-1 fertilizer N: N0) and nitrogen sufficient (120 kg ha-1 fertilizer N: N120) field conditions on total nitrogen accumulation in grain during **(A)** the 2019-kharif and during **(B)** the 2020-kharif cropping seasons in diverse rice genotypes. Values presented are Mean ±SE with three replications.

protein content. The N stored in the vegetative organs before anthesis plays an important role in maintaining high photosynthetic efficiency (Millard, 1988; Slafer and Satorre, 1999), but the higher N remobilization rate in the vegetative organs during grain filling may limit its accumulation (Rajcan and Tollenaar, 1999; Pommel et al., 2006). N movement takes place from source organs, mainly leaves, to sink organs, younger leaves during the vegetative stage and developing grains during the reproductive stage. Movement is dependent on the N status and developmental stage of the plant. When the N status is relatively low, plants remobilize N more efficiently. On the other hand, plants tend to retain N in source organs when N is sufficient (Assaf et al., 2014). This negative feedback regulation of N remobilization can act as a checkpoint to improve NRE in food crops. In our study, lower N during the vegetative stage was compensated by an uptake during the reproductive stage. Though the level of post-anthesis N uptake required for panicle yield and grain quality was not significant, it was very significant for total grain N accumulation. Post-anthesis N uptake and translocation are important for photosynthetic assimilation and grain filling in rice. Post-anthesis N uptake is critical as it is directly associated with N accumulation in rice grain. During reproductive development, the N absorbed by the plant is directly translocated to reproductive organs as the developing grain acts as a sink and the rate of N translocation is dependent on sink strength and activity. Higher N translocation to grain leads to higher total grain N accumulation and a high N Harvest Index (NHI). Improved coordination in N application and growth

stages in rice can enhance N uptake while maintaining a high N harvest index (NHI) (Zheng et al., 2017). Therefore, some recent studies have shown that increasing the N uptake of crops after anthesis and its transport to the grain can increase protein content. Nitrogen partitioning during vegetative growth is critical for reproductive growth and panicle yield. Because the N content of different vegetative organs is critical for grain N content, N content in storage organs is translocated to the panicle and contributes to the growth of the panicle. The grain-filling period is critical for the formation of grain and identifying the physiological mechanisms of grain filling is desirable for higher yield (Ding et al., 2014). Findings in our study suggested that the NHI and total grain accumulation were positively correlated. Higher N partitioning to grain resulted in a higher NHI value and also higher panicle yield.However, higher N accumulation and NHI values were inversely correlated. Higher total N accumulation in vegetative tissues resulted in low N partitioning to grain. An increase in the N content of vegetative tissues decreased the N recovery amount and also the panicle yield. There is an inverse relationship between grain yield and total N accumulation in the plant (Cox et al., 1986; Clarke et al., 1990). So, crop genotypes that are efficient in panicle yield under N deficient or scarcity conditions are more desirable. Genotypes with such traits can be categorized under the high NUE group that is selected for crop breeding for resource use efficiency.

Total nitrogen content and nitrogen loss determine nitrogen grain production efficiency

Nitrogen use efficiency is mainly determined by N uptake and its utilization by the plant. Any limitation to N uptake or utilization imposed by environmental, physiological, and agronomic processes is reflected in the form of yield loss and low NUE (Debaeke et al., 1996). Total grain yield or panicle yield per total available tissue N is variable. As more tissue N increased the NHI and grain protein content, the grain yield declined to show the opposite relationship between them. Higher grain yield or panicle yield resulted in dilution of N concentration in grain as well as in the plant. The grain N production efficiency (NUEg) was found higher with lower vegetative N accumulation and with the N0 treatment showing the inverse relationship between yield and total N accumulation. However, grain N accumulation had a positive relationship with yield. Higher grain N content was associated with higher grain growth activity and higher NUEg. The different hypotheses related to the inverse relationship between total N content and grain yield were: (i) dilution of N or protein in higher yield (Heitholt et al., 1990; Martre, 2003; Guarda et al., 2004; Barneix, 2007); (ii) higher rate of improvement in HI relative to NHI (Slafer et al., 1994); (iii) competition for energy and assimilates between biomass and N during the grain formation as some genotypes will continue to direct their energy and assimilate for vegetative growth after anthesis, and consequently less amount of assimilates for grain formation (Cox et al., 1985; Bogard et al., 2010); and (iv) difference in rate grain N and carbohydrates during the grain filling period (Jenner et al., 1991). Higher NUEg values were recorded in genotypes with no external N application as compared to the N120 application. However, grain N content was found higher in the N120 treatment. Other reasons for low NUEg are N loss or lower rate N gain at anthesis. The panicle yield will be lower if N present in the vegetative tissues is lost to the environment, which may happen through leaf fall or volatilization of secondary N compounds (Kanampiu et al., 1997; Wang et al., 2021). As N losses from the plant at anthesis were observed only in a few genotypes, the lower amount of N gain at anthesis may be the reason for low NUEg, though

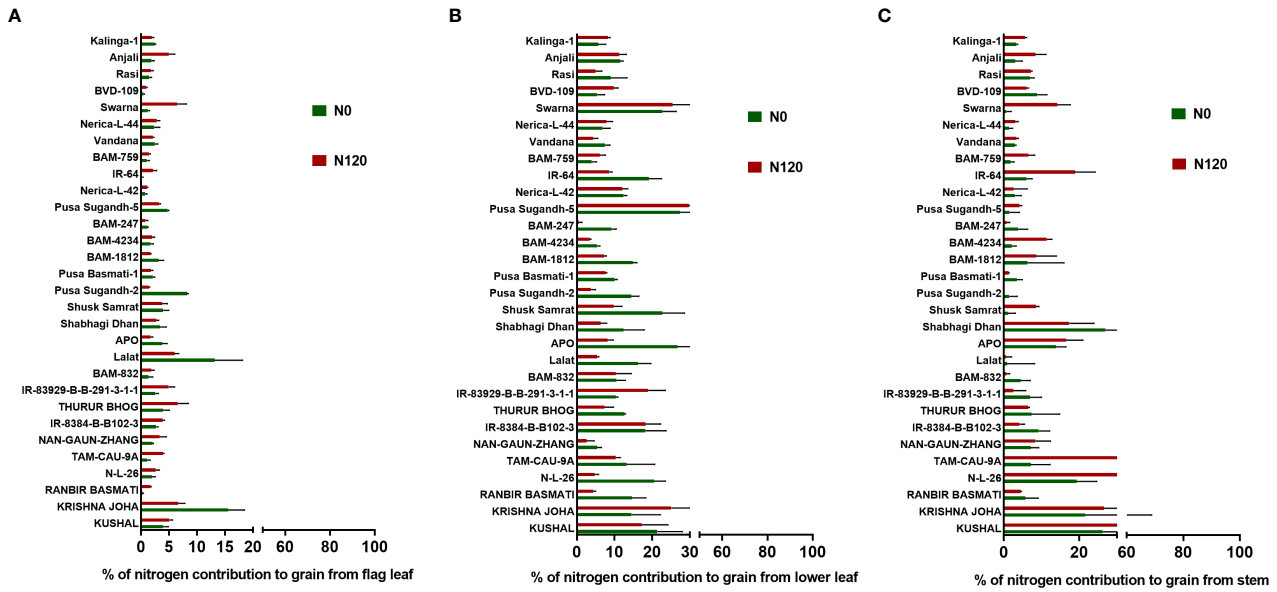

FIGURE 9
Effect of nitrogen deficient (0 kg ha-1 fertilizer N: N0) and nitrogen sufficient (120 kg ha-1 fertilizer N: N120) field conditions on **(A)** (%) percentage of nitrogen contribution to grain from flag leaf, **(B)**, (%) percentage of nitrogen contribution to grain from lower leaf, and **(C)** (%) percentage of nitrogen contribution to grain from the stem in field- grown diverse rice genotypes during the 2019-kharif season. Values presented are Mean±SE with three replications.

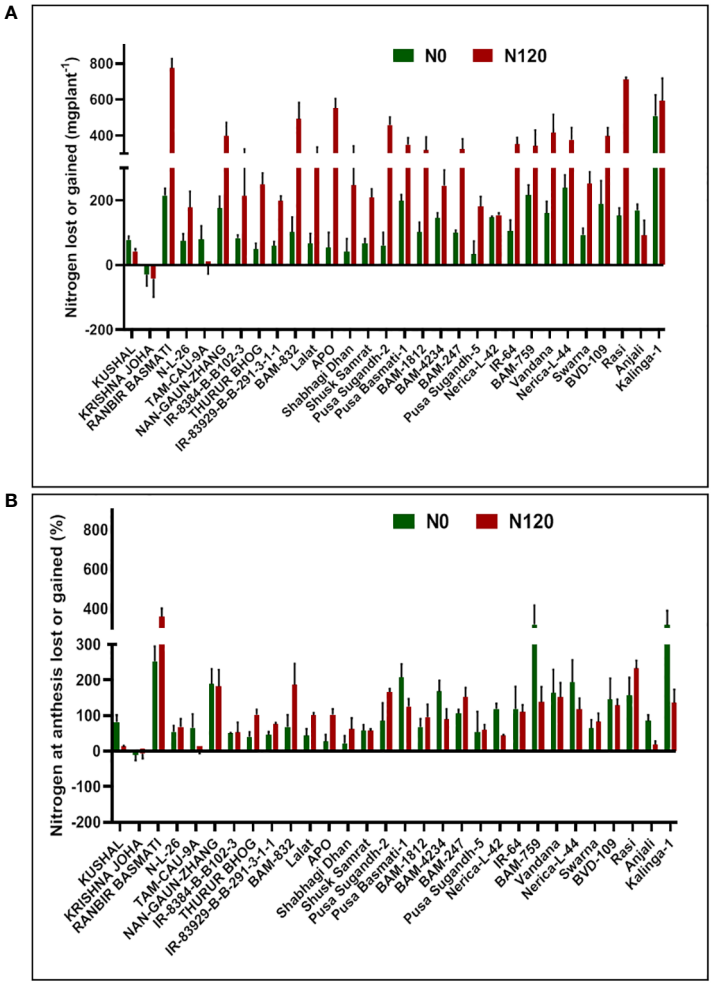

FIGURE 10
Effect of nitrogen deficient (0 kg ha^{-1} fertilizer N: N0) and nitrogen sufficient (120 kg ha^{-1} fertilizer N: N120) field conditions on **(A)** nitrogen lost or gained and **(B)** nitrogen at anthesis lost or gained in field-grown diverse rice genotypes during the 2019-*kharif* season. Values presented are Mean ± SE with three replications.

the grain yield and grain N content were high. As the N gain at anthesis through direct translocation to grain or remobilization from vegetative tissues promoted grain development, it had a positive relationship with yield. The lower value in gain of N anthesis also denotes the lower rate of N recovery; thus, N was lost from the vegetative biomass and lowering the in NUE.

Nitrogen Harvest Index and grain N concentration are essential for investigating changes in Nitrogen Use Efficiency (NUE) and grain quality attributes in rice (Heitholt et al., 1990). An increase in yield is usually reflected as a decline in grain N and protein concentration. As yield increment begins to stabilize at higher N uptake levels, grain N and protein concentration increases (McMullan et al., 1988; Barraclough et al., 2010; Sułek et al., 2023). Grain N concentration is usually source-limited (Borghi et al., 1986; Martre, 2003), particularly towards the end of the grain filling period, as opposed to grain yield being sink-limited (Jenner et al., 1991). When there is an N source limitation during grain filling, improving the coordination between soil N supply and crop N demand by N fertilizer management is a critical approach for simultaneously increasing the grain yield and protein content (Chen et al., 2011; Zhang et al., 2020; Qun et al., 2023). Therefore, in the case of no N application (N0 treatment), the source limitation was the major factor associated with higher N translocation to grain. In the N0 condition, the N uptake rate and the tissue N accumulation were lower. The N present in the vegetative tissues was remobilized efficiently to grain and displayed a higher NUEg. However, the gain in N content per plant in the N0 condition was lower.

IR-83929-B-B-291-3-1-1, Kalinga-1, APO, Pusa Basmati-1, and Nerica-L-44 were the rice genotypes that performed well for more than one N use efficiency component traits under both N deficient (N0) and N sufficient (N120) conditions (Figure 12). The N efficient rice genotypes had higher panicle yield and NUEg in comparison to inefficient genotypes under N scarcity. This is mainly due to larger sink size, higher sink strength, and improved filled grain percentage (Gallais and Hirel, 2004; Bahrani et al., 2011; Zhu et al., 2022; Qun et al., 2023). The genotypes performing better under N deficient conditions can be used as donors for N use efficiency component traits in breeding.

Conclusion

Reproductive stage N remobilization is important for grain yield, grain N as well as protein content in rice. Higher uptake under

10.3389/fpls.2023.1093581

sufficient N was associated with a high Normalized Difference Vegetation Index. N application promoted vegetative growth and more photosynthetic activity whereas an N deficient condition reduced panicle yield. Nitrogen application and its utilization increased the Harvest Index value and total N accumulation in plants. Soil N availability in the N0 plot was unable to support optimum plant growth and resulted in lower vegetative greenness and reduced yield. Though lower panicle yield was recorded under the N0 conditions, the nitrogen grain production efficiency was higher as most of the N present in the vegetative tissues were remobilized to grain and N recovery was high. More N accumulation under the N120 condition in vegetative tissues resulted in lower grain growth and yield. The N120 treatment enhanced pre-anthesis N uptake and more N remobilization to grain, resulting in high N remobilization efficiency. Post-anthesis N uptake and translocation to grain is an important determinant in improving grain yield as well as grain N content and higher Nitrogen Harvest Index. However, post-anthesis N uptake was lesser as compared to N uptake during the vegetative stage. So, the grain N content mainly relied upon vegetative N uptake and its remobilization during the reproductive stage to grain. N remobilization activity was found to be limited by source, hence lower N availability during the reproductive stage triggered more N translocation to developing grains. However, overall N remobilization, Nitrogen Harvest Index, and total N accumulation were higher in the case of the N120 treatment. Among various plant parts, the highest percentage of N remobilization from the total available N content was observed in the flag leaf, followed by the lower leaf, and the lowest percentage was observed in the stem. Unlike the percentage of N remobilization, total N remobilization was higher in quantity in lower leaf and stem as these parts contain higher total biomass. N loss from vegetative parts was also limited to N recovery and grain N accumulation. So, from these observations, it is

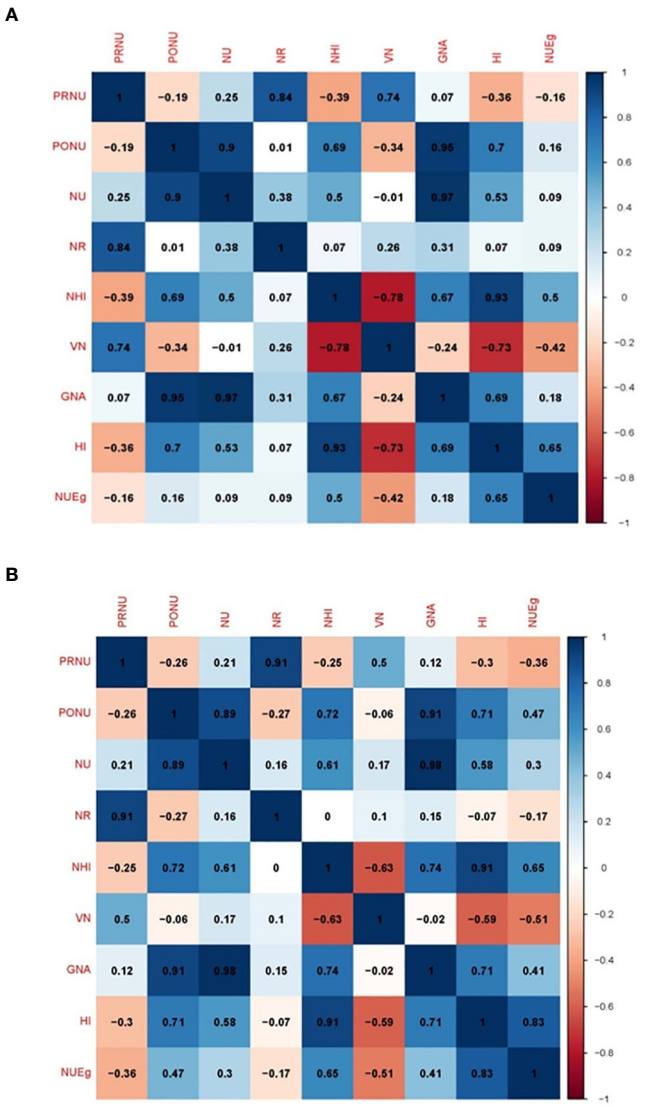

FIGURE 11
Pearson correlation matrix showing the relationship between PRNU (pre-anthesis nitrogen uptake), PONU (post-anthesis nitrogen uptake), NU (total nitrogen uptake), NR (nitrogen remobilization), NHI (nitrogen harvest index), VN (total vegetative nitrogen), GNA (total grain nitrogen accumulation), HI (harvest index), and NUEg (nitrogen grain production efficiency) under **(A)** nitrogen deficient (0 kg ha-1 fertilizer N: N0), **(B)** nitrogen sufficient (120 kg ha-1 fertilizer N: N120) field conditions.

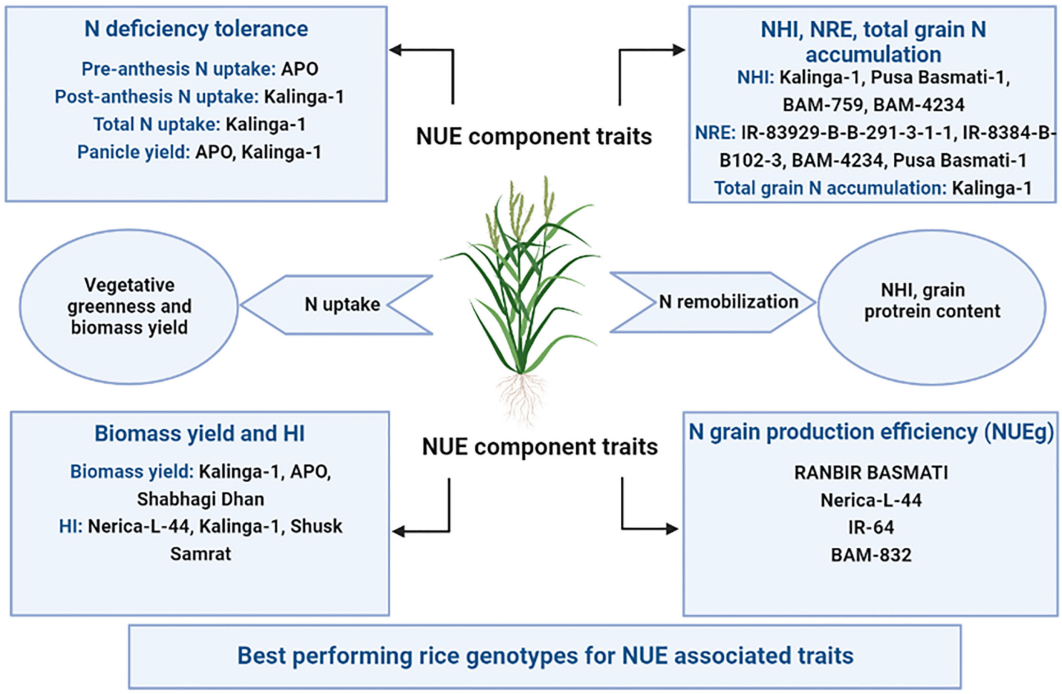

FIGURE 12
Schematic representation of N use efficiency (NUE) component traits in rice and best-performing genotypes under both nitrogen deficient (0 kg ha^{-1} fertilizer N: N0) and nitrogen sufficient (120 kg ha^{-1} fertilizer N: N120) field conditions. NHI, Nitrogen Harvest Index; NRE, Nitrogen Remobilization Efficiency; HI, Harvest Index; and NUEg, Nitrogen grain production efficiency.

concluded that genotypes under a low N environment with traits such as high N remobilization and partitioning, optimum yield, and higher NUEg are desirable for improving the N fertilizer economy and sustainable agriculture.

Data availability statement

The original contributions presented in the study are included in the article/Supplementary Material. Further inquiries can be directed to the corresponding author.

Author contributions

BK conducted experiments under the supervision of LS. BK performed the statistical analysis and wrote the manuscript. LS revised the manuscript. LS, VC, SK and AK finalized the experiments and manuscript. All authors contributed to the article and approved the submitted version.

Funding

The authors are thankful to the ICAR-Indian Agricultural Research Institute for funding and NAHEP-CAAST for providing the necessary facilities. BK acknowledges ICAR-IARI for the fellowship support received during the study. Authors also acknowledge the financial support received from NAHEP-CAAST, ICAR-IARI (Grant No. NAHEP/CAAST/2018-23).

Conflict of interest

The authors declare that the research was conducted in the absence of any commercial or financial relationships that could be construed as a potential conflict of interest.

Publisher's note

Supplementary material

The Supplementary Material for this article can be found online at: https://www.frontiersin.org/articles/10.3389/fpls.2023.1093581/full#supplementary-material

References

Asibi, A. E., Chai, Q., and Coulter, J. A. (2019). Mechanisms of nitrogen use in maize. *Agronomy*. 9, 775. doi: 10.3390/agronomy9120775

Assaf, D., Raz, A., and Andreas, M. (2014). Senescence, nutrient remobilization, and yield in wheat and barley. *Journal of Experimental Botany* 65 (14), 3783–3798. doi: 10.1093/jxb/ert477

Bahrani, A., Abad, H. H. S., and Aynehband, A. (2011). Nitrogen remobilization in wheat as influenced by nitrogen application and post-anthesis water deficit during grain filling. *Afr. J. Biotechnol.* 10 (52), 10585–10594. doi: 10.5897/AJB11.013

Barneix, A. J. (2007). Physiology and biochemistry of source-regulated protein accumulation in the wheat grain. *J. Plant Physiol.* 164, 581–590. doi: 10.1016/j.jplph.2006.03.009

Barraclough, P. B., Lopez-Bellido, R., and Hawkesford, M. J. (2014). Genotypic variation in the uptake, partitioning and remobilization of nitrogen during grain-filling in wheat. *F. Crops Res.* 156, 242–248. doi: 10.1016/j.fcr.2013.10.004

Barraclough, P. B., Howarth, J. R., Jones, J., Lopez-Bellido, R., Parmar, S., Shepherd, C. E., et al. (2010). Nitrogen efficiency of wheat: Genotypic and environmental variation and prospects for improvement. *Eur J Agron* 33 (1), 1–11. doi: 10.1016/j.eja.2010.01.005

Bhullar, N. K., and Gruissem, W. (2013). Nutritional enhancement of rice for human health: the contribution of biotechnology. *Biotechnol. Adv.* 31, 50–57. doi: 10.1016/j.biotechadv.2012.02.001

Bogard, M., Allard, V., Brancourt-Hulmel, M., Heumez, E., MacHet, J. M., Jeuffroy, M. H., et al. (2010). Deviation from the grain protein concentration- grain yield negative relationship is highly correlated to post-anthesis n uptake in winter wheat. *J. Exp. Bot.* 61, 4303–4312. doi: 10.1093/jxb/erq238

Borghi, B., Corbellini, M., Cattaneo, M., Fornasari, M. E., and Zucchelli, L. (1986). Modification of the sink/source relationships in bread wheat and its influence on grain yield and grain protein content. *J. Agron. Crop Sci.* 157, 245–254. doi: 10.1111/j.1439-037X.1986.tb00073.x

Bremner, J. M. (1960). Determination of nitrogen in soil by the kjeldahl method. *J. Agric. Science.* 55 (1), 11–33. doi: 10.1017/S0021859600021572

Cassman, K. G., Peng, S., Olk, D. C., Ladha, J. K., Reichardt, W., Dobenmann,, et al. (1998). Opportunities for increased nitrogen-use efficiency from improved resource management in irrigated rice systems. *Field Crops Res.* 56, 7–39. doi: 10.1016/S0378-4290(97)00140-8

Chamely, S. G., Islam, N., Hoshain, S., Rabbani, M. G., Kader, M. A., and Salam, M. A. (2015). Effect of variety and nitrogen rate on the yield performance of boro rice. *Progressive Agriculture.* 26 (1), 6–14. doi: 10.3329/pa.v26i1.24508

Chen, X., Cui, Z., Vitousek, P. M., Cassman, K. G., Matson, P. A., Bai, J., et al. (2011). Integrated soil-crop system management for food security. *Proc. Natl. Acad. Sci. U.S.A.* 108, 6399–6404. doi: 10.1073/pnas.1101419108

Chen, K., Ma, T., Ding, J., Yu, S. E., Dai, Y., He, P., et al. (2023). Effects of straw return with nitrogen fertilizer reduction on rice (*Oryza sativa* l.) morphology, photosynthetic capacity, yield and water–nitrogen use efficiency traits under different water regimes. *Agronomy*. 13 (1), 133. doi: 10.3390/agronomy13010133

Chen, Y., Wang, M., and Ouwerkerk, P. B. F. (2012). Molecular and environmental factors determining grain quality in rice. *Food Energy Secur.* 1, 111–132. doi: 10.1002/fes3.11

Ciampitti, I. A., and Vyn, T. J. (2014). Understanding global and historical nutrient use efficiencies for closing maize yield gaps. *Agron. J.* 106, 1–11. doi: 10.2134/agronj14.0025

Clarke, J. M., Campbell, C. A., Cutforth, H. W., Depauw, R. M., and Winkleman, G. E. (1990). Nitrogen and phosphorus uptake, translocation, and utilization efficiency of wheat in relation to environment and cultivar yield and protein levels. *Can. J. Plant Sci.* 70, 965–977. doi: 10.4141/cjps90-119

Cox, M. C., Qualset, C. O., and Rains, D. W. (1985). Genetic variation for nitrogen assimilation and translocation in wheat. i. dry matter and nitrogen accumulation. *Crop Sci.* 25, 430–435. doi: 10.2135/cropsci1985.0011183X002500030002x

Cox, M. C., Qualset, C. O., and Rains, D. W. (1986). Genetic variation for nitrogen assimilation and translocation in wheat. II. nitrogen translocation in relation to grain yield and protein. *Crop Sci.* 26, 737–740. doi: 10.2135/cropsci1986.0011183X002600040022x

Debaeke, P., Aussenac, T., Fabre, J. L., Hilaire, A., Pujol, B., and Thuries, L. (1996). Grain nitrogen content of winter bread wheat (*Triticum aestivum* l.) as related to crop management and to the previous crop. *Eur. J. Agron.* 5, 273–286. doi: 10.1016/S1161-0301(96)02038-2

Debata, A., and Murty, K. S. (1986). Influence of population density on leaf and panicle senescence in rice. *Indian J. Plant Physiol.* 29, 281–285.

Debata, A., and Murty, K. S. (1988). Leaf senescence characters in relation to tiller yield in early rice cultures. *Indian J. Agric. Res.* 22, 1299–1136.

Dey, P., and Sekhon, B. S. (2016). Nitrogen fertility status of the Indian soils I the world soils. *Indian J. Fert.* 12 (4), 36–43.

Ding, C., You, J., Chen, L., Wang, S., and Ding, Y. (2014). Nitrogen fertilizer increases spikelet number per panicle by enhancing cytokinin synthesis in rice. *Plant Cell Rep.* 33, 363–371. doi: 10.1007/s00299-013-1536-9

Dingkuhn, M. (1996). Modelling concepts for the phenotypic plasticity of dry matter and nitrogen partitioning in rice. *Agric. Systems.* 52 (2-3), 383–397. doi: 10.1016/0308-521X(95)00078-J

Duan, M., and Sun, S. S. M. (2005). Profling the expression of genes controlling rice grain quality. *Plant Mol. Biol.* 59, 165–178. doi: 10.1007/s11103-004-7507-3

DuPont, F. M., and Altenbach, S. B. (2003). Molecular and biochemical impacts of environmental factors on wheat grain development and protein synthesis. *J. Cereal Science.* 382, 133–146. doi: 10.1016/S0733-5210(03)00030-4

Elbasyoni, I. S., Abdallah, A. M., Morsy, S., and Baenziger, S. (2019). Effect of deprivation and excessive application of nitrogen on nitrogen use efficiency-related traits using wheat cultivars, lines, and landraces. *Crop Sci.* 59, 994–1006. doi: 10.2135/cropsci2018.09.0564

Fageria, N. K. (2014). Nitrogen harvest index and its association with crop yields. *J. Plant Nutr.* 37 (6), 795–810. doi: 10.1080/01904167.2014.881855

Gaju, O., Allard, V., Martre, P., Snape, J. W., Heumez, E., LeGouis, J., et al. (2011). Identification of traits to improve the NUE of wheat genotypes. *Field Crops Res.* 1232, 139–152. doi: 10.1016/j.fcr.2011.05.010

Gallais, A., and Hirel, B. (2004). An approach to the genetics of nitrogen use efficiency in maize. *J. Exp. botany.* 55 (396), 295–306.

Glangchai, P., and Rangsri, W. (2021). Effects of pressure soaking on elastic modulus of steamed-cooked glutinous rice kernel. *Trends Sci.* 18 (22), 501. doi: 10.48048/tis.2021.501

Good, A. G., Shrawat, A. K., and Muench, D. G. (2004). Can less yield more? is reducing nutrient input into the environment compatible with maintaining crop production? *Trends Plant science.* 9 (12), 597–605. doi: 10.1016/j.tplants.2004.10.008

Guarda, G., Padovan, S., and Delogu, G. (2004). Grain yield, nitrogen-use efficiency and baking quality of old and modern Italian bread-wheat cultivars grown at different nitrogen levels. *Eur. J. Agron.* 21, 181–192. doi: 10.1016/j.eja.2003.08.001

Hajibarat, Z., and Saidi, A. (2022). Senescence-associated proteins and nitrogen remobilization in grain filling under drought stress condition. *J. Genet. Eng. Biotechnol.* 20 (1), 1–14. doi: 10.1186/s43141-022-00378-5

Hameed, F., Xu, J., Rahim, S. F., Wei, Q., Rehman Khalil, A. U., and Liao, Q. (2019). Optimizing nitrogen options for improving nitrogen use efficiency of rice under different water regimes. *Agronomy.* 9 (1), 39. doi: 10.3390/agronomy9010039

He, X., Ma, H., Zhao, X., Nie, S., Li, Y., Zhang, Z., et al. (2016). Comparative RNA-seq analysis reveals that regulatory network of maize root development controls the expression of genes in response to n stress. *PloS One* 11, e0151697.

Heitholt, J. J., Croy, L. I., Maness, N. O., and Nguyen, H. T. (1990). Nitrogen partitioning in genotypes of winter wheat differing in grain n concentration. *F. Crop Res.* 23, 133–144. doi: 10.1016/0378-4290(90)90108-N

Herrera, J. M., Noulas, C., Stamp, P., and Pellet, D. (2016). Little potential of spring wheat genotypes as a strategy to reduce nitrogen leaching in central Europe. *Agronomy* 6, 29–3847. doi: 10.3390/agronomy6020029

Hirel, B., Gouis, J. L., Ney, B., and Gallais, A. (2007). The challenge of improving nitrogen use efficiency in crop plants: Towards a more central role for genetic variability and quantitative genetics within integrated approaches. *J. Exp. Botany.* 58 (9), 2369–2387. doi: 10.1093/jxb/erm097

Jagadhesan, B., Meena, H. S., Jha, S. K., Krishna, K. G., Kumar, S., Elangovan, A., et al. (2022). Association of nitrogen use efficiency in diverse rice genotypes with sustenance of reproductive stage photoassmilation and nitrogen metabolism. doi: 10.21203/rs.3.rs-2356439/v1

Jagadhesan, B., Sathee, L., Meena, H. S., Jha, S. K., Chinnusamy, V., Kumar, A., et al. (2020). Genome wide analysis of NLP transcription factors reveals their role in nitrogen stress tolerance of rice. *Sci. Rep.* 10 (1), 1–16.

Jenner, C., Ugalde, T., and Aspinall, D. (1991). The physiology of starch and protein deposition in the endosperm of wheat. *Aust. J. Plant Physiol.* 18, 211. doi: 10.1071/PP9910211

Kanampiu, F. K., Raun, W. R., and Johnson, G. V. (1997). Effect of nitrogen rate on plant nitrogen loss in winter wheat varieties. *J. Plant Nutr.* 20 (2-3), 389–404. doi: 10.1080/01904169709365259

Khwankaew, J., Bunnag, W., Pichakum, A., Songnuan, W., Dhammasamisorn, B. O., and Narawatthana, S. (2022). Differences in nutrient remobilization characteristics and relationship to senescence and grain nutrient content among rice varieties. *J. Crop Sci. Biotechnol.*, 1–13. doi: 10.1007/s12892-022-00141-9

Kraiser, T., Gras, D. E., Gutierrez, A. G., Gonzalez, B., and Gutierrez, R. A. (2011). A holistic view of n acquisition in plants. *J. Exp. Botany.* 624, 1455–1466.

Kumari, S., Sharma, N., and Raghuram, N. (2021). Meta-analysis of yield-related and n-responsive genes reveals chromosomal hotspots, key processes and candidate genes for nitrogen-use efficiency in rice. *Front. Plant Sci.* 12, 627955.

Lemaitre, T., Gaufichon, L., Boutet-Mercey, S., Christ, A., and Masclaux-Daubresse, C. (2008). Enzymatic and metabolic diagnostic of nitrogen deficiency in arabidopsis thaliana wassileskija accession. *Plant Cell Physiol.* 49, 1056–1065. doi: 10.1093/pcp/pcn081

Li, T., Raman, A. K., Marcaida, M. I., Kumar, A., Angeles, O., and Radanielson, A. M. (2013). Simulation of genotype performances across a larger number of environments for rice breeding using ORYZA2000. *Field Crops Res.* 149, 312–321. doi: 10.1016/j.fcr.2013.05.006

Li, S., Tian, Y., Wu, K., Ye, Y., Yu, J., Zhang, J., et al. (2018). Modulating plant growth–metabolism coordination for sustainable agriculture. *Nature.* 560, 595–600. doi: 10.1038/s41586-018-0415-5

Lim, Y. Y., and Quah, E. P. L. (2007). Antioxidant properties of different cultivars of portulaca oleracea. *Food Chem.* 1033, 734–740.

Lin, X., Zhou, W., Zhu, D., Chen, H., and Zhang, Y. (2006). Nitrogen accumulation, remobilization and partitioning in rice (*Oryza sativa* l.) under an improved irrigation practice. *Field Crops Res.* 96 (2-3), 448–454. doi: 10.1016/j.fcr.2005.09.003

Liu, X., Hu, B., and Chu, C. (2022). Nitrogen assimilation in plants: Current status and future prospects. *J. Genet. Genomics* 49 (5), 394–404. doi: 10.1016/j.jgg.2021.12.006

Mariotti, F., Tome, D., and Mirand, P. P. (2008). Converting nitrogen into protein–beyond 6.25 'nd jones' factors. *Crit. Rev. Food Sci. Nutr.* 48 (2), 177–184. doi: 10.1080/10408390701279749

Martin, A., Lee, J., Kichey, T., Gerentes, D., Zivy, M., Tatout, C., et al. (2006). Two cytosolic glutamine synthetase isoforms of maize are specifically involved in the control of grain production. *Plant Cell.* 18, 3252–3274. doi: 10.1105/tpc.106.042689

Martinoia, E., Heck, U., and Wiemken, A. (1981). Vacuoles as storage compartments for nitrate in barley leaves. *Nature* 289, 292–294.

Martre, P. (2003). Modeling grain nitrogen accumulation and protein composition to understand the sink/source regulations of nitrogen remobilization for wheat. *Plant Physiol.* 133, 1959–1967. doi: 10.1104/pp.103.030585

Masclaux-Daubresse, C., Daniel-Vedele, F., Dechorgnat, J., Chardon, F., Gaufichon, L., and Suzuki, A. (2010). Nitrogen uptake, assimilation and remobilization in plants: Challenges for sustainable and productive agriculture. *Ann. Bot.* 105, 1141–1157. doi: 10.1093/aob/mcq028

Masclaux-Daubresse, C., Reisdorf-Cren, M., and Orsel, M. (2008). Leaf nitrogen remobilization for plant development and grain filling. *Plant Biol.* 10 (s1), 23–36. doi: 10.1111/j.1438-8677.2008.00097.x

Masoni, A., Ercoli, L., Mariotti, M., and Arduini, I. (2007). Post-anthesis accumulation and remobilization of dry matter, nitrogen and phosphorus in durum wheat as affected by soil type. *Eur. J. Agron.* 26, 179–186. doi: 10.1016/j.eja.2006.09.006

McMullan, P. M., McVetty, P. B. E., and Urquhart, A. A. (1988). Dry matter and nitrogen accumulation and redistribution and their relationship to grain yield and grain protein in oats. *Can. J. Plant Sci.* 68, 311–322. doi: 10.4141/cjps88-041

Melino, V. J., Tester, M. A., and Okamoto, M. (2022). Strategies for engineering improved nitrogen use efficiency in crop plants *via* redistribution and recycling of organic nitrogen. *Curr. Opin. Biotechnol.* 73, 263–269. doi: 10.1016/j.copbio.2021.09.003

Millard, P. (1988). The accumulation and storage of nitrogen by herbaceous plants. *Plant Cell Environment.* 11 (1), 1–8. doi: 10.1111/j.1365-3040.1988.tb01769.x

Moll, R. H., Kamprath, E. J., and Jackson, W. A. (1982). Analysis and interpretation of factors which contribute to efficiency of nitrogen utilization. *Agron. J.* 74, 562–564.

Nelson, D. W., and Sommers, L. E. (1980). Total nitrogen analysis of soil and plant tissues. *J. Assoc. Off. Analytical Chemists.* 63 (4), 770–778. doi: 10.1093/jaoac/63.4.770

Nooden, L.D. Guiamet, J.J. John, I. (1997). Senescence mechanisms. *Physiologia Plantarum* 1014, 746–7. doi: 10.1111/j.1399-3054.1997.tb01059.x

Ntanos, D. A., and Koutroubas, S. D. (2002). Dry matter and n accumulation and translocation for indica and japonica rice under Mediterranean conditions. *Field Crops Res.* 74, 93–10. doi: 10.1016/S0378-4290(01)00203-9

Peng, B., Kong, H. L., Li, Y. B., Wang, L., Zhong, M., Sun, L., et al. (2007). Effect of different level of nitrogen on growth and yield of transplant aman rice cv brri dhan32. *Int. J. Sustain. Crop Production.* 2 (1), 28–34.

Peng, B., Kong, H., Li, Y., Wang, L., Zhong, M., Sun, L., et al. (2014). OsAAP6 functions as an important regulator of grain protein content and nutritional quality in rice. *Nat Commun* 5 (1), 4847.

Pommel, B., Gallais, A., Coque, M., Quillere, I., Hirel, B., Prioul, J. L., et al. (2006). Carbon and nitrogen allocation and grain filling in three maize hybrids differing in leaf senescence. *Eur. J. Agron.* 24, 203–211. doi: 10.1016/j.eja.2005.10.001

Qun, Z. H. O. U., Rui, Y. U. A. N., Zhang, W. Y., Gu, J. F., Liu, L. J., Zhang, H., et al. (2023). Grain yield, nitrogen use efficiency and physiological performance of indica/japonica hybrid rice in response to various nitrogen rates. *J. Integr. Agriculture.* 22 (1), 63–79.

Raddatz, N., Morales de los Rios, L., Lindahl, M., Quintero, F. J., and Pardo, J. M.. (2020). Coordinated transport of nitrate, potassium, and sodium. *Front. Plant Sci.* 11, 247. doi: 10.3389/fpls.2020.00247

Rajcan, I., and Tollenaar, M. (1999). Source: sink ratio and leaf senescence in maize: I. dry matter accumulation and partitioning during grain filling. *Field Crop Res.* 60, 245–253. doi: 10.1016/S0378-4290(98)00142-7

Rahman, M. H., Ali, M. H., Ali, M. M., and Khatun, M. M. (2007). Effect of different level of nitrogen on growth and yield of transplant Aman rice cv Brri dhan32. *Int. J. Sustain. Agric. Res. Crop Prod.* 2 (1), 28–34.

Salo-vaananen, P. P., and Koivistoinen, P. E. (1996). Determination of protein in foods: comparison of net protein and crude protein (N× 6.25) values. *Food Chem.* 57 (1), 27–31. doi: 10.1016/0308-8146(96)00157-4

Satyanarayana, T., Majumdar, K., Shahi, V., Kumar, A., Pampolino, M., Jat, M. L., et al. (2012). Economics of nitrogen fertilizer application in rice, wheat and maize grown in the indo-gangetic plains. *Indian J. Fert.* 8 (8), 62–71.

Slafer, G. A., Andrade, F. H., and Satorre, E. H. (1990). Genetic-improvement effects on pre-anthesis physiological attributes related to wheat grain-yield. *Field Crop Res.* 23, 255–263. doi: 10.1016/0378-4290(90)90058-J

Slafer, G. A., Connor, D. J., and Halloran, G. M. (1994). Rate of leaf appearance and final number of leaves in wheat: Effects of duration and rate of change of photoperiod. *Ann. Bot.* 74 (5), 427–436. doi: 10.1006/anbo.1994.1138

Slafer, G. A., and Satorre, E. H. (1999). An introduction to the physiological-ecological analysis of wheat yield. *Wheat: Ecology and physiology of yield determination*, 3–12.

Sułek, A., Cacak-Pietrzak, G., Rozewicz, M., Nierobca, A., Grabinski, J., Studnicki, M., et al. (2023). Effect of production technology intensity on the grain yield, protein content and amino acid profile in common and durum wheat grain. *Plants* 12 (2), 364. doi: 10.3390/plants12020364

Tabuchi, M., Abiko, T., and Yamaya, T. (2007). Assimilation of ammonium ions and reutilization of n in rice (*Oryza sativa* l). *J. Exp. Botany.* 589, 2319–2327. doi: 10.1093/jxb/erm016

Taulemesse, F., Le Gouis, J., Gouache, D., Gibon, Y., and Allard, V. (2015). Post-flowering nitrate uptake in wheat is controlled by n status at flowering, with a putative major role of root nitrate transporter nRT2.1. *PloS One* 10, e0120291. doi: 10.1371/journal.pone.0120291

Tilman, D., Cassman, K. G., Matson, P. A., Naylor, R., and Polasky, S. (2002). Agriculture sustainability and intensive production practices. *Nature.* 418, 671–677. doi: 10.1038/nature01014

Uauy, C., Distelfeld, A., Fahima, T., Blechl, A., and Dubcovsky, J. (2006). A NAC gene regulating senescence improves grain protein, zinc, and iron content in wheat. *Science.* 314, 1298–1301.

Wang, B., Li, R., Wan, Y., Cai, W., Guo, C., Qin, X., et al. (2021). Air warming and CO_2 enrichment cause more ammonia volatilization from rice paddies: An OTC field study. *Sci. Total Environment.* 752, 142071. doi: 10.1016/j.scitotenv.2020.142071

Wenefrida, I., Utomo, H. S., Blanche, S. B., and Linscombe, S. D. (2009). Enhancing essential amino acids and health benefit components in grain crops for improved nutritional values. *Recent Patents DNA Gene Sequences.* 3 (3), 219–225. doi: 10.2174/187221509789318405

West, P. C., Gerber, J. S., Engstrom, P. M., Mueller, N. D., Brauman, K. A., Carlson, K. M., et al. (2014). Leverage points for improving global food security and the environment. *Science.* 3456194, 325–328. doi: 10.1126/science.1246067

Xu, C. G., Li, X. H., and He, Y. Q. (2014). *OsAAP6* functions as an important regulator of grain protein content and nutritional quality in rice. *Nat. Commun.* 5, 4847.

Xue, L. H., and Yang, L. Z. (2008). Recommendations for nitrogen fertiliser topdressing rates in rice using canopy reflectance spectra. *Biosyst. Eng.* 100, 524–534. doi: 10.1016/j.biosystemseng.2008.05.005

Yoshida, H., Horie, T., and Shiraiwa, T. (2006). A model explaining genotypic and environmental variation of rice spikelet number per unit area measured by cross-locational experiments in Asia. *Field Crops Research* 97 (2–3), 337–343. doi: 10.1016/j.fcr.2005.11.004

Zebarth, B. J., Botha, E. J., and Rees, H. (2007). Rate and time of fertilizer nitrogen application on yield, protein and apparent efficiency of fertilizer nitrogen use of spring wheat. *Can. J. Plant Sci.* 87, 709–718. doi: 10.4141/CJPS06001

Zhang, Z. J., Chu, G., Liu, L. J., Wang, Z. Q., Wang, X. M., Zhang, H., et al. (2013). Mid-season nitrogen application strategies for rice varieties differing in panicle size. *Field Crops Res.* 150, 9–18. doi: 10.1016/j.fcr.2013.06.002

Zhang, L., Liang, Z. Y., He, X. M., Meng, Q. F., Hu, Y. C., Schmidhalter, U., et al. (2020). Improving grain yield and protein concentration of maize (*Zea mays* l.) simultaneously by appropriate hybrid selection and nitrogen management. *Field Crop Res.* 249, 107754. doi: 10.1016/j.fcr.2020.107754

Zheng, W., Liu, Z., Zhang, M., Shi, Y., Zhu, Q., Sun, Y., et al. (2017). Improving crop yields, nitrogen use efficiencies, and profits by using mixtures of coated controlled-released and uncoated urea in a wheat-maize system. *Field Crop Res.* 205, 106–115. doi: 10.1016/j.fcr.2017.02.009

Zhu, K. Y., Yan, J. Q., Yong, S. H. E. N., Zhang, W. Y., Xu, Y. J., Wang, Z. Q., et al (2022). Deciphering the morpho–physiological traits for high yield potential in nitrogen efficient varieties (NEVs): A japonica rice case study. *J. Integr. Agriculture* 21 (4), 947–963. doi: 10.1016/S2095-3119(20)63600-0

frontiers | Frontiers in Plant Science

TYPE Original Research
PUBLISHED 20 April 2023
DOI 10.3389/fpls.2023.1100318

OPEN ACCESS

EDITED BY
Petra Bauer,
Heinrich Heine University of Düsseldorf, Germany

REVIEWED BY
Vesna Dragicevic,
Maize Research Institute Zemun Polje, Serbia
Georgios Liakopoulos,
Agricultural University of Athens, Greece

*CORRESPONDENCE
Søren Husted
shu@plen.ku.dk

†These authors have contributed equally to this work and share first authorship

SPECIALTY SECTION
This article was submitted to Plant Nutrition, a section of the journal Frontiers in Plant Science

RECEIVED 16 November 2022
ACCEPTED 31 March 2023
PUBLISHED 20 April 2023

CITATION
Tougaard SL, Szameitat A, Møs P and Husted S (2023) Leaf age and light stress affect the ability to diagnose P status in field grown potatoes.
Front. Plant Sci. 14:1100318.
doi: 10.3389/fpls.2023.1100318

Leaf age and light stress affect the ability to diagnose P status in field grown potatoes

Stine Le Tougaard†, Augusta Szameitat†, Pauline Møs and Søren Husted*

Section for Plant and Soil Science, Department of Plant and Environmental Sciences, University of Copenhagen, Copenhagen, Denmark

Phosphorus (P) deficiency is a global issue which can severely impact the yield of crops, including the P demanding and important food crop potato. Diagnosis of P status directly in the field can be used to adapt P fertilization strategies to the needs of the evolving crop during the growing season and is often estimated by analyzing P concentrations in leaf tissue. In this study, we investigate how diagnosis of P status in field grown potato plants is affected by leaf position and time of measurement in a randomized block experiment. The concentrations of many essential plant nutrients are highly dynamic, and large differences in nutrient concentrations were found in potato leaves depending on leaf age and time of sampling. During tuber initiation, P concentrations decreased in a steep gradient from the youngest leaves (0.8%) towards the oldest leaves (0.2%). The P concentrations in the youngest fully expanded leaf decreased by 25-33% within just 7 days, due to a high remobilization of P from source to sink tissue during crop development. 40 days later P concentrations in all leaves were near or below the established critical P concentration of 0.22%. The P concentration in leaf tissue thus depends on sampling time and leaf position on the plant, which in a practical setting might prevent a meaningful interpretation in terms of fertilizer recommendation. The chlorophyll *a* fluorescence parameter "P-predict", derived from the fluorescence transients, is an alternative to the classical chemical analysis of nutrient concentrations in leaf tissue. P-predict values serve as a proxy for the bioavailable P pool in the leaf and can be measured directly in the field using handheld technology. However, in conditions of high solar irradiation, the P-predict values of the most light-exposed leaf positions, i.e. the younger leaves, were found to be severely impacted by photoinhibition, preventing accurate characterization of the P status in potatoes. Shading the plants can reverse or prevent photoinhibition and restore the diagnostic capabilities of the P-predict approach.

KEYWORDS

***Solanum tuberosum*, chlorophyll *a* fluorescence, phosphorus deficiency, nutrient remobilization, critical nutrient concentration**

1 Introduction

Potatoes are the third most important world crop, supplying food to more than a billion people worldwide (Birch et al., 2012). It is a nutritionally valuable staple crop used for various purposes, i.e. fresh consumption, processed food products and starch extraction, with many specific quality requirements which can be influenced by the availability of different plant nutrients. Potato is a highly phosphorus (P) demanding crop, and adequate P supply throughout the entire growth period is crucial for optimal yields and product quality. In the early growing season during the tuber initiation stage, P has a significant effect on tuber setting (Jenkins and Ali, 2000). The highest quantity of P is taken up during tuber bulking in the mid- to late growing season, and continues in the tuber maturation phase, where it improves tuber maturity (Rosen et al., 2014). P uptake continues even after uptake of other nutrients, such as nitrogen (N) and potassium (K), have ceased (Rosen et al., 2014). During tuber bulking, P has a critical role in carbon partitioning and starch synthesis, where key enzymes such as ADP-glucose pyrophosphorylase (AGPase) are tightly regulated by the phosphate concentration in amyloplasts. Moreover, P is essential for regulation of starch synthesis through phosphorylation of enzymes and carbohydrate intermediates (Geigenberger, 2011; MacNeill et al., 2017). Furthermore, phosphate is covalently bound in amylopectin of storage starch species in root and tuber crops, most prevalent in potato, where the degree of phosphate substitution affects the properties of potato starch paste (Noda et al., 2007).

Regulation of biochemical processes through phosphorylation is a central function of P in plant cells, but the most essential role of P is found in adenosine triphosphate (ATP) (de Bang et al., 2021). Hydrolysis of ATP is the primary source of biochemical energy in the plant and is necessary for generating the proton motive force (PMF) required for loading sucrose into the phloem. Phloem loading, translocation and unloading of sucrose is essential for the movement of photosynthates from leaves to tubers, and to synthesize and store starch in the tubers (Hammond and White, 2008). Phloem loading is also dependent on the essential nutrients Potassium (K) and Magnesium (Mg). During inadequate supply of either of these nutrients, carbohydrate distribution is affected, and sucrose accumulates in potato leaves (Cakmak et al., 1994; Ceylan et al., 2016; Koch et al., 2019a). This is related to the important role of Mg as an activator of ATP, making it a substrate for ATPase to generate the PMF (Hermans et al., 2005). Mg furthermore serves crucial functions in photosynthetic light harvesting as a co-factor of chlorophyll (Verbruggen and Hermans, 2013).

Both Mg and, especially, K serve as osmotic and enzymatic regulators within the plant. K establishes the osmotic pressure necessary for transport of sucrose via the phloem, and it regulates pH via charge balancing across membranes, which is essential to drive ATP production and optimize enzyme activity. In particular, K is an activator of starch synthase which is required for starch synthesis. It therefore has a central role in establishing tuber and starch yields (Koch et al., 2019b). K also influences quality traits such as storability and cooking type, which is mainly determined by starch content, and a sufficient supply helps reduce after-cooking darkening, black spot bruise and formation of acrylamide (Naumann et al., 2019). K is typically the most abundant element in potatoes at a concentration up to 6% in the leaves and 1.7-2.5% in the tubers (Koch et al., 2019b), with a maximum K uptake during tuber initiation and bulking and close to zero uptake during the maturation phase (Horneck and Rosen, 2008).

In addition to the above-mentioned nutrients, nitrogen (N) naturally has a large impact on potato yield. Though excessive N supply can reduce tuber maturity and quality, e.g. decreasing starch while increasing sucrose, free amino acids and reducing sugars, it is the nutrient with the greatest influence on tuber weight. N is primarily taken up during the tuber bulking phase, but it is also important for canopy development earlier in the growing season (Koch et al., 2019b).

In order to ensure optimal yield and quality of potato, it is therefore important to avoid nutrient deficiencies during the growing season. However, potatoes have a sparse and shallow root system, with up to 90% of roots located in the uppermost 25 cm of the soil (Tanner et al., 1982). This reduces their access to nutrients with limited mobility in soil, such as P, and results in a low P use efficiency. Placing P in or between the rows during planting increases root interception of the applied P, thus improving the P use efficiency (Hopkins et al., 2014). Before planting, it is common practice to perform a soil analysis to estimate the availability of plant nutrients, even though soil analyses repeatedly have shown a poor correlation between the extractable soil P and the plant available pool of P (Mundus et al., 2017). The availability of soil P furthermore depends on soil texture and environmental factors such as humidity, temperature and precipitation during the growth period (Rosen et al., 2014; Potarzycki and Grzebisz, 2019; Koch et al., 2019b). P deficiency therefore often occurs as a temporal disorder caused by climatic conditions. The crop might in such cases benefit from supplementation of P fertilizers applied to the foliage or incorporated into the soil (Rosen and Bierman, 2008; Rosen et al., 2014).

However, P deficiency often occurs without visible symptoms, and can be hard to diagnose by visual inspection (Carstensen et al., 2018a; Carstensen et al., 2018b). Monitoring the nutritional status and predicting yields can instead be done during the growing season by measuring nutrient concentrations in leaves or petioles. It has traditionally been reported that the youngest fully expanded leaf (YFEL) should have a P content above a critical P concentration of 0.22% at tuber bulking (Tindall et al., 1993; Rosen et al., 2014). The critical P concentration is the concentration below which the plant is considered P deficient, and the yields are expected to be affected. The YFEL is chosen due to its developmental stage, as it has a high photosynthetic activity but is not yet fully transformed from a net importer to a net exporter of photosynthates (Walworth and Muniz, 1993; Katoh et al., 2015; Grzebisz et al., 2018). Yet, regularly monitoring the nutrient composition can be both time consuming and expensive. Furthermore, it can be questioned how useful this classical approach is in potato, as recent research suggests it is insufficient to rely on macronutrient concentrations of the YFEL to predict yields (White et al., 2018; Grzebisz et al., 2020).

As an alternative to measuring nutrient concentrations, chlorophyll *a* fluorescence can diagnose physiological deficiencies of certain nutrients, when they affect nutrient specific functions of the photosynthetic machinery (Frydenvang et al., 2015; Carstensen et al., 2018a). Measurements of chlorophyll *a* fluorescence can be used to create a fluorescence transient, which is a polyphasic, time-dependent emission of fluorescent light, also known as an OJIP transient. In the OJIP transient, the fluorescence initially increases in three distinct steps (the O-, J-, and I-steps) before peaking (the P-step) at the maximum fluorescence (Fm) and subsequently decreasing. These steps are caused by discrete events in the linear electron transport from photosystem II (PSII) to photosystem I (PSI) and will be affected in different ways by distinct disruptions in the electron transport chain.

The P-predict parameter is a new chlorophyll *a* fluorescence parameter, which is derived from the fluorescence transients and has been developed to characterize P status in barley grown under different levels of P deficiency (Frydenvang et al., 2015; Carstensen et al., 2018a; Carstensen et al., 2018b). P deficiency is correlated with specific changes in the fluorescence transient and appears to be independent on most other nutrient deficiencies. Under P deficiency, a rapid lumen acidification decreases the rate of plastoquinone oxidation and erases the I-step (Carstensen et al., 2018a), resulting in a smooth curve between the J- and P-steps. The P-predict value is calculated largely based on the degree of I-step deletion (Frydenvang et al., 2015).

Chlorophyll *a* fluorescence can also be used to detect Manganese (Mn) deficiency, because it decreases the quantum yield (Fv/Fm) of PSII and results in a low maximum fluorescence. As a result, Mn deficiency distorts the shape of the fluorescence transients (Schmidt et al., 2016b). The effects of P deficiency on a fluorescence transient will therefore be obscured if it occurs simultaneously with Mn deficiency, preventing detection of both deficiencies at once.

Environmental stressors, such as excess light, extreme temperature or drought, can result in photoinhibition which affects chlorophyll *a* fluorescence patterns and the resulting P-predict values (Ruban, 2016; Guidi et al., 2019). The P-predict approach has primarily been developed and used in controlled conditions in greenhouses and climate chambers. However, field grown crops are inevitably exposed to various types of stresses during a growing season. Testing the applicability of the P-predict method in real field settings across different crop species and climates is therefore required to ensure the method's suitability for standard agronomical practices. It should be underlined that this method is suitable for diagnosing the immediate plant P status, but is unable to provide a prognosis of how the future plant P status might develop.

This study aims to investigate the P-predict responses under field conditions, and to determine best practice for diagnosing P deficiency in a P sensitive crop such as potato. This was done by following the nutrient concentrations at different leaf positions throughout the growing season and correlating the P concentrations with diagnosis of the P status based on chlorophyll *a* fluorescence analyses.

2 Materials and methods

2.1 Field experiment

The experiment was conducted in western Jutland, Denmark (55°36'13.4"N, 8°57'09.0"E) on a field where P deficiency had previously been observed in potatoes. Soil samples from the top 25 cm were randomly collected, air dried and sieved through a 2 mm mesh. The soil samples were analyzed by standard procedures and included: texture, pH, Olsen-P and ammonium extractable Mg and K at a commercial laboratory (Agrolab, Germany) (Table 1). Furthermore, P availability was determined by the C_{DGT} technique as presented by Tandy et al. (2011) and Christel et al. (2016) (Table 1). Seed potatoes *Solanum tuberosum* L., cv. Kuras were planted with a row distance of 0.75 m and a distance between tubers of 0.2 m. The experimental site was irrigated when there was no precipitation. Fertilizer was placed between the rows (10 cm from the tubers and 5 cm below tuber level) while planting. The following fertilization rate was used: 136.5 kg N ha^{-1}, 250 kg K ha^{-1}, 60 kg Mg ha^{-1}, 170 kg S ha^{-1} and it was provided as diammonium phosphate, N-S (27-4) and patentkali (25% K, 6% Mg, 17.5% S). Two soil P fertilizer treatments were used: P+ and P-. P+ was supplied with 30 kg P ha^{-1}, while P- did not receive P fertilizer.

Soil moisture (0-20 cm below the soil surface) and soil temperatures (6 cm below the surface, at the soil surface and 15 cm above ground) were monitored using two Standard TMS dataloggers (Tomst, Czech Republic) throughout the entire growing season. On the days when tissue sampling and chlorophyll *a* fluorescence measurements were made, the photosynthetically active radiation (PAR) was recorded for a period of at least 3 hours using a universal light meter (ULM-500, Heinz Walz GmbH, Germany).

TABLE 1 Soil properties at the field site in Hovborg, Denmark.

Soil content	Value
Clay <0.002mm (%)	4.3
Silt 0.002-0.02mm (%)	0.3
Fine sand 0.02-0.2mm (%)	22.9
Coarse sand 0.2-2mm (%)	69.4
SOM (Soil Organic Matter) (%)	3.1
pH (0.01 M $CaCl_2$)	5.4 ± 0.0
Olsen-P (mg P kg^{-1} soil)	4.6 ± 0.4 (>2.0)
C_{DGT} (µg P L^{-1})	66.8 ± 2.2 (>65)
K (mg K kg^{-1} soil)	29.5 ± 0.9 (>40)
Mg (mg Mg kg^{-1} soil)	35.5 ± 0.6 (>40)

Values in parenthesis indicate standard thresholds for sufficient soil nutrient concentrations. Results presented as mean ± SEM (n = 4).

2.2 Elemental analysis of potato leaves

All leaf positions were harvested from 4 field grown potato plants at each sampling date, giving a total of 4 independent replicates of each leaf position. Sampling occurred twice in June at 51 and 58 days after planting (DAP) during the tuber initiation stage, and twice in August at 99 and 113 DAP, during the tuber bulking stage. The leaves were dried at 50°C on the day of harvesting. Ultra-wave digestion of plant tissue was performed in a mixture of 500 µL ultra-pure acid (70% HNO_3) and 250 µL 15% H_2O_2 under an inert gas (N_2) at a pressure of 45 bars and 240°C for 15 min (Ultrawave, Milestone Inc., USA). When leaf tissue dry weight exceeded 150 mg, the leaves were pulverized and homogenized before taking a sub-sample. All samples were analyzed on a 5100 DW ICP-OES (Agilent Technologies, USA) with multi-element detection. Data were validated with the analysis of seven replicates of certified reference material (Apple leaves, NIST 1515, National Institute of Standards and Technology, USA). Only elemental data with accuracies and precision better than 95% were included (Chen et al., 2020).

2.3 Chlorophyll *a* fluorescence analysis

Chlorophyll *a* fluorescence analysis was performed on all leaf positions (n = 4) before harvesting at 51, 58, 99 and 113 DAP, using a HandyPEA chlorophyll fluorometer (Hansatech instruments, UK). Prior to measuring, leaves were dark adapted for 25 minutes using Hansatech leaf clips (Hansatech instruments, UK). Leaves were exposed to continuous saturating actinic light (3000 µmol m^{-2} s^{-1}) for 10 seconds. The resulting fluorescence emission was recorded by a PIN photodiode to construct a fluorescence transient (Kautsky and Hirsch, 1931). The transients were created by double normalizing the data between F0 and Fm to get the relative fluorescence, V(t), using the formula:

$$V(t) = \frac{F(t) - F0}{Fm - F0}$$

F0 and Fm correspond to the minimal fluorescence at time 0 and the maximum fluorescence, respectively, and F(t) is the measured fluorescence at time *t*. Furthermore, the fluorescence transients were used to evaluate the plant P status, by preprocessing and analysis using a Python 3.9 script based on a partial least square (PLS) model to quantify the level of P deficiency (Frydenvang et al., 2015) (Patent EP3049792B1). P-predict values can provide an indication of plant P status and identify P deficiency. Plants are considered P deficient at P-predict<0.40 and P sufficient at P-predict >0.65 while P-predict values in the range 0.40-0.65 indicate intermediate P status (Frydenvang et al., 2015; Carstensen et al., 2018a).

3 Results

3.1 Variability of leaf nutrient content

The experimental field site was chosen due to a historical yield response to P fertilization, which was confirmed by a pot trial that showed an increased barley biomass following P fertilization (data not shown). The soil has a high percentage of coarse sand (Table 1), which is suitable for potato cultivation. The soil type has a low water holding capacity often resulting in low P availability and drought stress in absence of irrigation, and for this reason irrigation was implemented. The volumetric soil moisture was maintained above 25% for the duration of the experiment (Supplementary Figure S1), thus exceeding the field capacity for the sandy soil (Zotarelli et al., 2019). Soil tests for P status showed that the soil was near deficiency according to C_{DGT}, which is the most reliable indicator of plant available soil P (Mundus et al., 2017), while it had sufficient P levels according to the Olsen-P value (Rubæk, 2015) (Table 1). The field experiment was fertilized according to standard practices and recommendations based on the soil tests, and the plants presented no visible symptoms of any nutrient deficiencies (Figure 1).

The elemental composition was measured in all leaves from four randomly selected plants at each sampling date and showed striking patterns of nutrient concentrations depending on leaf position and sampling date (Figure 2). P fertilization had a significant effect on the P concentration at the individual leaf positions during tuber initiation on the first sampling date 51 DAP (P<0.001), but no significant differences were found 7 days later, nor at the tuber bulking stage 99 and 113 DAP. During tuber initiation, halfway through the growing period at 51 DAP, P concentrations were very high in the youngest leaves (0.85-0.94% in leaf 1) and decreased markedly with increasing leaf age. Leaf 5 had P concentrations of 0.40-0.44%, while leaf 11 had P concentrations of 0.20-0.26%, which is within 1 standard deviation of the reported critical P concentration of 0.22% (Figure 2A). One week later, at 58 DAP, P concentrations in leaves 3-7 had decreased by a remarkable 19-40% compared to the previous week, with concentrations in older leaves (leaf 7-13) near the critical P concentration. During tuber bulking in the later part of the growing season (99 and 113 DAP), P concentrations in all leaves had stabilized at or below the critical P concentration (Figure 2B). Furthermore, no differences were found in tuber P concentration between P fertilization treatments (Supplementary Table S1).

The distribution patterns observed for Mg and K concentrations were opposite to the ones observed for P during tuber initiation (Figure 2). Mg and K did, however, resemble those of phloem immobile nutrients such as Ca, Mn and B, while the nutrients S, Fe, Zn and Cu all differed in distribution patterns with seemingly no relation to their phloem mobility (Supplementary Figures S2 and

FIGURE 1
Leaf positions. One replicate of all leaves from a single plant at 51 days after planting. Numbers indicate leaf position, 1 being the youngest and 12 the oldest.

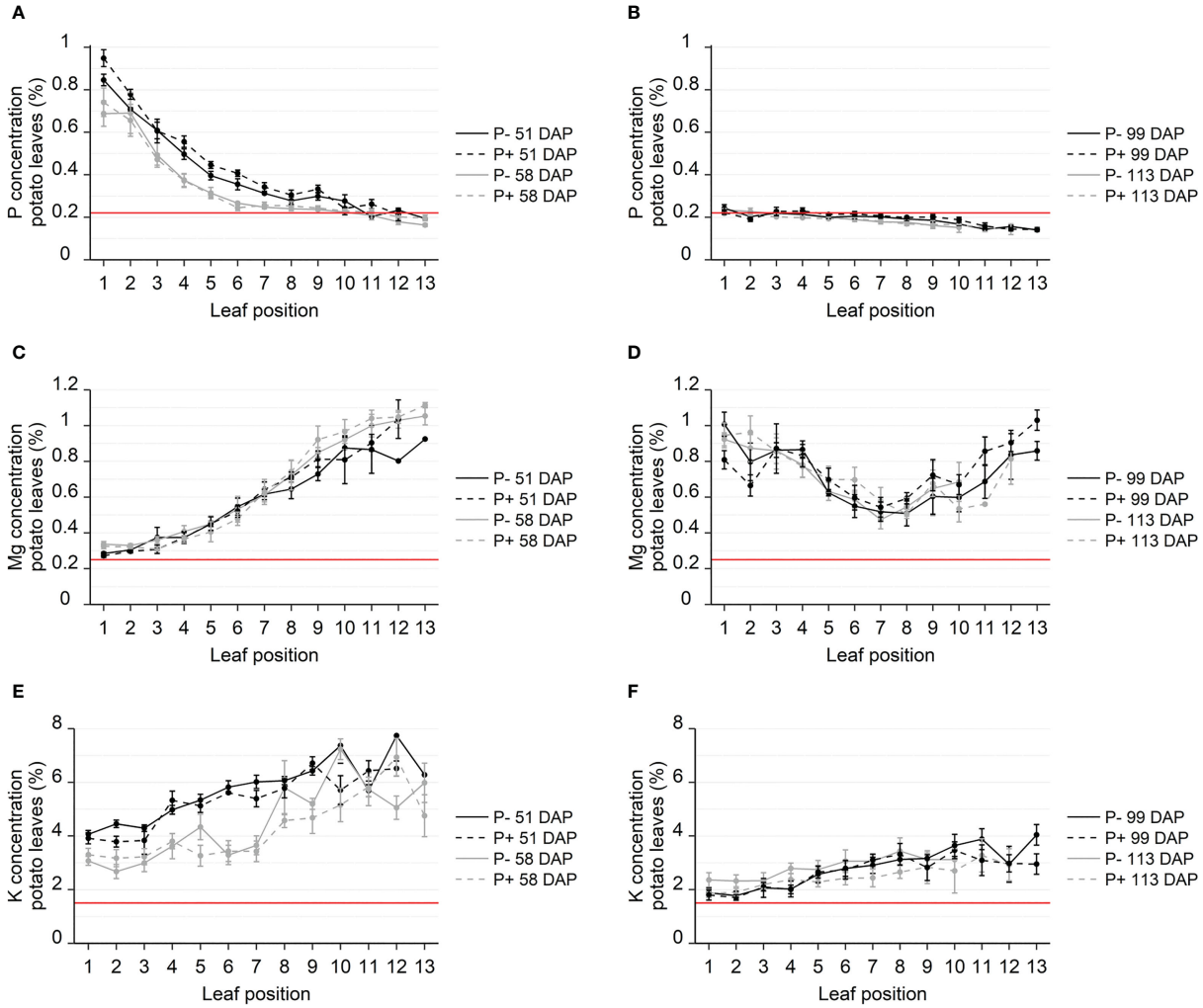

FIGURE 2
Concentration of P **(A, B)**, Mg **(C, D)** and K **(E, F)** in leaves from field grown potato. Leaves sampled from four replicate plants throughout the growing season, 51-113 days after planting (DAP), during tuber initiation **(A, C, E)** or tuber bulking **(B, D, F)**. Nutrient concentrations were analyzed using ICP-MS and reported in %. Leaf positions specify the location of the leaf on the plant with lower numbers being the topmost, younger leaves and higher numbers indicating increasing leaf age. Red lines show standard threshold values for deficiencies for each nutrient in potato. Error bars show SEM (n = 4).

S3). While the younger leaves had the highest P concentrations, they had the lowest Mg and K concentrations, (Figures 2C, E). The youngest leaves had Mg concentrations slightly above the critical Mg concentration of 0.25%, while Mg concentrations in leaf 11-13 were four times higher, peaking at around 1%. Similar to Ca and Mn, Mg concentrations did not decrease between 51 and 58 DAP. During tuber bulking, Mg concentrations in leaf 7 had fallen to 0.51%, while both older and younger leaves contained high levels of Mg (up to 0.81-1.0%) (Figure 2D). The K concentration decreased systematically over time. In the span of one week during tuber initiation, K concentrations were significantly reduced in all leaves (Figure 2E), similar to the P concentrations. The K concentrations had fallen by 50% at the time of tuber bulking 113 DAP (Figure 2F). In the time between tuber initiation and tuber bulking, the K concentration decreased from 4% to 1.7% in the youngest leaves and from 7% to 4% in the oldest.

These data indicate that the results of leaf nutrient analyses are highly dependent on leaf position and time of sampling, more so than on the availability of nutrients in the soil.

3.2 Diagnosis of P status with chlorophyll *a* fluorescence

Prior to the elemental analysis shown in Figure 2, chlorophyll *a* fluorescence was measured to generate P-predicts for all leaf positions. P-predict values are used to estimate the P status in plants, where values below 0.4 indicate a P concentration below the critical P concentration. Correlating P-predicts with leaf P concentrations during tuber initiation (51 DAP) shows that according to both P concentrations and P-predict values, 72% of the leaves were not P deficient (Figures 2A, 3A). Only 8% of the

leaves were classified as being P deficient according to both P-predict and leaf concentration, while 19.5% of the leaves were misclassified by P-predicts. Strikingly, the rate of P-predict misclassification increased to 43% at 58 DAP. Most of the misclassifications on both days came from P-predicts indicating P deficiency, although leaf concentrations were above the critical P concentration. At 51 DAP, most of the leaves misclassified as deficient by P-predict had relatively low P concentrations between 0.22% and 0.4%. At 58 DAP, leaves 1-11 were frequently misclassified as P deficient by P-predict, irrespective of their P concentration (Figure 3B). At 51 DAP, the P-predicts were highest in the YFELs at position 4-5, while the youngest, not fully expanded, leaf positions 1-3 showed decreasing P-predict values despite having the highest P concentrations. Two replicates of leaf 1 had P concentrations of nearly 1% but were classified as deficient by their P-predicts.

Given the increasing number of misclassifications, it is clear that the reliability of the P-predict as a diagnostic tool was affected prior to day 58. This indicates a disturbance in the photosynthetic machinery, as chlorophyll *a* fluorescence is tightly correlated with the linear electron flow from PSII to PSI. Besides nutrient deficiencies, fluorescence emissions can also be affected by stressors such as light or temperature. The irradiance was significantly higher on day 58 compared to day 51, which was likely contributing to the higher rate of misclassified P-predicts (Supplementary Figure S4). During fluorescence measurements on day 51, the irradiance fluctuated around 600 PAR, with single spikes at 1600, while the irradiance was significantly higher at 1400-1500 PAR on day 58, with short dips when clouds passed. Similarly, the air temperature was 26°C on day 50 and 51, but 32°C on day 57 and 58 (Supplementary Figure S5).

The fluorescence transients serving as input to the P-predict calculations were severely distorted on day 58, especially in the young and mid-level leaves (positions 1-7). These leaves represent the most sun-exposed parts of the plant, and their fluorescence transients lost their J- and I-steps and instead developed D-dips where the I-step is usually located. The transients of the older leaves, deep in the shaded canopy looked normal (Figure 4A).

To avoid light stress and potential photoinhibition, some plants were shaded from day 51, which resulted in normal transients and reliable P-predict values on day 58. The transients of shaded leaves showed distinct OJIP steps on day 58 and were markedly different from the distorted transients in the same leaf positions in unshaded plants (Figure 4B). The shading decreased the irradiance from 1400 to 600 PAR, while the temperature inside and outside the shaded areas were nearly identical. P-predict values ranged from –2 to 2 (average –0.07 ± 0.65) in the unshaded leaf 4, while shading of leaf 4 improved P-predict values to 0.62 ± 0.03. Shading thus enabled a correct P-predict diagnosis (Figure 4B).

4 Discussion

4.1 Distinct patterns of remobilization

In this study, we observed a steep gradient of leaf P concentrations through the canopy. The youngest leaves had a high P concentration during tuber initiation, while the older leaves had concentrations around or just above 0.22% (Figure 2A). When the nutrient supply becomes limiting, it is often observed that young leaves retain high nutrient levels at the expense of older leaves due to remobilization (Smith and Loneragan, 1997). In the current experiment, the observed P depletion of the older leaves was caused by a substantial remobilization of P from source to sink tissue, i.e. to the young leaves and the developing tubers of the potato plant. During tuber initiation, the P concentration in the YFEL fell by 25-33% in the span of just one week, indicating a large remobilization from shoot to tuber. Later in the growing season, during the tuber bulking period, all leaves ended up near or just below the critical P concentration of 0.22% which indicated that the shoot P was remobilized to the tubers and settling at the critical P concentration. The timing and leaf sampling prior to

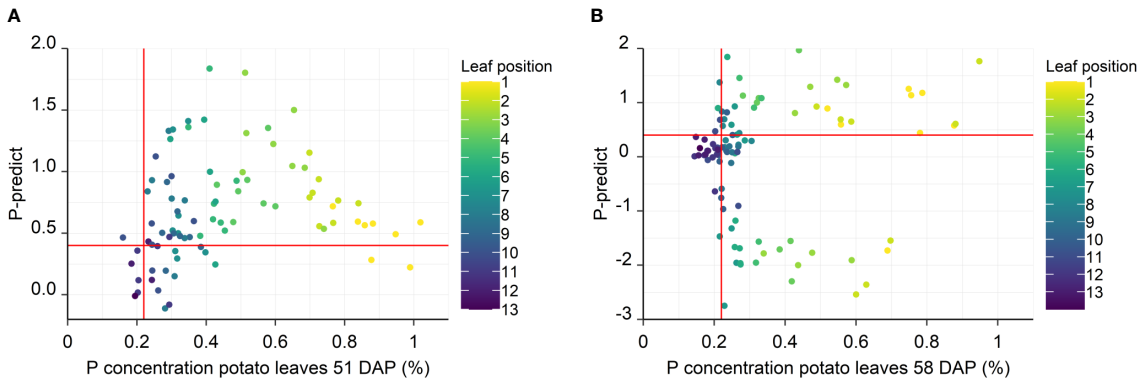

FIGURE 3
P-predict values correlated with the leaf P concentration at 51 DAP **(A)** and 58 DAP **(B)**. Each point corresponds to one measured leaf, color coded for leaf position. The vertical red line indicates the P concentration threshold for P deficiency at 0.22%, while the horizontal line represents the P-predict level indicating P deficiency at 0.4. Points located in the upper-left and lower-right are thus misclassified as being P sufficient or P deficient, respectively. 51 DAP: n = 90, 58 DAP: n = 97.

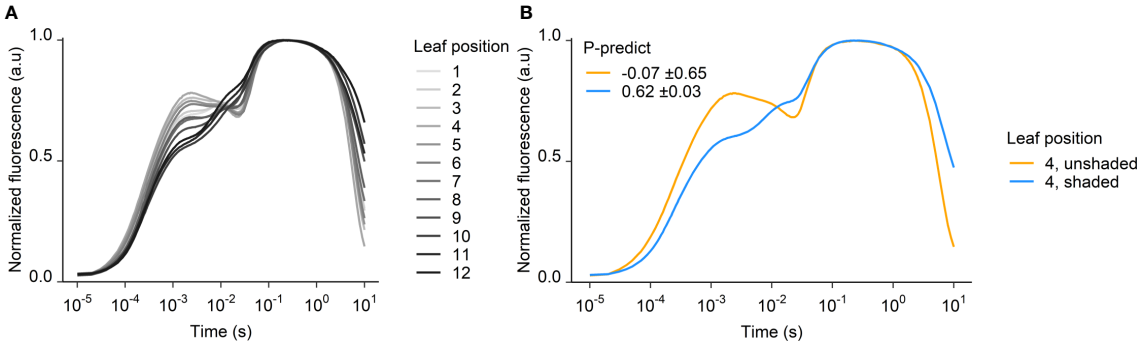

FIGURE 4
Fluorescence transients from 58 DAP at **(A)** different leaf positions and **(B)** shaded and unshaded YFEL. P-predict ± SEM is inserted for shaded and unshaded leaves in **(B)** (n = 4).

measurements is therefore incredibly important for a meaningful interpretation of leaf analysis data.

Interestingly, K and Mg distribution presented opposite patterns compared to P. The concentration of K and Mg were highest in the older leaves and did not exhibit deficiency levels in the late season. This indicates a sufficient K and Mg availability, even though the concentration of K fell significantly between 51 and 58 DAP and was close to the critical K concentration in the youngest leaves 113 DAP.

It is remarkable that the distribution patterns of K and Mg resemble those of the phloem immobile nutrients Ca and Mn during tuber bulking, despite Mg and K presumably having a high phloem mobility similar to that of P (Supplementary Figures S2, S3). P concentration in tubers at harvest was 0.15% (Supplementary Table S1), and from Figure 2B it is clear that P was remobilized fully until it reached the critical P concentration of the shoot. This did not occur to the same extent for Mg and K and indicates that the tubers were a stronger sink for P than for Mg and K (Figures 2D, F). This is likely because the primary involvement of K and Mg in starch synthesis occurs through phloem loading of photosynthates in the shoots. P is also engaged in phloem loading but is remobilized to the tubers due to a key-functionality in activating enzymes of the starch synthesis pathway in the amyloplasts (MacNeill et al., 2017).

However, although we observed remobilization of P from old to younger tissue, it is not clear whether P availability was actually limited in this experiment. In fact, no differences could be observed between fertilized and unfertilized plots, neither in P-predicts, P concentrations nor in the final yields. Across both treatments, we only observed P concentrations below 0.22% in the older leaves on the later sampling dates. The missing response to P fertilization could indicate that the availability of P from residual pools in the soil made the applied fertilizer P redundant. This has previously been observed during optimal water conditions, and is therefore a likely observation in the current study (Potarzycki and Grzebisz, 2019). It is also possible that the buffering capacity of the soil was sufficient to supply the plants with enough P to satisfy the functional requirement, although it would be unexpected, as the field was chosen due to a history of P fertilization responses.

The lack of fertilizer effect could also imply that the applied P was immobilized and not available for uptake by the roots. It is therefore unclear if the low P concentrations measured in the older leaves in the early growing season, and in all leaves in the late growing season, should be classified as a nutrient deficiency or a normal physiological consequence of massive P remobilization to the tubers. Once the shoot has become a P source for tuber development, any further P uptake is not likely to be reflected in leaf concentrations as it will be directed towards the tubers. The P response, which was not achieved under field conditions, could certainly have been obtained under controlled conditions (climate chamber or greenhouse). However, this would clearly have omitted all interactions with the environment that are so essential for an appropriate and "real-life" assessment of the P-predict method.

4.2 Diagnosing nutrient deficiencies

The nutrient concentrations are highly dynamic and observed to change drastically within a few days, which essentially prevents meaningful data interpretation based on single leaf analysis. Furthermore, the nutrient demand of plants fluctuates during a growth cycle, and a tissue analysis cannot foresee if deficiencies will arise later in the season. The tissue concentration would therefore need to be regularly monitored, which is both labor and cost intensive. The critical P concentration of 0.22% in the YFEL is widely used as a threshold for diagnosing P deficiency (Rosen et al., 2014). This critical P concentration is set for mid- to late season potatoes, but the critical concentration is higher in the early growth stages (Walworth and Muniz, 1993; Huett et al., 1997). The critical concentration of 0.22% corresponds well with the concentration at which most leaves are classified as deficient by P-predict. The P concentration in the YFEL of P sufficient potato plants decreases from 0.6% in early season to 0.4% in mid-season and 0.2% in late season (Walworth and Muniz, 1993). A concentration of 0.3% might therefore be indicative of P deficiency in the early growth phases, but not in the late growing season. In this study, the YFEL (leaf 4) had a P concentration around 0.4% in the mid-season (51

and 58 DAP), which would also be deemed sufficient by these standards.

When chlorophyll *a* fluorescence is measured, thresholds are also used to evaluate the P status of plants. The fluorescence parameter P-predict is used to indicate when P deficiency physiologically affects the functionality of the photosynthetic processes in the plants (Frydenvang et al., 2015; Carstensen et al., 2018a). In this study, the different leaf positions presented a wide range of P status, from severely deficient in the older leaves late in the season to very high concentrations in the youngest leaves early in the season. A positive correlation between leaf P concentration and P-predict was observed for leaf positions 4-13 (Figure 3A). However, the three youngest leaves had lower P-predicts despite having higher P-concentrations. These leaves are not yet fully evolved and have thus not yet transitioned from being sink to source tissue which is reflected in the fluorescence signal. Measuring a fully expanded leaf is therefore necessary for correct classification of P status.

The advantages of chlorophyll-based diagnosis in field settings, as an alternative to measuring the nutrient concentration in leaves, include the cheap cost and rapid on-site classification compared to plant tissue analysis by external laboratories, where it can take up to several weeks to receive the result of tissue sampling. Obtaining data about the crop nutrient status in real time will allow immediate fertilization efforts to alleviate P deficiencies, before the deficiency can affect yield outcomes.

It can be valuable to measure tissue P concentration during the growing season to add P fertilizers in response to low P status (Rosen et al., 2014), and P concentration and yields have been found to correlate (Fernandes et al., 2014). Yet, research has also shown that macronutrient concentrations in leaves can be poor indicators of yield, for both P (White et al., 2018) and N (Grzebisz et al., 2020). White et al. (2018) grew 66 potato genotypes and found a positive effect of P fertilization on both yield and leaf P concentration. However, within the tested cultivars there was no correlation between P concentration in the YFEL and tuber yields. In previous studies, P concentration and P-predict could only predict yield effects in the first few weeks of the barley growing season (Carstensen et al., 2018b). Later in the season, the size of the plant had adjusted to the available P levels, and the P status of each leaf was therefore at sufficient levels, despite a significant yield response. In this study, a transient P effect of P fertilization was observed during the early tuber initiation phase (Figure 2A) but disappeared at the next sampling time 7 days later. The transient P response indicates that the plant adapts its size to the available P. However, in this case P fertilization would be expected to influence measured yield which was not found.

4.3 Photoinhibition and shading

Despite the high correlation between leaf P concentration and P-predict on day 51, field grown crops are often exposed to environmental stresses which may interfere with chlorophyll *a* fluorescence. In this study we observed that high solar irradiance (>1400 PAR) on measurement days impaired the reliability of the fluorescence-based diagnosis of P status. The chlorophyll *a* fluorescence response in the leaves were severely affected, leading to erroneous P-predict estimates of P status. The fluorescence transients showed indications of photoinhibition, including the development of D-dips in the OJIP transients following the I-step at approximately 0.07 seconds (Figure 4). The D-dips that developed at day 58 under high irradiance might be related to degradation of the Mn cluster of the oxygen evolving complex at PSII (Pospíšil and Dau, 2000; Schmidt et al., 2016a). D-dips have also been observed in transients of Mn deficient plants, which are severely affected by photoinhibition (Schmidt et al., 2016b). Photoinhibition is a light-induced inhibition of PSII. It is a mechanism plants employ to protect the photosystems from photodamage caused by excess energy from absorbed light and is part of non-photochemical fluorescence quenching (NPQ). The primary components of NPQ respond to thylakoid lumen acidification and reverse quickly during dark adaptation. Photoinhibition (qI), however, is only induced over prolonged exposure to excess light, and is caused by inactivation or degradation of the D1 subunit of PSII, or from permanent damage to the photosynthetic systems (Ruban, 2016; Guidi et al., 2019). It therefore reverses slowly, over the span of hours or days, as the reversion depends on D1 repair mechanisms. In order to understand the cause of the distorted transients at the mechanistic level, detailed PAM fluorometry would be required to identify the individual NPQ components (qE, qT, qI). Moreover, to further elucidate the correlations between high light intensity and the shape of the distorted transients, it would be necessary to perform experiments with a range of light levels and plant P tissue levels under controlled growth conditions. Such experiments could determine the intensity at which high light causes distortion at a given P status, and how low the intensity should be to subsequently restore the fluorescence transients for diagnosis of nutrient status.

To understand the cause of the distorted transients in the field, some plants were shaded for one week prior to measuring chlorophyll a fluorescence on a day with high light intensity. In this experiment it was observed that shading the plants resulted in fluorescence transients comparable to those obtained at low light, either measured on a cloudy day or on the leaves shaded in the canopy (Figures 3, 4). Leaves deep in the canopy will always be shaded, and as a result their transients will be unaffected by photoinhibition, which consequently makes them useful for diagnosing P status. However, these older leaves without exposure to high light were P depleted early in the season due to P remobilization, and a diagnosis based on these leaves would therefore indicate P deficiency, even when the plant might be fully supplied with P. In effect, measuring chlorophyll a fluorescence for diagnosis of nutrient status should be avoided on days with extreme light intensity. If this is not possible, it will therefore be necessary to shade the plants for several hours prior to chlorophyll *a* based diagnosis of P status.

In order to use these techniques for reliable diagnosis of P deficiency and fertilizer planning, P status needs to be monitored throughout the season. Due to the highly dynamic P concentrations, meaningful interpretation is incredibly challenging when using the traditionally established critical P concentrations. Chlorophyll *a* fluorescence analysis provides a cheaper and immediate diagnosis, but threshold values for P-predict at the different growth stages are not yet established. Furthermore, interpretation of both methods is

complicated by the highly dynamic P concentrations and thresholds for P deficiency which vary throughout the growth season.

5 In conclusion

While the traditional practice of measuring tissue concentrations gives an exact measure of the P content of the plant, the interpretation is not straightforward. The nutrient concentrations in potato plants are highly dynamic, with large variations over time and across different leaf positions. Attention to sampling time is therefore incredibly important for a meaningful interpretation, as P concentrations fell by 19-40% in the span of just 7 days during tuber initiation. The picture is further complicated when attempting to characterize the status of several nutrients at once, as the distribution of different nutrients are distinctly different, even when comparing nutrients which are generally considered to be equally phloem mobile, such as P, Mg and K. In the current experiment, the tubers acted as a strong sink for P and to a lesser degree K, consequently depleting the shoot of these nutrients to deficiency levels at the end of the growing season. Thus, frequent sampling and analysis are required to monitor the P status of potatoes and to prevent P deficiency from occurring.

This study shows that chlorophyll *a* fluorescence is able to rapidly estimate the bioactive P pool across a range of leaf positions to characterize the P status of field grown potatoes. However, in the field high solar irradiation may affect the photosynthetic machinery, induce photoinhibition, and thereby disturb the resulting fluorescence signals. It was shown that photoinhibition may be reversed by shading the plants. Future research should investigate the interactions between NPQ and leaf P status at different PAR to potentially develop an algorithm capable of delivering P-predicts at high light.

Data availability statement

The raw data supporting the conclusions of this article will be made available by the authors, without undue reservation.

Author contributions

ST and AS designed and carried out the experiments. AS did the data analysis, ST and PM wrote the manuscript, and SH designed the experiments and reviewed the manuscript. All authors contributed to the article and approved the submitted version.

Funding

This work is supported by Innovation Fund Denmark (Grand Solution Programs, grant 7045-00010A).

Acknowledgments

The field work was assisted by staff at Plant and Soil Section, University of Copenhagen: Francesco Minutello, Andrea Pinna, Thomas Hesselhøj Hansen, Mette Sylvan, and Birgit Andersen. ICP measurements were performed by Thomas Hesselhøj Hansen and Lena Byrgesen. Thanks to BJ Agro, Hovorg, Denmark, for competent assistance with setting up and maintaining the field trials, and their generous hospitality throughout the experimental period.

Conflict of interest

Author SH is co-founder of SpectraCrops ApS, marketing hand-held devices to diagnose P deficiency under field conditions using chlorophyll a fluorescence analysis. It should be noted that similar OJIP transients, as the ones recorded in this study, can be obtained by a wide range of standard chlorophyll a fluorescence instruments, including Photon Systems Instruments PSI, Walz, Hansatech, Opti Sciences, Phenospex and MultispeQ.

The remaining authors declare that the research was conducted in the absence of any commercial or financial relationships that could be construed as a potential conflict of interest.

Publisher's note

Supplementary material

The Supplementary Material for this article can be found online at: https://www.frontiersin.org/articles/10.3389/fpls.2023.1100318/full#supplementary-material

References

Birch, P. R. J., Bryan, G., Fenton, B., Gilroy, E. M., Hein, I., Jones, J. T., et al. (2012). Crops that feed the world 8: potato: are the trends of increased global production sustainable? *Food Secur.* 4 (4), 477–508. doi: 10.1007/s12571-012-0220-1

Cakmak, I., Hengeler, C., and Marschner, H. (1994). Changes in phloem export of sucrose in leaves in response to phosphorus, potassium and magnesium deficiency in bean plants. *J. Exp. Bot.* 45 (9), 1251–1257. doi: 10.1093/jxb/45.9.1251

Carstensen, A., Herdean, A., Schmidt, S. B., Sharma, A., Spetea, C., Pribil, M., et al. (2018a). The impacts of phosphorus deficiency on the photosynthetic electron transport chain. *Plant Physiol.* 177 (1), 271–284. doi: 10.1104/pp.17.01624

Carstensen, A., Szameitat, A. E., Frydenvang, J., and Husted, S. (2018b). Chlorophyll a fluorescence analysis can detect phosphorus deficiency under field conditions and is an effective tool to prevent grain yield reductions in spring barley (Hordeum vulgare l.). *Plant Soil* 434 (1-2), 79–91. doi: 10.1007/s11104-018-3783-6

Ceylan, Y., Kutman, U. B., Mengutay, M., and Cakmak, I. (2016). Magnesium applications to growth medium and foliage affect the starch distribution, increase the grain size and improve the seed germination in wheat. *Plant Soil* 406 (1-2), 145–156. doi: 10.1007/s11104-016-2871-8

Chen, A., Hansen, T. H., Olsen, L. I., Palmgren, M., Husted, S., Schjoerring, J. K., et al. (2020). Towards single-cell ionomics: a novel micro-scaled method for multi-element analysis of nanogram-sized biological samples. *Plant Methods* 16, 31. doi: 10.1186/s13007-020-00566-9

Christel, W., Lemming, C., Mundus, S., Bruun, S., Magid, J., and Jensen, L. S. (2016). Measuring phosphorus availability in recently fertilized soils with the diffusive gradient in thin films (DGT) method – challenges and opportunities. *Commun. Soil Sci. Plant Anal.* 47 (5), 563–570. doi: 10.1080/00103624.2016.1141920

de Bang, T. C., Husted, S., Laursen, K. H., Persson, D. P., and Schjoerring, J. K. (2021). The molecular-physiological functions of mineral macronutrients and their consequences for deficiency symptoms in plants. *New Phytol.* 229 (5), 2446–2469. doi: 10.1111/nph.17074

Fernandes, A. M., Soratto, R. P., and Pilon, C. (2014). Soil phosphorus increases dry matter and nutrient accumulation and allocation in potato cultivars. *Am. J. Potato Res.* 92 (1), 117–127. doi: 10.1007/s12230-014-9422-8

Frydenvang, J., van Maarschalkerweerd, M., Carstensen, A., Mundus, S., Schmidt, S. B., Pedas, P. R., et al. (2015). Sensitive detection of phosphorus deficiency in plants using chlorophyll a fluorescence. *Plant Physiol.* 169 (1), 353–361. doi: 10.1104/pp.15.00823

Geigenberger, P. (2011). Regulation of starch biosynthesis in response to a fluctuating environment. *Plant Physiol.* 155 (4), 1566–1577. doi: 10.1104/pp.110.170399

Grzebisz, W., Frąckowiak, K., Potarzycki, J., Diatta, J., and Szczepaniak, W. (2020). The unexploited potential of nutrient analysis in potato tissues at the onset of tuberization for tuber yield prediction. *Agronomy* 10 (1), 103. doi: 10.3390/agronomy10010103

Grzebisz, W., Potarzycki, J., and Biber, M. (2018). The early prognosis of tuber yield based on nitrogen status in potato tops. *Plant Soil Environ.* 64 (11), 539–545. doi: 10.17221/388/2018-PSE

Guidi, L., Lo Piccolo, E., and Landi, M. (2019). Chlorophyll fluorescence, photoinhibition and abiotic stress: does it make any difference the fact to be a C3 or C4 species? *Front. Plant Sci.* 10, 174. doi: 10.3389/fpls.2019.00174

Hammond, J. P., and White, P. J. (2008). Sucrose transport in the phloem: integrating root responses to phosphorus starvation. *J. Exp. Bot.* 59 (1), 93–109. doi: 10.1093/jxb/erm221

Hermans, C., Bourgis, F., Faucher, M., Strasser, R. J., Delrot, S., and Verbruggen, N. (2005). Magnesium deficiency in sugar beets alters sugar partitioning and phloem loading in young mature leaves. *Planta* 220 (4), 541–549. doi: 10.1007/s00425-004-1376-5

Hopkins, B. G., Horneck, D. A., and MacGuidwin, A. E. (2014). Improving phosphorus use efficiency through potato rhizosphere modification and extension. *Am. J. Potato Res.* 91 (2), 161–174. doi: 10.1007/s12230-014-9370-3

Horneck, D. A., and Rosen, C. J. (2008). Measuring nutrient accumulation rates of potatoes - tools for better management. *Better Crops* 92 (1), 4–6.

Huett, D. O., Maier, N. A., Sparrow, L. A., and Piggott, T. J. (1997). "Vegetable crops," in *Plant analysis: an interpretation manual*. Eds. D. J. Reuter and J. B. Robinson (Collingwood, Australia: CSIRO Publishing).

Jenkins, P. D., and Ali, H. (2000). Phosphate supply and progeny tuber numbers in potato crops. *Ann. Appl. Biol.* 136 (1), 41–46. doi: 10.1111/j.1744-7348.2000.tb00007.x

Katoh, A., Ashida, H., Kasajima, I., Shigeoka, S., and Yokota, A. (2015). Potato yield enhancement through intensification of sink and source performances. *Breed Sci.* 65 (1), 77–84. doi: 10.1270/jsbbs.65.77

Kautsky, H., and Hirsch, A. (1931). Neue versuche zur kohlensäureassimilation. *Naturwissenschaften* 19, 964. doi: 10.1007/BF01516164

Koch, M., Busse, M., Naumann, M., Jakli, B., Smit, I., Cakmak, I., et al. (2019a). Differential effects of varied potassium and magnesium nutrition on production and partitioning of photoassimilates in potato plants. *Physiol. Plant* 166 (4), 921–935. doi: 10.1111/ppl.12846

Koch, M., Naumann, M., Pawelzik, E., Gransee, A., and Thiel, H. (2019b). The importance of nutrient management for potato production part I: plant nutrition and yield. *Potato Res.* 63 (1), 97–119. doi: 10.1007/s11540-019-09431-2

MacNeill, G. J., Mehrpouyan, S., Minow, M. A. A., Patterson, J. A., Tetlow, I. J., Emes, M. J., et al. (2017). Starch as a source, starch as a sink: the bifunctional role of starch in carbon allocation. *J. Exp. Bot.* 68 (16), 4433–4453. doi: 10.1093/jxb/erx291

Mundus, S., Carstensen, A., and Husted, S. (2017). Predicting phosphorus availability to spring barley (hordeum vulgare) in agricultural soils of Scandinavia. *Field Crops Res.* 212, 1–10. doi: 10.1016/j.fcr.2017.06.026

Naumann, M., Koch, M., Thiel, H., Gransee, A., and Pawelzik, E. (2019). The importance of nutrient management for potato production part II: plant nutrition and tuber quality. *Potato Res.* 63 (1), 121–137. doi: 10.1007/s11540-019-09430-3

Noda, T., Kottearachchi, N. S., Tsuda, S., Mori, M., Takigawa, S., Matsuura-Endo, C., et al. (2007). Starch phosphorus content in potato (Solanum tuberosum l.) cultivars and its effect on other starch properties. *Carbohydr. Polymers* 68 (4), 793–796. doi: 10.1016/j.carbpol.2006.08.005

Pospíšil, P., and Dau, H. (2000). Chlorophyll fluorescence transients of photosystem II membrane particles as a tool for studying photosynthetic oxygen evolution. *Photosynthesis Res.* 65 (1), 41–52. doi: 10.1023/A:1006469809812

Potarzycki, J., and Grzebisz, W. (2019). Trends in phosphorus concentrations in potato organs during the growing season. *J. Elementology* 24(3), 935–952. doi: 10.5601/jelem.2019.24.1.1777

Rosen, C. J., and Bierman, P. M. (2008). Potato yield and tuber set as affected by phosphorus fertilization. *Am. J. Potato Res.* 85 (2), 110–120. doi: 10.1007/s12230-008-9001-y

Rosen, C. J., Kelling, K. A., Stark, J. C., and Porter, G. A. (2014). Optimizing phosphorus fertilizer management in potato production. *Am. J. Potato Res.* 91 (2), 145–160. doi: 10.1007/s12230-014-9371-2

Rubæk, G. H. (2015). "Validity and analytical robustness of the Olsen soil p test and other agronomic soil p tests used in northern Europe," in *DCA report* (Tjele, Denmark: DCA - Danish Centre for Food and Agriculture), 071.

Ruban, A. V. (2016). Nonphotochemical chlorophyll fluorescence quenching: mechanism and effectiveness in protecting plants from photodamage. *Plant Physiol.* 170 (4), 1903–1916. doi: 10.1104/pp.15.01935

Schmidt, S. B., Jensen, P. E., and Husted, S. (2016a). Manganese deficiency in plants: the impact on photosystem II. *Trends Plant Sci.* 21 (7), 622–632. doi: 10.1016/j.tplants.2016.03.001

Schmidt, S. B., Powikrowska, M., Krogholm, K. S., Naumann-Busch, B., Schjoerring, J. K., Husted, S., et al. (2016b). Photosystem II functionality in barley responds dynamically to changes in leaf manganese status. *Front. Plant Sci.* 7, 1772. doi: 10.3389/fpls.2016.01772

Smith, F. W., and Loneragan, J. F. (1997). "Interpretaton of plant analysis: comcepts and principles," in *Plant analysis: an interpretation manual*. Eds. D. J. Reuter and J. B. Robinson (Collingwood Australia: CSIRO Publishing), 1–34.

Tandy, S., Mundus, S., Yngvesson, J., de Bang, T. C., Lombi, E., Schjoerring, J. K., et al. (2011). The use of DGT for prediction of plant available copper, zinc and phosphorus in agricultural soils. *Plant Soil* 346 (1-2), 167–180. doi: 10.1007/s11104-011-0806-y

Tanner, C. B., Weis, G. G., and Curwen, D. (1982). Russet burbank rooting in sandy soils with pans following deep plowing. *Am. Potato J.* 59, 107–112. doi: 10.1007/BF02866365

Tindall, T. A., Westerman, D. T., Stark, J. C., Ojala, J. C., and Kleinkopf, G. E. (1993). *Phosphorus nutrition of potatoes* Vol. 903 (Idaho, USA: University of Idaho College of Agriculture, Current information series).

Verbruggen, N., and Hermans, C. (2013). Physiological and molecular responses to magnesium nutritional imbalance in plants. *Plant Soil* 368 (1-2), 87–99. doi: 10.1007/s11104-013-1589-0

Walworth, J. L., and Muniz, J. E. (1993). A compendium of tissue nutrient concentrations for field-grown potatoes. *Am. Potato J.* 70, 579–597. doi: 10.1007/BF02850848

White, P. J., Bradshaw, J. E., Brown, L. K., Dale, M. F. B., Dupuy, L. X., George, T. S., et al. (2018). Juvenile root vigour improves phosphorus use efficiency of potato. *Plant Soil* 432 (1-2), 45–63. doi: 10.1007/s11104-018-3776-5

Zotarelli, L., Dukes, M. D., and Morgan, K. T. (2019). "Interpretation of soil moisture content to determine soil field capacity and avoid over-irrigating sandy soils using soil moisture sensors #AE460," in *Agricultural and biological engineering department, UF/IAS extension* (Florida, USA: University of Florida).

frontiers | Frontiers in Plant Science

TYPE Original Research
PUBLISHED 26 June 2023
DOI 10.3389/fpls.2023.1018984

OPEN ACCESS

EDITED BY
Petra Bauer,
Heinrich Heine University of Düsseldorf, Germany

REVIEWED BY
Toshiro Shigaki,
The University of Tokyo, Japan
Agnieszka Sirko,
Polish Academy of Sciences, Poland

*CORRESPONDENCE
Tzu-Yin Liu
tzliu@life.nthu.edu.tw

†These authors have contributed equally to this work and share first authorship

RECEIVED 14 August 2022
ACCEPTED 23 May 2023
PUBLISHED 26 June 2023

CITATION
Lin L-Y, Chow H-X, Chen C-H, Mitsuda N, Chou W-C and Liu T-Y (2023) Role of autophagy-related proteins ATG8f and ATG8h in the maintenance of autophagic activity in *Arabidopsis* roots under phosphate starvation.
Front. Plant Sci. 14:1018984.
doi: 10.3389/fpls.2023.1018984

Role of autophagy-related proteins ATG8f and ATG8h in the maintenance of autophagic activity in *Arabidopsis* roots under phosphate starvation

Li-Yen Lin[1†], Hong-Xuan Chow[1†], Chih-Hao Chen[1], Nobutaka Mitsuda[2], Wen-Chun Chou[1] and Tzu-Yin Liu[1,3*]

[1]Institute of Bioinformatics and Structural Biology, College of Life Sciences and Medicine, National Tsing Hua University, Hsinchu, Taiwan, [2]Bioproduction Research Institute, National Institute of Advanced Industrial Science and Technology (AIST), Tsukuba, Japan, [3]Department of Life Science, College of Life Sciences and Medicine, National Tsing Hua University, Hsinchu, Taiwan

Nutrient starvation-induced autophagy is a conserved process in eukaryotes. Plants defective in autophagy show hypersensitivity to carbon and nitrogen limitation. However, the role of autophagy in plant phosphate (Pi) starvation response is relatively less explored. Among the core autophagy-related (*ATG*) genes, *ATG8* encodes a ubiquitin-like protein involved in autophagosome formation and selective cargo recruitment. The *Arabidopsis thaliana ATG8* genes, *AtATG8f* and *AtATG8h*, are notably induced in roots under low Pi. In this study, we show that such upregulation correlates with their promoter activities and can be suppressed in the *phosphate response 1* (*phr1*) mutant. Yeast one-hybrid analysis failed to attest the binding of the *At*PHR1 transcription factor to the promoter regions of *AtATG8f* and *AtATG8h*. Dual luciferase reporter assays in *Arabidopsis* mesophyll protoplasts also indicated that *At*PHR1 could not transactivate the expression of both genes. Loss of *At*ATG8f and *At*ATG8h leads to decreased root microsomal-enriched ATG8 but increased ATG8 lipidation. Moreover, *atg8f/atg8h* mutants exhibit reduced autophagic flux estimated by the vacuolar degradation of ATG8 in the Pi-limited root but maintain normal cellular Pi homeostasis with reduced number of lateral roots. While the expression patterns of *AtATG8f* and *AtATG8h* overlap in the root stele, *AtATG8f* is more strongly expressed in the root apex and root hair and remarkably at sites where lateral root primordia develop. We hypothesize that Pi starvation-induction of *At*ATG8f and *At*ATG8h may not directly contribute to Pi recycling but rely on a second wave of transcriptional activation triggered by PHR1 that fine-tunes cell type-specific autophagic activity.

KEYWORDS

***Arabidopsis*, phosphate starvation, autophagy, autophagy-related protein 8 (ATG8), lateral root**

Introduction

Autophagy is a highly conserved catabolic process in eukaryotes that maintains cellular homeostasis and contributes to stress adaptation (Marshall and Vierstra, 2018; Gross and Graef, 2020). It begins with the induction and nucleation of isolation membranes, followed by the formation of cup-shaped pre-autophagosome structures called phagophores, which eventually mature into closed double-membrane autophagosomes (Yoshimoto and Ohsumi, 2018; Wun et al., 2020). During the process, damaged or dispensable cytoplasmic components, protein aggregates, and dysfunctional organelles are enclosed in the autophagosome (Yoshimoto and Ohsumi, 2018; Wun et al., 2020). As the autophagosome reaches the vacuole or the lysosome, its outer membrane fuses with the vacuolar/lysosomal membrane and releases the autophagic bodies for degradation (Yoshimoto and Ohsumi, 2018; Wun et al., 2020). The breakdown products are then recycled for energy production or usage in biosynthetic pathways (Yoshimoto and Ohsumi, 2018; Wun et al., 2020). The biogenesis of autophagosome is stepwise and dynamic, and is driven by a large number of autophagy-related (ATG) genes that can be categorized into four functional groups (Yoshimoto and Ohsumi, 2018; Wun et al., 2020). The ATG1/ATG13 kinase complex stimulates autophagosome formation in response to the phosphorylation status of ATG13 (Kamada et al., 2000; Suttangkakul et al., 2011). The class III phosphatidylinositol 3-kinase (PI3K) complex containing VACUOLAR PROTEIN SORTING 34 (VPS34), ATG6 and ATG14, incorporates the phosphatidylinositol 3-phosphate (PI3P) phospholipids into the expanding phagophore (Russell et al., 2013). The ATG2-ATG18-ATG9 complex localizes to the edge of phagophore and delivers the lipid molecules for its expansion (Mari and Reggiori, 2007; Zhuang et al., 2017). The ATG12 and ATG8 ubiquitin-like conjugation systems, which consist of the E1-like ATG7, the E2-like ATG3 and ATG10 and the E3-like ATG12-ATG5 conjugate together with ATG16, participate in autophagosome maturation (Geng and Klionsky, 2008). Of note, the ubiquitin-like protein ATG8, through its covalent conjugation to the lipid phosphatidylethanolamine (PE), plays a central role in both bulk and selective autophagy (Marshall and Vierstra, 2018; Bu et al., 2020). Although ATG8 interacts with diverse receptors or adaptor proteins to recruit specific cargos for degradation, autophagy-independent function of ATG8 has also been reported (Marshall and Vierstra, 2018; Bu et al., 2020). In addition, ATG8 is used as a reliable marker to monitor autophagic degradation activity upon the inhibition of vacuolar/lysosomal degradation by protease inhibitors (Klionsky et al., 2021).

Unlike a single-copy *ATG8* gene in yeast and algae, the plant *ATG8* gene family has significantly expanded and some members are upregulated under various biotic and abiotic stresses (Kellner et al., 2017; Bu et al., 2020; Qi et al., 2021). Selective interaction of various ATG8 isoforms (ATG8s) with their protein targets may contribute to the diversification of autophagy pathways in plants (Svenning et al., 2011; Kellner et al., 2017; Boycheva Woltering and Isono, 2020; Jung et al., 2020; Wu et al., 2021). In the model plant *Arabidopsis thaliana*, nine *ATG8* genes were identified and classified into three separate groups. Intriguingly, the *AtATG8h-i* group have a characteristic C-terminal exposed glycine residue that does not require ATG4 protease-dependent cleavage prior to their lipidation (Seo et al., 2016; Kellner et al., 2017). Although the analysis of the *At*ATG8 gene family is incomplete, the expression of several *At*ATG8 genes showed different yet partially overlapping patterns (Sláviková et al., 2005; Boycheva Woltering and Isono, 2020), supporting that different ATG8s share redundant roles while individual ATG8 members may have distinct and specific functions. Therefore, it remains challenging to distinguish the impact of each ATG8 isoform merely based on characterization of single knockouts due to functional redundancy.

Although most of the plant *ATG* genes are expressed at a ubiquitous and basal level, they can be induced by various developmental cues and environmental stimuli (Yoshimoto et al., 2004; Sláviková et al., 2005; Thompson et al., 2005; Rose et al., 2006; Peng et al., 2007; Chung et al., 2009; Avin-Wittenberg et al., 2018; Rodriguez et al., 2020; Qi et al., 2021). Ectopic overexpression of certain *ATGs* in plants successfully upregulated autophagy for plant fitness and stress tolerance (Xia et al., 2012; Li et al., 2015; Wang et al., 2016; Wang et al., 2017a; Wang et al., 2017b; Avin-Wittenberg et al., 2018; Minina et al., 2018; Sun et al., 2018a; Sun et al., 2018b). Compared to the extensive identification of transcription factors (TFs) regulating *ATGs* in animal and yeast cells, only a few TFs were discovered for their role in activation or repression of *ATGs* in plants. In cassava, WRKY20 was identified as a transcriptional activator of *ATG8a* (Yan et al., 2017). In nitrogen (N)-starved tomato leaves, the brassinosteroid (BR)-activated TF BRASSINAZOLE-RESISTANT1 (BZR1) binds to the promoters of *ATG2* and *ATG6* and induces autophagosome formation (Wang et al., 2019). The tomato heat shock TF HsfA1a was shown to upregulate the expression of *ATG10* and *ATG18f* and thereby inducing autophagy for drought tolerance (Wang et al., 2015). Recently, a study using yeast one-hybrid (Y1H) screening has revealed the binding of 225 TFs to the promoter of several *AtATG8s* (Wang et al., 2020). However, only the basic leucine-zipper protein TF TGA9 was further validated to transcriptionally upregulate the expression of *AtATG8b* and *AtATG8e* (Wang et al., 2020).

Inorganic phosphate (Pi) is an essential nutrient to plants for their growth and reproduction, but is poorly accessible to plants in most soils (Manning, 2008). To cope with the low availability of Pi, plants acquire a series of metabolic and morphological strategies, including enhancing Pi acquisition and remobilization, increasing exudation of organic acid and phosphatase, and remodeling of root architecture (Crombez et al., 2019; Wang et al., 2021; Paz-Ares et al., 2022). Several TFs were identified to be responsible for the regulation of Pi starvation-responsive (PSR) genes (Jain et al., 2012). Among them, PHOSPHATE STARVATION RESPONSE1 (PHR1) has been extensively studied and shown to act as a master regulator of PSR genes (Rubio et al., 2001; Bustos et al., 2010). In *Arabidopsis*, nearly 2,000 PSR genes are controlled by PHR1, perhaps *via* binding to the PHR1-binding sites (P1BS) (Castrillo et al., 2017). Although PHR1 is weakly transcriptionally responsive to low Pi stress, its activity is regulated by the nuclear SPX (SYG1/Pho81/XPR1) domain proteins (Bari et al., 2006; Puga et al., 2014; Wang et al., 2014). Moreover, an increased number of lateral roots is often regarded as a typical adaptive response to Pi limitation in *Arabidopsis* and in species that produce cluster roots (Desnos, 2008; Crombez et al., 2019). Such phenotypic change may generate a greater number of root tips to enlarge the potential hotspots for Pi uptake (Kanno et al., 2016). Nevertheless, the results from many other studies in *Arabidopsis* as well as in other species were occasionally in disagreement with the increased lateral root response upon Pi starvation (Crombez et al., 2019).

Compared to the wealth of investigations on carbon (C) and N starvation-induced autophagy (Avila-Ospina et al., 2014; Havé et al., 2017), the mechanism by which plant cells sense Pi limitation and induce autophagy is relatively less explored. An early study using tobacco BY-2 cells expressing aggregate-prone fluorescent proteins showed that Pi deprivation induced autophagy to remove the aggregates (Toyooka et al., 2006; Tasaki et al., 2014). Recent analysis of GFP-*At*ATG8a-labeled autophagic structures also suggested that low P induced the autophagosome formation in *Arabidopsis* root tips and such responses were exaggerated in the *pdr2* but attenuated in the *pdr2/ire1a* mutants, thereby linking Pi limitation-induced autophagy to the ER stress-dependent signaling pathway (Naumann et al., 2019). In addition, when Pi limitation was combined with a reduced C/N ratio, Rubisco-containing body (RCB)-mediated chlorophagy was induced (Yoshitake et al., 2021). Our recent study revealed that low Pi preferentially increased the autophagic flux in the differential zone of the *Arabidopsis* root and most *AtATG* genes are highly induced by N starvation but moderately upregulated by Pi starvation (Chiu et al., 2023). Among the *AtATG8* family, *AtATG8a*, *AtATG8f*, *AtATG8g* and *AtATG8h* were upregulated by Pi starvation in the shoot, but only *AtATG8f* and *AtATG8h* were strikingly upregulated in the Pi-deprived root (Chiu et al., 2023). In this study, we further investigated the Pi starvation-induced transcriptional regulation of *AtATG8f* and *AtATG8h* and their spatial expression patterns. We also explored the physiological implication of Pi starvation-induced upregulation of *AtATG8f* and *AtATG8h*. Characterization of the *atg8f/atg8h* double mutants showed that loss of *At*ATG8f and *At*ATG8h reduces the autophagic activities of root under Pi starvation but does not affect the cellular Pi levels. In addition, the *atg8f/atg8h* double mutants exhibited decreased number of lateral roots under both Pi-replete and Pi-deplete conditions but not under N-starved conditions. Although Pi starvation-induced upregulation of *AtATG8f* and *AtATG8h* is PHR1-dependent, the results of Y1H and dual luciferase analyses indicated that PHR1 may not directly transactivate these two genes. As *AtATG8f* and *AtATG8h* are strongly expressed in the root stele tissues and involved in the lateral root development, we hypothesize that PHR1 may act upstream of *At*ATG8f and *At*ATG8h to fine-tune the root cell type-specific autophagic activity under Pi starvation.

Results

Pi deficiency induces the expression of *AtATG8f* and *AtATG8h* in a *At*PHR1-dependent manner

Our recent study has revealed that Pi limitation upregulated the expression of *AtATG8f* and *AtATG8h* among the *ATG8* family (Chiu et al., 2023). We further monitored the expression of these two genes in the wild-type (WT) plants at 24-, 48-, and 72-hour time points following Pi deprivation as well as in the *pho1-2* mutant, which exhibits extremely low shoot levels of Pi (Poirier et al., 1991). The progressive increase of *AtATG8f* and *AtATG8h* transcripts during Pi limitation (Figure 1A) as well as the exacerbated

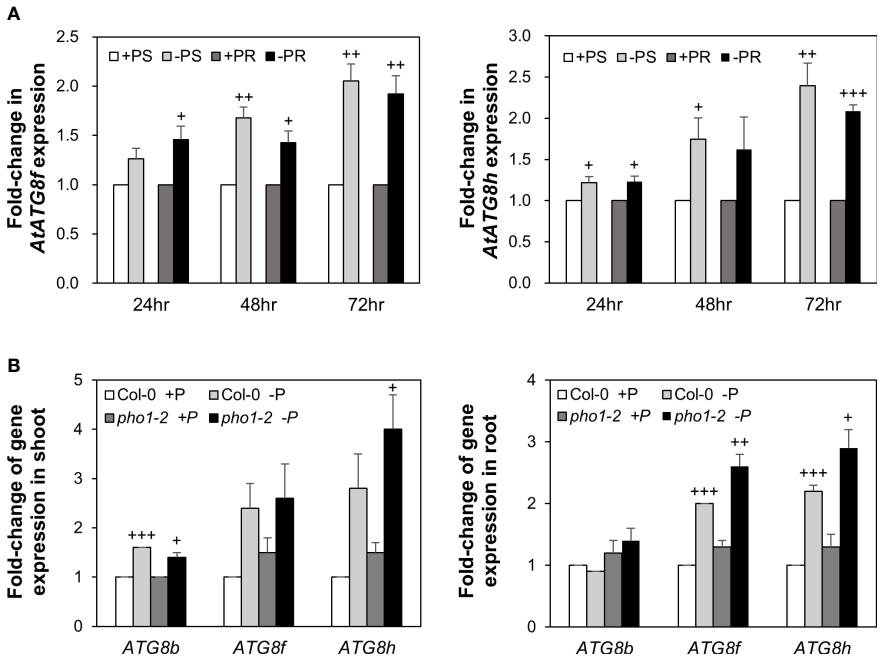

FIGURE 1
Low Pi induction of *AtATG8f* and *AtATG8h* is progressive and exacerbated in the *pho1-2* mutant. **(A)** Fold-change of expression of *AtATG8f* and *AtATG8h* in the shoot (S) and root (R) of 11-day-old *Arabidopsis* WT seedling following 24, 48 and 72 hours of Pi starvation (–P, 0 μM KH_2PO_4) conditions as determined by qRT-PCR. Error bars represent SE (n = 3, biological replicate pools of 20 seedlings collected from three independent experiments). $^{+++}$P< 0.001 $^{++}$P< 0.01, $^{+}$P< 0.05 compared to Pi-sufficient conditions; Student's *t*-test; two-tailed. **(B)** Fold-change of expression of *AtATG8f* and *AtATG8h* expression in the shoot and root of 11-day-old *Arabidopsis* WT and *pho1-2* seedling under Pi-sufficient (+P, 250 μM KH_2PO_4) and Pi-deficient (–P, 0 μM KH_2PO_4, 3 days of starvation) conditions as determined by qRT-PCR. *AtATG8b* expression was used for comparison. Error bars represent SE (n = 3, biological replicate pools of 20 seedlings collected from three independent experiments). $^{+++}$P< 0.001 $^{++}$P< 0.01 $^{+}$P< 0.05 compared to Pi-sufficient conditions within the same genotype; Student's *t*-test; two-tailed.

10.3389/fpls.2023.1018984

upregulation of *AtATG8f* and *AtATG8h* in the shoot and/or root of *pho1-2* under Pi limitation (Figure 1B) suggested that *AtATG8f* and *AtATG8h* are induced according to the magnitude of Pi deficiency. We were then prompted to determine which TFs are involved in such upregulation. To find out whether *AtATG8f* and *AtATG8h* could be upregulated by *At*PHR1, we set out to search for potential *cis*-elements in the promoter region of *AtATG8f* and *AtATG8h* that may be recognized by *At*PHR1. By using the PlantPan3.0 server (Chow et al., 2019), we found two and three putative P1BS elements in the proximal promoter of *AtATG8f* and *AtATG8h*, respectively (Figure 2A; Table S1). To validate whether *At*PHR1 participates in the regulation of *AtATG8f* and *AtATG8h*, we examined the expression of *AtATG8f* and *AtATG8h* in the *phr1-3* mutant (Rubio et al., 2001; Ren et al., 2012). The Pi starvation upregulation of *AtATG8f AtATG8h* was suppressed in both the shoot and root of *phr1-3* (Figure 2B), indicating that Pi limitation induces the expression of *AtATG8f* and *AtATG8h* in a PHR1-dependent manner.

*At*PHR1 does not directly transactivate the expression of *AtATG8f* and *AtATG8h* in *Arabidopsis* mesophyll protoplasts

In our initial attempt to search for potential TFs that bind to the promoter region of *AtATG8f* and *AtATG8h* by Y1H, we surprisingly failed to identify *At*PHR1 as a positive candidate (Figure S1). In parallel, we performed transient dual-luciferase reporter assays using *Arabidopsis* mesophyll protoplasts to test whether *At*PHR1 transactivates the expression of *AtATG8f* and *AtATG8h in planta*. For the reporter constructs encoding firefly luciferase (LUC) and *Renilla* luciferase (REN), the genomic sequences of each promoter were cloned into the pGreenII-0800-Luc vector (Hellens et al., 2005) (Figure 3A). For the effector construct, we used the ß-estradiol-inducible XVE expression system in the pGPTVII backbone to express TFs (Schlücking et al., 2013) (Figure 3A). In addition, the reporter construct carrying the promoter sequences of *AtIPS1* containing two P1BS elements was used as the positive control (Figure 3A) (Bustos et al., 2010). When *At*PHR1 was co-expressed with P_{IPS1}:LUC/P_{35S}:REN, the ratio of LUC : REN was increased to 2.9-fold as compared to the negative control in which GFP was co-expressed (Figure 3B). When we co-expressed the NAC domain TF *At*ATAF2 as a positive control with P_{ATG8h}:LUC/P_{35S}:REN (Wang et al., 2020), the ratio of LUC : REN was increased by 1.8-fold (Figure 3B). In comparison, when *At*PHR1 was co-expressed with P_{ATG8f}:LUC/P_{35S}:REN or P_{ATG8h}:LUC/P_{35S}:REN, the ratio of LUC : REN was similar to that of the GFP control (Figure 3B). These results indicated that *At*PHR1 may not directly transactivate *AtATG8f* and *AtATG8h*.

Loss of *At*ATG8f and *At*ATG8h does not impair cellular Pi homeostasis

To investigate the physiological role of *AtATG8f* and *AtATG8h*, we obtained the homozygous T-DNA lines for each gene: *atg8f-2*,

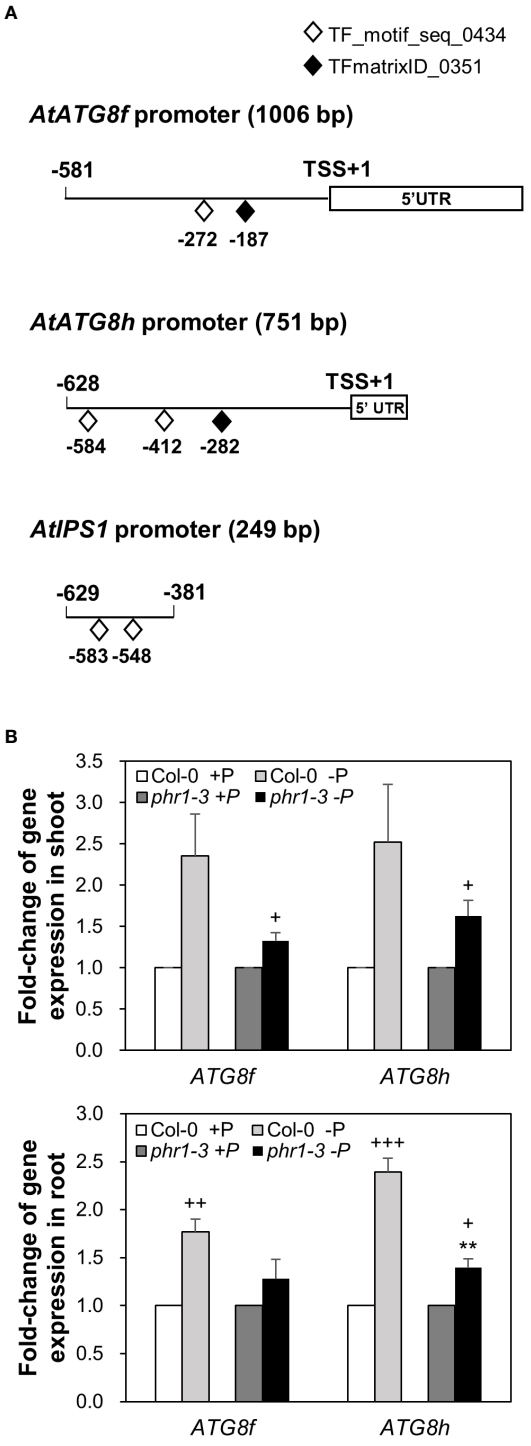

FIGURE 2
PHR1-dependent Pi starvation-induced upregulation of *AtATG8f* and *AtATG8h*. **(A)** Putative PHR1 binding sites (P1BS) predicted by the matrix TF_motif_seq_0434 (white diamond) and TFmatrixID_0351 (black diamond) in the proximal promoter of *AtATG8f, AtATG8h*, and *AtIPS1*. TSS, transcription start site; UTR, untranslated region. **(B)** Fold-change of expression of *AtATG8f* and *AtATG8h* in the shoot and root of 11-day-old *Arabidopsis* WT and *phr1-3* seedlings grown under Pi-sufficient (+P, 250 μM KH_2PO_4) and Pi-deficient (–P, 0 μM KH_2PO_4, 3 days of starvation) conditions as determined by qRT-PCR. Error bars represent SE (n = 3, biological replicate pools of 20 seedlings collected from three independent experiments). $^{+++}$P< 0.001 $^{++}$P< 0.01 $^{+}$P< 0.05 compared to Pi-sufficient conditions within the same genotype; **P< 0.01, compared to Pi-deficient WT; Student's *t*-test; two-tailed.

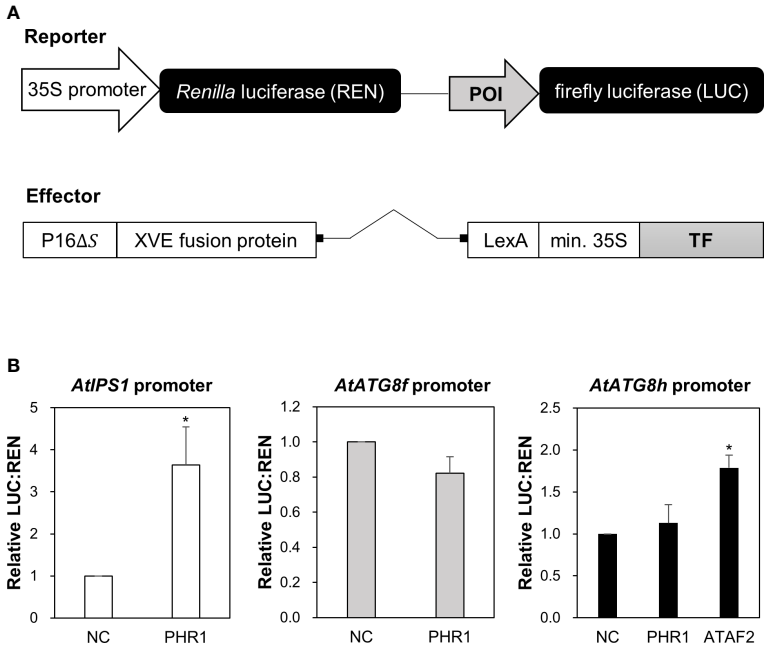

FIGURE 3
Transactivation of *AtATG8f* and *AtATG8h* promoters not by *At*PHR1 in *Arabidopsis* mesophyll protoplasts. **(A)** Schematic design of the reporter and effector constructs used for dual-luciferase assay (not drawn in scale). 35S promoter: CaMV 35S promoter; POI, promoter of interest; P16ΔS: a constitutive promoter; XVE: a chimeric transcription activator; LexA: an operator; min.35S: minimal 35S promoter; TF, transcription factor. **(B)** The relative LUC: REN ratios for the co-expression of the reporter construct containing the *AtIPS1*, *AtATG8f*, or *AtATG8h* promoter with the effector construct containing the transcription factor *At*PHR1 or *At*ATAF2. The co-expression of the effector construct expressing GFP and the corresponding reporter construct was taken as the negative control (NC). Data represent mean ± S.E. of biological replicates from independent experiments (n = 4 for the *AtATG8f* promoter and n = 3 for the *AtIPS1* and *AtATG8h* promoters). *P< 0.05, compared to NC; Student's *t*-test; two-tailed.

atg8f-3, *atg8f-5*, and *atg8f-6* for *AtATG8f* and *atg8h-2* and *atg8h-3* for *AtATG8h* (Figure S2; Table S2). By reverse transcription polymerase chain reaction (RT-PCR), we validated that the full-length transcripts of *AtATG8f* were absent in the *atg8f-2* and *atg8f-5* homozygotes (Figure S2), indicating that these two mutants carry null alleles. We only chose *atg8f-5* (hereafter referred to as *atg8f*) for further study because the T-DNA insertion site in this mutant was closer to the 5' untranslated region (UTR) of *AtATG8f*, which likely resulted in complete disruption of the transcription. On the other hand, the full-length transcripts of *AtATG8h* were not detected in both the *atg8h-2* and *atg8h-3* mutants. Nevertheless, we were able to detect some truncated transcripts in *atg8h-2* (Figure S2), and therefore *atg8h-3* (hereafter referred to as *atg8h*) was used. Through crosses we also successfully generated the *atg8f-5/atg8h-3* double mutant (hereafter referred to as *atg8f/atg8h*). The expression of *AtATG8f* and *AtATG8h* was induced in the WT Pi-starved roots but not detectable in *atg8f/atg8h* under both Pi-replete and Pi-deplete conditions (Figure S2). Of note, the transcript expression of the other *AtATG8* genes was comparable in WT and *atg8f/atg8h* (Figure S3), suggesting no compensatory upregulation of the other *AtATG8* members for the loss of *AtATG8f* and *AtATG8h* in the double mutant. To investigate whether *At*ATG8f and *At*ATG8h could be involved in the maintenance of cellular Pi homeostasis, we measured the shoot and root Pi levels of *atg8f, atg8h*, and *atg8f/atg8h*. All of them showed no difference from WT under both Pi-replete and Pi-deplete conditions (Figures 4A, B), suggesting that defective *AtATG8f* and *AtATG8h* do not affect cellular Pi levels.

*At*ATG8f and *At*ATG8h account for the maintenance of autophagic flux in the root under Pi starvation

To evaluate whether the low Pi induction of *AtATG8f* and *AtATG8h* may change autophagic activities, we attempted to compare autophagic flux between WT and *atg8f/atg8h*. The GFP-ATG8 cleavage assay is a widely accepted tool to measure autophagic flux by calculating the ratio of the amount of cleaved GFP to the amount of full-length GFP-ATG8 (Klionsky et al., 2021). However, this approach would unfortunately introduce additional ATG8s into *atg8f/atg8h*. We therefore conducted the ATG8 degradation assay to estimate the autophagic flux in the root of *atg8f/atg8h*. As the steady-state abundance of ATG8s can be influenced by autophagy activation or blockage of downstream steps such as inefficient vacuolar fusion or decreased degradation (Zhang et al., 2013), the vacuolar H^+-ATPase inhibitor concanamycin A (Conc A) was applied to prevent ATG8s from vacuolar degradation (Dröse et al., 1993; Bowman and Bowman, 2005). Without the availability of *At*ATG8f and *At*ATG8h-specific antibodies, we performed immunoblotting with a polyclonal anti-ATG8s antibody that recognize all the *At*ATG8 isoforms (ATG8s).

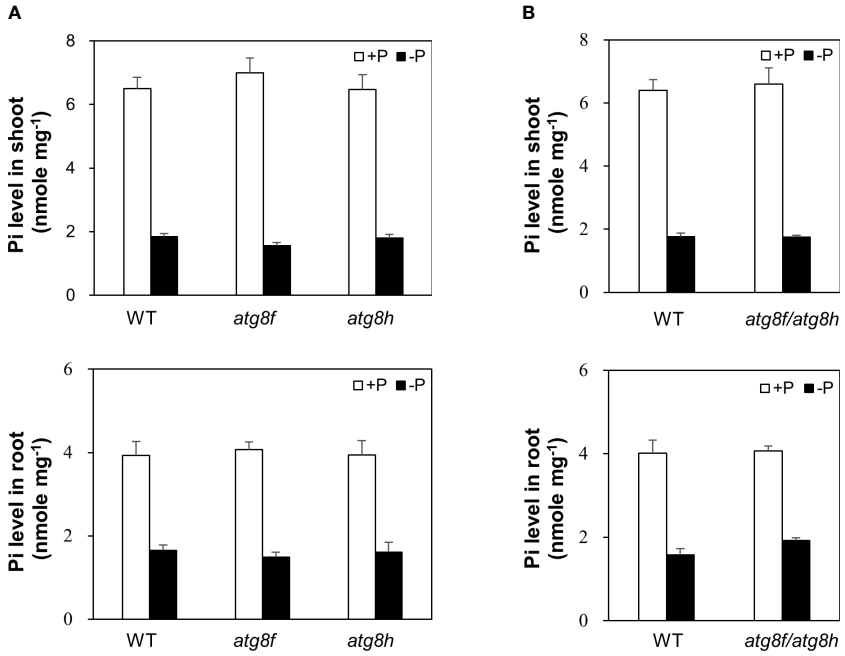

FIGURE 4
Pi levels of *atg8f*, *atg8h* and *atg8f/atg8h* mutants. **(A, B)** The shoot and root Pi levels of 11-day-old *Arabidopsis* seedlings of WT, *atg8f*, and *atg8h* **(A)** and *atg8f/atg8h* **(B)** under Pi-sufficient (+P, 250 μM KH_2PO_4) and Pi-deficient (−P, 0 μM KH_2PO_4, 3 days of starvation) conditions. Error bars represent SE (n = 9, biological replicate pools of 10 seedlings collected from three independent experiments).

Regardless of Pi status, ATG8s were found to accumulate in the WT root upon Conc A treatment (Figure 5A). In the absence of Conc A, the abundance of ATG8s in the total root proteins was comparable in *atg8f/atg8h* and WT (Figure 5A). This may be because only a small proportion of ATG8s were contributed by *At*ATG8f and *At*ATG8h transcripts (Figure S3). Nonetheless, the relative autophagic flux in the WT root calculated based on the changes of ATG8s between DMSO control and Conc A treatment showed no differences between Pi-replete and Pi-depleted conditions (Figure 5B). These results were in good agreement with our recent findings (Chiu et al., 2023). Notably, the autophagic flux was comparable in the Pi-repleted root of *atg8f/atg8h* and WT but reduced in the Pi-depleted root of *atg8f/atg8h* (Figures 5A, B). Given that the abundance of membrane-associated ATG8s would correlate with autophagic activity, we then compared the amount of ATG8s in the root microsomal fraction between WT and *atg8f/atg8h*. While the microsomal-enriched ATG8s was missing in the autophagy-defective *atg7-3* mutant, it was slightly reduced in the Pi-deplete root of WT (Figure S4). There was a substantial decrease of microsomal-enriched ATG8s in the root of *atg8f/atg8h* as compared to WT, but no significant difference was found between Pi-replete and Pi-deplete root of *atg8f/atg8h* (Figure S4). We then further examined ATG8s lipidation in WT and *atg8f/atg8h* by immunoblot. Because to distinguish lipidated ATG8s from non-lipidated ATG8s using immunoblot analyses was reported to be technically challenging due to the multiple variants in plants (Yoshimoto et al., 2004; Chung et al., 2010), we applied phospholipase D (PLD) treatment, which hydrolyzes the terminal phosphodiester bonds of phospholipids to produce phosphatidic acid (PA). The PLD-mediated cleavage of ATG8-PE yields ATG8-ethanolamine and PA, thus helping identify bands that correspond to lipidated ATG8s. The lipidated ATG8s migrated faster than the unmodified form during SDS-PAGE in the presence of urea and were sensitive to PLD digestion and absent in the *atg5* and *atg7* backgrounds (Yoshimoto et al., 2004; Chung et al., 2010; Suttangkakul et al., 2011; Li et al., 2014; Zhuang et al., 2017; Luo and Zhuang, 2018). Our results indicated that Pi starvation did not change the abundance of lipidated ATG8s in the WT root, but the lipidated ATG8s was unexpectedly increased in the Pi-replete root of *atg8f/atg8h* and remained a similar level or slightly declined following Pi starvation (Figure S5).

Besides ATG8s, NBR1 known as a selective autophagy receptor is itself a substrate degraded in the vacuole (Svenning et al., 2011; Zhou et al., 2013; Ji et al., 2020; Jung et al., 2020). Disruption of *At*NBR1 conferred increased sensitivity to heat, drought, and salt stresses (Zhou et al., 2013; Ji et al., 2020). However, *At*NBR1 does not play an essential role in regulating N deprivation-induced autophagy (Lin et al., 2020). To answer whether *At*NBR1 is involved in Pi starvation-induced autophagy and thus its degradation could be used as an alternative method for measuring autophagic flux in the root, we monitored the expression changes of *At*NBR1 in the WT root following 12, 24, 48, 72 hours of Pi deprivation. The specificity of anti-NBR1 antibodies was validated with the *nbr1-2* and *atg7-3* mutants by the absence and accumulation of *At*NBR1 proteins, respectively (Figure S6). Either with 6 or 12 hours of Conc A treatment, *At*NBR1 accumulated in the WT root to a similar extent at different time point of Pi starvation (Figure S6). Of note, the expression changes of

10.3389/fpls.2023.1018984

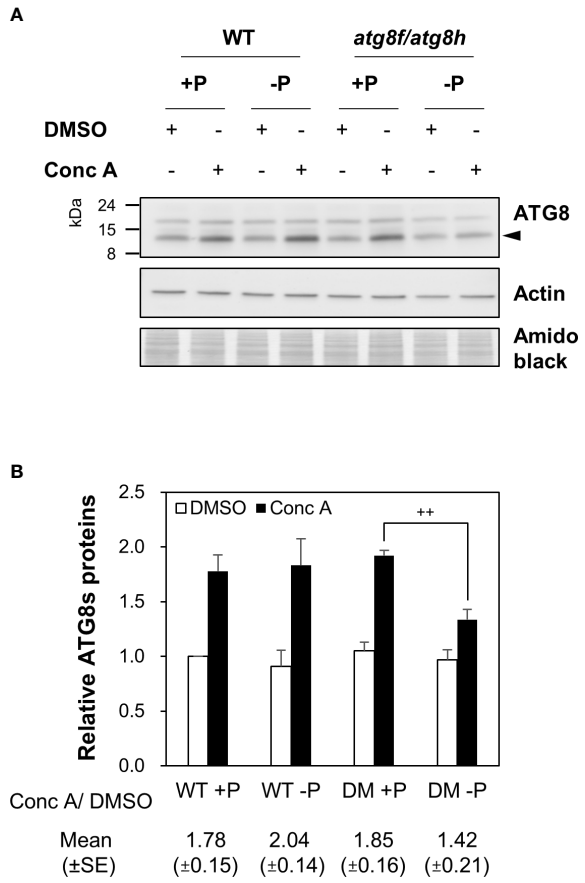

FIGURE 5
AtATG8f and *AtATG8h* are required for the maintenance of autophagic flux in the Pi-starved roots. **(A)** Immunoblot analysis of the expression of ATG8s in the root of 11-day-old *Arabidopsis* WT and *atg8f/atg8h* seedlings under Pi-sufficient (+P, 250 μM KH_2PO_4) and Pi-deficient (−P, 0 μM KH_2PO_4, 3 days of starvation) conditions with or without Conc A treatment (1 μM, 6 h). Representative images are shown. Arrowhead indicates the bands of ATG8s. **(B)** The expression change of ATG8s and the autophagic flux in the root of *Arabidopsis* WT and DM (*atg8f/atg8h*) seedlings. The expression level of ATG8s was normalized with the corresponding actin. Error bars represent SE (n = 3, biological replicate pools of 20 seedlings collected from three independent experiments). $^{++}$P< 0.01, compared to Pi-sufficient DM with Conc A treatment; Student's *t*-test; two-tailed. The relative autophagic flux was calculated by dividing the normalized ATG8s signal intensity of Conc A-treated samples by that of DMSO controls. Amido black staining was used for total protein detection.

*At*NBR1 in the WT root upon Conc A treatment appeared to be smaller than that of ATG8s (Figures 5A, S6). It is possible that *At*NBR1 is subjected to selective autophagic degradation only under certain stress conditions. Accordingly, Pi deprivation did not alter the vacuolar degradation of *At*NBR1 in the WT root (Figure S6). There was also no difference of *At*NBR1 degradation between *atg8f/atg8h* and WT (Figure S7), indicating that *At*NBR1 may not participate in Pi starvation-induced autophagy. Overall, these results revealed that *At*ATG8f and *At*ATG8h contribute to a substantial proportion of microsomal-enriched ATG8s and may regulate the autophagic flux under Pi starvation through a mechanism other than promoting ATG8s lipidation.

Expression of *AtATG8f* and *AtATG8h* in the root stele and at the sites where lateral root primordia develop

To examine the spatial expression patterns of *AtATG8f* and *AtATG8h* under Pi starvation, we generated GFP reporter lines, designated P_{ATG8f}:GFP and P_{ATG8h}:GFP. The promoter sequence of *AtATG8f* we used starts from 2386 bp upstream of the putative transcription start site (TSS) to 606 bp downstream of the TSS within the second exon as shown (Figure 6A). This is much longer than the one used by Di Berardino et al., which contains the 1651 bp upstream of the TSS and the 176 bp downstream of the TSS (Di Berardino et al., 2018). The upstream region of the TSS in our construct is also longer than the one used by Sláviková et al., which includes the 1906 bp upstream of ATG codon plus the entire coding regions of *AtATG8f*, a total of 3125-bp genomic sequence containing the exons and introns (Sláviková et al., 2005). While the study of Di Berardino et al. indicated the expression of *AtATG8f* in the veins of the pericarp and in the seed embryo, the study of Sláviková et al. displayed the expression of *AtATG8f* in the root of seedlings with relatively poor resolution at the cell-type level. As for *AtATG8h*, due to the short intergenic region between *AtATG8h* and the upstream gene At3g06430, two *AtATG8h* promoter regions were considered in our study. The shorter one contains a total of 553 bp, starting from 221 bp upstream of the TSS to 312 bp downstream of the TSS. The longer one contains the partial genomic sequences of At3g06430 and extending to 312 bp downstream of the TSS within the second exon (Figure 6A). Overall, there were no differences in the expression levels and patterns of GFP between the *AtATG8h* reporter lines with different promoter lengths (data not shown), so we chose the transgenic lines with the longer *AtATG8h* promoter for our further investigation. Confocal analysis of the root of P_{ATG8f}:GFP lines showed that the expression of *AtATG8f* was in the root apical meristem, root cap, stele tissues, and root hairs of the primary root under Pi sufficiency (Figure 6B). By comparison, the GFP signals in P_{ATG8h}:GFP lines were much weaker and mainly detected in the root stele tissues (Figure 6C). Of note, GFP signals were hardly detected in the root cap and root hairs of P_{ATG8h}:GFP lines under Pi sufficiency (Figure 6C). Under Pi deficiency, the GFP expression patterns of P_{ATG8f}:GFP and P_{ATG8h}:GFP lines were similar as those under Pi sufficiency and the signals in the root hair showed stronger intensities (data not shown). Further quantitative real-time PCR analysis of GFP expression in the Pi-starved root of P_{ATG8f}:GFP and P_{ATG8h}:GFP lines also supported the upregulation of GFP expression by low Pi (Figure 6D), which was in good agreement with the increased endogenous *AtATG8f* and *AtATG8h* transcripts in these reporter lines (Figure S8). These results suggested that *AtATG8f* and *AtATG8h* can be upregulated by Pi starvation at the transcriptional level.

To assess the promoter activities of *AtATG8f* and *AtATG8h* in the shoot, we also generated P_{ATG8f}:GUS and P_{ATG8h}:GUS lines, in which the promoter sequences used were the same as those used in the GFP lines. The expression of *AtATG8f* was mainly found in the shoot vascular tissues and mesophylls (Figure 7A). Similarly, the GUS staining of P_{ATG8h}:GUS lines was predominantly in the similar shoot tissues yet with weaker signals (Figure 7B). Moreover, the P_{ATG8f}:GUS lines showed the expression patterns of *AtATG8f* in the

10.3389/fpls.2023.1018984

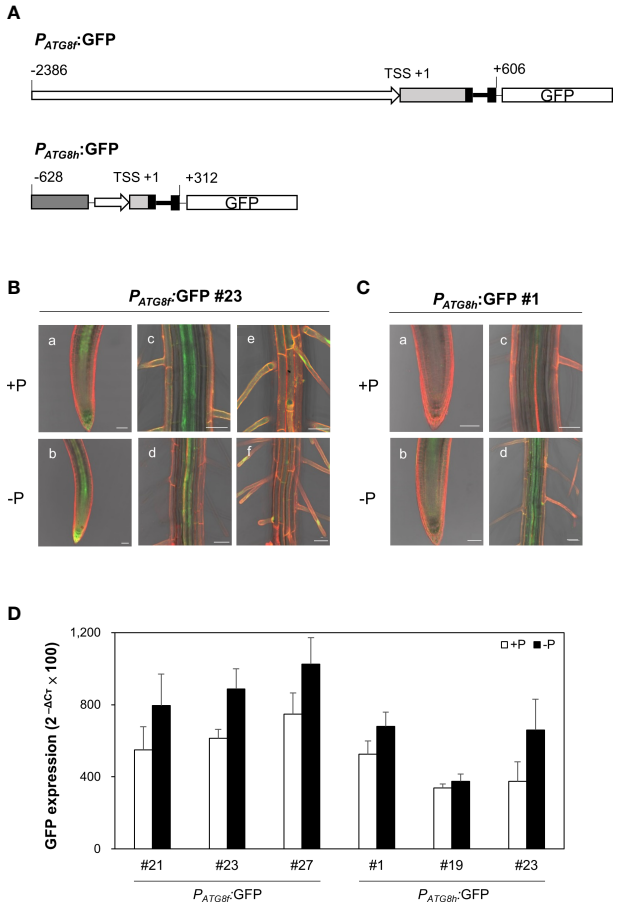

FIGURE 6
Expression patterns of *AtATG8f* and *AtATG8h* in *Arabidopsis* GFP reporter lines. **(A)** Schematic design of *AtATG8f* and *AtATG8h* promoter-fused GFP reporter constructs. The upstream region of the putative transcription starts site (TSS) in *AtATG8f* and *AtATG8h* were indicated by rightwards thick arrows. Black, light gray and dark gray boxes represent exons, 5´UTR and the gene At3g06430, respectively. Thick and thin lines indicate introns and linkers, respectively. The schematic structure is drawn according to scale. **(B, C)** GFP expression in the root of 3-day-old seedlings of P_{ATG8f}:GFP **(B)** and P_{ATG8h}:GFP **(C)** germinated under Pi-sufficient (a, c, and e; +P, 250 μM KH_2PO_4) and Pi-deficient (b, d, and f; −P, 0 μM KH_2PO_4) conditions. GFP signals in the root apical meristem (a, b), the vascular tissue **(C, D)** and the root hair (E, F). Scale bars = 50 μm. At least two independent lines were examined for each construct and representative images are shown. Propidium iodide (PI) was used as a root cell wall stain. **(D)** qRT-PCR analysis of GFP expression in the root of 11-day-old P_{ATG8f}:GFP and P_{ATG8h}:GFP seedlings grown under Pi-sufficient (+P, 250 μM KH_2PO_4) and Pi-deficient (−P, 0 μM KH_2PO_4, 3 days of starvation) conditions. Error bars represent SE (n = 3, biological replicate pools of 20 seedlings from three independent experiments).

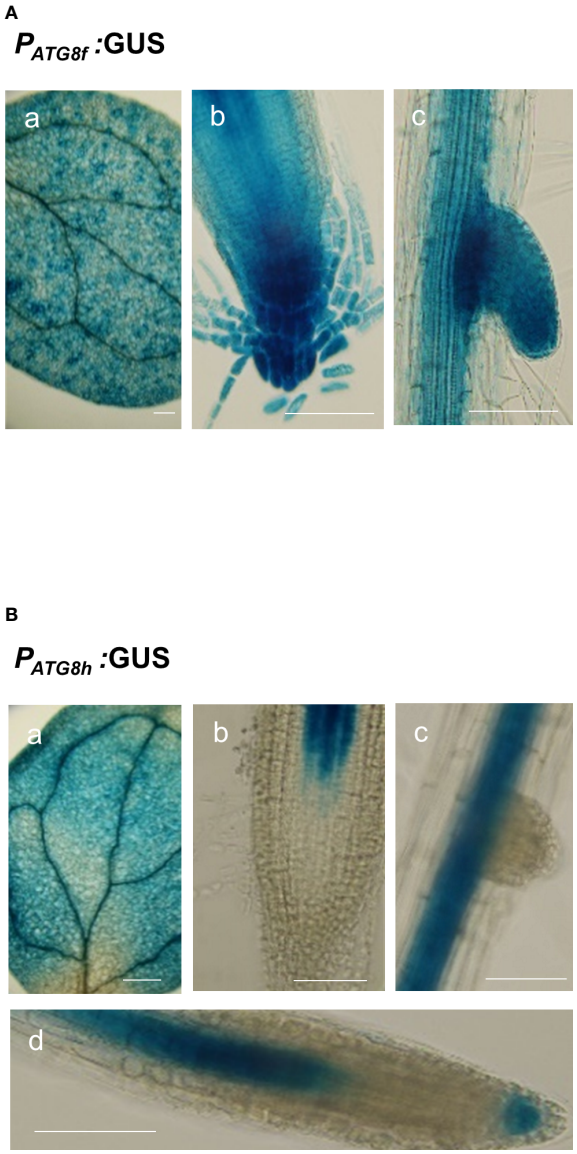

FIGURE 7
Expression patterns of *At*ATG8f and *At*ATG8h in *Arabidopsis* GUS reporter lines. **(A, B)** GUS staining in the 8-day-old seedlings of P_{ATG8f}:GUS **(A)** and P_{ATG8h}:GUS **(B)** seedlings under full nutrient (+PN, 250 μM KH_2PO_4 and 7.5 mM NO_3-) conditions. GUS signals in the cotyledon (a), root apical meristem (b), lateral root primordia (c), and lateral root tip (d). Scale bars, 50 μm. The time of GUS staining for P_{ATG8f}:GUS and P_{ATG8h}:GUS, was 1 and 2 hours, respectively. At least two independent lines were examined for each construct and representative images are shown.

root stele tissues of both primary and lateral roots as well as in fully emerged lateral root primordia (Figure 7A). Of note, the promoter activity of *AtATG8f* was detected throughout the development of lateral root (Figure 7A), which was consistent with P_{ATG8f}:GFP lines (Figure S9). By comparison, the promoter activity of *AtATG8h* was absent in the primary root apical meristem but detectable in the basal meristem (Figure 7B). Importantly, the GUS staining of *AtATG8h* reporter lines was neither detectable in the lateral root primordia nor at early stages of lateral root development (Figure 7B). Only after the establishment of lateral root meristem, we could detect the expression of *AtATG8h* in the stele and columella of lateral root (Figure 7B), which was also consistent with P_{ATG8h}:GFP lines (Figure S9).

Loss of *At*ATG8f and *At*ATG8h suppresses the lateral root number

Next, we focused to characterize the root phenotypes of *atg8f/atg8h* mutants and used the *atg7-3* mutant for comparison (Huang et al.,

2019). Pi starvation is known to induce the synthesis of extracellular acid phosphatases and organic acids for P mobilization (Marschner, 1995). Considering that the phytochemical or metabolite crosstalk between plants under nutrient deficiency may affect the root phenotypes of different genotypes when grown on the same plate, we grew four seedlings for each genotype *per* plate to avoid the mutual effect of root exudates from different genotypes. Under our full nutrient and Pi- and N-deprived conditions, the primary root length showed no difference between WT and *atg8f/atg8h* but was shorter in *atg7-3* (Figures 8A, B). These results suggested that unlike the impairment of the single-copy *ATG* gene, loss of *At*ATG8f and *At*ATG8h does not retard the primary root growth. Because strong *AtATG8f* and *AtATG8h* expression was observed during the lateral root development, we set out to analyze the number of lateral roots for *atg8f/atg8h*. Similar to the results of previous studies showing the inhibition of lateral growth under severe N starvation (Krouk et al., 2010; Gruber et al., 2013), we observed a reduction of lateral root number *per* seedling in all genotypes grown on N-limited media (Figure 8C). The lateral root number was strikingly reduced in the autophagy-defective *atg7-3* mutant under all the growth conditions, implying that functional autophagy is required for the lateral root development (Figure 8C). Intriguingly, the lateral root number was also significantly reduced in the *atg8f/atg8h* relative to the WT under Pi-rich and Pi-starved conditions (Figure 8C), indicating that *ATG8f* and *ATG8h* are involved in the regulation of lateral root growth. While under N starvation the lateral root number of *atg7-3* was reduced relative to the WT, no significant differences were found between WT and *atg8f/atg8h* (Figure 8C), indicating that the other *At*ATG8 may share redundant roles in lateral root development during N starvation.

Discussion

PHR1 acts upstream of the transcriptional regulation of *AtATG8f* and *AtATG8h*

A chromatin immunoprecipitation sequencing (ChIP-seq) study has revealed *AtATG8f* to be a direct target of *At*PHR1 (Castrillo et al., 2017), while a previous Y1H screen discovered that *At*PHR1 was not among the 32 TFs interacting with the *AtATG8h* promoter (Wang et al., 2020). In our Y1H assay, we failed to identify *At*PHR1 as a positive TF binding to the promoter of *AtATG8f* and *AtATG8h* (Figure S1). Results of our dual luciferase reporter assays also did not support a direct transactivation of *AtATG8f* and *AtATG8h* by *At*PHR1. Recently, a chromatin remodeling analysis of *Arabidopsis* Pi-starved roots suggested that *At*PHR1 activates a set of TFs triggering a second wave of epigenetic changes required for upregulation of PSR genes (Barragán-Rosillo et al., 2021). Intriguingly, the association of *AtATG8h* with increased chromatin accessibility (upDARs) was found in Pi-limited root of WT but not *phr1/phl2* (Barragán-Rosillo et al., 2021) (Table S3), indicating that PHR1 and/or its paralogues may engage transcriptional activation of *AtATG8h* in response to Pi limitation by enhancing chromatin accessibility. According to the ChIP-seq data (Castrillo et al., 2017), we found that only less than 20% of PHR1/PHL2-dependent Pi starvation-induced genes are direct targets of PHR1 (Barragán-Rosillo et al., 2021). This could in part explain the discrepancy among conclusions due to different methods or

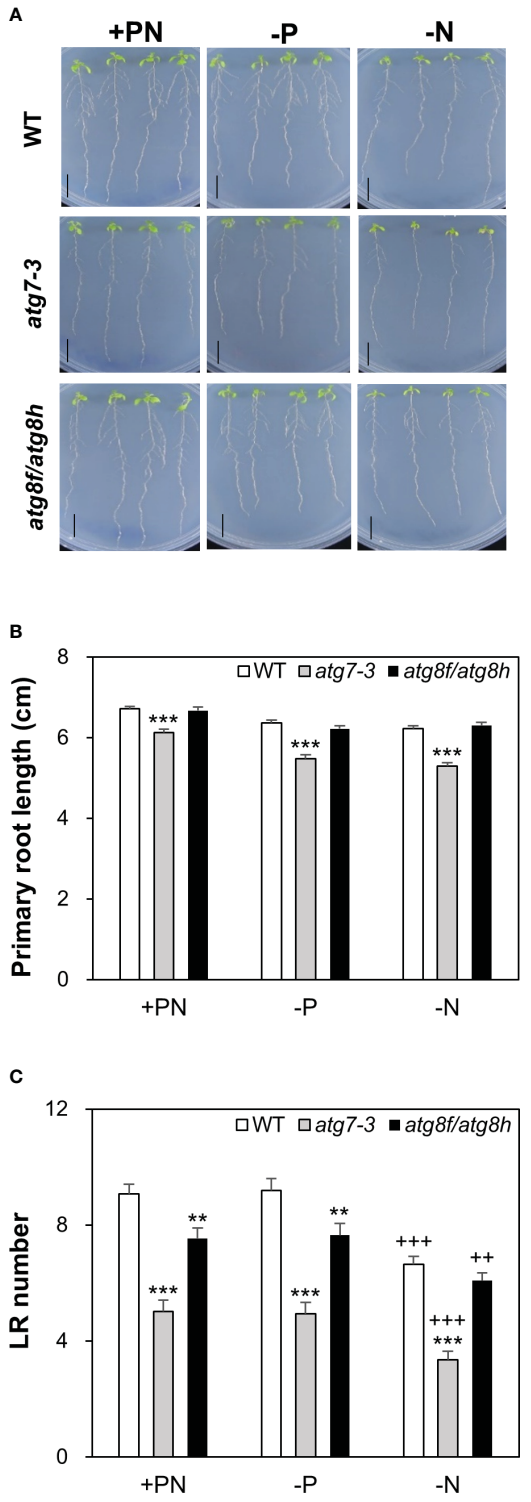

FIGURE 8
Loss of *At*ATG8f and *At*ATG8h suppresses lateral root development. **(A)** Representative images of 10-day-old WT, *atg7-3*, and *atg8f/atg8h* seedlings under full nutrient (+PN, 250 μM KH_2PO_4 and 7.5 mM NO_3^-), Pi-deficient (−P, 0 μM KH_2PO_4, 5 days of starvation) and N-deficient (−N, 0.1 mM NO_3^-, 5 days of starvation) conditions. Scale bars = 1 cm. **(B, C)** Data are presented for the primary root (PR) length **(B)** and the lateral root (LR) number **(C)** of WT, *atg7-3* and *atg8f/atg8h* seedlings. Error bars represent SE (n = 35–40, collected from three independent experiments). $^{+++}$P< 0.001 $^{++}$P< 0.01, compared to Pi-sufficient conditions within the same genotype; ***P< 0.001 **P< 0.01, compared to WT under the same conditions; Student's *t*-test; two-tailed.

test systems. Nevertheless, it warrants further investigation as to whether other TFs are responsible for the transcriptional regulation of *AtATG8f* and *AtATG8h* under Pi limitation and whether low Pi induction of *AtATG8f* and *AtATG8h* involves the coordination of epigenetic and transcriptional changes.

AtATG8f and *AtATG8h* finetune the autophagic flux in response to Pi starvation

ATG8 itself is degraded together with cargos and serves as a faithful proxy for autophagy activity readout (Klionsky et al., 2021). In this study, we showed that the expression changes of endogenous ATG8s were not prominent in the Pi-depleted root of WT and *atg8f/atg8h* relative to their respective Pi-replete controls (Figures 5A, B). This may be explained, at least in part, by the modest upregulation of *AtATG8f* and *AtATG8h* in certain root cell types. It is also likely that the abundance of the other ATG8s masks the small expression changes of *At*ATG8f and *At*ATG8h by Pi starvation (Figure S3). On the other hand, we could detect the reduction of microsomal-enriched ATG8s in the root of *atg8f/atg8h*, indicating that loss of *At*ATG8f and *At*ATG8h indeed decreased the abundance of membrane-associated ATG8s (Figure S4). Intriguingly, neither the autophagic flux nor the *At*ATG8s lipidation was increased by Pi starvation in the WT root, which reinforced the view of the two recent studies that nutrient starvation-induced autophagy is likely tissue- or cell type-specific (Dong et al., 2022; Chiu et al., 2023). While based on the expression changes of ATG8s between DMSO control and Conc A treatment, the relative autophagic flux was reduced in the Pi-starved root of *atg8f/atg8h* (Figures 5A, B), the autophagic flux estimated by NBR1 degradation failed to support this conclusion (Figure S7). We thought that NBR1 may not play a direct role in Pi starvation-induced autophagy, at least at the whole-root level. Nevertheless, we found the increased amount of lipidated ATG8s in the *atg8f/atg8h* root (Figure S5). The discrepancy between the reduced autophagic flux and the increased lipidated ATG8s in the Pi-depleted root of *atg8f/atg8h* might hint that the lipidation/de-lipidation of the other isoforms is altered and/or that *At*ATG8f and *At*ATG8h fine-tune the autophagic flux under Pi starvation through an unknown ATG8s lipidation-independent pathway. In mammalian cells, knockout of all the ATG8 family members suggested that the ATG8s are dispensable for autophagosome formation but crucial for autophagosome–lysosome fusion (Nguyen et al., 2016). However, it remains to discover whether the plant ATG8s are also important at this step to regulate the autophagic flux. It is worth noting that there are intrinsic limitations in measuring autophagic flux changes based on the steady-state abundance of ATG8s in the whole root. Even in the presence of vacuolar inhibitors that isolate autophagy induction from inhibition of autophagic degradation, this assay obscures estimates of substrate clearance – the most ideal measure of autophagic flux (Klionsky et al., 2021) and thus cannot determine the autophagic flux at the cellular level. The development of tool that allows to quantify autophagic responses at cell-type specific resolution as well as generation of *At*ATG8f and *At*ATG8h-specific antibodies may advance these issues (Stephani and Dagdas, 2020).

Role of *AtATG8f* and *AtATG8h* in the lateral root development

In our recent study of *Arabidopsis* autophagy-defective mutants, we showed that the *atg5-1*, *atg7-3* and *atg10-1* mutants exhibited impaired Pi homeostasis and compromised plant fitness in response to fluctuating Pi availability (Chiu et al., 2023). However, we did not observe similar phenotypes for *atg8f, atg8h*, and *atg8f/atg8h* (Figures 4A, B). Regardless of nutrient conditions, the primary root length showed no difference between WT and *atg8f/atg8h* but was shorter in *atg7-3* (Figures 8A, B). Rather, we found a reduction in the lateral root number of both *atg7-3* and *atg8f/atg8h* (Figure 8C). The development of lateral root primordia is sensitive to the availability of N (Banda et al., 2019; Santos Teixeira and ten Tusscher, 2019). Under severe N starvation, the primary root length, the lateral root length, and the number of lateral roots *per* primary root were reported to be inhibited in *atg4a4b-1* (Yoshimoto et al., 2004). We also found that compared to WT, *atg7-3* but not *atg8f/atg8h* had a decreased lateral root number under relatively mild N deficiency (Figure 8C). We reasoned that while *At*ATG8f and *At*ATG8h are critical for lateral root development under full nutrient and Pi-starved conditions, some other ATG8s are induced under N limitation and thus compensate for the loss of *At*ATG8f and *At*ATG8h. It is known that nutrient cues can affect lateral root formation *via* crosstalk with hormone signaling at four key developmental steps: initiation, primordium establishment, emergence, and elongation (Jia et al., 2021). As *AtATG8f* is present throughout the lateral root formation and *AtATG8h* starts to express likely after vascular tissue differentiation, we speculate that *AtATG8f* and *AtATG8h* may be involved in the lateral root development at different stages, which needs to be further studied. Intriguingly, we found that *AtATG8f* but not *AtATG8h* is expressed in the root cap. The periodicity of lateral root formation is driven by programmed cell death of the root cap (Xuan et al., 2016). Prior to the root cap cell death, autophagy has been shown to be required for organelle clearance and organized cell separation (Goh et al., 2022). In addition, selective autophagy was previously proposed to promote the lateral root development upon Pi starvation through ARK2-PUB9 module-dependent auxin accumulation (Deb et al., 2014; Sankaranarayanan and Samuel, 2015). However, the underlying mechanism remains to be elucidated on a molecular basis.

Materials and methods

Plant material and growth conditions

Seeds of the *Arabidopsis thaliana atg7-3* (SAIL_11_H07), *atg8f-2* (SALK_052510C), *atg8f-3* (SALK_039231), *atg8f-5* (SALK_133008), *atg8f-6* (SALK_004370), *atg8h-2* (SALK_021495), *atg8h-3* (SALK_136493), *phr1-3* (SALK_067629), *nbr1-2* (GK-246H08), and *pho1-2* (Poirier et al., 1991) mutants used in this study were in the Columbia (Col) background and obtained from the Arabidopsis Biological Resource Center (ABRC). The *Arabidopsis* seeds were surface-sterilized and germinated on agar plates with one-half modified Hoagland's solution containing 1% Suc and 0.8% Bacto agar (BD Difcom 204010), and grown in the growth chamber at 22°

C with a 16 h light/8 h dark cycle. The full nutrient (+PN) or Pi-sufficient (+P) and Pi-deficient (−P) media were supplemented with 250 μM and 0 or 10 μM KH_2PO_4, respectively, unless specified otherwise. The full nutrient (+PN) and N-deficient (−N) media were supplemented with 7.5 mM and 0 or 0.1 mM μM $Ca(NO_3)_2/KNO_3$, respectively, unless specified otherwise.

Construct design

All the insert fragments of interest were amplified by polymerase chain reaction (PCR) and cloned into pJET1.2/blunt vector for sequencing and then subcloned into the desired vectors. For the constructs used for dual-luciferase assay, the promoter sequences of *AtATG8f*, *AtATG8h* and *AtIPS1* were subcloned into the pGreenII-0800-Luc vector (Hellens et al., 2005). The full-length coding sequences of *At*ATAF2 and *At*PHR1 were subcloned into the β-estradiol-inducible P16ΔS:sXVE:S10 vector (Liu et al., 2018). For the constructs used for Y1H analysis, the promoter sequences of *AtATG8f* and *AtATG8h* were as same as those used for dual-luciferase reporter constructs and were cloned into the pHISi2 vector in which extra start codons of pHISi (Clontech/Takara bio Inc.) residing within 5' untranslated region of the reporter gene HIS3 are mutated. For the GFP or GUS reporter constructs, the P_{ATG8f}:GFP or P_{ATG8h}:GFP constructs were obtained by inserting the promoter sequences of *AtATG8f* and *AtATG8h* in the binary vector pMDC111. The P_{ATG8f}:GUS or P_{ATG8h}:GUS constructs were made by inserting the genomic sequences into the binary vector pMDC163. Primer sequences used for gene cloning are listed in Table S4.

Yeast one-hybrid analysis

The yeast strain YM4271 was employed for Y1H analysis of the *AtATG8f* and *AtATG8h* promoters, which was performed as described previously (Mitsuda et al., 2010) but with some modifications. The promoter-cloned pHISi construct was linearized with the restriction enzyme ApaI (for *AtATG8f*) or NcoI (for *AtATG8h*) and the promoter::*HIS3* fusion was then integrated into the YM4271 genome. A total of 1,736 *Arabidopsis* transcription factor genes were cloned into pGADT7 vector (Clontech/Takara bio Inc.), divided into 384 mini pools and individual interactions between each promoter and mini pool were examined by the yeast growth on the selective media lacking leucine (L), uracil (U) or histidine (H) with or without the addition of 3-amino-1,2,4-triazole (3-AT) as indicated.

Arabidopsis mesophyll protoplast isolation and transfection

Leaves of 4-week-old *Arabidopsis* plants grown under 12 h light/12 h dark were harvested and protoplasts were isolated following the tape-*Arabidopsis* sandwich method (Wu et al., 2009) with minor modifications. About 2.5×10^4 cells were transfected by the PEG/calcium-mediated method (Yoo et al., 2007). An equal volume of the freshly-prepared PEG 4000 solution containing 40% (w/v) PEG, 0.1 M $CaCl_2$, and 0.2 M mannitol was added, completely mixed, and incubated at RT for 10 min. A 600 μL of modified W5 solution (154 mM NaCl, 125 mM $CaCl_2$, 5 mM KCl, 5 mM glucose, and 2 mM MES) was added and gently mixed to stop the transfection. Transfected protoplasts were collected by centrifugation at 100 g for 2 min and were re-suspended in 0.5 mL of W5 solution. The final protoplasts were incubated in a 1% BSA pre-coated 12-well plate at 22°C for 16 hours in light. 10 μg/mL (36.7 μM) β-estradiol in ethanol was added 8 hours before performing the dual-luciferase assay.

Dual-luciferase assay in *Arabidopsis* protoplasts

Dual-luciferase assays were carried out as described with slight modifications (Hellens et al., 2005). Briefly, after 8 hours of induction, the transfected protoplast suspension was transferred to a 1.5 mL centrifugation tube and centrifuged at 100 g for 10 min. The supernatant was discarded and the pellets were re-suspended in 100 μL of 1X passive lysis buffer (PLB) provided in the Dual Luciferase Reporter Assay System kit (Promega). Protoplasts were disrupted by vortex for 10 s followed by centrifugation at 10,000 g for 2 min. A 5 μL of the supernatant sample was loaded into a well of a white flat bottom Costar 96 well plate (Corning). Dual-luciferase assays were performed in Synergy™ HTX Multi-Mode Microplate Reader (BioTek). A 40 μL luciferase assay reagent and a 40 μL Stop and Glo reagent (Promega) were injected *per* well. The ratio of LUC to REN was measured to represent the activity of the corresponding promoter when the effector plasmid DNA was co-transfected.

Phosphate concentration analysis

Pi concentrations were analyzed as described (Ames, 1966) with minor modifications. For the measurement of Pi concentrations, fresh tissue was frozen with liquid nitrogen and homogenized with 1% glacial acetic acid and incubated at 42°C for 30 min followed by centrifugation at 13,000 g for 5 min. The supernatant aliquot was mixed with the assay solution (0.35% NH_4MoO_4, 0.86 N H_2SO_4, and 1.4% ascorbic acid) and incubated at 42°C for 30 min. Pi content determined by colorimetric assay based on the formation of phosphomolybdate was measured at A_{750}.

RNA isolation, reverse transcription PCR, quantitative real-time RT-PCR

Total RNA from samples was isolated using GENEzol™ TriRNA Pure Kit with DNase (Geneaid, GZXD200). The first strand cDNA was synthesized from 0.5 μg total RNA using PrimeScript™ 1st strand cDNA Synthesis Kit (TaKaRa, 6110A) with oligo(dT) primer. qRT-PCR was performed using KAPA SYBR® FAST qPCR Master Mix (2X) Kit on StepOnePlus™ Real-Time PCR System (Applied Biosystems) according to the manufacturer's instructions. Relative expression levels were

normalized to that of an internal control *ACT8* (At1g49240). Sequences of primers used are listed in Table S5.

Immunoblot analysis

For extraction of total root protein, the roots of WT and mutant seedlings were ground in liquid nitrogen and dissolved in protein lysis buffer containing 60 mM 2-amino-2-(hydroxymethyl)-1,3-propanediol (Tris)-HCl (pH 8.5), 2% Sodium dodecyl sulfate (SDS), 2.5% glycerol, 0.13 mM EDTA, 1 mM phenylmethylsulfonyl fluoride (PMSF) and Protease Inhibitor Cocktail (Sigma-Aldrich P9599). A total of 25 μg root protein from each sample was loaded onto 12% Q-PAGE™ Bis-Tris Precast Gel (SMOBIO) or NuPAGE 4–12% Bis-Tris Gels (Thermo Fisher Scientific) and transferred to polyvinylidene difluoride (PVDF) membranes. The membrane was blocked with 1 or 2% BSA in 1X PBS solution with 0.2% Tween 20 (PBST, pH 7.2) at room temperature for 1 h and hybridized with primary antibodies of ATG8 (1:1000; Agrisera AS14 2811), NBR1 (1:4000; Agrisera AS14 2805) and actin (1:4000; Abcam, ab197345) for 1 h at room temperature in blocking solution. The membrane was washed four times with 1X PBST for 5 min followed by hybridization with the horseradish peroxidase–conjugated secondary antibody (1:10,000–20,000 dilution; GeneTex GTX213110-01) in blocking solution for 1 h. After four washes in 1× PBST for 5 min and a rinse with distilled water, chemiluminescent substrates (Advansta, WesternBright ECL) for signal detection were applied.

Isolation of root microsomal protein and ATG8 lipidation assay

Root microsomal protein was isolated with the Minute Plant Microsomal Membrane Extraction Kit (Invent, MM-018) according to the manual instruction. The resultant pellets (microsomal protein) were resuspended in the solubilization buffer containing 350 mM sucrose, 0.5% Triton X-100, 10 mM Tris-MES (pH 7.0), 1 mM Dithiothreitol (DTT) and Protease Inhibitor Cocktail (Sigma-Aldrich P9599). A total of 10 μg root microsomal protein from each sample was loaded onto NuPAGE 4–12% Bis-Tris Gels (Thermo Fisher Scientific) and transferred to PVDF membranes for further immunoblot analysis as described above, except with 3% BSA-containing blocking solution. Phospholipase D (PLD; Enzo Lifesciences BML-SE301) treatment was performed by mixing 10 μg root microsomal protein with 80 U PLD in reaction buffer containing 10 mM Tris-HCl (pH 8.0), 1% glycerol, 0.01% Triton X-100 and incubated at 37°C for 1 h. Each sample was loaded onto 15% mPAGE® TurboMix Bis-Tris Gel (TMKIT, Merck) with 6 M urea for electrophoresis according to the manual instruction and transferred to PVDF membranes for further immunoblot analysis as described above.

Arabidopsis transformation and transgenic plant selection

The binary plasmid was introduced into *A. tumefaciens* strain GV3101:pMP90 and selected on 5 μg ml^{-1} rifampicin, 50 μg ml^{-1} gentamycin and 50 μg ml^{-1} kanamycin. The *Arabidopsis* plants were transformed using standard floral dip method, and T1 transgenic plants were selected on half-strength MS medium supplemented with 1% sucrose plates containing appropriate antibiotics. T2 transgenic lines with a segregation ratio of 3 resistant: 1 sensitive were used for further study as presumably having single insertion of T-DNA.

GUS staining

GUS activity was detected as previously described with modifications (Jefferson et al., 1987). Briefly, seedlings were placed in 90% acetone on ice after sampling and vacuum infiltrated in freshly prepared GUS assay buffer containing 500 mM NaH_2PO_4, 500 mM Na_2HPO_4 $7H_2O$, 1mM $K_3Fe(CN)_6$, 1 mM $K_4Fe(CN)_6$, 10 mM EDTA, 0.1% Triton X-100, and 2.25 mM X-Gluc (5-bromo-4-chloro-3-indoyl-β-D-glucuronide sodium salt; Cyrusbioscience) for 20 min followed by incubation at 37°C, 1 and 2 hours for P_{ATG8f}:GUS and P_{ATG8h}:GUS reporter lines, respectively. Destaining was made with ethanol to remove chlorophyll. GUS staining was observed under the stereomicroscope and Leica DM2000 microscope.

Confocal microscopy

Confocal microscopy images were acquired using Zeiss LSM 800 with objectives Plan-Apochromat 40x/1.3 Oil DIC M27 in multi-track mode with line switching and averaging of two – four readings. The excitation/emission wavelengths for GFP and propidium iodide (PI) were 488 nm/530 nm and 548 nm/561 nm, respectively.

Analysis of root morphology

Seedlings were germinated on one-half modified Hoagland's media containing full nutrient (+PN) for 5 days and then transferred for vertical growth under full nutrient (+PN), Pi-deficient (0 μM KH_2PO_4) or N-deficient (0.1 mM NO_3^-) conditions for another 5 days. For each independent experiment, the plates were prepared with the same volume of medium from the same batch. For the lateral root analyses, at least 9 plates were taken for the total sample collection. Photos were taken by PowerShot G16 Camera. The length of the primary roots and the number of lateral roots with length longer than 0.25 cm *per* seedlings were calculated or counted using ImageJ (Schneider et al., 2012).

Chemical treatments

The Concanamycin A (Conc A; 1 mM; Cayman 11050) and Acetosyringone (150 mM; Sigma-Aldrich D134406) stock solutions were prepared in dimethyl sulfoxide (DMSO). The PI working solution (20 μg/ml) was prepared from the stock solution (1 mg/ml; Invitrogen P3566). A six-hour of 1μM Conc A or DMSO treatment was applied in the sample preparation for immunoblot analysis of ATG8s and NBR1 proteins. β-estradiol (36.7 mM; Sigma-Aldrich

E2758) and acetosyringone (150 mM; Sigma-Aldrich D134406) stock solutions were prepared in ethanol and DMSO, respectively.

Data availability statement

The raw data supporting the conclusions of this article will be made available by the authors, without undue reservation.

Author contributions

T-YL designed the research. L-YL, H-XC, C-HC, W-CC, T-YL and NM performed experiments. T-YL, L-YL, H-XC, C-HC and NM analyzed data. T-YL, L-YL, H-XC and NM wrote the manuscript. All authors contributed to the article and approved the submitted version.

Funding

This work was supported by grants from the Ministry of Science and Technology of the Republic of China (MOST 105-2621-M-007-001-MY3 and 108-2311-B-007-003-MY3).

Acknowledgments

We thank Dr Tzyy-Jen Chiou at Academia Sinica, Taiwan, for kindly providing the *pho1-2* and *phr1-3* seeds and the technical support from Ms. Fumie Tobe at AIST and Ms. Ya-Hsien Chou at the confocal imaging core in National Tsing Hua University (sponsored by MOST 108-2731-M-007-001 and MOST 110-2731-M-007-001). We also thank Dr Wen-Chi Chang at National Cheng Kung University, Taiwan, for personal advice and additional help on using PlantPAN3.0.

Conflict of interest

The authors declare that the research was conducted in the absence of any commercial or financial relationships that could be construed as a potential conflict of interest.

Publisher's note

All claims expressed in this article are solely those of the authors and do not necessarily represent those of their affiliated organizations, or those of the publisher, the editors and the reviewers. Any product that may be evaluated in this article, or claim that may be made by its manufacturer, is not guaranteed or endorsed by the publisher.

Supplementary material

The Supplementary Material for this article can be found online at: https://www.frontiersin.org/articles/10.3389/fpls.2023.1018984/full#supplementary-material

References

Ames, B. N. (1966). Assay of inorganic phosphate, total phosphate and phosphatases. *Meth. Enzymol.* 8, 115–118. doi: 10.1016/0076-6879(66)08014-5

Avila-Ospina, L., Moison, M., Yoshimoto, K., and Masclaux-Daubresse, C. (2014). Autophagy, plant senescence, and nutrient recycling. *J. Exp. Bot.* 65, 3799–3811. doi: 10.1093/jxb/eru039

Avin-Wittenberg, T., Baluška, F., Bozhkov, P. V., Elander, P. H., Fernie, A. R., Galili, G., et al. (2018). Autophagy-related approaches for improving nutrient use efficiency and crop yield protection. *J. Exp. Bot.* 69, 1335–1353. doi: 10.1093/jxb/ery069

Banda, J., Bellande, K., von Wangenheim, D., Goh, T., Guyomarc'h, S., Laplaze, L., et al. (2019). Lateral root formation in *Arabidopsis*: a well-ordered LRexit. *Trends Plant Sci.* 24, 826–839. doi: 10.1016/j.tplants.2019.06.015

Bari, R., Datt Pant, B., Stitt, M., and Wolf-Rüdiger, S. (2006). PHO2, microRNA399, and PHR1 define a phosphate-signaling pathway in plants. *Plant Physiol.* 141, 988–999. doi: 10.1104/pp.106.079707

Barragán-Rosillo, A. C., Peralta-Alvarez, C. A., Ojeda-Rivera, J. O., Arzate-Mejía, R. G., Recillas-Targa, F., and Herrera-Estrella, L. (2021). Genome accessibility dynamics in response to phosphate limitation is controlled by the PHR1 family of transcription factors in *Arabidopsis*. *Proc. Natl. Acad. Sci. U.S.A.* 118, 33. doi: 10.1073/pnas.2107558118

Bowman, E. J., and Bowman, B. J. (2005). V-ATPases as drug targets. *J. Bioenerg. Biomembr.* 37, 431–435. doi: 10.1007/s10863-005-9485-9

Boycheva Woltering, S., and Isono, E. (2020). Knowing when to self-eat - fine-tuning autophagy through ATG8 iso-forms in plants. *Front. Plant Sci.* 11, 579875. doi: 10.3389/fpls.2020.579875

Bu, F., Yang, M., Guo, X., Huang, W., and Chen, L. (2020). Multiple functions of ATG8 family proteins in plant autophagy. *Front. Cell Dev. Biol.* 8. doi: 10.3389/fcell.2020.00466

Bustos, R., Castrillo, G., Linhares, F., Puga, M. I., Rubio, V., Pérez-Pérez, J., et al. (2010). A central regulatory system largely controls transcriptional activation and repression responses to phosphate starvation in *Arabidopsis*. *PloS Genet.* 6, 9. doi: 10.1371/journal.pgen.1001102

Castrillo, G., Teixeira, P. J., Paredes, S. H., Law, T. F., de Lorenzo, L., Feltcher, M. E., et al. (2017). Root microbiota drive direct integration of phosphate stress and immunity. *Nature* 543, 513–518. doi: 10.1038/nature21417

Chiu, C.-Y., Lung, H.-F., Chou, W.-C., Lin, L.-Y., Chow, H.-X., Kuo, Y.-H., et al. (2023). Autophagy-mediated phosphate homeostasis in *Arabidopsis* involves modulation of phosphate transporters. *Plant Cell Physiol.* 64, 519–535. doi: 10.1093/pcp/pcad015

Chow, C.-N., Lee, T.-Y., Hung, Y.-C., Li, G.-Z., Tseng, K.-C., Liu, Y.-H., et al. (2019). PlantPAN3.0: a new and updated resource for reconstructing transcriptional regulatory networks from ChIP-seq experiments in plants. *Nucleic Acids Res.* 47, 1155–1163. doi: 10.1093/nar/gky1081

Chung, T., Phillips, A. R., and Vierstra, R. D. (2010). ATG8 lipidation and ATG8-mediated autophagy in *Arabidopsis* require ATG12 expressed from the differentially controlled ATG12A AND ATG12B loci. *Plant J.* 62, 483–493. doi: 10.1111/j.1365-313X.2010.04166.x

Chung, T., Suttangkakul, A., and Vierstra, R. D. (2009). The ATG autophagic conjugation system in maize: ATG transcripts and abundance of the ATG8-lipid adduct are regulated by development and nutrient availability. *Plant Physiol.* 149, 220–234. doi: 10.1104/pp.108.126714

Crombez, H., Motte, H., and Beeckman, T. (2019). Tackling plant phosphate starvation by the roots. *Dev. Cell.* 48, 599–615. doi: 10.1016/j.devcel.2019.01.002

Deb, S., Sankaranarayanan, S., Wewala, G., Widdup, E., and Samuel, M. A. (2014). The s-domain receptor kinase *Arabidopsis* receptor kinase2 and the U box/armadillo repeat-containing E3 ubiquitin ligase9 module mediates lateral root development under phosphate starvation in *Arabidopsis*. *Plant Physiol.* 165, 1647–1656. doi: 10.1104/pp.114.244376

Desnos, T. (2008). Root branching responses to phosphate and nitrate. *Curr. Opin. Plant Biol.* 11, 82–87. doi: 10.1016/j.pbi.2007.10.003

Di Berardino, J., Marmagne, A., Berger, A., Yoshimoto, K., Cueff, G., Chardon, F., et al. (2018). Autophagy controls resource allocation and protein storage accumulation in *Arabidopsis* seeds. *J. Exp. Bot.* 69, 1403–1414. doi: 10.1093/jxb/ery012

Dong, Y., Aref, R., Forieri, I., Schiel, D., Leemhuis, W., Meyer, C., et al. (2022). The plant TOR kinase tunes autophagy and meristem activity for nutrient stress-induced developmental plasticity. *Plant Cell* 34, 3814–3829. doi: 10.1093/plcell/koac201

Dröse, S., Bindseil, K. U., Bowman, E. J., Siebers, A., Zeeck, A., and Altendorf, K. (1993). Inhibitory effect of modified bafilomycins and concanamycins on p- and V-type adenosinetriphosphatases. *Biochemistry* 32, 3902–3906. doi: 10.1021/bi00066a008

Geng, J., and Klionsky, D. J. (2008). The ATG8 and ATG12 ubiquitin-like conjugation systems in macroautophagy. *EMBO Rep.* 9, 859–864. doi: 10.1038/embor.2008.163

Goh, T., Sakamoto, K., Wang, P., Kozono, S., Ueno, K., Miyashima, S., et al. (2022). Autophagy promotes organelle clearance and organized cell separation of living root cap cells in *Arabidopsis* thaliana. *Development* 149, 11. doi: 10.1242/dev.200593

Gross, A. S., and Graef, M. (2020). Mechanisms of autophagy in metabolic stress response. *J. Mol. Biol.* 432, 28–52. doi: 10.1016/j.jmb.2019.09.005

Gruber, B. D., Giehl, R. F. H., Friedel, S., and von Wirén, N. (2013). Plasticity of the *Arabidopsis* root system under nutrient deficiencies. *Plant Physiol.* 163, 161–179. doi: 10.1104/pp.113.218453

Havé, M., Marmagne, A., Chardon, F., and Masclaux-Daubresse, C. (2017). Nitrogen remobilization during leaf senescence: lessons from *Arabidopsis* to crops. *J. Exp. Bot.* 68, 2513–2529. doi: 10.1093/jxb/erw365

Hellens, R. P., Allan, A. C., Friel, E. N., Bolitho, K., Grafton, K., Templeton, M. D., et al. (2005). Transient expression vectors for functional genomics, quantification of promoter activity and RNA silencing in plants. *Plant Methods* 1, 13. doi: 10.1186/1746-4811-1-13

Huang, L., Yu, L.-J., Zhang, X., Fan, B., Wang, F.-Z., Dai, Y.-S., et al. (2019). Autophagy regulates glucose-mediated root meristem activity by modulating ROS production in *Arabidopsis*. *Autophagy* 15, 407–422. doi: 10.1080/15548627.2018.1520547

Jain, A., Nagarajan, V. K., and Raghothama, K. G. (2012). Transcriptional regulation of phosphate acquisition by higher plants. *Cell. Mol. Life Sci.* 69, 3207–3224. doi: 10.1007/s00018-012-1090-6

Jefferson, R. A., Kavanagh, T. A., and Bevan, M. W. (1987). GUS fusions: beta-glucuronidase as a sensitive and versatile gene fusion marker in higher plants. *EMBO J.* 6, 3901–3907. doi: 10.1002/j.1460-2075.1987.tb02730.x

Ji, C., Zhou, J., Guo, R., Lin, Y., Kung, C.-H., Hu, S., et al. (2020). AtNBR1 is a selective autophagic receptor for AtEXO70E2 in *Arabidopsis*. *Plant Physiol.* 184, 777–791. doi: 10.1104/pp.20.00470

Jia, Z., Giehl, R. F., and von Wirén, N. (2021). Local auxin biosynthesis acts downstream of brassinosteroids to trigger root foraging for nitrogen. *Nat. Commun.* 12, 5437. doi: 10.1038/s41467-021-25250-x

Jung, H., Lee, H. N., Marshall, R. S., Lomax, A. W., Yoon, M. J., Kim, J., et al. (2020). *Arabidopsis* cargo receptor NBR1 mediates selective autophagy of defective proteins. *J. Exp. Bot.* 71, 73–89. doi: 10.1093/jxb/erz404

Kamada, Y., Funakoshi, T., Shintani, T., Nagano, K., Ohsumi, M., and Ohsumi, Y. (2000). Tor-mediated induction of autophagy *via* an Apg1 protein kinase complex. *J. Cell Biol.* 150, 1507–1513. doi: 10.1083/jcb.150.6.1507

Kanno, S., Arrighi, J.-F., Chiarenza, S., Bayle, V., Berthomé, R., Péret, B., et al. (2016). A novel role for the root cap in phosphate uptake and homeostasis. *eLife* 5, e14577. doi: 10.7554/eLife.14577.022

Kellner, R., de la Concepcion, J. C., Maqbool, A., Kamoun, S., and Dagdas, Y. F. (2017). ATG8 expansion: a driver of selective autophagy diversification? *Trends Plant Sci.* 22, 204–214. doi: 10.1016/j.tplants.2016.11.015

Klionsky, D. J., Abdel-Aziz, A. K., Abdelfatah, S., Abdellatif, M., Abdoli, A., Abel, S., et al. (2021). Guidelines for the use and interpretation of assays for monitoring autophagy (4th edition). *Autophagy* 17, 1–382. doi: 10.1080/15548627.2020.1797280

Krouk, G., Lacombe, B., Bielach, A., Perrine-Walker, F., Malinska, K., Mounier, E., et al. (2010). Nitrate-regulated auxin transport by NRT1.1 defines a mechanism for nutrient sensing in plants. *Dev. Cell.* 18, 927–937. doi: 10.1016/j.devcel.2010.05.008

Li, W.-w., Chen, M., Zhong, L., Liu, J.-m., Xu, Z.-s., Li, L.-c., et al. (2015). Overexpression of the autophagy-related gene SiATG8a from foxtail millet (Setaria italica l.) confers tolerance to both nitrogen starvation and drought stress in *Arabidopsis*. *Biochem. Biophys. Res. Commun.* 468, 800–806. doi: 10.1016/j.bbrc.2015.11.035

Li, F., Chung, T., and Vierstra, R. D. (2014). Autophagy-related 11 plays a critical role in general autophagy- and senescence-induced mitophagy in *Arabidopsis*. *Plant Cell* 26, 788–807. doi: 10.1105/tpc.113.120014

Lin, Y., Guo, R., Ji, C., Zhou, J., and Jiang, L. (2020). New insights into AtNBR1 as a selective autophagy cargo receptor in *Arabidopsis*. *Plant Signal. Behav.* 16, 1839226. doi: 10.1080/15592324.2020.1839226

Liu, T. Y., Chou, W. C., Chen, W. Y., Chu, C. Y., Dai, C. Y., and Wu, P. Y. (2018). Detection of membrane protein-protein interaction *in planta* based on dual-intein-coupled tripartite split-GFP association. *Plant J.* 94, 426–438. doi: 10.1111/tpj.13874

Luo, M., and Zhuang, X. (2018). Analysis of autophagic activity using ATG8 lipidation assay in *Arabidopsis thaliana*. *Bio-protoc* 8, 12. doi: 10.21769/BioProtoc.2880

Manning, D. A. C. (2008). Phosphate minerals, environmental pollution and sustainable agriculture. *Elements* 4, 105–108. doi: 10.2113/GSELEMENTS.4.2.105

Mari, M., and Reggiori, F. (2007). ATG9 trafficking in yeast s*accharomyces cerevisiae*. *Autophagy* 3, 145–148. doi: 10.4161/auto.3608

Marschner, H. (1995). *Mineral nutrition of higher plants, 2nd edn* Vol. 889 (London: Academic Press).

Marshall, R. S., and Vierstra, R. D. (2018). Autophagy: the master of bulk and selective recycling. *Annu. Rev. Plant Biol.* 69, 173–208. doi: 10.1146/annurev-arplant-042817-040606

Minina, E. A., Moschou, P. N., Vetukuri, R. R., Sanchez-Vera, V., Cardoso, C., Liu, Q., et al. (2018). Transcriptional stimulation of rate-limiting components of the autophagic pathway improves plant fitness. *J. Exp. Bot.* 69, 1415–1432. doi: 10.1093/jxb/ery010

Mitsuda, N., Ikeda, M., Takada, S., Takiguchi, Y., Kondou, Y., Yoshizumi, T., et al. (2010). Efficient yeast one-/two-hybrid screening using a library composed only of transcription factors in *Arabidopsis thaliana*. *Plant Cell Physiol.* 51, 2145–2151. doi: 10.1093/pcp/pcq161

Naumann, C., Müller, J., Sakhonwasee, S., Wieghaus, A., Hause, G., Heisters, M., et al. (2019). The local phosphate deficiency response activates endoplasmic reticulum stress-dependent autophagy. *Plant Physiol.* 179, 460–476. doi: 10.1104/pp.18.01379

Nguyen, T. N., Padman, B. S., Usher, J., Oorschot, V., Ramm, G., and Lazarou, M. (2016). ATG8 family LC3/GABARAP proteins are crucial for autophagosome–lysosome fusion but not autophagosome formation during PINK1/Parkin mitophagy and starvation. *J. Cell Biol.* 215, 857–874. doi: 10.1083/jcb.201607039

Paz-Ares, J., Puga, M. I., Rojas-Triana, M., Martinez-Hevia, I., Diaz, S., Poza-Carrión, C., et al. (2022). Plant adaptation to low phosphorus availability: core signaling, crosstalks, and applied implications. *Mol. Plant* 15, 104–124. doi: 10.1016/j.molp.2021.12.005

Peng, M., Bi, Y.-M., Zhu, T., and Rothstein, S. J. (2007). Genome-wide analysis of *Arabidopsis* responsive transcriptome to nitrogen limitation and its regulation by the ubiquitin ligase gene NLA. *Plant Mol. Biol.* 65, 775–797. doi: 10.1007/s11103-007-9241-0

Poirier, Y., Thoma, S., Somerville, C., and Schiefelbein, J. (1991). Mutant of *Arabidopsis* deficient in xylem loading of phosphate. *Plant Physiol.* 97, 1087–1093. doi: 10.1104/pp.97.3.1087

Puga, M. I., Mateos, I., Charukesi, R., Wang, Z., Franco-Zorrilla, J. M., de Lorenzo, L., et al. (2014). SPX1 is a phosphate-dependent inhibitor of phosphate starvation response 1 in *Arabidopsis*. *Proc. Natl. Acad. Sci. U.S.A.* 111, 14947–14952. doi: 10.1073/pnas.1404654111

Qi, H., Xia, F. N., and Xiao, S. (2021). Autophagy in plants: physiological roles and post-translational regulation. *J. Integr. Plant Biol.* 63, 161–179. doi: 10.1111/jipb.12941

Ren, F., Guo, Q.-Q., Chang, L.-L., Chen, L., Zhao, C.-Z., Zhong, H., et al. (2012). Brassica napus PHR1 gene encoding a MYB-like protein functions in response to phosphate starvation. *PloS One* 7, 8. doi: 10.1371/journal.pone.0044005

Rodriguez, E., Chevalier, J., Olsen, J., Ansbøl, J., Kapousidou, V., Zuo, Z., et al. (2020). Autophagy mediates temporary reprogramming and dedifferentiation in plant somatic cells. *EMBO J.* 39, 4. doi: 10.15252/embj.2019103315

Rose, T. L., Bonneau, L., Der, C., Marty-Mazars, D., and Marty, F. (2006). Starvation-induced expression of autophagy-related genes in *Arabidopsis*. *Biol. Cell.* 98, 53–67. doi: 10.1042/BC20040516

Rubio, V., Linhares, F., Solano, R., Martín, A. C., Iglesias, J., Leyva, A., et al. (2001). A conserved MYB transcription factor involved in phosphate starvation signaling both in vascular plants and in unicellular algae. *Genes Dev.* 15, 2122–2133. doi: 10.1101/gad.204401

Russell, R. C., Tian, Y., Yuan, H., Park, H. W., Chang, Y.-Y., Kim, J., et al. (2013). ULK1 induces autophagy by phosphorylating beclin-1 and activating VPS34 lipid kinase. *Nat. Cell Biol.* 15, 741–750. doi: 10.1038/ncb2757

Sankaranarayanan, S., and Samuel, M. A. (2015). A proposed role for selective autophagy in regulating auxin-dependent lateral root development under phosphate starvation in *Arabidopsis*. *Plant Signal. Behav.* 10, 3. doi: 10.4161/15592324.2014.989749

Santos Teixeira, J. A., and ten Tusscher, K. H. (2019). The systems biology of lateral root formation: connecting the dots. *Mol. Plant* 12, 784–803. doi: 10.1016/j.molp.2019.03.015

Schlücking, K., Edel, K. H., Köster, P., Drerup, M. M., Eckert, C., Steinhorst, L., et al. (2013). A new β-estradiol-inducible vector set that facilitates easy construction and efficient expression of transgenes reveals CBL3-dependent cytoplasm to tonoplast translocation of CIPK5. *Mol. Plant* 6, 1814–1829. doi: 10.1093/mp/sst065

Schneider, C. A., Rasband, W. S., and Eliceiri, K. W. (2012). NIH Image to ImageJ: 25 years of image analysis. *Nat. Methods* 9, 671–675. doi: 10.1038/nmeth.2089

Seo, E., Woo, J., Park, E., Bertolani, S. J., Siegel, J. B., Choi, D., et al. (2016). Comparative analyses of ubiquitin-like ATG8 and cysteine protease ATG4 autophagy genes in the plant lineage and cross-kingdom processing of ATG8 by ATG4. *Autophagy* 12, 2054–2068. doi: 10.1080/15548627.2016.1217373

Sláviková, S., Shy, G., Yao, Y., Glozman, R., Levanony, H., Pietrokovski, S., et al. (2005). The autophagy-associated ATG8 gene family operates both under favourable growth conditions and under starvation stresses in *Arabidopsis* plants. *J. Exp. Bot.* 56, 2839–2849. doi: 10.1093/jxb/eri276

Stephani, M., and Dagdas, Y. (2020). Plant selective autophagy-still an uncharted territory with a lot of hidden gems. *J. Mol. Biol.* 432, 63–79. doi: 10.1016/j.jmb.2019.06.028

Sun, X., Huo, L., Jia, X., Che, R., Gong, X., Wang, P., et al. (2018a). Overexpression of *MdATG18a* in apple improves resistance to *Diplocarpon mali* infection by enhancing antioxidant activity and salicylic acid levels. *Hortic. Res.* 5, 57. doi: 10.1038/s41438-018-0059-5

Sun, X., Wang, P., Jia, X., Huo, L., Che, R., and Ma, F. (2018b). Improvement of drought tolerance by overexpressing *MdATG18a* is mediated by modified antioxidant system and activated autophagy in transgenic apple. *Plant Biotechnol. J.* 16, 545–557. doi: 10.1111/pbi.12794

Suttangkakul, A., Li, F., Chung, T., and Vierstra, R. D. (2011). The ATG1/ATG13 protein kinase complex is both a regulator and a target of autophagic recycling in *Arabidopsis*. *Plant Cell* 23, 3761–3779. doi: 10.1105/tpc.111.090993

Svenning, S., Lamark, T., Krause, K., and Johansen, T. (2011). Plant NBR1 is a selective autophagy substrate and a functional hybrid of the mammalian autophagic adapters NBR1 and p62/SQSTM1. *Autophagy* 7, 993–1010. doi: 10.4161/auto.7.9.16389

Tasaki, M., Asatsuma, S., and Matsuoka, K. (2014). Monitoring protein turnover during phosphate starvation-dependent autophagic degradation using a photoconvertible fluorescent protein aggregate in tobacco BY-2 cells. *Front. Plant Sci.* 5. doi: 10.3389/fpls.2014.00172

Thompson, A. R., Doelling, J. H., Suttangkakul, A., and Vierstra, R. D. (2005). Autophagic nutrient recycling in *Arabidopsis* directed by the ATG8 and ATG12 conjugation pathways. *Plant Physiol.* 138, 2097–2110. doi: 10.1104/pp.105.060673

Toyooka, K., Moriyasu, Y., Goto, Y., Takeuchi, M., Fukuda, H., and Matsuoka, K. (2006). Protein aggregates are transported to vacuoles by a macroautophagic mechanism in nutrient-starved plant cells. *Autophagy* 2, 96–106. doi: 10.4161/auto.2.2.2366

Wang, Y., Cai, S., Yin, L., Shi, K., Xia, X., Zhou, Y., et al. (2015). Tomato HsfA1a plays a critical role in plant drought tolerance by activating *ATG* genes and inducing autophagy. *Autophagy* 11, 2033–2047. doi: 10.1080/15548627.2015.1098798

Wang, Y., Cao, J.-J., Wang, K.-X., Xia, X.-J., Shi, K., Zhou, Y.-H., et al. (2019). BZR1 mediates brassinosteroid-induced autophagy and nitrogen starvation in tomato. *Plant Physiol.* 179, 671–685. doi: 10.1104/pp.18.01028

Wang, Z., Kuo, H.-F., and Chiou, T.-J. (2021). Intracellular phosphate sensing and regulation of phosphate transport systems in plants. *Plant Physiol.* 187, 2043–2055. doi: 10.1093/plphys/kiab343

Wang, P., Nolan, T. M., Yin, Y., and Bassham, D. C. (2020). Identification of transcription factors that regulate ATG8 expression and autophagy in *Arabidopsis*. *Autophagy* 16, 123–139. doi: 10.1080/15548627.2019.1598753

Wang, Z., Ruan, W., Shi, J., Zhang, L., Xiang, D., Yang, C., et al. (2014). Rice SPX1 and SPX2 inhibit phosphate starvation responses through interacting with PHR2 in a phosphate-dependent manner. *Proc. Natl. Acad. Sci. U.S.A.* 111, 14953–14958. doi: 10.1073/pnas.1404680111

Wang, P., Sun, X., Jia, X., and Ma, F. (2017a). Apple autophagy-related protein MdATG3s afford tolerance to multiple abiotic stresses. *Plant Sci.* 256, 53–64. doi: 10.1016/j.plantsci.2016.12.003

Wang, P., Sun, X., Jia, X., Wang, N., Gong, X., and Ma, F. (2016). Characterization of an autophagy-related gene MdATG8i from apple. *Front. Plant Sci.* 7. doi: 10.3389/fpls.2016.00720

Wang, W., Xu, M., Wang, G., and Galili, G. (2017b). Autophagy: an important biological process that protects plants from stressful environments. *Front. Plant Sci.* 7. doi: 10.3389/fpls.2016.02030

Wu, J., Michaeli, S., Picchianti, L., Dagdas, Y., Galili, G., and Peled-Zehavi, H. (2021). ATI1 (ATG8-interacting protein 1) and ATI2 define a plant starvation-induced reticulophagy pathway and serve as MSBP1/MAPR5 cargo receptors. *Autophagy* 17, 3375–3388. doi: 10.1080/15548627.2021.1872886

Wu, F.-H., Shen, S.-C., Lee, L.-Y., Lee, S.-H., Chan, M.-T., and Lin, C.-S. (2009). Tape-*Arabidopsis* sandwich - a simpler *Arabidopsis* protoplast isolation method. *Plant Methods* 5, 16. doi: 10.1186/1746-4811-5-16

Wun, C.-L., Quan, Y., and Zhuang, X. (2020). Recent advances in membrane shaping for plant autophagosome biogenesis. *Front. Plant Sci.* 11. doi: 10.3389/fpls.2020.00565

Xia, T., Xiao, D., Liu, D., Chai, W., Gong, Q., and Wang, N. N. (2012). Heterologous expression of ATG8c from soybean confers tolerance to nitrogen deficiency and increases yield in *Arabidopsis*. *PloS One* 7, 5. doi: 10.1371/journal.pone.0037217

Xuan, W., Band, L. R., Kumpf, R. P., Van Damme, D., Parizot, B., De Rop, G., et al. (2016). Cyclic programmed cell death stimulates hormone signaling and root development in *Arabidopsis*. *Science* 351, 384–387. doi: 10.1126/science.aad2776

Yan, Y., Wang, P., He, C., and Shi, H. (2017). MeWRKY20 and its interacting and activating autophagy-related protein 8 (MeATG8) regulate plant disease resistance in cassava. *Biochem. Biophys. Res. Commun.* 494, 20–26. doi: 10.1016/j.bbrc.2017.10.091

Yoo, S.-D., Cho, Y.-H., and Sheen, J. (2007). *Arabidopsis* mesophyll protoplasts: a versatile cell system for transient gene expression analysis. *Nat. Protoc.* 2, 1565–1572. doi: 10.1038/nprot.2007.199

Yoshimoto, K., Hanaoka, H., Sato, S., Kato, T., Tabata, S., Noda, T., et al. (2004). Processing of ATG8s, ubiquitin-like proteins, and their deconjugation by ATG4s are essential for plant autophagy. *Plant Cell* 16, 2967–2983. doi: 10.1105/tpc.104.025395

Yoshimoto, K., and Ohsumi, Y. (2018). Unveiling the molecular mechanisms of plant autophagy-from autophagosomes to vacuoles in plants. *Plant Cell Physiol.* 59, 1337–1344. doi: 10.1093/pcp/pcy112

Yoshitake, Y., Nakamura, S., Shinozaki, D., Izumi, M., Yoshimoto, K., Ohta, H., et al. (2021). RCB-mediated chlorophagy caused by oversupply of nitrogen suppresses phosphate-starvation stress in plants. *Plant Physiol.* 185, 318–330. doi: 10.1093/plphys/kiaa030

Zhang, X.-j., Chen, S., Huang, K.-x., and Le, W.-d. (2013). Why should autophagic flux be assessed? *Acta Pharmacol. Sin.* 34, 595–599. doi: 10.1038/aps.2012.184

Zhou, J., Wang, J., Cheng, Y., Chi, Y.-J., Fan, B., Yu, J.-Q., et al. (2013). NBR1-mediated selective autophagy targets insoluble ubiquitinated protein aggregates in plant stress responses. *PloS Genet.* 9, 1. doi: 10.1371/journal.pgen.1003196

Zhuang, X., Chung, K. P., Cui, Y., Lin, W., Gao, C., Kang, B.-H., et al. (2017). ATG9 regulates autophagosome progression from the endoplasmic reticulum in *Arabidopsis*. *Proc. Natl. Acad. Sci. U.S.A.* 114, 426–435. doi: 10.1073/pnas.1616299114

Frontiers in
Plant Science

Cultivates the science of plant biology and its applications

The most cited plant science journal, which advances our understanding of plant biology for sustainable food security, functional ecosystems and human health.

Discover the latest Research Topics

See more →

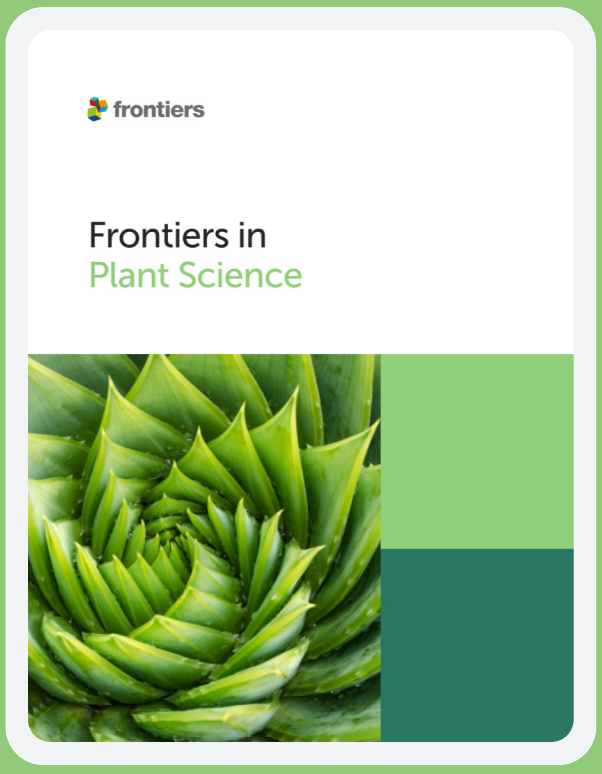

Frontiers

Avenue du Tribunal-Fédéral 34
1005 Lausanne, Switzerland
frontiersin.org

Contact us

+41 (0)21 510 17 00
frontiersin.org/about/contact